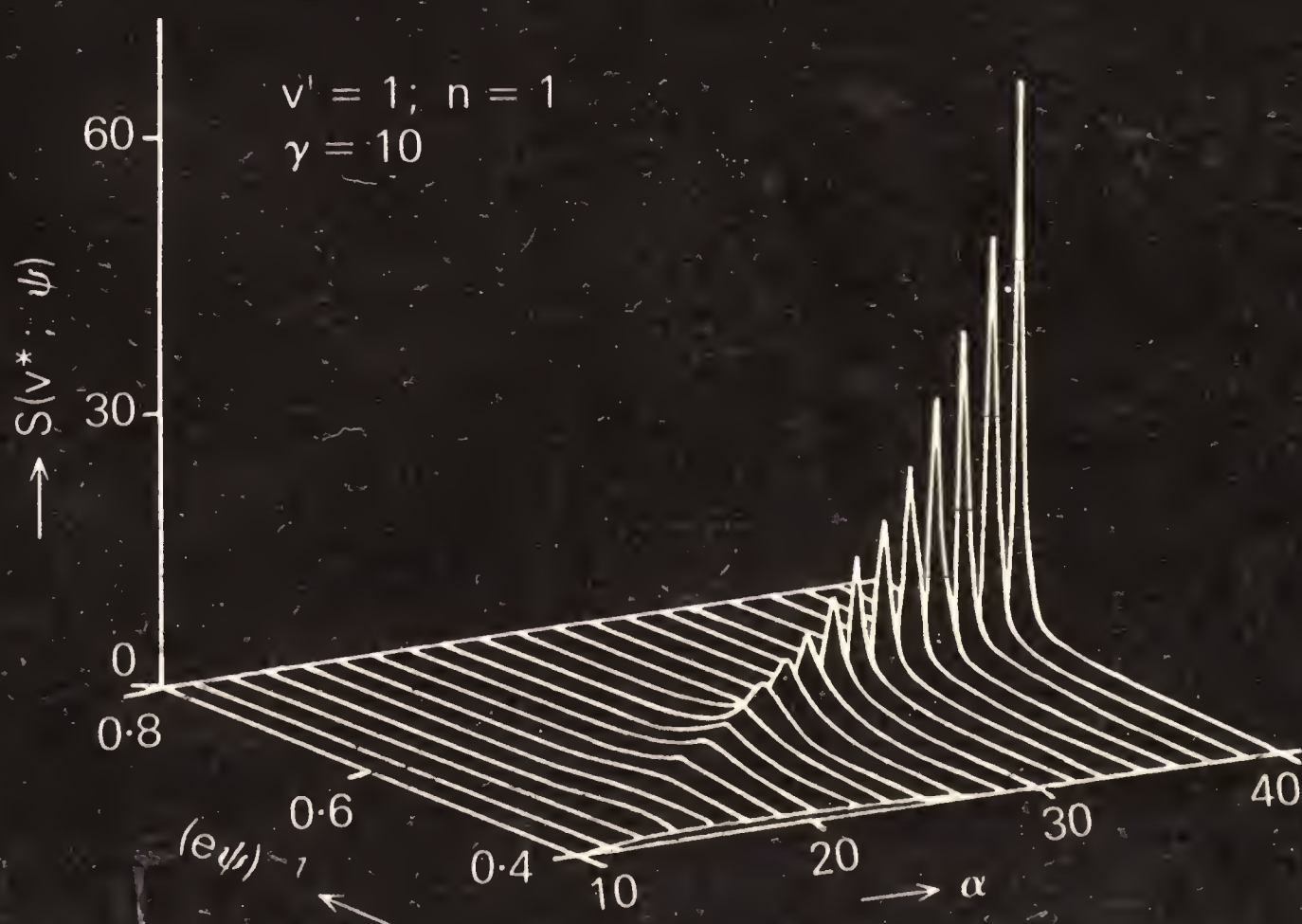


# REACTIONS AND REACTION ENGINEERING

Edited by  
R A MASHELKAR  
R KUMAR



INDIAN ACADEMY OF SCIENCES  
Bangalore 560 080









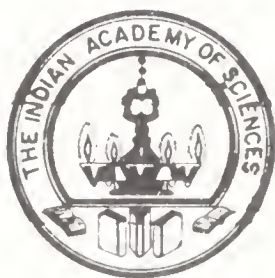
# REACTIONS AND REACTION ENGINEERING

Edited by  
R. A. MASHELKAR

National Chemical Laboratory, Pune

R. KUMAR

Indian Institute of Science, Bangalore



1 9 8 7

INDIAN ACADEMY OF SCIENCES  
BANGALORE 560 080

The cover shows normalized parametric sensitivity in reacting systems from the  
paper by Morbidelli and Varma

© 1987 by the Indian Academy of Sciences

Reprinted from *Sādhanā* – Academy Proceedings in Engineering Sciences  
Volume 10, pp. 1–317, 1987

Edited by R. A. Mashelkar and R. Kumar and printed for the Indian  
Academy of Sciences by Phoenix Printing Co.  
Attibele Industrial Area, Bangalore-562 107, India

# C O N T E N T S

Foreword	i
A Tribute	
List of Publications	
XIAO-HUI SONG and RUTHERFORD ARIS: A global study of Kondepudi's pitchfork	1
DRAGOMIR B BUKUR: The counter-current backmixing model for fluid bed reactors – computational aspects and model modifications	13
J R GRACE, C J LIM, C M H BRERETON and J CHAOUKI: Circulating fluidized bed reactor design and operation	35
C LAGUERIE and D BARRETEAU: Gas desulphurization by sorption of SO <sub>2</sub> on CuO/Al <sub>2</sub> O <sub>3</sub> solid sorbent in a counterflow multistage fluidized bed reactor. Experimental analysis and modelling of the reactor	49
R MURALIDHAR, S GUSTAFSON and D RAMKRISHNA: Population balance modelling of bubbling fluidized beds. II. Axially dispersed dense phase	69
R HUGHES, V DAKESSIAN and A BRITO-ALAYON: Coking and re-generation of fixed bed catalytic reactors	87
M S ANANTH and VINOD JALAN: A comparative study of mathematical models for gas-solid non-catalytic reactions	99
C G DASSORI, J W TIERNEY and Y T SHAH: Transient analysis of the particle-pellet model with structural changes in the solid phase	115
MASSIMO MORBIDELLI and ARVIND VARMA: Parametric sensitivity and runaway in chemical reactors	133
K B ARCURI, L H SCHWARTZ and J B BUTT: Olefin incorporation on supported FeCo alloy Fischer-Tropsch catalysts	149
V G GAIKAR and M M SHARMA: New strategies for separations through reactions	163
H LIVBJERG, T S CHRISTENSEN, T T HANSEN and J VILLADSEN: Theoretical foundation of cluster formation in supported liquid-phase catalysis	185
PETER LEWIS SILVESTON: Periodic operation of chemical reactors – a review of the experimental literature	217
A TSUTSUMI, Y H KIM, S TOGAWA and K YOSHIDA: Classification of three-phase reactors	247
Y H KIM, A TSUTSUMI and K YOSHIDA: Effect of particle size on gas holdup in three-phase reactors	261

P A RAMACHANDRAN, M P DUDUKOVIC and P L MILLS: Recent advances in the analysis and design of trickle-bed reactors	269
KENNETH B BISCHOFF and PAMELA G COXSON: Lumping analysis in the presence of measurement error	299
T FUNAZUKURI and N WAKAO: Supercritical fluid extraction of Chinese Maoming oil shale with water and toluene	307
Author Index	319
Subject Index	000

## Foreword

It gives us great pleasure to present this volume on 'Reaction and Reaction Engineering' which has been brought out in honour of Dr L K Doraiswamy, an outstanding chemical engineer of this country. This festschrift has been brought out to commemorate Dr Doraiswamy's reaching the age of 60 in May 1987.

This volume is essentially a collection of specially invited research papers from various eminent scientists around the world. The contributions reflect directly on the areas in which Doraiswamy has been making consistent and valuable contributions over the past three decades. As editors of this issue we have attempted to bring together top scholars in chemical reaction engineering, an area in which Doraiswamy has carved out a special niche for himself at an international level.

Doraiswamy's contributions to chemical reaction engineering have been extensive and remarkably varied. He has contributed significantly to our understanding of gas-solid reactions (both catalytic and non-catalytic), gas-liquid reactions, solid-solid reactions, poisoning mechanisms and fixed and fluid bed reactors. In each of these areas he has made signal contributions. In recent years he has focussed on fundamental problems associated with adsorption and oscillations in catalytic reactions. In both these areas his work has opened up new vistas. The bulk of his analysis has been concerned with rate forms of the autocatalytic type. Xiao-Hui Song and Aris in their own incisive and elegant way present an analysis of Kondepudi's Pitchfork in their contribution to this volume. The question of selectivity dependence in complex network on the stability considerations is very well-known and the paper draws a parallel on the results in the early work of Doraiswamy with the results presented here.

Doraiswamy has combined theory and practice in chemical reaction engineering in an elegant way. In the area of fluidized bed reactors (FBR) not only has he provided intuitively appealing and elegant analyses of these reactors but has also been instrumental in designing complex commercial fluidised bed reactors such as for chloromethanes. The real problems of modelling FBR are rather complex and engineers need to build models by balancing the complexities of real behaviour with the simplicity of solutions. Doraiswamy's work on the conversion of a difficult two-point boundary value problem into a simple initial value problem is an example of this approach. The contribution by Bukur entitled 'The counter-current backmixing model for fluid bed reactors – Computational aspects and model modifications' relates rather closely to this approach.

Doraiswamy's interest in developing innovative strategies for operation of fluid bed reactors links rather closely with the contribution of Grace and co-workers entitled 'Circulating fluidized bed reactor design and operation' and Laguerie and Barreteau's contribution on gas desulphurization by sorption of  $\text{CO}_2$  on  $\text{CuO}/\text{Al}_2\text{O}_3$  solid sorbent in a counterflow, in this volume.

Doraiswamy's early efforts on deterministic modelling turned to stochastic modelling when he realised the inevitable randomness of the events that occurred



in fluidized bed reactors. Muralidhar, Gustafson and Ramkrishna's contribution on population balance modelling of bubbling fluidized beds, in this volume, pursues a parallel approach in an elegant way.

Doraiswamy has been credited with making major contributions to our efforts on modelling of gas-solid catalytic and non-catalytic systems (moving from pellet to reactors). Not generally satisfied with gross models which brought out 'integral' description of overall performance, he was keen on examining the details of the concentration profiles using sophisticated techniques such as ESCA, EPMA etc. Hughes, Dakessian and Brito-Alayon's contribution entitled 'Coking and regeneration of fixed bed catalytic reactors' provides a nice link with this approach. Doraiswamy's experimental data often provided a basis for comparative evaluation of different models. This spirit is reflected in the contribution by Ananth and Jalan entitled 'A comparative study of mathematical models for gas-solid non-catalytic reactions'.

Doraiswamy was an early contributor who looked at the question of gas-solid structural models and Dassori, Tierney and Shah's article entitled 'Transient analysis of the particle-pellet model with structural changes in the solid phase' looks at this problem including the transients.

Doraiswamy's work in the early seventies on parametric sensitivity in fixed beds and the delineation based on the controlling regimes is considered to be a major effort in chemical reaction engineering. We were fortunate to get a fine contribution from Morbidelli and Varma entitled 'Parametric sensitivity and runaway in chemical reactors' which investigates this problem in its full generality by including the pseudo-homogeneous, heterogeneous and the non-isothermal cases of CSTR.

Doraiswamy's work on catalytic deactivation, especially with reference to the mechanism of deactivation and the attendant mathematical analysis of deactivated catalytic systems is well-known. Arcuri, Schwartz and Butt's contribution on the analysis of the specific problem related to the olefin incorporation on supported FeCo alloy Fischer-Tropsch catalysts is a major contribution in the vital area of Fischer-Tropsch synthesis, whose importance is increasing in modern days.

Doraiswamy's contributions have been so broad and varied that we thought it appropriate to add contributions in other areas of chemically reacting systems, which reflect on the modern trends of building innovative systems or operational modes for 'intensification', to this volume. The papers by Gaikar and Sharma entitled 'New strategies for separations through reactions' and by Villadsen and co-workers entitled 'Theoretical foundation of cluster formation in supported liquid-phase catalysts' provide elegant examples of this. The reactor performance can be improved by novel modes of operations and Silveston's paper entitled 'Periodic operation of chemical reactors – A review of the experimental literature' gives an impressive summary of the benefits that can be reached by periodic operations. The increasing interest in operations of three-phase reactors in chemical industry is reflected in the contributions of Yoshida and co-workers on three-phase reactors, and by Ramachandran, Dudukovic and Mills entitled 'Recent advances in the analysis and design of trickle-bed reactors'. The elegant analysis concerning lumping procedures presented in the article by Bischoff and Coxson entitled 'Lumping analysis in presence of measurement errors' reflects the general thinking Doraiswamy followed in his research and practical endeavours. Although

this entire volume is based on reacting systems, Funazukuri and Wakao's contribution entitled 'Supercritical fluid extraction of Chinese Maoming oil shale with water and toluene' has been included so that Doraiswamy's early work on pulsed extraction columns may be remembered for its quality and timeliness.

We wish to express our grateful thanks to all the contributors for readily agreeing to contribute to this special issue. We are grateful to all those who gave valuable help in processing and editing this issue. We would like to end by expressing the hope that this issue will have some lasting place in the chemical engineering literature not only due to the quality of the contributions but also due to the cause it serves in honouring one of the most distinguished chemical engineers this country has produced.

R A MASHELKAR  
R KUMAR





## Errata

1. p. 11, line immediately before 'References', 'heir' should be 'their'.
2. p. 62, line just after (23), ' $\tilde{C}_{pi}$ ' should be ' $\tilde{C}_{pj}$ '.  
Equations (28) and (29), the denominators in the terms just before the square brackets should be  $(m_{1i} - m_{2i})$ .
3. p. 63, the last two equation numbers on the page are (34) and (35), respectively.  
Line just after (33), 'concentrations' has been misspelt.
4. pp. 69–86 – in the running heads, "Ramkrishna" and "bubbling" have been misspelt.
5. p. 105, (3), 2nd line, ' $De$ ' should be ' $D_e$ '.
6. p. 112, particle diffusivity ' $De$ ' should be ' $D_e$ '.
7. p. 119, on the 2 lines just after (12) –  $T_c$  should be  $T_c^*$ .
8. p. 130, List of symbols – Nu\*, 'Nusselt' has been misspelt.
9. p. 131,  $\rho_g$  is the dimensionless radius of a particle at time  $\theta$ .  
 $\phi$  is the Thiele modulus, defined in (29), not (30).
10. p. 185, Abstract, line 3, read 'reacting' for 'reaching'.
11. p. 190, 2nd para, last line – reference cited is Schubert (1982), not (1922).
12. p. 200, lines 1 and 6, the symbol for pore volume is  $V_p$ .
13. p. 202, first term in brackets after the integral sign should be  $(1/x)$  instead of  $(2/x)$ .
14. p. 329, under the entries ' $\text{CuO}/\text{Al}_2\text{O}_3$ ', 'desulphurization' and 'experimental data' – ' $\text{CO}_2$ ' should be ' $\text{SO}_2$ '.
15. p. 330, under the entries 'modelling', 'multistage fluidized bed' and 'sorption' – ' $\text{CO}_2$ ' should be ' $\text{SO}_2$ '.



Dedicated to Dr L K Doraiswamy on his sixtieth birthday.



*Dr L K Doraiswamy*

## A Tribute

Lakshmangudi Krishnamurthy Doraiswamy, LKD to many of us, is the first chemical engineer to have firmly placed research from an Indian establishment on the world map. He has had a long, fruitful and rewarding career of 33 years with the National Chemical Laboratory (NCL), which is a CSIR laboratory.

LKD started off well, early in his career, with the group contribution method for the estimation of thermodynamic properties and this was included in the standard text of Reid and Sherwood. As a student at Bombay, I was very impressed with this work and I made it a point, later as a teacher, to impress upon my students this important contribution from India. My first encounter with him in 1958 at NCL was due to my own, albeit somewhat short-lived, infatuation with thermodynamics. However, I had no inkling whatsoever at that time that we would have a long and enduring professional and personal relationship. We worked together for several years to publish our two-volume encyclopaedic 'Heterogeneous reactions – analysis, examples, and reactor design' (Wiley-Interscience, USA, 1984).

The NCL duly recognised the importance of chemical engineering, predominantly due to LKD's leadership in process development even for very heavily organic chemistry-oriented projects and Prof. B D Tilak, who was the Director of NCL from 1966 to 1978, gave a pre-eminent role to the Chemical Engineering Division. LKD's heavy involvement in process development for a variety of intricate cases did not, however, come in the way of his first love – engineering science-oriented research.

LKD has made original, innovative and substantial contributions in a variety of fields in chemical reaction engineering. In fact LKD is among the few scientists in the world who have used an integrated approach that includes basic kinetics and catalysis, internal and external field problems, as well as practical reactor design for the industry.

LKD's contributions have been varied and although there is a lot that he has accomplished, it is worthwhile summarizing some of the key features of his work in different areas especially in gas-solid catalytic reactions, multiplicity and instability, stochastic modelling and gas-solid noncatalytic reactions.

LKD has pioneered the surface science approach to catalysis in the solution of reaction engineering problems. A significant contribution was the exact solution of the adsorption integral equation with realistic upper and lower limits of the heat of adsorption. While analysing the diffusion-reaction systems, he proposed an original, intuitive transformation that reduces the mathematical complexities to a bare minimum and has generalised it to include a variety of rate forms.

In the area of catalytic reactor design he showed that runaway criteria can be drastically influenced by transport limitations. He undertook extensive studies on fluidized-bed reactors for complex reactions and showed that dilution of catalysts with inert solids can lead to substantial enhancement of selectivity in fluidized-bed reactors. This finding is of fundamental importance in reactor design.



In gas-solid noncatalytic reactions LKD was among the first to observe and explain an unusual model for complex reactions, where reactions started at the pellet centre. This has subsequently been called the rotten apple model (since the apple rots from the centre). Two other aspects of his contributions in this field are particularly noteworthy. In the case of solids with inerts (as in ores) he has established that the reaction is enhanced in the presence of inerts. He also established rigorously the finite reaction zone model. He has demonstrated experimentally, using for the first time in these reactions such techniques as ESCA and EPMA, the applicability of this general macroscopic model.

LKD's contributions to multiplicity and instability in reactors have brought some fresh insights. He suggested some novel concepts such as feedback of active centres as a possible reason for nonunique behaviour, nonsystemic autocatalytic forms to explain exotic features and transformations among adsorbed species on the catalyst surface as a possible cause of instability, leading to the concept of a priori instability.

In the area of stochastic modelling, his publications are just beginning to appear. These are the first in the CRE literature to note the shortcomings of the conventional macroscopic methods of modelling and provide suitable corrective stochastic formalisms invoking fundamental considerations. All these concepts have been included in his book which he has coauthored with his former student, now his colleague, B D Kulkarni, and will appear later this year. A particularly original and noteworthy contribution has been the hypothesis that oscillations may not be the consequence of any built-in chemical step, but are governed solely by noise.

All the above contributions have academic excellence of the highest order. Indeed LKD has often behaved as an academic and I have always wondered why he did not take a position in academia, even though he has had tempting offers from within India and overseas. It is truly remarkable that, as amply demonstrated by the contributions mentioned above, he has been able to weave academic fibre-oriented ideas into the web of the mundane world of chemical industry with a characteristic finesse of his own.

One of the refreshing features of LKD's contributions to chemical reaction engineering has been his fine blend of theory and practice. About a dozen processes involving reactors of varying degrees of complexity have been developed by LKD. The most novel has been the multi-tubular reactor for dimethylaniline (DMA) from methanol and aniline. This was the first vapour phase reaction of DMA in the world, and employs an additive with the feed which continuously activates the catalyst. This was acclaimed in the *Chemtator* of Chemical Engineering followed by an invited article in its *Process Technology* section.

LKD has had an intense desire to make NCL an institution *par excellence* and he has succeeded admirably as is evident from its work culture and its entry into high-tech closely-guarded areas, particularly novel catalysts and polymers, which have been internationally recognised. NCL has now become a place of 'pilgrimage' for any chemically oriented person in India.

LKD has high respect for the views of other persons even though he may not agree with them. We have also often held very different views on several occasions but it has in no way affected our relationship. I hazard a guess that our predictive capabilities fail when it comes to assessing our views on new issues! He is a very



patient listener – a trait hard to find these days and I am perhaps guilty of making him somewhat more talkative!

The LKD tree has many strong branches which have resplendent flowers and fruits. A number of his former students have earned a name for themselves and one of them has even become a successful entrepreneur! LKD firmly believes that no one is indispensable. He has worked hard to create successors and he has indeed succeeded very well. LKD has an innate desire to write good English and is, therefore, always charmed by literature which elevates him. He is undoubtedly one of our most gifted writers in chemical engineering.

LKD is a person of sharp intellect and imposing personality. He has a penchant for excellence and for him compromise with principles is just not possible. After a long career of 33 years with the NCL, CSIR has aptly honoured LKD by giving him an extension of two years well ahead of his retirement. I am sure with his love for the highest standards of achievements and excellence, he will continue to provide active and inspiring leadership. Indeed he does provide an excellent model for inspiration.

The Indian Academy of Sciences should be congratulated for bringing out this Festschrift.

M M SHARMA  
APRIL 1987



## List of Publications

S. No.	Title	Author(s)	Reference
<i>A. Adsorption and catalysis</i>			
1.	Applications of gas-chromatography in catalysis	V R Choudhary L K Doraiswamy	Ind. Eng. Chem., Prod. Res. Dev., 10(3), 218 (1971), plenary article
2.	The adsorption integral equation: A new method of solution	S D Prasad L K Doraiswamy	Phys. Lett. A, 60(1), 11 (1977)
3.	Instabilities due to surface transformations of adsorbed species: The case of hydrocarbon oxidation	V Ravikumar B D Kulkarni L K Doraiswamy	Chem. Eng. Commun., 20, 367 (1983)
4.	Statistical rates for reactions on heterogeneous surfaces	S D Prasad L K Doraiswamy	Chem. Phys. Lett., 97, 31 (1983)
5.	High coverage adsorption on heterogeneous surfaces: The validity of a limiting isotherm	S D Prasad L K Doraiswamy	Phys. Lett. A, 94, 219 (1983)
6.	Statistical rates for reactions on heterogeneous surfaces: The influence of non-ideal collisions	S D Prasad L K Doraiswamy	Chem. Phys. Lett., 99, 129 (1983)
7.	State of the art of the theory of adsorption and catalysis on heterogeneous surfaces	S D Prasad L K Doraiswamy	"Frontiers in chemical reaction engineering", Vol. 1, eds. L K Doraiswamy and R A Mashelkar, Wiley Eastern (1984), p. 85
8.	Kinetics of catalysis on heterogeneous surfaces: Some unusual pressure relationships	S D Prasad L K Doraiswamy	"Frontiers in chemical reaction Engineering", Vol. 2, eds. L K Doraiswamy and R A Mashelkar, Wiley Eastern (1984), p. 3
9.	Influence of site energy distribution on catalytic rates with multicomponent chemisorption	Y S Bhat S D Prasad L K Doraiswamy	AIChE J. 31, 1585 (1985)
10.	Effects of interaction and mobility on selectivity of a simple reaction scheme	Y S Bhat S D Prasad L K Doraiswamy	J. Catal. 31, 1585 (1985)
11.	Enhancement of steady states through cooperative adsorption	P C Prasannan S D Prasad L K Doraiswamy	Chem. Eng. Commun., 31, 131 (1984)
12.	Characterization of site energy distribution through the estimation of pressure derivatives	S D Prasad L K Doraiswamy	Chem. Phys. Lett., 104, 315 (1984)

S. No.	Title	Author(s)	Reference
13.	Control and prediction of selectivity for reactions occurring on a heterogeneous surface	Y S Bhat S D Prasad L K Doraiswamy	"Catalysis on the energy scene", eds. S Kaliaguine and A Mahay, Elsevier Science Publishers, Amsterdam (1984), p. 419
14.	Exact solution of the adsorption integral equation for a heterogeneous surface	S D Prasad L K Doraiswamy	Chem. Phys. Lett., 108, 83 (1984)
15.	Fixed bed reactor design with non-isothermal catalytic kinetic effects of surface heterogeneity	Y S Bhat S D Prasad L K Doraiswamy	Ind. Eng. Chem., Fundam., (accepted)
16.	Effects of interaction and mobility on the performance of fixed bed reactors	L K Doraiswamy S D Prasad	Chem. Eng. Commun., (Amundson Memorial issue) (expected late 1987)
<i>B. Catalytic reaction and reactor analysis</i>			
17.	The reactor unit concept in process design	G Narsimhan L K Doraiswamy	Br. Chem. Eng., 5, 845 (1960)
18.	Applied reaction kinetics and reactor design	L K Doraiswamy	Br. Chem. Eng., 5, 315 (1961)
19.	Reaction kinetics and reactor design	S P Mukherjee L K Doraiswamy	Br. Chem. Eng., 10, 93 (1965)
20.	Kinetics of the catalytic vapour-phase hydrogenation of nitrobenzene to aniline	D N Rihani T K Narayan L K Doraiswamy	Ind. Eng. Chem., Process Des. Dev., 4, 403 (1965)
21.	A new adiabatic MT reactor system	K Babu Rao S P Mukherjee L K Doraiswamy	AIChE J. 11, 741 (1965)
22.	Reaction kinetics and reactor design, Part I	S P Mukherjee L K Doraiswamy	Br. Chem. Eng., 11, 1380 (1966)
23.	Reaction kinetics and reactor design - Part II	S P Mukherjee L K Doraiswamy	Br. Chem. Eng., 12, 70 (1966)
24.	A kinetic model for the catalyst vapour phase hydrolysis of chlorobenzene	V D Deo L K Doraiswamy	Indian J. Technol., 5, 174 (1967)
25.	A generalised equation for solids distribution in the semifluidized MT reactor	K Babu Rao L K Doraiswamy	AIChE J. 13, 397 (1967)
26.	Controlling mechanisms in benzene oxidation	K Vaidyanathan L K Doraiswamy	Chem. Eng. Sci., 23, 537 (1968)
27.	Controlling mechanisms in the selective oxidation of toluene to benzaldehyde	K A Reddy L K Doraiswamy	Chem. Eng. Sci., 24, 1415 (1969)

S. No.	Title	Author(s)	Reference
28.	Controlling mechanisms in the catalytic vapour-phase ethylation of aniline	Prakash Goyal L K Doraiswamy	Ind. Eng. Chem., Process Des. Dev., 9, 26 (1970)
29.	Combined reactors: Formulation of criteria and operation of mixed tubular semi-fluidized reactor	K Babu Rao L K Doraiswamy	AIChE J. 16, 273 (1970)
30.	A generalised effectiveness factor plot for second-order reactions	Ajit Sadana L K Doraiswamy	Chem. Age India, 22(2), 85 (1971)
31.	Isomerization of <i>n</i> -butene to isobutene. I: Selection of catalyst by group screening	V R Choudhary L K Doraiswamy	J. Catal. 23, 54 (1971)
32.	Effect of catalyst fouling in fixed-, moving and fluid-bed	Ajit Sadana L K Doraiswamy	J. Catal. 23, 147 (1971)
33.	Development of continuous-stirred gas-solid reactors for studies in kinetics and catalyst evaluation	V R Choudhary L K Doraiswamy	Ind. Eng. Chem., Process Des. Dev., 11, 420 (1972)
34.	Effect of fouling in a fixed-bed reactor for a complex reaction: Test of proposed model and formulation of an optimal policy	K B S Prasad L K Doraiswamy	J. Catal. 32, 384 (1974)
35.	Laboratory catalytic reactors	D G Tajbl L K Doraiswamy	Cat. Rev. Sci. Eng., 10, 177 (1974)
36.	A kinetic model for the isomerization of <i>n</i> -butene to isobutene	V R Choudhary L K Doraiswamy	Ind. Eng. Chem. Process Des. Dev., 14, 227 (1975)
37.	Effectiveness factors in gas-liquid reactions	B D Kulkarni L K Doraiswamy	AIChE J. 21, 501 (1975)
38.	Parametric sensitivity in fixed-bed reactors	R A Rajadhyaksha K Vasudeva L K Doraiswamy	Chem. Eng. Sci., 30, 1399 (1975)
39.	Effectiveness factors in gas-liquid reactions: The general <i>n</i> th order case	B D Kulkarni L K Doraiswamy	AIChE J. 22, 597 (1976)
40.	Effectiveness factors in Langmuir-Hinshelwood and general order kinetics	R A Rajadhyaksha K Vasudeva L K Doraiswamy	J. Catal., 41, 61 (1976)
41.	Falsification of kinetic parameters by transport limitations and its role in discerning the controlling regime	R A Rajadhyaksha L K Doraiswamy	Catal. Rev. Sci. Eng., 13, 1209 (1976)
42.	Effective diffusivities under reaction conditions (isobutene in fluorinated alumina)	N S Raghavan L K Doraiswamy	Ind. Eng. Chem., Process Des. Dev., 16, 519 (1977)
43.	On the validity of kinetic modelling for vapour phase catalytic reactions: Isomerization of <i>n</i> -butene to isobutene	N S Raghavan L K Doraiswamy	J. Catal., 48, 21 (1977)

Continued



S. No.	Title	Author(s)	Reference
44.	Generalized dehydration models for <i>n</i> -aliphatic monohydric alcohols	S M Abhyankar L K Doraiswamy	Can. J. Chem. Eng., 57, 481 (1979)
45.	Some unusual observations concerning the adsorption of thiophene on copper chromite	S D Sansare V R Choudhary L K Doraiswamy	J. Catal., 60, 21 (1979)
46.	Transport accompanied by chemical reaction in stagnation flow	K S Balaraman R A Mashelkar L K Doraiswamy	AIChE J., 26, 635 (1980)
47.	Estimation of effective transport properties in packed-bed reactors	B D Kulkarni L K Doraiswamy	Cat. Rev. Sci. Eng., 22, 431 (1980)
48.	Effectiveness factors in bidispersed catalysts: The general <i>n</i> th order case	B D Kulkarni V K Jayaraman L K Doraiswamy	Chem. Eng. Sci., 36, 943 (1981)
49.	Transient analysis of a stirred gas-solid reactor	S D Prasad L K Doraiswamy	J. Catal., 67, 21 (1981)
50.	Influence of catalyst deactivation on the nature of the steady state solution for reactions on catalytic surfaces	V Ravi Kumar B D Kulkarni L K Doraiswamy	Chem. Eng. Commun., 17, 305 (1982)
51.	A simple method for solution of a class of reaction-diffusion problems	V K Jayaraman B D Kulkarni L K Doraiswamy	AIChE J. 29, 521 (1983)
52.	Dynamics of coupled CSTRs operating at different steady state conditions	V Ravi Kumar V K Jayaraman B D Kulkarni L K Doraiswamy	Chem. Eng. Sci., 35, 673 (1983)
53.	Some aspects of diffusion interference in complex catalytic reactions	V K Jayaraman L K Doraiswamy	Curr. Sci., 52, 283 (1983)
54.	An initial value approach to reaction-diffusion problems	Asha Namjoshi B D Kulkarni L K Doraiswamy	AIChE J. 30, 915 (1984)
55.	Multiplicity and instability in isothermal homogeneous reactions in CSTR: The case of autocatalysis	V Ravi Kumar B D Kulkarni L K Doraiswamy	AIChE J. 30, 649 (1984)
56.	Kinetics of vapour phase deamination of diethylenetriamine over an alumina catalyst	Y S Bhat B D Kulkarni L K Doraiswamy	Ind. Eng. Chem., Process Des. Dev., 24, 525 (1985)
57.	Carbonylation of nitrobenzene to phenyl isocyanate using palladium complex catalysts	S B Halligudi R V Chaudhari L K Doraiswamy	Ind. Eng. Chem., Process Des. Dev., 23, 794 (1983)
58.	Reversible adsorption of thiophene on copper chromite	S D Sansare V R Choudhary L K Doraiswamy	J. Chem. Technol. Bio-technol, 33A, 140 (1983)

S. No.	Title	Author(s)	Reference
59.	Effectiveness factors in bidispersed catalysts under conditions of catalyst fouling	Asha Datar B D Kulkarni L K Doraiswamy	Chem. Eng. Commun., 32, 377 (1985)
60.	Effectiveness factors for bidispersed catalyst under non-isothermal conditions	Asha Datar B D Kulkarni L K Doraiswamy	AIChE J. 32, 859 (1986)
61.	New catalyst revised dimethylaniline production	G R Venkitakrishnan S P Mukherjee L K Doraiswamy	Chem. Eng., 88, 78 (1981)
<i>C. Gas-solid reactions</i>			
62.	Mass transfer model for Kolbe-Schmitt carbonation of 2-naphthol	P G Phadtare L K Doraiswamy	Ind. Eng. Chem., Process Des. Dev., 4, 274 (1965)
63.	Kolbe-Schmitt carbonation of 2-naphthol: Confirmation of the mass transfer model and process optimization	P G Phadtare L K Doraiswamy	Ind. Eng. Chem., Process Des. Dev., 8, 165 (1969)
64.	A model for solid-gas reactions	A N Gokarn L K Doraiswamy	Chem. Eng. Sci., 26, 1521 (1971)
65.	Measurement of diffusion in the "ash layer" in gas-solid reactions	A N Gokarn L K Doraiswamy	Chem. Eng. Sci., 27, 1515 (1972)
66.	Solid-gas reactions: Effect of solid shape on proposed diffusion model	A N Gokarn L K Doraiswamy	Chem. Eng. Sci., 28, 401 (1973)
67.	Gas-solid reactions: An unusual observation in the disproportionation of potassium benzoate to terephthalate	M V Goghale A T Naik L K Doraiswamy	Chem. Eng. Sci., 30, 1409 (1975)
68.	Analysis of gas-solid reactions formulation of general model	V B Mantri A N Gokarn L K Doraiswamy	Chem. Eng. Sci., 31, 779 (1976)
69.	A delayed diffusion model for an unusual reaction (disproportionation of potassium benzoate to terephthalate) involving an expanding reaction zone	B D Kulkarni L K Doraiswamy	Chem. Eng. Sci., 35, 817 (1980)
70.	Modelling of noncatalytic gas-solid reactions	P A Ramachandran L K Doraiswamy	AIChE J. 28, 898 (1982)
71.	Gas-solid reactions: Experimental evaluation of the zone model	P C Prasannan L K Doraiswamy	Chem. Eng. Sci., 37, 925 (1982)
72.	Analysis of gas-solid reactions with zero order dependency on both gas and solid: Concept of jumping reaction zones	P A Ramachandran L K Doraiswamy	AIChE J., 28, 881 (1982)

Continued



S. No.	Title	Author(s)	Reference
73.	Gas-solid reactions: A method of direct solution for solid conversion profiles	P C Prasannan P A Ramachandran L K Doraiswamy	Chem. Eng. J., 33, 19 (1986)
74.	An evaluation of the expanding core model in the disproportionation of potassium benzoate	V V S Revankar B D Kulkarni L K Doraiswamy	Chem. Eng. Sci., (in press)
75.	A model for gas-solid reactions with structural changes in presence of inert solids	P C Prasannan P A Ramachandran L K Doraiswamy	Chem. Eng. Sci., 40, 1251 (1985)
76.	Catalytic gasification of carbon by steam: Effect of sodium salts	V V S Revankar A N Gokarn L K Doraiswamy	Third International Conference on Coal Science, Sydney (Australia) (1985),
<i>D. Fluidization</i>			
77.	Chlorination of ilmenite in a fluidized bed	H C Bijawat M V Kunte L K Doraiswamy	Chem. Eng. Prog., 55(10), 80 (1959)
78.	Effect of catalyst dilution on the performance of a fluid bed reactor for complex first-order reactions	R K Irani B D Kulkarni L K Doraiswamy	Ind. Eng. Chem., Process Des. Dev., 18, 648 (1979)
79.	Analysis of complex reaction schemes in a fluidized bed: Application of the Kunii-Levenspiel model	R K Irani B D Kulkarni L K Doraiswamy	Ind. Eng. Chem., Process Des. Dev., 19, 24 (1980)
80.	Analysis of fluid-bed reactors for reactions involving a change in volume	R K Irani B D Kulkarni L K Doraiswamy	Ind. Eng. Chem., Fundam., 19, 424 (1980)
81.	Criteria for temperature multiplicity in fluidized bed reactors	B D Kulkarni P A Ramachandran L K Doraiswamy	Proceedings of the Conf. on Fluidization (Engineering Foundation of USA), "Fluidization", eds. J R Grace and J M Matsen (1980), p. 589
82.	Optimal production of intermediate for zero-first and first-first order reactions sequences in fluidized bed reactors	R K Irani V K Jayaraman B D Kulkarni L K Doraiswamy	Chem. Eng. Sci., 36, 29 (1981)
83.	An initial value approach to the counter-current backmixing model of the fluid bed	V K Jayaraman B D Kulkarni L K Doraiswamy	ACS Symp. Series, No. 168, Chemical Reactors, ed. H. C. Fogler (1981), p. 19
84.	Catalyst dilution to improve the selectivity of intermediate in complex reactions in fluid beds: An experimental verification	R K Irani B D Kulkarni S Z Hussain L K Doraiswamy	Ind. Eng. Chem., Process Des. Dev., 21, 188 (1982)

S. No.	Title	Author(s)	Reference
<i>E. Stochastic modelling of chemically reacting systems</i>			
85.	A stochastic approach to the analysis of chemically reacting systems, Part I: Analysis of the role of fluctuations in reacting systems	S S Tambe B D Kulkarni L K Doraiswamy	Chem. Eng. Sci., 40, 1943 (1985)
86.	A stochastic approach to the analysis of chemically reacting systems, Part II: Sustained oscillations on catalytic surfaces	S S Tambe V Ravi Kumar B D Kulkarni L K Doraiswamy	Chem. Eng. Sci., 40, 1951 (1985)
87.	A stochastic approach to the analysis of chemically reacting systems, Part III: Critical slowing down in reacting systems	S S Tambe B D Kulkarni L K Doraiswamy	Chem. Eng. Sci., 40, 1959 (1985)
88.	A stochastic approach to the analysis of chemically reacting systems, Part IV: Critical slowing down in autocatalysis	S S Tambe B D Kulkarni L K Doraiswamy	Chem. Eng. Sci., 40, 2293 (1985)
89.	A stochastic approach to the analysis of chemically reacting systems, Part V: Estimation of mean passage time for reaching a threshold value using the asymptotic theory of Fokker-Planck processes	S S Tambe B D Kulkarni L K Doraiswamy	Chem. Eng. Sci., 40, 2297 (1985)
90.	A stochastic approach to the analysis of chemically reacting systems, Part VI: The case of autocatalysis followed by non-elementary reaction	S S Tambe V Ravikumar B D Kulkarni L K Doraiswamy	Chem. Eng. Sci., 40, 2303 (1985)
91.	A stochastic approach to the analysis of chemically reacting systems, Part VII: Influence of external noise on the behaviour of fluid-bed with non-linear reaction rates	N S Dabke B D Kulkarni L K Doraiswamy	Chem. Eng. Sci., 41 1771 (1986)
92.	On the origin of oscillations in chemically reacting systems	B D Kulkarni N S Dabke L K Doraiswamy	Chem. Eng. Sci., 40, 2007 (1985)
93.	Role of external white and non-white Poisson noise on the behaviour of chemically reacting systems: The case of single variable multistationary systems	N S Dabke B D Kulkarni L K Doraiswamy	Chem. Eng. Sci., 41, 2891 (1986)
94.	Stochastic analysis of a model reaction system: The occurrence of noise induced transitions	N S Dabke B D Kulkarni L K Doraiswamy	Presented at ISCRE-9, Philadelphia, USA, Chem Eng. Sci., 41, 891 (1986)

Continued

S. No.	Title	Author(s)	Reference
95.	Stochastic modelling of fluid bed reactor	N S Dabke B D Kulkarni L K Doraiswamy	"Advances in transport processes", eds. A S Mujumdar and R A Mashelkar (1987)
96.	On the relevance of stochastic modelling in chemically reacting systems	B D Kulkarni L K Doraiswamy	Ind. Eng. Chem., Fundam. (Hougen memorial issue), (1986)
<i>F. Thermodynamic and transport properties</i>			
97.	Diffusion in binary gaseous systems	L K Doraiswamy	Chem. Eng., 64, No. 6 334 (1957)
98.	Thermodynamic properties of vinyl chloride	S C Banerjee L K Doraiswamy	Br. Chem. Eng., 3, 316 (1958)
99.	Estimation of gaseous densities	M V Kunte L K Doraiswamy	Chem. Process Eng. 39, 157 (1958)
100.	Enthalpy-concentration chart for the system urea-water	S C Banerjee L K Doraiswamy	Br. Chem. Eng., 5, 269 (1960)
101.	A generalised method for estimating heats of vaporization	M V Kunte L K Doraiswamy	Chem. Eng. Sci., 12, 1 (1960)
102.	Binary vapour-liquid equilibria involving 1,2-dichloroethane and 1,1,1 and 1,1,2-trichloroethane	D C Bigg S C Banerjee L K Doraiswamy	J. Chem. Eng. Data, 9, 17 (1964)
103.	Catalytic vapour phase hydrogenation of acetone to isopropyl alcohol: A process development study	N K Maitra K D Pathak B S Subba Rao L K Doraiswamy	Indian J. Technol., 2, 293 (1964)
104.	Thermodynamic properties of organic compounds, Part I: normal symmetrical ethers	S C Banerjee L K Doraiswamy	Br. Chem. Eng., 9, 311 (1964)
105.	Thermodynamic properties of organic compounds, Part II: normal alkylbenzene sulphuric acids	D C Bigg S C Banerjee L K Doraiswamy	Br. Chem. Eng., 9, 688 (1964).
106.	Alternate method for vapour heat capacity	M S Kothari L K Doraiswamy	Hydrocarbon Process Pet. Refiner, 43, 133 (1964)
107.	Estimation of the heat capacity of organic compounds from group contributions	D N Rihani L K Doraiswamy	Ind. Eng. Chem., Fundam., 4(1), 17 (1965)
108.	Estimation of heats of formation of organic compounds	K K Varma L K Doraiswamy	Ind. Eng. Chem., Fundam., 4(4), 389 (1965)
109.	Estimating liquid densities	P Goyal L K Doraiswamy	Hydrocarbon Process. Pet. Refiner, 45, 200 (1966)
110.	Generalised charts for viscosity estimation	K Babu Rao L K Doraiswamy	Indian J. Technol., 4, 141 (1966)
111.	Acetone-isopropanol system: Equilibrium and enthalpy-concentration chart	S N Balasubramanian S C Banerjee L K Doraiswamy	Br. Chem. Eng., 11, 1540 (1966)

S. No.	Title	Author(s)	Reference
112.	An equation for estimating liquid diffusivities	R Pratap L K Doraiswamy	Indian J. Technol., 5, 145 (1967)
113.	Estimating liquid diffusivities	K A Reddy L K Doraiswamy	Ind. Eng. Chem., Fundam., 6, 77 (1967)
114.	Estimation of the ideal/gas entropy of organic compounds	D N Rihani L K Doraiswamy	Ind. Eng. Chem., Fundam., 7, 375 (1968)
115.	A generalised method for estimating the latent heat of vaporization of organic compounds	S R S Sastri M V Ramana Rao K A Reddy L K Doraiswamy	Br. Chem. Eng., 14, 959 (1968)
116.	Physical properties in the reaction of ethylene and hydrogen chloride in liquid media: Diffusivities and solubilities	R V Chaudhari L K Doraiswamy	J. Chem. Eng. Data, 17, 428 (1972)
<i>G. Miscellaneous</i>			
117.	Study of the kinetics of semi-chemical pulping	J N McGovern L K Doraiswamy	Report of the Annual Tech. Conf. of the American Paper & Pulp Organization, Report No. 6, May 13, 1952, p. 13.
118.	Emulsion paints	R L Carlisle L K Doraiswamy	Encycl. of Chem. Technol., Intersci. Encycl. Inc. New York, 9, 795 (1952)
119.	Fundamental chemical relations	J N McGovern L K Doraiswamy	Report of the Annual Tech. Conf. of the American Paper & Pulp Organization, Report No. 9, June 2, 1953, p. 15
120.	Behaviour of active carbons in the catalytic dehydrochlorination of ethylene dichloride to vinyl chloride	M U Pai L K Doraiswamy	J. Sci. Ind. Res., 87, 15B (1956)
121.	Production of polyvinyl chloride from alcohol (a complete review)	M U Pai L K Doraiswamy	Popular Plastics, 11, 35 (1957)
122.	Performance of a pulsed heat exchanger	N B Patel L K Doraiswamy	J. Sci. Ind. Res., 18A, 522 (1959)
123.	A process study of the polymerization of vinyl chloride	P H Brahme M U Pai L K Doraiswamy	J. Sci. Ind. Res., 18B, 17 (1959)
124.	Upping column extraction efficiency by pulse application in packed columns	H C Bijawat G V Potnis L K Doraiswamy	Ind. Eng. Chem., 51, 645 (1959)
125.	Thermal dehydrochlorination of ethylene dichloride	P H Brahme M U Pai S Chidambaram L K Doraiswamy	Br. Chem. Eng., 5, 618 (1960)

Continued



S. No.	Title	Author(s)	Reference
126.	Nomogram for heat transfer coefficient in agitated kettles	L K Doraiswamy	Br. Chem. Eng., 6, 196 (1961)
127.	Active carbons as catalysts in the chlorination of ethylene	S P Mukherjee M Goswami L K Doraiswamy	Proceedings of the Symposium on Active Carbons, Hyderabad (1964)
128.	Statistical approach to indanthrone production	S N Balasubramanian R Shantaram L K Doraiswamy	Br. Chem. Eng., 12, 377 (1967)
129.	Falsification of the kinetics of azobis-isobutyronitrile decomposition	M G Kulkarni R A Mashelkar L K Doraiswamy	J. Polym. Sci. (Lett), 17, 713 (1979)
130.	Solvent and viscosity effects in the decomposition of azobis-isobutyronitrile	M G Kulkarni R A Mashelkar L K Doraiswamy	Chem. Eng. Sci., 35, 823 (1980)
131.	A mass transfer model for ethylene dichloride formation in a stirred tank reactor	S N Balasubramanian D N Rihani L K Doraiswamy	Ind. Eng. Chem., Fundam., 5, 184 (1966)
132.	Absorption of phosphine in an aqueous solution of formaldehyde and hydrochloric acid	R V Chaudhari L K Doraiswamy	Chem. Eng. Sci., 29, 129 (1974)
133.	Simultaneous absorption and reaction of two gases in a liquid/formation of ethyl chloride from ethylene and hydrogen chloride	R V Chaudhari L K Doraiswamy	Chem. Eng. Sci., 29, 675 (1974)
134.	Simultaneous absorption of two gases accompanied by a complex chemical reaction: Approximate solutions	R V Chaudhari B D Kulkarni V A Juvekar L K Doraiswamy	Chem. Eng. Sci., 30, 945 (1975)

### Books

1. *Heterogeneous reactions: analysis, examples and reactor design* L K Doraiswamy and M M Sharma, Vol. I, John Wiley, New York, 1984
2. *Heterogeneous reactions: analysis, examples and reactor design* L K Doraiswamy and M M Sharma, Vol. II, John Wiley, New York, 1984
3. *Recent advances in the engineering analysis of chemically reacting systems* ed. L K Doraiswamy, Wiley Eastern, New Delhi, 1984
4. *Frontiers in chemical reaction engineering: Proceedings of the International Chemical Reaction Engineering Conference* eds. L K Doraiswamy and R A Mashelkar, Vol. I, Wiley Eastern, New Delhi, 1984
5. *Frontiers in chemical reaction engineering: Proceedings of the International Chemical Reaction Engineering Conference* eds. L K Doraiswamy and R A Mashelkar, Vol. II, Wiley Eastern, New Delhi, 1984
6. *Transport processes in fluidized-bed reactors*, eds. L K Doraiswamy and B D Kulkarni, Wiley Eastern, New Delhi, 1987
7. *Analysis of chemically reacting systems – a stochastic approach*, L K Doraiswamy and B D Kulkarni, Gordon and Breach, London, 1987

**Chapters in books**

1. Instabilities in nonlinear reaction and reaction-diffusion systems, in *Recent advances in the engineering analysis of chemically reacting systems* ed. L K Doraiswamy, Wiley Eastern, New Delhi, pp. 156–190, 1984.
2. Modelling of gas-solid reactions, in *Handbook for heat and mass transfer: Vol. II. Mass transfer and reactor design* ed. N P Cheremisinoff, Gulf Publishing, Houston, pp. 1107–1136, 1986
3. Gas-solid reactions in *Chemical reaction and reactor analysis* ed. J J Carberry and A Verma, Marcel Dekker, New York, pp. 293–372, 1986
4. Stochastic modelling of fluidized-bed reactors, in *Transport processes in fluidized-bed reactors* – a special issue in the series *Advances in transport processes* ed. L K Doraiswamy and B D Kulkarni (series editors, A S Mujumdar and R A Mashelkar), Wiley Eastern, New Delhi, 1987





# A global study of Kondepudi's pitchfork

XIAO-HUI SONG and RUTHERFORD ARIS

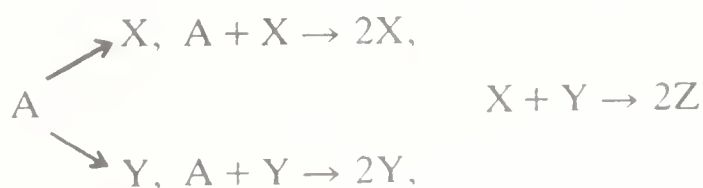
Department of Chemical Engineering, University of Minnesota, 421 Washington Avenue SE, Minneapolis, MN 55455, USA

**Abstract.** This model reaction, studied so effectively by Kondepudi and his co-workers, is transferred here to a stirred tank. It is shown that, though the rate constants for the two pathways are identical, the stable steady state can still be one in which one or the other pathway is favoured enormously.

**Keywords.** Kondepudi's pitchfork reaction; stirred tank reactor, stable steady state.

## 1. Introduction

There is scarcely a topic in the field of chemical reaction engineering or the development of industrial reactors that would not be suitable as a tribute to L K Doraiswamy on his 60th anniversary. The system of reactions examined in this paper is rather distantly connected to the work of Doraiswamy and his colleagues on stochastic effects in chemical reactors (Tambe *et al* 1985a-f; Dabke *et al* 1986) for it is a system that has been used by Kondepudi and his coworkers (Kondepudi & Nelson 1983, 1984) to examine the effect of fluctuations at the bifurcation point. It takes its motivation from studies of chirality since X and Y in the schema



may well be optical isomers. Kondepudi showed that such a system in which the rate constants for the two pathways differed in activation energy by as little as  $10^{-15}$  might still exhibit distinct chiral selectivity under the influence of external fluctuations.

Though it is with similarly difficult questions of stochastic analysis that Doraiswamy and his coworkers have been concerned, his experience of actual reactors has led him to consider realistic systems. It is hoped therefore that he will appreciate the value of studying these reactions in the stirred tank reactor in a purely traditional way.

We shall show that if the autocatalytic steps are sufficiently dominant, the stable steady state of the stirred tank is not the symmetric one with equal concentrations of X and Y, but one in which X or Y dominates even though the rate constants in the two pathways are identical. When one path is slightly preferred the corresponding asymmetric state has an enhanced region of attraction.

## 2. Model of autocatalytic alternative reactions and their steady state solutions

Consider the reactions in the scheme above and take the rate constants of the steps  $A \rightarrow X$  and  $A \rightarrow Y$  as  $k_1$  and  $k'_1$ , those of the autocatalytic steps as  $k_2$  and  $k'_2$  and of the last step as  $k_3$ . We use  $a, x, y$  to represent the concentrations of species A, X and Y. In the stirred tank of volume  $V$  with a feed of pure A at concentration  $a_0$ , and flow rate  $q$ ,

$$V(da/dt) = q(a_0 - a) - V[k_1a + k_2ax + k'_1a + k'_2ay],$$

$$V(dx/dt) = -qx + V[k_1a + k_2ax - k_3xy],$$

$$V(dy/dt) = -qy + V[k'_1a + k'_2ay - k_3xy].$$

We wish to use dimensionless variables and parameters and to isolate the effect of residence time ( $V/q$ ) in a distinguished parameter  $\theta$ ,

$$(V/q) = \theta, \quad u = (a/a_0) \quad v = (x/a_0) \quad w = (y/a_0), \quad \tau = k_3a_0t,$$

$$\mu = k_3a_0\theta, \quad k_1/k_3a_0 = \alpha + \varepsilon, \quad k'_1/k_3a_0 = \alpha - \varepsilon, \quad k_2/k_3 = \beta + \eta,$$

$$k'_2/k_3 = \beta - \eta,$$

then

$$\mu \dot{u} = 1 - u - \mu[2\alpha + (\beta + \eta)v + (\beta - \eta)w]u, \quad (1)$$

$$\mu \dot{v} = -v + \mu[(\alpha + \varepsilon) + (\beta + \eta)v]u - \mu vw, \quad (2)$$

$$\mu \dot{w} = -w + \mu[(\alpha - \varepsilon) + (\beta - \eta)w]u - \mu vw. \quad (3)$$

In the steady state,  $\dot{u} = \dot{v} = \dot{w} = 0$ , and the values of  $u, v, w$ , denoted by  $\bar{u}, \bar{v}, \bar{w}$ , satisfy

$$\mu \bar{u} = \mu / \{1 + \mu[2\alpha + (\beta + \eta)\bar{v} + (\beta - \eta)\bar{w}]\} \quad (4)$$

$$= [\bar{v}(1 + \mu\bar{w})] / [(\alpha + \varepsilon) + (\beta + \eta)\bar{v}] \quad (5)$$

$$= [\bar{w}(1 + \mu\bar{v})] / [(\alpha - \varepsilon) + (\beta - \eta)\bar{w}] \quad (6)$$

$$= \{\mu[1 - (\bar{v} + \bar{w}) - 2\mu\bar{v}\bar{w}]/1\}, \quad (7)$$

where (7) is derived from the previous three by adding their numerators and their denominators. From (5) and (6)

$$[\alpha - \mu\beta(\bar{v}\bar{w})](\bar{v} - \bar{w}) = \varepsilon[\bar{v} + \bar{w} + 2\mu\bar{v}\bar{w}] + \eta[2 + \bar{v} + \bar{w}]\bar{v}\bar{w}. \quad (8)$$

Consider the case  $\varepsilon = \eta = 0$ , first. We have

$$\bar{v} = \bar{w}, \quad (9)$$

or

$$\bar{v}\bar{w} = \alpha/\mu\beta, \quad (10)$$

for the symmetric and the unsymmetric branches respectively. On the symmetric branch, let us set the common value of  $\bar{v} = \bar{w} = x$  so that from (7)  $\bar{u} = 1 - 2x - 2\mu x^2$ . Using (5), (6) and (7) we have

$$2\beta\mu^2x^3 + \mu(1 + 2\beta + 2\alpha\mu)x^2 + [1 + (2\alpha - \beta)\mu]x - \alpha\mu = 0, \quad (11)$$

which has just one positive root for any  $\alpha, \beta, \mu$ .

Rather than solve this cubic for  $x$  we may treat  $x$  as a parameter and the equation as a quadratic in  $\mu$ , giving

$$\mu = \{P \pm (P^2 - 2xQ)^{1/2}\}/Q, \quad (12)$$

$$P = \alpha - (2\alpha - \beta)x - (1 + 2\beta)x^2, \quad Q = 4(\alpha + \beta x)x^2.$$

As  $x$  varies from 0 to  $X$ , the value which makes  $P^2 = 2xQ$ ,  $\mu_+$  varies from  $\infty$  to  $M$  and  $\mu_-$  from 0 to  $M$ .  $X$ , which is always less than  $1/2$ , satisfies

$$\alpha + \beta X = \{X/[1 - (2X)^{1/2}]\}^2, \quad (13)$$

$$M = [1 - (2X)^{1/2}]/(2X^3)^{1/2}. \quad (14)$$

Figure 1 shows the lines of constant  $M$ , or  $X$ , in the  $\alpha, \beta$ -plane; those for  $M = 0.5, 1, 2$  are shown. They have vertical and horizontal asymptotes given by

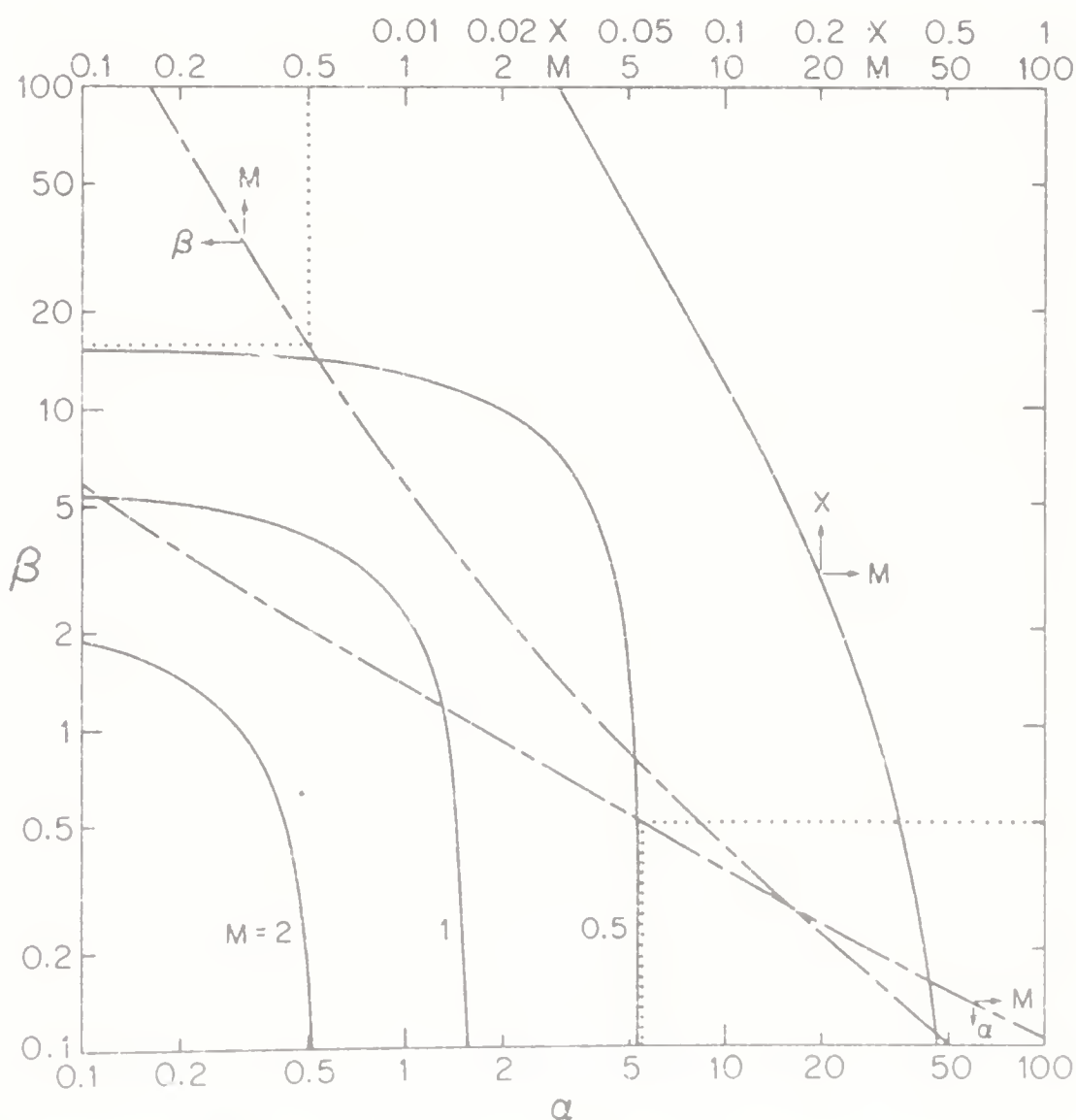


Figure 1. Loci of constant  $M(\alpha, \beta)$ . Auxiliary broken curves give asymptotes for any  $M$  as shown by the dotted lines. Relation between  $X$  and  $M$  shown at right

$X/[1 - (2X)^{1/2}]^2$  and  $X/[1 - (2X)^{1/2}]^2$ , respectively, shown by the broken lines. The relation (14) between  $M$  and  $X$  is shown by the solid curve on the right which has the vertical asymptote  $X = 0.5$ .

Thus the locus of symmetric steady states is a loop

$$\begin{aligned} U^2 - [1 + 2x - x^2/(\alpha + \beta x)]U + 2x &= 0, \\ U &= 1 - \bar{u}, \quad \bar{v} = \bar{w} = 0, \end{aligned} \quad (15)$$

connecting  $\bar{u} = 1, \bar{v} = \bar{w} = 0$  ( $\mu = 0$ ) to the origin ( $\mu = \infty$ ) as shown in figure 2. The asymptotic properties near  $x = 0$  are:

$$\alpha \neq 0$$

$$\mu_+ = \frac{1}{2x^2} - \frac{1}{x} - \frac{1}{2\alpha} + \frac{\beta - 2\alpha}{2\alpha^2}x$$

$$u_+ = \frac{x^2}{\alpha} - \frac{(\beta - 2x)x^3}{\alpha^2} \dots$$

$$\mu_- = \frac{x}{\alpha} + \frac{2\alpha - \beta}{\alpha^2}x^2 + \frac{1 + 2\beta}{\alpha^2}x^3$$

$$u_- = 1 - 2x - \frac{2}{\alpha}x^3 \dots$$

$$\alpha = 0$$

$$\mu_+ = \frac{1}{2x^2} - \frac{1}{x} - \frac{1}{\beta} \dots$$

$$u_+ = \frac{x}{\beta}(1 + 2x) \dots$$

$$\mu_- = \frac{1}{\beta} + \frac{1 + 2\beta}{\beta^2}x \dots$$

$$u_- = 1 - 2x - 2x^2/\beta.$$

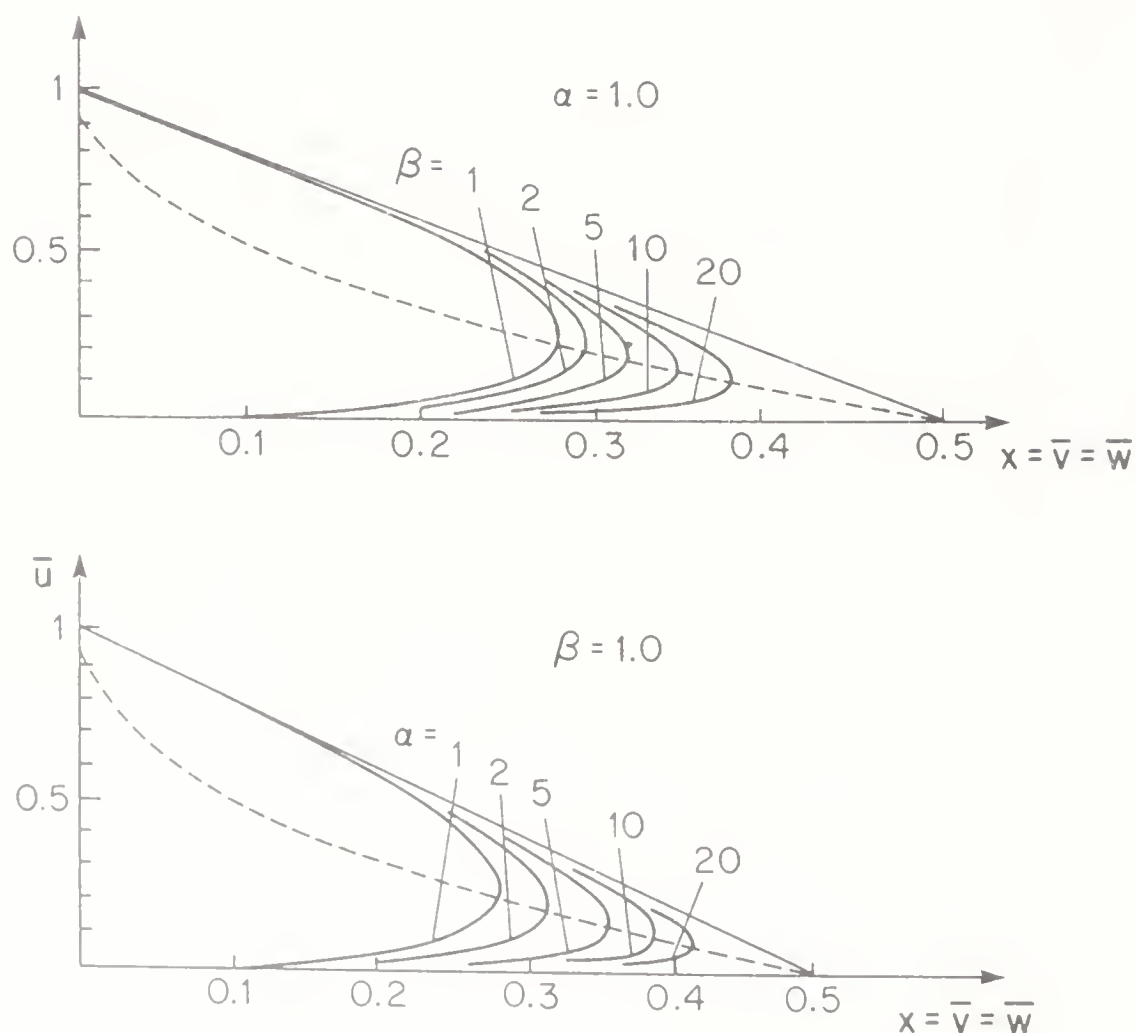


Figure 2. Typical loci of steady states for fixed  $\alpha$  and  $\beta$ .

Turning to the unsymmetric branch for which  $\bar{v}\bar{w} = \alpha/\beta\mu$  we have from (4) and (7)

$$1 = [1 - (\bar{v} + \bar{w}) - 2\alpha/\beta] [1 + 2\alpha\mu + \beta\mu(\bar{v} + \bar{w})]. \quad (16)$$

Putting  $y = \bar{v} + \bar{w}$  gives a quadratic that factorizes as

$$(\mu\beta y + 1 - \mu\beta + 2\alpha\mu)(y + 2\alpha/\beta) = 0. \quad (17)$$

The second factor is irrelevant, since  $y$  cannot be negative and the first gives a positive root if

$$\mu > 1/(\beta - 2\alpha) \quad \text{and} \quad \beta > 2\alpha. \quad (18)$$

Knowing

$$\bar{v} + \bar{w} = 1 - (1 + 2\alpha\mu)/\beta\mu \quad \text{and} \quad \bar{v}\bar{w} = \alpha/\beta\mu,$$

immediately gives

$$\bar{v} = \frac{1}{2} \left( 1 - \frac{1 + 2\alpha\mu}{\beta\mu} \right) \pm \left[ \frac{1}{4} \left( 1 - \frac{1 + 2\alpha\mu}{\beta\mu} \right)^2 - \frac{\alpha}{\beta\mu} \right]^{1/2}, \quad (19)$$

$$\bar{w} = \frac{1}{2} \left( 1 - \frac{1 + 2\alpha\mu}{\beta\mu} \right) \pm \left[ \frac{1}{4} \left( 1 - \frac{1 + 2\alpha\mu}{\beta\mu} \right)^2 \right]^{1/2} - \frac{\alpha}{\beta\mu}, \quad (20)$$

whence

$$\bar{u} = 1/\beta\mu. \quad (21)$$

Now  $\bar{v}$  and  $\bar{w}$  will only be real if  $\mu$  is sufficiently small or sufficiently large, in fact, outside the interval  $(\mu_*, \mu^*)$  between the roots

$$\mu^*, \mu_* = \{(\beta - 2\alpha + 2\alpha\beta) \pm [4\alpha\beta(\beta - 2\alpha + \alpha\beta)]^{1/2}\}/(\beta' - 2\alpha)^2. \quad (22)$$

These are real since  $\beta > 2\alpha$  but  $\mu_* < 1/(\beta - 2\sigma)$  so the condition for real  $\bar{v}$  and  $\bar{w}$  is

$$\mu \geq \mu^* = \{(\beta - 2\alpha + 2\alpha\beta) \pm [4\alpha\beta(\beta - 2\alpha + \alpha\beta)]^{1/2}\}/(\beta - 2\alpha)^2, \quad (23)$$

and the inequality (18) is always satisfied if  $\beta > 2\alpha$ .

When  $\mu = \mu^*$  the symmetric steady state from which it bifurcates is

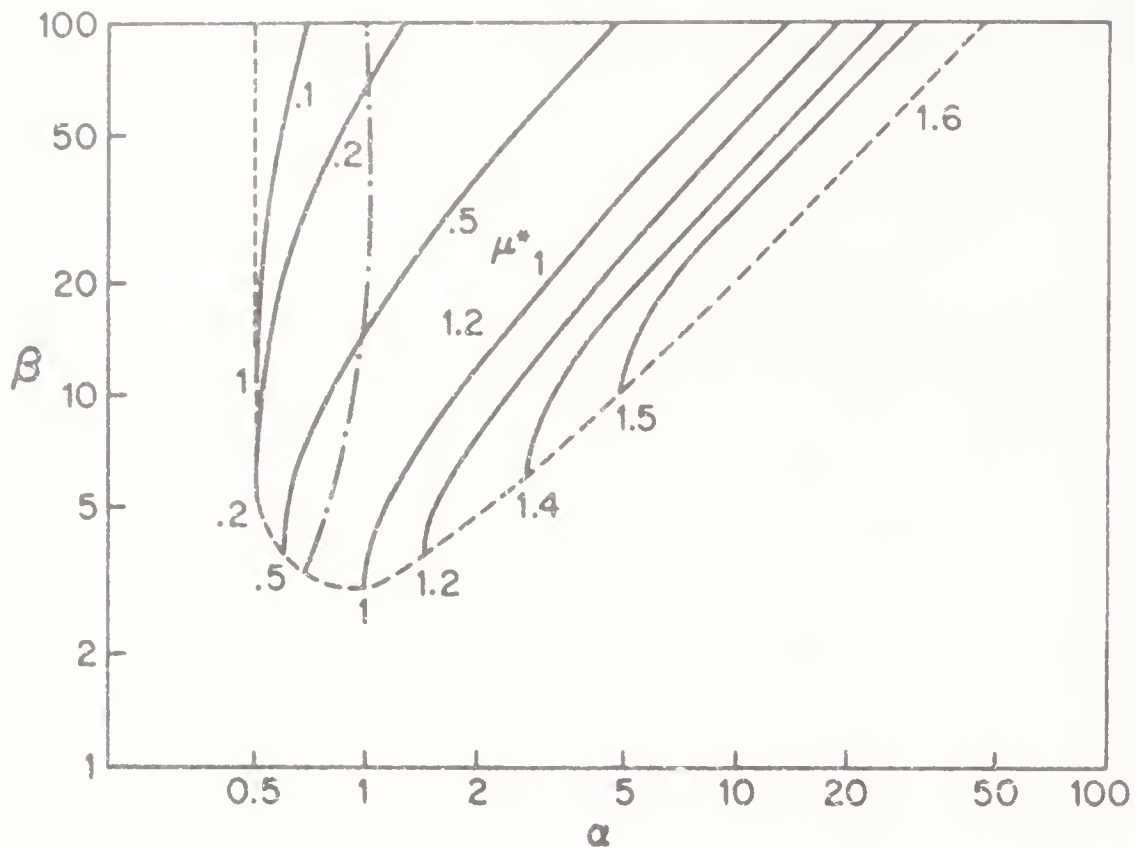
$$\begin{aligned} \bar{v}^* &= \bar{w}^* = \alpha \left\{ \left( 1 + \frac{\beta - 2\alpha}{\alpha\beta} \right)^{1/2} - 1 \right\}, \\ \bar{u}^* &= 2\alpha \left\{ 1 + \frac{\beta - 2\alpha}{2\alpha\beta} - \left( 1 + \frac{\beta - 2\alpha}{\alpha\beta} \right)^{1/2} \right\}. \end{aligned} \quad (24)$$

By writing

$$\bar{v}, \bar{w} = \left( \frac{\beta - 2\alpha}{2\beta} - \frac{1}{2\beta\mu} \right) \pm \left[ \left( \frac{\beta - 2\alpha}{2\beta} - \frac{1}{2\beta\mu} \right)^2 - \frac{\alpha}{\beta\mu} \right]^{1/2}, \quad (25)$$

we see that as  $\mu$  increases from  $\mu^*$  to infinity one branch goes to  $\bar{u} = \bar{w} = 0$ ,  $\bar{v} = 1 - 2(\alpha/\beta)$  and the other to  $\bar{u} = \bar{v} = 0$ ,  $\bar{w} = 1 - 2(\alpha/\beta)$ . Now by (18) the



Figure 3. Loci of constant  $\mu^*(\alpha, \beta)$ .

unsymmetric branch can only exist if  $\beta - 2\alpha \geq 1/\mu$ , which will certainly be the case if  $\beta - 2\alpha \geq 1/\mu^*$ , since  $\mu \geq \mu^*$ . In figure 3 are drawn the loci of constant  $\mu^*$  in the  $\alpha, \beta$ -plane. They are most easily obtained by letting  $\bar{v} = \bar{w}$  in (19) and (20) giving

$$4\alpha\beta\mu = [(\beta - 2\alpha)\mu - 1]^2,$$

which can be treated as a quadratic in  $\beta$ . Only the larger root

$$\beta = \{2\alpha(1 + \mu) + 1 + [(2\alpha(1 + \mu) + 1)^2 - \mu^2(2\alpha\mu + 1)^2]^{1/2}\}/\mu$$

need be considered, for on the locus of equal roots the condition  $\beta - 2\alpha = 1/\mu$  is just satisfied. This locus (shown as a broken curve) is

$$\alpha = (1 + \mu)/2(1 + \mu - \mu^2), \quad \beta = (1/\mu + 2)/(1 + \mu - \mu^2), \quad (26)$$

for  $0 \leq \mu \leq (1 + 5^{1/2})/2 = 1.6180$ . The locus of  $\mu^* = M$ , i.e., where the unsymmetric solution breaks away from the turning point of the symmetric solution, is shown with the dash-dot curve. Translating these logarithmic planes into linear ones, figure 4 shows the general disposition of the curves in the case  $\varepsilon = \eta = 0$ .

### 3. The stability of the steady states

The Jacobian of the dynamical equations (1)–(3) at steady state is

$$\begin{bmatrix} -\{1 + \mu(2\alpha + \beta(\bar{v} + \bar{w}))\} & -\beta\mu\bar{u} & -\beta\mu\bar{u} \\ \mu(\alpha + \beta\bar{v}) & -\{1 + \mu(\bar{w} - \beta\bar{u})\} & -\mu\bar{v} \\ \mu(\alpha + \beta\bar{w}) & -\mu\bar{w} & -\{1 + \mu(\bar{v} - \beta\bar{u})\} \end{bmatrix} \quad (27)$$

Consider first the unsymmetric steady state for which by (17) and (21),  $\beta\mu\bar{u} = 1$  and  $1 + 2\mu + \beta\mu(\bar{v} + \bar{w}) = \beta\mu$ . This allows us to write the matrix more simply as

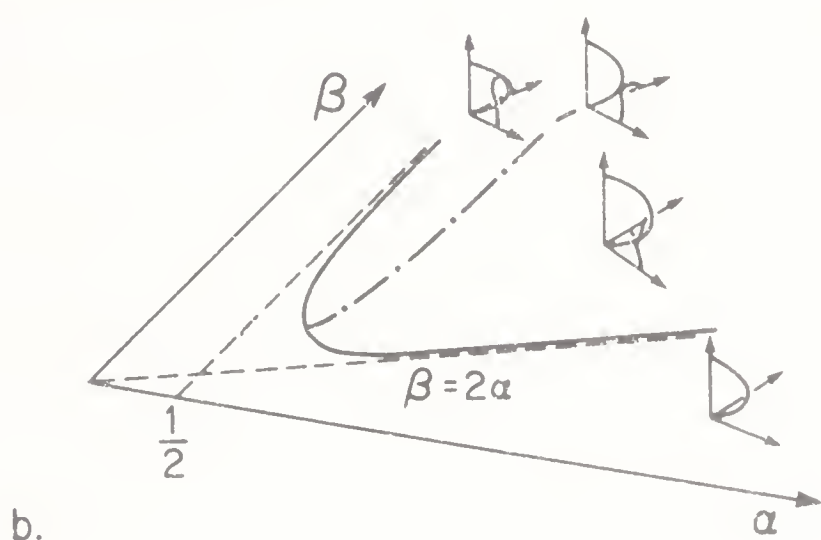
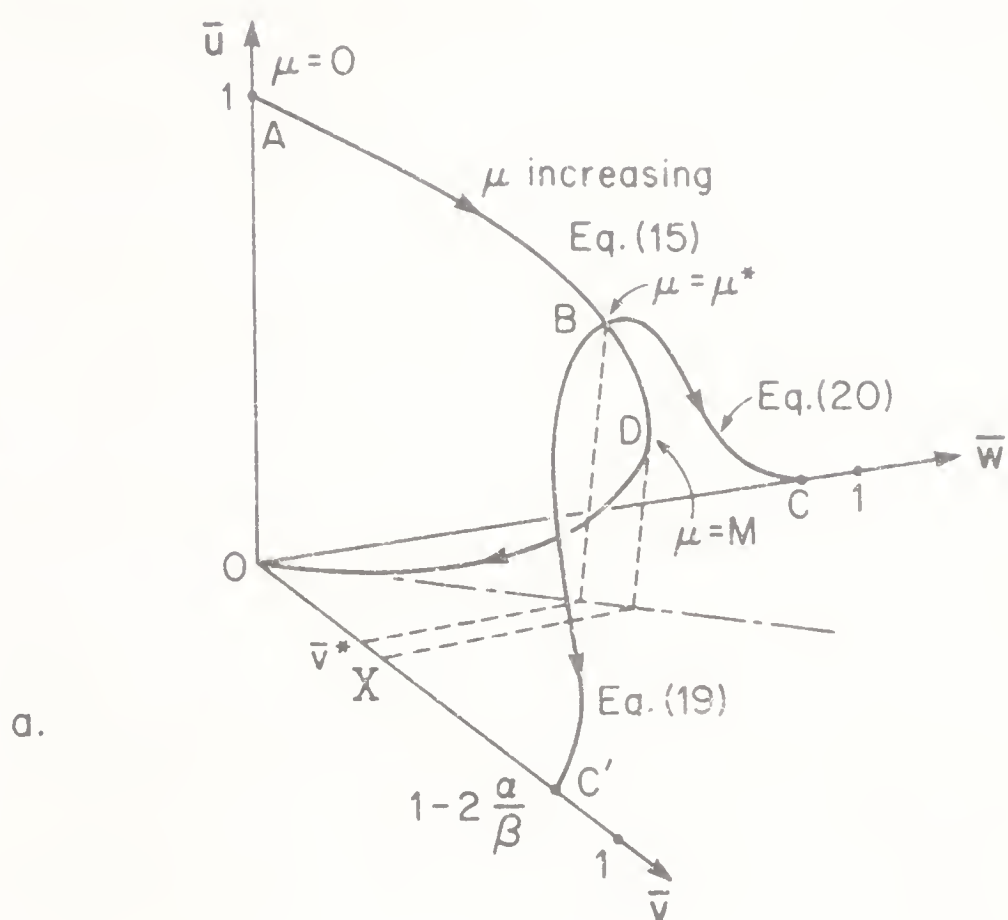


Figure 4. a) Three dimensional locus of steady states for  $\varepsilon = \eta = 0$ ; b) types of such loci for  $\alpha, \beta$ .

$$\begin{bmatrix} -\beta\mu & -1 & -1 \\ \mu(\alpha + \beta\bar{v}) & -\mu\bar{w} & -\mu\bar{v} \\ \mu(\alpha + \beta\bar{w}) & -\mu\bar{w} & -\mu\bar{v} \end{bmatrix}$$

giving a characteristic equation

$$\lambda^3 + \lambda^2\mu(\beta + \bar{v} + \bar{w}) + \lambda\mu[2\alpha + (1 + \beta\mu)(\bar{v} + \bar{w})] + \mu^2\beta(\bar{v} - \bar{w})^2 = 0. \quad (28)$$

All the coefficients in this cubic are positive and so the real parts of  $\lambda$  will be negative providing only that

$$[2\alpha + (1 + \beta\mu)(\bar{v} + \bar{w})]\mu(\bar{v} + \bar{w}) - \mu^2\beta(\bar{v} - \bar{w})^2 > 0. \quad (29)$$

But we see that the only negative term  $-\mu^2(\bar{v} - \bar{w})^2$  can be combined with the term  $\mu^2\beta(\bar{v} + \bar{w})^2$  to give  $4\mu^2\beta\bar{v}\bar{w}$  which is certainly positive. Hence the unsymmetric state, when it exists, is always stable.

On the symmetric path  $\bar{v} = \bar{w} = x$  we can make use of (4), (5) and (6) to simplify the Jacobian to

$$\begin{bmatrix} -1/\bar{u} & -\beta\mu\bar{u} & -\beta\mu\bar{u} \\ \mu(\alpha + \beta x) & -\alpha\mu\bar{u}/x & -\mu x \\ \mu(\alpha + \beta x) & -\mu x & -\alpha\mu\bar{u}/x \end{bmatrix} \quad (30)$$

The determinant of this matrix is

$$\mu^2(x^2 - \alpha\bar{u}) \{x^2 + (\alpha + \beta x)\beta x\mu\bar{u}^2\} - \bar{u}x^2, \quad (31)$$

which vanishes only when

$$x^2 = \alpha\bar{u}(1 - 2x - 2\mu x^2). \quad (32)$$

Now if  $\beta < 2\alpha$ , the curve of  $\alpha\bar{u}$  lies above  $x^2$  and the only intersection is the trivial  $x = \bar{u} = 0$ ,  $\mu = \infty$ . Thus the determinant is negative when the symmetric state is unique. On the other hand, if  $\beta > 2\alpha$ ,  $\alpha\bar{u} - x^2$ , which is asymptotically  $-(\beta - 2\alpha)x^3\alpha$  near the origin, is negative at first, and  $\alpha\bar{u}$  must have a unique intersection with  $x^2$  since it increases monotonically as  $x$  increases to  $X$  and then decreases again to zero. Thus for  $\mu > \mu^*$ , the symmetric steady state is unstable, and a similar analysis of the characteristic equations shows it to be stable when  $\alpha\bar{u} > x^2$  i.e.  $\mu < \mu^*$ .

This exchange of stability at  $\mu = \mu^*$  is known as the ‘‘pitchfork’’ bifurcation and Kondepudi’s system affords an excellent example of it.

#### 4. The asymmetric case

In turning to the asymmetric case in which the rate constants on the paths are not identical (i.e.  $\eta$  and  $\varepsilon$  not both zero), it is useful to change the variables from  $u, v, w$  to  $u, p, q$

$$p = \frac{1}{2}(v - w), \quad q = \frac{1}{2}(v + w). \quad (33)$$

The equations are then

$$\mu\dot{u} = 1 - u - 2\mu(\alpha + \eta p + \beta q)u, \quad (34)$$

$$\mu\dot{p} = -p + \mu(\varepsilon + \beta p + \eta q)u, \quad (35)$$

$$\mu\dot{q} = -q + \mu(\alpha + \eta p + \beta q)u - \mu(q^2 - p^2). \quad (36)$$

The special form of these equations is illustrated by defining

$$P(p, q) = \alpha + \eta p + \beta q, \quad (37)$$

$$Q(p, q) = \varepsilon + \beta p + \eta q$$

$$R(p, q) = q^2 - p^2,$$

$$m = 1/\mu, \quad (38)$$

and the steady states satisfy either

$$\begin{aligned} 2\mu uP &= 1 - u, \\ \mu uQ &= p, \\ \mu uP &= q + \mu R, \end{aligned} \tag{39}$$

or

$$\begin{aligned} 2uP &= m(1 - u), \\ uQ &= mp, \\ uP &= mq + R. \end{aligned} \tag{40}$$

It is useful to note that

$$1 - u - 2q + \mu R = 0 \quad \text{or} \quad R = -m(1 - u - 2q). \tag{41}$$

Clearly if  $\bar{u}(\mu; \alpha, \beta; \varepsilon, \eta)$ ,  $\bar{p}(\mu; \alpha, \beta; \varepsilon, \eta)$ ,  $\bar{q}(\mu; \alpha, \beta; \varepsilon, \eta)$  is a solution, so also is  $\bar{u}(\mu; u, \beta; -\varepsilon, -\eta)$ ,  $-\bar{p}(\mu; \alpha, \beta; -\varepsilon, -\eta)$ ,  $\bar{q}(\mu; \alpha, \beta; -\varepsilon, -\eta)$ .

In case  $\varepsilon = \eta = 0$  the equations simplify, the second giving either  $p = 0$  or  $u = 1/\mu\beta$ , whence, substituting in the other equations, the known symmetric and unsymmetric solutions [(12) and (19)–(21)] can be recovered. It is not hard to show that the steady state when  $\mu \rightarrow \infty$  is either  $(0, 0, 0)$ ,  $(0, 1 - 2\alpha/\beta, 0)$  or  $(0, 0, 1 - 2\alpha/\beta)$ ; in fact by expanding in powers of  $m$  the approach to the state  $(0, 1 - 2\alpha/\beta, 0)$  is given by

$$\begin{aligned} u &= m/\beta, \quad v = 1 - (2\alpha/\beta) - m(\beta - 2\alpha + \alpha\beta)/\beta(\beta - 2\alpha), \\ w &= \alpha m/(\beta - 2\alpha). \end{aligned} \tag{42}$$

Since  $P$  and  $Q$  are linear in  $p$  and  $q$ , the first two equations of (39) or (40) can be solved for  $p$  and  $q$  and these substituted in (41). This gives a quintic in  $u$  with coefficients which are functions of the five parameters  $\mu$  (or  $m$ ),  $\alpha$ ,  $\beta$ ,  $\varepsilon$  and  $\eta$ . This equation is of ferocious complexity and its solution to find the possible steady states is clearly not the way to go! Instead we recognize that  $\varepsilon$  and  $\eta$  destroy the symmetry of the curves ABO and CBC' in figure 4 by cleaving the locus into two parts ABC (or ABC') and OB'C' (or OB'C). On the curve ABC,  $\mu$  increases from zero at A to infinity at C, while, on OB'C',  $\mu$  decreases from infinity to a minimum  $\bar{\mu}$  at B' and then increases again (or  $m$  increases from zero to  $\bar{m} = 1/\bar{\mu}$  and returns again to zero). Since we know the starting points A and 0 we have only to develop differential equations for  $u$ ,  $p$ ,  $q$  and  $\mu$  or  $m$  along the paths.

Let a prime denote differentiation with respect to an arc length to be defined later, then the first two equations of (39) and (41) give

$$\begin{aligned} -(1 + 2\mu P)u' - 2\mu uP_p p' - \mu uP_q q' - 2uP\mu' &= 0, \\ \mu Qu' - (1 - \mu uQ_p)p' + \mu uQ_q q' + uQ\mu' &= 0, \\ -u' + \mu R_p p' - (2 - \mu uR_q)q' + R\mu' &= 0. \end{aligned} \tag{43}$$

These three equations can be regarded as determining the three ratios if the four derivatives,

$$u'/A = p'/B = q'/\Gamma = \mu'/\Delta \tag{44}$$

where  $A$ ,  $B$ ,  $\Gamma$  and  $\Delta$  are the minors obtained by deleting each column in turn, e.g.,

$$A = \begin{vmatrix} -2\mu u P_p & -2\mu u P_q & -2uP \\ -(1 - \mu u Q_p) & \mu u Q_q & uQ \\ \mu R_p & -(2 - \mu R_q) & R \end{vmatrix}$$

If we define the variable, with respect to which we differentiate, as arc length in  $u, v, w, \mu$ -space we may set the common ratio of the quantities in (44) equal to  $1/E$ , where

$$E^2 = A^2 + B^2 + \Gamma^2 + \Delta^2. \quad (45)$$

Then simultaneous integration of

$$u' = A/E, \quad v' = B/E, \quad w' = \Gamma/E, \quad \mu' = \Delta/E, \quad (46)$$

will trace out the locus of steady states and will only fail when  $E$  vanishes i.e.  $A, B, C, D$  vanish simultaneously. This only happens in the symmetric case,  $\varepsilon = \eta = 0$ , and at the pitchfork point  $\mu = \mu^*$ .

In any other case, if the four simultaneous equations are integrated from  $(1, 0, 0, 0)$  one branch of the solution will be traced out. It is the branch ABC of figure 5, descending from the  $u$ -axis, that will be so calculated. The other branch coming up from the origin is best calculated using the parameter  $m = 1/\mu$ , substituted throughout for  $\mu$  and satisfying

$$m' = -m^2 \Delta/E. \quad (47)$$

For this branch the starting point is  $(0, 0, 0, 0)$  since  $m = 0$  where  $\mu \rightarrow \infty$ , namely the origin. On this branch  $m$  increases to a maximum  $\tilde{m}$ , of magnitude close to  $1/\mu^*$  ( $\alpha/\beta$ ), and then decreases again to zero. This is ODC' in figure 5.

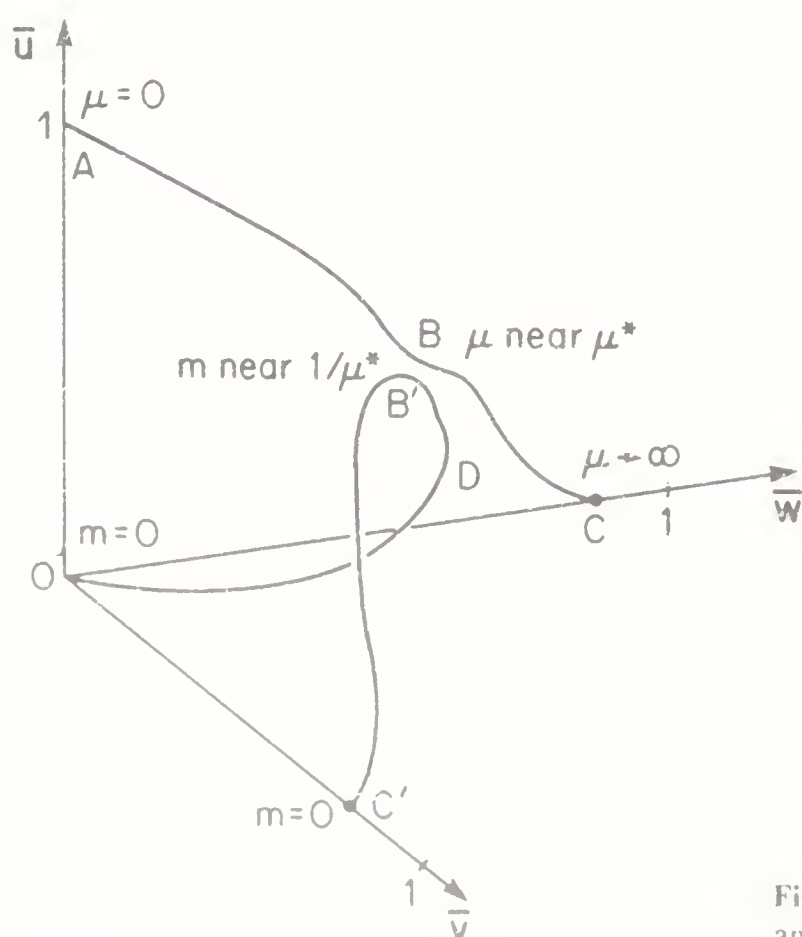


Figure 5. Locus of steady states for given  $\alpha, \beta$  and  $\varepsilon, \eta$ , the latter pair not being zero.



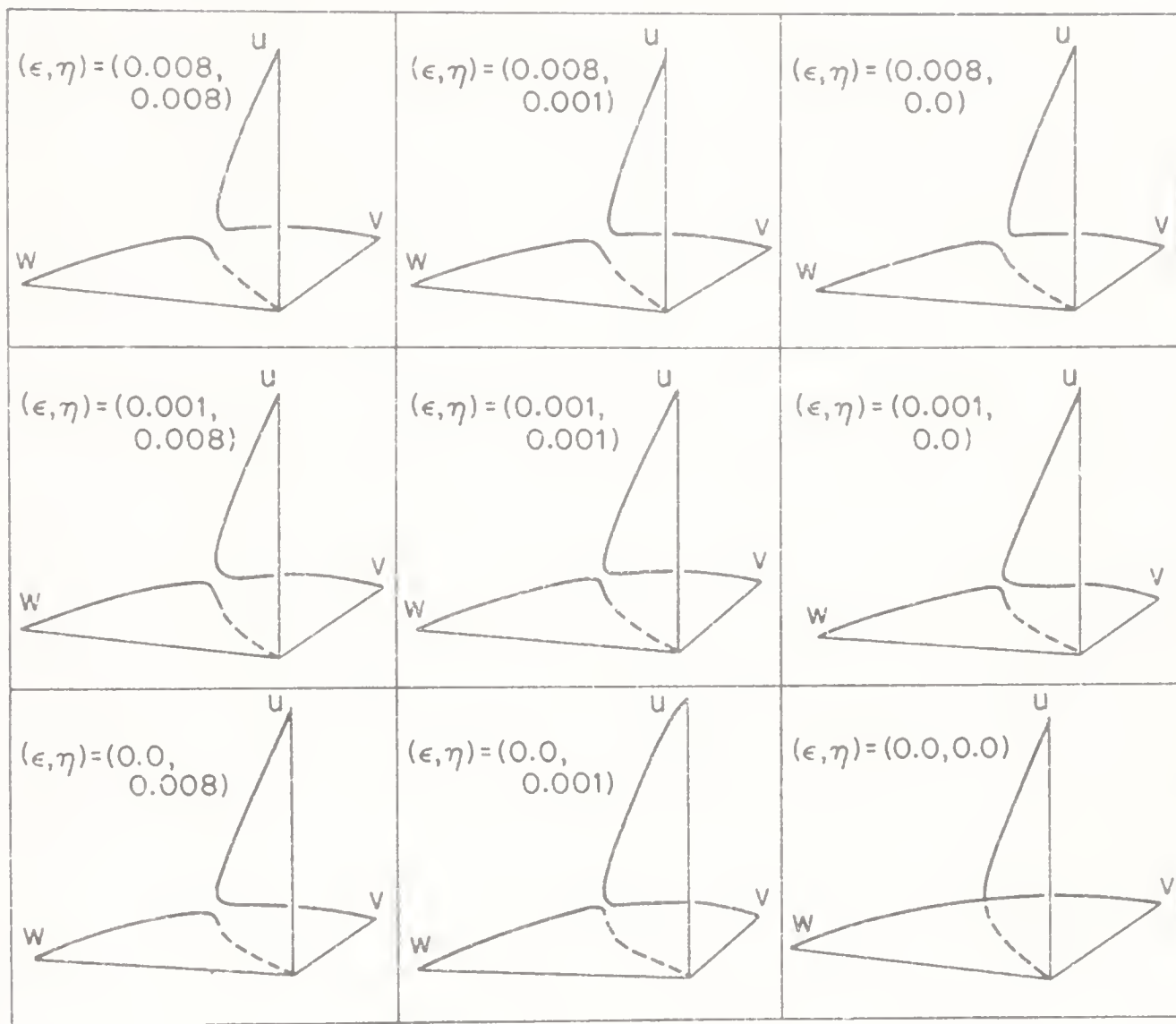


Figure 6. Loci of steady states for various  $\epsilon$  and  $\eta$ ;  $\alpha = 1$ ,  $\beta = 16.8$ .

In figure 6 eight combinations of non-zero  $\epsilon$  and  $\eta$  are shown; the ninth, at the bottom right, is the symmetric case which is being perturbed. It is clear that quite small values of  $\epsilon$  and  $\eta$  move the two branches away from one another quite substantially. This is not surprising and corresponds to the extreme sensitivity to small variations that Kondepudi and his colleagues have found in the stochastic context. For values of  $\mu$  greater than  $1/\tilde{\mu}$  there are three steady states. Of them the one on the branch that goes to the origin is unstable (shown broken in figure 6) and the other two are stable. The phase space is divided by a separatrix surface into two regions of attraction to the two stable states. We had hoped to describe the evolution of this separatrix from the plane  $v = w$ , but this must await further study.

We are indebted for partial support to the National Science Foundation through their grant CPE 8112292.

## References

- Dabke N S, Kulkarni B D, Doraiswamy L K 1986 *Chem Eng. Sci.* 41, 1765–1770  
 Kondepudi D K, Nelson G W 1983 *Phys. Rev. Lett.* 50: 1023–1026  
 Kondepudi D K, Nelson G W 1984 *Physica A* 125, 465–496

- Tambe S. S., Kulkarni B. D., Doraiswamy L. K. 1985a *Chem. Eng. Sci.* 40: 1943–1949  
Tambe S. S., Kulkarni B. D., Ravikumar V., Doraiswamy L. K. 1985b *Chem. Eng. Sci.* 40: 1951–1957  
Tambe S. S., Kulkarni B. D., Doraiswamy L. K. 1985c *Chem. Eng. Sci.* 40: 1959–1964  
Tambe S. S., Kulkarni B. D., Doraiswamy L. K. 1985d *Chem. Eng. Sci.* 40: 2293–2296  
Tambe S. S., Kulkarni B. D., Doraiswamy L. K. 1985e *Chem. Eng. Sci.* 40: 2297–2302  
Tambe S. S., Kulkarni B. D., Doraiswamy L. K. 1985f *Chem. Eng. Sci.* 40: 2303–2309

# The counter-current backmixing model for fluid bed reactors – computational aspects and model modifications

DRAGOMIR B BUKUR

Kinetics, Catalysis and Reaction Engineering Laboratory, Department of Chemical Engineering, Texas A&M University, College Station, Texas 77843, USA

**Abstract.** Numerical solution of differential equations describing the counter-current backmixing model of Fryer and Potter is very difficult due to the boundary value nature of the problem. Several numerical methods (shooting, superposition and finite difference) have been described and tested on a problem with a single first-order reaction in an isothermal fluid bed reactor. It was found that the finite difference method is the most stable method and provides accurate solution over the entire range of parameters that were investigated, while the shooting and the superposition methods could not produce accurate solutions for some parameter values. Also, some modifications of the Fryer and Potter model such as: compartment models and conversion to an initial value type of problem (Jayraman-Kulkarni-Doraiswamy model), have been described. Results obtained from compartment models are in close agreement with predictions obtained from the original Fryer and Potter model.

**Keywords.** Fluid bed reactors; mathematical modelling; counter-current backmixing model.

## 1. Introduction

The possibility of flow reversal of gas in the emulsion phase in the bubbling region of a fluidized bed was suggested independently by several authors (Stephens *et al* 1967; Van Deemter 1967, pp. 334–347; Kunii & Levenspiel 1968a). Several mathematical models for fluid bed reactors based on this concept have been developed. Kunii & Levenspiel (1968b), Kato & Wen (1969), and Mori & Wen (1976, pp. 179–203) made the simplifying assumption in their models that the bulk flow of gas in the cloud-wake phase and the emulsion phase is negligible. The predictions obtained from these models were found to be in good agreement with experimental data for various catalytic reaction systems (e.g. Kato & Wen 1969;

Mori & Wen 1976, pp. 179–203; Chavarie & Grace 1975; Shaw *et al* 1972). Fryer & Potter (1972a) developed a more rigorous model, which will be referred to as the counter-current backmixing model (CCBM). The unique feature of the CCBM is that it predicts the existence of a minimum in the average gas concentration value within the reactor under the emulsion gas flow reversal conditions. This prediction was confirmed experimentally in the study by Fryer & Potter (1974, pp. 440–453, 1976).

Recently, Peters *et al* (1982) proposed a new three-phase model for fluid bed reactors, which like the CCBM of Fryer and Potter predicts the flow reversal of the emulsion phase gas. The two models have similar structures, and the main difference arises from the assumptions made concerning the division of gas flow between the phases. The model of Peters *et al* (1982) takes into account the bubble size variation with height and allows for axial variations in the division of gas flow among the phases. Another difference between the two models is in the boundary conditions employed at the reactor outlet. Peters *et al* (1982) found that their model predictions compare favourably with some of previously reported experimental data on the division of gas flow, steady state axial profiles and the overall conversion.

In spite of the apparent success of simplified versions of the CCBM, the rigorous form of the CCBM proposed by Fryer & Potter (1972a) has not found widespread use in the literature. One reason for this lies in the difficulties associated with numerical solution of the governing equations which represent a two-point boundary value problem. Fryer & Potter (1972a) reported that the numerical solution of the CCBM could not be obtained for some values of the model parameters and Jayraman *et al* (1981) allude to this by stating that the boundary value presentation leads to severe stability and convergence problems. In this paper I shall describe our experience with numerical solution of the Fryer & Potter CCBM, and several approaches to this difficult problem will be discussed. They can be divided into two categories, i.e. (1) numerical techniques for solution of the model equations which allow for continuous variation of bubble size with distance; (2) the model modifications which include conversion of a boundary value problem to initial value problem (Jayraman *et al* 1981) and compartment models of Fryer & Potter (1974, pp. 440–453) and Peters *et al* (1982). Also, some results illustrating the effect of additional mass transfer due to crossflow arising from axial variations in the fluid bed properties and of modified boundary conditions, proposed by Peters *et al* (1982), on conversion will be presented.

## 2. Model equations

### 2.1 Crossflow model (CFM)

Figure 1a shows the schematic diagram of the counter-current backmixing model as well as the notation employed. The basic assumptions are the same as in the Fryer & Potter's (1972a) model and will not be restated here. When the bubble size and the superficial gas phase velocities vary with height, the steady state mass balance equations for the reactant in each of the phases can be written as

Bubble phase:

$$-\frac{d}{dz} (U_{GB} C_B) - K_{BC} \epsilon_B (C_B - C_C) - P_{BC} C_B = 0. \quad (1)$$



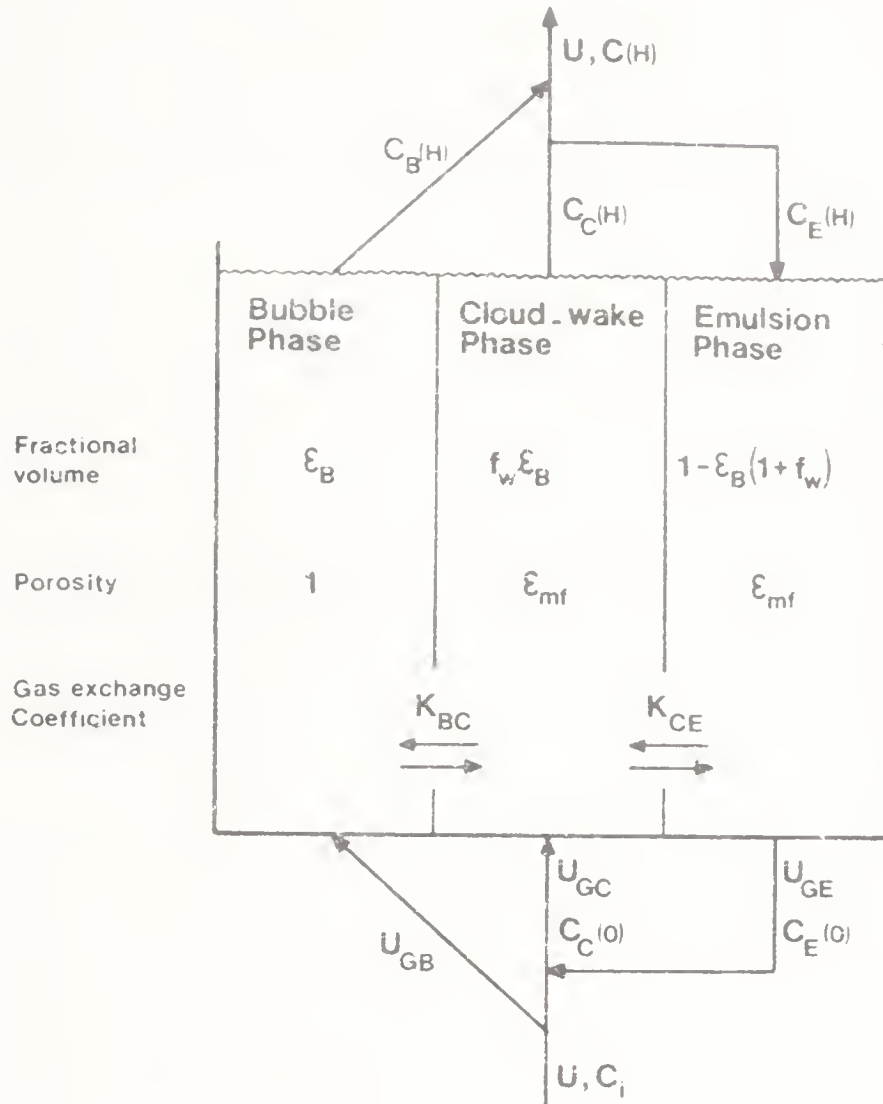


Figure 1. Schematic representation of the counter-current backmixing model of Frver and Potter

Cloud-wake phase:

$$\begin{aligned} & \frac{d}{dz} (U_{GC} C_C) + K_{BC} \epsilon_B (C_B - C_C) - K_{CE} \epsilon_B (C_C - C_E) + P_{BC} C_B \\ & - P_{CE} C_C - k(1 - \epsilon_{mf}) \epsilon_B f_w C_C = 0. \end{aligned} \quad (2)$$

Emulsion (dense) phase:

$$\begin{aligned} & - \frac{d}{dz} (U_{GE} C_E) + K_{CE} \epsilon_B (C_C - C_E) + P_{CE} C_C \\ & - k[1 - \epsilon_B(1 + f_w)](1 - \epsilon_{mf}) C_E = 0. \end{aligned} \quad (3)$$

The crossflow terms,  $P_{BC}$  and  $P_{CE}$ , represent the change of volumetric flow rate of the bubble gas and the emulsion phase gas, respectively, per unit volume of bed due to axial variations in fluid bed properties. They give rise to additional bulk transport of material between the phases. The concept of additional bulk flow due to changes in volumetric flow rates that are caused either by chemical reactions which proceed with a change in total number of moles or by bubble coalescence was first introduced by Litz (1973) and used later by Peters *et al* (1982) and Kai & Furusaki (1984). Here we consider a reaction without changes in total number of moles (i.e.  $U = \text{const}$ ) and the crossflow terms arise due to axial variations of fluid bed properties. In such a case they can be expressed as



$$P_{BC} = -dU_{GB}/dz, \quad (4a)$$

$$P_{CE} = dU_{GE}/dz = -[(dU_{GB}/dz) + (dU_{GC}/dz)]. \quad (4b)$$

Referring to figure 1a the boundary conditions under the emulsion gas flow reversal are as follows. At the distributor level a fraction of the incoming gas forms the bubble gas,

$$C_B = C_i, \quad \text{at } z = 0, \quad (5)$$

while the remainder combines with the downflowing emulsion gas to form the cloud-wake gas,

$$(U - U_{GB})C_i + (-U_{GE})C_E(0) = U_{GC}C_C(0). \quad (6)$$

At the top of the bed ( $z = H$ ) the exit gas is composed of all the bubble gas and some cloud-wake gas. The remainder of the cloud-wake gas provides the downflowing gas in the emulsion phase, thus

$$C_C = C_E, \quad \text{at } z = H. \quad (7)$$

The reactant conversion is given by

$$X = 1 - [U_{GB}C_B(H) + (U - U_{GB})C_C(H)]UC_i. \quad (8)$$

If one introduces the dimensionless variables defined as

$$s = z/H, \quad x_j = C_j/C_i (j = B, C, E), \quad (9)$$

the mass balance equations and the boundary conditions can be brought into the following form:

$$\frac{dx_B}{ds} = \frac{N_{BC}}{\beta_B} (x_C - x_B), \quad (10)$$

$$\frac{dx_C}{ds} = \left( \frac{N_{BC} + P'_{BC}}{\beta_C} \right) (x_B - x_C) - \frac{N_{CE}}{\beta_C} (x_C - x_E) - \frac{\varepsilon_B f_w N_r}{\beta_C} x_C, \quad (11)$$

$$\frac{dx_E}{ds} = \left( \frac{N_{CE} + P'_{CE}}{\beta_E} \right) (x_C - x_E) - \frac{[1 - \varepsilon_B(1 + f_w)]N_r}{\beta_E} x_E, \quad (12)$$

$$x_B = 1, \quad \text{at } s = 0, \quad (13)$$

$$x_C = (1 - \beta_B)/\beta_C - (\beta_E/\beta_C)x_E, \quad \text{at } s = 0, \quad (14)$$

$$x_C = x_E, \quad \text{at } s = 1, \quad (15)$$

where:

$$\begin{aligned} N_{BC} &= K_{BC}\varepsilon_B H/U; \quad N_{CE} = K_{CE}\varepsilon_B H/U; \\ P'_{BC} &= P_{BC}H/U; \quad P'_{CE} = P_{CE}H/U; \end{aligned} \quad (16)$$

$$\beta_j = U_{Gj}/U (j = B, C, E); \quad N_r = kH(1 - \varepsilon_{mf})/U.$$

The expression (8) for reactant conversion becomes

$$X = 1 - [\beta_B x_B(1) + (1 - \beta_B)x_C(1)]. \quad (17)$$

The average dimensionless concentration which would be expected if gas were sampled continuously at a point in the reactor in proportion to the fraction of the phases present is calculated from

$$x_{av} = \epsilon_B x_B + f_w \epsilon_B x_C + [1 - \epsilon_B(1 + f_w)] x_E. \quad (18)$$

## 2.2 Modified boundary conditions (MBC)

Peters *et al* (1982) proposed that at the top of the bed the downflowing emulsion gas is provided by a fraction of the exit gas, while the latter is made up of all the bubble gas and all the cloud-wake gas. Then, instead of (15) one uses

$$x_E = (\beta_B x_B + \beta_C x_C) / (\beta_B + \beta_C), \text{ at } s = 1, \quad (19)$$

and the conversion is calculated as

$$X = 1 - x_E(1). \quad (20)$$

Boundary conditions at the distributor level ( $s = 0$ ) remain unchanged.

## 2.3 Model with negligible crossflow (NCFM)

This model represents a special case of the model developed in §2.1, where one assumes that the effect of bulk flow transport due to changes in gas flow rates is negligible in comparison to the mass transport due to convection and diffusion. (The latter two mechanisms of mass transport are embodied in the gas exchange coefficient  $K_{BC}$ , while  $K_{CE}$  is based on the diffusion mechanism only.) Mass balances for this model are given by (10)–(12) with  $P'_{BC} = P'_{CE} = 0$ . It should be noted that numerical values of all other dimensionless parameters still vary axially along the reactor.

## 3. Model parameters

The expressions used for calculation of the superficial gas velocities, the bubble volume fraction and the gas exchange coefficients are summarized in table 1. The value of wake-volume to bubble-volume ratio has been varied between 0.5 and 1.0.

Table 1. Parameter definitions for the counter-current backmixing model

Parameter	Definition
Absolute bubble gas velocity, $U_B$	$U - U_{mf} + 0.711(gd_B)^{1/2}$
Volume fraction of bubbles in the bed $\epsilon_B$	$(U - U_{mf}) / [U_B - U_{mf}(1 + f_w)]$
Superficial gas velocity in the bubble phase, $U_{GB}$	$(U - U_{mf}) / [1 - (1 + f_w)U_{mf}/U_B]$
Superficial gas velocity in the cloud-wake phase, $U_{GC}$	$U_{GB} f_w \epsilon_{mf}$
Superficial gas velocity in the emulsion phase, $U_{GE}$	$U_{mf} [1 - \epsilon_B(1 + f_w)] (1 + \epsilon_{mf} f_w) - U f_w \epsilon_{mf}$
Gas interphase coefficient between the bubble and the cloud-wake phase per unit bubble volume, $K_{BC}$	$4.5(U_{mf}/d_B) + 5.85(D_G^{1/2} g^{1/4}/d_B^{3/4})$
Gas interphase coefficient between the cloud-wake and the emulsion phase per unit bubble volume, $K_{CE}$	$6.78(\epsilon_{mf}^2 D_G U_B / d_B^3)^{1/2}$

The latter value was suggested by Fryer & Potter (1976) on the basis of their experimental data which exhibited a minimum in the concentration profile within the reactor. On the other hand in experiments by Rowe & Partridge (1965) and Woolard & Potter (1968) it was found that  $f_w = 0.25-0.60$ . Thus the wake to bubble volume ratio must be regarded as an adjustable model parameter.

A correlation by Darton *et al* (1977), which was found to fit experimental data of various investigators, was employed for prediction of bubble size variation with height,

$$d_B = 0.54(U - U_{mf})^{0.4} [z + 4(A_0^{1/2})]^{0.8} / g^{0.2} \quad (21)$$

The "catchment" area  $A_0$  was calculated by specifying the initial bubble size at the distributor level ( $z = 0$ ), or by specifying the number and size of holes in the orifice plate distributor.

For a given value of bed height at minimum fluidization conditions  $H_{mf}$  the expanded bed height is calculated by numerical quadrature:

$$H = H_{mf} / \left( 1 - \int_0^1 \epsilon_B ds \right) \quad (22)$$

The solution of this equation requires iteration since  $H$  appears also in the expression for  $\epsilon_B$ .

Numerical values for the operating conditions, catalyst particle properties and kinetic parameters employed in calculations are listed in table 2. Computations have been made for two types of solid particles, one belonging to group A and the other one to group B powders in Geldart's (1973) classification. The values in parentheses represent the range of variables studied.

#### 4. Numerical methods

In this section several methods for solution of the mass balance equations (10)–(12) subject to the boundary conditions (13)–(15) will be described and numerical

**Table 2.** Standard values of model parameters

	Powder A	Powder B
<i>Catalyst particle properties:</i>		
Minimum fluidization velocity, m/s	0.035	0.05(0.012–0.19)
Catalyst particle size, m	$1 \times 10^{-4}$	$2 \times 10^{-4}$ ( $1 \times 10^{-4}$ – $4 \times 10^{-4}$ )
Particle density, kg/m <sup>3</sup>	1000	2500
Voidage at minimum fluidization	0.50	0.50
<i>Operating conditions and model parameters:</i>		
Superficial gas velocity, m/s	0.35(0.175–0.525)	0.50(0.25–1.0)
Initial bubble size, m	0.03(0.02–0.05)	0.03(0.001–0.09)
Bed height at minimum fluidization, m	3(0–5)	0.75(0–3.0)
Gas diffusivity, m <sup>2</sup> /s	$2 \times 10^{-5}$	$2 \times 10^{-5}$
Ratio of wake volume to bubble volume	1.0	0.5–1.0
<i>Kinetic parameters:</i>		
Reaction rate constant based on unit volume of solids, s <sup>-1</sup>	1.0(0.2–3.0)	2.0(0.2–16)

results will be presented. Their comparison and relative merits will also be discussed.

#### 4.1 Analytical solution

When the bubble diameter and other parameters are invariant with position an explicit solution of the mass balance equations is possible for the case of a first-order reaction. With these restrictions one has to solve a system of three linear differential equations with constant coefficients. Although this solution is applicable only to a rather limited class of problems, it also serves as the base case for comparison of results obtained from numerical methods. For the case of a single reaction the solution of (10)–(12) was first presented by Fryer & Potter (1972a), who employed the method of elimination. Here we present the solution of these equations in terms of matrix theory, since this approach can handle an arbitrary number of equations and would be applicable to the case of multiple first-order reactions. The equations (10)–(12) can be written in the matrix form as:

$$dx/ds = Ax, \quad (23)$$

where,  $x$  is a  $3 \times 1$  vector of dimensionless concentrations, and  $A$  is a  $3 \times 3$  matrix of constant coefficients

$$x = \begin{bmatrix} x_B(s) \\ x_C(s) \\ x_L(s) \end{bmatrix}$$

$$A = \begin{bmatrix} -N_{BC}/\beta_B & N_{BC}/\beta_L & 0 \\ N_{BC}/\beta_C & -(N_{BC} + N_{CE} + \varepsilon_B f_w N_r)/\beta_C & N_{CE}/\beta_B \\ 0 & N_{CE}/\beta_F & -(N_{CE} + [1 - \varepsilon_B(1 + f_w)]N_r)/\beta_E \end{bmatrix} \quad (24)$$

The general solution of the system (23) is

$$x = \sum_{j=1}^3 m_j v^{(j)} e^{\lambda_j s}, \quad (25)$$

where,  $v^{(j)}$  is an eigenvector corresponding to the eigenvalue  $\lambda_j$  of the matrix  $A$  and  $m_j$  is an arbitrary constant. In the above solution it is assumed that all eigenvalues are distinct. The constants,  $m_j$  ( $j = 1 \rightarrow 3$ ), are determined from the boundary conditions (13)–(15) by solving the following system of linear algebraic equations

$$Bm = d, \quad (26)$$

where

$$d = \begin{bmatrix} 1 \\ (1 - \beta_B)/\beta_C \\ 0 \end{bmatrix}$$



$$B = \begin{bmatrix} v_1^{(1)} & v_1^{(2)} & v_1^{(3)} \\ v_1^{(2)} + \frac{\beta_I}{\beta_C} v_1^{(3)} & v_2^{(2)} + \frac{\beta_E}{\beta_C} v_2^{(3)} & v_3^{(2)} + \frac{\beta_E}{\beta_C} v_3^{(3)} \\ [v_1^{(2)} - v_1^{(3)}] e^{\lambda_1} & [v_2^{(2)} - v_2^{(3)}] e^{\lambda_2} & [v_3^{(2)} - v_3^{(3)}] e^{\lambda_3} \end{bmatrix} \quad (27)$$

For a given set of model parameters, the eigenvalues and eigenvectors of matrix  $A$  were calculated using the IMSL subroutine EIGRF, and  $m_j$  values were calculated using the subroutine LEQT2F.

#### 4.2 Shooting method

This is a method where one converts a boundary value problem (BVP) into an initial value problem (IVP), by assuming values for the missing conditions at either  $s = 0$  or  $s = 1$ . The resulting IVP is then solved iteratively until the boundary conditions are satisfied. This method has been used extensively in chemical reaction engineering literature to solve problems where axial dispersion is taken into account (e.g. tubular and fixed bed reactors) and it can be used to solve nonlinear problems. For the CCBM only one condition is missing at  $s = 0$ , while two conditions are missing at  $s = 1$ , and thus the forward shooting (starting integration from  $s = 0$ ) is more straightforward than the backward shooting. For the CCBM described by (10)–(15) the BVP is converted to an IVP as follows:

$$dx/ds = A(s)x, \quad (28)$$

and

$$x(0) = \begin{bmatrix} 1 \\ q \\ (1 - \beta_B)/\beta_E - (\beta_E/\beta_E)q \end{bmatrix} \quad (29)$$

where,  $q$  is an assumed value for  $x_C(0)$ . Then the system of equations (28) can be integrated using a straightforward marching technique (the Runge-Kutta and/or Gear's method were employed in this work). The objective is to find  $q^*$  such that the boundary condition (15) at  $s = 1$  is satisfied, i.e.

$$F(q^*) = x_C(1; q^*) - x_I(1; q^*) = 0, \quad (30)$$

This is done by iteration where the improved values of  $q$  are obtained using the Newton-Raphson method

$$q^{(i+1)} = q^{(i)} - [F(q^{(i)})/F'(q^{(i)})], \quad i = 0, 1, 2, \dots, \quad (31)$$

where

$$F' = dF/dq = [dx_C(1)]/dq - [dx_I(1)]/dq. \quad (32)$$

The derivatives in (32) were calculated by defining the auxiliary variables as suggested by McGinnis (1965),

$$y = \frac{dx}{dq}, \quad (33)$$



and solving the system of variational equations

$$\frac{dy}{ds} = A(s)y; \quad y(0) = \begin{bmatrix} 0 \\ 1 \\ -(\beta_C/\beta_E) \end{bmatrix} \quad (34)$$

Then,

$$q^{(i+1)} = q^{(i)} - [x_C(1) - x_L(1)]/[y_2(1) - y_3(1)]. \quad (35)$$

Thus, for each iteration one has to solve the system of six first-order differential equations. A similar procedure was used for the backward shooting method, but in this case the number of simultaneous differential equations per iteration is nine.

The elements of matrix  $A$  in (28) are given by (24), but when the bubble diameter varies with height these elements also vary with distance which is indicated using the notation  $A(s)$ . Also, when the crossflow terms are taken into account  $P'_{BC}$  has to be added to numerators of the elements  $a_{21}$  and  $a_{22}$ , and  $P'_{CL}$  to numerators of the elements  $a_{32}$  and  $a_{33}$ .

#### 4.3 Superposition method

The method of superposition of solutions is applicable only to linear differential equations but unlike the analytical solution (§4.1) it can also be used for problems with variable coefficients. The solution of the system of equations (28) by this method is given by:

$$\mathbf{x} = \mathbf{u} + c\mathbf{v}, \quad (36)$$

where  $\mathbf{u}$  and  $\mathbf{v}$  are the solutions of the following two initial value problems

$$\frac{d\mathbf{u}}{ds} = A(s)\mathbf{u}; \quad \mathbf{u}(0) = \begin{bmatrix} 0 \\ -(\beta_F K_1/\beta_C) \\ K_1 \end{bmatrix} \quad (37, 37a)$$

$$\frac{d\mathbf{v}}{ds} = A(s)\mathbf{v}; \quad \mathbf{v}(0) = \begin{bmatrix} 1 \\ (1 - \beta_B)/\beta_C - (\beta_E/\beta_C)K_2 \\ K_2 \end{bmatrix} \quad (38, 38a)$$

where  $K_1$  and  $K_2$  are arbitrary constants and

$$c = [v_3(1) - v_2(1)]/[u_2(1) - u_3(1)]. \quad (39)$$

It can be easily shown that the solution given by (36) satisfies the differential equations and the boundary conditions of the original problem (10)–(15). In this case one needs to solve the system of six differential equations, but no iterations are required. The differential equations were solved by the Runge-Kutta method (IMSL routine DVERK).

#### 4.4 Finite difference method

In this method the interval  $[0, 1]$  is portioned into  $(N + 1)$  intervals, which need not be of equal size

$$0 = s_0 < s_1 < \dots < s_{N+1} = 1; h_n = s_{n+1} - s_n, \quad (40)$$

and the derivatives and functions are approximated by finite differences. The system of differential equations (28) is approximated by the system of difference equations

$$\frac{x_n - x_{n-1}}{h_n} - \frac{1}{2} [A(s_n)x_n + A(s_{n-1})x_{n-1}] = 0; \\ n = 1, 2, \dots, N+1, \quad (41)$$

which have to be solved simultaneously with the boundary conditions (13)–(15). The latter can be written as

$$x_{B,0} - 1 = 0, \\ x_{C,0} - (1 - \beta_B)/\beta_C + (\beta_E/\beta_C)x_{E,0} = 0, \\ x_{C,N+1} - x_{E,N+1} = 0. \quad (42)$$

Equations (41) and (42) represent a system of  $(3N+6)$  linear sparse algebraic equations, which can be solved using a standard computer library software. The finite difference (FD) approximation (41) is equivalent to a trapezoidal rule and has an error of the order of  $h^2$  where  $h = \max_n h_n$ . Higher-order approximations can be obtained by deferred corrections. In actual computations we have employed the IMSL routine DVCPR which is based on Lentini and Pereyra's PASVA3 program described by Pereyra (1978, pp. 67–88). This is a sophisticated program with an adaptive non-uniform mesh chosen to make the local error of approximately the same size everywhere. Also, global error estimates and higher-order approximations are made to improve the accuracy and to control the computations. This routine can be used to solve nonlinear BVP problems, in which case the resulting nonlinear algebraic system is solved by Newton's method, while the linearized sparse system is solved by a special form of Gaussian elimination that preserves the sparseness.

### 5. Numerical results and comparisons

In this section results obtained from different numerical methods are compared with the ones obtained using the analytical solution. Also, results illustrating the effect of some model parameters on the reactant conversion and/or concentration profiles are presented.

The numerical results are summarized in tables 3 and 4. Table 3 summarizes results obtained using the standard values of parameters for Powder B catalyst (table 2), while varying the bed height at minimum fluidization,  $H_{mf}$ . All computations were made with  $f_w = 0.50$  and a constant bubble diameter of 0.15 m. It is found that the superposition and the FD method give identical results (four significant digits) as the analytical solution for all values of  $H_{mf}$ . The forward

**Table 3.** Comparison of numerical methods (powder B catalyst with  $f_w = 0.50$  and base values for other parameters given in table 2)

$H_{mf}$ (m)	Analytical method				Forward shooting method			
	$X$	$x_B(1)$	$x_C(1)$	$x_E(1)$	$X$	$x_B(1)$	$x_C(1)$	$x_F(1)$
0.3	0.2247	0.7829	0.6150	0.6150	0.2247	0.7829	0.6150	0.6150
0.90	0.4666	0.5386	0.4261	0.4261	0.4666	0.5386	0.4261	0.4261
1.50	0.6316	0.3719	0.2942	0.2942	0.6323	0.3713	0.2910	0.2598
1.80	0.6939	0.3091	0.2445	0.2445	0.6770	0.3233	0.3163	1.015
2.10	0.7456	0.2568	0.2032	0.2032	0.5157	0.4511	1.181	10.70
2.70	0.8243	0.1474	0.1403	0.1403	-48.7	42.03	210.9	2261.00
3.00	0.8540	0.1474	0.1166	0.1166	N/A	128.6	646.7	6940.00

The results obtained from the finite difference and superposition method are identical with the results obtained from the analytical solution.

**Table 4.** Comparison of numerical methods (powder A catalyst with standard values of model parameters given in table 2)

$H_{mf,m}$	Analytical method				Finite difference method				Superposition method				
	$X$	$x_B(1)$	$x_C(1)$	$x_E(1)$	$X$	$x_B(1)$	$x_C(1)$	$x_E(1)$	$X$	$x_B(1)$	$x_C(1)$	$x_F(1)$	$d_B^{H,m}$
1.0	0.5009	0.5026	0.4118	0.4118	0.5009	0.5026	0.4118	0.4118	0.5009	0.5026	0.4118	0.4118	0.124
2.0	0.5937	0.4117	0.3002	0.3002	0.5937	0.4117	0.3002	0.3002	0.5937	0.4117	0.3002	0.3002	0.194
3.0	0.6331	0.3737	0.2482	0.2482	0.6331	0.3737	0.2482	0.2482	0.6331	0.3737	0.2482	0.2482	0.255
4.0	0.6565	0.3513	0.2155	0.2155	0.6565	0.3513	0.2155	0.2155	0.6566	0.3512	0.2156	0.2148	0.312
5.0	0.6728	0.3358	0.1922	0.1922	0.6728	0.3358	0.1922	0.1922	0.6722	0.3364	0.1934	0.2500	0.365

shooting method works well up to  $H_{mf} = 1.5$  m, where it starts to deviate from the analytical solution. At this point the boundary condition at  $s = 1$  was not satisfied within the specified accuracy [ $x_C(1) - x_E(1) < 10^{-4}$ ], but the exit bubble phase concentration and the conversion are still very close to the exact values. For higher  $H_{mf}$  values the shooting method produces meaningless results. The concentration profiles obtained from the analytical solution and the forward shooting method are shown in figure 2 for  $H_{mf} = 1.8$  m. It can be seen that the shooting method gives results which are in excellent agreement with the analytical solution over the major portion of the reactor ( $s \leq 0.7$ ), but the numerical solution becomes unstable as  $s \rightarrow 1$ . (When the backward shooting technique was employed, the instability occurred as  $s \rightarrow 0$ .) The reasons for the failure of the shooting method are not completely understood, since the concentration profiles are not very steep and the resulting IVP does not represent a "stiff" problem.

Similar problems, with the shooting method, were encountered in the solution of the CCBM equations with the bubble size variation with height. Numerical instabilities developed for the following values of parameters:  $f_w = 0.50$  and  $H_{mf} > 1.3$  m or  $f_w = 0.50$  and  $k > 4 \text{ s}^{-1}$  while using the standard values for other parameters (Powder B, table 2).

Results of computations with the standard values of model parameters corresponding to Powder A catalyst (table 2) are summarized in table 4. In these calculations, for each value of the bed height at minimum fluidization the effective bubble diameter, which gives the same expanded height as predicted from (22)

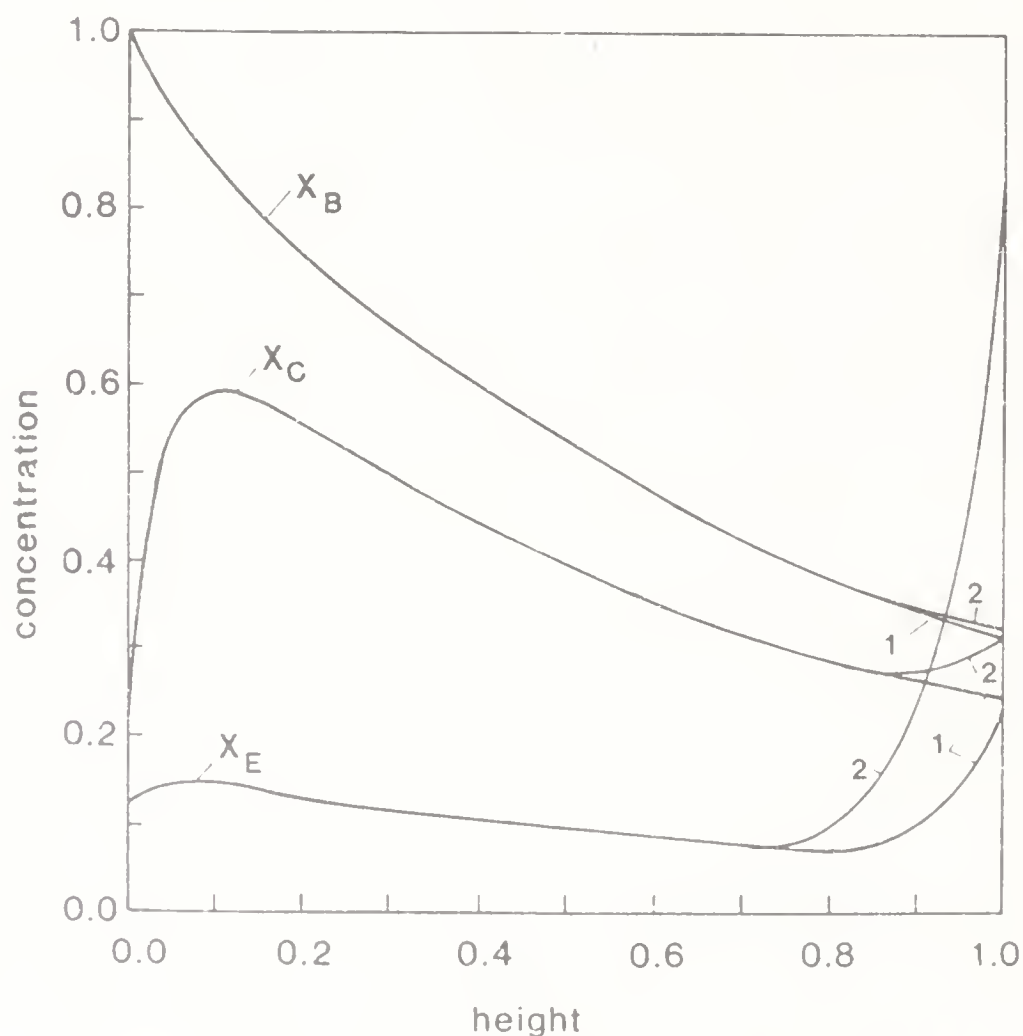


Figure 2. Comparison of concentration profiles obtained from the CCBM with constant bubble size ( $d_B = 0.15$  m,  $f_w = 0.50$ ,  $H_{mf} = 1.8$  m, other parameters at their standard values given in table 2, powder B; 1-Analytical solution; 2-Forward shooting method).



using the Darton *et al* (1977) correlation for  $d_B(s)$ , is calculated from

$$d_B^H = \left( \frac{H_{mf}}{H - H_{mf}} \frac{U - U_{mf}}{(0.71 \text{ g}^{0.5})} \right)^2 \quad (43)$$

The values of  $d_B^H$  are listed in the last column of table 4, and all dimensionless groups defined by (16) were evaluated using  $d_B = d_B^H = \text{constant}$ . The shooting method was not employed in these calculations.

Like in the previous case, results obtained from the FD method and the analytical solution are the same for all values of  $H_{mf}$ . The superposition method gives essentially the same results as the analytical solution for  $H_{mf} \leq 4$  m. For  $H_{mf} = 4$  and 5 m, the boundary condition at  $s = 1$  is not satisfied within the specified accuracy, but this has small effect on the values of conversion. Thus, on the basis of this limited comparison it appears that the finite difference method is the most stable numerical method for this problem and gives results which are in excellent agreement with the ones obtained from the analytical solution over the entire range of parameters that was investigated.

The mass balance equations for the CCBM with bubble size variation have been solved numerically over the wide range of parameters given in table 2. Only selected results will be presented here since the more comprehensive discussion and additional results are presented elsewhere (Bukur 1985; Nasif 1985).

For Powder A type of material the forward shooting and the FD method were employed in calculations, and no numerical problems with either of the two methods were encountered. The effect of the crossflow and the boundary conditions on predictions of conversion for different values of  $H_{mf}$  is shown in figure 3. The effect of additional bulk transport (i.e. crossflow) of reactant is small

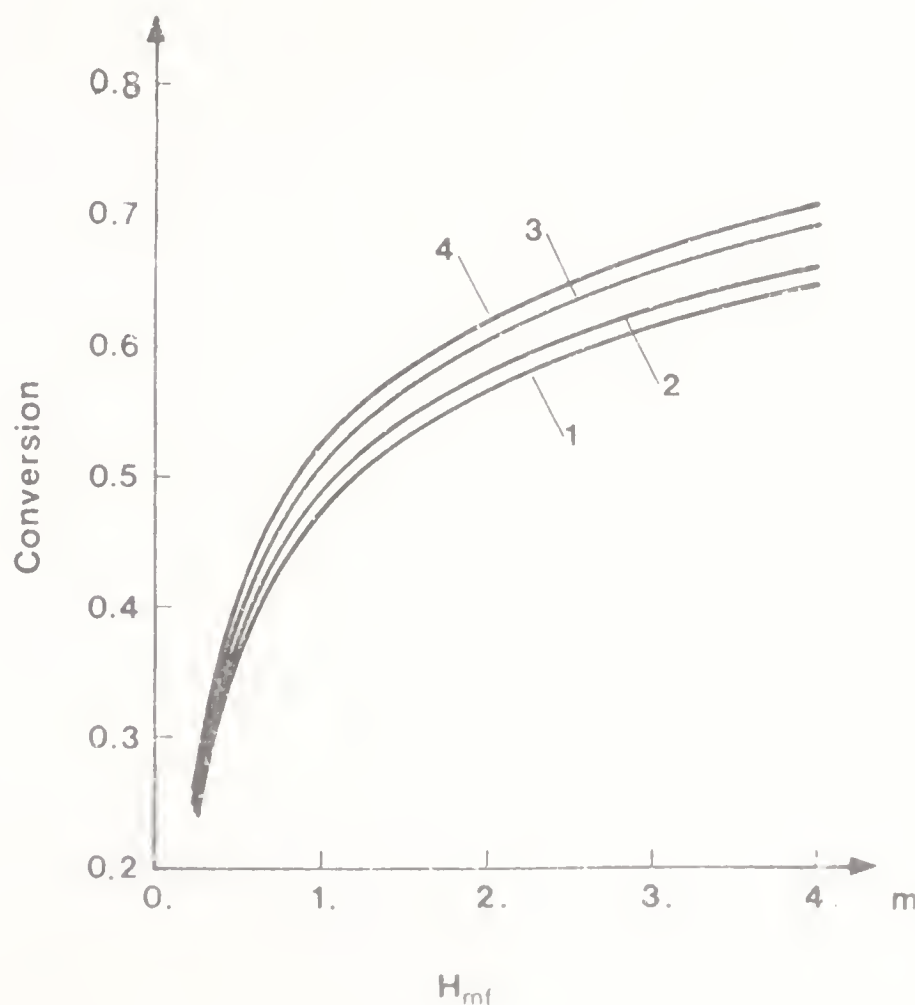


Figure 3. Effects of bed height at minimum fluidization, crossflow and boundary conditions on conversion. Other parameters at their standard values given in table 2: powder A, 1-CEM, 2-NCEM, 3-CEM (MBC), 4-NCEM(MBC).



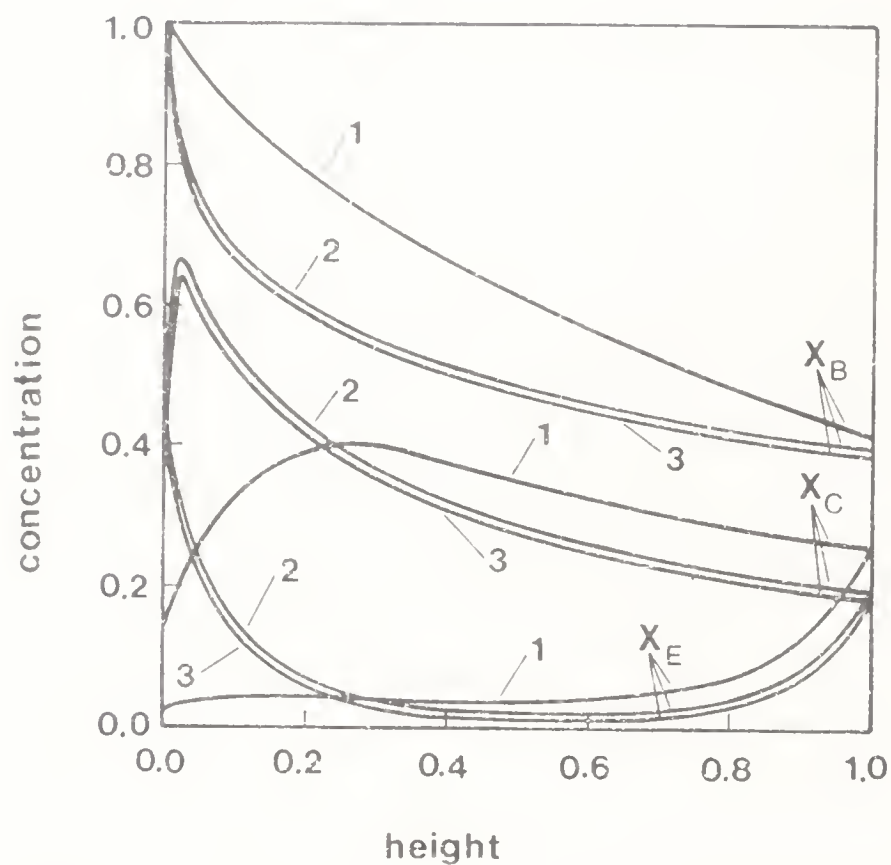


Figure 4. Comparison of axial concentration profiles (powder A with standard values of model parameters; 1 -  $d_B = d_B^H$ ; 2-CFM; 3-NCFM).

and it results in lower values of conversion in comparison to the case where this effect is neglected (curves 2 and 4 for the NCFM are above the corresponding curves 1 and 3 for the CFM). This somewhat unexpected result is caused by catalyst distribution between the cloud-wake and the emulsion phases and flow patterns that are characteristic of the CCBM of Fryer and Potter. The effect of modified boundary conditions is more pronounced but is not sufficiently large for the model discrimination studies.

Concentration profiles obtained from the CCBM which incorporates the bubble growth with height are compared with the ones obtained from the same model using a constant bubble diameter, calculated from (43), in figures 4 and 5. The

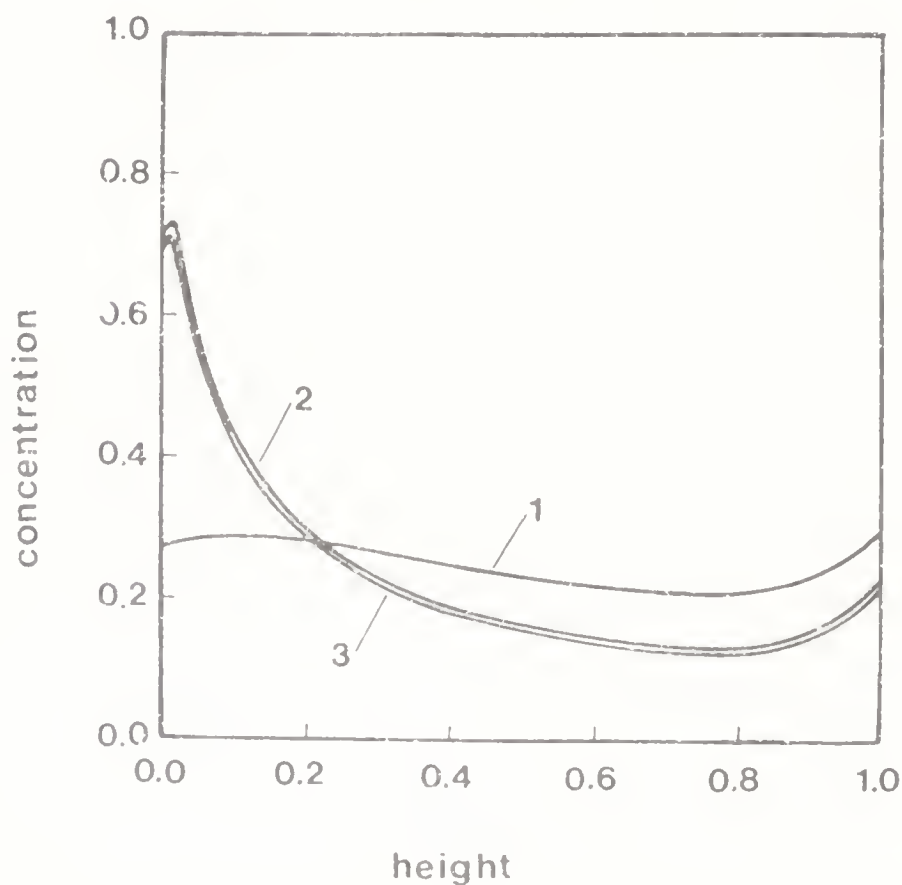


Figure 5. Comparison of average concentration profiles (powder A with standard values of model parameters; 1 -  $d_B = d_B^H$ ; 2-CFM; 3-NCFM).

concentration profiles obtained from the CFM and the NCFM are similar to each other, while the concentration profiles obtained using the constant bubble diameter,  $d_B^{II}$ , are quite different although the predicted values of conversion are similar in all three cases (CFM: 0.615; NCFM: 0.627;  $d_B^{II} = 0.255$  m: 0.633). Similar results were obtained for other values of model parameters (Bukur 1985), which demonstrates that model discrimination on the basis of conversion alone may not be possible. Additional information on the use of effective bubble diameters in modelling of fluid bed reactors can be found in Fryer & Potter (1972b), Bukur & Nasif (1985) and Bukur *et al* (1986).

Figure 6 illustrates the influence of several variables on predictions of conversion for a catalyst belonging to the class B powders. Conversion increases with the increase of  $f_w$  (curves labeled 1 and 2), but for a given set of parameters the maximum allowable value for  $f_w$  is 0.67. This limitation arises from a requirement that the volume fraction of bubbles and wakes has to be less than or equal to one, i.e.

$$\varepsilon_B(1 + f_w) \leq 1. \quad (44)$$

Since the volume fraction of bubbles decreases with height this condition will be satisfied for all values of  $z$  if it is satisfied at the distributor level. One can use larger values of  $f_w$  by reducing the value of  $\varepsilon_B(0)$ . The latter can be accomplished by either increasing the initial bubble size while keeping the constant gas flow rate (curve 3, figure 6), or by decreasing the gas flow rate while keeping the initial

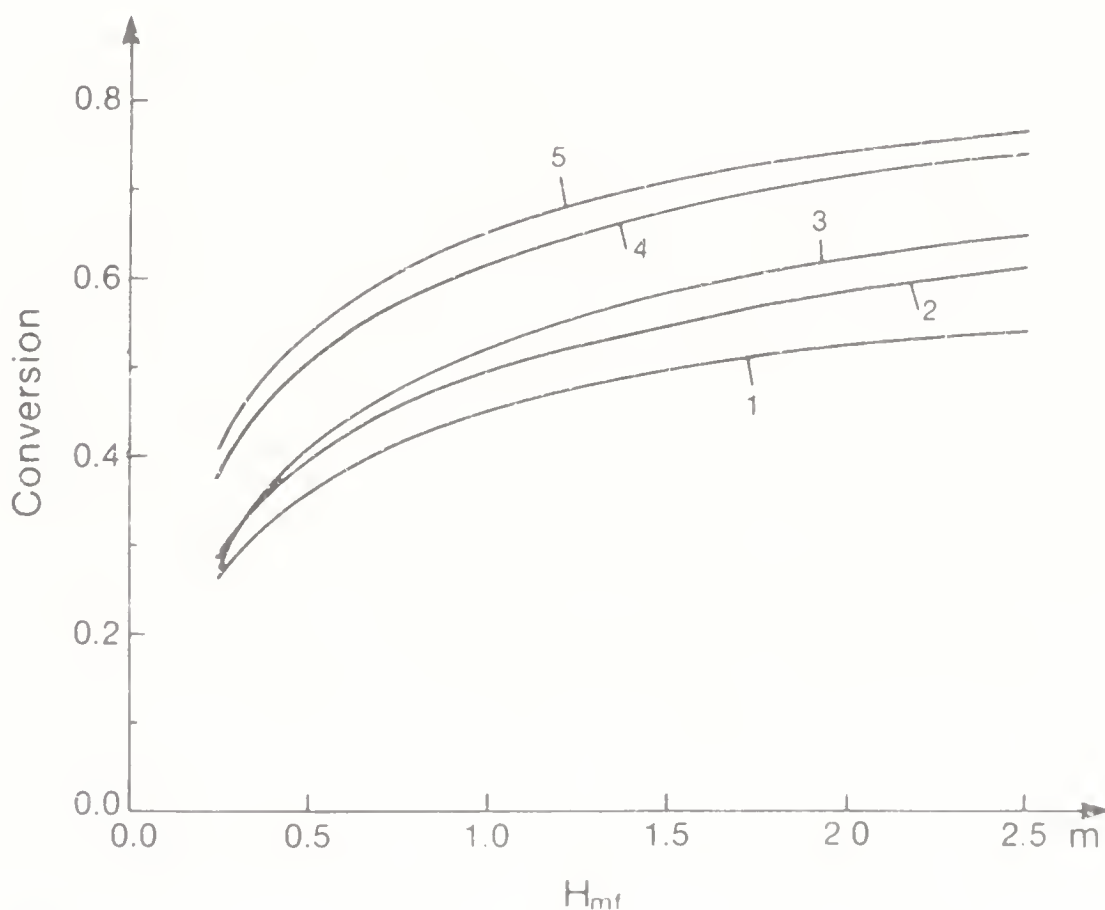


**Figure 6.** Effect of model parameters on predictions of conversion-CFM. (1 -  $U/U_{mf} = 10$ ,  $d_{B0} = 0.03$  m,  $f_w = 0.5$ ; 2 -  $U/U_{mf} = 10$ ,  $d_{B0} = 0.03$  m,  $f_w = 0.67$ ; 3 -  $U/U_{mf} = 10$ ,  $d_{B0} = 0.06$  m,  $f_w = 1.0$ ; 4 -  $U/U_{mf} = 7$ ,  $d_{B0} = 0.03$  m,  $f_w = 0.96$ ; 5 -  $U/U_{mf} = 6$ ,  $d_{B0} = 0.03$  m,  $f_w = 1.0$ . Other parameters at their standard values given in table 2, powder B)

bubble size constant (curves 4 and 5). In practice, the required changes could be made by changing the number and/or the size of holes in a perforated distributor plate. For curves 2–4 the values of  $U$ ,  $d_{B0}$  and  $f_w$  were chosen so that  $\varepsilon_B(0)(1+f_w) = 1$ .

Curve 3 shows that further increase in the value of  $f_w$  gives higher values of conversion even though the initial bubble size is doubled. As expected, decrease in the gas flow rate (i.e.  $U$ ) leads to increase in predicted values of conversions (curves 4 and 5).

## 6. Compartment models

These models were developed to describe performance of the fluid bed reactors with axial variation of the fluidized bed properties due to bubble growth with height. The concept whereby the fluid bed is divided axially into a number of cells (compartments), within each of which a constant bubble diameter is used, was first introduced by Kato & Wen (1969). They used a simplified version of the CCBM in which the gas flow through the emulsion phase was neglected. Subsequently, this concept was applied to different models (e.g. Fryer & Potter 1972b, 1974, pp. 440–453; Darton 1979; Peters *et al* 1982) and its application to the CCBM will be described in this section. Two alternative approaches will be discussed and some numerical results will be presented.

### 6.1 Fryer and Potter algorithm

Fryer & Potter (1972b, 1974) proposed a version of the compartment model where the bed is divided into a number of compartments within each of which a constant bubble size is used. The schematic representation of their approach is shown in figure 7. The size of compartment is chosen such that the fractional increase in bubble size is the same in each compartment, i.e.

$$d_B(z_n)/d_B(z_{n-1}) = R = \text{constant}, \quad 1 \leq n \leq N. \quad (45)$$

The mean bubble diameter in a typical compartment  $n$ , is defined as

$$d_{B_n} = \frac{1}{2} [d_B(z_n) + d_B(z_{n-1})]. \quad (46)$$

All superficial gas velocities, gas exchange coefficients and volume fractions in a given compartment are calculated using the mean bubble diameter. Material balances over a differential element of height within each compartment yield a set of equations which are identical to those obtained from the CCBM with constant bubble size (§4.1). The analytical solution is given by (25) which is valid only within a given compartment. The eigenvalues and eigenvectors are calculated for each compartment, and there are  $3N$  unknown coefficients  $m_i$  (3 per compartment). They are determined from the three boundary conditions, and the  $3(N-1)$  continuity conditions requiring that concentrations at the top of the  $n$ th compartment ( $z_n$ ) be the same as concentrations at the bottom of the next compartment, i.e.

$$x_n(z_n) = x_{n+1}(z_n), \quad 1 \leq n \leq N-1. \quad (47)$$

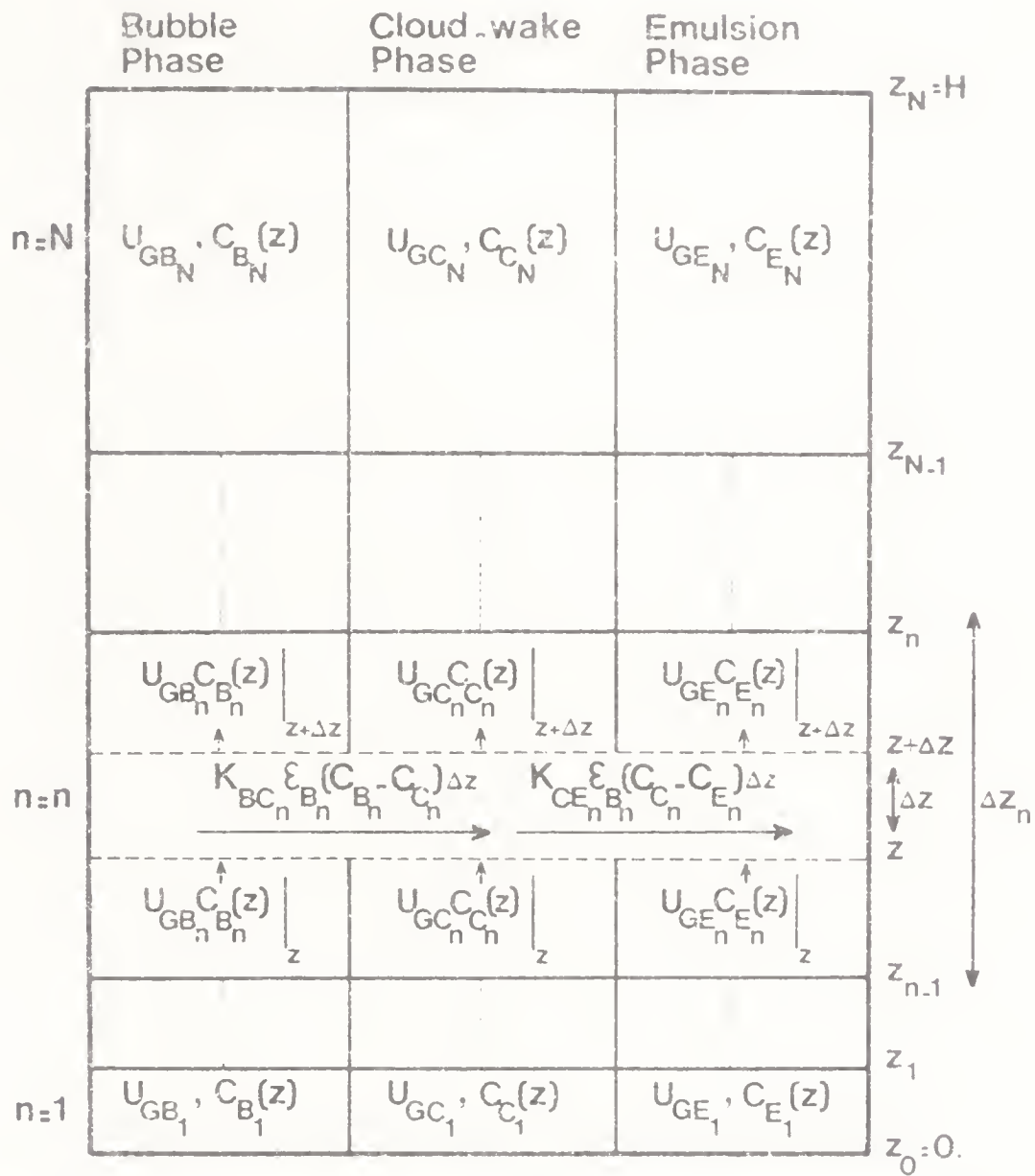


Figure 7. Schematic representation of the Fryer and Potter compartment model.

From these conditions one obtains the system of  $3N$  linear algebraic equations in  $3N$  unknowns. The details of solution of the resulting system of algebraic equations can be found elsewhere (Nasif 1985).

This algorithm can be applied to the NCFM (§2.3) only since the mass balances are based on the differential element of height within each compartment where the bubble size is constant. This, however, does not represent a serious drawback since the effect of crossflow terms was found to be small (§5).

## 6.2 Peters-Fan-Sweeney algorithm

Peters *et al* (1982) proposed a model similar to the CCBM and solved the resulting mass balance equations by dividing the bed into  $N$  compartments (see figure 8). The size of each compartment is given by the cloud diameter at a given bed height. The cloud diameter is calculated from the bubble diameter in the  $n$ th compartment by an iterative procedure. It is assumed that the gas is perfectly mixed within each phase of a compartment in which case the steady state material balance equations over a typical compartment  $n$  are

Bubble phase:

$$U_{GB_n} C_{B_n} A - U_{GB_n} C_{B_n} A - P_{12_n} A C_{B_n} - K_{BC_n} \epsilon_{B_n} (C_{B_n} - C_{C_n}) A \Delta z_n = 0. \quad (48)$$



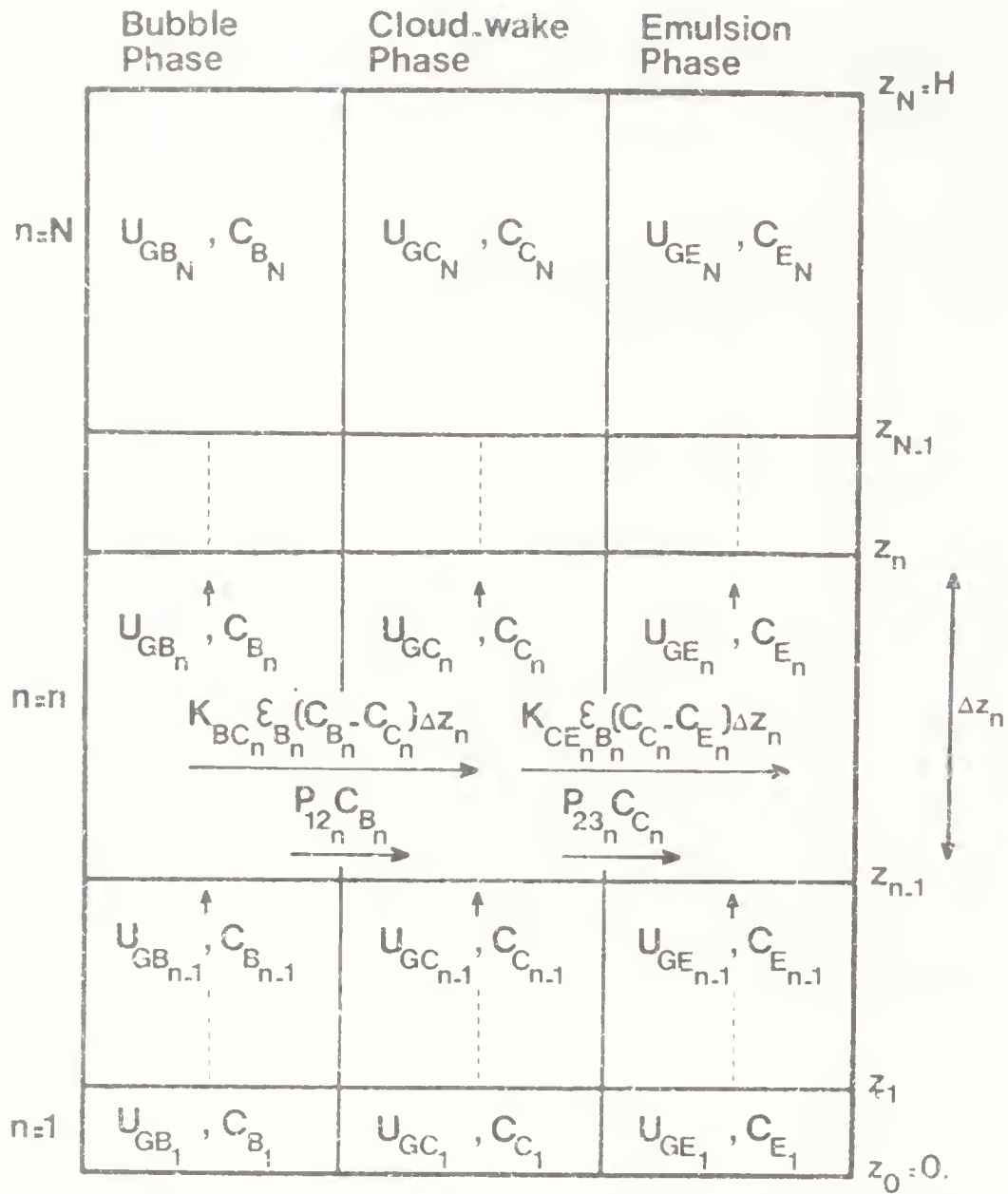


Figure 8. Schematic representation of the algorithm of Peters and others.

Cloud-wake phase:

$$U_{GC_{n-1}}AC_{C_{n-1}} - U_{GC_n}AC_{C_n} + P_{12_n}AC_{B_n} + K_{BC_n}\epsilon_{B_n}(C_{B_n} - C_{C_n})A\Delta z_n - P_{23_n}AC_{C_n} - K_{CE_n}\epsilon_{B_n}(C_{C_n} - C_{E_n})A\Delta z_n - k(1 - \epsilon_{mf})f_w\epsilon_{B_n}C_{C_n}A\Delta z_n = 0. \quad (49)$$

Emulsion phase:

$$U_{GE_{n-1}}AC_{E_{n-1}} - U_{GE_n}AC_{E_n} + P_{23_n}AC_{C_n} + K_{CF_n}\epsilon_{B_n}(C_{C_n} - C_{E_n})A\Delta z_n - k(1 - \epsilon_{mf})[1 - \epsilon_{B_n}(1 + f_w)]C_{E_n}A\Delta z_n = 0. \quad (50)$$

The crossflow terms  $P_{12}$  and  $P_{23}$  represent the additional bulk transport of material from bubble to cloud-wake, and from cloud-wake to emulsion phase, respectively. They are given by

$$P_{12_n} = U_{GB_{n-1}} - U_{GB_n}, \quad (51)$$

and

$$P_{23_n} = P_{12_n} + U_{GC_{n-1}} - U_{GC_n}. \quad (52)$$

Equations (48)–(50) together with the boundary conditions (13)–(15) represent the system of the  $3N + 3$  linear algebraic equations in  $(3N + 3)$  unknowns. A detailed procedure to solve these equations is described elsewhere (Nasif 1985).



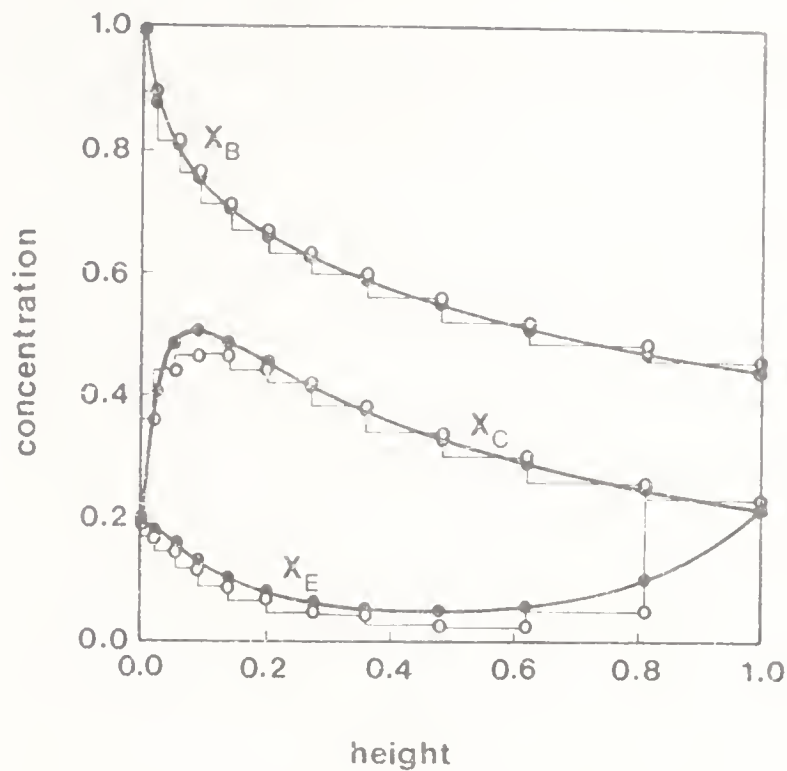


Figure 9. Comparison of concentration profiles. ( $d_{B0} = 0.06$  m,  $f_w = 1.0$ ,  $H_{mf} = 1.25$  m, other variables at their standard values given in table 2, powder B; — forward shooting method; • algorithm of Fryer and Potter; ○ algorithm of Peters and others).

### 6.3 Numerical results and comparison of methods

In this section the results obtained from the compartment models are compared with those obtained from the CCBM with continuous bubble size variation with height. In the latter case, the differential equations were solved by the forward shooting method. Comparison is made for the case where the crossflow terms are neglected and concentration profiles obtained using different methods are shown in figures 9 and 10. Fryer and Potter's (1972b, 1974, pp. 440–453) algorithm with  $R = 1.2$  gives results that are virtually identical to those obtained from the CCBM with continuous bubble size variation. According to the Peters *et al* (1982) algorithm, the concentrations in each compartment are assumed to be constant and as a result stepwise profiles are obtained. These stepwise profiles approximate well the continuous profiles as shown in figures 9 and 10. Similar results were obtained

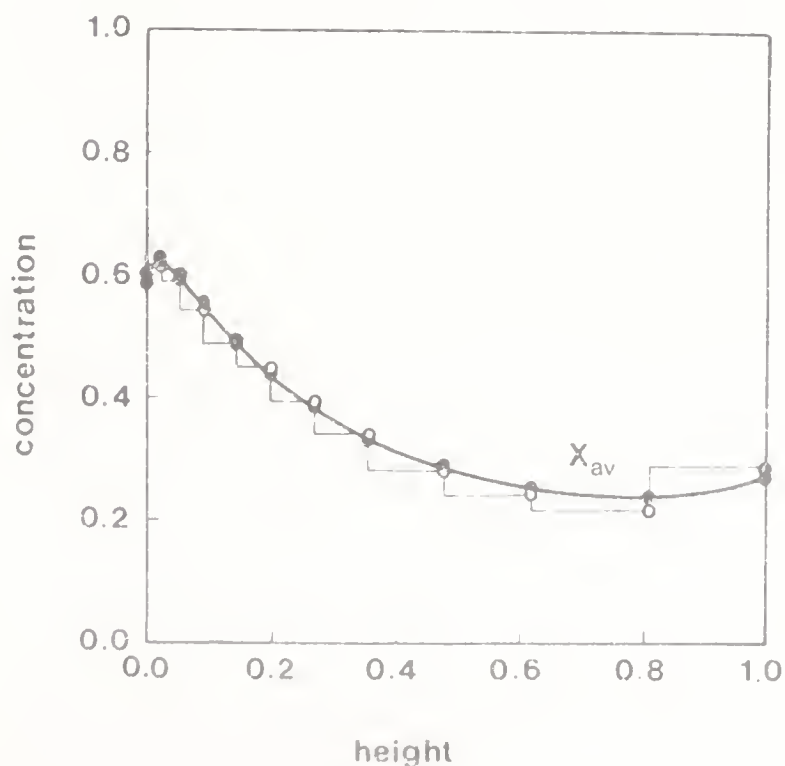


Figure 10. Comparison of average concentration profiles. ( $d_{B0} = 0.06$  m,  $f_w = 1.0$ ,  $H_{mf} = 1.25$  m, other variables at their standard values given in table 2, powder B; — forward shooting method; • algorithm of Fryer and Potter; ○ algorithm of Peters and others).

for some other values of model parameters. As a consequence of these studies, it can be concluded that the compartment models give satisfactory results and require less computations. Also, they can be used to describe performance of fluid bed reactors with non-linear reaction rate expressions.

### 7. A simplified initial value (Jayaraman-Kulkarni-Doraiswamy) model

Jayaraman *et al* (1981) modified the CCBM of Fryer and Potter by assuming that the emulsion phase gas is perfectly mixed. This assumption is probably closer to physical reality in large diameter industrial reactors, and it leads to the conversion of the original two-point BVP to a simpler IVP. Conversions obtained from this model were found to be in excellent agreement with those of the original model, over a range of model parameters. However, agreement between the average concentration profiles predicted by the two models was found to be less satisfactory. In particular, the model of Jayaraman *et al* (1981) does not predict the existence of a minimum in the average concentration profile which represents the unique feature of the Fryer and Potter model (see figure 5). The model of Jayaraman and others was derived for a constant bubble size in which case a closed form analytical solution is possible. In the case of bubble size variation with height the mass balances for the bubble and the cloud-wake phase are given by (10) and (11), while the mass balance for the reactant in the emulsion phase is

$$\begin{aligned}
 & -\beta_E(1)(x_C(1) - x_E) + \int_0^1 P'_{CE} x_C \, ds \\
 & + \int_0^1 N_{CF}(x_C - x_E) \, ds - N_r x_E \int_0^1 [1 - \varepsilon_B(1 + f_w)] \, ds = 0.
 \end{aligned} \tag{53}$$

Equations (13) and (14) are still valid, but in this case they represent the initial conditions. The resulting system of equations could be solved by an iterative procedure whereby one initially assumes a value of  $x_E$  and integrates numerically the differential equations (10) and (11) subject to initial conditions (13) and (14). Then calculated  $x_C(s)$  values would be inserted into (53) to check whether this balance is satisfied. This would yield a new value for  $x_E$  and the whole procedure would be repeated until (53) is satisfied within a desired accuracy.

### 8. Summary and conclusions

The counter-current backmixing model in its rigorous form proposed by Fryer & Potter (1972a) represents a two-point boundary value problem whose numerical solution is difficult to obtain. Numerical solution of this problem was attempted using several numerical methods (shooting, superposition and finite difference) for solution of boundary value problems. It was found that the forward shooting and the superposition method are not stable for some values of model parameters, while the finite difference method is stable and produces accurate results over the entire range of parameters that was investigated.

The compartment models are also suitable for solution of the CCBM which incorporates the bubble size variation with height. The modification of the original

Fryer & Potter model, proposed by Jayraman *et al* (1981), which converts it from the BVP into an IVP represents an attractive alternative which needs to be explored further. Additional studies of the type reported here are required with nonlinear reaction rate expression and/or nonisothermal fluid bed reactors before definite conclusions can be drawn as to which method is the most suitable for solving the counter-current backmixing model equations.

The effect of additional bulk transport of material (crossflow) and modified boundary conditions on predictions of conversions and concentration profiles were found to be rather small. Differences in the model predictions are too small to be used as a basis for model discrimination from experimental data.

This paper is dedicated to Dr L K Doraiswamy on his sixtieth birthday. Computations reported in this paper were carried out by N Nasif, J G Daly and S H Lane.

### List of symbols

$A$	cross-sectional area of the bed,
$A_0$	catchment area in Darton <i>et al</i> 's (1977) correlation, $\text{m}^2$ ,
$C$	reactant concentration, $\text{mol}/\text{m}^3$ ,
$d_B$	local value of bubble diameter, m,
$d_{B0}$	initial value of bubble diameter, m,
$D_G$	molecular gas diffusivity, $\text{m}^2/\text{s}$ ,
$f_w$	ratio of wake volume to bubble volume,
$g$	gravitational acceleration, $\text{m}/\text{s}^2$ ,
$H$	expanded bed height, m,
$k$	reaction rate constant based on unit volume of solids, $\text{s}^{-1}$ ,
$K_{BC}$	volumetric rate of gas exchange between bubble and cloud-wake phase per unit bubble volume, $\text{s}^{-1}$ ,
$K_{CE}$	volumetric rate of gas exchange between cloud-wake and emulsion phase per unit bubble volume, $\text{s}^{-1}$ ,
$N_{BC}$	number of mass transfer units based on $K_{BC}$ , (16),
$N_{CE}$	number of mass transfer units based on $K_{CE}$ , (16),
$N_r$	number of reaction units, (16),
$P_{BC}$	crossflow coefficient between bubble and cloud-wake phase, (4a), $\text{s}^{-1}$ ,
$P_{CE}$	crossflow coefficient between cloud-wake and emulsion phase, (4b), $\text{s}^{-1}$ ,
$P'_{BC}, P'_{CE}$	dimensionless crossflow coefficients, (16),
$U$	total superficial gas velocity, $\text{m}/\text{s}$ ,
$U_B$	absolute bubble rise velocity, $\text{m}/\text{s}$ ,
$U_{Gj}$	superficial gas velocity in phase $j$ ( $j = B, C, E$ ), $\text{m}/\text{s}$ ,
$x$	dimensionless concentration, ( $x = C/C_i$ ),
$x_{av}$	dimensionless average concentration, (18),
$X$	reactant conversion,
$z$	axial distance from distributor, m,



$\beta_j$	fraction of gas that passes through phase $j$ , $j = B, C, E$ ; (16),
$\varepsilon_B$	volume fraction of bed occupied by bubbles,
$\varepsilon_{mf}$	bed voidage at minimum fluidization.

### Subscripts

$B^*$	bubble phase,
$C$	cloud-wake phase,
$E$	emulsion (dense) phase
$i$	inlet of reactor,
$mf$	minimum fluidization,
$n$	compartment number ( $n = 1 \rightarrow N$ ).

### References

- Bukur D B 1985 Paper No. 61d, Annual AIChE Meeting, Chicago, Illinois
- Bukur D B, Nasif N 1985 *Chem. Eng. Sci.* 40: 1925–1933
- Bukur D B, Nasif N, Daly J G 1986 *Chem. Eng. Sci.* (accepted for publication)
- Chavarie C, Grace J R 1975 *Ind. Eng. Chem., Fundam.* 14: 79–86
- Darton R C 1979 *Trans. Inst. Chem. Eng.* 57: 134–138
- Darton R C, La Nauze R D, Davidson J F, Harrison D 1977 *Trans. Inst. Chem. Eng.* 55: 274–280
- Fryer C, Potter O E 1972a *Ind. Eng. Chem., Fundam.* 11: 338–344
- Fryer C, Potter O E 1972b *Powder Technol.* 6: 317–322
- Fryer C, Potter O E 1974 Proc. Int. Symp. on Fluidization and its Applications, Toulouse (October 1973), *ste. Chimie Industrielle*, 440–453
- Fryer C, Potter O E 1976 *AIChE J.* 22: 38–47
- Geldart D 1973 *Powder Technol.* 7: 285–292
- Jayraman V K, Kulkarni B D, Doraiswamy L K 1981 *ACS Symp. Ser.* 168: 19–29
- Kai T, Furusaki S 1984 *Chem. Eng. Sci.* 39: 1317–1319
- Kato K, Wen C Y 1969 *Chem. Eng. Sci.* 24: 1351–1367
- Kunii D, Levenspiel O 1968a *Ind. Eng. Chem., Fundam.* 7: 446–452
- Kunii D, Levenspiel O 1968b *Ind. Eng. Chem., Process Des. Dev.* 7: 481–492
- Litz W 1973 *Chem.-Ing.-Tech.* 45: 382–387
- McGinnis P H 1965 *Chem. Eng. Prog., Symp. Ser.* 61(55): 2–10
- Mori S, Wen C Y 1976 *Fluidization technology* (ed.) D L Keairns (Washington D C: Hemisphere Publishing Co.) vol. 1
- Nasif N 1985 *Mathematical modeling of fluidized bed reactors* M.Sc. thesis, Texas A&M University
- Pereyra V 1978 *Codes for boundary value problems in ordinary differential equations—Lecture notes in computer science* 76 (Berlin: Springer-Verlag)
- Pereyra V 1978 *Codes for boundary value problems in ordinary differential equations—Lecture notes in computer science* 76 (Berlin: Springer-Verlag)
- Shaw I D, Hoffman T W, Orlickas A, Reilly P M 1972 *Can. J. Chem. Eng.* 50: 637–643
- Stephens G K, Sinclair R J, Potter O E 1967 *Powder Technol.* 1: 157–166
- Van Deemter J J 1967 *Proceedings of the international symposium on fluidization*, (ed.) A A H Drinkenburg (Netherlands University Press: Amsterdam)
- Woolard I N M, Potter O E 1968 *AIChE J.* 3: 388–391

# Circulating fluidized bed reactor design and operation

J R GRACE, C J LIM, C M H BRERETON and J CHAOUKI

Department of Chemical Engineering, University of British Columbia, Vancouver, Canada V6T 1W5

**Abstract** The circulating fluidized bed reactor has unique qualities which differentiate it from other gas-solid contactors and make it promising for a wide range of reactions. A  $0.15\text{ m} \times 0.15\text{ m} \times 7.3\text{ m}$  tall circulating bed reactor with solids returned via an *L*-valve has been established at the University of British Columbia for combustion of a wide range of solid and heavy liquid fuels. The reactor is heavily instrumented to allow reaction characteristics to be related to reactor hydrodynamics and transfer processes. Novel features are incorporated to permit measurement of solids circulation rates and in the configuration of secondary gas entry ports. Preliminary heat transfer data, temperature profiles and pressure profiles are reported for operation at high temperatures.

**Keywords.** Circulating fluidized bed reactor; reactor hydrodynamics; transfer processes.

## 1. Introduction

The earliest fluidized bed reactors used for the catalytic cracking of hydrocarbons dating from the early 1940's operated at high superficial gas velocities now associated with the regime of fast fluidization. However, methods used to separate and return entrained solids were crude, and these early reactors were soon replaced by fluidized beds operating at much lower gas velocities (Yerushalmi & Cankurt 1978; Jahnig *et al* 1980). The circulating bed as it has evolved in recent years follows from its development by Reh (1971) for calcining of alumina. Since that time, the circulating fluidized bed has been adopted or tested for a variety of gas-solid reactions and solid-catalysed gas phase reactions.

The so-called circulating fluidized bed is, in reality, not a bed at all, having no distinct upper surface. Instead, it is intermediate in density between dense phase fluidization and dilute pneumatic conveying. Boundaries showing the approximate operating range of circulating beds, in comparison with other common types of gas-solid contactors, are shown in figure 1 (Grace 1986a) on dimensionless gas



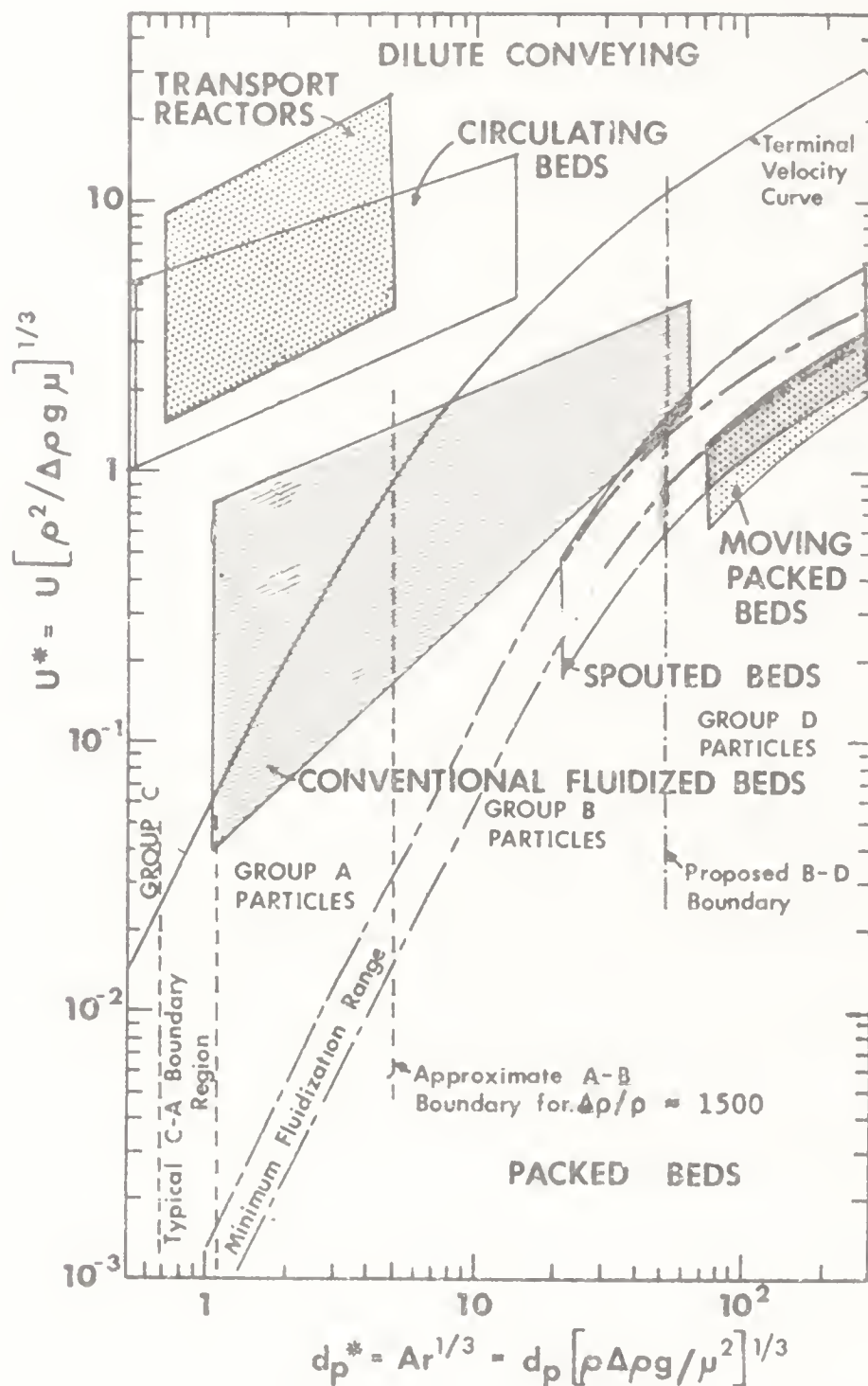


Figure 1. Regime map for gas-solid systems in dimensionless gas velocity vs dimensionless particle diameter coordinates according to Grace (1986a) showing regions occupied by different principal types of gas-solid reactors and approximate boundaries between Geldart powder groups.

velocity versus dimensionless particle diameter coordinates. It is seen that circulating beds are quite distinct from "conventional" (i.e. bubbling and slugging) fluidized beds, whereas they overlap substantially with transport reactors. In current applications, circulating bed reactors encompass primarily Groups A and B of the Geldart (1973) classification, but it would seem to be possible to operate with Group C solids if these can be successfully recycled. Future applications appear likely to extend circulating beds to larger particle sizes classified as Group D.

The key features of circulating fluidized bed reactors which distinguish them from competing reactor configurations are as follows:

- vertical upflow reactor column with superficial gas velocity of the order of 4–12 m/s;
- no distinct upper bed surface in the column;

- overall void fraction in the range 0.85–0.99;
- the gas, rather than an emulsion of solid particles with interstitial gas, forms the continuous phase;
- some means, external or internal, for returning the vast majority of particles reaching the top of the vessel back to its base.

Some specific applications of circulating fluidized beds as reactors, satisfying the above requirements, are listed in table 1. It is clear that circulating beds have a wide potential applicability to many industrial chemical processes practised in industry, in competition with other principal reactor types such as the fixed bed, entrained flow reactors, dense phase fluidized beds and rotary kilns.

## 2. Circulating fluidized bed combustion

The circulating fluidized bed has been especially successful for combustion of a wide range of solid fuels including coal, biomass, peat, petroleum coke, oil shale, and refuse-derived fuels. Advantages of circulating fluidized bed combustion (CFBC) relative to conventional pulverized and grate type burners include:

- ability to capture sulphur *in situ* and with good sorbent utilization by feeding limestone or dolomite with the fuel;
- low emissions of nitrogen oxides due to low combustion temperatures (typically 840–900°C) and staged introduction of combustion air;
- fuel flexibility, with ability to switch from one fuel to another and burn low quality and agglomerating fuels;
- excellent combustion efficiency, commonly > 99%;

Table 1. Application of circulating fluidized beds.

Application	Reference	Status
Calcination of aluminium phosphate rock, clay	Reh 1971	Approximately 30 units with capacity up to 1500 tonnes/day in operation
Combustion of coal, peat, wood wastes, petroleum coke, shale	Reh <i>et al</i> 1980; Schwieger 1985, among many	Being widely adopted for industrial uses, cogeneration of power and steam, district heating. Up to >100 MW <sub>e</sub> in capacity
Gasification of coal, wood wastes, biomass	Reh 1986; Hirsch <i>et al</i> 1986	Commercial units being installed
Catalytic cracking*	Matsen 1980	In wide usage in many countries
Fisher-Tropsch synthesis of hydrocarbons	Hoogendoorn 1973	In operation in Sasol plants
Low temperature adsorption from waste gas streams including flue gas desulphurization	Graf 1986	Several industrial reactors in operation
Prereduction of iron and nickel ores	Hirsch <i>et al</i> 1986	Pilot plant tests completed
Roasting of sulphide ores	Reh 1986	Pilot plant tests completed

\* Modern riser reactors employed in catalytic cracking appear to fall generically within the circulating bed category

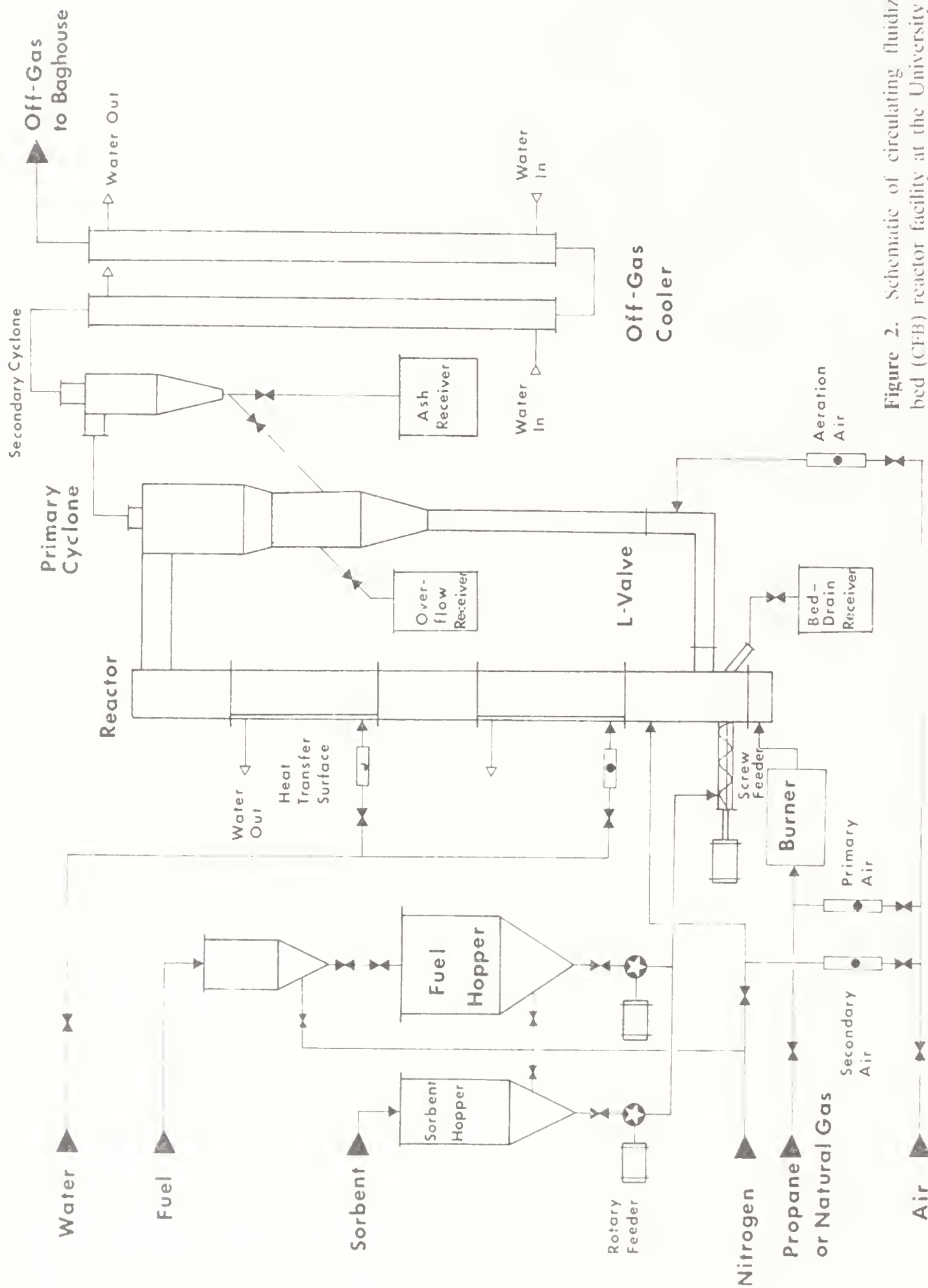


Figure 2. Schematic of circulating fluidized bed (CFB) reactor facility at the University of British Columbia.

— favourable turndown (typically 4:1) and good load following capabilities.

This paper describes a pilot plant scale circulating fluidized bed unit recently designed, constructed and put into operation in the Pulp and Paper Centre at the University of British Columbia for combustion and reactor characterization studies. The unique experimental set-up and operation of the unit are described, showing how the unit can be operated and illustrating key differences from other common reactor types. Some early data are also presented.

### 3. Experimental facility

An overall schematic of the experimental equipment appears in figure 2. The principal reactor chamber is composed of five refractory-lined flanged sections

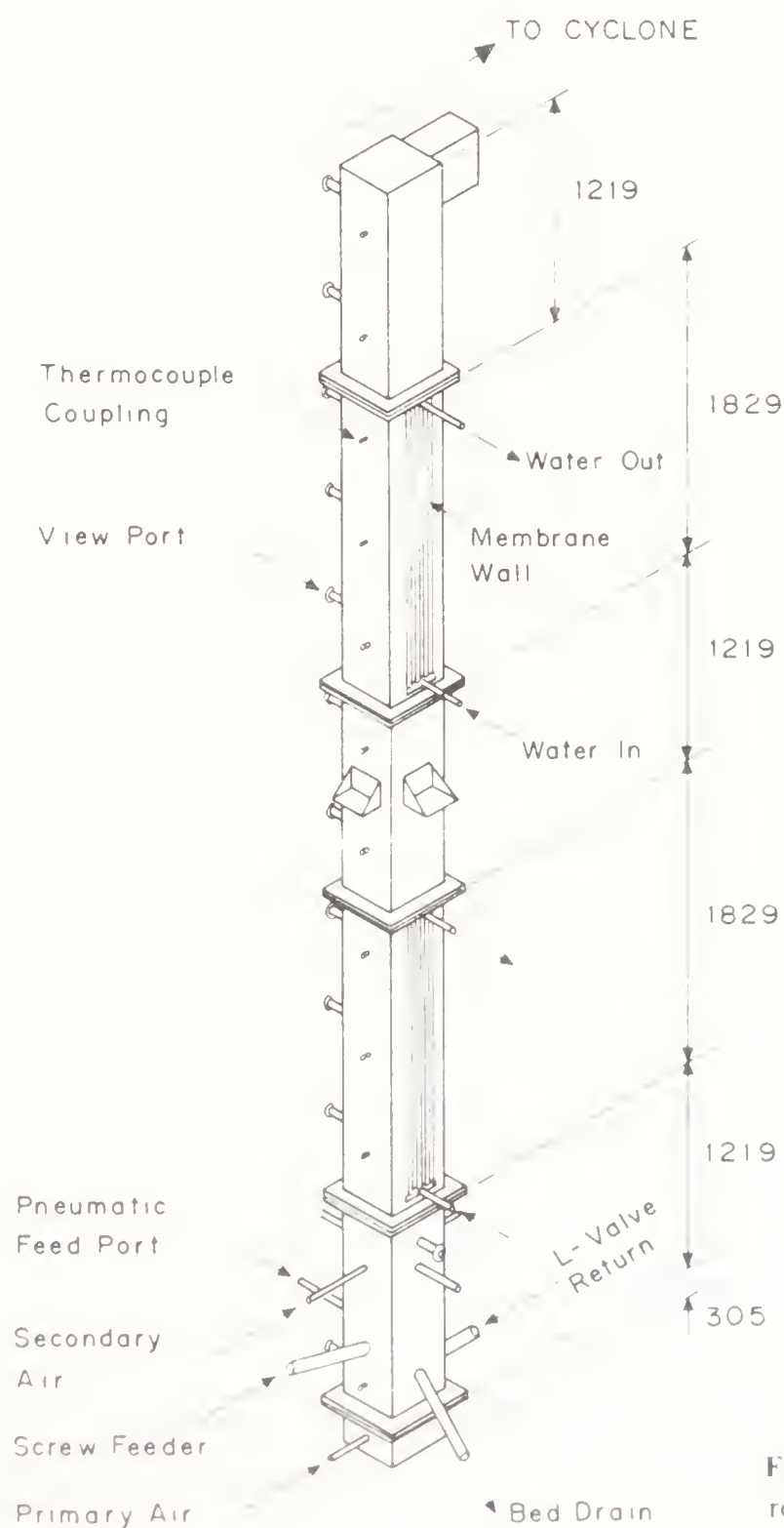


Figure 3. View of principal refractory lined reactor chamber



providing a chamber of 152 mm square cross-section with an overall height of 7.32 m. A view of the reactor is shown in figure 3. The refractory is erosion-resistant and held in place by pins welded to the outer steel walls. Pressure taps and thermocouples are located at 610 mm intervals along opposite faces of the column. In addition, there are a series of twelve regularly spaced 41 mm diameter ports which can be used as viewing ports, for withdrawal of gas and/or solids samples, or for insertion of probes.

A distributor plate and plenum chamber are suspended from the bottom of the reactor for easy removal. Primary air is introduced to the bottom of the reactor through three tuyeres, each consisting of a 38 mm o.d. stainless steel pipe capped and drilled with six holes of 9 mm diameter at an angle of 30° downwards to the horizontal as shown in figure 4a to prevent solids from flowing back into the plenum chamber during shutdown. An inclined stainless steel frame around the outer periphery of the grid plate protects the refractory at the base from erosion. For start-up of the unit, the primary air is preheated in an external burner chamber by burning natural gas or propane.

Secondary air is fed to the reactor through four ports located 0.9 m above the primary air distributor plate. This secondary air can either be injected through two pairs of directly opposed orifices (ports a, b, d and e in figure 4b) or through four off-centre ports (ports b, c, e and f in figure 4b) in order to introduce swirl. The primary air and secondary air are metered and controlled separately so that their ratio can be varied with a fixed total air flow.

Solid fuel and sorbent are fed to the unit by means of a 125 mm diameter screw feeder inclined downward at an angle of 15° to the horizontal. The fuel and sorbent are contained in separate sealed hoppers. The feed rate is controlled by means of rotary valves, one per hopper, with rubber impellers and a transparent front to allow visual verification that the feeder is operating properly at all times. The hoppers will be mounted on load cells to allow the feed rates to be determined accurately. A purge of nitrogen or air is introduced at the drive end of the screw feeder to prevent dust from entering the bearings and to cool the screw feeder. In experiments where the fuel is a heavy liquid, e.g., tar or pitch from heavy oil or tar sands upgrading operations, the fuel is pumped into the reactor through a 25 mm orifice 720 mm above the distributor plate. For feeding of hog fuel and other wood wastes, the hopper has a live bottom emptying directly into the screw feeder.

Heat can be removed from the reactor either by one or two membrane waterwall cooling surfaces mounted on one wall of the column, one beginning 1.22 m and the other 4.27 m above the distributor plate as indicated in figure 3. Four vertical stainless steel tubes of 21.3 mm o.d. and 13.9 mm i.d., separated by longitudinal flat fins welded along their lengths, comprise the two cooling surfaces. Thermocouples are positioned at 152 mm intervals inside one of the central tubes and at the inlet and outlet for the cooling water to allow heat transfer rates to be determined for different sections of the assemblies. Each of the cooling surfaces has a total exposed surface area of 0.30 m<sup>2</sup> and a projected surface area of 0.23 m<sup>2</sup>. Each can be removed and replaced by a refractory-lined section if less heat transfer surface area is required.

Gas and entrained solids leaving the top of the reactor enter a refractory-lined medium-efficiency primary cyclone of inside diameter 305 mm. Solids captured in the primary cyclone drop into a conical recycle hopper which serves also as an



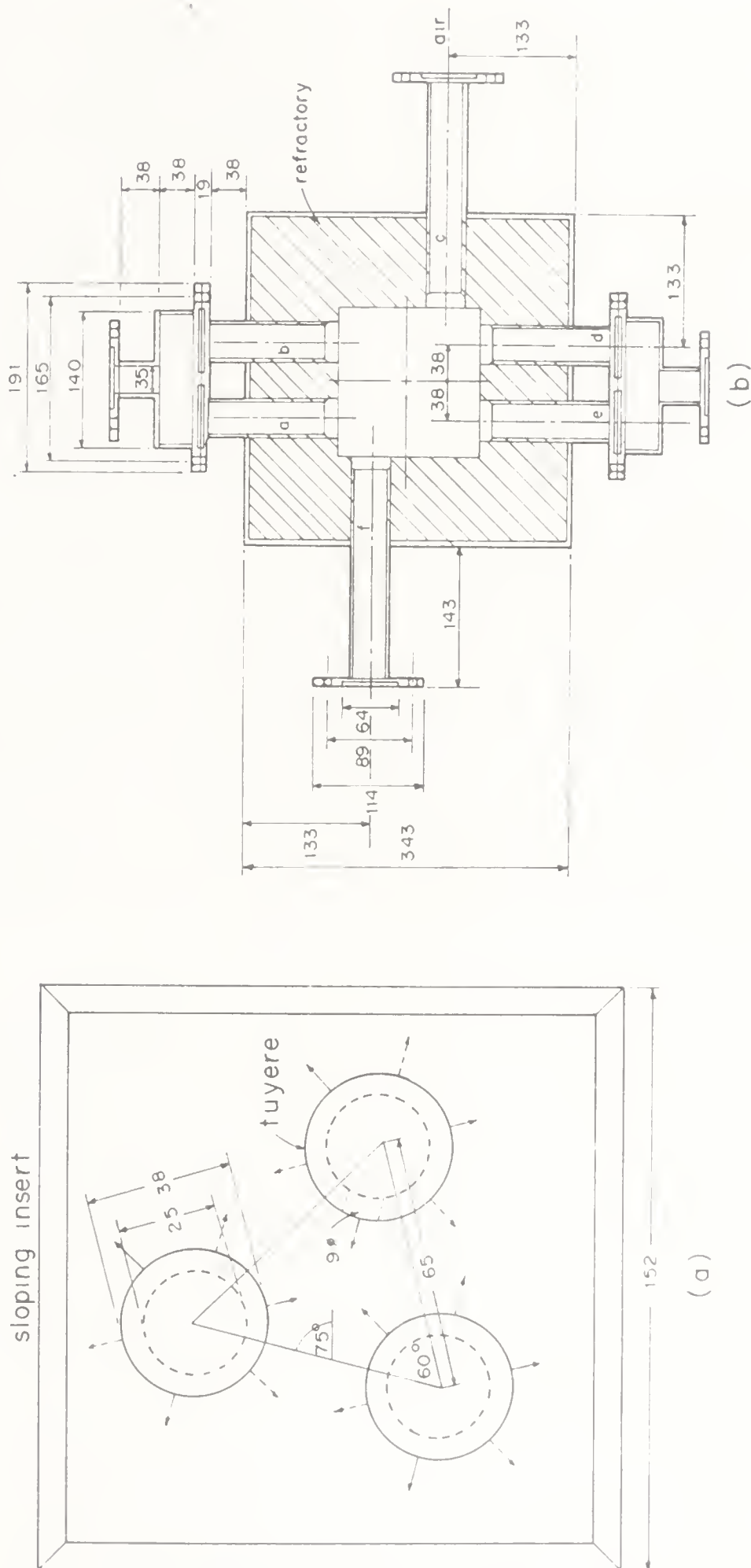


**Figure 4.** (a) Primary air distributor plate configuration. Solid and broken arrows indicate lower and upper holes, respectively. (b) Secondary air entry configuration. All dimensions are in mm.

overflow or inventory vessel if the inventory of solids builds up. Make-up inert particles can also be added into this vessel from a small external hopper. From the bottom of the vessel, the solids descend in moving packed bed flow in a 102 mm i.d., 4.42 m long externally insulated stainless steel standpipe, forming the vertical leg of an *L*-valve. There is a bellows-type expansion joint near the top of the standpipe to allow for thermal expansion. The solids are returned to the principal reactor vessel 381 mm above the grid plate through the horizontal section of the *L*-valve which is 810 mm long and of 102 mm diameter. The circulation rate is controlled by the amount of aeration air fed to the *L*-valve at a single point whose placement is as recommended by Knowlton & Hirsan (1978).

The circulation rate of solids through the *L*-valve can be measured by two independent methods. First, a transparent quartz window of length 330 mm and width 25 mm has been incorporated in the standpipe 770 mm above the bottom of the horizontal leg of the *L*-valve. Identifiable particles can be timed visually or on video film as they travel a known distance along the window. Experiments in a room temperature circulating bed unit in our laboratory (Burkell 1986) show that the assumption of plug flow of solids at the loose-packed bed voidage through the standpipe leads to reliable estimates of particle flow through an *L*-valve providing that the measuring interval terminates several pipe diameters upstream of the *L*-valve elbow. The second method employed to measure the flux of solids involves simple calorimetry. Cooling water or air is passed through a jacket surrounding a 450 mm long section of the standpipe. The jacket is insulated on the outside. Determination of the coolant flow rate and its temperature at the entrance and exit allows the total heat removed to be calculated. By measuring the temperature of the solids entering and leaving the jacketed section of pipe and ignoring the contribution of interstitial gas to the energy loss, we can then estimate the mass flow rate of solid particles.

Gas and entrained solids leaving the primary cyclone are directed to a 203 mm i.d. high-efficiency secondary cyclone. This is made of stainless steel and is insulated externally. Solids captured in the secondary cyclone can be returned to the reactor via the standpipe and *L*-valve or collected in a separate vessel. Gas leaving the secondary cyclone is sampled for gas analysis, cooled in a U-tube heat-exchanger and then discharged to the building ventilation system. A baghouse will soon be added between the cooler and the ventilation duct. Gas samples are analysed for oxygen, SO<sub>2</sub>, CO, CO<sub>2</sub>, and NO<sub>x</sub> using a gas chromatograph and continuous gas analysers.

Solid samples can be withdrawn from five positions in the reactor system: (a) from the bottom of reaction chamber through a gate valve; (b) at the corner of the *L*-valve, again via a gate valve; (c) obliquely from the recycle hopper below the primary cyclone; (d) by diverting the discharged solids from the secondary cyclone; (e) downstream of the secondary cyclone either by isokinetic sampling or, when available, by capture in the baghouse. Provision for in-reactor solids and gas sampling will soon be added.

Data acquisition is provided by an AT&T 6300 computer equipped with a Metrabyte interface permitting 4000 samples per second in BASIC language and up to 8 multiplexer boards with 16 channels on each board. Electrical outputs from thermocouples, pressure transducers, load cells, gas analysers etc. can be stored and processed by the computer.

#### 4. Operation of the circulating fluidized bed reactor

Operation of a circulating bed reactor is more complex than that of a conventional fluidized bed reactor or of an entrained flow reactor. The combustion case illustrates the principles of successful operation. At high solid-circulation rates and steady state operation, the temperature in the entire loop (upflow reactor, primary cyclone, recycle hopper, and *L*-valve) is approximately uniform. For burning of high sulphur fuels, the temperature is usually chosen to optimize sulphur capture by sorbent particles while retaining a high combustion efficiency. Typically this results in a temperature in the range 840–900°C and 90% sulphur capture with a Ca:S molar ratio of about 1.5 for 10–15% excess air. For wood and other low sulphur fuels, lower or higher temperatures can be adopted. Combustion efficiencies for circulating beds are generally of the order of 99% (Reh *et al* 1980).

The University of British Columbia (UBC) CFBC unit is capable of operating over a broad range of load because of the capability of extensively varying the heat removal from the reactor. This is because the heat transfer to vertical surfaces exposed to a circulating bed varies almost linearly with the density of the suspension (Grace 1986b). The suspension density in turn can be controlled over a broad range by varying the solids circulation rate at constant primary and secondary gas flow rates by small changes in the aeration rate to the *L*-valve. This principle can be used to control large-scale CFB boilers (Kobro & Brereton 1986). Its usefulness in smaller units, such as the pilot scale unit at UBC, is more problematic because uncontrollable heat losses, e.g., from the *L*-valve and through the refractory of the reactor, represent a much larger fraction of the total heat dissipation, reducing the degree of control. For the UBC unit, typical steady state energy losses and transfer rates for 10% excess air, full load (superficial velocity of 8 m/s) and a temperature of 850°C are as follows:

Heat removed by gaseous products of combustion:	48 kW
Heat losses through reactor walls (refractory-lined):	9 kW
Heat losses through cyclone, recycle vessel, expansion joint, standpipe and <i>L</i> -valve:	8 kW
Heat removed by calorimetric jacketted standpipe section (air as coolant):	3 kW
Heat removed by discharged solids:	0–1 kW
Heat removed by one membrane waterwall surface:	20–74 kW
<hr/>	
Total heat removal and loss:	88–143 kW

Maintaining steady state operation for this case requires a fuel of lower heating value 21,000 to 34,000 kJ/kg (9000 to 15000 BTU/lb) on a moisture and ash free basis. Some control of the reactor at a given fuel feed rate can also be exercised by varying the amount of excess air, the inventory of solids in the system and the amount of external insulation on the recycle vessel and *L*-valve. Increasing the superficial gas velocity beyond about 10 m/s reduces the residence time of gas and solids unduly, resulting in a drop in combustion efficiency and sulphur capture as well as increased erosion. Increasing the ratio of secondary to primary air generally reduces NO<sub>x</sub> emissions.



One disadvantage of the circulating bed unit is that it takes longer to achieve steady state temperatures than conventional reactors. This is because heat-up of the return portion of the cycle loop can only be achieved by the solids which are in free fall or in moving packed bed flow. Heat transfer coefficients to the wall are then much less than within the principal reactor vessel. Start-up of the UBC CFBC unit is initiated by using the gas burner and circulating inert solids to heat the entire system to about 400°C. Just enough secondary air is fed to keep the orifices unblocked. The limitation on windbox temperature (maximum 950°C) imposes an upper limit on the heat input during this phase of the start-up which requires 3–4 hours.

Once the temperature in the entire system exceeds 400°C, the primary air flow is decreased to a point where a dense bed is formed on the distributor. With the windbox temperature maintained at 950°C, the dense bed is then heated rapidly to a point (525–750°C depending on fuel) where ignition of the intended fuel can be sustained. Fuel feeding is then begun, slowly at first. A delicate process is then carried out where the solid (or liquid) fuel feed is gradually increased, the natural gas or propane fuel is decreased, air flow is increased and solid-circulation is initiated to provide cooling in the main reactor and heating of the recycle leg. The objective is to bring the entire system up to full load and an operating temperature of about 850°C as rapidly as possible. Where sorbent is required for sulphur capture, sorbent feeding is initiated once the average system temperature has reached 750°C. The secondary-to-primary air ratio is gradually increased during the heat-up phase, being established in the 1:2 to 4:1 range during full operation.

## 5. Preliminary experimental results

The UBC CFBC reaction system will be used to test the combustion characteristics of a number of fuels which are of interest in Canada (low and high sulphur coals, wood wastes, tar and pitch residues from heavy oil upgrading processes) as well as to study the high temperature characteristics of circulating fluidized beds.

Some heat transfer coefficients measured at suspension temperatures of 150–400°C, at superficial gas velocities of 4–7 m/s and for sand of mean particle size 188  $\mu\text{m}$  are plotted in figure 5. These coefficients are suspension-to-exposed-surface values averaged over the entire tube length. The suspension densities are determined from static pressure profiles ignoring frictional losses and acceleration effects which are generally minor for fast fluidization (Hartge *et al* 1986). The results show a strong influence of suspension density as in earlier work (see Grace 1986b), and virtually no influence of secondary-to-primary air ratio, superficial gas velocity and temperature within the ranges investigated. Our results show a considerable influence of the length of the cooling surface (Wu *et al* 1987), the heat transfer coefficient decreasing with increasing length.

In figure 6 we have plotted some heat transfer results for the upper membrane waterwall surface under combustion conditions (780–850°C), with a bituminous coal. The mean particle size measured in the *L*-valve was 303  $\mu\text{m}$  during these measurements. For comparison purposes, fitted lines obtained at lower temperatures (150–400°C) for sand of mean size 188  $\mu\text{m}$  and 356  $\mu\text{m}$  are also shown. It is clear that the higher temperature of operation results in an increase in the

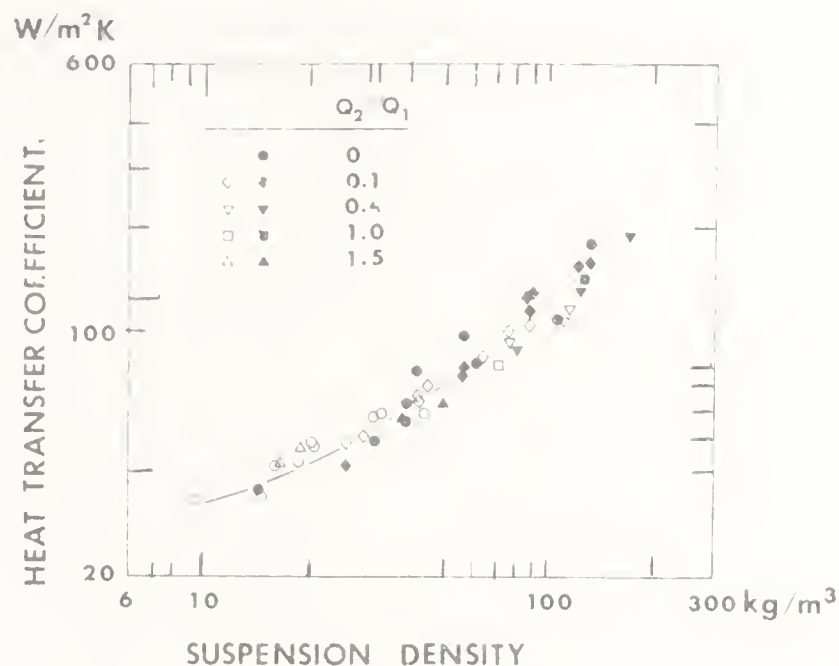


Figure 5. Typical experimental suspension-to-exposed surface heat transfer coefficients at intermediate temperatures (150–400°C) with negligible radiation: 188  $\mu\text{m}$  sand particles with superficial gas velocities of 4–7 m/s.  $Q_2/Q_1$  is the secondary-to-primary air ratio. For full details see Wu *et al* (1987).

suspension-to-waterwall heat transfer coefficient of about 60 W/m<sup>2</sup>K. This is of the same order as the increase measured by Kobro & Brereton (1986), and indicates that radiation plays an important role in the heat transfer process under combustion conditions.

In figure 7 we show temperatures measured at different positions around the circulating fluidized bed flow loop during typical combustion conditions. It is seen that the temperature rises slightly in the main reactor, except in the vicinity of the membrane cooling surface. The temperature drops somewhat in the return *L*-valve, but the overall variation of temperature is less than 30°C.

Some typical pressure profiles obtained under combustion conditions appear in figure 8. These are seen to be qualitatively similar to those presented by earlier workers (e.g., Yerushalmi & Cankurt 1978; Li & Kwauk 1980) for room temperature fast fluidization. There appear to be no radical changes in bed hydrodynamics which result from an increase in the temperature of operation. We have, however, noted that operation of the *L*-valve becomes smoother at elevated temperatures, the circulating solids showing less tendency to flow in stick-slip motion. This is consistent with recent findings by Grace (1986a) that solids which

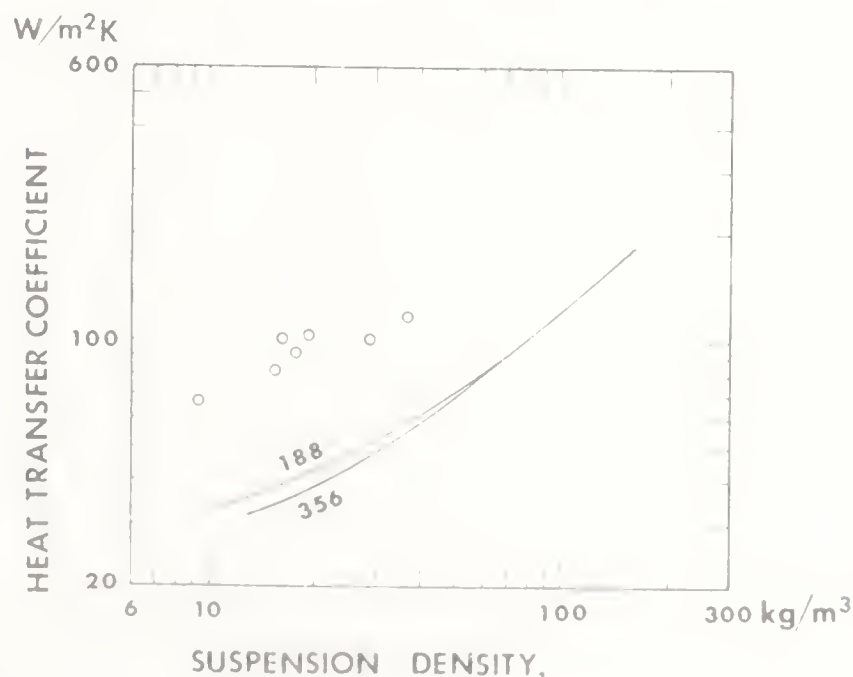


Figure 6. Suspension-to-exposed-surface heat transfer coefficients (points) under combustion conditions (suspension temperature 750–850°C, mean particle size 303  $\mu\text{m}$ , superficial gas velocity 6–10 m/s) in comparison with data (represented by line) under conditions (temperature 150–400°C) where radiation is negligible.



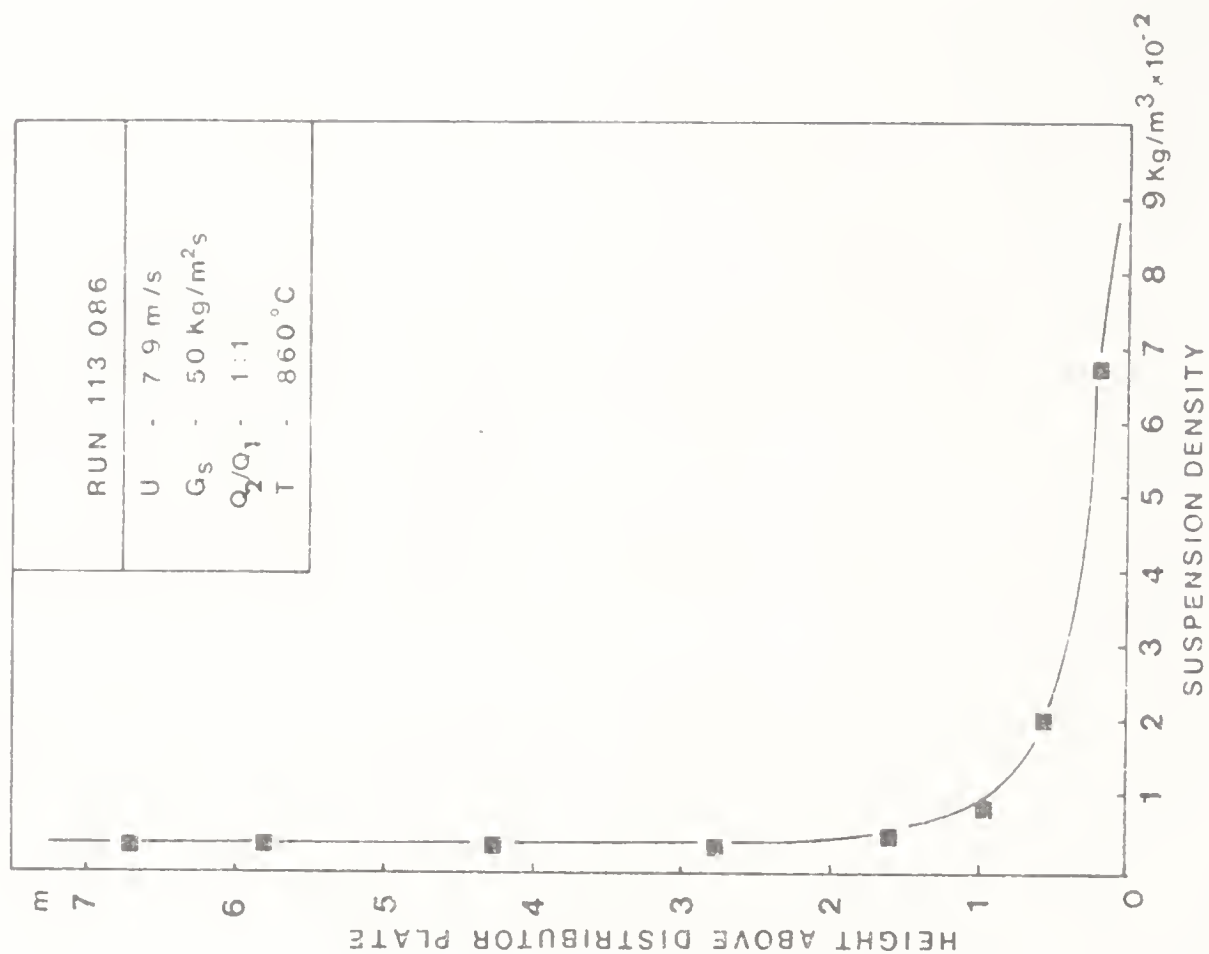


Figure 8. Suspension density profile derived from pressure profile for typical combustion conditions.

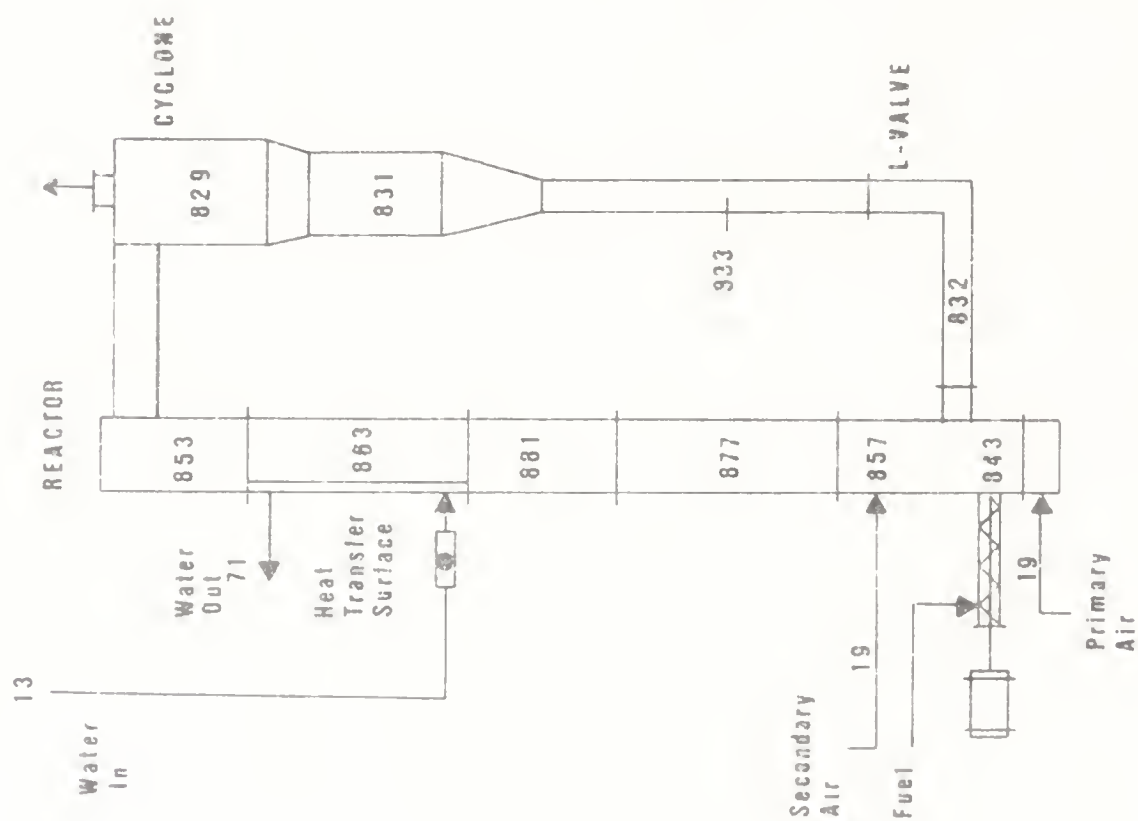


Figure 7. Temperature readings obtained with thermocouple during typical combustion run. Temperature accuracy is  $\pm 3^\circ\text{C}$ .

belong to Group B at room temperature tend to have their behaviour shifted towards Group A with increasing temperature

## 6. Discussion and conclusion

The circulating fluidized bed reactor has interesting characteristics which may be of interest for a wide range of gas-solid reactions or reactions where gas is treated in the presence of solid particles. Whereas gas is approximately in plug flow, recycle of the solids causes their residence time distribution to approximate perfect mixing (Reh 1978). Moreover, the residence time and loading of particles in the reactor can be varied over a broad range by judiciously altering the solids circulation rate, secondary-to-primary gas feed rate and the overall gas velocity. Heat removal from the unit can be controlled over a broad range, especially if an external heat exchanger is incorporated within the recycle loop. Circulating fluidized beds can also be operated at elevated pressures, which further reduces their cross-sectional areas.

While the circulating bed shows great promise for combustion and other reactions, there remain a number of research areas requiring future study. Radial mixing of volatiles and oxygen when fuel is fed from one side or from a small number of feed points may be relatively slow. The effect of column geometry, e.g., the exit geometry and solids re-entry height, may be profound (Brereton 1987), but this factor has received little attention. Different solid species, differing in size or density, clearly have different circuit times and histories, but there is no reported work on this aspect. Erosion and attrition have not been reported to be serious problems in installations to date, but have remained sources of concern. Comprehensive reactor models and control strategies for circulating bed reactors have not yet been developed. These topics are among those that are receiving attention in the programme at the University of British Columbia.

This paper is dedicated to Dr L K Doraiswamy on his sixtieth birthday. We are grateful to Energy, Mines and Resources, Canada, and to the Natural Sciences and Engineering Research Council of Canada, for financial support and to C Desjardins, R L Wu, W Yu and J Zhao for assistance with the design, improvement and operation of the experimental facility.

## References

- Brereton C M H 1987 *Fluid mechanics of circulating fluidized beds* Ph.D. thesis, University of British Columbia
- Burkell J J 1986 *Solids circulation rate measurement in a circulating fluidized bed* M.A.Sc. thesis, University of British Columbia
- Geldart D 1973 *Powder Technol.* 7: 285-492
- Grace J R 1986a *Can. J. Chem. Eng.* 64: 352-363
- Grace J R 1986b *Circulating fluidized bed technology* (ed.) P Basu (Toronto: Pergamon) pp 63-80
- Graf R 1986 in *Circulating fluidized bed technology* (ed.) P Basu (Toronto: Pergamon) pp 317-327

- Hartge E U, Li Y, Werther J 1986 in *Circulating fluidized bed technology* (ed.) P Basu (Toronto: Pergamon) pp. 329-339
- Hirsch M, Janssen K, Serbent R 1986 in *Circulating fluidized bed technology* (ed.) P Basu (Toronto: Pergamon)
- Hoogendoorn J C 1973 in *Clean fuels from coal* (Chicago: Inst. of Gas Technology) pp. 353
- Jahrig C E, Campbell D L, Martin H Z 1980 in *Fluidization* (eds) J R Grace, J M Matsen (New York: Plenum Press) pp. 3-24
- Knowlton T M, Hirsan I 1978 *Hydrocarb. Proc.* (No. 3): 149-156
- Kobro H, Brereton C 1986 in *Circulating fluidized bed technology* (ed.) P Basu (Toronto: Pergamon) pp. 263-272
- Li Y, Kwauk M 1980 in *Fluidization* (eds) J R Grace, J M Matsen (New York: Plenum) pp. 537-544
- Matsen J M 1980 in *Handbook of multiphase systems* (ed.) G Hetsroni (Washington: Hemisphere) pp. 8-154
- Reh L 1971 *Chem. Eng. Prog.* 67 (2): 58-63
- Reh L 1978 *German Chem. Eng.* 1: 319-329
- Reh L 1986 in *Circulating fluidized bed technology* (ed.) P Basu (Toronto: Pergamon) pp. 105-118
- Reh L, Schmidt H W, Daradimos G, Petersen V 1980 Circulating fluid bed combustion an efficient technology for energy, supply and environmental protection, Inst. of Energy Symp. Ser. 4, paper VI-2
- Schwieger B 1985 *Power* (No. 2): S1-16
- Wu R L, Lim C J, Chaouki J, Grace J R 1987 *AIChE J.* (in press)
- Yerushalmi J, Cankurt N T 1978 *Chemtech.* 8: 564-572

# Gas desulphurization by sorption of SO<sub>2</sub> on CuO/Al<sub>2</sub>O<sub>3</sub> solid sorbent in a counterflow multistage fluidized bed reactor: Experimental analysis and modelling of the reactor

C LAGUERIE and D BARRETEAU

Laboratoire de Génie Chimique (UA-CNRS 192), ENSIGC, Chemin de la Loge, 31078 Toulouse, Cédex, France

**Abstract.** This paper gives a review of several works performed in the Laboratory of Chemical Engineering of Toulouse (France) on the desulphurization of gas mixtures by chemical sorption of sulphur dioxide on cupric oxide deposited on porous alumina particles in a counterflow multistage fluidized bed reactor.

The first part of the paper presents experimental results concerning effects of gas and solids flow rates, hold up of solids in the reactor, temperature and concentrations of SO<sub>2</sub> and other gases (CO<sub>2</sub>, H<sub>2</sub>O and NO<sub>x</sub>). Desulphurization yields exceeding 90% were obtained using a four-stage reactor and sulphur dioxide content could be reduced from 3000 ppm to less than 300 ppm with a small gas pressure drop. The presence of other components in the flue gas led to slight changes in the desulphurization yield. This could be corrected by a better choice of the operating conditions.

The second part of the article presents the modelling of the reactor by taking into account the residence time distribution of the solid particles through it. Comparison between the model predictions and experimental results showed that the assumptions of Davidson and Harrison are sophisticated enough to describe reactor operation under steady state conditions.

**Keywords.** Desulphurization; sorption; CuO/Al<sub>2</sub>O<sub>3</sub>; multistage fluidized bed; experimental data; modelling.

## 1. Introduction

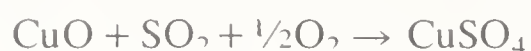
Pollution of the environment by sulphur compounds remains a major problem in industrialized countries. Coal or oil fired power stations account for more than 50% of the sulphur dioxide emissions. They lead to acid rains which are thought to be the main cause of forest destruction in northern Europe for instance. Therefore large amounts of money are being spent to reduce such emissions and very numerous desulphurization as well as denitrification projects have been undertaken for more than fifteen years. A recent bibliography published by the US



Department of Energy (1985) lists 3920 references to flue gas desulphurization and denitrification projects current to the end of 1983, even though one wonders whether flue gas desulphurization is the answer to these environmental problems (Woodburn 1986). It would probably be better to clean fuels before burning but this is still expensive especially in the case of coal.

Nevertheless, among the flue gas desulphurization processes studied or being operated, those using reactions of sulphur dioxide with solid metal oxides are of particular interest (Van Hootte 1973). These processes are carried out at temperatures ranging between 300 and 400°C which correspond to the usual temperatures of flue gas. However, the sulphates formed are sometimes difficult to decompose. To overcome this difficulty, manganese oxide, alkalized alumina or cupric oxide may be used, provided that the mechanical strength of solid particles is high enough to prevent dust pollution, and the pressure drop is kept small. An example of this kind of treatment is the Shell process (Dautzenberg & Nader 1971; Hollinden & Elder 1974; Slack & Hollinden 1975) in which two fixed bed reactors operate alternatively in sorption and regeneration modes at the same temperature (between 300 and 400°C). The sorbent used is cupric oxide deposited on porous alumina particles.

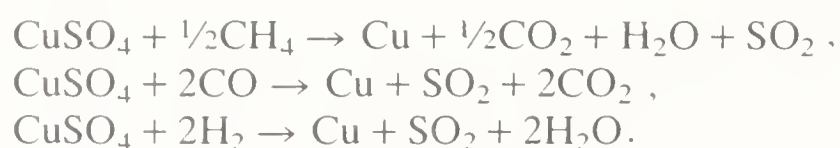
The sorption reaction needs a small amount of oxygen:



and it is slightly exothermic.

It is to be noted that if the copper concentration is not sufficiently high (is less than 3% wt), other compounds resulting from the reaction of sulphur dioxide with alumina appear and the activity of the solids decreases.

The regeneration is performed by reduction of the sulphate formed with methane or carbon monoxide and hydrogen mixtures into copper which is then readily oxidized by oxygen:



The exit gas from the regeneration reactor contains about 30–35% of sulphur dioxide. It can be either converted to elemental sulphur in a Claus process or oxidized into sulphur trioxide on a catalyst and then transformed into sulphuric acid.

The Shell process is not really continuous. Therefore it could be conveniently carried out in a fluidized bed reactor. The main advantage of this procedure is to make the operation continuous and the exit sulphur dioxide concentration constant.

A series of work was carried out for nearly ten years at the Laboratory of Chemical Engineering of Toulouse with the aim of testing the feasibility of the process in a fluidized bed reactor. Only the sorption reaction was studied. Regeneration was carried out separating by reduction of the copper sulphate with methane. Performance of the desulphurization operation was investigated for a wide range of operating conditions and a model of a counterflow multistage fluidized bed reactor, taking into account the distribution of residence time of solids, and its consequences on the kinetic aspects was derived (Barreteau 1977; Barreteau & Angéline 1978; Barreteau *et al* 1978; Vizcarra-Mendoza 1979;



Vizcarra-Mendoza & Laguérie 1981; Laguérie & Vizcarra-Mendoza 1982; Laguérie *et al* 1982; Barreteau & Laguérie 1983, 1984; Barreteau *et al* 1983, 1984).

The purpose of this paper is to sum up the main results obtained in all these studies.

## 2. Experimental study

### 2.1 Apparatus

The apparatus is shown schematically in figure 1. It has been described in full detail elsewhere (Vizcarra-Mendoza 1979; Vizcarra-Mendoza & Laguérie 1981). The reactor is made of refractory steel. Four stages 150 mm high and 98 mm in diameter are stacked vertically. The distributor for each stage is a perforated plate. Solids flow down from one stage to the other through downcomers. Pressure gauges, thermocouples, gas and solids sampling valves are provided. Solids, added from a hopper, and gas mixtures are preheated in two auxiliary fluidized beds before being fed into the reactor. Gas mixtures are analysed either by gas chromatography or infrared spectrometry. A commutating valve selects the gas samples from different stages. Solids leaving the reactor are stored and regenerated periodically in another reactor.

### 2.2 Preparation of the solid sorbent

Alumina particles are first sieved and dried. They are then immersed in an aqueous copper sulphate solution ( $0.76 \text{ k mol/m}^3$ ) and dried at  $80^\circ\text{C}$ . The sulphate is reduced by methane in the regeneration reactor and the product is oxidized in air at  $300^\circ\text{C}$  to give copper oxide. The physical properties of the solid are presented in table 1. The solids were analysed for their copper, sulphur and sulphate contents.

### 2.3 Experiments and results

The overall desulphurization yield is defined as:

$$Y_G = (C_{\text{in}} - C_{\text{out}}) / C_{\text{in}}, \quad (1)$$

where  $C_{\text{in}}$  and  $C_{\text{out}}$  are the respective inlet and outlet concentrations of sulphur dioxide in gas.

Likewise for stage  $i$  a stage yield is defined as:

$$Y_i = (C_{i+1} - C_i) / C_{i+1}, \quad (2)$$

Table 1. Physical properties of the sorbent.

Property	Value
Density	$1600 \text{ kgm}^{-3}$
Particle diameter	$400 \mu\text{m}$
Minimum fluidization velocity at $20^\circ\text{C}$	$0.30 \text{ ms}^{-1}$
Specific area of unreacted sorbent	$184 \text{ m}^2\text{g}^{-1}$
Specific area of $\text{SO}_2$ saturated sorbent	$164 \text{ m}^2\text{g}^{-1}$
Mean pore diameter	$55 \text{ \AA}$
Weight fraction of copper	$3.77\text{--}4.12\%$

- A - hopper
- B - solid valve
- C - solid preheater
- D - reactor
- E - gas preheater
- F - flowmeter
- G - solid storage
- H - commutation valve
- J - solid cooler
- M - manometer

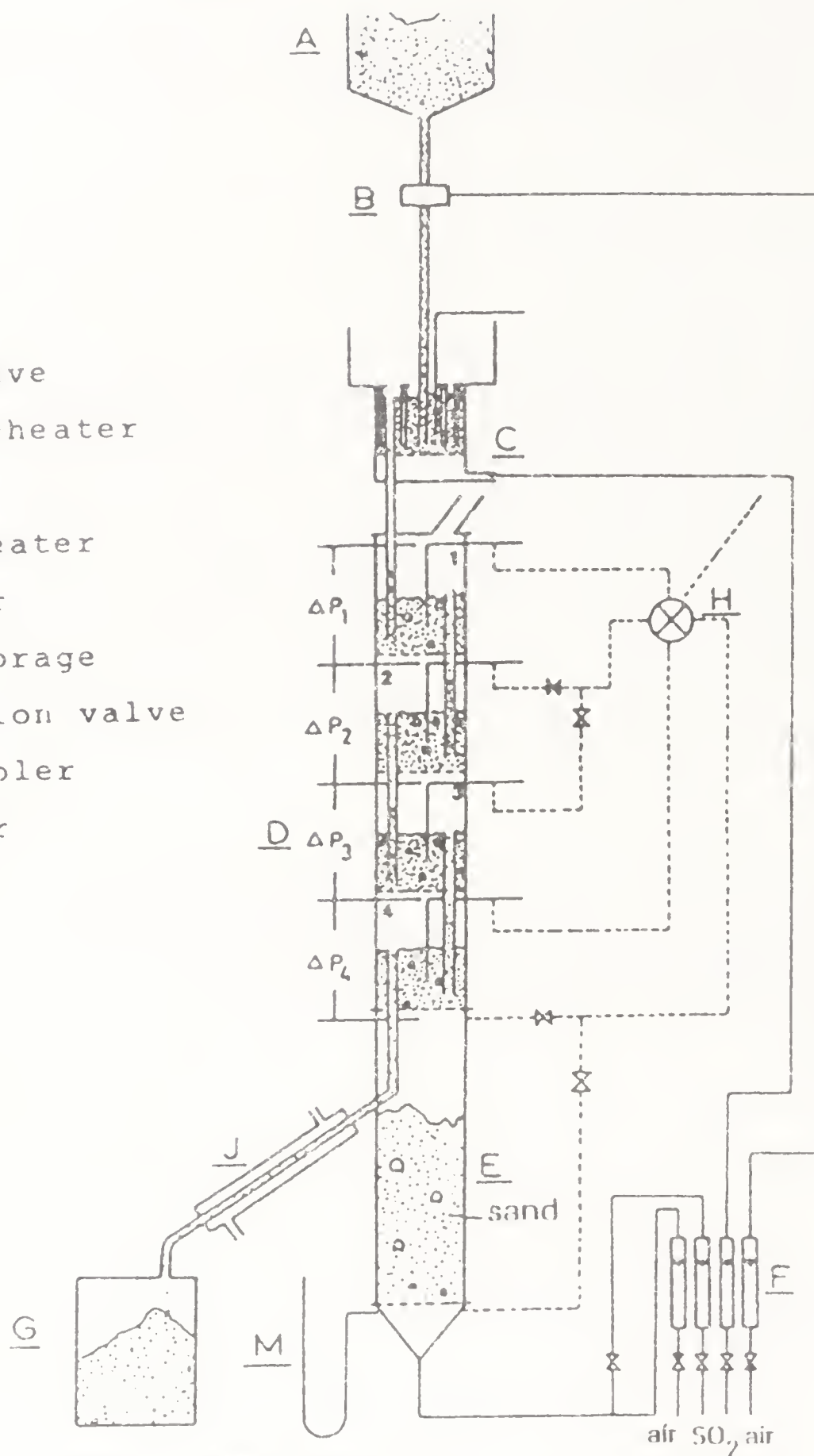


Figure 1. Desulphurization unit.

where  $C_i$  and  $C_{i+1}$  are the outlet and inlet sulphur dioxide concentrations, respectively, for this.

These yields depend on the gas flow rate  $Q_g$ , the solids flow rate  $Q_s$ , the solids hold up in each stage, defined in terms of the height of the downcomer  $L$ , temperature  $T$ , and water vapour, carbon dioxide and nitrogen dioxide concentrations.

**2.3a Effect of the gas and solids flow rate and the solids hold up:** The first series of experiments, carried out at a temperature of 300°C and an inlet sulphur dioxide concentration of 2000 ppm, was concerned with the dioxide mixtures. The experiments were performed according to a  $2^3$  factorial design. The experimental conditions led to a mean residence time for solids between 6 and 30 min, and gas velocity between 0.77 and 1.4 m/s. Thus contact times between solids and gas were between 0.08 and 0.3 s. In order to determine the experimental error variance, the experiment was repeated four times for the average values of the three parameters. The results are presented in table 2. The overall yield was always above 48%, and it could be as high as 98%. Gas pressure drop was less than 140 mm water, the outlet sulphur dioxide concentration less than 1000 ppm and usually less than 300 ppm. It should be noted that in France the maximum allowable sulphur dioxide concentration is about 1400 ppm, while in other countries, like the USA, Japan or Germany, it is about 350 ppm. If the solids flow rate was suitably chosen, the exit sulphur dioxide concentration would fall below 300 ppm. It may also be observed that the mechanical strength of the solid was good. This was confirmed by comparing the particle size analyses made before and after 150 hours of operation. It seems that the presence of copper renders the alumina particles more resistant to attrition (Barreteau & Angéline 1978; Vizcarra-Mendoza & Laguérie 1981). On comparing the results of the experiments, it can be seen that the desulphurization yields are higher when the flow rate and hold up of solids are higher, and the gas flow rate lower. These observations have been confirmed by statistical analysis (Vizcarra-Mendoza & Laguérie 1981).

**2.3b Effect of the temperature and inlet concentration of  $SO_2$ :** In a second series of experiments the effects of temperature (300–400°C) and of the inlet sulphur dioxide concentration (500–5000 ppm) were determined. The results are presented in table 3 and figures 2 and 3.

The reaction rate depends on temperature (Yates & Best 1976). Therefore it is not surprising that the overall desulphurization yield increases with temperature (figure 2). The value of the yield  $Y_1$  obtained in the first stage at 400°C is certainly wrong because of the error in measurement of  $C_1$  and  $C_2$  concentrations which in

**Table 2.** Effects of gas and solid flow rates and height of downcomers on desulphurization yields.

Run No.	101	102	103	104	105	106	107	108	109	110	111	112
$Q_s$ (kg hr <sup>-1</sup> )	2	5	2	5	2	5	2	5	3.5	3.5	3.5	3.5
$Q_g$ (m <sup>3</sup> hr <sup>-1</sup> )	10	10	18	18	10	10	18	18	14	14	14	14
$L$ (mm)	30	30	30	30	60	60	60	60	45	45	45	45
$C_{in}$ (ppm)	1950	1924	1924	1933	1927	1965	1973	1998	1903	1888	1922	1913
$T_{gin}$ (°C)	297	298	293	292	298	297	291	295	296	293	294	294
$T_{pin}$ (°C)	375	314	376	328	380	380	346	340	350	354	360	360
$C_1$ (ppm)	273	42	998	568	95	30	705	243	250	265	294	200
$C_2$ (ppm)	636	140	1316	932	370	50	1135	558	647	710	755	592
$C_3$ (ppm)	910	330	1494	1195	798	184	1465	1000	978	1038	1097	942
$C_4$ (ppm)	1381	902	1694	1557	1212	567	1706	1402	1355	1400	1450	134
$T_1$ (°C)	303	300	299	300	298	305	300	303	306	307	306	305
$T_2$ (°C)	298	297	302	302	295	292	302	293	304	304	301	302
$T_3$ (°C)	301	300	304	303	300	292	303	300	306	304	303	304
$T_4$ (°C)	306	306	305	306	308	305	308	306	310	306	306	307
$\Delta P$ (mm H <sub>2</sub> O)	84	84	86	86	125	140	131	146	93	93	93	93

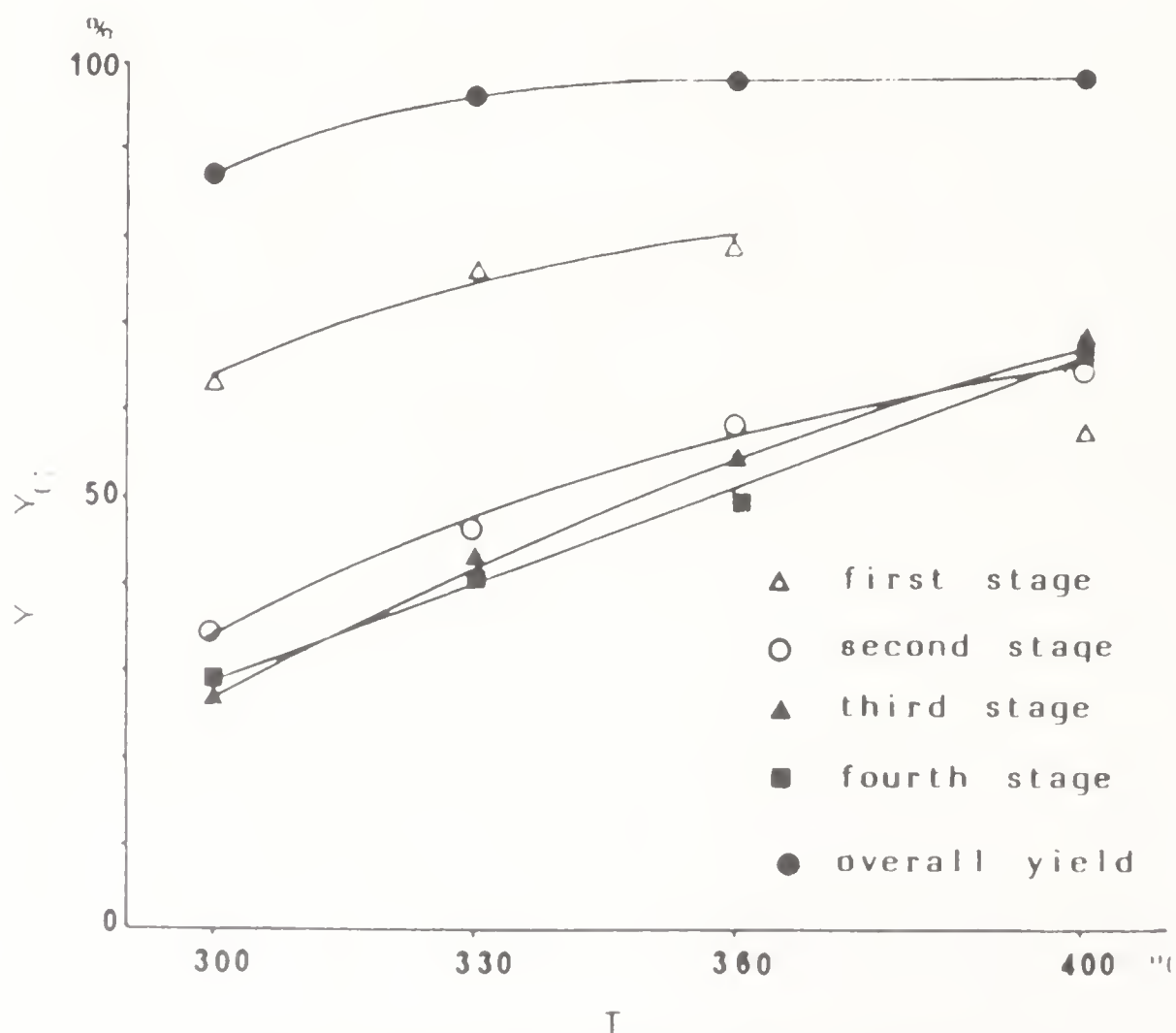


**Table 3.** Influence of temperature and inlet sulphur dioxide concentration on desulphurization yields. $Q_s = 3.5 \text{ kg hr}^{-1}$ ;  $Q_g = 14 \text{ m}^3 \text{ hr}^{-1}$ ;  $L = 45 \text{ mm}$ .

Run Number	201	202	203	301	302	303	304	305	306
$C_{in}$ (ppm)	1910	1924	1924	495	986	1500	2908	3963	4850
$T_{gin}$ ( $^{\circ}\text{C}$ )	326	351	398	290	289	290	291	297	294
$T_{pin}$ ( $^{\circ}\text{C}$ )	330	435	480	347	367	353	348	350	340
$C_1$ (ppm)	83	40	31	10	40	92	558	913	1583
$C_2$ (ppm)	348	189	73	30	112	316	1267	2013	2950
$C_3$ (ppm)	643	444	207	68	242	568	1692	2600	3608
$C_4$ (ppm)	1130	957	650	158	480	902	2158	3200	4133
$T_1$ ( $^{\circ}\text{C}$ )	330	358	395	301	308	301	309	308	309
$T_2$ ( $^{\circ}\text{C}$ )	328	355	389	301	302	299	307	305	308
$T_3$ ( $^{\circ}\text{C}$ )	329	357	394	302	300	299	306	305	307
$T_4$ ( $^{\circ}\text{C}$ )	334	364	406	304	302	302	306	309	307
$\Delta P$ (mm $\text{H}_2\text{O}$ )	99	98	96	98	101	97	101	105	101

this case amounts to less than 100 ppm. The overall desulphurization yield,  $Y_G$ , approaches 100% at temperatures higher than  $330^{\circ}\text{C}$ .

Increasing inlet sulphur dioxide concentration affects the desulphurization yield adversely (figure 3) due to an increase in the sulphate concentration, which results in a decrease of the sorbent activity. It should be noted that in all the experiments the first stage yield is always the higher because the solid which enters this stage does not contain any copper sulphate yet.

**Figure 2.** Desulphurization yields versus temperature

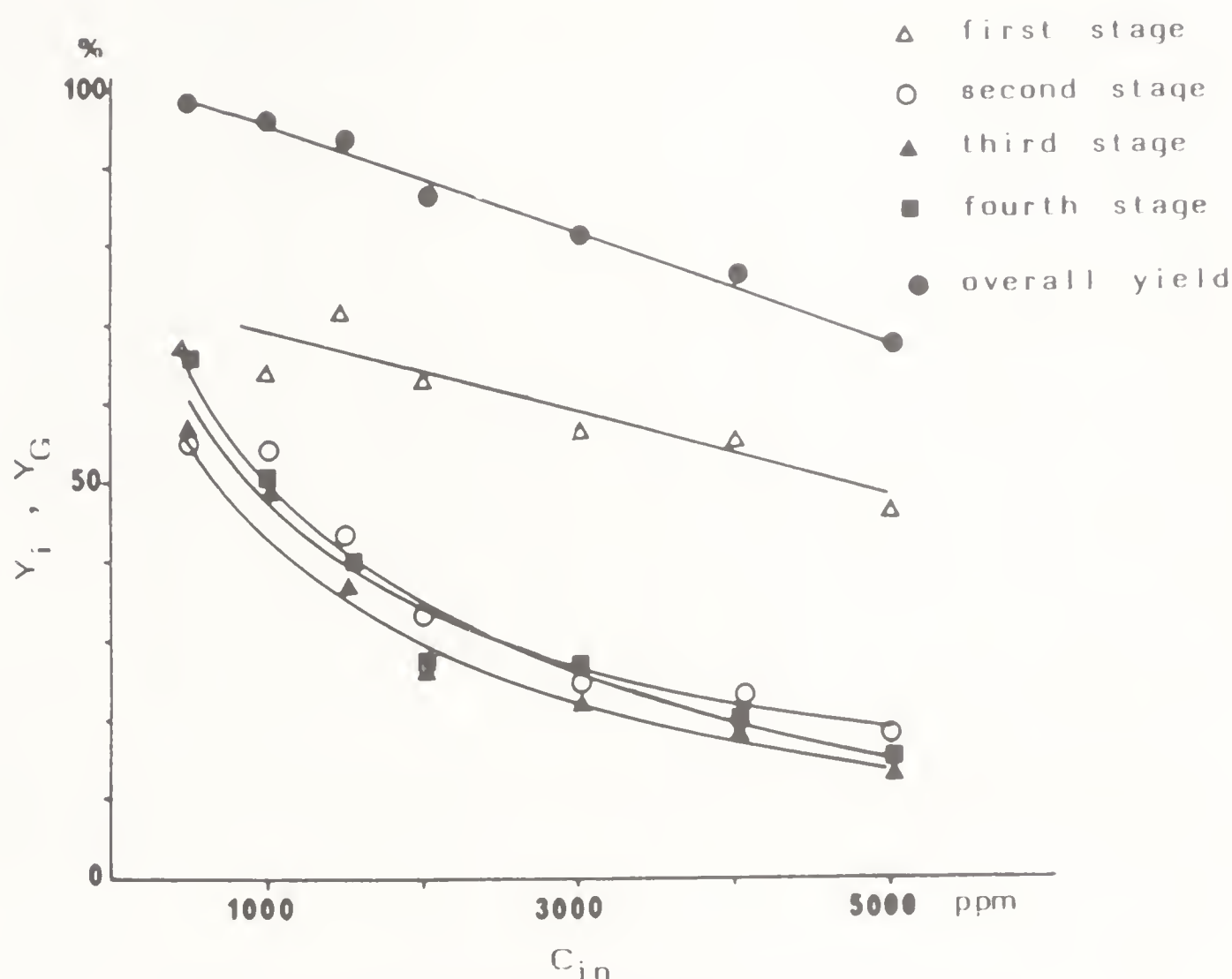


Figure 3. Desulphurization yields versus inlet  $\text{SO}_2$  concentration.

**2.3c Effect of carbon dioxide, nitrogen dioxide and water vapour concentrations:** The first two series of experiments were performed by treating air-sulphur dioxide mixtures. Composition of flue gas from stacks strongly differs from that of the synthesis mixtures used previously. Therefore a third series of experiments was undertaken to assess the effect of carbon dioxide, nitrogen dioxide and water vapour concentration. Note that the effect of the oxygen concentration was not considered though it might be thought that it would affect the reaction kinetics.

As only one stage of the reactor was used, the desulphurization yield was less than in the preceding experiments.

A factorial design was still chosen with carbon dioxide concentration between 11 and 17%, water vapour between 2 and 10%, and nitrogen dioxide between 100 and 150 ppm. The results were compared with those for experiments without carbon dioxide, nitrogen dioxide and hydrogen oxide (table 4).

Nitric oxide does not influence the desulphurization yield which in presence of carbon dioxide decreases slightly. Carbon dioxide molecules are bigger than the others ( $\text{N}_2$ ,  $\text{O}_2$ ,  $\text{H}_2\text{O}$ ), thus they can slow down the diffusion of sulphur dioxide in the pores of the solid and reduce the desulphurization yield.

It is the water vapour which exhibits the strongest influence. This observation was confirmed by statistical analysis (Barreateau & Laguérie 1984; Barreateau *et al* 1984). Therefore to analyse the effect of the concentration of water independently of that of the other components added to the air- $\text{SO}_2$  mixtures, other experiments were performed by using mixtures of air, sulphur dioxide and water. The results are



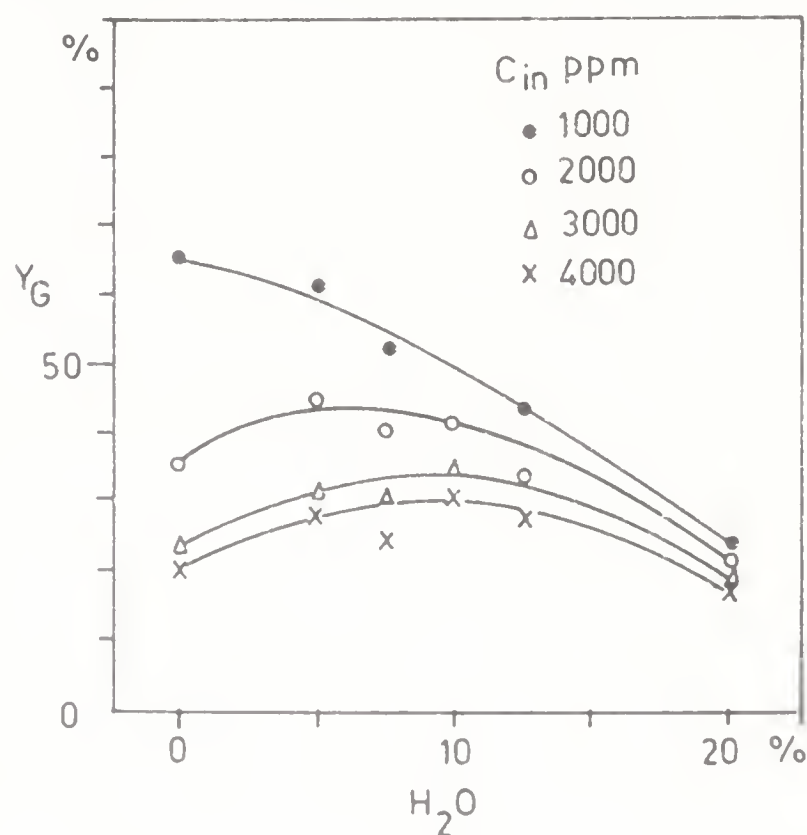
**Table 4.** Influence of nitrogen dioxide, carbon dioxide and water vapour concentration on desulphurization yields. $Q_v = 3.5$  kg/hr;  $Q_r = 6.67$  m<sup>3</sup>/hr;  $L = 45$  mm

CO <sub>2</sub> %	% (Vol) H <sub>2</sub> O (ppm)	ppm NO <sub>2</sub>	C <sub>in</sub> (ppm) SO <sub>2</sub>	T <sub>gin</sub> (°C)	T <sub>pin</sub> (°C)	T (°C)	ΔP (mm) H <sub>2</sub> O	C <sub>1</sub> (ppm) SO <sub>2</sub>	Y <sub>G</sub> %
11	2	100	2026	298	299	296	23	1114	45.0
17	2	100	2172	299	300	296	23	1279	41.1
11	10	100	2125	303	298	299	24	1296	39.0
17	10	100	2121	300	304	301	23	1379	35.0
11	2	500	2190	301	308	302	22	1204	45.0
17	2	500	1913	300	301	299	23	1088	43.1
11	10	500	2176	304	302	301	24	1284	41.0
17	10	500	2106	302	301	299	23	1326	37.0
14	6	300	1837	304	299	305	23	1186	35.4
14	6	300	1990	300	306	306	23	1278	35.8
14	6	300	1891	299	295	302	23	1186	37.3
14	6	300	1972	298	307	301	23	1195	39.4
0	0	0	2054	301	305	301	22	1161	43.5
0	0	0	1990	299	309	301	23	1240	37.7
0	0	0	1880	298	300	302	22	1031	45.2
0	0	0	2050	299	299	300	23	1177	42.6

reported in figure 4. It can be noted that the maximum yield is attained at water concentration between 6 and 10% except for sulphur dioxide concentration of 1000 ppm. At low concentrations, water seems to promote the desulphurization, but an opposite effect is observed at higher concentrations.

Influence of water concentration can be explained in two different ways:

- As in corrosion of metals, which is enhanced by the presence of water, the oxidation of sulphur dioxide to sulphur trioxide is promoted by water vapour so that the sulphatation of copper oxide becomes faster.
- Water can interact with alumina and copper sulphate to give hydrated salts. The blue-green colour of some particles tends to confirm this supposition. The hydration of the sorbent could reduce its activity.

**Figure 4.** Effect of SO<sub>2</sub> and water vapour concentrations on desulphurization yields.

These two opposing effects could explain the observed variations of the yield. For experiments at the lowest sulphur dioxide concentration, the second effect is more likely.

### 3. Modelling of the reactor

Most of the fluidized bed reactor models proposed in the literature are relative to catalytic reactions without macroscopic transformation of the solid particles. Other models have been derived for gasification or combustion of coal in fluidized beds. To our knowledge, nothing has been done in the case of multistage fluidized bed reactors through which solids are submitted to a change without any size variation. A first attempt was made by Barreteau and coworkers (Barreteau & Angéline 1978; Barreteau *et al* 1978) who proposed a model for desulphurization. They only focussed on the variation of SO<sub>2</sub> concentration in the gas, ignoring the variation of the distribution of copper sulphate concentration on the solid sorbent. Though the predictions of their model were not entirely satisfactory, they could conclude that under the conditions chosen the assumptions of the Davidson & Harrison model (1963) for bubbling beds were sophisticated enough. Therefore, it was decided to derive a model based on the same concept, but taking into account the residence time distribution of solids on each stage and in turn the distribution of concentrations of the species in the solid phase.

#### 3.1 Choice of a kinetic model

From a kinetic point of view, Yates & Best (1976) showed that a two-step mechanism involving cupric oxysulphate as an intermediate compound fits rather well with their experimental test runs:



Each reaction is first-order with respect to sulphur dioxide and to the active component of the solid. Rate constants have been expressed according to Arrhenius' law:

$$k_1 = 2.147 \exp(-2118/T), \quad (3)$$

$$\text{and } k_2 = 0.143 \exp(-1748/T). \quad (4)$$

#### 3.2 Assumptions of the model

The assumptions underlying the model are the following:

- i) all the gas in excess of that required for incipient fluidization passes through the bed as bubbles;
  - ii) bubbles are spherical, of constant size and evenly distributed in the bed at any time. They do not contain any solids;
  - iii) the gas in the bubbles is perfectly mixed;
  - iv) as they rise, bubbles exchange gas with the rest of the bed (emulsion phase).
- The interphase mass transfer results from two superimposed independent mechanisms: throughflow of gas and diffusion;

v) solid particles are perfectly mixed in the emulsion phase.

Two limiting cases are considered for the behaviour of the gas flowing through the emulsion phase:

- i) The gas in the entire emulsion phase is perfectly mixed;
- ii) The gas circulates through the emulsion phase in plug flow. The above-mentioned assumptions characterize the model of Davidson & Harrison (1963) for catalytic reactions.

Additional assumptions were made to describe the continuous flow of solid particles:

- i) the flow of solids through the beds does not affect their hydrodynamic behaviour;
- ii) all the stages operate under the same conditions of fluidization;
- iii) hold up of solids is the same on each stage;
- iv) all the particles entering the first stage (the upper one) present the same concentration in active species.

Assumptions (i) and (ii) lead in fact to two distinct models: the EGPM model (emulsion gas perfectly mixed), and the EGPF model (emulsion gas in plug flow). They are schematically represented in figures 5 and 6.

### 3.3 Equations of the model

3.3a *Mass balance equations on sulphur dioxide: Bubble phase* – The mass balance on sulphur dioxide through the bubble phase of the  $i$ th stage is independent of the assumption relative to the behaviour of gas in the emulsion phase. It can be written:

$$(u - u_{mf}) \frac{dc_{bi}}{dz} = N_b Q (c_{pi} - c_{bi}). \quad (5)$$

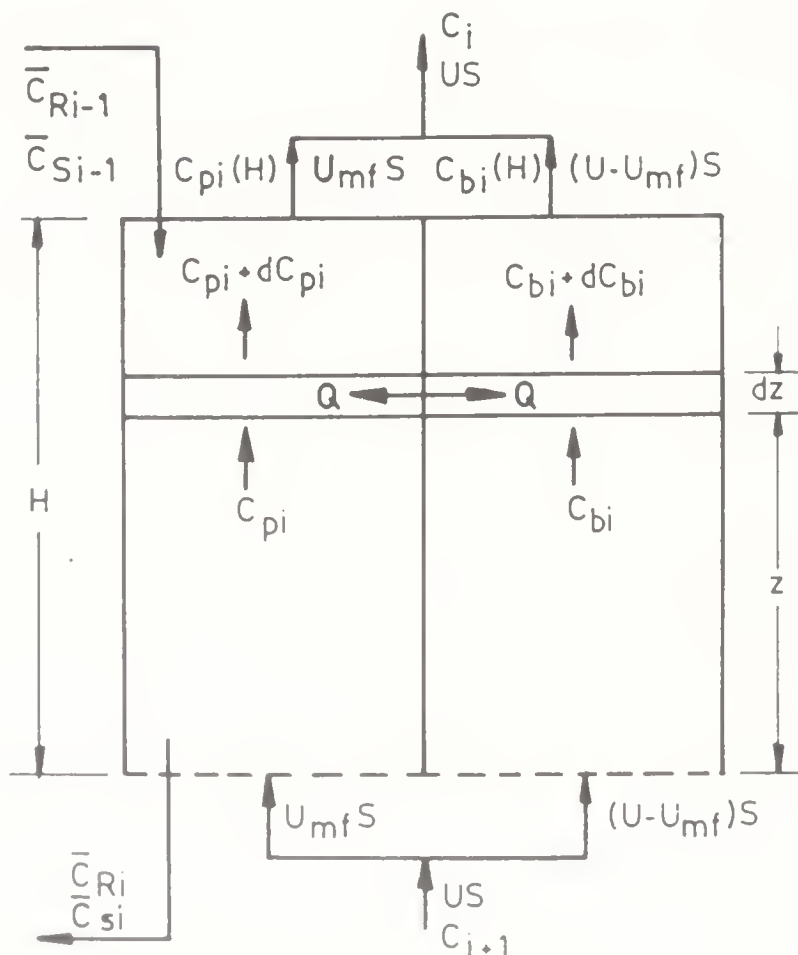


Figure 5. EGPF model.

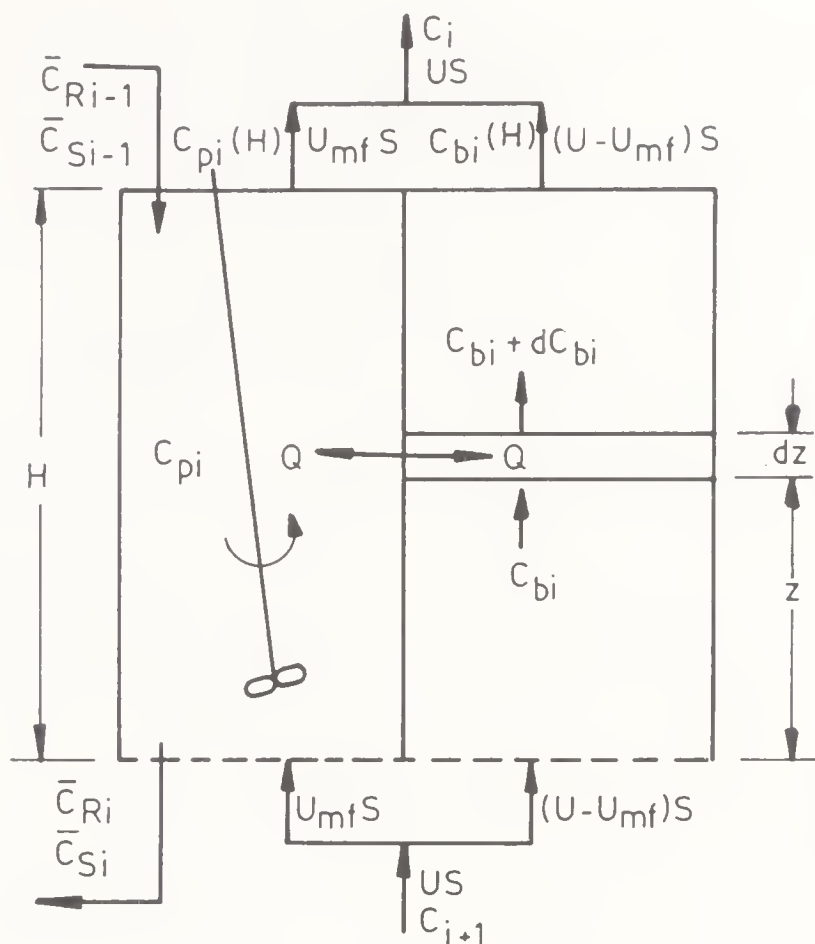


Figure 6. EGPM model.

*Emulsion phase* The mass balance equation depends on the model:

i) EGPM model:

$$u_{mf}(c_{i+1} - c_{pi}) = N_b Q \int_0^H (c_{pi} - c_{bi}) dz + (1 - N_b V_b) H \bar{r}_i, \quad (6)$$

where the  $\text{SO}_2$  concentration in the emulsion,  $C_{pi}$ , is independent of  $z$ .  $H$  is the height of the expanded bed assumed equal to the height of the downcomers over each distributor ( $L$ ), and  $\bar{r}$  is the average rate of disappearance of  $\text{SO}_2$  in the entire emulsion phase.

ii) EGPF model:

$$u_{mf} dc_{pi}/dz = N_b Q (c_{bi} - c_{pi}) - (1 - N_b V_b) \bar{r}_i dz, \quad (7)$$

where  $c_{pi}$  and  $\bar{r}_i$  are functions of  $z$ .

Relations used to calculate the parameters of the models are given in table 5.

**3.3b Continuity balance on solids:** The residence time distribution of solids (RTD) in the  $i$ th stage can be expressed by:

$$E_i(\tau_i) = (1/\tau_i) \exp(-\tau_i/\bar{\tau}), \quad (8)$$

where  $\bar{\tau}$  is the mean residence time of solids in each stage.

Among the solid particles held up in the  $i$ th stage for time  $\tau_i$ , only the fraction  $E_{i-1}(\tau_{i-1})$  had stayed for a time  $\tau_{i-1}$  in the  $(i-1)$ th stage. By repeating this reasoning it can easily be shown that the fraction of solids staying successively for times  $\tau_1, \tau_2, \dots, \tau_i$ , in the first, second,  $\dots$   $i$ th stages is:



Table 5. Parameters of the model.

Parameter	Definition	Formula
$N_b$	Number of bubbles per unit bed volume	$N_b = (u - u_{mf}) / u_b V_b$
$V_b$	Bubble volume	$V_b = \pi D_b^3 / 6$
$D_b$	Bubble diameter (Mori & Wen 1975)	$\frac{D_{b\max} - D_b(z)}{D_{b\max} - D_{b0}} = \exp(-0.3 z / D_T)$
$D_{b\max}$	Maximum bubble diameter for total coalescence	$D_{b\max} = 0.652 [S(u - u_{mf})]^{0.4}$
$D_{b0}$	Initial bubble diameter	$D_{b0} = 0.347 [S(u - u_{mf}) / n_d]^{0.4}$
$n_d$	Number of orifices of each distributor	$n_d = 87$
$D_T$	Diameter of the reactor	$D_T = 0.098 \text{ (m)}$
$u_b$	Bubble rise velocity (Davidson and Harrison 1963)	$u_b = (u - u_{mf}) + 0.711 (g D_b)^{1/2}$
$\bar{D}_b$	Average bubble diameter	$\bar{D}_b = D_{b\max} - (D_{b\max} - D_{b0}) \times (D_T / 0.3 H) \times [1 - \exp(-0.3 H / D_T)]$
$H_{mf}$	Height of the bed at rest	$H_{mf} = H [1 - (u - u_{mf}) / u_b]$
$Q$	Interphase mass transfer (Davidson & Harrison 1963)	$Q = [3/4 u_{mf} + 0.975 D_g^{1/2} \times (g D_b)^{1/4}] \pi D_b^2$
$D_g$	Diffusivity of gaseous reactant	$D_g = 0.39 \times 10^{-4} \text{ m}^2 \text{ s}^{-1}$

$$E'_i(\tau_1, \tau_2, \dots, \tau_i) = (1/\bar{\tau}) \exp \left[ (-1/\bar{\tau}) \left( \sum_{j=1}^i \tau_j \right) \right]. \quad (9)$$

All the particles belonging to this population have undergone the same transformations since they were fed into the reactor. Concentrations of the different species are the same for all of them.

**3.3c Mass balance on the sorbent particles:** At any time over the  $i$ th stage and for the population of particles mentioned above the disappearance rate of copper oxide ( $R$ ) according to the first reaction can be written:

$$dc_{Ri}/dt = -k_1 c_{Ri} c_{pi}. \quad (10)$$

As for copper oxisulphate ( $S$ ) which is formed according to the first reaction and disappears according to the second reaction, it is given by:

$$dc_{Si}/dt = (k_1 c_{Ri} - k_2 c_{Si}) c_{pi}, \quad (11)$$

where  $t$  is allowed to vary between 0 and  $\tau_i$ .

Initial conditions for these particles at the entry of the  $i$ th stage are the following:

$$c_{Ri0} = c_{Ri-1}(\tau_1, \tau_2, \dots, \tau_{i-1}), \quad (12)$$

$$c_{Si0} = c_{Si-1}(\tau_1, \tau_2, \dots, \tau_{i-1}), \quad (13)$$

EGPM model: the copper oxide concentration is

$$c_{Ri} = c_{Ri0} \exp(-k_1 c_{pi} \tau_i), \quad (14)$$

which can be expressed as a function of the copper oxide concentration,  $c_{R0}$ , of the particles entering the first stage of the reactor:

$$c_{Ri} = c_{R0} \exp \left( -k_1 \sum_{j=1}^i c_{pj} \tau_j \right). \quad (15)$$

From (10) and (11), one obtains:

$$dc_{Si}/dc_{Ri} = (k_2/k_1)/(c_{Si}/c_{Ri}) - 1. \quad (16)$$

Integrating this equation gives:

$$c_{Si} = \frac{k_1 c_{Ri}}{(k_2 - k_1)} \left[ 1 - \left( \frac{c_{Ri}}{c_{Ri0}} \right)^{\left( \frac{k_2 - k_1}{k_1} \right)} \left( 1 - \frac{k_2 - k_1}{k_1} \frac{c_{Si0}}{c_{Ri0}} \right) \right]. \quad (17)$$

Assuming the oxysulphate concentration of the particles entering the reactor to be zero leads to:

$$c_{Si} = [k_1 c_{R0}/(k_2 - k_1)] \left[ \exp \left( -k_1 \sum_{j=1}^i c_{pj} \tau_j \right) - \exp \left( -k_2 \sum_{j=1}^i c_{pj} \tau_j \right) \right]. \quad (18)$$

EGPF model: The sulphur dioxide concentration of gas varies throughout the emulsion phase but the solid particles which are perfectly mixed, have at any time, an equal probability of contacting an element of gas volume, whose concentration  $c_{pi}$  lies between  $c_{i+1}$  and  $c_{pi}(H)$ . Therefore, it can be accepted that considering all the particles, the sulphur dioxide concentration of the gas is  $\bar{c}_{pi}$  which is defined by the equation:

$$\bar{c}_{pi} = (1/H) \int_0^H c_{pi} dz. \quad (19)$$

Thus, except for this restriction, (15) and (18) are still valid by substituting  $\bar{c}_{pj}$  for  $c_{pj}$ .

3.3d *Mean concentration of solid species on the sorbent particles:* Mean concentrations  $\bar{c}_{Ri}$  and  $\bar{c}_{Si}$  of copper oxide and copper oxysulphate for all the particles at any time on the  $i$ th stage are defined by:

$$\bar{c}_{Ri} = \int_{\tau_1=0}^{\infty} \int_{\tau_2=0}^{\infty} \cdots \int_{\tau_i=0}^{\infty} c_{Ri} E'(\tau_1, \tau_2, \dots, \tau_i) d\tau_1 d\tau_2 \dots d\tau_i, \quad (20)$$

and

$$\bar{c}_{Si} = \int_{\tau_1=0}^{\infty} \int_{\tau_2=0}^{\infty} \cdots \int_{\tau_i=0}^{\infty} c_{Si} E'(\tau_1, \tau_2, \dots, \tau_i) d\tau_1 d\tau_2 \dots d\tau_i. \quad (21)$$

Integration of (20) and (21) leads to:

$$\bar{c}_{Ri} = c_{R0} / \left[ \prod_{j=1}^i (1 + k_1 \bar{c}_{pj} \bar{\tau}) \right], \quad (22)$$

and,

$$\begin{aligned} \bar{c}_{Si} = [k_1 c_{R0} / (k_2 - k_1)] & \left\{ 1 / \left[ \prod_{j=1}^i (1 + k_1 \bar{c}_{pj} \bar{\tau}) \right] - \right. \\ & \left. 1 / \left[ \prod_{j=1}^i (1 + k_2 \bar{c}_{pj} \bar{\tau}) \right] \right\}, \end{aligned} \quad (23)$$

where  $\bar{c}_{pi}$  is either  $c_{pj}$  in the EGPM model, or  $\bar{c}_{pj}$ , defined by (19), in the EGPF model.

3.3e *Sulphur dioxide concentration in the exit gas stream from the  $i$ th stage:* The rate of  $\text{SO}_2$  disappearance in the  $i$ th stage can be expressed as:

$$r_i = (k_1 \bar{c}_{Ri} + k_2 \bar{c}_{Si}) c_{pi}. \quad (24)$$

The term in brackets remains constant over the entire emulsion phase so that the reaction rate can be considered as first order. Integration of (5) and (6) or (7) thus gives – for the EGPM model:

$$c_{pi} = [c_{i+1} (1-\beta) e^{-X}] / [1-\beta e^{-X} + (H_{mf}/u) (k_1 \bar{c}_{Ri} + k_2 \bar{c}_{Si})], \quad (25)$$

$$c_{bi}(H) = C_{pi} + (c_{i+1} - c_{pi}) e^{-X}, \quad (26)$$

and for the concentration of the gas stream leaving the  $i$ th stage:

$$c_i = \beta c_{bi}(H) + (1-\beta) c_{pi}, \quad (27)$$

where  $\beta$  is the fraction of the gas flow associated to the bubble phase ( $\beta = 1 - u_{mf}/u$ ), and  $X$ , the number of transfer units ( $X = QH/V_b u_b$ ).

For the EGPF model:

$$\begin{aligned} c_{pi}(H) = \frac{c_{i+1}}{m_{1i} - m_{2i}} & \left[ m_{1i} \left( 1 + \frac{H}{X} m_{2i} \right) \exp(m_{2i} H) - \right. \\ & \left. m_{2i} \left( 1 + \frac{H}{X} m_{1i} \right) \exp(m_{1i} H) \right], \end{aligned} \quad (28)$$

$$c_{bi}(H) = \frac{c_{i+1}}{m_{1i} - m_{2i}} \left[ m_{1i} \exp(m_{2i} H) - m_{2i} \exp(m_{1i} H) \right]. \quad (29)$$

Concentration of the resulting stream is still given by (28) by substituting  $c_{pi}(H)$  for  $c_{pi}$ .

$m_{1i}$  and  $m_{2i}$  are defined by:

$$m_{1i} \text{ or } m_{2i} = \frac{1}{2} \frac{X + K_i}{H(1-\beta)} \pm \frac{1}{2} \left[ \left( \frac{X + K_i}{H(1-\beta)} \right)^2 - 4 \frac{X K_i}{H^2 (1-\beta)} \right]^{1/2}, \quad (30)$$

where  $K_i$  is the number of reaction units in the emulsion phase:

$$K_i = (k_1 c_{Ri} + k_2 c_{Si}) H_{mf} / u. \quad (31)$$

The mean concentration of the emulsion gas is given by:

$$c_{pi} = \frac{1}{H} \frac{c_{i+1}}{m_{1i} - m_{2i}} \left[ \frac{m_{1i}}{m_{2i}} \left( 1 + \frac{H}{X} m_{2i} \right) \right. \\ \left. [\exp(m_{2i}H) - 1] - \frac{m_{2i}}{m_{1i}} \left( 1 + \frac{H}{X} m_{1i} \right) [\exp(m_{1i}H) - 1] \right]. \quad (32)$$

### 3.4 Comparison of predictions with experiments

The concentrations of the gas stream exiting each stage can be calculated by solving the equations of the models. All the experiments presented in table 2 were treated. The copper oxide concentration ( $c_{R0}$ ) of the sorbent particles entering the reactor, expressed in moles of copper oxide per unit volume of solids, was determined by analysing samples of solids for a few experiments. For the experiments where no analysis was done,  $c_{R0}$  was assumed to be equal to the average value of all the other runs.

Besides, in order to make the model treatment easier, all the stages were considered to operate at the same temperature (300°C) and the mass of solids held up was calculated by taking the mean value of the pressure drops:

$$W = (1/4) S \sum_{i=1}^4 \Delta P_i. \quad (33)$$

The basic concentrations,  $\bar{c}_{pi}$  for the EGPM model and  $c_{pi}$  for the EGPF model, were identified by using the Gauss-Newton algorithm. The results of the mathematical treatment are presented in table 6.  $\text{SO}_2$  concentrations have been converted into ppm. Likewise, the comparison between the predicted and experimental values of the overall desulphurization yield is shown in figure 7.

It can be observed by comparing tables 2 and 6 that the concentrations predicted by the EGPF model are nearer to the experimental ones than those predicted by the EGMP model. Surprisingly, experimental concentrations are sometimes smaller than those predicted by the EGPF model. However, it must be noted that the mass of sorbent particles held up on each stage at any time may differ up to 15% from that calculated (Vizcarra-Mendoza, 1979).

Figure 7 shows that, except for experiments 104 and 108, both the models predict rather well the overall desulphurization yield but with a slight advantage for the EGPM model. This is confirmed by calculating two deviation criteria respectively defined by:

$$\sigma_q = (1/7) [\sum (Y_{Gi} \text{ expt} - Y_{Gi} \text{ calc})^2]^{1/2}, \quad (33)$$

and

$$\sigma_m = (1/7) [\sum (Y_{Gip} \text{ expt} - Y_{Gi} \text{ calc})], \quad (34)$$



Table 6. Predictions of the models.

	Experiment number									Average values for central point
	101	102	103	104	105	106	107	108	112	
$Q_v$ (kg/hr)	2	5	2	5	2	5	2	5	3.5	3.5
$Q_g$ (m <sup>3</sup> /hr)	10	10	18	18	10	18	18	18	14	14
$H$ (mm)	30	30	30	30	60	60	60	45	45	4.5
$C_{in}$ (ppm)	1950	1924	1924	1933	1927	1965	1973	1998	1913	1907
$C_{Bo}$ (mol/m <sup>3</sup> )	311	349	311	290	263	311	311	263	357	311

*EGPM model*

$c_1$ (ppm)	361	201	1073	924	123	52	655	554	266	333
$c_2$ (ppm)	610	368	1312	1143	284	135	977	815	462	546
$c_3$ (ppm)	972	661	1545	1392	614	347	1338	1156	781	869
$c_4$ (ppm)	1509	1213	1829	1732	1239	905	1761	1633	1323	1389
$Y_G$ (%)	81	90	44	52	94	97	67	72	86	83

*EGPF model*

$c_1$ (ppm)	264	107	1056	892	42	8	612	493	183	241
$c_2$ (ppm)	511	235	1305	1118	145	35	956	760	359	453
$c_3$ (ppm)	900	505	1540	1372	446	150	1335	1117	677	784
$c_4$ (ppm)	1410	1030	1749	1648	1083	604	1686	1544	1195	1274
$Y_G$ (%)	86	94	45	54	98	100	69	75	90	87

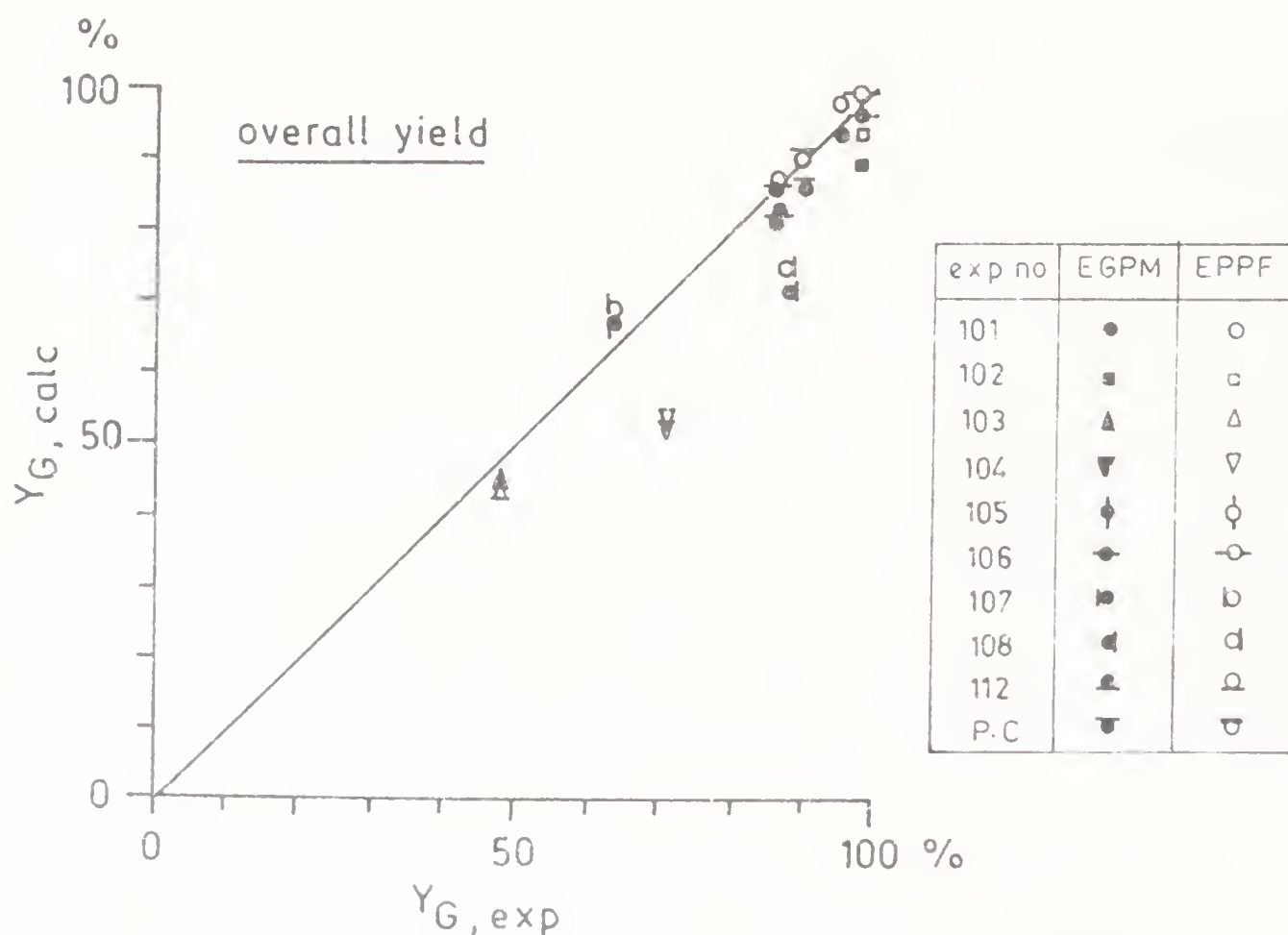


Figure 7. Predictions of the EGPM and EPPF models (calc = calculated; exp = experimental).

which do not take into account experiment 104 and 108.

For the EGPM model:  $\sigma_g = 3.5\%$ ,  $\sigma_m = -2.3\%$ ,  
and for the EGPF model:  $\sigma_g = 2.6\%$ ,  $\sigma_m = 1.0\%$ .

This shows the tendency of the EGPM model to underestimate the yields while the EGPF model tends to slightly overestimate them. Predictions for experiments 104 and 108 differ more strongly from data. These experiments have been performed for the highest values of gas and solid flow rates. The mean residence times of solids were respectively 88 and 180 s, while they were greater than 220 s for all other experiments. It can be considered that under these conditions, the solids cannot be assumed to be perfectly mixed.

The slight difference observed between the predictions of the two models tends to indicate that the gas interchange between the bubbles and the emulsion phase is not the limiting step in this process. This is probably a consequence of the rather narrow bed height. This interpretation was confirmed by Laguérie & Vizcarra-Mendoza (1982).

#### 4. Conclusions

From a practical point of view, desulphurization yields of more than 90% can be obtained by chemical sorption of sulphur dioxide on copper oxide deposited on porous alumina particles in a fluidized bed reactor working at about 300°C. The sulphur dioxide content of the exit gas can be reduced to less than 300 ppm. The gas pressure drop is not prohibitive and the mechanical strength of the solids is sufficient to avoid dust pollution. The presence of other components in the flue gas leads to a slight decrease in the desulphurization yield. This could be corrected by a better choice of the operating conditions. The process could then be used to control sulphur dioxide pollution by flue gas.

A model based on the assumptions of Davidson & Harrison (1963) has been developed for simulating the operation of the reactor. The assumption of plug flow of the gas percolating through the emulsion phase leads to slightly better predictions than the assumption of perfect mixing of the emulsion phase.

Even though some of the conclusions are specific to this study, the model could be considered general enough to be used for predicting the performance of a counterflow multistage fluidized bed reactor for solid-gas treatment, without changing the size of particles, by using an appropriate kinetic law.

This paper is dedicated to Dr L K Doraiswamy on his sixtieth birthday. The authors wish to acknowledge Dr M Vizcarra-Mendoza, Dr H Yi-Duran and Dr K Iovtchev for their decisive contributions to the studies.

#### List of symbols

$c_b$	Sulphur dioxide concentration of bubbles ( $\text{mol m}^{-3}$ );
$c_i$	sulphur dioxide concentration of gas leaving the $i$ th stage ( $\text{mol m}^{-3}$ or ppm);

$c_{in}$	sulphur dioxide concentration of gas to be treated ( $\text{mol m}^{-3}$ or ppm);
$c_{out}$	sulphur dioxide concentration of the exit gas ( $\text{mol m}^{-3}$ or ppm);
$c_p$	sulphur dioxide concentration of emulsion phase ( $\text{mol m}^{-3}$ );
$c_R$	copper oxide concentration of solids ( $\text{mol m}^{-3}$ );
$c_S$	copper oxisulphate concentration of solids ( $\text{mol m}^{-3}$ );
$D_b$	bubble diameter (m);
$D_b^{\max}$	maximum bubble diameter for total coalescence (m);
$D_{b0}$	initial bubble diameter (m);
$D_g$	diffusivity of gaseous reactant ( $\text{m}^2 \text{s}^{-1}$ );
$D_T$	diameter of the reactor (m);
$E_i, E'_i$	residence time distribution of solids in the $i$ th stage ( $\text{s}^{-1}$ );
$g$	acceleration due to gravity ( $\text{m.s}^{-2}$ );
$H$	height of the bed (m or mm);
$H_{mf}$	minimum fluidization height of the bed (m);
$K$	number of reaction units;
$k_1, k_2$	reaction rate constants ( $\text{m}^3 \text{mol}^{-1} \text{s}^{-1}$ );
$L$	height of downcomers (m);
$m_1, m_2$	constants;
$N_b$	number of bubbles per unit bed volume ( $\text{m}^{-3}$ );
$n_d$	number of orifices of each distributor;
$\Delta P$	pressure drop of gas (mm $\text{H}_2\text{O}$ );
$Q$	interphase mass transfer flux ( $\text{m}^3 \text{s}^{-1}$ );
$Q_g$	gas flow rate ( $\text{m}^3 \text{hr}^{-1}$ );
$Q_s$	solid flow rate ( $\text{kg hr}^{-1}$ );
$r_1, r_2$	reaction rates ( $\text{mol m}^{-3} \text{s}^{-1}$ );
$r$	average rate of $\text{SO}_2$ disappearance ( $\text{mol m}^{-1} \text{s}^{-1}$ );
$S$	cross-sectional area of the reactor ( $\text{m}^2$ );
$T$	temperature ( $^{\circ}\text{C}$ or $\text{K}$ );
$T_{gm}$	inlet gas temperature ( $^{\circ}\text{C}$ );
$T_{pin}$	inlet solids temperature ( $^{\circ}\text{C}$ );
$t$	time (s or hr);
$u$	superficial velocity of gas ( $\text{m s}^{-1}$ );
$u_b$	bubble rise velocity ( $\text{m s}^{-1}$ );
$u_{mf}$	incipient fluidization velocity ( $\text{m s}^{-1}$ );
$v_b$	bubble volume ( $\text{m}^3$ );
$W$	mass of solid on each stage (kg);
$X$	number of transfer units;
$Y_G$	(overall) desulphurization yield;
$Y_i$	$i$ th stage desulphurization yield;
$z$	height in the bed (m);
$\beta$	fraction of gas flow associated with bubbles (m);
$\sigma_m, \sigma_q$	deviation criteria;
$\tau$	mean residence time of solids on each stage (s);
$\tau_i$	residence time of solids on the $i$ th stage (s);

## References

- Barreteau D 1977 *Etude d'une réaction gaz-solide en lit fluidisé alimenté en continu en solide* Dr. Ing. Thesis, Univ. Paul Sabatier, Toulouse
- Barreteau D, Angéline H 1978 *Can. J. Chem. Eng.* 56: 570-77
- Barreteau D, Laguérie C, Angéline H 1978 in *Fluidization, Proc. of the 2nd Engineering Foundation Conf.* (eds) J F Davidson, D L Keairns (Cambridge: Univ. Press) pp. 297-302
- Barreteau D, Laguérie C 1983 in *Studies in environmental sciences, Proc. of the Int. Symp. on Chemistry and Protection of Environment* (eds) A J Verdier, L Pawlowski (Amsterdam: Elsevier) pp. 597-602
- Barreteau D, Laguérie C 1984 *Environ. Prot. Eng.* 10(3): 69-78
- Barreteau D, Yi-Duran H, Iovtchev K, Laguérie C 1984 *Environ. Technol. Lett.* 4: 325-331
- Barreteau D, Yi-Duran H, Laguérie C 1983 *Entropie* 19: 80-88
- Dautzenberg F M, Nader J E 1971 *Chem. Eng. Prog.* 67: 8-13
- Davidson J F, Harrison D 1963 *Fluidized particles* (Cambridge: Univ. Press)
- Hollinden G A, Elder H W 1974 Paper Coal Utilization Symposium, Washington
- Laguérie C, Vizcarra-Mendoza M, Yi-Duran H 1982 32nd Canadian Chemical Engineering Conference, Vancouver
- Laguérie C, Vizcarra-Mendoza 1982 *Entropie* 106: 46-57
- Mori S, Wen C Y 1975 *AIChE J.* 21: 109-117
- Slack A V, Hollinden G A 1975 *Pollut. Technol. Rev.* 21: 17-24
- United State Department of Energy 1985 Report on flue gas desulphurization and denitrification, DOE/TIC-3402
- Van Hootte G 1973 *Soixante procédés de désulfuration*, Office International de la Librairie, Bruxelles
- Vizcarra-Mendoza M 1979 *Etude de la désulfuration d'un gaz dans un réacteur multiétagé à couches fluidisées fonctionnant en continu*, Dr. Ing. Thesis, INP, Toulouse
- Vizcarra-Mendoza M, Laguérie C 1981 *Environ. Technol. Lett.* 2: 215-224
- Woodburn T 1986 *The Chemical Engineer* November: 36-39
- Yates J G, Best R J 1976 *Ind. Eng. Chem., Process Des. Dev.* 15: 2-12





# Population balance modelling of bubbling fluidized beds.

## II. Axially dispersed dense phase

R MURALIDHAR, S GUSTAFSON and D RAMKRISHNA\*

School of Chemical Engineering, Purdue University, West Lafayette,  
Indiana 47907, USA

**Abstract.** The population balance model of Sweet, Gustafson and Ramkrishna for a steady state gas-solid fluidized bed reactor is extended in this work to include axial mixing in the dense phase. A trivariate population balance equation for the bubble phase, and an axial dispersion equation for the dense phase are solved simultaneously by combining a Monte Carlo simulation technique with the method of successive approximations. Conversion for a first-order reaction is analysed in terms of five dimensionless groups including: a coalescence parameter controlling the extent of coalescence, a Peclet number measuring the amount of mixing in the dense phase, a Damkohler number which relates the dispersive mixing time in the dense phase to the reaction time, a dimensionless group representing the ratio of the dispersive mixing time to the time scale of mass transfer, and a dimensionless reaction rate constant.

The computations show that coalescence can significantly affect reactor conversion. It appears that the effect of mixing is less significant particularly at higher reaction rates. Comparison of these results with those obtained earlier in which the dense phase was assumed to be perfectly mixed shows that higher conversions could be obtained in the latter case for sufficiently fast reactions while the opposite is true for slow reactions.

**Keywords.** Population balances; fluidization; Monte Carlo simulation.

### 1. Introduction

In Part I of this paper, Sweet *et al* (1986) have analysed the effect of bubble by-passing on conversion of a first-order reaction in a fluidized bed reactor using a population balance model for coalescence of bubbles. They assumed that the dense phase was perfectly mixed while individual bubbles exchanged gas with the dense

---

\*To whom correspondence should be addressed  
A list of symbols is given at the end of the paper

phase. In this paper, we retain the population balance model of the earlier paper but assume that the dense phase satisfies an axial dispersion model. Such would be a more realistic description of the mixing in the dense phase so that together with the population balance model for the bubble phase we have a relatively realistic picture of the fluidized bed reactor. With a view towards making this paper independently readable we briefly present the relevant features and equations of the population balance model, presented in detail in Part I.

The extent of axial mixing in the dense phase is related to the hydrodynamics of the bubbles, the local turbulence as well as the density of the catalyst particles. There have been models in the literature to describe backmixing in the dense phase. The countercurrent backmixing model developed by Potter and co-workers is discussed by Yates (1983). The investigators show that for velocities greater than a critical velocity, strong backmixing may occur leading to downward flow of the emulsion phase. The model divides the bed into emulsion, bubble and wake phases. Bubble coalescence is accounted for in an indirect way by assuming, based on experimental evidence, a linear profile of bubble diameters. Reactant balance equations are identified for each of the three phases and the overall reactant concentration is a weighted average over the three phases. The model predictions have been successfully tested with experimental data. The Kato-Wen bubble assemblage model described in detail by Yates (1983) again assumes a linear profile of bubble diameters to account for coalescence. The bed is divided into many compartments the thickness of each being equal to the average bubble diameter corresponding to that location. In each compartment the emulsion and bubble phase are assumed to be perfectly mixed and appropriate reactant mass balance equations are identified for both the phases. The predicted concentration profiles show good agreement with experimental data.

A deficiency of the above models is that mixing is not characterized quantitatively in a simple manner. Moreover, bubble dynamics are lumped so that fluctuations cannot be predicted. Indeed even under steady state conditions, the bubble population is not strictly invariant but fluctuates as a consequence of which there may be fluctuations in reactor conversion. In this paper, a detailed population balance model is derived for a gas-solid fluidized bed reactor with an axially mixed dense phase wherein mixing is characterized by means of an axial dispersion coefficient. The population balance framework directly yields the distribution of bubbles over their possible states. The objective is to observe the concentration profiles in the two phases under different levels of mixing and coalescence and to investigate the importance of bubble coalescence as well as axial mixing (in the dense phase) on the overall reactor performance.

## 2. The population balance model

The object of interest is an isothermal gas-solid fluidized bed reactor in which the first-order chemical reaction,



occurs in the dense particulate phase. Bubbles of uniform size are formed at the feed plate. Any known variations in bubble size are of course readily incorporated.

The bubbles coalesce randomly as they rise through the bed. Although bubble splitting occurs in conjunction with coalescence, the latter is the dominant phenomenon and in this analysis bubble splitting is neglected. As the bubbles rise through the bed, mass transfer to the particulate phase occurs due to bulk exchange as well as diffusion. These are discussed by Davidson & Harrison (1963, 1971).

The mass exchange between the bubbles and the dense-phase clearly depends on the height of the bubble and its size as well as the reactant concentration. In accordance with Ramakrishna (1985), a vector  $[v, z, c]^T$  characterizes the state of a bubble. In order to estimate the reaction conversion, it is necessary to know the distribution of the bubble population with respect to their possible states. Let  $f_1(v, z, c)$  denote the steady state number density function for the bubble population, i.e.,  $f_1(v, z, c)dv dz dc$  represents the average number of bubbles of volume between  $v$  and  $v + dv$ , height between  $z$  and  $z + dz$  and reactant concentration between  $c$  and  $c + dc$ , in the bed. Clearly the domain of  $f_1(v, z, c)$  is given by  $0 < v < v_{\max}$ ,  $0 \leq z \leq H$  and  $0 \leq c \leq c_0$ . The population balance equation (PBE) is a conservation equation for the trivariate number density accounting for bubble events such as coalescence, mass exchange, vertical motion etc.

In order to write the PBE, the rates for various bubble processes need to be identified. The rate of change of volume of a bubble of volume  $v$  at location  $z$  is given by

$$\dot{V}(v, z) = [vu(v)]/[H - z + p_a/\rho_p z], \quad (2)$$

where  $\rho_p$  is the density of the particulate phase and  $H$  is the height of the bed. The upward velocity of a bubble of volume  $u$  is estimated by Davidson & Harrison (1963, 1971) to be

$$u(v) = U - U_{mf} + 0.71[6v/\pi]^{1/6}. \quad (3)$$

The rate of change of reactant concentration of a bubble of volume  $v$ , at height  $z$  and concentration  $c$  is again obtained from Davidson & Harrison (1963, 1971).

$$v\dot{C}(v, z, c) = (q + K_G a)(c_p - c) = R(c_p - c), \quad (4)$$

$$q = 3\pi[3v/4\pi]^{2/3} U_{mf}. \quad (5)$$

In (4), we have accounted for change due to bulk exchange rate  $q$  and due to mass transfer via the mass transfer coefficient times the interfacial area. To account for bubble coalescence, we use the coalescence model of Argyriou *et al* (1971), modified slightly by Shah *et al* (1977a). The model yields for the coalescence frequency the expression

$$Q(v, z, v', z') = \begin{cases} 0 & |z - z'| > d(v, v') \\ k_2(v^{1/3} + v'^{1/3})^2/k_3^{2/3} & |z - z'| < d(v, v') \end{cases}, \quad (6)$$

where

$$d(v, v') = \frac{1}{2} \left[ (v/k_3)^{1/3} + (v'/k_3)^{1/3} \right]. \quad (7)$$

The rate expressions are discussed in greater detail by Sweet *et al* (1986).



With the identification of the above rate expressions, the relevant equation for the steady state expected number density is readily identified as

$$\begin{aligned}
 & \frac{\partial}{\partial v} [\dot{V}(v, z) f_1(v, z, c)] + \frac{\partial}{\partial z} [u(v) f_1(v, z, c)] + \frac{\partial}{\partial c} [\dot{C}(v, z, c) f_1(v, z, c)] = \\
 & \frac{1}{2} \left\{ \int_0^{v/2} dv' \int_{z-d(v', v-v')}^{z+d(v', v-v')} dz' \int_0^{\max[c_0, vc/v']} dc' k_2 \left[ \left( \frac{v-v'}{k_3} \right)^{1/3} + \left( \frac{v'}{k_3} \right)^{1/3} \right]^2 \right. \\
 & \times f_2(v-v', z, \frac{vc-v'c'}{v-v'}; v', z', c') \\
 & + \int_{v/2}^v dv' \int_{z-d(v', v-v')}^{z+d(v', v-v')} dz' \int_0^{\max[c_0, vc/v']} dc' k_2 \left[ \left( \frac{v-v'}{k_3} \right)^{1/3} + \left( \frac{v'}{k_3} \right)^{1/3} \right]^2 \\
 & \times f_2\left(v', z, c'; v-v', z', \frac{vc-v'c'}{v-v'}\right) \left. \right\} \\
 & - \int_0^{v_{\max}} dv' \int_{z-d(v', v)}^{z+d(v', v)} dz' \int_0^{c_0} dc' k_2 \left[ \left( \frac{v}{k_3} \right)^{1/3} + \left( \frac{v'}{k_3} \right)^{1/3} \right]^2 \\
 & \times f_2(v, z, c; v', z', c'). \tag{8}
 \end{aligned}$$

In the above, the function  $f_2(v, z, c; v', z', c')$  is the second order product density (Ramkrishna & Borwanker 1973; Ramkrishna *et al* 1976). The initial condition for (8) is given by the inlet bubble distribution which in this case is

$$f_1(v, 0, c) = N_0 \delta(v - v_0) \delta(c - c_0). \tag{9}$$

In (9),  $v_0$  and  $c_0$  are the volume and concentration of entering bubbles while  $N_0$  is the number density of bubbles entering the bed over the entire cross-section  $S$  and is given by

$$N_0 = S(U - U_{mf})/u_0 v_0, u_0 \equiv u(v_0). \tag{10}$$

In order to assess the significance of coalescence in determining the distribution of bubbles, it is convenient to non-dimensionalize the PBE. We define the following dimensionless quantities.

$$\begin{aligned}
 \xi & \equiv c/c_0, \eta \equiv v/v_0, \zeta \equiv z/H_{mf}, \tau \equiv H_{mf}/u_0, \dot{\xi} = \dot{C}\tau/c_0, \\
 \dot{\eta} & \equiv \dot{V}\tau/v_0, \dot{\zeta} = u/u_0, \\
 \phi_1(\eta, \zeta, \xi) & \equiv (v_0 c_0 / N_0) f_1(v, z, c),
 \end{aligned} \tag{11}$$

$$\phi_2(\eta, \zeta, \xi; \eta', \zeta', \xi') \equiv (v_0 c_0 / N_0)^2 f_2(v, z, c; v', z', c').$$

Using the above, one obtains from (8)

$$\begin{aligned} & \frac{\partial}{\partial \eta} \left[ \dot{\eta} \phi_1(\eta, \zeta, \xi) \right] + \frac{\partial}{\partial \zeta} \left[ \dot{\zeta} \phi_1(\eta, \zeta, \xi) \right] + \frac{\partial}{\partial \xi} \left[ \dot{\xi} \phi_1(\eta, \zeta, \xi) \right] \\ &= \omega \left\{ \frac{1}{2} \int_{\eta/2}^{\eta} d\eta' \int_{\zeta - \Delta(\eta - \eta', \eta')}^{\zeta + \Delta(\eta - \eta', \eta')} d\zeta' \int_0^{\text{Max}[1, \xi \eta' / \eta]} d\xi' [(\eta - \eta')^{1/3} + (\eta')^{1/3}] \right. \\ & \times \phi_2(\eta - \eta', \zeta, \frac{\eta \xi - \eta' \xi'}{\eta - \eta'}; \eta', \zeta', \xi') \\ & + \frac{1}{2} \int_{\eta/2}^{\eta} d\eta' \int_{\zeta - \Delta(\eta - \eta', \eta')}^{\zeta + \Delta(\eta - \eta', \eta')} d\zeta' \int_0^{\text{Max}[1, \xi \eta' / \eta]} d\xi' \left[ (\eta - \eta')^{1/3} + (\eta')^{1/3} \right]^2 \\ & \times \phi_2\left(\eta', \zeta, \xi'; \eta - \eta', \zeta', \frac{\eta \xi - \eta' \xi'}{\eta - \eta'}\right) \\ & - \int_0^{\eta_{\max}} d\eta' \int_{\zeta - \Delta(\eta, \eta')}^{\zeta + \Delta(\eta, \eta')} d\zeta' \int_0^1 d\xi' \left[ (\eta)^{1/3} + (\eta')^{1/3} \right]^2 \\ & \left. \times \phi_2(\eta, \zeta, \xi; \eta', \zeta', \xi') \right\}, \end{aligned} \quad (12)$$

where

$$\Delta(\eta, \eta') \equiv d(v, v') / H_{mf}, \quad (13)$$

and  $\omega$ , the dimensionless coalescence parameter is given by

$$\omega \equiv k_2(v_0/k_3)^{2/3}(N_0 H_{mf}^2 / u_0). \quad (14)$$

The initial condition given by (9) is transformed to

$$\phi_1(\eta, \xi, 0) = \delta(\eta - 1)\delta(\xi - 1). \quad (15)$$

As the value of the coalescence parameter increases, the importance of coalescence in determining the distribution of bubble states increases.

The mass balance for the dense phases depends on the degree of mixing brought about by the bubbles and the catalyst particles. It is convenient to describe the mixing effects by means of the axial dispersion model,

$$D \frac{d^2 c_p}{dz^2} - U_{mf} \frac{dc_p}{dz} - k c_p = \frac{1}{S} \int_0^{c_0} dc \int_0^{v_{\max}} dv v \dot{C}(v, z, c) f_1(v, z, c), \quad (16)$$

together with the Danckwerts' boundary conditions at the inlet and exit

$$D \frac{dc_p}{dz} - U_{mf} c_p = -U_{mf} c_0, \text{ at } z = 0, \quad (17a)$$

$$D(dc_p/dz) = 0, \text{ at } z = H. \quad (17b)$$

In (16), (17a) and (17b),  $D$  is the axial dispersion coefficient. When  $D \rightarrow 0$ , the dense phase is in plug flow and when  $D \rightarrow \infty$ , the dense phase becomes perfectly mixed. The term on the right hand side of (16) accounts for the net transfer of reactants from the bubbles to the dense phase.

Substituting for  $v\dot{C}(v, z, c)$  in (16) from (4) and introducing dimensionless variables, one obtains

$$-\frac{d^2\xi_p}{d\zeta^2} + \alpha \frac{d\xi_p}{d\zeta} + \beta \xi_p = -\mu \int_0^1 d\xi \int_0^{\eta_{m,ax}} d\eta (\xi_p - \xi) \phi_1(\eta, \zeta, \xi), \quad (18)$$

$$(d\xi_p/d\zeta) - \alpha \xi_p = -\alpha, \text{ at } \zeta = 0, \quad (19a)$$

$$(d\xi_p/d\zeta) = 0, \text{ at } \zeta = \bar{\zeta}. \quad (19b)$$

In the above,  $\alpha$  is the Peclet number ( $U_{mf}H_{mf}/D$ ) representing the relative importance of convection over diffusion,  $\beta = (kH_{mf}^2/D)$  is a dimensionless Damkohler number depicting the relative importance of chemical reaction over dispersive mixing and  $\mu = (RN_0H_{mf}^2/DS)$  is a dimensionless number showing the relative importance of mass transfer from the bubble phase over dispersion in the dense phase. Another useful dimensionless parameter  $k' = kH_{mf}/U$  represents the ratio of the residence time in the bed to the characteristic reaction time.

### 3. Solution of the population balance model

The steady state solution of the population balance model with an axially dispersed dense phase involves

- (a) the determination of the steady state trivariate density function for the bubble phase from the solution of (12) with the boundary condition given by (15), and
- (b) the determination of the steady state dense phase concentration profile from the solution of (18) along with the boundary conditions given by (19a) and (19b).

One of the major sources of difficulty in solving the population balance equation and the axial dispersion equation arises due to the coupling introduced by the mass transfer term  $\dot{\xi}(\eta, \zeta, \xi)$ . Clearly the solution of (12) requires a knowledge of the dense phase concentration profile which in turn cannot be determined from (18) without the knowledge of the trivariate bubble population density. Thus (12) and (18) must be solved simultaneously and a trial and error or successive approximation scheme is essential.

For a given trivariate density function, the solution for the dense phase is given by

$$\xi_p(\zeta) = 1 + \int_0^{\bar{\zeta}} G(\zeta, \rho) \left[ \mu \int_0^1 d\eta \int_0^{\eta_{\max}} d\gamma (\xi_p - \xi) \phi_I(\eta, \rho, \xi) + \beta \right] \times e^{-\alpha\rho} d\rho, \quad (20)$$

where  $G(\zeta, \rho)$  is the *Green's function* associated with (18), (19a) and (19b) and is given by

$$G(\zeta, \rho) = \begin{cases} A[e^{m_1\rho} - (m_2/m_1)e^{m_2\rho}][e^{m_2\zeta} - (m_2/m_1)e^{(m_2-m_1)\bar{\zeta}}e^{m_1\zeta}] & 0 < \rho < \zeta \\ A[e^{m_2\rho} - (m_2/m_1)e^{(m_2-m_1)\bar{\zeta}}e^{m_1\rho}][e^{m_1\rho} - (m_2/m_1)e^{m_2\zeta}] & \zeta < \rho < \bar{\zeta} \end{cases} \quad (21)$$

$$A = (m_1/m_2) / \left[ e^{(m_2-m_1)\bar{\zeta}} \frac{(m_2^2 - m_1m_2)}{m_1} + \frac{(\alpha - m_2)}{(\alpha - m_1)} (m_1 - m_2) \right], \quad (22)$$

$$m_1 = [\alpha + (\alpha^2 + 4\beta)^{1/2}]/2, \quad m_2 = [\alpha - (\alpha^2 + 4\beta)^{1/2}]/2. \quad (23)$$

This enables a *successive approximation* scheme to be established. The dense phase profile is initially guessed and this enables the solution of the population balance equation (12) for the steady state trivariate bubble density  $\phi_I(\eta, \zeta, \xi)$ . This computed trivariate density function is used to establish the dense phase concentration profile via (20). If the calculated and guessed dense phase concentration profiles are not the same, the calculated profile is taken as the next guess for the dense phase profile, the trivariate distribution is again established and the dense phase profile recalculated. The procedure is repeated until the calculated and guessed dense phase profiles are in agreement. In other words, the  $n$ th approximation for the dense phase concentration profile is given by

$$\xi_{p,n}(\zeta) \equiv \mathbf{T}\xi_{p,n-1}(\zeta) = 1 + \int_0^{\bar{\zeta}} d\rho e^{-\alpha\rho} G(\zeta, \rho) \times \left[ \mu \int_0^1 d\xi \int_0^{\eta_{\max}} d\eta (\xi_{p,n-1} - \xi) \phi_{I,n-1}(\eta, \rho, \xi) + \beta \right]. \quad (24)$$

Although the convergence of the above for arbitrary initial guesses  $\xi_{p,0}(\zeta)$  requires the mapping  $\mathbf{T}$  to be a contraction (see, for instance, Ramkrishna and Amundson 1985), this is in general a very strong condition and convergence may be possible, even if  $\mathbf{T}$  is not a contraction, provided the initial guess is reasonable. Such a guess is facilitated in this case from the fact that the dimensionless concentration must lie between 0 and 1.



The solution of the population balance equation (12) can be extremely cumbersome. Further, a second equation needs to be identified for the second-order density function which would again involve an unknown third-order density function and so on. Thus one is faced with a 'closure problem'. The above difficulties are obviated by a Monte Carlo solution of (12). The simulation technique of Shah *et al* (1977b) requires the updating of particle states during randomly generated quiescence intervals. Several sample pathways or realizations are constructed from the prescribed initial condition and the trivariate density is obtained as an average over the ensemble of realizations. Ramkrishna (1981) has established the equivalence of the Monte Carlo approach and the direct solution of population balance equations. Indeed, this successive approximation approach may appear to be computationally overburdened. However, there are several redeeming features. First, because the random coalescence rates have been assumed to be independent of reactant concentration the generation of quiescence intervals required for the simulation is also independent of the concentration of the reactant either in the bubbles or in the dense phase. (Of course the updating of particle states during a quiescence interval does depend upon the reactant concentration in both phases.) Thus if steps are taken to exploit the sequence of quiescence intervals generated at the beginning for each iteration, and only repeat the bubble state-updating procedure, then considerable amount of computation time can be saved. Second, since we are interested in the steady state fluidized bed reactor, a further simplification is possible. Recognizing that the process is stationary at steady state, the trivariate distribution may be simply obtained as a time average over a single realization.

### 3.1 The simulation algorithm

The volume interval  $[0, v_{\max}]$ , the height interval  $[0, H]$  and the concentration interval  $[0, c_0]$  are discretized into  $N_v$ ,  $N_z$  and  $N_c$  cells, respectively, the end points of which are given by

$$\begin{aligned} v_i &= 2(i-1)v_0, \quad i = 1, 2, \dots, N_v+1, \\ z_j &= (H/N_z)(j-1), \quad j = 1, 2, \dots, N_z+1, \\ c_k &= (c_0/N_c)(k-1), \quad k = 1, 2, \dots, N_c+1. \end{aligned} \quad (25)$$

The characteristic values corresponding to these units are given by

$$\begin{aligned} \bar{v}_i &= (v_i + v_{i+1})/2, \quad i = 1, 2, \dots, N_v, \\ \bar{z}_j &= (z_j + z_{j+1})/2, \quad j = 1, 2, \dots, N_z, \\ \bar{c}_k &= (c_k + c_{k+1})/2, \quad k = 1, 2, \dots, N_c. \end{aligned} \quad (26)$$

It is possible to use other methods of discretization such as for example the division of bed height by Kato and Wen (see Yates 1983). The number of units depends on the size of the bubble population in the bed as well as the number of sampling times. Clearly for the same level of discretization, the smaller the bubble population, the larger is the number of sampling times for a reliable average distribution to be estimated.

Let  $f_1(i, j, k)$  denote the expected number of bubbles of volume in interval  $i$ , location in interval  $j$  and concentration in interval  $k$ . During the transient period,  $f_1(i, j, k)$  will depend on time. Let  $f_1^l(i, j, k)$  denote the distribution of the population at the  $l$ th sampling time after steady state is reached. Bubbles entering the bed are

characterized by their state vector  $[\mathbf{v}_0, \mathbf{0}, \mathbf{c}_0]^T$ . Bubble dynamics is simulated using the interval of quiescence approach of Shah *et al* (1977b). The number of bubbles with location in height cell  $j$  at  $l$ th sampling time is given by

$$n_j^l = \sum_{i=1}^{N_v} \sum_{k=1}^{N_c} f_1^l(i, j, k), \quad j = 1, 2, \dots, N_z. \quad (27)$$

Clearly the total number of bubbles in the bed at the  $l$ th sampling time is given by

$$N_b^l = \sum_{j=1}^{N_z} n_j^l, \quad (28)$$

The average population density after  $N_s$  sample times is given by

$$f_1(i, j, k) = \frac{1}{N_s} \sum_{l=1}^{N_s} f_1^l(i, j, k), \quad i = 1, 2, \dots, N_v; \quad j = 1, 2, \dots, N_z; \\ k = 1, 2, \dots, H_c. \quad (29)$$

The above is used to calculate the array of dense phase concentrations from the discretized version of (20).

#### 4. Results and discussion

The solution procedure is illustrated by numerical examples. The values of the fluidized bed parameters used in the simulations are given in tables 1 and 2. In all computations twenty equal bed slices, fifteen equal concentration slices and fifty volume slices were employed. Expansion of rising bubbles was neglected. The maximum absolute difference between the guessed and calculated dense phase concentration profiles decreased as the successive approximation proceeded as expected. When this error became sufficiently small, fluctuations in the expected trivariate distribution caused the maximum error to fluctuate and not decrease monotonically. The concentration profiles obtained during these states are all extremely close and any may be chosen as the solution. In our computations, the number of sample times was increased to a maximum of one thousand as the absolute error decreased in order to minimize the effects of fluctuations in the estimated mean population distribution. When the absolute error became smaller than a prescribed tolerance level, the estimated trivariate distribution was fixed at the current value and the dense phase concentration profiles was evaluated very

**Table 1.** Constant parameters during simulations.

$U_{mf}$	0.042 in/s (1 in = 2.54cm)
$U$	0.08652 in/s
$k_1$	14.0 in <sup>1/2</sup> /s
$k_3$	0.125
$H$	30.8 in
$H_{mf}$	30.685 in
Bed diameter	11.5 in
$v_0$	0.037 in <sup>3</sup>
$c_0$	0.0000029 lb mol/in <sup>3</sup> (1 lb = 0.4536 kg)

**Table 2.** Fluidized bed parameters used in the simulations.

$k$ ( $s^{-1}$ )	$D$ ( $in^2/s$ )	$D_g$ ( $in^2/s$ )	$k_2$ ( $in^{-1}s^{-1}$ )	Conversion	Standard deviation	Maximum simulations
0.02	0.02232	0.01	3.64	0.759	0.0043	500
0.02	0.02232	0.01	0.364	0.881	0.019	100
0.005	0.02232	0.1	3.64	0.713	0.0022	1000
0.005	2.232	0.1	3.64	0.665	0.0022	1000
0.005	0.02232	0.001	3.64	0.570	0.0025	1000
0.005	0.2232	0.001	3.64	0.562	0.0024	1000
0.005	2.232	0.001	3.64	0.530	0.0033	1000
0.02	0.02232	0.1	3.64	0.905	0.0025	1000
0.02	2.232	0.1	3.64	0.887	0.0015	1000
0.005	0.02232	0.01	3.64	0.627	0.0018	1000

accurately by successive approximation. In order to verify that the calculated dense phase and bubble phase concentration profiles were indeed correct, a test simulation was carried out using the established dense phase concentration profile. The bubble and dense phase concentration profiles obtained were found to be in very good agreement with the same established earlier. The progress of iterations for a single numerical experiment is shown in table 3. All computations were carried out on the Gould PN9800 computer at Purdue University.

Since the concentrations of all the exiting bubbles are not the same, the reactor conversion fluctuates as every bubble exits the bed. The conversions and the standard deviations of the conversions for the various cases considered are shown in table 2. In figure 1, the expected number of bubbles and the standard deviation are plotted as a function of the dimensionless bed length for the lower of the two coalescence frequencies employed. The average number of bubbles decreases along the length of the reactor due to coalescence. The relative uncertainty is also

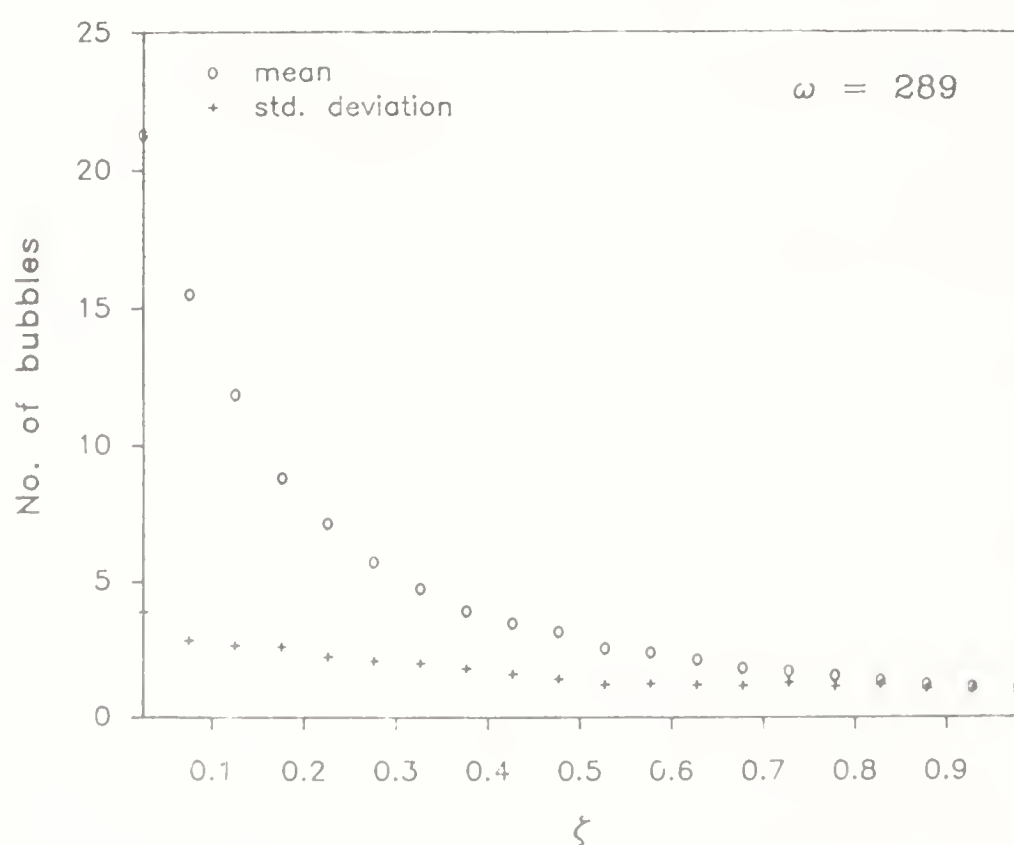
**Figure 1.** Profile of bubble population size.

Table 3. Progress of iterations for the last case in table 2.

Iteration (number of simulations)	Location, Z (inches)					
	0.77	5.39	11.55	17.71	23.87	30.03
Initial guess	$c_p$	$0.27 \times 10^{-5}$	$0.27 \times 10^{-5}$	$0.27 \times 10^{-5}$	$0.27 \times 10^{-5}$	$0.27 \times 10^{-5}$
1	$c$	$0.29 \times 10^{-5}$	$0.29 \times 10^{-5}$	$0.27 \times 10^{-5}$	$0.27 \times 10^{-5}$	$0.27 \times 10^{-5}$
(10)	$c_p$	$0.254 \times 10^{-5}$	$0.155 \times 10^{-5}$	$0.813 \times 10^{-6}$	$0.208 \times 10^{-6}$	$0.106 \times 10^{-6}$
2	$c$	$0.29 \times 10^{-5}$	$0.269 \times 10^{-5}$	$0.250 \times 10^{-5}$	$0.182 \times 10^{-5}$	$0.459 \times 10^{-6}$
(10)	$c_p$	$0.256 \times 10^{-5}$	$0.164 \times 10^{-5}$	$0.101 \times 10^{-5}$	$0.606 \times 10^{-6}$	$0.371 \times 10^{-6}$
3	$c$	$0.29 \times 10^{-5}$	$0.269 \times 10^{-5}$	$0.248 \times 10^{-5}$	$0.199 \times 10^{-5}$	$0.180 \times 10^{-5}$
(40)	$c_p$	$0.255 \times 10^{-5}$	$0.165 \times 10^{-5}$	$0.101 \times 10^{-5}$	$0.489 \times 10^{-6}$	$0.341 \times 10^{-6}$
4	$c$	$0.29 \times 10^{-5}$	$0.269 \times 10^{-5}$	$0.247 \times 10^{-5}$	$0.181 \times 10^{-5}$	$0.160 \times 10^{-5}$
(40)	$c_p$	$0.255 \times 10^{-5}$	$0.167 \times 10^{-5}$	$0.104 \times 10^{-5}$	$0.559 \times 10^{-6}$	$0.438 \times 10^{-6}$
5	$c$	$0.29 \times 10^{-5}$	$0.269 \times 10^{-5}$	$0.247 \times 10^{-5}$	$0.195 \times 10^{-5}$	$0.173 \times 10^{-5}$
(1000)	$c_p$	$0.255 \times 10^{-5}$	$0.166 \times 10^{-5}$	$0.102 \times 10^{-5}$	$0.522 \times 10^{-6}$	$0.414 \times 10^{-6}$
6	$c$	$0.29 \times 10^{-5}$	$0.269 \times 10^{-5}$	$0.245 \times 10^{-5}$	$0.194 \times 10^{-5}$	$0.172 \times 10^{-5}$
(1000)	$c_p$	$0.255 \times 10^{-5}$	$0.166 \times 10^{-5}$	$0.103 \times 10^{-5}$	$0.514 \times 10^{-6}$	$0.394 \times 10^{-6}$
7	$c$	$0.29 \times 10^{-5}$	$0.269 \times 10^{-5}$	$0.245 \times 10^{-5}$	$0.193 \times 10^{-5}$	$0.170 \times 10^{-5}$
(1000)	$c_p$	$0.256 \times 10^{-5}$	$0.166 \times 10^{-5}$	$0.102 \times 10^{-5}$	$0.523 \times 10^{-6}$	$0.399 \times 10^{-6}$
$c_p$ final	$0.256 \times 10^{-5}$	$0.166 \times 10^{-5}$	$0.102 \times 10^{-5}$	$0.706 \times 10^{-6}$	$0.526 \times 10^{-6}$	$0.409 \times 10^{-6}$
Test run using $c_p$ final	$c$	$0.29 \times 10^{-5}$	$0.269 \times 10^{-5}$	$0.246 \times 10^{-5}$	$0.193 \times 10^{-5}$	$0.171 \times 10^{-5}$
	$c_p$	$0.256 \times 10^{-5}$	$0.166 \times 10^{-5}$	$0.103 \times 10^{-5}$	$0.530 \times 10^{-6}$	$0.420 \times 10^{-6}$



observed to increase along the reactor length owing to the smaller sizes of the bubble populations. In figure 2, the profile of average bubble volumes and the standard deviations are plotted. The average bubble volume increases due to coalescence along the length of the bed. Even before the mid-point of the bed, the standard deviations begin to exceed the average values. This is representative of the extent of fluctuations in bubble volumes. However, towards the end of the bed, the relative uncertainty again begins to decrease, possibly due to a smoothing effect of several coalescence events.

The performance of the fluidized bed reactor is governed by the values of the dimensionless numbers  $\alpha$ ,  $\beta$ ,  $\mu$ ,  $\omega$  and  $k'$  defined earlier. It is convenient to also consider the dimensionless group  $\mu/\beta$  which represents the relative importance of mass exchange between the two phases and dispersive mixing in the dense phase. The simulation results corresponding to table 2 are shown as functions of the above dimensionless groups in table 4, and are depicted graphically in figures 3–6. Figure 3 shows the concentration profiles in the dense phase and bubble phase at two coalescence frequencies (2 values of  $\omega$ ). For the lower of the two coalescence frequencies used, the bubble concentrations are significantly smaller. This is because lower coalescence frequencies imply smaller bubbles and as such more efficient reactant transfer to the dense phase. The dense phase concentrations corresponding to the lower frequency are naturally higher for most part of the reactor. In the entrance region since the dense phase and bubble phase concentrations are not very different for the low dispersion coefficients and because the disparity between average bubble sizes is not very significant, the dense phase profile corresponding to the two frequencies are almost identical. Towards the end of the bed the profiles again become very close, due to the offsetting effect of higher reaction rates in the dense phase corresponding to the lower coalescence frequency. The difference in conversion was more than ten percent, thus

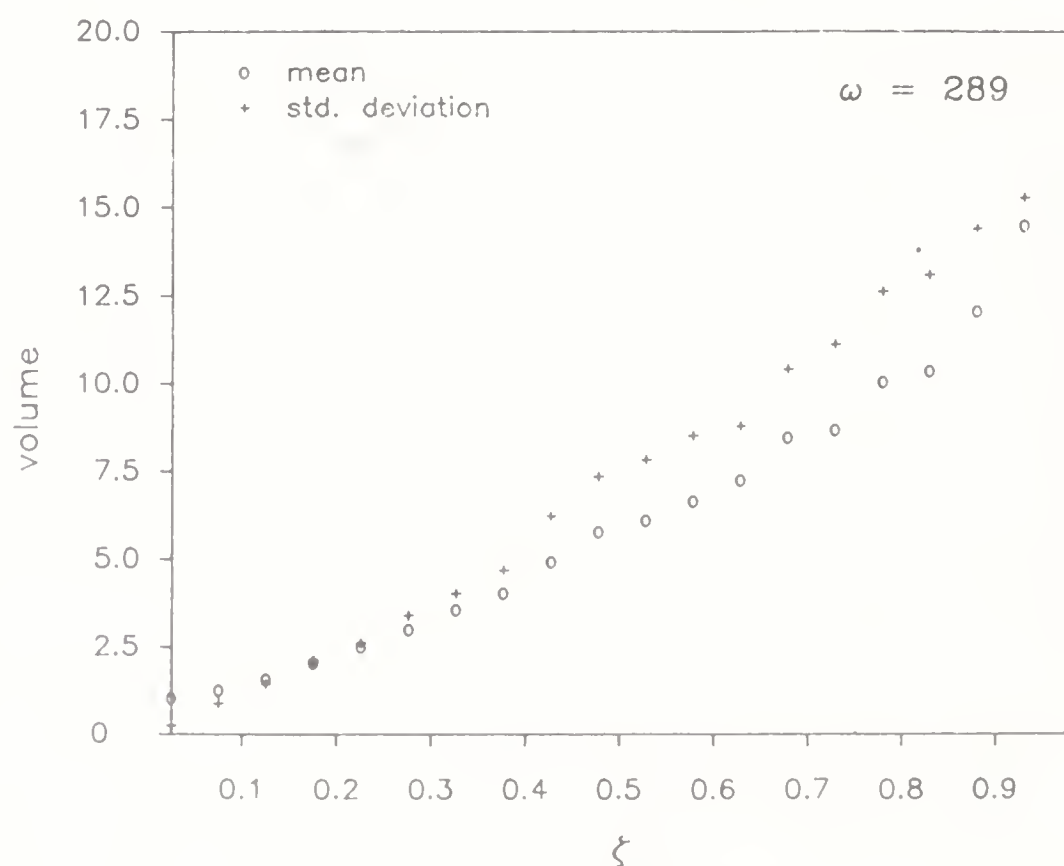


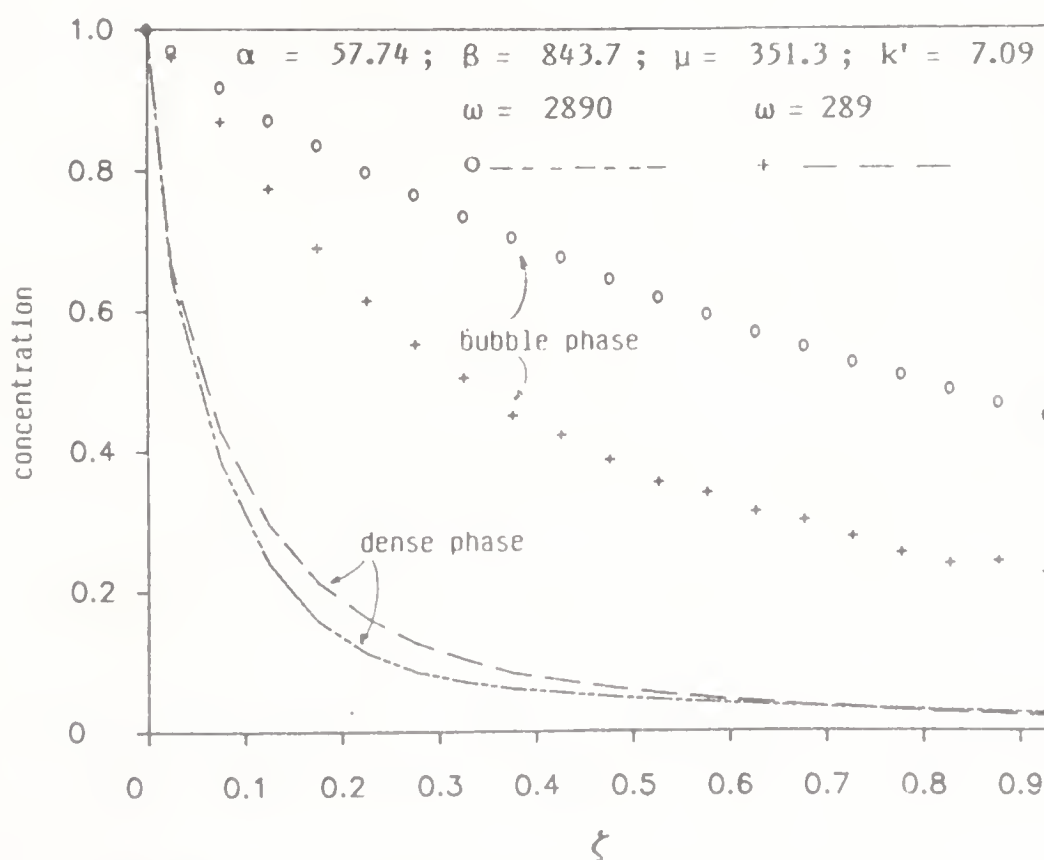
Figure 2. Profile of bubble volumes.

**Table 4.** Simulation results in terms of dimensionless numbers.

Figure number	$\omega$	$\alpha$	$\beta$	$\mu$	$k'$	Conversion
3	2890	57.74	843.7	351.3	7.09	0.759
	289	57.74	843.7	351.3	7.09	0.881
4	2890	57.74	210.9	881.7	1.77	0.713
	2890	0.58	2.1	8.82	1.77	0.665
5	2890	57.74	210.9	183.4	1.77	0.570
	2890	0.58	2.1	1.83	1.77	0.530
6	2890	57.74	843.7	881.7	7.09	0.905
	2890	0.58	8.4	8.82	7.09	0.887

emphasizing the importance of coalescence in affecting the overall reactor performance.

In figures 4–6, the effect of axial mixing is considered. Two dispersion coefficients differing by a factor of one hundred were considered. On changing the dispersion coefficient, the three dimensionless groups  $\alpha$ ,  $\beta$ , and  $\mu$  change by the same factor so that the relative values of  $\alpha$ ,  $\beta$  and  $\mu$  remain the same. However  $k'$  and  $\omega$  are unaffected. Figure 4 portrays the concentration profiles of both the phases for both values of the axial dispersion coefficient. The concentration profile in the dense phase clearly reveals the smoothing effect of dispersion. The disparities in the bubble phase concentration profiles increase initially but again approach each other. This can be understood as follows. In the case of higher mixing, the dense phase concentration near the inlet is significantly smaller than in the case of lower mixing thus facilitating significantly more mass exchange from the

**Figure 3.** Concentration profiles for two coalescence numbers

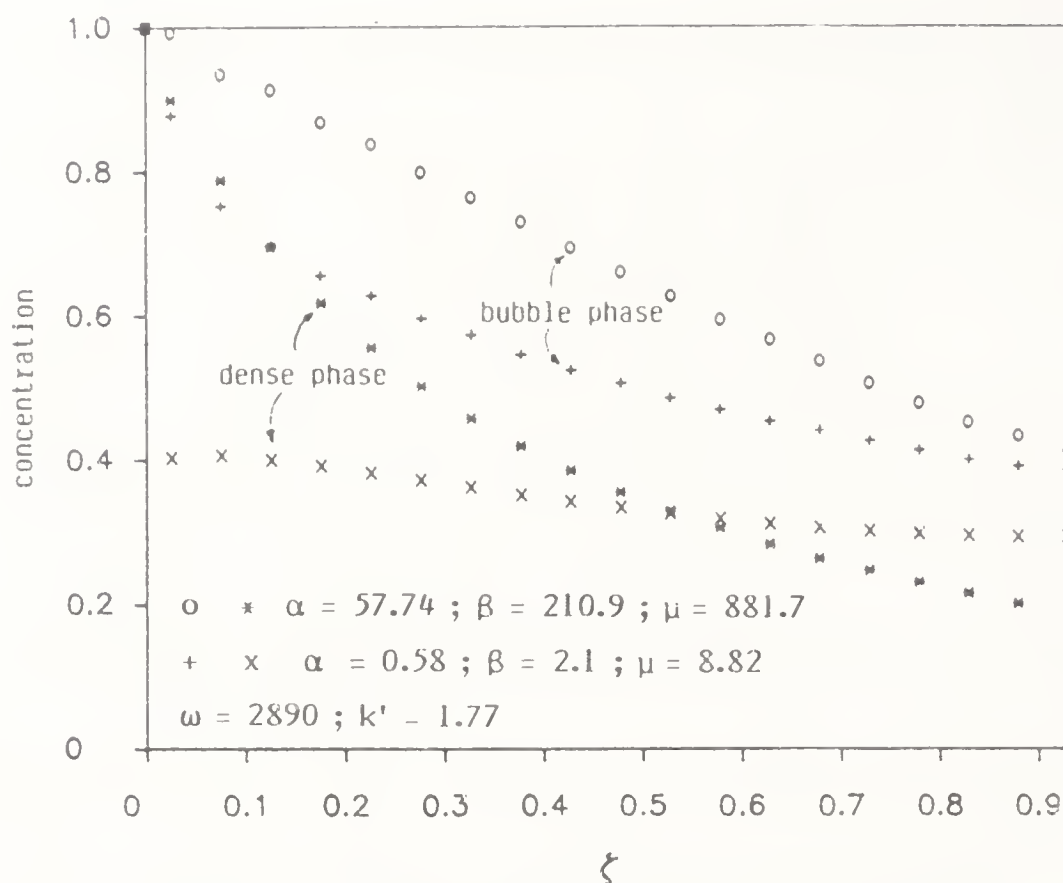


Figure 4. Concentration profiles for two dispersion coefficients.

bubbles. However, in the case of lower mixing, we observe a larger concentration gradient between the two phases for the most part of the reactor. Hence, although bubble coalescence effects have the effect of retarding reactant transfer to the dense phase, this is offset by a larger concentration difference for most of the reaction length. The higher values of  $\mu$ ,  $\alpha$  and  $\beta$  for the case of lower dispersion coefficient contribute to an increased conversion ( $\omega$ ,  $k'$  are the same in both cases).

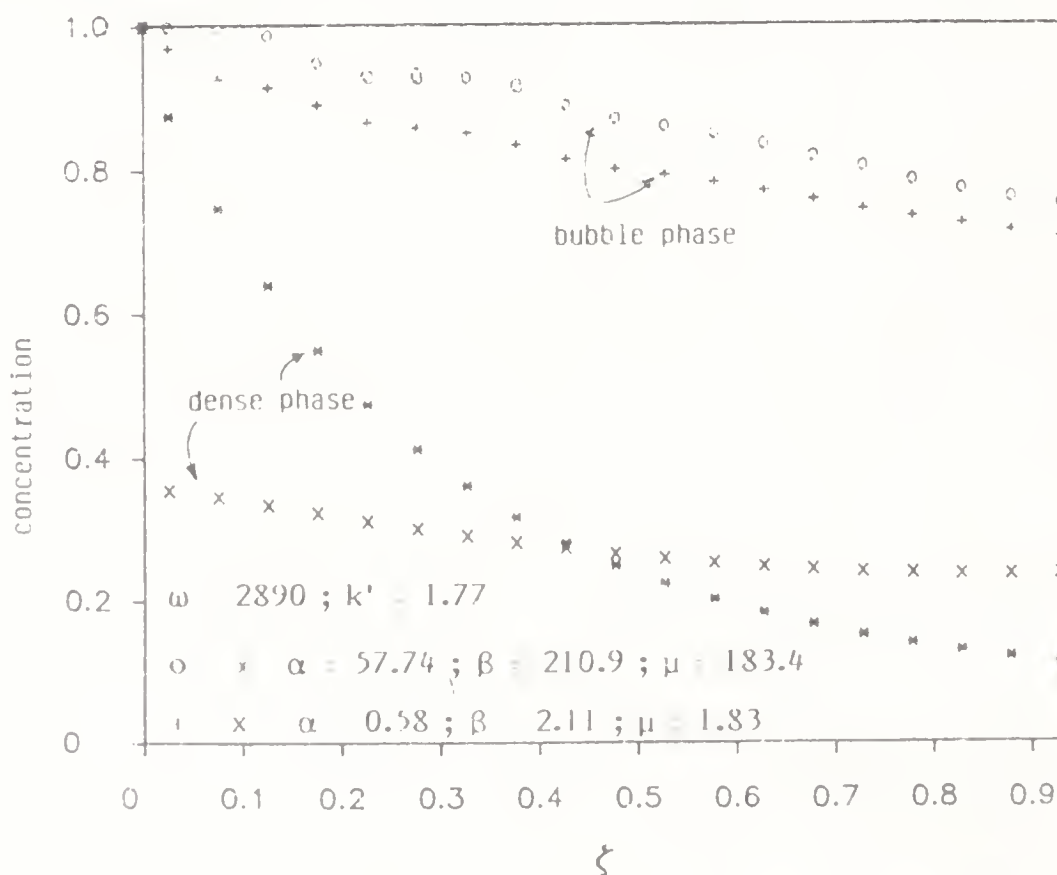


Figure 5. Concentration profiles for two dispersion coefficients

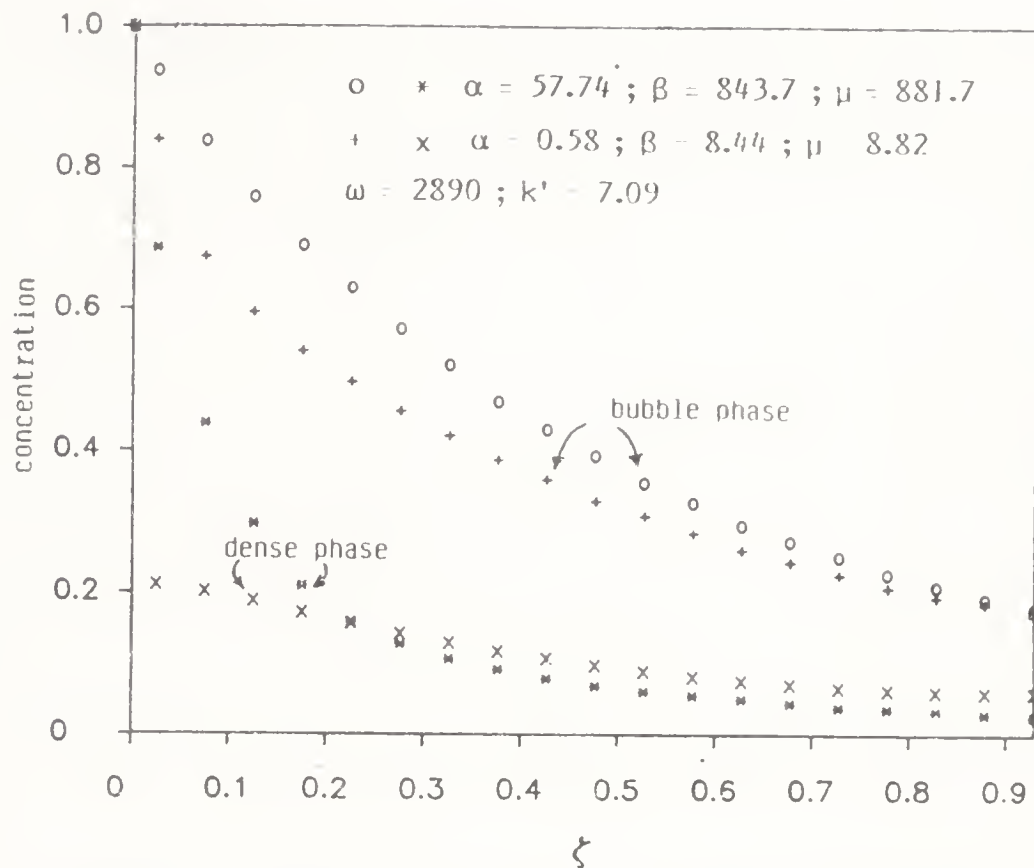


Figure 6. Concentration profiles for two dispersion coefficients.

Although the profiles differ quite significantly, the increase in conversion for decreased mixing was only about seven percent. In figure 5, the lowest mass exchange factor is considered. The trends are similar to the previous case with approximately seven percent increase in conversion on decreasing the level of mixing. The conversions are lower than the corresponding cases in figure 4 because the  $\mu$  values are greater in the latter case.

On changing the reaction rate constant,  $k$ ,  $\beta$  and  $k'$  change, while  $\alpha$ ,  $\beta$  and  $\omega$  remain unchanged. Figures 4 and 6 depict the effect of increasing rate constant on the reactor performance. As expected, the reactor conversion increases on increasing the rate constant. However, the change in reactor conversion on decreasing the dispersion coefficient was only two percent emphasizing that mixing effects become less important at higher reaction rates (a situation paradoxically at variance from that for homogeneous reactions).

Table 5 and figure 7 depict the exit concentrations predicted by this model along with those predicted in Part I. The predictions of the models of Davidson & Harrison (1963, 1971) are also shown. As expected, the exit concentrations predicted in this

Table 5. Exit concentrations predicted by different models.

$k'$	$\omega$	$\alpha$	$\beta$	$\mu$	$\xi'$ (model)	$\xi'$ (Part I)	$\xi'$ (Davidson & Harrison 1963)
1.0	2890	5.8	11.88	24.36	0.521	0.562	0.502
2.0	2890	5.8	23.75	24.36	0.395	0.438	0.338
5.0	2890	5.8	58.86	24.36	0.304	0.326	0.173
11.0	2890	5.8	130.5	24.36	0.274	0.273	0.093
19.0	2890	5.8	225.7	24.36	0.268	0.252	0.059
30.0	2890	5.8	356.2	24.36	0.263	0.241	0.041



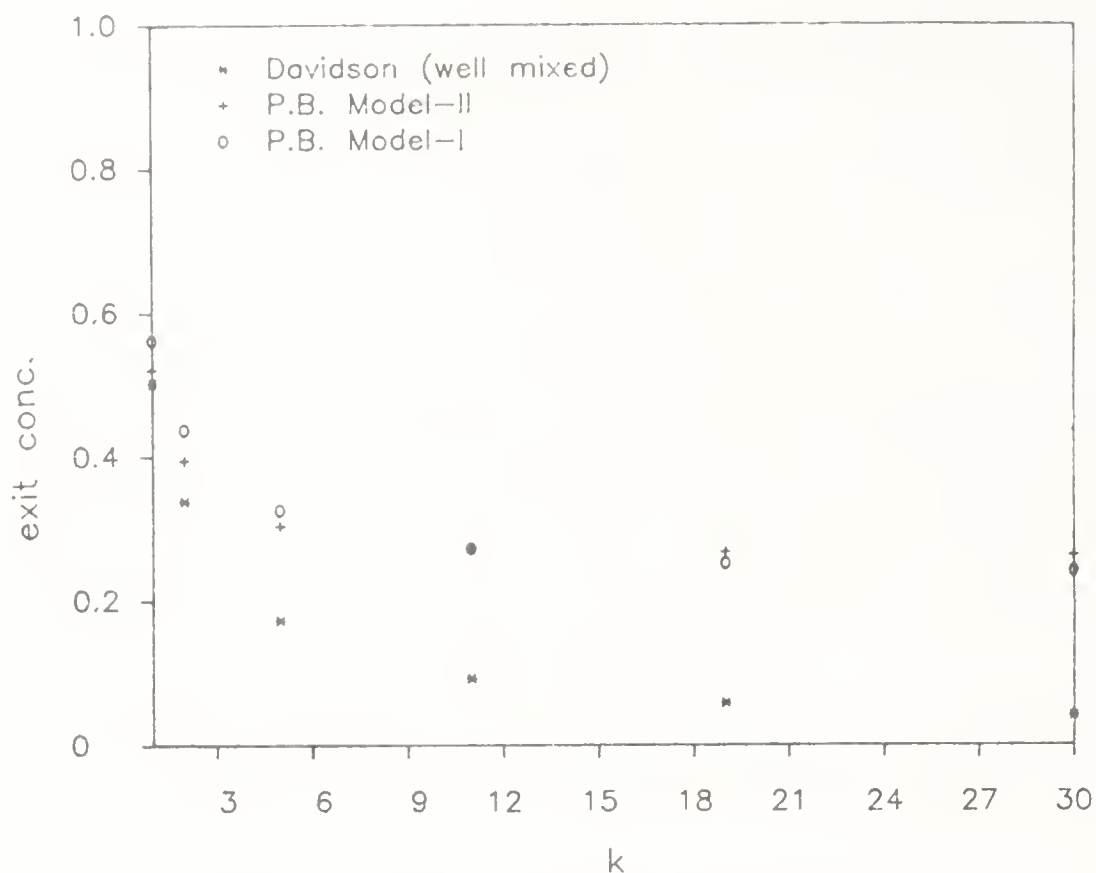


Figure 7. Exit concentration for different  $k'$ .

paper are smaller than the values predicted using the perfectly mixed dense phase in Part I of this paper. However for sufficiently large values of  $k'$ , the conversion obtained from a perfectly mixed dense phase exceeds that from an axially dispersed dense phase. This is due to the fact that in the perfectly mixed case, the reactant transfer from the smallest bubbles (of high interfacial area) to the dense phase is exploited better near the reactor inlet with a large concentration difference between the two phases. In other words, the perfectly mixed dense phase draws more reactant from the bubble phase as compared to the axially dispersed dense phase. Owing to the difficulties of relating mixing effects incorporated in the countercurrent back-mixing model and bubble assemblage model (see Yates 1983) with the axial dispersion coefficient, comparison of these models is difficult.

## 5. Summary and conclusions

A population balance model of a gas-solid fluidized bed is derived in §2 featuring an axial dispersion equation for the continuous phase and a population balance equation for the bubble phase. The model is ideally suited to describe bubble dynamics in a realistic manner. Mass exchange between the two phases couples the equations. The two equations are solved simultaneously by Monte Carlo simulation of the bubble population for an assumed dense phase concentration profile followed by successive approximation to determine progressively better estimates of the latter. Numerical examples are considered to illustrate the solution procedure. For the cases considered, coalescence proved significant in determining the overall reactor performance (figure 3). The effect of mixing was less significant and differences in conversion were only about seven percent for two values of the dispersion coefficient differing two orders in magnitude. The effect of mixing would

however be more significant at fluidizing velocities just greater than the minimum fluidizing velocity because of negligible reactant bypass with bubbles. The results of computation using high and low mass exchange rates show that the nature of mass exchange may not significantly affect the influence of mixing in terms of relative increase in conversion obtained on decreasing the dispersion coefficient. Further, at a higher reaction rate, the influence of mixing was further diminished (figure 6). A comparison of results with those in Part I (Sweet *et al* 1986) shows that for slow reactions the axially dispersed dense phases yield a higher conversion compared to a perfectly mixed dense phase. The opposite is true for sufficiently fast reactions. The conversions predicted differ significantly from those obtained using simple models such as that of Davidson & Harrison (1963, 1971) with a well-mixed dense phase. It is thus important to recognize the identity of the bubbles and not lump them as a homogeneous phase. In fact, the population balance model predicts that such a lumping is only reasonable at low coalescence numbers. The model can be extended to study non-isothermal reactions and to investigate the influence of mixing on the selectivity in complex first-order reaction mechanisms. Clearly, non-linear kinetics may also be accommodated by such simulations in which case convergence of the successive approximation scheme would be a special item of investigation. Large bubble populations place heavy burdens on computation so that *ad hoc* time-saving schemes will play an important compensating rule.

This paper is dedicated to Dr L K Doraiswamy on his sixtieth birthday. The authors gratefully acknowledge the National Science Foundation for an International Grant INT-8206424 which made this research possible. One of us (DR) is also grateful to the Indian Institute of Science, Bangalore, where part of this research was accomplished.

### List of symbols

$a$	interfacial area of bubble;
$c$	concentration of reactant in bubble;
$c_p$	concentration of reactant in the dense phase;
$c_0$	concentration of reactant in feed gas;
$\dot{C}$	rate of change of reactant concentration in the bubble;
$d_g$	gas phase diffusion coefficient;
$D$	axial dispersion coefficient;
$H$	height of bed;
$H_{mf}$	height of bed at incipient fluidization;
$k$	rate constant of reaction;
$k'$	dimensionless reaction rate constant;
$k_2$	constant in coalescence frequency;
$k_3$	shape factor for non-spherical bubbles;
$K_G$	mass transfer coefficient for reactant exchange with dense phase;
$f_1$	average number density function (product density of order 1);
$f_2$	average number of bubble pairs (product density of order 2);
$N_0$	number of bubbles per unit volume in feed;

$q$	gas exchange rate between bubble and dense phase;	
$Q$	coalescence frequency;	
$R$	factor defined in (4);	
$S$	bed cross-sectional area;	
$u$	bubble velocity;	
$U$	superficial velocity of fluidization;	
$U_{mf}$	superficial velocity at incipient fluidization;	
$v$	bubble volume;	
$v_{\max}$	maximum bubble volume;	
$\dot{V}$	rate of change of bubble volume;	
$z$	location measured from grid plate.	
$\alpha$	Peclet number;	
$\beta$	dimensionless number ( $kH_{mf}^2/D$ );	
$\delta$	Dirac delta function;	
$\xi$	concentration;	dimensionless
$\xi'$	overall exit concentration;	
$\eta$	bubble volume;	
$\dot{\eta}$	rate of increase of bubble volume;	
$\phi_1$	number density function;	
$\phi_2$	bubble pair density function;	
$\mu$	parameter in (17);	
$\chi$	exchange rate for bubbles;	
$\omega$	coalescence number defined in (13);	
$\zeta$	height of bubble location;	
$\dot{\zeta}$	bubble velocity.	

## References

- Argyriou D T, List H L, Shinnar R 1971 *AIChE J.* 17: 122–130  
Davidson J F, Harrison D 1963 *Fluidized particles* (Cambridge: University Press)  
Davidson J F, Harrison D 1971 *Fluidization* (London: Academic Press)  
Ramakrishna D 1981 *Chem. Eng. Sci.* 36: 1203–1209  
Ramakrishna D 1985 *Rev. Chem. Eng.* 3: 49  
Ramakrishna D, Amundson N R 1985 *Linear operator methods in chemical engineering with applications to transport and chemical reaction systems* (Englewood Cliffs, NJ: Prentice Hall)  
Ramakrishna D, Borwanker J D 1973 *Chem. Eng. Sci.* 28: 1423–1435  
Ramakrishna D, Shah B H, Borwanker J D 1976 *Chem. Eng. Sci.* 31: 435  
Shah B H, Ramakrishna D, Borwanker J D 1977a *Chem. Eng. Sci.* 32: 1419  
Shah B H, Ramakrishna D, Borwanker J D 1977b *AIChE J.* 23: 897–904  
Sweet I R, Gustafson S S, Ramakrishna D 1986 *Chem. Eng. Sci.* (in press)  
Yates J G 1983 *Fundamentals of fluidized-bed chemical processes* (London: Butterworths)



# Coking and regeneration of fixed bed catalytic reactors

R HUGHES, V DAKESSIAN and A BRITO-ALAYON\*

Department of Chemical and Gas Engineering, University of Salford, Salford M5 4WT, England

\* Present address: Departamento Quimica Tecnica, Universidad de La Laguna, Tenerife, Spain

**Abstract.** Coke concentration profiles have been determined by a non-invasive method for the catalytic reaction of xylenes over a silica-alumina bead catalyst. Coking was observed to be of the parallel type with the reactant xylene as the immediate coke precursor. Temperature profiles on regeneration of these coked reactors have been investigated experimentally and show that the maximum temperature increase occurs near the reactor inlet for this type of *coking*. The coke deposit has been analysed and found to have the composition  $\text{CH}_{0.55}$ ; this was reasonably uniform throughout the bed.

**Keywords.** Coking; catalyst regeneration; silica-alumina bead catalyst.

## 1. Introduction

During the operation of catalytic reactors the activity of the catalyst frequently decreases with time on stream. This deactivation may be due to a number of causes but coke deposition, or coking, of the catalyst is one of the most common of these. Coking presents a problem in that it occurs in side reactions to the main reaction and, therefore, in contrast to impurity poisoning and sintering, which can be minimised by feed purification and careful temperature control respectively, coking cannot be completely eliminated. Fortunately, if the catalyst has become coked, the coke deposit can usually be removed by oxidation at temperatures between 400 and 600°C, using a gas stream containing a small percentage of oxygen.

Because of the industrial importance of catalytic processes, many papers have been published on the subject of coking and regeneration in both fluidised and fixed bed reactors. Since fluidised beds can have continuous circulation of the catalyst in the reactor and regenerator sections and in addition have excellent heat transfer characteristics, deactivation due to coking can be overcome adequately. In fixed beds, however, the temperature rise on regeneration, caused by combustion of the coke on the catalyst, can become excessive if care is not exercised, with consequent sintering and loss of catalyst surface area.



Despite the attention directed to the problem of catalyst coking and regeneration, many areas of uncertainty remain. This is especially true of the nature of the coke deposits. The term "coke" represents many chemical species, the common factor being representation by the empirical formula  $\text{CH}_n$ . Values of  $n$  vary widely and Wolf & Alfani (1982) report experimental values from 0.1 to 1.8. This is hardly surprising as not only does  $n$  vary with the coke precursor but also depends on reaction temperature and time (Takahashi & Watanabe 1978; Plank & Nace 1955).

The morphology of coke may also be very different. Albright *et al* (1979) identified seven types of coke formed from the pyrolysis of light hydrocarbons and found that the surface on which the coke deposits is of major importance in determining the properties of the coke formed. The size of the coke aggregates deposited on the surface of the catalyst is also important since this may determine whether pore-blocking can occur (Mann *et al* 1984). Haldeman & Botty (1959) give the size of the aggregates as less than 10 nm, while Gavrilov *et al* (1983) and Hughes & Shettigar (1971) suggest that values of 3 nm and 4 nm are more usual. Recently Beeckman & Froment (1982) have adopted a statistical approach to incorporate the effects of both site coverage and plugged pore behaviour.

The form and distribution of the coke deposits may influence the regeneration behaviour. For example, if significant plugging of the pores by coke deposits occurs, regeneration behaviour may be significantly different from that with a more uniform distribution of the coke aggregates.

When the catalyst bed is regenerated it is vital to limit the temperature rise resulting from the combustion of coke. Numerous theoretical investigations have been made to predict temperature profiles resulting from regeneration under various conditions. Earlier investigations by Van Deempter (1953) using simplified kinetics established that movement of combustion and heat fronts occurred in the bed during the regeneration process.

This was confirmed by Johnson *et al* (1962) and by Schulman (1963), the former adopting an adiabatic model while the latter also included wall heat transfer terms in his model. All the above used a homogeneous model to describe the regeneration process, a procedure which was probably justified since Olson *et al* (1968) showed that the temperature difference between the solid surface and the gas was usually small. However, it was also shown that the combustion and temperature waves travelled downstream with time. Ozawa (1969) modelled the regeneration of a zeolitic bed of catalyst and at the lower temperature employed (420°C) showed that chemical control was now dominant and significant differences occurred for the temperature and concentration profiles between the bulk gas and the surface. Additionally, a minimum in the coke concentration profile was shown to occur.

Experimental work on catalyst regeneration has been much less. Johnson *et al* (1962) verified that temperature and concentration peaks traversed the bed, while Menon & Sreeramamurthy (1967) using the reaction between  $\text{H}_2\text{S}$  and oxygen also found that travelling reaction zone peaks occurred. On the other hand unpublished work in this laboratory has indicated that in certain circumstances travelling peaks do not always occur. The latter effect may be due to a number of factors, including flow rate, reactant concentration and temperature, but one possibility which has not been considered previously is the distribution of coke in the reactor.

All the above reported regeneration results assume that the coke is composed of carbon only and that the coke is uniformly distributed. If the coke has the composition  $\text{CH}_n$  it is important to allow for the hydrogen contribution to the overall combustion process. Whether the combustion of coke should be regarded as separate contributions by the hydrogen and the carbon components as suggested by Massoth (1967) or whether the coke combustion should be regarded as similar to that of a condensed hydrocarbon as suggested by Nascimento (1982) has still not been resolved.

The importance of coke distribution as a result of coking by reactions in parallel and series to the main reaction was first pointed out by Froment & Bischoff (1961, 1962). When coking occurs by a reaction in parallel with the main reaction, the coke concentration is greatest at the water inlet and decreases with distance from the water inlet. With series coking, the coke precursor is now the product and since the product concentration increases towards the reactor outlet, the coke profile will follow the same pattern. It is also important to recognise that average coke values for the whole reactor, obtained from analysing the oxides of carbon at the reactor exit, can be misleading. Thus a low overall value may disguise quite high coke concentrations in certain regions of the reactor and as the temperature rise during regeneration is dependent on the amount of coke present, the distribution of coke is very important.

## 2. Methods of determining coke distribution in a fixed bed catalytic reactor

Various methods have been adopted in the past to determine the coke distribution in a fixed bed reactor. The method generally used has been to remove pellets from known positions in the reactor and to analyse the coke by standard methods, such as oxidation to  $\text{CO}_2$  and water. The procedure is well documented by Richardson (1972). There are obviously problems with this approach, apart from the time consuming nature of the analysis when the whole reactor length has to be analysed. The major disadvantage of this method is that the bed is necessarily disturbed during this sampling process, and repacking the bed is often difficult, with the result that regeneration cannot be studied on the same bed as was used for determining the coke distribution. Use of a non-invasive, non-destructive technique for determining the coke distribution after the coking period, which can then be followed by the normal regeneration procedure on the same bed, would clearly enable a better understanding of the whole coking-regeneration cycle.

A technique has been developed by us in which the coke distribution in the fixed bed is determined by attenuation of a neutron beam at different axial positions along the reactor. Initial experiments using neutron radiography were found to be not completely satisfactory and were superseded by neutron counting measurements which gave much better results. The method is described fully elsewhere (Byrne *et al* 1985). Also, since this method depends on the hydrogen content of the coke, it is important to determine the coke compositional variation along the reactor length.

The present paper describes some results obtained using the non-invasive neutron technique to determine coke profiles and the effect of these non-uniform coke profiles on the resultant temperature profiles obtained during regeneration of



the fixed bed. Coking of the silica-alumina bead catalyst employed was achieved using a xylene feedstock.

### 3. Experimental

#### 3.1 Equipment

This consisted of a feed system, a preheater and the fixed bed reactor. The reactor was constructed from type 316 stainless steel tubing 0.6 m long and 25 mm i.d. with a wall thickness of 0.15 mm. An external heating element was removed prior to the neutron irradiations. Temperatures up to 600°C could be achieved over the whole effective length of the catalyst bed. Temperatures within the bed were measured using six Chromel-Alumel thermocouples, 0.5 mm in diameter and the maximum temperature variation of the bed under non-reactive conditions with a flow of nitrogen was found to be  $\pm 5^\circ\text{C}$ . The reactor was packed with 4–6 mm silica-alumina bead catalyst.

#### 3.2 Procedure

For the coking experiments the reactor was heated to the appropriate temperature (usually 400°C or higher) in a preheated stream of nitrogen. When the correct temperature had been attained the nitrogen stream was switched to a mixture of xylene in nitrogen. The xylene was vaporised prior to being carried into the reactor by the nitrogen stream. The coking operation was continued for various times and/or temperatures depending on the amount of coke deposition desired. The coked catalyst bed was then analysed for coke content and distribution using either a thermobalance or the neutron attenuation technique.

*3.2a Thermobalance experiments:* A conventional thermobalance was used to analyse the coke distribution in the catalyst bed in some experiments. To do this, the coked catalyst bed was divided into sections and a sample of each was oxidised at 550°C in the thermobalance using a synthetic air mixture (79%  $\text{N}_2$  : 21%  $\text{O}_2$ ). The water originally adsorbed on the catalyst was removed in the initial heating period by passing a nitrogen stream over the sample. When the sample achieved constant weight the 79% : 21%  $\text{N}_2/\text{O}_2$  mixture was substituted for the nitrogen. The loss in weight due to oxidation of the coke was recorded continuously, while the exit gases were passed through infrared analysers to determine the amounts of carbon dioxide and carbon monoxide evolved during the oxidation. The hydrogen content of the coke was determined by measuring the water produced in an independent gravimetric experiment.

*3.2b Neutron attenuation experiments:* A collimated neutron beam of wavelength 0.15 nm from the DIDO reactor at AERE, Harwell, was passed through different sections of the coked reactor. Attenuation of the neutron beam occurred from which the amount of coke deposited could be estimated using a neutron counting technique. In this method a boron trifluoride counter was employed, the counter being fitted with a ceramic end window. The exposure time per sample count was

10 seconds and an average of 8 independent counts were taken for each section of the catalyst bed.

The neutron attenuation method exploits the fact that the slow-neutron-scattering cross-section,  $\sigma$ , for a proton is substantially higher than that for any other element likely to be found in a tubular catalytic reactor. The determination of coke thus depends on there being hydrogen present in the coke; the validity of this is confirmed below. The theory has been presented in full elsewhere (Byrne *et al* 1985). Briefly, for two initially identical, catalyst-filled reactor tubes, one of which has been subjected to coking, the ratio of the transmissions of the two tubes,  $I_1/I_2$ , at a specific axial position is given by

$$I_1/I_2 = \exp\left[-tN_{\text{CH}_n} \sigma_{\text{CH}_n}^T\right],$$

where  $\text{CH}_n$  is the atomic composition of the coke,  $t$  the specimen thickness,  $N$  the number of  $\text{CH}_n$  species and  $\sigma_{\text{CH}_n}^T$  the total cross-section (scattering and absorption of the species  $\text{CH}_n$ ). Since  $t$ ,  $\sigma_C^T$  and  $\sigma_H^T$  are known,  $\sigma_{\text{CH}_n}$  can be estimated if  $n$  is known. This was determined for the coked catalyst as described below.

**3.2c Regeneration of the catalyst bed:** The coked reactor was heated to the regeneration temperature with nitrogen flowing through the bed. When the required steady state temperature was attained, the nitrogen flow was discontinued and an air or air/nitrogen supply was switched to the reactor. Temperature changes were continuously monitored and recorded by a data logger and microprocessor at a minimum of six axial positions, using the 0.5 mm Chromel-Alumel thermocouples. Simultaneously, the carbon dioxide and carbon monoxide concentrations in the exit stream were monitored during the oxidation by the use of the infrared gas analysers. A combination of valves positioned between the gas analysers and the reactor outlet ensured that equal amounts of gases passed through the analysers.

## 4. Results

### 4.1 Composition of coke

It was essential to establish this in order to determine the value of  $n$  in the coke species,  $\text{CH}_n$ . Even though the ratio of hydrogen/carbon of coke has been widely reported in the literature for some reactions under different conditions (often using only small amounts of catalyst) there has been no published work on the variation of this ratio along a deactivated bed. Due to the sensitivity of the neutron counting technique to this hydrogen/carbon ratio, it was important not only to evaluate this ratio but also to measure its variation along the axial direction.

A catalyst bed deactivated under similar conditions as those used in the deactivation experiments was divided into equal sections and analysed as mentioned in the experimental section.

To check that an average value for the hydrogen/carbon ratio can be used, the neutron counting results obtained for one experiment were processed by two different means. First, the average value for the hydrogen/carbon ratio was used to obtain the coke profiles along the reactor. Secondly, a new coke profile was obtained by changing the values of the hydrogen/carbon ratio for each position of



**Table 1.** Hydrogen/carbon ratio as a function of position in reactor tube for the xylene coked catalyst.

Position in reactor (m)	H/C ratio	Coke (%)
0.05	0.64	0.75
0.15	0.59	0.50
0.25	0.53	0.30
0.35	0.54	0.26
0.45	0.46	0.20
0.55	0.52	0.18

the reactor according to the results in table 1 below. These ratios were obtained by gravimetric chemical analysis as described above. The differences obtained in the coke profiles were negligible. Therefore, a constant value of H/C ratio of 0.55 has been used throughout this work. The H/C ratio obtained for xylene as the coke precursor is close to the value of 0.5 reported for xylene coking by Takahashi *et al* (1978) for an equivalent reaction temperature.

#### 4.2 Coke profiles by neutron counting

Coking was accomplished by feeding a premixed reactant-nitrogen stream over a fixed bed of the catalyst. The flow rates used were 3 ml of xylene/min in a carrier gas of 1000 ml/min of nitrogen. Reactor temperatures during the coking period were 457 or 477°C.

The profiles obtained after coking were determined by neutron attenuation using a BF<sub>3</sub> detector as the neutron counter. It is important that the profiles obtained by neutron attenuation be checked independently. In order to do this, subsequent to one neutron irradiation experiment, different sections of the catalyst bed were removed from the reactor tube and analysed by oxidising the coke deposit and determining the weight change using the thermobalance. From this the percentage of coke on the catalyst could be estimated and the results so obtained compared to the profile estimated from the neutron attenuation results. A comparison is given in figure 1, which shows that the agreement between the two sets of results is, on the

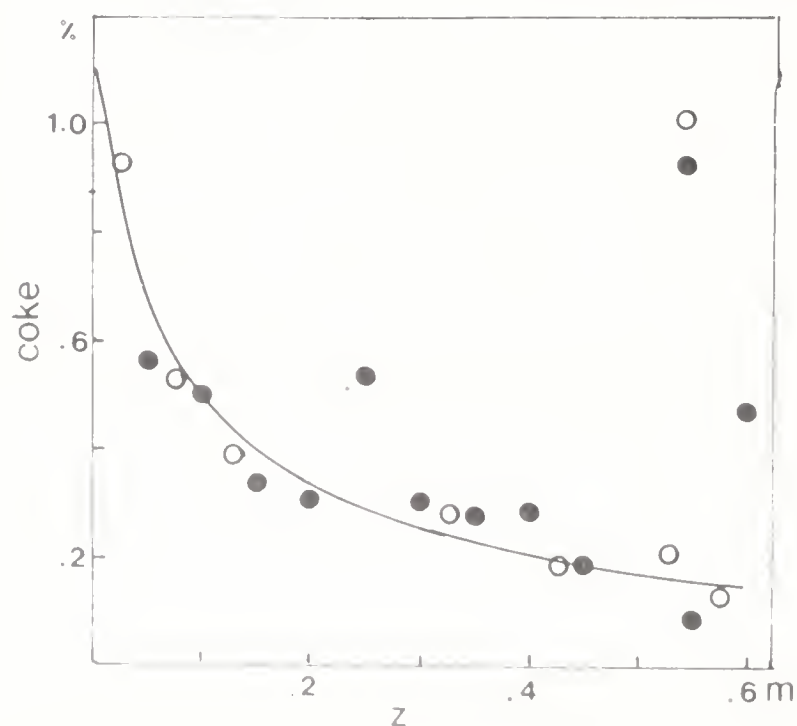


**Figure 1.** Comparison of coke profiles by neutron attenuation and weight loss methods (● Neutron counting; ○ thermobalance)

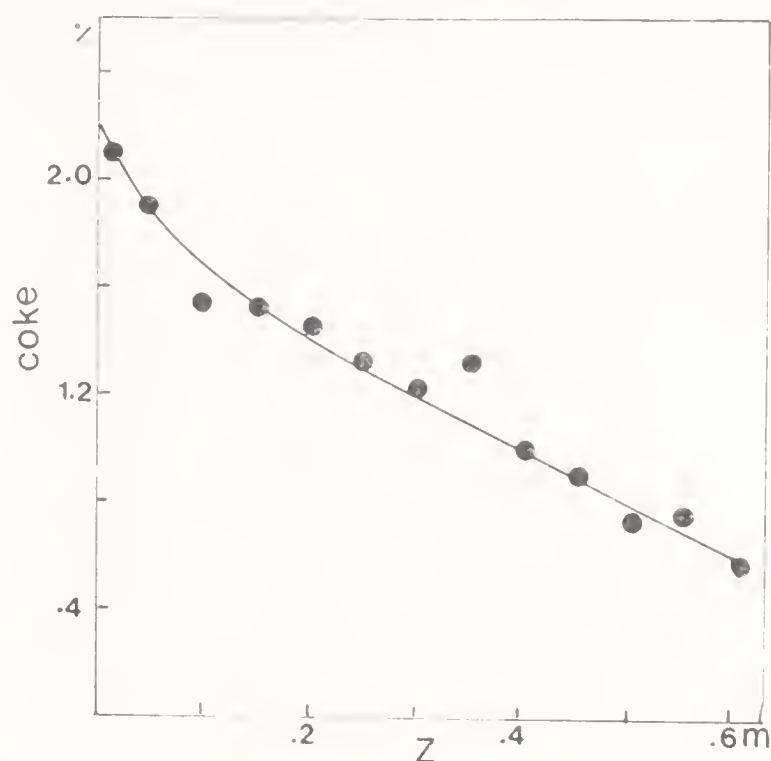


Figure 2. Experimental coke profile determined by neutron attenuation. Inlet temperature 457°C; deposition time 6 hr.

whole, good. The major exception is the result at the reactor exit (0.6 m); this high value could be explained by a ring of coke which was found to have deposited on the inside of the reactor tube at this point. This deposit would give a higher reading for the neutron attenuation while not influencing the thermobalance test on the catalyst pellets.

Figures 2 and 3 show coke profiles obtained by the neutron method. Both exhibit the characteristic of parallel fouling, with the coke deposit greatest at the reactor inlet and decreasing monotonically with distance towards the reactor exit. Thus the coking of the silica-alumina catalyst by xylene proceeds by a parallel mechanism.

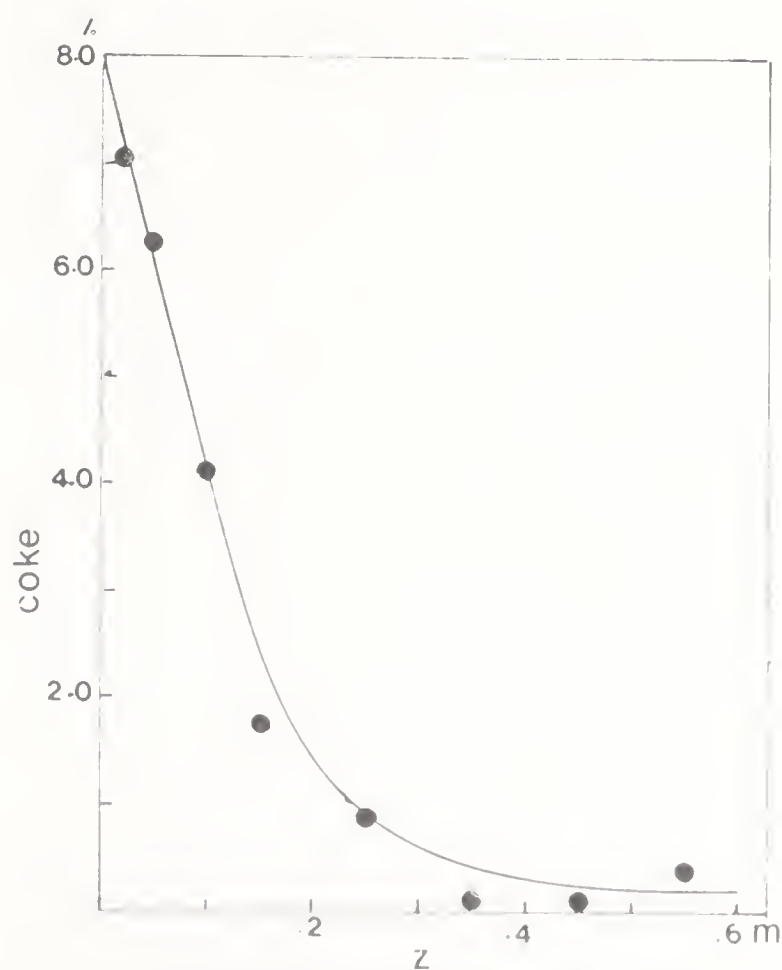


Figure 3. Experimental coke profile determined by neutron attenuation. Inlet temperature 474°C; deposition time 6 hr.

Coke levels of between 1 and 2% averaged over the whole bed were obtained which were substantiated by the measurement of  $\text{CO}_2$  and CO evolved when each bed was regenerated.

Figure 2 shows the profile obtained when the reactor was coked by xylene at a temperature of  $457^\circ\text{C}$  for a period of 6 hours. The initial coke deposit was 2.3% at the reactor inlet and decreased continuously with distance along the reactor until at 0.6 m from the front of the bed, the coke concentration had decreased to 0.6%. The average coke level along the reactor was 1.26%. This experiment was repeated under identical conditions and the average coke level was found to be 1.29%, and with a slightly increased maximum of 2.6% at the reactor inlet. However, in view of the small differences in catalyst packing which could occur, the agreement is good and shows that the method gives reproducible results.

On raising the overall reactor temperature to  $474^\circ\text{C}$ , larger amounts of coke were deposited especially at the inlet of the reactor as figure 3 shows. Again the time of coking was 6 hours and it can be observed that under these conditions the high initial coke level is followed by a very steep decrease in coke deposition. In this experiment the coke concentration dropped to a very low value 0.35 m from the reactor inlet. Despite the high inlet value of 8% coke the average coke concentration in the bed was 1.65%.

### 4.3 Regeneration results

**4.3a Coke levels:** The reactor tubes, which had been coked and subsequently irradiated to determine the coke profile, were not disturbed physically by this method, so it was possible to perform the regeneration experiments on the whole catalyst bed with the coke profiles now well established.

During the regeneration experiments the amounts of  $\text{CO}_2$  and CO evolved were monitored continuously and the areas under the curves were used to evaluate the amounts of carbon deposited on the catalyst. The average carbon concentrations calculated by this means were in fair agreement with the coke results obtained by neutron counting as can be seen from a comparison of columns 1 and 2 in table 2. To obtain the average coke concentration from these carbon percentages it is necessary to know the composition of the coke. From table 1 and the discussion of the results obtained an average coke composition of  $\text{CH}_{0.55}$  was obtained which was assumed to be constant throughout the bed. Using this result the coke percentages in column 3 of table 2 were obtained and it can be seen that much closer agreement is now obtained between the neutron counting and analyser results.

**Table 2.** Comparison of neutron counting and carbon oxides analysis for average coke and carbon content.

Run number	1 % coke using counting	2 % carbon using $\text{CO}$ , $\text{CO}_2$ analysers	3 % coke from 2 using $\text{CH}_{0.55}$
2	1.26	1.04	1.09
3	1.29	1.10	1.15
4	1.65	1.48	1.55
5	1.95	1.82	1.90



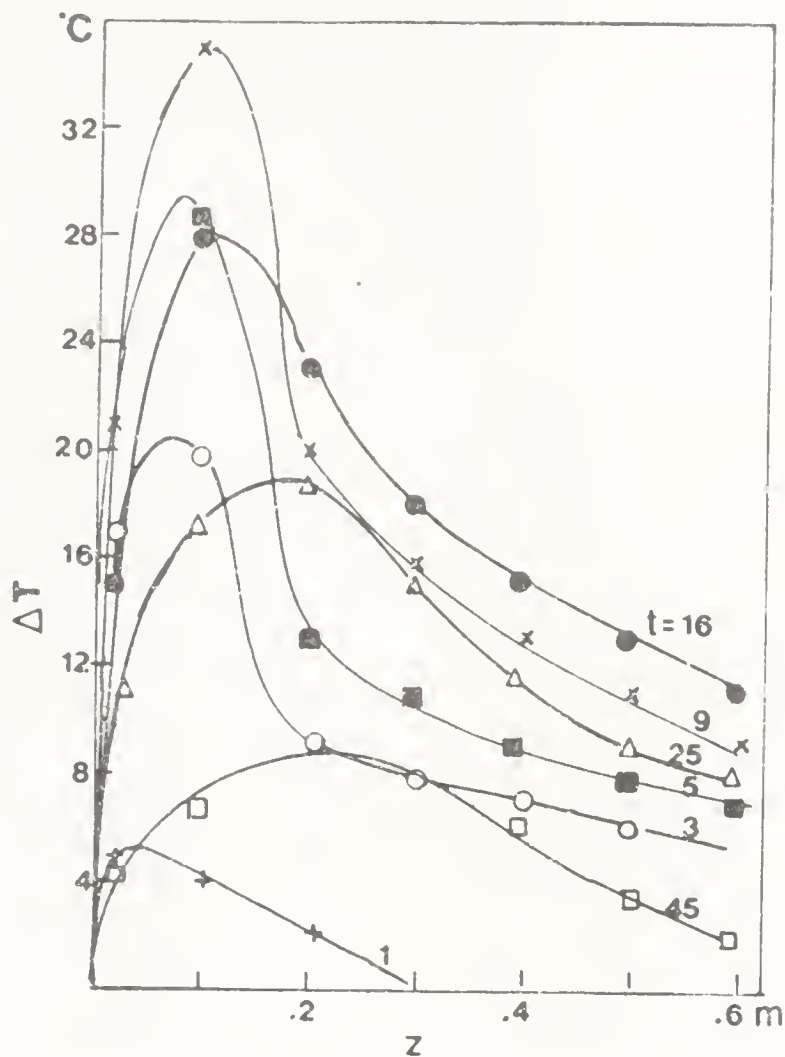


Figure 4. Temperature profiles during regeneration of coked reactor corresponding to figure 2.  $T = 525^{\circ}\text{C}$ ; flow =  $1.0 \times 10^{-3} \text{ m}^3/\text{min}$  of 21%  $\text{O}_2$ :79%  $\text{N}_2$  (+ = 1 min, O = 3 min, ■ = 5 min, X = 9 min, ● = 16 min, △ = 25 min, □ = 45 min).

4.3b *Temperature profiles during regeneration:* The regenerations were carried out using the 21%  $\text{O}_2$ , 79%  $\text{N}_2$  mixture at a flow rate of  $10^{-3} \text{ m}^3/\text{min}$ . All experiments were conducted at the initial bed temperature of  $525^{\circ}\text{C}$ , so that the only variable was the coke distribution along the reactor.

Figure 4 shows the axial distribution of temperature at various times for the regeneration of the coked reactor, the profile of which was illustrated in figure 2. The average coke concentration in this case was about 1.3%. A maximum temperature rise of  $35^{\circ}\text{C}$  occurred at a time of 9 minutes at a point about 0.1 m from the reactor inlet. The chief characteristic of the temperature profiles observed is that the high temperature observed in the inlet portion of the reactor is followed by a relatively low increase in temperature towards the end of the bed. This is a consequence of the small amount of coke present in this region of the bed. Another feature observed is that the maximum temperature tends to propagate downstream during the regeneration. This could be explained by the existence of a relatively narrow combustion zone where coke burn-off occurs and which slowly moves downstream during the regeneration period. The regenerative heating of the combustion gas, as it passes over the portion of the bed from which the coke has been burnt (but still retains heat), results in a build-up of the temperature profile as this moves through the bed.

The maximum value of the temperature obtained ( $35^{\circ}\text{C}$ ) is in broad agreement with the result observed by Sampath (1975) of  $40^{\circ}\text{C}$ . This was obtained for an average initial coke level of 1.2% when the regeneration was carried out at this same reactor temperature of  $525^{\circ}\text{C}$ .

The temperature profiles obtained when the reactor containing the coke profile



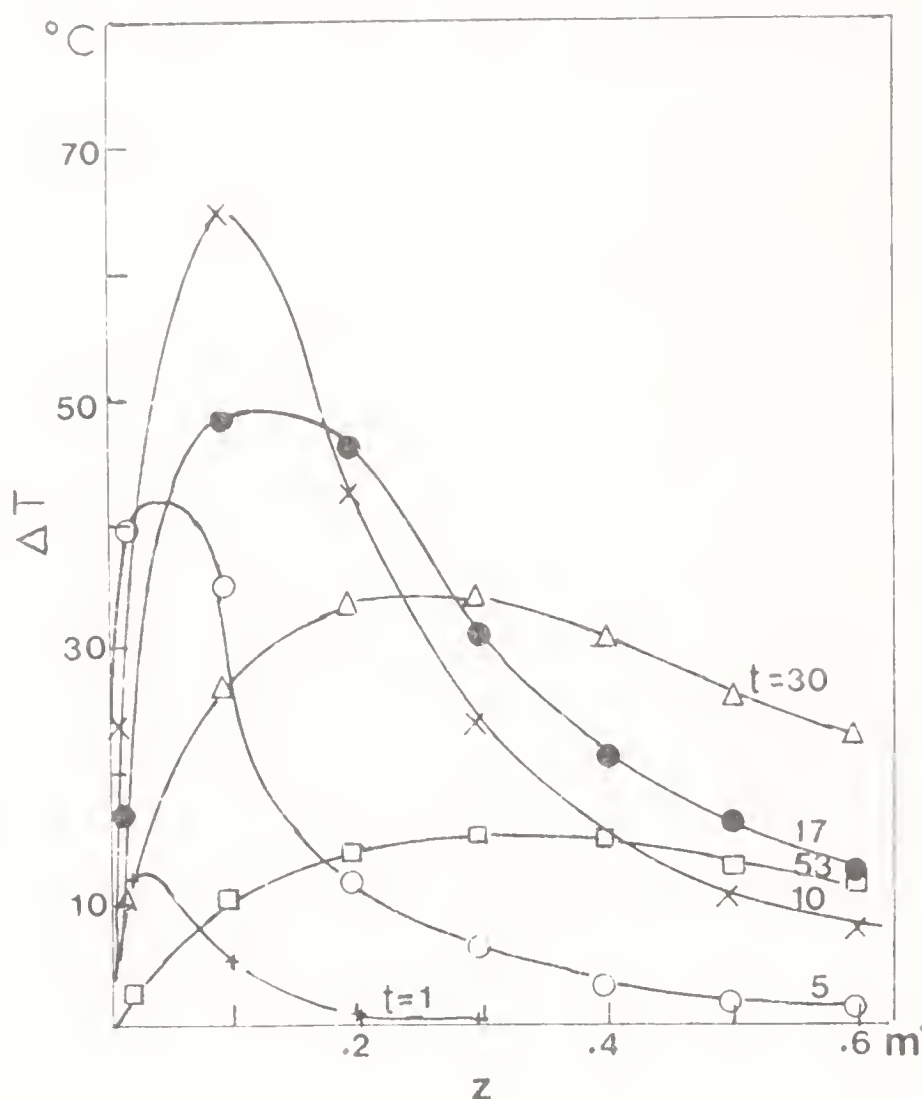


Figure 5. Temperature profiles during regeneration of coked reactor corresponding to figure 3.  $T = 525^{\circ}\text{C}$ ; flow =  $1.0 \times 10^{-3} \text{ m}^3/\text{min}$  of 21%  $\text{O}_2$ :79%  $\text{N}_2$  (+ = 1 min. O = 5 min, x = 10 mins, • = 17 mins,  $\Delta$  = 30 mins,  $\square$  = 53 mins).

given in figure 3 was regenerated are illustrated in figure 5. Because of both the higher average coke level and the high percentage of coke at the bed inlet (8%), the maximum temperature rise is now much higher at  $65^{\circ}\text{C}$ . A comparison with figure 4 demonstrates that the peak temperature occurs at approximately the same point, 0.1 m from the reactor inlet, and occurs at almost the same time of about 9 to 10 minutes. The moving maximum is now more pronounced, however, although the profiles reflect the same general shape as in figure 4. Again the maximum temperature attained is in reasonable agreement with previous work; Parvinian (1977) observed a maximum temperature rise of  $78^{\circ}\text{C}$  for an average coke concentration of 2.16% at an initial bed temperature of  $525^{\circ}\text{C}$ .

To compare the manner in which the maximum temperature changes with time irrespective of bed position, maximum temperatures have been plotted against time corresponding to the regenerations in figures 4 and 5. The resulting curves are shown in figure 6. Both curves show the same features with a very fast rise in the maximum temperature caused by the larger concentration of coke at the inlet of the catalyst bed, followed by a more gradual decrease following the peak temperature. The peak temperatures occur at approximately the same time as noted above but the maximum temperatures attained are quite different. As expected, the higher coke concentration gives the larger temperature rise but it should be noted that from these results there is no direct proportionality between the maximum temperature rise and either the average or the maximum coke concentrations. Thus while the maximum temperature rises are in the ratio 1.86:1 the average coke concentrations are only 1.31:1, while the maximum coke concentrations are in the ratio 3.64:1. This illustrates the difficulty in deriving any direct proportionality

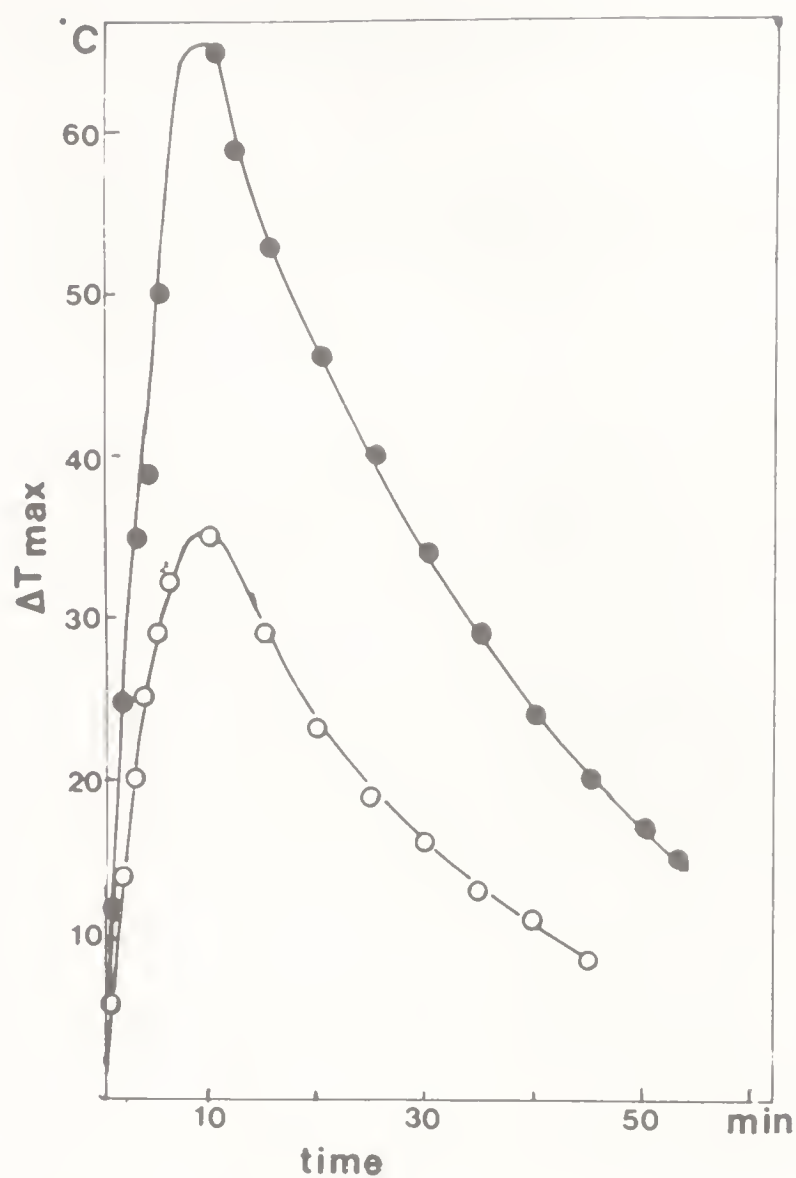


Figure 6. Effect of coke concentration on maximum temperature profiles (○ corresponding to regeneration in figure 4; ● corresponding to regeneration in figure 5).

relationship between coke concentrations and maximum temperatures in the reactor, even when the coke profile is well established.

## 5. Conclusions

By use of a newly developed non-invasive technique, the pattern of coke deposition for a fixed bed reactor has been established under various conditions when employing the reaction of xylene over a silica-alumina bead catalyst. It has been established unequivocally that coking with xylene occurs by a parallel mechanism with xylene acting as the coke precursor. Under these conditions most of the coke is deposited at or near the inlet to the reactor.

From these known coke reactor profiles, regenerations of the catalytic reactors have been carried out under well-defined conditions. The temperature profiles so obtained have been related to the corresponding coke profiles and certain general features have emerged. A well-defined maximum temperature developed rapidly near the reactor inlet, which subsequently diminished with elapsed time, giving ultimately a broad shallow maximum situated approximately at the mid-point of the reactor.

The composition of the coke has also been determined and, for the present set of conditions using xylene as coking agent, the coke composition is given by the empirical formula  $\text{CH}_{0.55}$ . This composition does not change significantly with

position in the reactor, thus enabling the coke profile determination to be carried out with confidence.

This paper is dedicated to Dr L K Doraiswamy on his sixtieth birthday. We gratefully acknowledge the financial support of the SERC for this work.

## References

- Albright L F, McDonnell C F, Welther C 1979 *Adv. Chem. Ser.* 183: 175–184
- Beeckman J W, Froment G F 1982 *Ind. Eng. Chem. Fundam.* 21: 243–250
- Byrne A, Dakessian V, Hughes R, Santamaria-Ramiro J M, Wright C J 1985 *J. Catal.* 96: 146–168
- Froment G F, Bischoff K B 1961 *Chem. Eng. Sci.* 16: 189–201
- Froment G F, Bischoff K B 1962 *Chem. Eng. Sci.* 17: 105–114
- Gavrilov V Y, Ferelov V B, Rachkovskaya L N 1983 *Kinet. Catal. (Eng. Transl.)* 24(5): 977–981
- Haldeman R G, Botty M C 1959 *J. Phys. Chem.* 63: 489–496
- Hughes R, Shettigar U R 1971 *J. Appl. Chem. Biotechnol.* 21: 35–38
- Johnson B H, Froment G F, Watson C C 1962 *Chem. Eng. Sci.* 17: 835–848
- Mann R, El-Kady F Y A, Moore I R 1984 8th Int. Symp. Chem. Reaction Eng., Edinburgh, Inst. Chem. Eng. Symposium Series, 87: 25–32
- Massoth F E 1967 *Ind. Eng. Chem., Process Des. Dev.* 6: 200–207
- Menon P G, Sreeramurthy R 1967 *J. Catal.* 8: 95–97
- Nascimento C A O 1982 Ph.D. thesis, University of Salford
- Olson K E, Luss D, Amundson N R 1968 *Ind. Eng. Chem., Process Des. Dev.* 7: 96–100
- Ozawa Y 1969 *Ind. Eng. Chem., Process Des. Dev.* 8: 378–383
- Parvinian M 1977 Ph.D. thesis, University of Salford
- Plank C J, Nace D M 1955 *Ind. Eng. Chem.* 47(11): 2374–2379
- Richardson J T 1972 *Ind. Eng. Chem., Process Des. Dev.* 11: 8–11
- Sampath B S 1975 Ph.D. thesis, University of Salford
- Schulman B L 1963 *Ind. Eng. Chem.* 55(12): 44–52
- Takashi T, Watanabe K 1978 *J. Jpn. Pet. Inst.* 21(2): 85–92
- Van Deempter J J 1953 *Ind. Eng. Chem.* 45: 1227–1238
- Wolf E E, Alfani F 1982 *Catal. Rev. Sci. Eng.* 24: 329–371

# A comparative study of mathematical models for gas-solid non-catalytic reactions

M S ANANTH<sup>1</sup> and VINOD JALAN<sup>2</sup>

<sup>1</sup>Department of Chemical Engineering, Indian Institute of Technology, Madras 600 036, India

<sup>2</sup>Electrochem, 400 W Cummings Park, Woburn, MA 01801, USA

**Abstract.** Experimental data on desulphurisation of a simulated coal gas mixture containing 200 ppm H<sub>2</sub>S, using CuO/ZnO mixed oxide sorbent in a fluidised bed reactor, are used to evaluate four representative structural models for gas-solid non-catalytic reactions. The four models chosen for evaluation are the spherical changing-grain-size model of Georgakis and co-workers, the rectangular grains version of the general formulation of Szekely and co-workers, the single-pore model of Ramachandran and Smith and the random pore model of Bhatia and Perlmutter. All the model parameters except the reaction rate constant are calculated from experimental measurements or from literature correlations. The rate constant alone is adjusted so as to obtain good agreement between the model and the experiment. It is shown that at any given temperature all the models describe the data well. However, the random pore model predicts conversions lower than experiment at large times while the rectangular grains model predicts conversions higher than experiment for small times. The rate constants decrease as temperature increases indicating an inadequacy of all the models in this regard. The models also predict much smaller variations in conversion with change in particle size than those observed experimentally.

**Keywords.** Gas-solid reactions; non-catalytic reactions; mathematical models; hot gas desulphurisation.

## 1. Introduction

Non-catalytic gas-solid reactions have received considerable attention in the last three decades. Major mathematical developments in the area have been reviewed in a book (Szekely *et al* 1976) and in an edited monograph (Sohn & Wadsworth 1979). Ramachandran & Doraiswamy (1982) presented a comprehensive critical



review of the modelling of non-catalytic gas-solid reactions. The major applications are in both the chemical and the metallurgical industries. A recent application is in the context of fuel cells. Molten carbonate fuel cell power plants appear to provide the most attractive method for converting coal or other fossil fuels to electricity. However, the successful development of molten carbonate cells, especially their integration with a coal gasifier, requires the removal of hydrogen sulphide from fuel gases down to one ppm or lower levels. The desulphurisation of fuel gases is usually carried out as a two-stage process, the first stage reducing  $\text{H}_2\text{S}$  from about 6000 ppm to about 200 ppm and the second stage from 200 ppm to one ppm or lower. One of the promising sorbents for this secondary high temperature desulphurisation is a mixed oxide of  $\text{CuO}/\text{ZnO}$  (Jalan 1983).

In this paper, a few experimental results are presented for the desulphurisation of a simulated coal gas mixture containing 200 ppm  $\text{H}_2\text{S}$  using a  $\text{CuO}/\text{ZnO}$  mixed oxide sorbent in a fluidized bed reactor. The results include the effects of changes in particle size, initial water concentration in the gas and temperature on the solid conversion.

Several mathematical models have been proposed to interpret laboratory data on gas-solid reactions. In this paper the experimental data are interpreted using different representative models. As far as possible parameters in the different models were estimated using literature correlations and independent measurements. The models are compared with one another in so far as they are capable of interpreting the different physical phenomena that are observed in the experiments.

## 2. Experiment

The fluidized bed reactor used is schematically shown in figure 1. The reactor consisted of a quartz tube 5 cm in diameter. A coarse quartz frit served as the gas distributor. The reactor was heated over 60 cm of its length with the distributor located in the isothermal region of the heated zone. Fines were entrained using a loose wad of quartz wool. The sorbent studied was a  $\text{CuO}/\text{ZnO}$  mixed oxide (G 66 B, United Catalysts Inc.) of mean chemical composition:  $\text{CuO}$  33%,  $\text{ZnO}$  65%,  $\text{Al}_2\text{O}_3$  2%. Table 1 summarizes the properties of the sorbent. The sorbent, supplied in the form of tablets, was ground to different-sized particles for the experiments. Particle sizes varied from 450 microns to 250 microns. Temperature

**Table 1.** Chemical and physical properties of  $\text{ZnO}/\text{CuO}$  sorbent (G66B, United Catalysts Inc.).

Chemical composition	$\text{CuO } 33 \pm 3$ , $\text{ZnO } 65 \pm 3$ , $\text{Al}_2\text{O}_3$ 2(max), S 0.04(max), Na 0.10(max)
Bulk density	$1.32 \pm 0.08$ g/cc
Surface area	30–60 $\text{m}^2/\text{g}$
Pore volume	0.22 cc/g
Pore diameter	0.01 cc/g in the range 175–0.08 $\mu$ 0.19 cc/g in the range 0.08–0.014 $\mu$ 0.02 cc/g in the range 0.014–0.0029 $\mu$
Particle size	450 $\mu$ , 250 $\mu$
Diluent	80% $\text{Al}_2\text{O}_3$
Solid density	4.33 g/cc

$\text{ZnO}/\text{CuO}$  concentration in particle,  $\rho_B = 0.00612$  g mol/cc

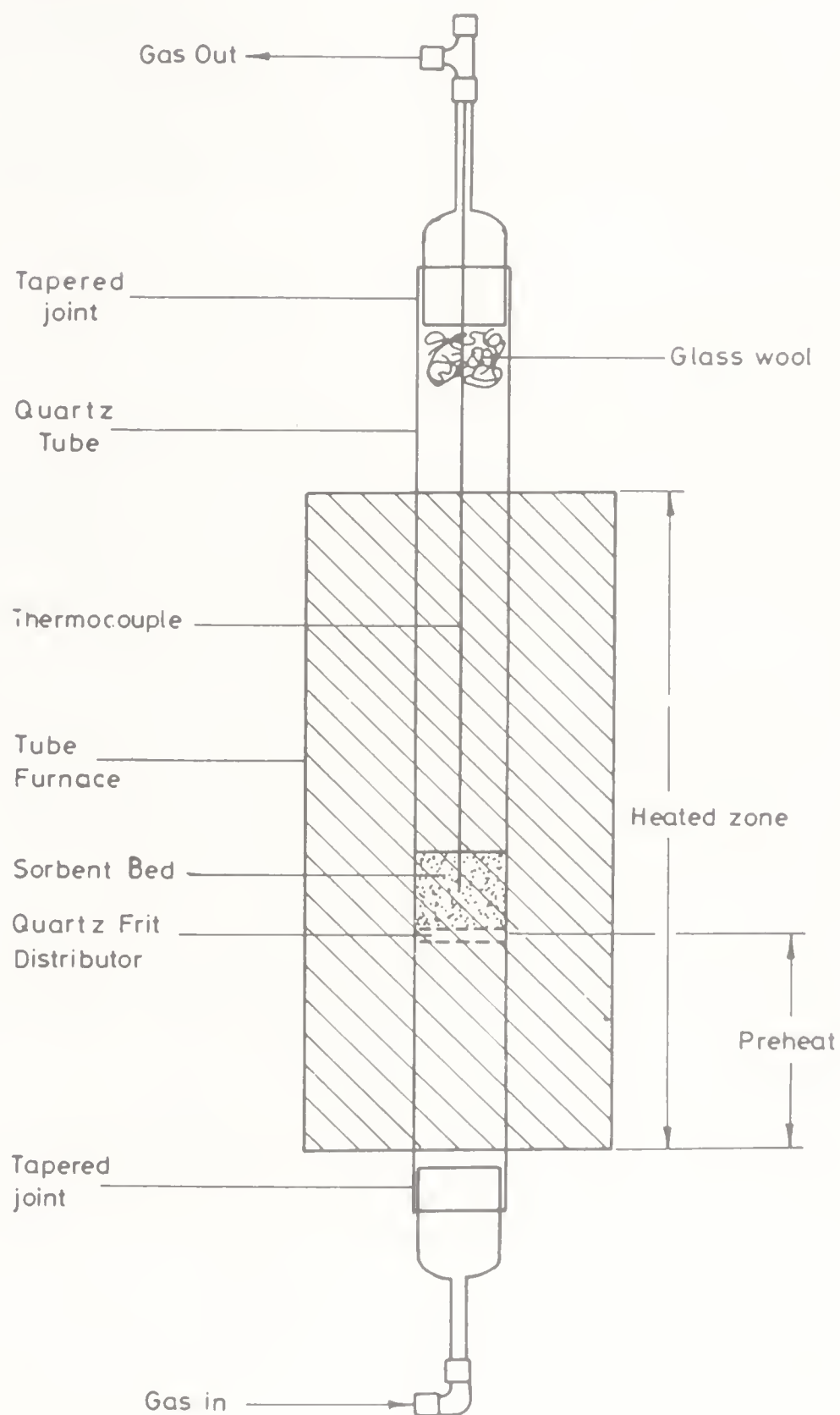


Figure 1. Fluidized bed reactor.

was varied from 650°C to 500°C. Water content in the inlet gas was varied from 26% to 9%. In all the experimental runs the bed was a mixture of 80% inert  $\text{Al}_2\text{O}_3$  and 20% active  $\text{ZnO/CuO}$  material. All the experiments were carried out with a simulated coal gas mixture (25.8%  $\text{H}_2$ , 47.2%  $\text{N}_2$ , 15.5%  $\text{CO}_2$  and 11.5%  $\text{CO}$  on dry basis) containing 200 ppm  $\text{H}_2\text{S}$  and varying quantities of  $\text{H}_2\text{O}$ . The desulphurisation runs were carried out until the exit  $\text{H}_2\text{S}$  concentration was between 14 and 20 ppm.

Further details of these experiments as well as other extensive studies involving high temperature desulphurisation/regeneration reactions of metal oxides have been reported elsewhere (Jalan 1983). The purpose of this presentation is to compare the ability of different representative models of gas-solid non-catalytic reactions to correctly interpret the data presented here. Table 2 is a summary of the conditions of these runs.

### 3. Experimental observations

The important experimental observations that are of special relevance to the selection and evaluation of representative models are as follows:

- (i) The CuO/ZnO mixed oxide particle was highly porous. The particles had an average initial pore volume of  $0.22 \text{ cm}^3/\text{g}$  and a very large average specific surface area of  $45 \text{ m}^2/\text{g}$  suggesting an average initial pore diameter of about  $200 \text{ \AA}$ . This means both molecular and Knudsen diffusion will play a role in mass transfer into the pores.
- (ii) The molal density ratio,  $Z$ , of the product ZnS/CuS to the reactant ZnO/CuO is about 1.6. This means that the structural changes due to reaction are significant. This has also been established using electron microscopy of the sorbent in the sulphided and regenerated states. During sulphidation, a finer grain structure develops due to the creation of relatively fine crystallites of the sulphided metals, copper and zinc. After oxidative regeneration the coarse open pore structure is re-established.
- (iii) All the experiments were carried out under isothermal conditions. So the energy balance need not be considered in the analysis as an integral part of the modelling exercise.
- (iv) Sintering was not at all significant during sulphidation although it was one of the major causes for loss of surface area during regeneration.
- (v) Kinetic studies of the ZnO-H<sub>2</sub>S reaction using powdered samples of reagent grade ZnO have been reported (Westmoreland *et al* 1977). The reaction was found to be first-order with respect to H<sub>2</sub>S concentration with a rate constant given by

$$k = k_0 \exp[-E/RT] = 94.6 \exp(-7236/RT).$$

The units of  $k$  are  $\text{cm}^4/\text{g mol min}$ .

No kinetic data are available for the mixed-oxide-H<sub>2</sub>S reaction.

**Table 2.** Summary of desulphurisation tests in fluidized bed reactors that have been analysed in this paper

Run number	Sorbent weight (g)	Particle size ( $\mu$ )	Temperature ( $^{\circ}\text{C}$ )	Inlet H <sub>2</sub> O (%)	Space velocity ( $\text{hr}^{-1}$ )	Test duration (mins)	$t_{id}$ (mins)	Log mean $C_{av}$ (ppm)
211	1	450	650	9	1990	170	376	57.6
210	1	450	650	26	1990	125	376	58.6
213	1	450	600	26	2330	135	322	63.4
214	1	450	550	26	2660	105	281	57.6
216	1	450	500	26	2790	140	268	58.6
217	1	250	600	26	1200	180	626	43.0



#### 4. Choice of models

One of primary aims of this study was to evaluate the different models for their ability to describe the experimental data without recourse to extensive curve fitting. As far as possible, the model parameters were therefore estimated from independent experiments or from literature correlations. It is also important to only evaluate those models that are derived on the basis of physically acceptable assumptions about the system of interest. Since the solid reactant is highly porous, the sharp interface model was not considered. The most appropriate models appeared to be the grain models. Two versions were considered—the spherical changing grain size model (Georgakis *et al* 1979) (GCSM), which accounts for density changes during reaction, and the rectangular grains version of the general formulation described by Szekeley *et al* (1976) (SESM). There appears to be a close analogy between grain shape factor and the order of reaction, with respect to the solid reactant in the volume reaction model, when diffusion of gas through the product layer tends to be very large. Zero-order corresponds to rectangular grains (Ramachandran & Doraiswamy 1982). Since the present data were (as shown later) adequately described by these models, the sophistication of varying the grain radius was unnecessary. The single pore model of Ramachandran & Smith (1977) (RSM) and the random pore model of Bhatia & Perlmutter (1980) (BPM) were considered because of their direct physical appeal and the relative ease of parameter estimation. The latter model unifies many of the earlier approaches and makes the separate evaluation of some of them redundant. The effect of inerts was only taken into account through the use of the actual density of the active material as the appropriate parameter in the models. The effect observed was similar to those accounted for by the more sophisticated treatment of Prasanna *et al* (1985).

All the four models chosen for interpreting the data provide information on conversion of the solid reactant in a single particle exposed to the gaseous reactant of fixed composition. When applying the models to batch fluidised bed data one should take into account the variation in composition with time as well as with axial position in the bed. Fortunately in the case of reactions which are first-order with respect to the gaseous reactant, Levenspiel (1979) has shown that it is enough to treat the problem as the reaction of a single particle with the gaseous reactant at a uniform concentration equal to the log mean concentration.

Ramachandran & Smith (1977) have analysed the simulations of their single pore model to develop simple criteria to determine the relative importance of reaction and diffusion rates: for the present system, the Thiele modulus for the pore is of the order of 0.07, the ratio of effective pore length to pore radius is about 1200 and the Biot number is of the order of  $10^{-9}$ . Hence it can be safely concluded that the sulphidation process is reaction controlled, that diffusional effects are relatively unimportant and that the effect of diffusion through the product layer is also likely to be insignificant. Finally, the initial porosity of the particle, 0.49 is greater than  $(Z - 1)/Z$ , 0.38, while the diffusional effects are relatively unimportant. This means that according to the model complete conversion of the solid is ensured before pore closure occurs. Since the experimental runs reported here were restricted to a maximum of about 50% conversion of the solid reactant, pore closure effects have not been considered separately in this paper. It is also clear from the results of Ramachandran & Smith (1977) that pore models are relatively insensitive to



changes in the rate constant when the diffusivity through the product layer is much less than the molecular diffusivity.

## 5. Parameter evaluation

The only unknown parameter was the rate constant. A starting value for iterative search is that given by Westmoreland *et al* (1977). The variation of the rate was carried out through changes in Biot number. The other parameters were calculated as follows:

- (i) The pore volume  $V_0$  and the solid density  $\rho_s$  in the particle (80% alumina and 20% ZnO/CuO) were  $0.22 \text{ cm}^3/\text{g}$  (measured) and  $4.33 \text{ g/cm}^3$  (calculated from densities of individual oxides given in handbooks). Hence the initial porosity  $\varepsilon_0$  was 0.49.
- (ii) The surface area was reported to be between 30 to  $60 \text{ m}^2/\text{gm}$  (manufacturer's specification). A mean value of  $45 \text{ m}^2/\text{gm}$  was used (however, variations between 30 and  $60 \text{ m}^2/\text{gm}$  were tried and found to have little effect on the model predictions). The corresponding surface area per unit volume,  $S_0$ , was  $0.908 \times 10^6 \text{ cm}^{-1}$ .
- (iii) The initial pore diameter was calculated as  $4\rho_p V_0/S_0$  while the effective pore length  $l$  in the SPM was calculated, as recommended by the authors, as  $R/3\varepsilon_0^{1/2}$  where  $R$  is the mean size of the particle. In the grain models, the grain radius was calculated as  $(3/S_0)$ .
- (iv) The particle diffusivity was calculated as suggested by Gibson & Harrison (1980),

$$D_e = D \varepsilon_0^2,$$

where  $D$  is given by a combination of molecular and Knudsen diffusivities,

$$1/D = 1/D_M + 1/D_K.$$

The molecular diffusivity  $D_M$  and the Knudsen diffusivity  $D_K$  are evaluated using the formulae given in Reed *et al* (1977), and Satterfield (1970), respectively.

- (v) The mass transfer coefficient was calculated using the correlation given by Davidson & Harrison (1971) for fluidized beds:

**Table 3.** Summary of parameters used in the calculations.

Particle density, $\rho_p = 2.21 \text{ gm/cc}$				
Initial porosity, $\varepsilon_0 = 0.49$				
$Z = \text{molar volume ratio of solid product to solid reactant} = 1.6$				
Molecular weight of dry inlet gas = 23.9				
Initial grain radius, $R_0 = 3.3 \times 10^{-6} \text{ cm}$			(GCSM, SESM)	
Aspect ratio, $A_r = 500$			(SESM)	
Slab height, $L = 0.064 \times (\text{particle radius})$			(SESM)	
Pore length, $l = (\text{particle radius})/3\varepsilon_0^{1/2}$			(RSM)	
Initial length of pore system, $L_0 = 1.4 \times 10^{11} \text{ cm}^{-2}$			(BPM)	
Initial effective diffusivity in particle = $D \varepsilon_0^2$			(GCSM, SESM)	
Diffusivity in product layer, $D_0 = D[1 - (1 - \varepsilon_0)(Z - 1)/\varepsilon_0]^2$			(BPM, SESM)	
Radius of pore, $R_p = 1.07 \times 10^{-6} \text{ cm}$			(RSM)	
Product porosity, $\varepsilon_c = 0.001$				
Temperature $^\circ\text{C}$	650	600	550	500
Rate constant: $10^3 \text{ k cm}^3 \text{ s}$ (GCSM) and (SESM)	0.467	0.462	0.521	0.565
(RSM)	0.243	0.253	0.289	0.304
(BPM)	5.610	4.470	5.440	5.650

$$\varepsilon_0 k_m / u = 0.81 Re^{-0.5} Sc^{-2/3}.$$

(vi) As discussed in the previous section, diffusional resistance was not likely to be as important as the reaction rate. The diffusivity in the product layer is taken to be equal to the diffusivity through the pores,  $D$ . In RPM and SESM, this  $D$  was naturally multiplied by the appropriate functions of  $\varepsilon_0$  and  $Z$ .

(vii) The aspect ratio for rectangular grains in the SESM was assumed to be 500. This was in keeping with the anticipation that the diffusion resistance in the grain is negligible.

Table 3 is a summary of parameter values used in each model.

## 6. Numerical procedure

All of the models considered here are of the form:

$$\frac{1}{\eta^a} \frac{\partial}{\partial \eta} \left[ \eta^a f(y) \frac{\partial C}{\partial \eta} \right] = h(y) C, \quad (1)$$

$$\partial y / \partial \tau = g(y) C, \quad (2)$$

where  $C$  is the dimensionless concentration of the gaseous reactant while  $y$  is a dimensionless variable which is related directly to the local conversion. The value of  $a$  and the form of functions  $f$ ,  $g$  and  $h$  for the four models are given in tables 4a and 4b. These tables also indicate the physical quantity represented by  $y$  and the dimensionless form of  $\eta$  and  $\tau$  for each model. The associated boundary conditions are:

$$\eta = 0, \frac{\partial C}{\partial \eta} = 0 \quad (\text{all models}),$$

$$\eta = 1, 1 - C = \frac{De/D}{Sh} \frac{\partial C}{\partial \eta} \quad (\text{BPM}),$$

$$C = 1 \quad (\text{SESM, GCSM, RSM}),$$

and

$$\tau = 0, C = 1, y = 0 \quad (\text{BPM, RSM}),$$

$$C = 1, y = 1 \quad (\text{SESM, GCSM}). \quad (3)$$

In the case of the grain models, the above equations and boundary conditions are valid till the conversion at the pellet surface is complete. Thereafter, the ash layer moves inwards and the equations are solved in two zones—a zone of completely reacted solid reactant through which only diffusion occurs, and a zone of partially reacted solid where diffusion and reaction occur simultaneously—and matched at the moving boundary,  $\eta = \eta_m$ , for continuity of the concentration as well as its first derivative. The equations for the two zones and the boundary conditions are given in detail by Dudukovic & Lamba (1978). The only difference is in the notation. The equations are solved using a finite difference formulation and the Crank-Nicholson

**Table 4a.** Variables and functions in RSM and BPM.

Function or variable	RSM	BPM
$\eta$	$x/l$	$r/R$
	$\frac{tD}{R_p^2} \frac{b C_{A0} Z}{\rho_B(1 - \varepsilon_G)}$	$\frac{tk S_0}{(1 - \varepsilon_0)} \frac{C_{av}}{\rho_B}$
$a$	0	2
$h$	$\frac{2l^2}{R_p^2} \frac{(1 + \delta_2)}{\psi}$ , where  $\delta_2 = -1 + \{[(1 - y)^2 - Z]/(1 - Z)\}^{1/2}$ ,  $\psi = \frac{D}{k R_p} + \frac{D}{D_e} (1 + \delta_2) \ln \left\{ \frac{1 + \delta_2}{1 - y} \right\}$	$\frac{\phi^2(1 - y) [1 - \psi \ln(1 - y)]^{1/2}}{1 + (\beta Z/\psi) \{[1 - \psi \ln(1 - y)]^{1/2} - 1\}}$ where $\psi = 4\pi L_0(1 - \varepsilon_0)/S_0^2$ , $\beta = 2k(1 - \varepsilon_0)/DS_0f(1)$ , $\phi^2 = R^2 k S_0/D_e$
$f$	$(1 - y)^2$	$[1 - (1 - \varepsilon_0)(Z - 1)y/\varepsilon_0]^2$
$g$	$(1/\psi) \{1 + (1 - y)/[(Z - 1)(1 + \delta_2)]\}^{-1}$	$h/\phi^2$
$y$	$\delta_1$ (radial distance of product surface from original surface of pore)	local conversion

**Table 4b.** Variables and functions in GCSM and SESM.

Function or variable	GCSM	SESM
$\eta$	$r/R_0$	$x/(L/2)$
	$\frac{t k C_{av}}{R_0 \rho_B}$	$\frac{t k C_{av}}{R_0 \rho_B} \frac{(A_r + 1)}{A_r}$
$a$	2	0
$h$	$\frac{\beta \phi^2 y^2}{\beta + y(1 - y/\nu)}$ , where  $\nu = [Z + (1 - Z)y^3]^{1/3}$ , $\phi^2 = [3(1 - \varepsilon_0)k R^2]/R_0 D_e$	$\frac{y k l^2}{2 D_e R_0} \frac{A_r + 1}{A_r} (1 - \varepsilon_0)$
$f$	$\left[ 1 - \frac{(1 - \varepsilon_0)(Z - 1)(1 - y^3)}{\varepsilon_0} \right]^2$	$1 - y^2$
$g$	$-\beta [\beta + y(1 - y/\nu)]$	-1
$y$	$r_2/R_0$ ( $r_2$ is radius of unreacted core)	$r_1/R_0$ ( $r_1$ is thickness of unreacted portion at any time)

method. While orthogonal collocation methods have been shown to be more efficient (Dudukovic & Lamba 1978), particularly for grain models, the finite difference scheme described above took less than five minutes on an IBM 370/155 for calculating solid conversions up to 50% as a function of time for each of the models. In any case the emphasis in the present paper is on the comparison between the models and not on the numerical technique.

## 7. Results and discussion

Figure 2 compares the conversions calculated using the four models with experiment at 600°C. The only parameter that was fitted was the rate constant. All the models correlate the experimental data well. The best model is the RSM. The BPM predicts conversions lower than the experiment at high conversions. The SESM predicts conversions higher than experiment at low conversions. The GCSM is in good agreement with experiment. These trends have been observed in all the runs

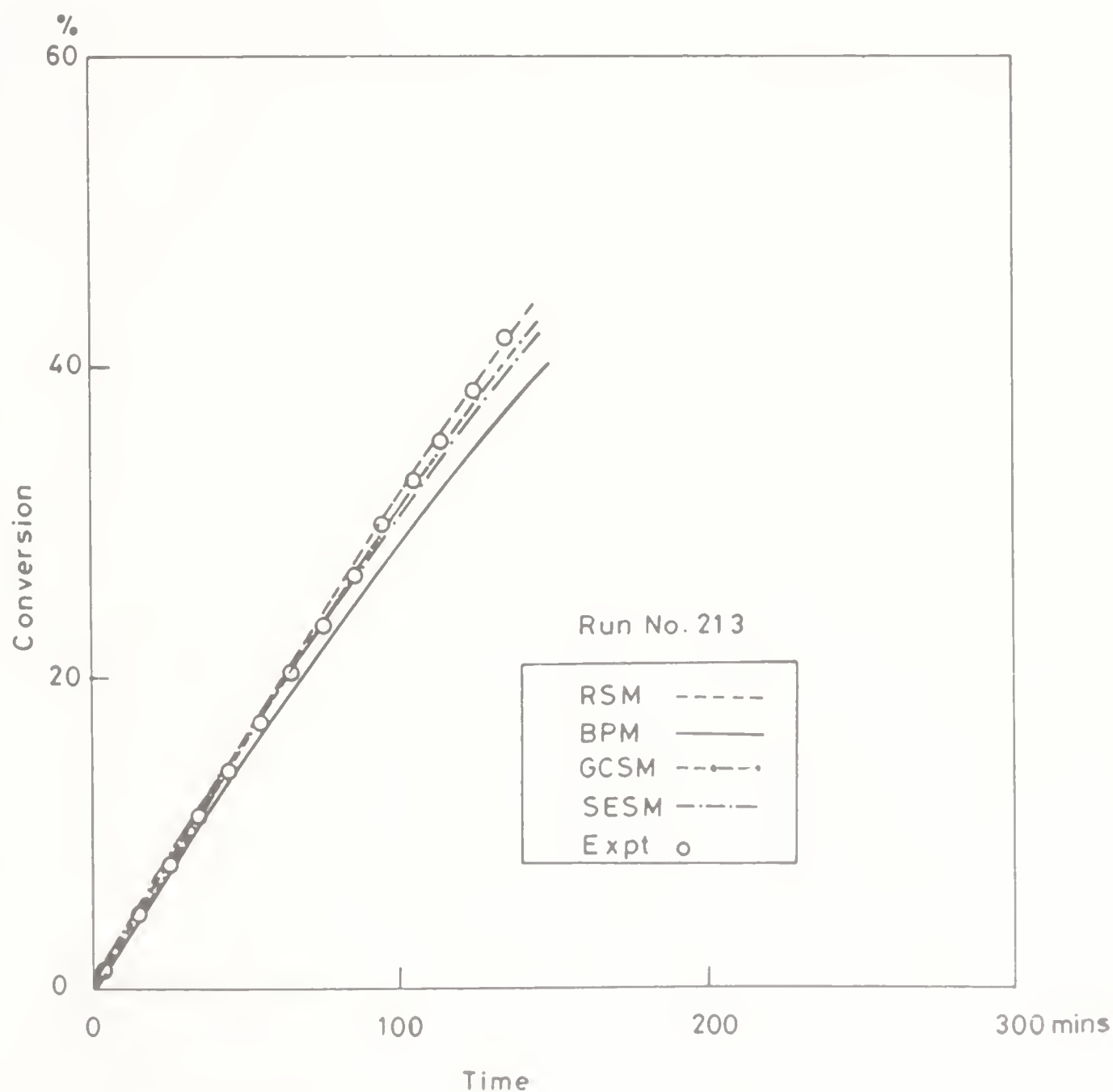


Figure 2. Comparison of GCSM, SESM, RSM and BPM with experiment



although only one run is illustrated here. The rate constants required to fit the data differ from model to model. Both the grain models (GCSM, SESM) correlate data with the same value of the rate constants. The RSM requires a rate constant that is somewhat lower while the BPM requires a rate that is an order of magnitude higher.

Figures 3 and 4 compare the ability of the GCSM and RSM to correlate the experimental data at different temperatures. The abscissa is time in minutes. To compare conversions in different experiments with one another the abscissa for each curve should be divided by the 'ideal breakthrough time',  $t_{id}$ , which is also given in table 2 for each run. This is the time required to reach 100% conversion of solid assuming that all the  $H_2S$  entering the bed reacts. The agreement with experiment is good but the rate constants required to fit the data increase as temperature decreases. This is true of all the four models evaluated and is certainly indicative of the inadequacy of the models in this regard. Jalan (1983) has studied the mixed oxide sorbent with a view to characterizing it *vis a vis* the pure oxides. The desulphurising capacity of the mixed oxide was considerably greater than would be expected based on the capacities of the individual oxides CuO and ZnO

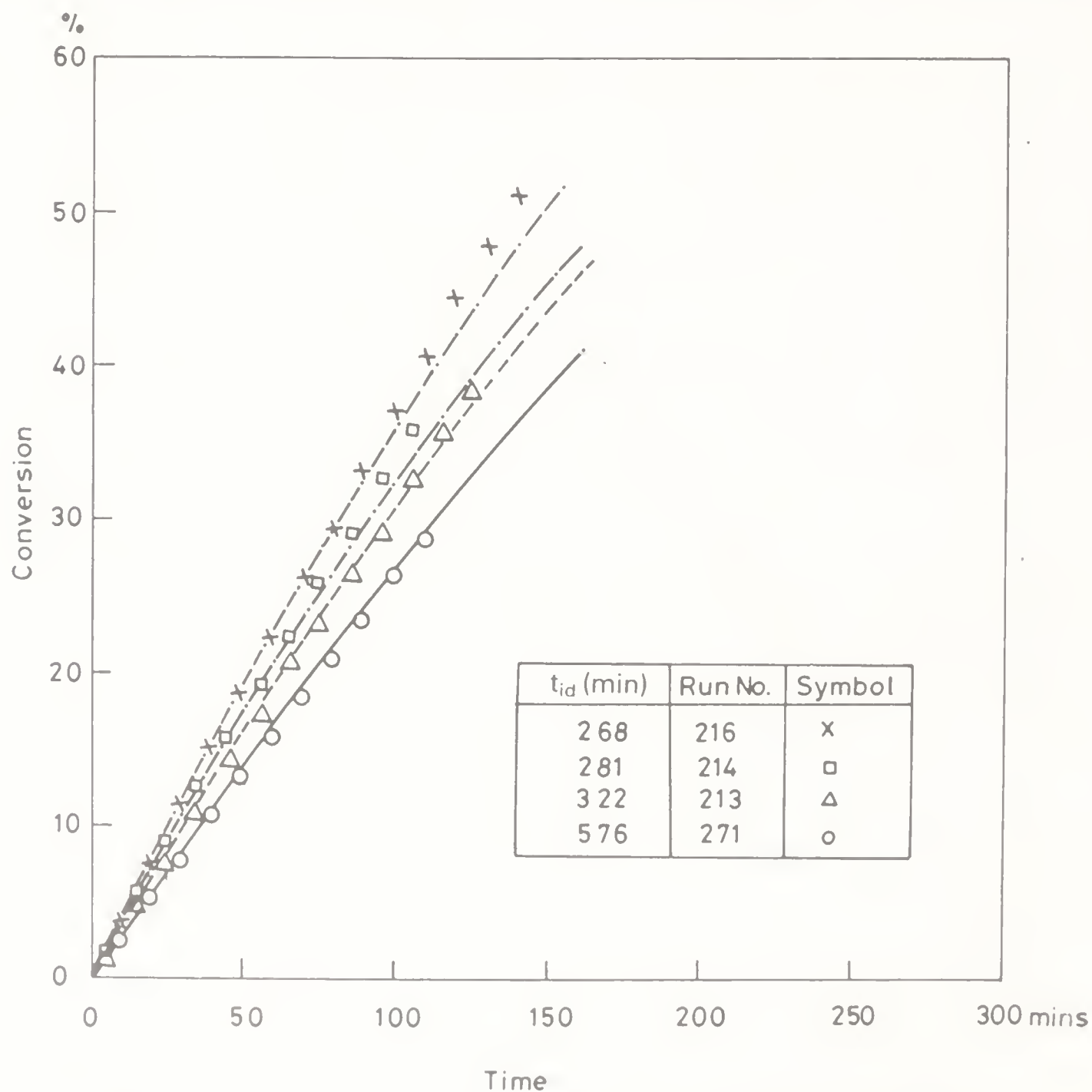


Figure 3. Comparison of GCSM with experiment at different temperatures.

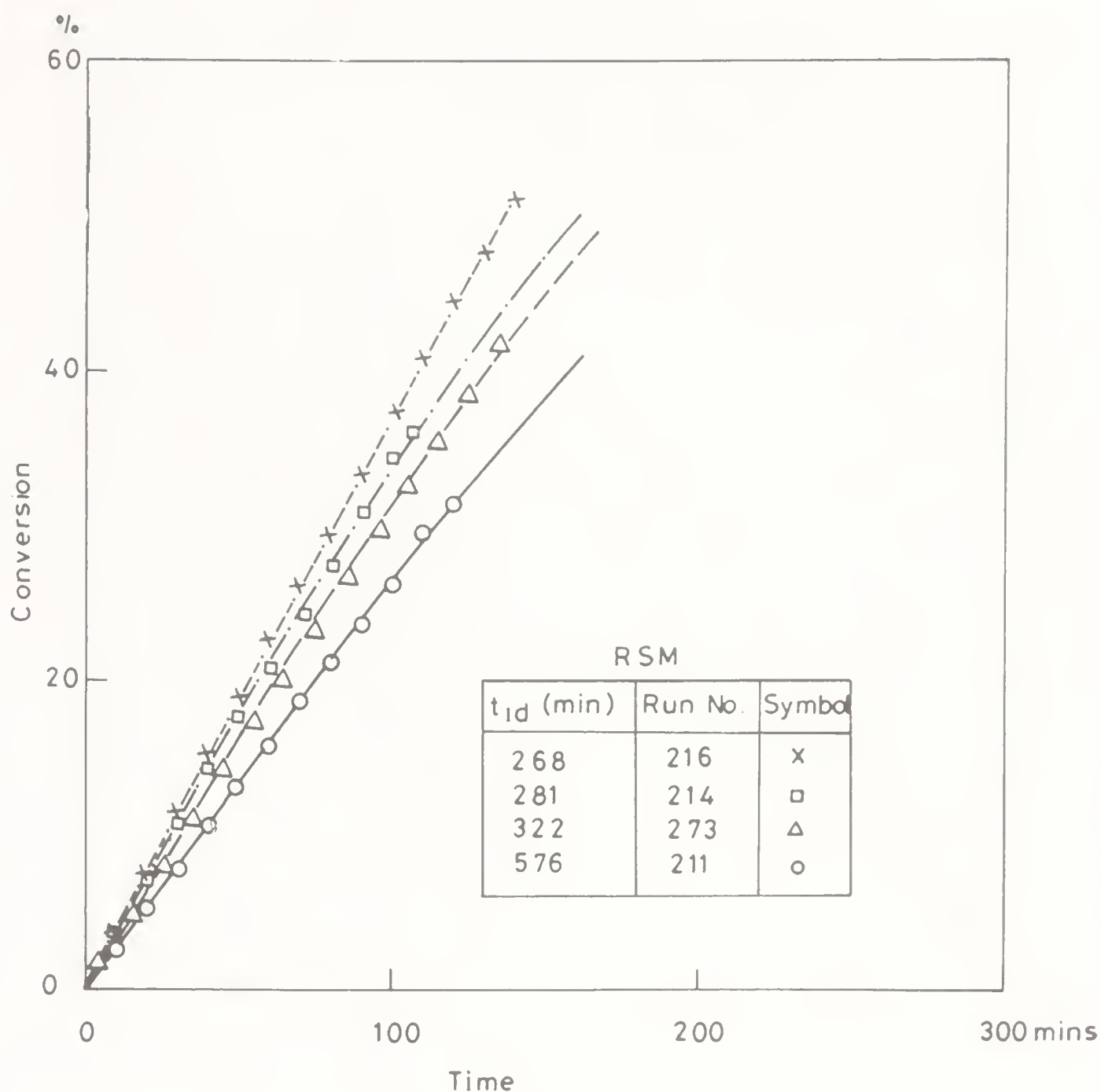


Figure 4. Comparison of RSM with experiment at different temperatures.

alone, suggesting a synergistic effect. Electron microscopy studies of the mixed oxide clearly showed extensive surface structural reorganisation: oxidative regeneration created a rough fissured oxide scale; hydrogen reduction led to a sintering of the oxide scale platelets; and the sulphidation process generated small crystallites of the new sulphide phases,  $\text{Cu}_2\text{S}$  and  $\text{ZnS}$ , on the surface of the reduced and sintered platelets of the metal oxide scale. The mixed oxide thus provides a 'structurally self-regenerating' system. Perhaps the activation energies for the sulphidation of the individual oxides in the mixed oxide are affected by the presence of the other oxide/sulphide differently at different temperatures. If this mechanism can be established independently then the models can be re-examined for their a priori predictive abilities.

Figures 5 and 6 compare the ability of the models to correlate data at two different particle sizes. The rate constant in each case was chosen to fit the data for  $450\ \mu$  particles. The predicted conversions for  $250\ \mu$  particles are clearly in poor agreement with the data, being always much higher than the experimentally

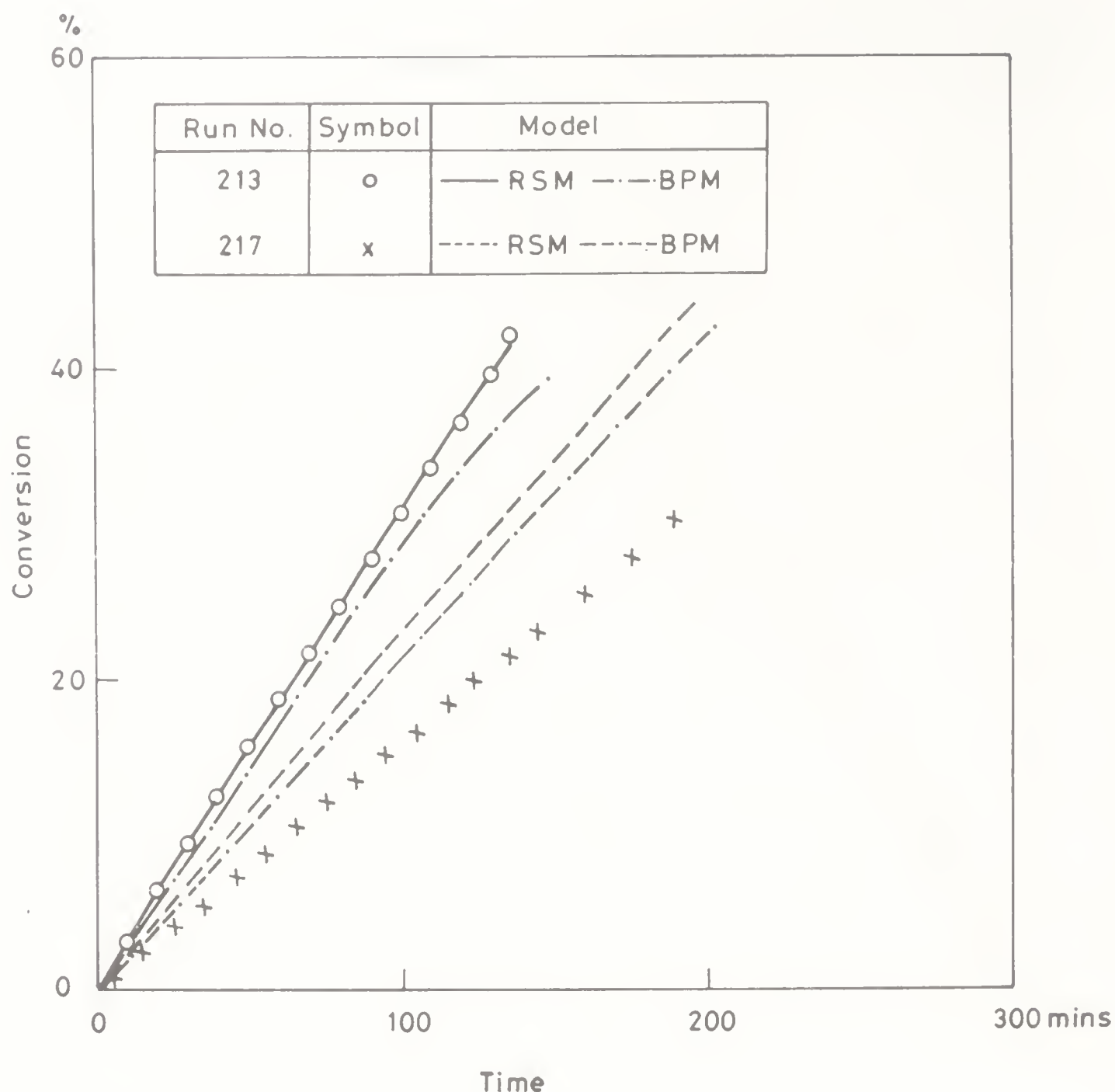


Figure 5. Comparison of pore models with experiment for two different particle sizes.

observed values. None of the models gives an accurate representation of the conversion vs time data as a function of particle size.

Figure 7 compares the ability of GCSM and RSM to correlate data at two different values of the initial moisture content. In this case neither the data nor the models show any significant effect of variations in moisture content of the inlet gas.

## 8. Conclusion

Experimental data on hot gas desulphurisation using ZnO/CuO as sorbent have been interpreted using four representative models for gas-solid non-catalytic reactions. In each case, all the parameters except the rate constant were calculated either from the conditions of the experiment or from literature correlations. The rate constant was varied at each temperature so as to obtain a fit of the data for one particle size and one value of the initial moisture content. It is found that all the models describe the experimental observations well at the four different tempera-

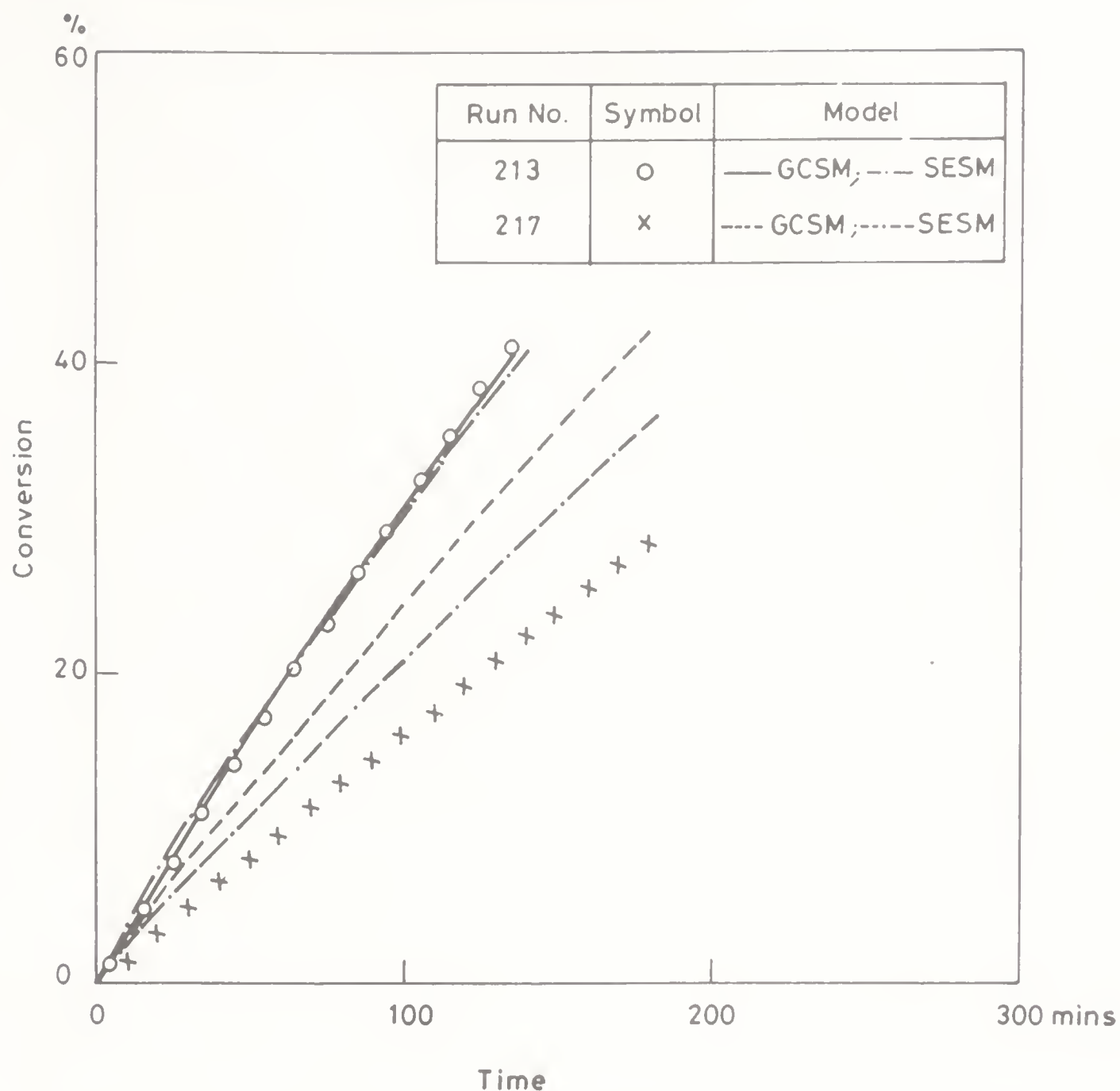


Figure 6. Comparison of grain models with experiment for two different particle sizes.

tures and for two different values of the initial moisture content. However the rate constant values required increase with decrease in temperature. Further the models do not adequately describe the changes in conversion with particle size observed in the experiments. Of the four models compared in this work the single pore model of Ramachandran & Smith (1977) gave the best correlation of the data while the model of Georgakis *et al* (1979) was the next best. The rectangular grain model of Szekeley & Evans (1970) was found to predict too high a conversion for small times while the random pore model of Bhatia & Perlmutter (1980) predicted too low a conversion for relatively large times.

#### List of symbols

- $A$  gaseous reactant,
- $A_r$  aspect ratio,
- $a$  parameter in (1),



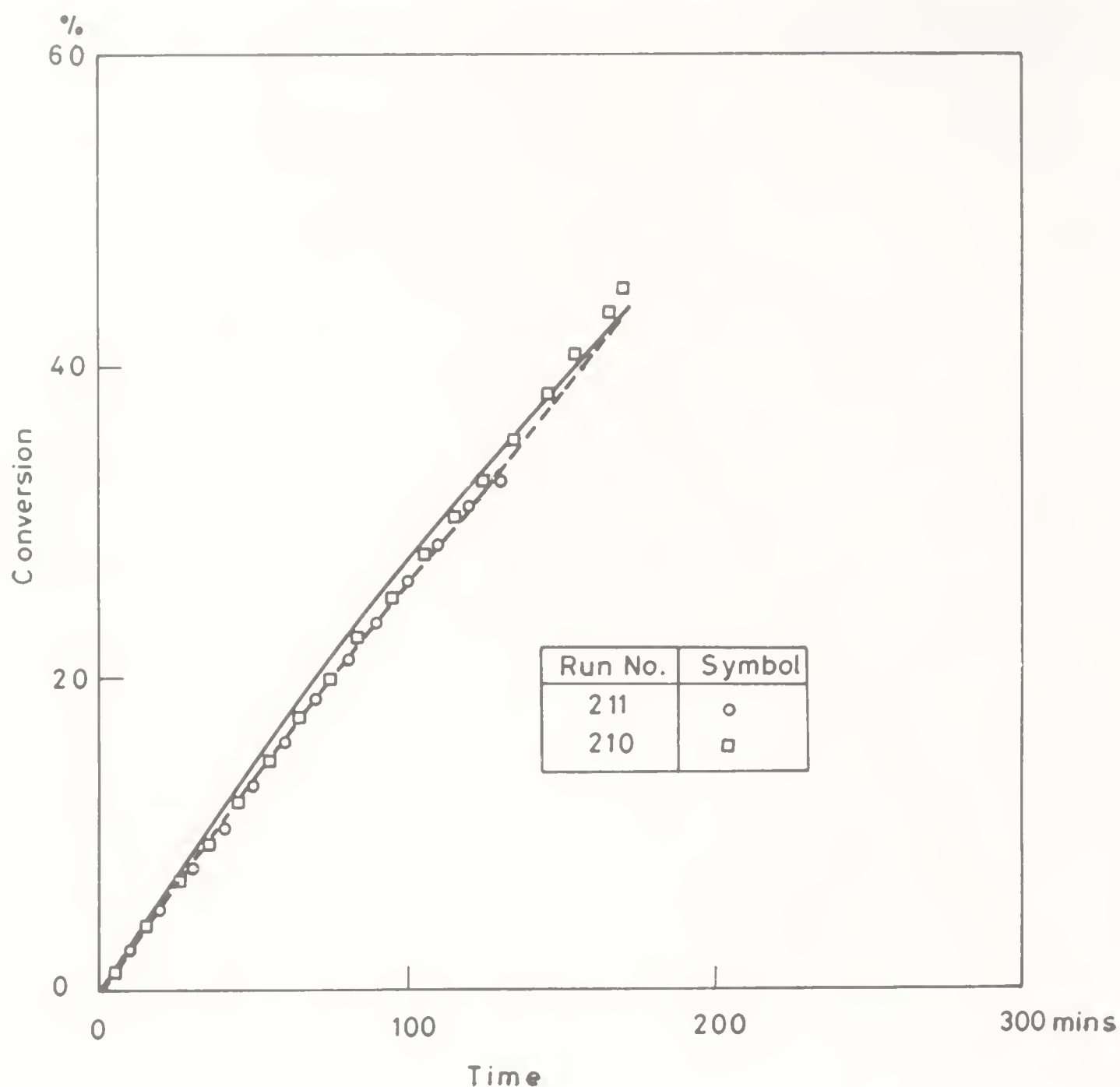


Figure 7. Comparison between GCSM (—) and RSM (---) and experiment for two different initial moisture contents.

- $B$  solid reactant,  
 $b$  stoichiometric coefficient,  
 $C$  concentration, dimensionless,  
 $C_{av}$  log mean concentration,  
 $D$  diffusivity in the pores,  
 $De$  particle diffusivity,  
 $D_K$  Knudsen diffusivity,  
 $D_M$  molecular diffusivity,  
 $f$  function in (1),  
 $G$  solid product,  
 $g$  function in (2),  
 $h$  function in (1),  
 $k$  reaction rate constant,  
 $L$  parameter in SESM and BPM,  
 $l$  parameter in RSM,  
 $R$  radius of particle,

$R_0$	grain radius,
$R_p$	pore radius,
$Re$	Reynolds number,
$S_0$	surface area per unit volume,
$Sc$	Schmidt number,
$Sh$	Sherwood number,
$V_0$	pore volume/g,
$x$	axial distance,
$y$	variable in (2),
$Z$	ratio of solid product molal volume to solid reactant molal volume,
$\beta$	parameter in GCSM and BPM,
$\psi$	parameter in BPM and RSM,
$\phi$	parameter in GCSM and BPM,
$C_0$	initial voidage,
$\lambda$	parameter in RSM,
$\eta$	dimensionless length,
$\nu$	parameter in GCSM,
$\rho_B$	solid reactant density,
$\rho_p$	particle density,
$\rho_s$	solid density,
$\tau$	dimensionless time,
$\delta_1$	parameter in RSM,
$\delta_2$	parameter in RSM.

## References

- Bhatia S K, Perlmutter D D 1980 *AIChE J.* 26: 379–386
- Davidson J F, Harrison D 1971 *Fluidization* (London: Academic Press)
- Dudukovic M P, Lamba H S 1978 *Chem. Eng. Sci.* 33: 303–314
- Georgakis C C, Chang W, Szekely J 1979 *Chem. Eng. Sci.* 34: 1072–1075
- Gibson J B, Harrison D P 1980 *Ind. Eng. Chem., Process Des. Dev.* 19: 231–237
- Jalan V 1983 Studies involving high temperature desulfurisation/regeneration reactions of metal oxides for fuel cell development (DE 84003096). NTIS, US Department of Commerce, Springfield, Virginia
- Levenspiel O 1979 *The chemical reactor omnibook* (Corvallis: OSU Book Stores)
- Prasannan P C, Ramachandran P A, Doraiswamy L K 1985 *Chem. Eng. Sci.* 40: 1251–1261
- Ramachandran P A, Smith J M 1977 *AIChE J.* 23: 353–361
- Ramachandran P A, Doraiswamy L K 1982 *AIChE J.* 28: 881–900
- Reid R C, Prausnitz J M, Sherwood T K 1977 *The properties of gases and liquids* (New York: McGraw-Hill)
- Satterfield C N 1970 *Mass transfer in heterogeneous catalysis* (Cambridge: MIT Press)
- Sohn H Y, Wadsworth M E (eds) 1979 *Process of extractive metallurgy* (New York: Plenum Press)
- Szekely J, Evans J W, Sohn H Y 1976 *Gas-solid reactions* (New York: Academic Press)
- Westmoreland P R, Gibson J B, Harrison D P 1977 *Environ. Sci. Technol.* 11: 488–491



# Transient analysis of the particle-pellet model with structural changes in the solid phase

C G DASSORI, J W TIERNEY and Y T SHAH

Department of Chemical and Petroleum Engineering, University of Pittsburgh, Pittsburgh, PA 15261, USA

**Abstract.** A transient analysis based on the particle-pellet model, which includes the effect of structural changes is presented for non-catalytic gas-solid reactions. Changes in the conversion-time relationship and in temperature profiles in the pellet are considered. The numerical solution of the resulting non-linear partial differential equations is performed using the method of lines, whereby finite difference discretization in the spatial variable yields a stiff system of ordinary differential equations in the time variable. The resulting initial value problem is solved with a general-purpose ordinary differential equation solver. The results obtained using this transient model have been compared with those using a simplified model in which a pseudo-steady state is assumed. Significant differences were found for cases in which structural changes are large.

**Keywords.** Heterogeneous reaction kinetics; non-catalytic gas-solid reactions; transient analysis; structural changes.

## 1. Introduction

It is well recognized that structural changes within the solid pellet play an important role in gas-solid non-catalytic reactions. Various mathematical models have been presented in the literature that deal with the structural change phenomena (Ramachandran & Doraiswamy 1982).

The distinguishing feature of non-catalytic gas-solid reactions, which causes most of the difficulties met in their mathematical modelling, is the evolution of the pore structure of the solid that takes place because of the physicochemical changes that the reacting solid undergoes. Ramachandran & Smith (1977) developed a theory to account for the effects of structural changes on the reacting system behaviour. The theory was based on the particle-pellet concept and accounts for differences in density between reactant and product solids and for changes of porosity and pore interconnections due to sintering. The rate of sintering was assumed to obey an Arrhenius-type equation. Georgakis *et al* (1979) developed a similar model, the

---

A list of symbols is given at the end of the paper



changing-grain-size one, which also accounts for density changes during isothermal reaction. They presented an analytical expression for the pore plugging time, which is the time at which the pore at the pellet surface is blocked if the initial porosity is not larger than the critical value. Ranade & Harrison (1979) also modified the grain model to take into account structural changes in the solid pellet. The structural properties were described in terms of the specific surface area. Lindner & Simonsson (1981) proposed a partially sintered spheres model that considers the initial solid structure to consist of aggregates of spheres in an initial stage of sintering. It takes into account the decreasing gas-solid interfacial area due to growing and overlapping product layers. Prasannan *et al* (1985) developed a mathematical model that accounts for the presence of inert material in the solid pellet that undergoes the gas-solid reaction accompanied by structural changes. Sotirchos & Yu (1985) used a random pore model approach to deal with any type of pore size distribution and studied the transient isothermal behaviour of solid pellets reacting under intraparticle diffusional limitations with structural changes.

The present work deals with the transient analysis of gas-solid non-catalytic reactions undergoing significant structural changes, and takes into account the thermal effects of the system. It employs the same approach as Ramachandran & Smith (1977) to depict the porosity and sintering evolution. A significant difference is that the pseudo-steady state assumption at the pellet level is not used. Instead a solution of the transient system of partial differential equations is obtained. The conversion of solid reactant and temperature and porosity profiles are compared with those obtained using the pseudo-steady state assumption.

## 2. The physical model and assumptions

In the particle-pellet model, the spherical pellet is assumed to be made out of an assembly of non-porous particles (of uniform size at the beginning of the reaction). In this case we have assumed a spherical shape for the grains (figure 1). The gaseous reactant diffuses through the pellet to reach the reactive surface of a particle. Consider a reaction of the form:



As the reaction evolves, a product layer of porous G grows around the non-reacted core of the particles. When there is a difference in stoichiometric coefficients and in the molal density of the product and reactant, the particles expand or shrink, resulting in a change in their radius. In this way, the porosity of the pellet is changed and, as a consequence, the effective diffusivity changes. Moreover, if substantial heat effects are present, sintering can also lead to structural changes by removing pore interconnections.

Within the frame of the particle-pellet model, the following assumptions are made.

- 1) The size and shape of the pellet do not change.
- 2) The shape of the particles is spherical and they retain their shape through the course of reaction.
- 3) Sintering affects the structure of the macroporosity of the pellet but not the porosity of the product layer in the particles.

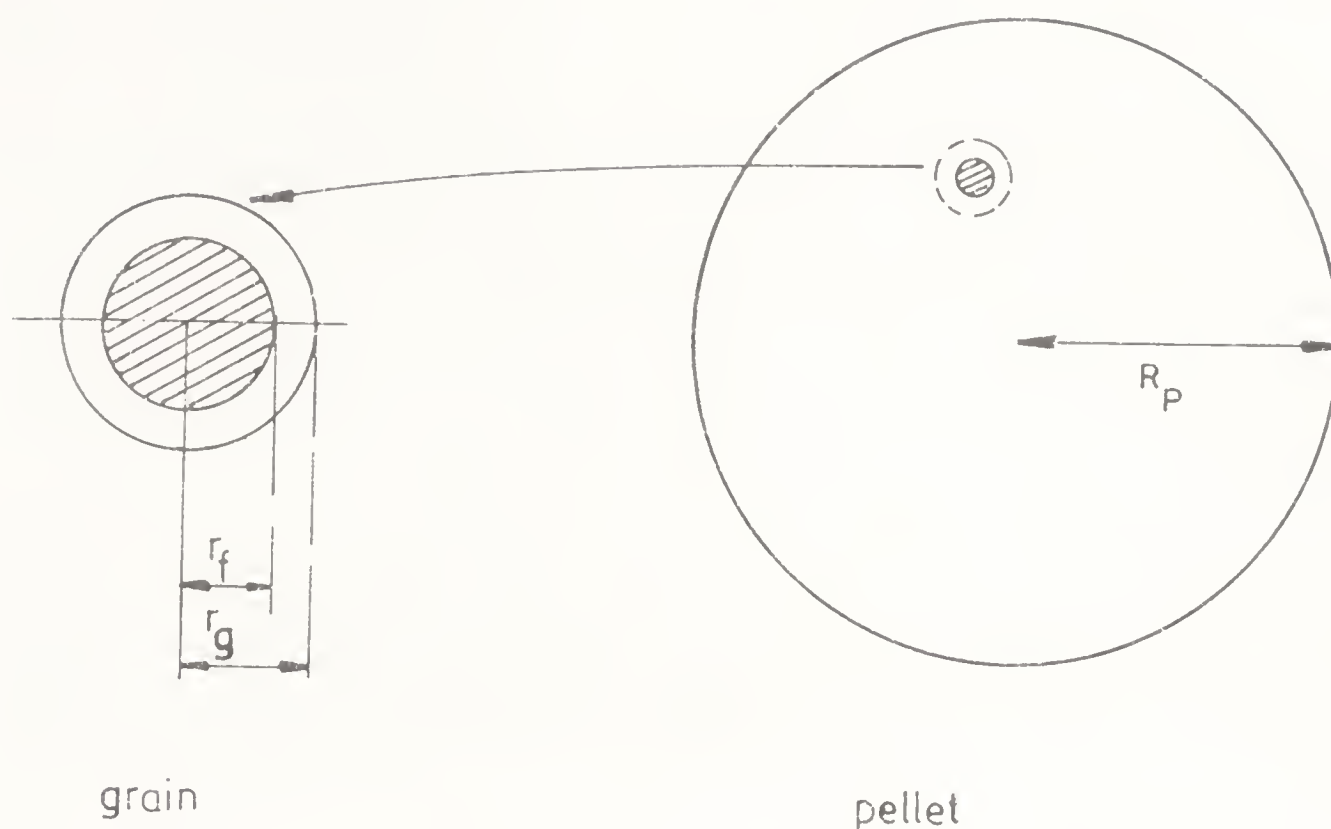


Figure 1. Schematic representation of the model.

- 4) The solid product layer is assumed to sinter, but not the solid reactant.
- 5) The effective thermal conductivity does not change with the extent of reaction.
- 6) The reaction is first-order irreversible with respect to the gaseous reactant and first-order with respect to the reactive surface. An equation of the following form is used;

$$-dn_A/dt = kC_A S_B. \quad (1)$$

This implies that the course of reaction at the particle level is complete according to the sharp interface model.

- 7) The temperature gradients inside the particles are not considered, but they are considered at the pellet level.

### 3. Formulation of the problem

The complete set of equations for the pellet are as follows. Mass conservation for gas reactant A:

$$\frac{1}{r^2} \frac{\partial}{\partial r} \left[ r^2 D_e(r) \frac{\partial C_A}{\partial r} \right] - r_A = \frac{\partial C_A}{\partial t}, \quad (2)$$

where  $D_e(r)$  is the effective diffusivity of A through the pellet, and equimolar counter-diffusion is assumed. Making the assumption of a constant number of spherical particles per unit volume, expressed as  $3(1-\epsilon)/4\pi r_0^3$ , the rate of reaction per unit volume of pellet ( $r_A$ ) can be written in the same way as Ramachandran & Smith (1977):

$$r_A = 3(1 - \varepsilon_0)r_f^2 k C_A \left\{ r_0^3 \left[ 1 + \frac{r_f k}{D_p} \left( 1 - \frac{r_f}{r_g} \right) \right] \right\}^{-1}, \quad (3)$$

where  $r_f$  is the position of the reaction front, which can be predicted by

$$-\frac{dr_f}{dt} = M_B b k C_A \left\{ \rho_B \left[ 1 + \frac{r_f k}{D_p} \left( 1 - \frac{r_f}{r_g} \right) \right] \right\}^{-1} \quad (4)$$

The first-order reaction rate constant ( $k$ ) is taken to be an Arrhenius function of temperature:

$$k = A \exp(-E/RT^*). \quad (5)$$

The radius of each grain ( $r_g$ ) is a function of time  $t$  and radial position ( $r$ ) within the pellet, whether shrinking or swelling is occurring in the solid phase. It can be computed by making a mass balance for the product layer, and it can be put in terms of the densities of the reactant and product solids as follows:

$$r_g = [r_f^3 + f(r_0^3 - r_f^3)]^{1/3}, \quad (6)$$

where  $f$  is the molal volume ratio defined as:

$$f = g\rho_B M_G / [b\rho_G (1 - \varepsilon_G) M_B]. \quad (7)$$

The energy balance for the pellet, assuming a constant heat of reaction ( $\Delta H$ ) and a constant effective thermal conductivity  $k_e$ , is:

$$k_e \left( \frac{\partial^2 T^*}{\partial r^2} + \frac{2}{r} \frac{\partial T^*}{\partial r} \right) + (-\Delta H)r_A = \rho_P C_P \frac{\partial T^*}{\partial t}, \quad (8)$$

where  $C_p$  is the solid phase specific heat, assumed to be constant and  $\rho_p$  is the pellet density, which can be expressed as follows:

$$\rho_p = [r_f^3 \rho_B + (r_g^3 - r_f^3) \rho_G (1 - \varepsilon_G)] (1 - \varepsilon_0) / r_0^3. \quad (9)$$

To take into account structural changes, one has to supply an expression for the pellet's porosity evolution through the course of reaction, as well as a relation to link it to the effective diffusivity. The simplest way to account for this is to use the random pore model with a correction for the tortuosity factor [ $g(z)$ ] to account for sintering. According to this model, the effective diffusivity is given by

$$D_e = [D/g(z)] \varepsilon^2. \quad (10)$$

The function  $g(z)$  accounts for the fractional increase in tortuosity due to sintering.  $D$  is a diffusivity coefficient, whose value results from the contributions of molecular and Knudsen diffusivity. It was taken as a constant for this work. Finally, to express the porosity variation we must consider not only the effect of changes in the particle radius but also the decrease of pore interconnections due to sintering. This can be expressed as:

$$\varepsilon = [1 - (1 - \varepsilon_0) (r_g/r_0)^3] (1 - z), \quad (11)$$

where  $z$  is the fraction of pores in the pellet that have been removed owing to sintering. The  $z$  evolution with time was modelled in the same way as

Ramachandran & Smith (1977).

$$dz/dt = (1 - z) A_\phi \exp \left\{ -[E_s/R(T^* - T_c^*)] \right\}, \quad (12)$$

where  $E_s$  is the activation energy for sintering and  $T_c$  is a characteristic temperature corresponding to the onset of sintering. The value of  $T_c$  is usually the Tamman temperature, which is approximately half the melting point of the solid. In order to integrate (2), (4), (8) and (12) in time and space, the following constraints are imposed on physical grounds.

Boundary conditions:

$$D_e \partial C_A / \partial r = k_g (C_A^g - C_A), \text{ at } r = R_P, \quad (13)$$

$$k_e \partial T / \partial r = h_f (T^{*g} - T^*), \text{ at } r = R_P, \quad (14)$$

$$\partial C_A / \partial r = \partial T^* / \partial r = 0, \text{ at } r = 0. \quad (15)$$

Equations (13) and (14) take into account external mass and heat transfer resistances, while (15) accounts for symmetry.

The initial conditions are:

$$C_A = C_A^i, \text{ at } t = 0, \quad (16)$$

$$T^* = T^{*i}, \text{ at } t = 0, \quad (17)$$

$$r_f = r_0, \text{ at } t = 0, \quad (18)$$

$$z = 0, \text{ at } t = 0. \quad (19)$$

The average conversion of the solid reactant B for the whole pellet can be obtained from the following integral:

$$X_B = 3 \int_0^{R_P} \{1 - (r_f/r_0)^3\} r^2 dr. \quad (20)$$

#### 4. Dimensionless equations

In order to get a general result from the system of equations to be solved, it is appropriate to put the set of equations in dimensionless form. These are

$$\frac{1}{\xi^2} \frac{\partial}{\partial \xi} \left( \xi^2 \delta \frac{\partial C}{\partial \xi} \right) - \phi^2 \rho^2 CF = P_1 \psi \frac{\partial C}{\partial \theta}, \quad (21)$$

$$\frac{\partial^2 T}{\partial \xi^2} + \frac{2}{\xi} \frac{\partial T}{\partial \xi} + \beta \phi^2 \rho^2 CF = P_2 \kappa \frac{\partial T}{\partial \theta}, \quad (22)$$

$$\partial \rho / \partial \theta = -CF, \quad (23)$$

$$dz/d\theta = (1 - z) \exp[-\gamma_s/(T - \chi)], \quad (24)$$

where,

$$\xi = r/R_P, \quad (25)$$



$$C = C_A/C_A^g, \quad (26)$$

$$T = T^*/T^{*g}, \quad (27)$$

$$\rho = r_f/r_0, \quad (28)$$

$$\phi = R_p[3k_0(1 - \varepsilon_0)/(D_{e0} r_0)]^{1/2}, \quad (29)$$

$$\beta = [(-\Delta H) D_{e0} C_A^g]/(T^{*g} k_e), \quad (30)$$

$$F = \exp [\gamma(1 - 1/T)/[1 + \rho/Bi(1 - \rho/\rho_g) \exp [\gamma(1 - 1/T)]], \quad (31)$$

$$\rho_g = r_g/r_0, \quad (32)$$

$$\gamma = E/RT^{*g}, \quad (33)$$

$$Bi = D_p/r_0 k_0, \quad (34)$$

$$P_1 = (\varepsilon_0 R_p^2 M_B C_A^g b k_0)/(D_{e0} \rho_B r_0), \quad (35)$$

$$P_2 = (R_p^2 \rho_P^0 C_P M_B C_A^g b k_0)/(k_e \rho_B r_0), \quad (36)$$

$$\delta = D_e/D_{e0}, \quad (37)$$

$$\psi = \varepsilon/\varepsilon_0, \quad (38)$$

$$\kappa = \rho_P/\rho_P^0, \quad (39)$$

$$\theta = t M_B C_A^g b k_0/\rho_B r_0, \quad (40)$$

$$\gamma_s = E_s/RT^{*g}, \quad (41)$$

$$\alpha = A_\phi \rho_B r_0/M_B C_A^g b k_0, \quad (42)$$

$$\chi = T_c^*/T^{*g}. \quad (43)$$

Using (9)–(11), expressions for  $\delta$ ,  $\psi$ , and  $\kappa$  can be obtained:

$$\delta = [1/g(z)] (\varepsilon/\varepsilon_0)^2, \quad (44)$$

$$\psi = [1 - (1 - \varepsilon_0) \rho_g^3] (1 - z)/\varepsilon_0, \quad (45)$$

$$\kappa = \rho^3 + f. (1 - \rho^3) (\rho_G/\rho_B) (1 - \varepsilon_G). \quad (46)$$

The boundary and initial conditions are as follows:

$$\partial C/\partial \xi = (Sh^*/\delta) (1 - C), \text{ at } \xi = 1, \quad (47)$$

$$\partial T/\partial \xi = Nu^* (1 - T), \text{ at } \xi = 1, \quad (48)$$

$$\partial C/\partial \xi = \partial T/\partial \xi = 0, \text{ at } \xi = 0, \quad (49)$$

$$C = C^i, \text{ at } \xi = 0, \quad (50)$$

$$T = T^i, \text{ at } \xi = 0, \quad (51)$$

$$\rho_f = 1, \text{ at } \xi = 0, \quad (52)$$

$$z = 0, \text{ at } \xi = 0, \quad (53)$$

where,

$$Sh^* = k_g R_p / D_e^0, \quad (54)$$

$$Nu^* = h_f R_p / k_e. \quad (55)$$

The average conversion of the solid reactant B can now be written as:

$$X_B = 3 \int_0^1 (1 - \rho^3) \xi^2 d\xi. \quad (56)$$

## 5. Method of lines solution

The numerical method that we used to solve the system of differential equations (21)–(24), (47)–(53) is the method of lines. It consists of discretizing the spatial variables, rewriting each of the differential equations as a set of ordinary differential equations in the corresponding discrete dependent variables, and solving the resulting ordinary differential equation system with a robust general purpose integrator (Davis 1984).

In order to compare the transient analysis solution with the corresponding pseudo-steady state solution, it is necessary to carry out computations by both methods. The transient equations above can be modified for the pseudo-steady state by replacing (21) and (22) with

$$\frac{1}{\xi^2} \frac{\partial}{\partial \xi} \left( \xi^2 \delta \frac{\partial C}{\partial \xi} \right) - \phi^2 \rho^2 CF = 0, \quad (57)$$

$$\frac{\partial^2 T}{\partial \xi^2} + \frac{2}{\xi} \frac{\partial T}{\partial \xi} + \beta \phi^2 \rho^2 CF = 0. \quad (58)$$

The rest of the formulation remains the same for both cases.

In order to get the solution for the pseudo-steady state analysis we adopted the same strategy as that used by Johnson & Hindmarsh (1983) and by Sohn *et al* (1985). That is, we have solved a nearly equivalent system in which the time-independent differential equations (57) and (58) are replaced by a set of time-dependent ones:

$$\frac{1}{\xi^2} \frac{\partial}{\partial \xi} \left( \xi^2 \delta \frac{\partial C}{\partial \xi} \right) - \phi^2 \rho^2 CF = \alpha_1 \frac{\partial C}{\partial \theta}, \quad (59)$$

$$\frac{\partial^2 T}{\partial \xi^2} + \frac{2}{\xi} \frac{\partial T}{\partial \xi} + \beta \phi^2 \rho^2 CF = \alpha_2 \frac{\partial T}{\partial \theta} \quad (60)$$

The  $\alpha_1$  and  $\alpha_2$  coefficients have no physical basis and require no physical derivation. They are chosen sufficiently small to ensure that the solution is not sensitive to the value selected. This is the same procedure used by Johnson & Hindmarsh (1983) and Sohn *et al* (1985). In particular,  $\alpha_1$  and  $\alpha_2$  were set equal to  $10^{-4}$ .

For both approaches reported in this work, the solution of the ordinary differential equation system was calculated by using a general purpose ODE system solver (for stiff and nonstiff initial value problems) called LSODE (Hindmarsh 1980).

## 6. Results and discussion

### 6.1 No structural changes

We can begin our analysis by considering a system in which the structure does not change with reaction. In this system the effects of sintering and molal density changes are not present; the parameters  $\alpha$ ,  $\chi$  and  $\gamma_s$  are not involved, and  $f = 1$ .

As can be seen in figure 2 conversion profiles eventually become similar. Most of the differences are present during the earlier stages of reaction, where the transient analysis differs from the pseudo-steady state analysis. In general, for the case of  $\alpha = 0$ , conversions computed with the pseudo-steady state analysis are slightly higher than those arising from the transient analysis. But the difference diminishes as time of reaction increases. The temperature profiles agree with previously reported trends for transient analysis of systems which have no structural change (Sampath *et al* 1975).

As can be seen in figure 3, at a fixed dimensionless time,  $\theta = 0.2$ , the pseudo-steady solution shows a monotonic decline as  $\xi$  tends to 1. That is, the

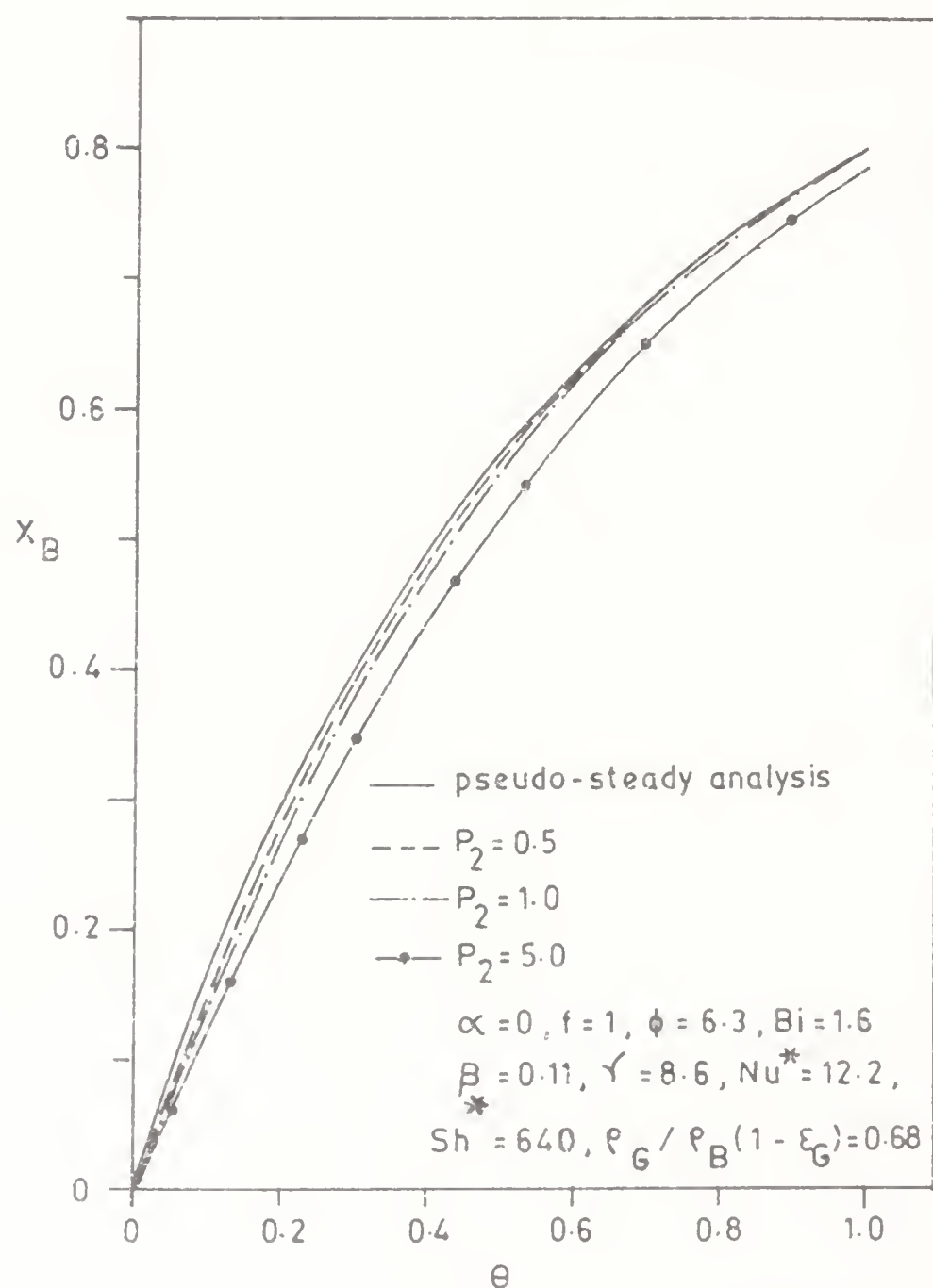


Figure 2. Solid reactant conversion as a function of dimensionless time.

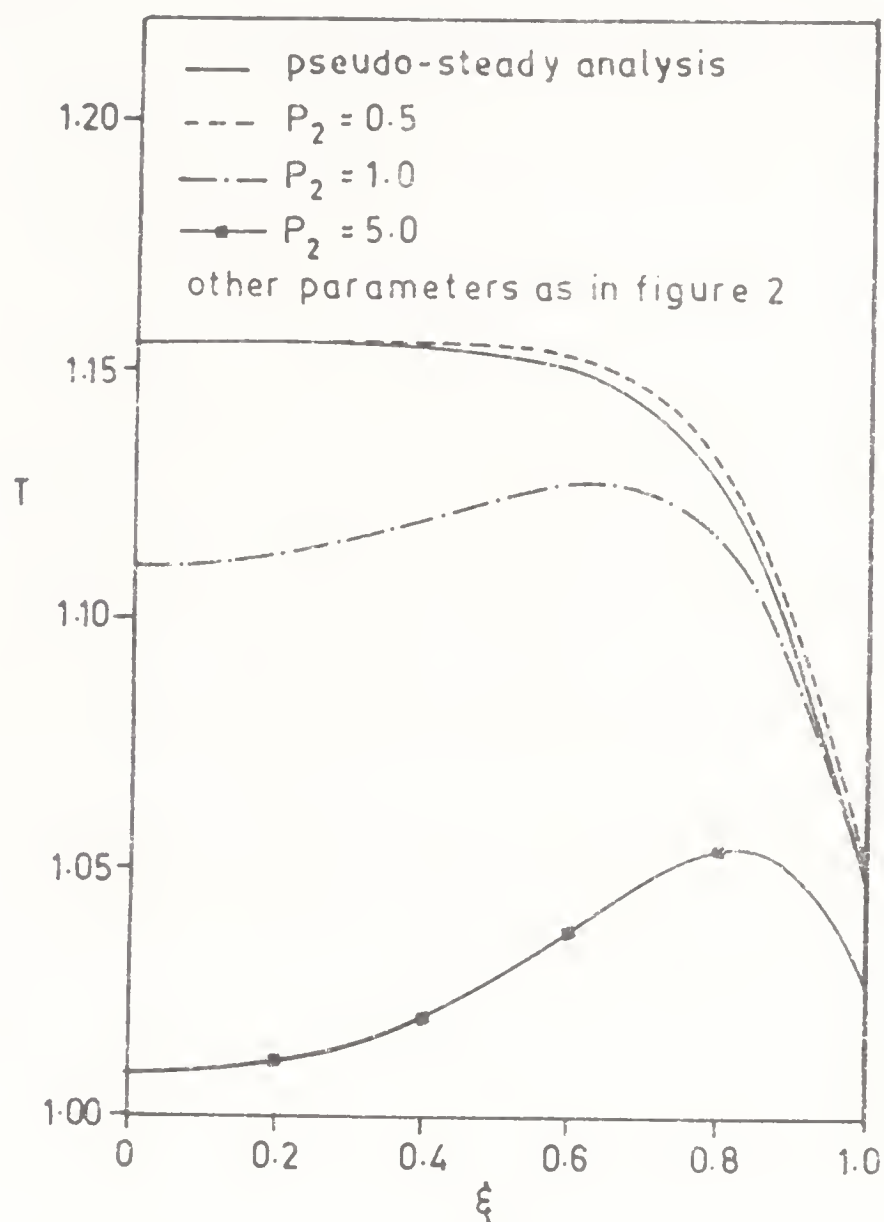


Figure 3. Temperature inside the pellet as a function of radial position.

pseudo-steady behaviour of the temperature profile always has a maximum with respect to  $\xi$  at  $\xi = 0$  (the centre of the pellet). Note that as  $P_2$  is increased, the maximum temperature shifts towards the outer part of the pellet. Also, the maximum temperature attained during the course of reaction is greater for the pseudo-steady analysis.

It was also found that for  $\alpha = 0$  and  $f > 1$ , the porosity inside the pellet always reaches a minimum at the pellet external surface, while for  $f < 1$ , the porosity has a maximum value at the external surface.

## 6.2 Structural changes present

The analysis for systems undergoing both sintering and variation of molal density was carried out for the set of data shown in table 1. These values correspond to

Table 1. Numerical values for the dimensionless parameters in this work.

$\theta = 7$	$\chi = 0.9$
$\beta = 0.15$	$Sh^* = 700$
$\epsilon_0 = 0.6$	$Nu^* = 20$
$Bi = 2$	$\alpha = 0; 3500; 7000$
$\gamma = 8$	$f = 0.5; 1.0; 1.5$
$(\rho_G/\rho_B) \cdot (1-\epsilon_G) = 0.7$	$P_1 = 0.025$
$\gamma_r = 1.6$	$P_2 = 0.5; 1.0; 5.0$



intermediate values for the physical parameters as reported in Costa & Smith (1971), and Ramachandran & Smith (1977).

In figures 4, 5, 6 and 7 the conversion, temperature and porosity profiles are shown for the case in which there is moderate sintering ( $\alpha = 3500$ ) and swelling ( $f = 1.5$ ). The transient analysis indicates higher conversion than the pseudo-steady state analysis. Differences of as much as 30% for conversion are found at moderate times (figure 4).

It was pointed out by Prasannan *et al* (1985) that for systems which do not have structural change the ratio  $P_2/P_1$  is an indicator for the transient character of the system. We found the same for systems which do have structural change. This can be seen in figures 4–7, where we used a fixed value for  $P_1$  and we varied  $P_2$  values.

The temperature inside the pellet, for a fixed dimensionless time,  $\theta = 0.2$ , shows (figure 5) a decline of temperature with the increase of  $\xi$  for the pseudo-steady analysis. At this time,  $\theta = 0.2$ , the curve for  $P_2 = 0.5$  is similar to the pseudo-steady solution; for  $P_2 = 1.0$  it can be seen that it still retains some of the transient character (a maximum at a different position from the centre of the pellet).

Figure 6 shows the temperature profile for  $P_2 = 0.5$  at a much smaller time ( $\theta = 0.05$ ) and here the transient nature of the response is even more evident. Temperature profiles for  $P_2 = 5.0$  are also shown, and it is clear that for this condition the system is controlled by transient behaviour.

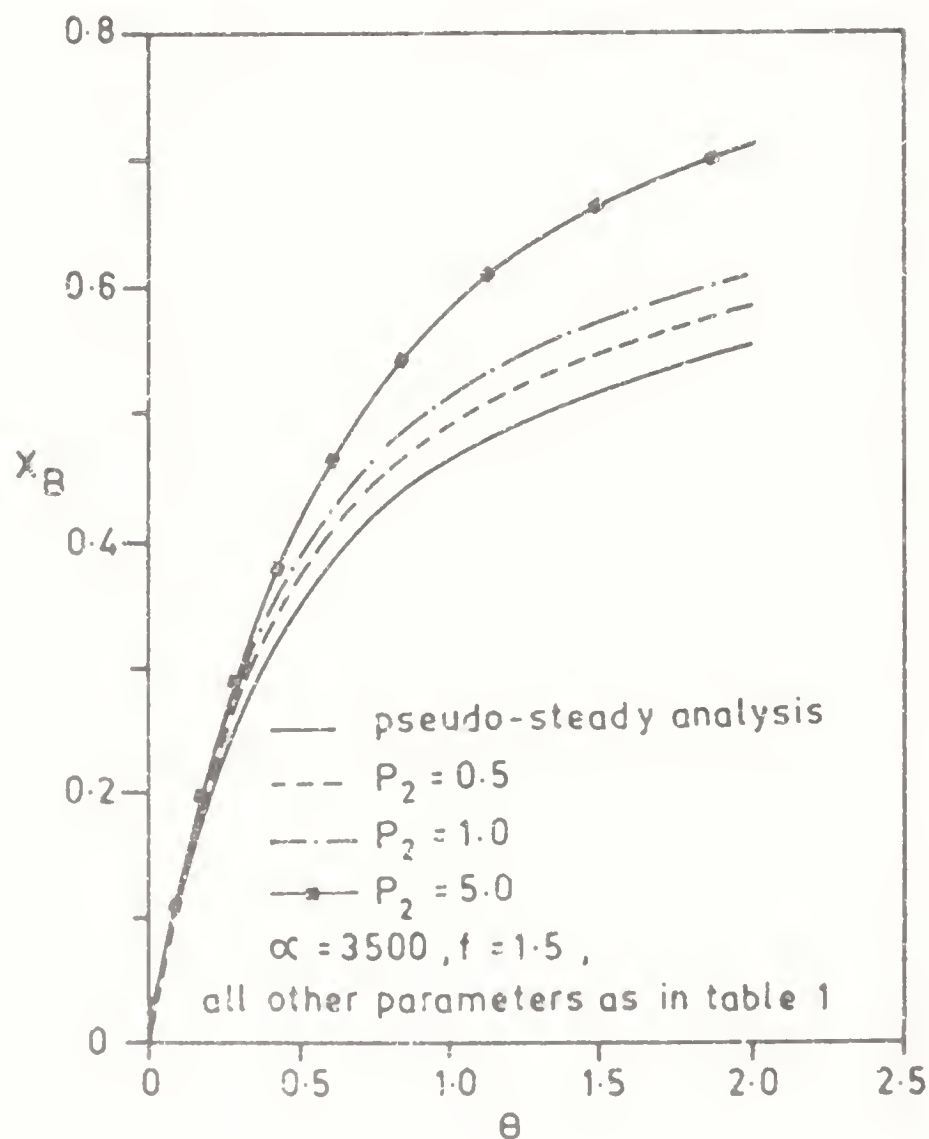


Figure 4. Solid reactant conversion as a function of dimensionless time.

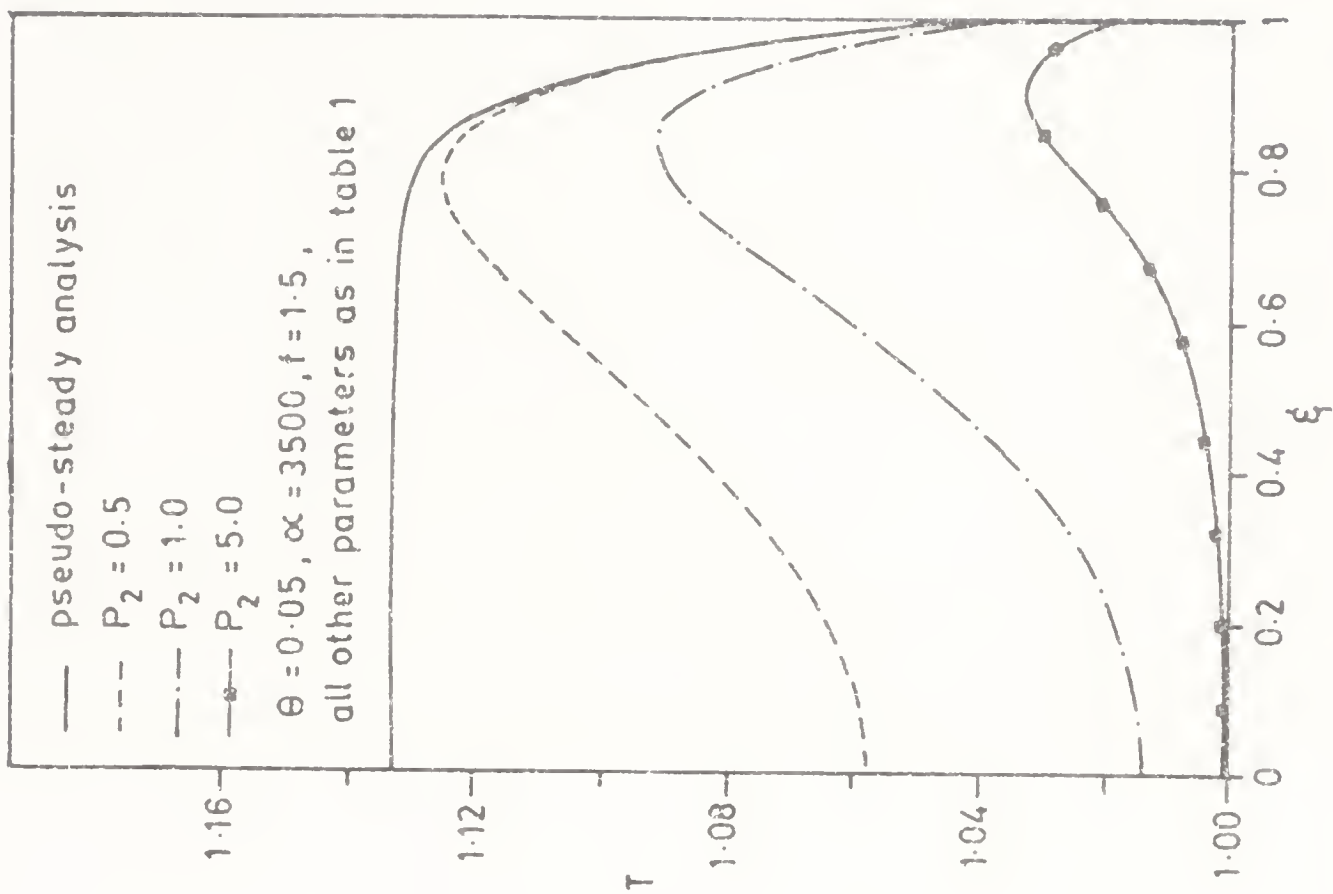


Figure 5. Temperature inside the pellet as a function of radial position.

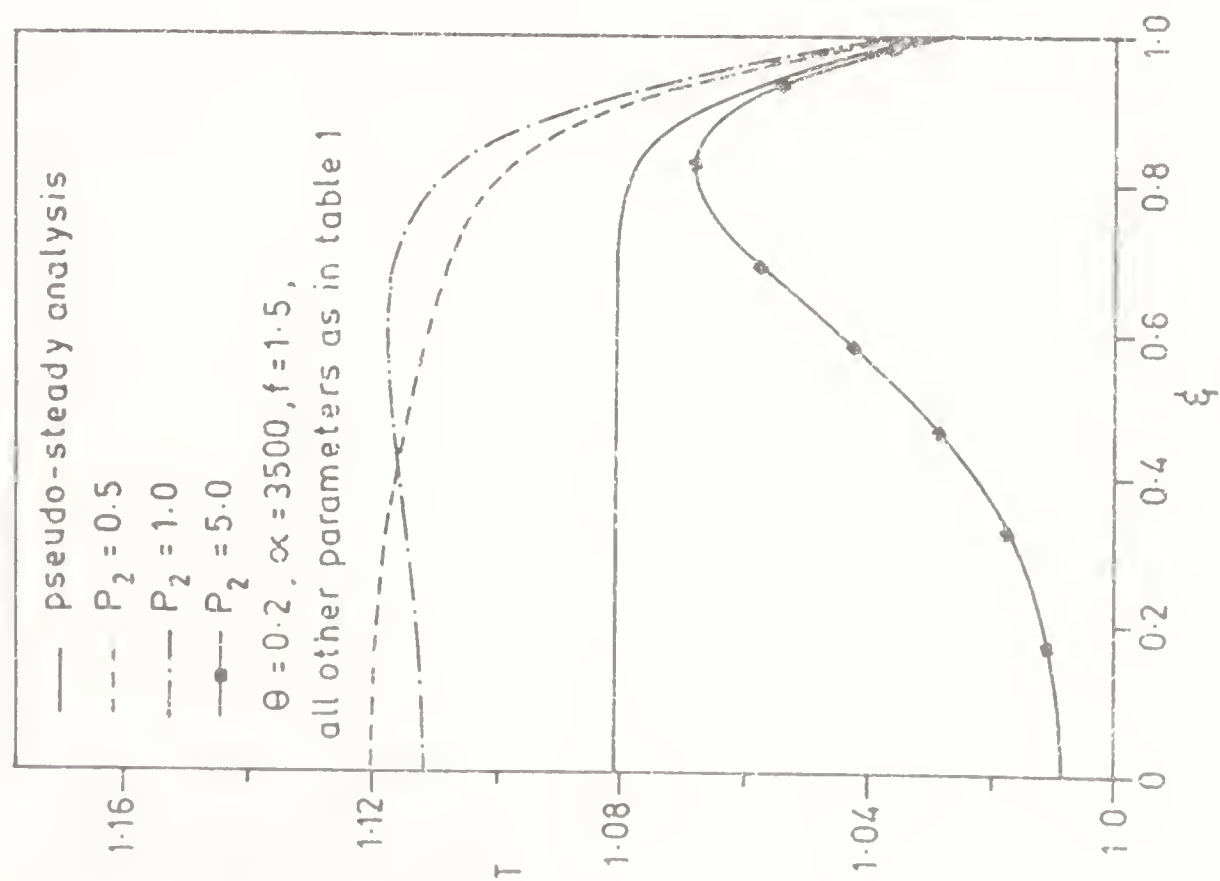


Figure 6. Temperature inside the pellet as a function of radial position.

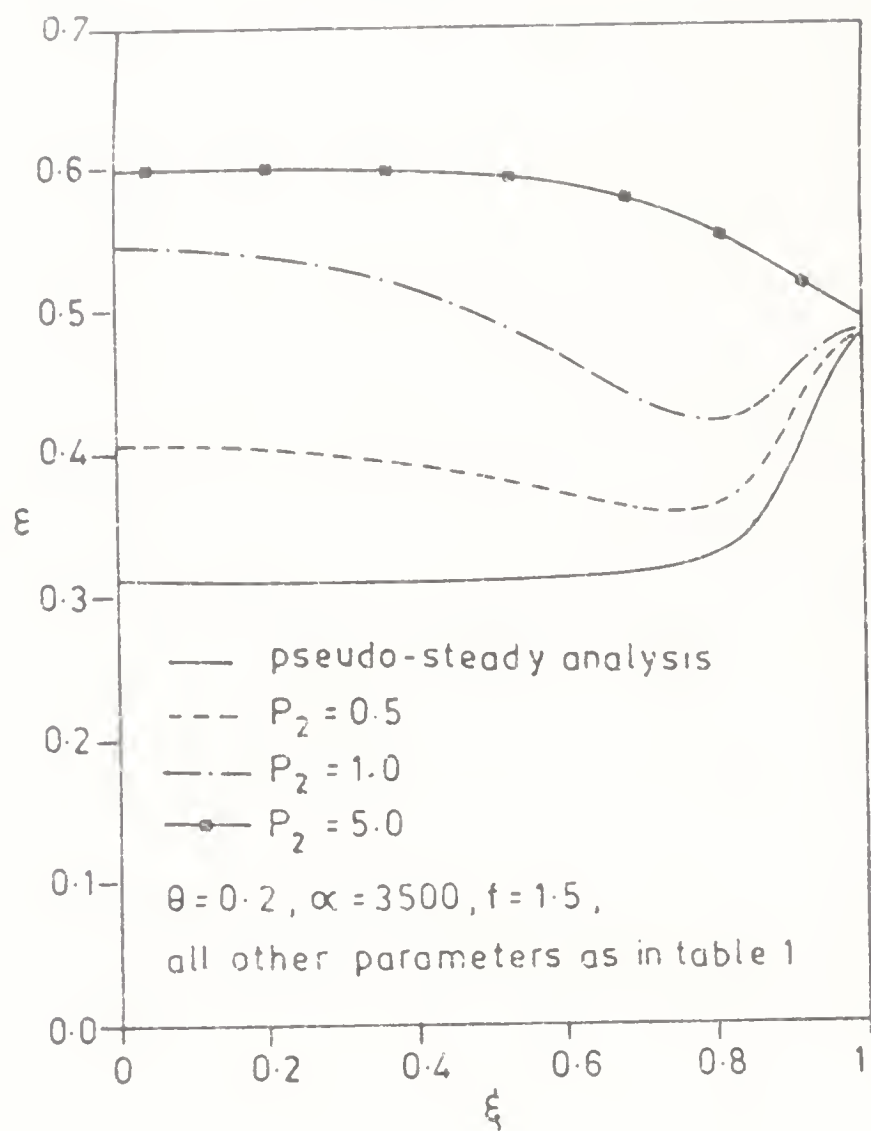


Figure 7. Porosity inside the pellet as a function of radial position.

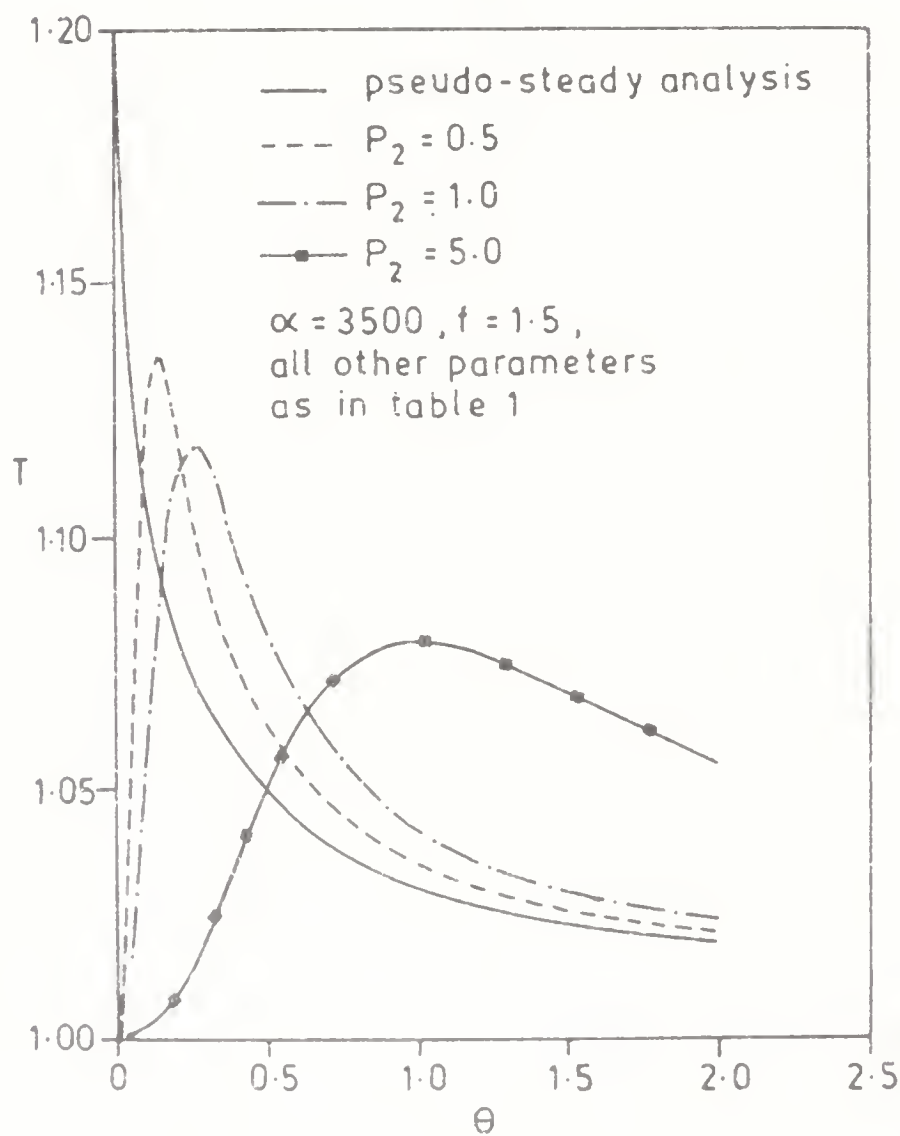


Figure 8. Temperature at the centre of the pellet. Solid line; pseudo-steady analysis.

The highest temperatures encountered during the course of reaction are found using the pseudo-steady state analysis. Figure 8 shows the temperature at the centre of the pellet as a function of the dimensionless time of reaction  $\theta$ . The higher temperatures computed using the pseudo-steady analysis, especially at the early stages of reaction, explain why, under significant sintering effects, conversion for the pseudo-steady analysis is always less than for the transient case. The computed temperatures attained result in higher conversions during the very early stages of reaction, and a larger amount of sintering. As a result, the porosity decreases much more in the pseudo-steady analysis (figure 7), increasing the diffusional resistance for transport, and thus decreasing the conversions attained relative to the transient analysis with an increase in time. This difference can be seen in figure 4.

In general, the temperature reaches a maximum and then diminishes with time at any point in the particle using either analysis. Figure 8 shows a typical plot for the centre of the pellet.

The difference between the transient and pseudo-steady analysis increases as  $P_2/P_1$  increases, and this difference is enhanced when the sintering effect is present. Figures 9–11 show the effect that  $\alpha$  (one of the parameters that determines the sintering behaviour) has on the conversion, temperature and porosity for  $P_2 = 1.0$  and  $P_1 = 0.025$ . Conversions attained without sintering, for  $f > 1$ , are far larger than those undergoing moderate ( $\alpha = 3500$ ) or high ( $\alpha = 7000$ ) sintering (figure 7). It can be seen from figures 10 and 11 that although higher temperatures are attained in the absence of sintering, the porosity profile is not significantly affected.

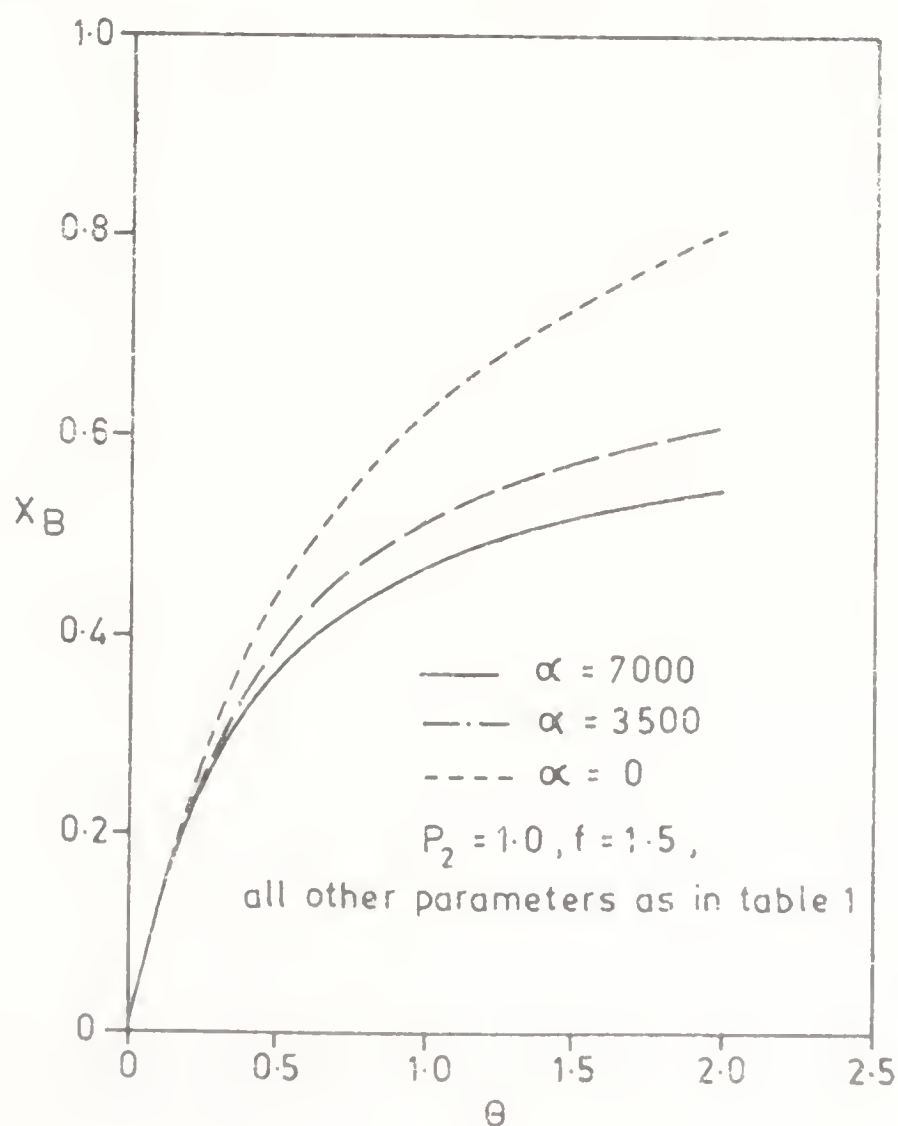


Figure 9. Solid reactant conversion as a function of dimensionless time.



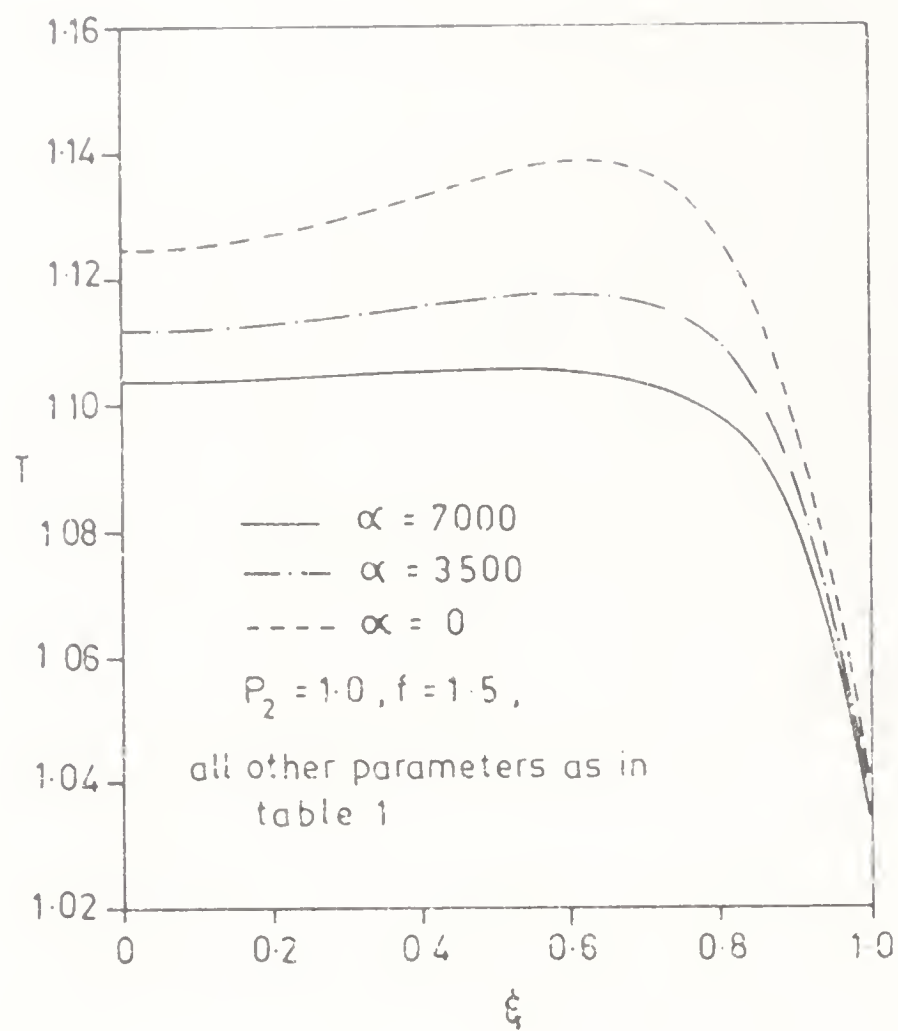


Figure 10. Temperature inside the pellet as a function of radial position.

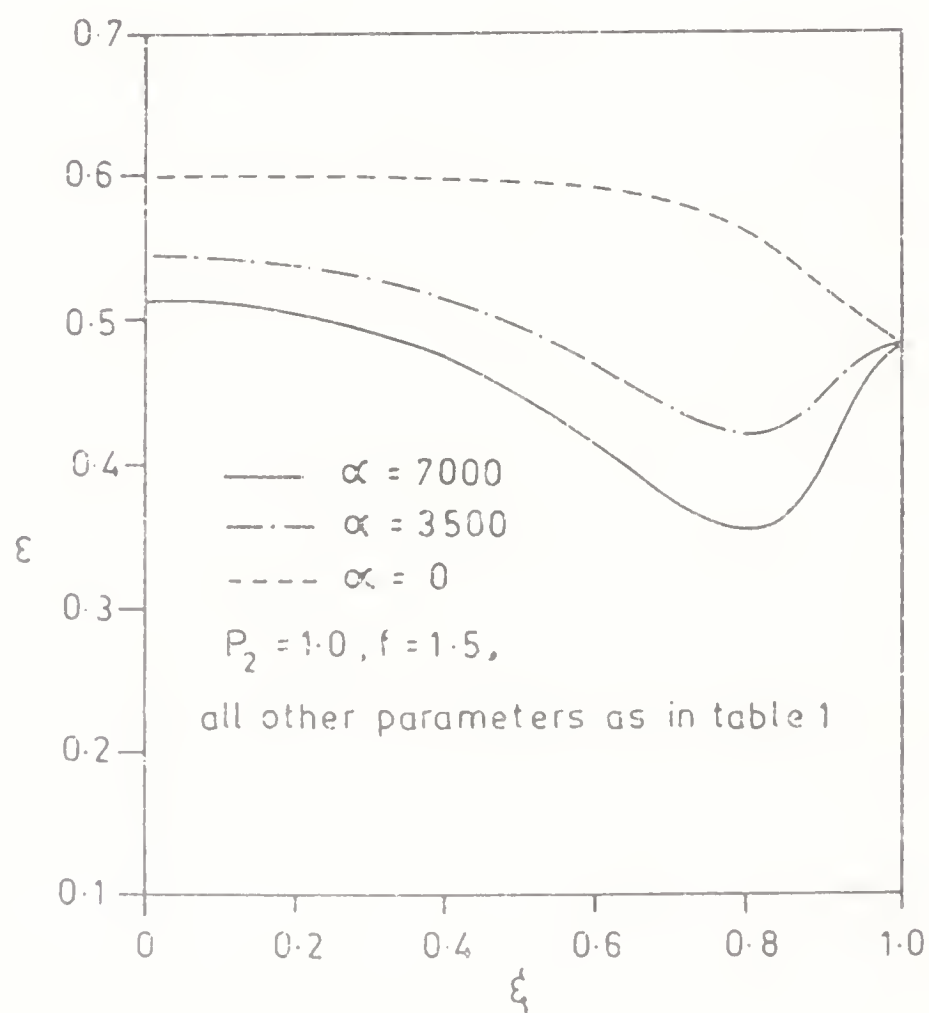


Figure 11. Porosity inside the pellet as a function of radial position.

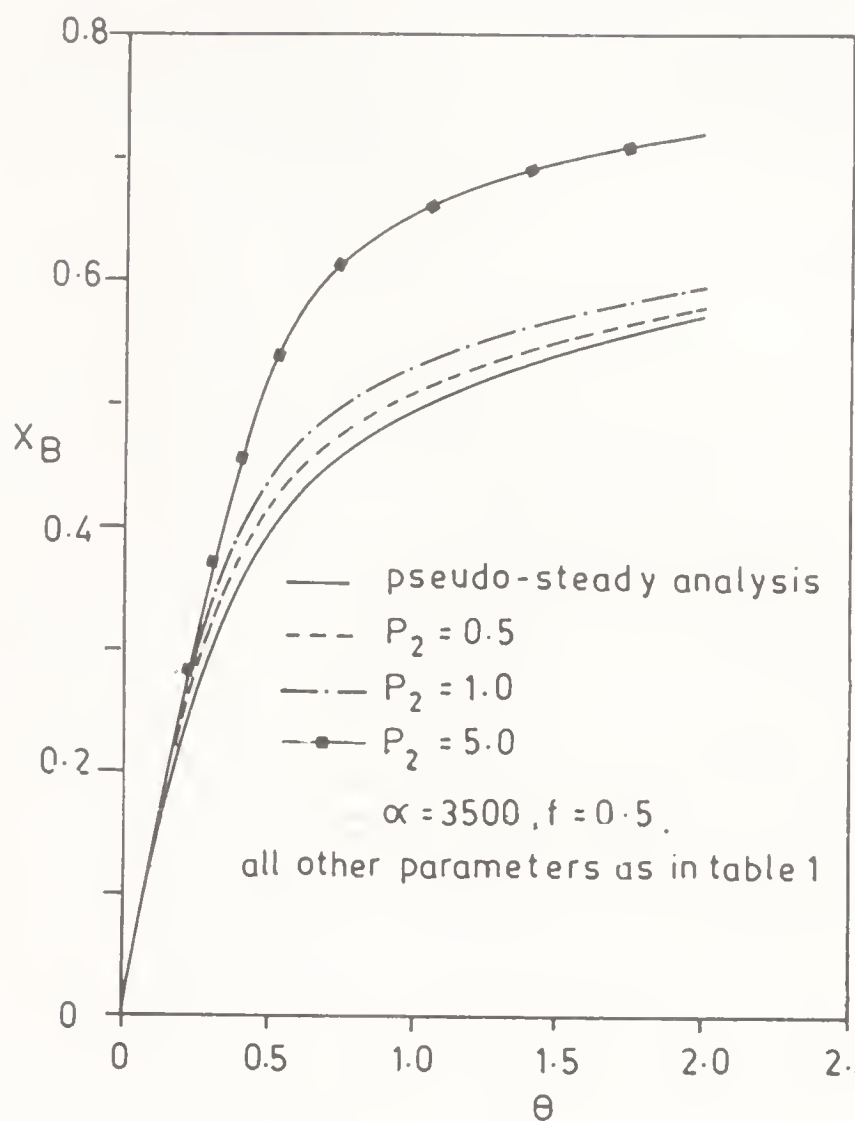


Figure 12. Solid reactant conversion as a function of dimensionless time.

However, slightly lower temperatures cause the porosity to diminish when sintering is present. This can be seen from (24) and (45).

Figure 12 shows the effect of shrinkage ( $f < 1$ ) coupled with sintering on conversions. In this case both phenomena have opposite effects, and for the smaller values of  $P_2$  the difference with the pseudo-steady analysis is less important than for the swelling case.

## 7. Conclusions

A complete transient analysis has been developed to describe the combined effects of sintering and molal density changes during the course of a non-catalytic gas-solid reaction. The results using this transient model have been compared with results obtained using a simplified model in which a pseudo-steady state is assumed. We find significant differences between the results in certain cases. The ratio  $P_2/P_1$  is a good parameter for estimating the differences between the two methods. As this parameter increases, the differences become more pronounced. Furthermore, if sintering is present, the differences are accentuated. For larger values of  $P_2/P_1$ , the conversion, the temperature profiles and the porosity profiles within the pellet can be significantly in error.

This paper is dedicated to Dr L K Doraiswamy on his sixtieth birthday. We are grateful to Consejo Nacional de Investigaciones Cientificas y Tecnicas de la Republica Argentina for a fellowship to one of us (C G Dassori) which made this research possible.

### List of symbols

$A$	frequency factor in the Arrhenius equation,
$A_b$	frequency factor in the rate equation for sintering,
$b$	stoichiometric coefficient of the solid reactant B,
$Bi$	$D_p/k_0r_0$ , Biot number in the particle,
$C$	dimensionless concentration of gas A at any point in the pellet,
$C_A$	concentration of gas A at any point in the pellet,
$C_p$	solid heat capacity,
$D$	diffusivity coefficient,
$D_p$	diffusivity of A through the product layer around the particles,
$D_e$	effective diffusivity of A in the pellet,
$D_{e0}$	initial effective diffusivity of A in the pellet,
$E$	activation energy for the reaction,
$E_s$	activation energy for the sintering process,
$f$	molal volume ratio, defined in (7),
$F$	factor defined in (31),
$g$	stoichiometric coefficient of the solid product G,
$g(z)$	factor by which the tortuosity is increased owing to sintering,
$h_f$	heat transfer coefficient in the gas film,
$\Delta H$	heat of reaction per mole of A,
$k$	first-order reaction rate constant, $\text{cm s}^{-1}$ ,
$k_e$	effective thermal conductivity of the solid,
$k_g$	gas-film mass transfer coefficient,
$M$	molecular weight,
$n_A$	number of moles of A
$Nu^*$	$h_f R_p/k_e$ , modified Nusselt number,
$P_1$	factor defined in (35),
$P_2$	factor defined in (36),
$r$	radial distance inside the pellet,
$r_A$	rate of disappearance of A per unit volume of pellet,
$r_f$	radius of the unreacted core in the particle,
$r_g$	radius of a particle at time $t$ ,
$r_0$	initial radius of the particle,
$R$	gas constant,
$R_p$	radius of the pellet,
$S_B$	reactive surface area per particle,
$Sh$	$k_g R_p/D_{e0}$ , modified Sherwood number,
$t$	time,
$T$	dimensionless temperature,
$T$	temperature,
$T_c$	Tamman temperature,
$X_B$	conversion of the solid reactant B in the pellet,

$z$	fraction of pores removed owing to sintering.
$\alpha$	dimensionless rate constant for sintering, defined in (42).
$\beta$	thermicity factor, defined in (30).
$\gamma$	Arrhenius number, defined in (33).
$\gamma_s$	Arrhenius number for sintering, defined in (43).
$\delta$	$D_c/D_{c0}$ .
$\varepsilon$	porosity.
$\varepsilon_0$	initial porosity.
$\theta$	dimensionless time.
$\kappa$	$\rho_P/\rho_{P0}$ .
$\xi$	dimensionless radial distance inside the pellet.
$\rho$	dimensionless radius of the unreacted core in the particle.
$\rho_B$	density of solid B.
$\rho_g$	dimensionless radius of a particle at time $\phi$ .
$\rho_G$	density of solid G.
$\rho_P^0$	density of the pellet.
$\rho_P$	initial density of the pellet.
$\phi$	Thiele modulus, defined in (30).
$\chi$	$T_c^*/T^{*g}$ .
$\psi$	$\varepsilon/\varepsilon_0$ .

### Superscripts

$g$	= bulk gas phase.
$i$	= initial condition.

### Subscripts

A	= gas reactant A.
B	= solid reactant B.
G	= solid product G.

### References

- Costa E C, Smith J M 1971 *AIChE J.* 17: 947-958  
 Davis M E 1984 *Numerical methods & modeling for chemical engineers* (New York: J Wiley & Sons)  
 Georgakis C H, Chang C W, Szekeley J 1979 *Chem. Eng. Sci.* 34: 1072-1075  
 Hindmarsh A C 1980 *ACM SIGNUM Newsl.* 15: 10  
 Johnson S H, Hindmarsh A C 1983 *J. Comput. Phys.* 52: 503-523  
 Lindner B, Simonsson D 1981 *Chem. Eng. Sci.* 36: 1519-1527  
 Prasannan P C, Ramachandran P A, Doraiswamy L K 1985 *Chem. Eng. Sci.* 40: 1251-1261  
 Ramachandran P A, Doraiswamy L K 1982 *AIChE J.* 28: 881-890  
 Ramachandran P A, Smith J M 1977 *Chem. Eng. J.* 14: 137  
 Ranade P V, Harrison D P 1979 *Chem. Eng. Sci.* 34: 427-432  
 Sampath B S, Ramachandran P A, Hughes R 1975 *Chem. Eng. Sci.* 30: 125-134  
 Sohn H Y, Johnson S H, Hindmarsh A C 1985 *Chem. Eng. Sci.* 40: 2185-2190  
 Sotirchos S V, Yu H-Ch 1985 *Chem. Eng. Sci.* 40: 2039-2052





# Parametric sensitivity and runaway in chemical reactors

MASSIMO MORBIDELLI<sup>†</sup> and ARVIND VARMA\*

Department of Chemical Engineering, University of Notre Dame,  
Notre Dame, IN 46556, USA

<sup>†</sup> Present address: Dipartimento di Ingegneria Chimica e Materiali,  
Universita di Cagliari, Piazza D Armi, 3, Cagliari, Italy

**Abstract.** In certain regions of operating conditions, chemical reactors may exhibit parametric sensitivity; i.e., small changes in one or more of the reactor input parameters lead to much larger changes in the output variables. Since such behaviour leads to deleterious performance, it is of practical interest to identify regions of parametric sensitivity in the reactor parameter space. Until recently, this could be done only to describe thermal runaway, and only for those systems where a temperature profile could be defined. Both of these limitations can be removed by considering *the generalized criterion for parametric sensitivity*, whereby sensitivity of *any* output of the model to *any* input can be treated. Applications of the generalized criterion are discussed, with specific examples including pseudohomogeneous and heterogeneous model tubular reactors, a nonisothermal CSTR, and a polymerization reactor.

**Keywords.** Parametric sensitivity; runaway behaviour; chemical reactors; reactor models.

## 1. Introduction

The concept of parametric sensitivity and runaway in the context of chemical reactors was first introduced by Bilous & Amundson (1956). This indicates a situation where the reactor output variables are sensitive to small variations of the input parameters. The classic example of such behaviour is given by a nonisothermal nonadiabatic tubular reactor, where an exothermic reaction occurs. Here the temperature profile almost inevitably exhibits a maximum value along the reactor length, which is usually referred to as the *hot-spot*. In this case parametrically sensitive behaviour appears in the form of thermal *runaway*, i.e. small variations of any of the reactor inlet or operating conditions (such as inlet or

---

\*To whom correspondence should be addressed.

A list of symbols is given at the end of the paper

cooling temperature) lead to large variations in the axial temperature profile, and particularly in the magnitude of the hot-spot.

Clearly this behaviour has to be avoided in industrial applications, because excessive temperature excursions may promote undesired side reactions, or seriously damage catalyst activity, and eventually may even affect safety of plant operation. Thus, the most attractive solution is to be able to avoid parametrically sensitive behaviour at the earliest stages of reactor design. This can be most conveniently done once the regions of parametric sensitivity in the reactor parameter space have been identified. This has been the goal of most previous work in this area, which will be discussed later in this paper.

The first step towards identification of parametrically sensitive regions is the definition of an a priori criterion which identifies, in mathematical terms, runaway and non-runaway reactor operations. It should be emphasized that such a criterion needs to be intrinsic and a priori, i.e., it should not refer to any characteristic contingent to the specific process under examination (such as the maximum temperature value for catalyst stability etc.).

## 2. Criteria for parametric sensitivity

Most sensitivity criteria used in chemical reactor theory in fact originated in the context of thermal explosion theory (cf. Semenov 1928; Zeldovich *et al* 1985). The reference system here is a homogeneous batch reactor, where an exothermic irreversible  $n$ th order reaction occurs. Using the dimensionless quantities defined in the list of symbols, the relevant mass and heat balances can be written as follows:

$$dx/ds = A(1-x)^n \exp[\gamma(v-1)/v], \quad (1)$$

$$dv/ds = B^0(1-x)^n \exp[\gamma(v-1)/v] - C(v-1), \quad (2)$$

with initial conditions: at time  $s = 0$ ,  $x = 0$  and  $v = v^i$ . The connection with chemical reactor theory is quite evident: (1) and (2) can also be regarded as the steady state mass and heat balances in a tubular pseudohomogeneous plug-flow reactor, with an  $n$ th order reaction and constant temperature external cooling, where  $s$  now represents dimensionless reactor length.

In the context of thermal explosions, two criteria based on some geometric feature of the temperature profile during the reaction have previously been presented by Thomas & Bowes (1961), and Adler & Enig (1964). They indicated runaway as the situation where the temperature profile exhibits a region with positive second-order derivative somewhere before the hot-spot, in the temperature-time or temperature-conversion planes, respectively. Thus *criticality* (viz., the situation separating runaway from non-runaway behaviour), occurs when the region with positive second-order derivative is just at the verge of appearing, i.e., when at the inflexion point also the third derivative vanishes. This corresponds to the condition

$$d^2v/ds^2 = dv^3/ds^3 = 0, \quad (3)$$

for the Thomas & Bowes (1961) criterion, and to

$$d^2v/dx^2 = dv^3/dx^3 = 0, \quad (4)$$

for the Adler & Enig (1964) criterion.

Using (3) or (4), it is possible to evaluate the critical value of one parameter (say, the dimensionless heat of reaction  $\alpha_c = B/A$ ), with all the other parameters fixed, such that for  $\alpha > \alpha_c$  the reactor exhibits parametrically sensitive behaviour, while for  $\alpha < \alpha_c$  it does not. For example, the critical value of the Semenov number,  $\psi = \alpha/\beta$  as computed by the Adler & Enig (1964) criterion is shown in figure 1 as a function of the heat of reaction parameter,  $\alpha$  for various values of the reaction order,  $n$  and for  $\gamma = \infty$ ,  $v^i = 1$ . It appears that as  $\alpha \rightarrow \infty$ ,  $\psi_c \rightarrow e^{-1}$ , which represents the critical value predicted by the classical Semenov theory. The latter is based on the assumption of negligible reactant consumption, and large activation energy for the reaction rate constant, so that (1) and (2) reduce to

$$dv/ds = B^0 \exp[\gamma(v-1)] - C(v-1). \quad (5)$$

It can be readily shown that (5) admits a finite, stable steady state for  $\psi < e^{-1}$ , while for  $\psi > e^{-1}$  the temperature increases unbounded in time. Thus  $\psi = e^{-1}$  could be considered as the boundary separating ignited from the non-ignited regimes. When properly accounting for reactant consumption, as in (1) and (2), the system exhibits a unique stable steady state for all parameter values, so that stability can no longer be considered as a criterion for determining ignition to thermal explosion. In such cases the parametric sensitivity criteria, such as those proposed by Thomas & Bowes (1961) and Adler & Enig (1964) discussed above, can then be used.

These two criteria have been applied in the context of chemical reactors by Dente & Collina (1964), and Morbidelli & Varma (1982), respectively. The first criterion was also adopted by van Welsenaere & Froment (1970), who also

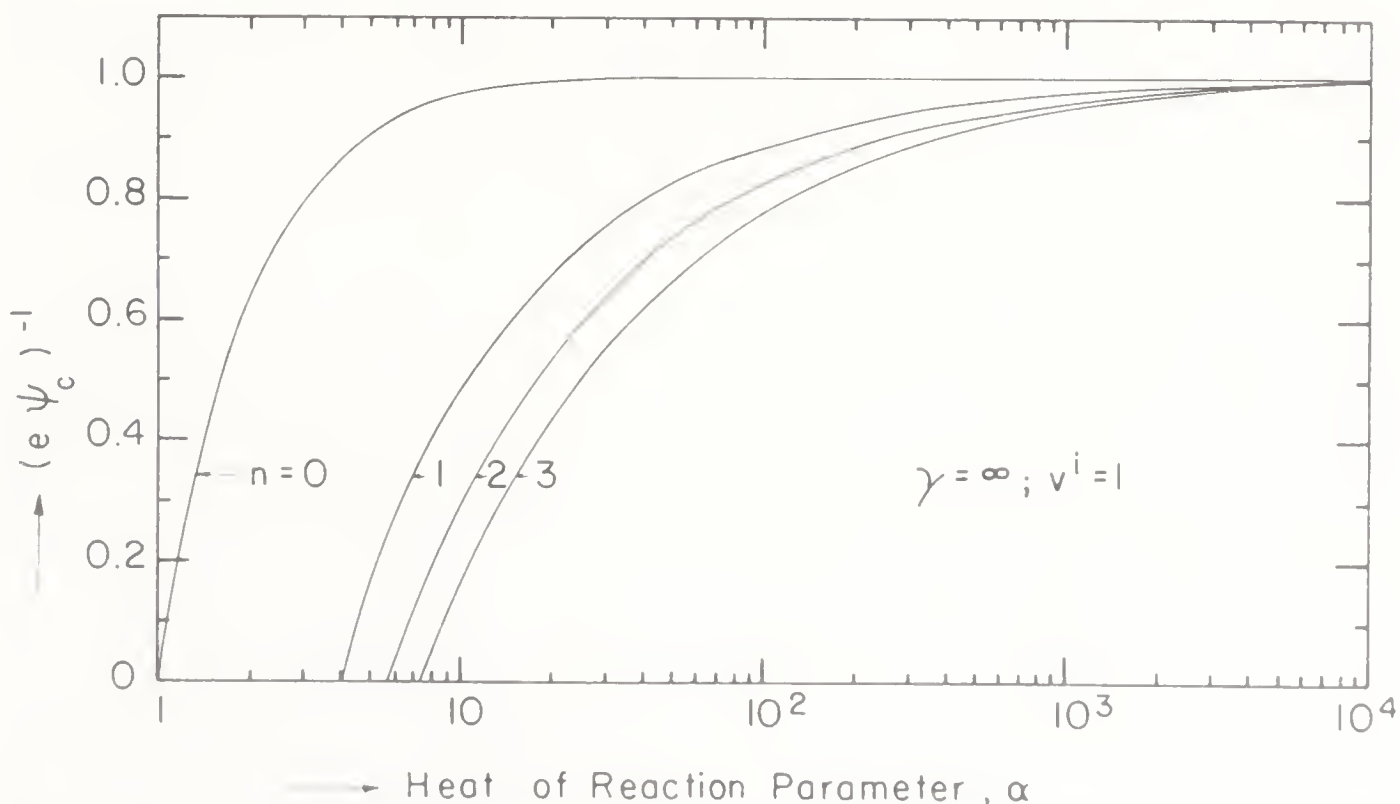


Figure 1. Values of the quantity  $(e\psi_c)^{-1}$  as a function of the heat of reaction parameter,  $\alpha$  for various values of the reaction order,  $n$ , using the Adler & Enig (1964) criterion [from Morbidelli & Varma 1987a].



developed approximate simple relationships for establishing the boundary between runaway and non-runaway conditions.

A detailed comparison among these and other criteria of this type has been reported recently (Morbidelli & Varma 1985). As a conclusion, the Adler & Enig (1964) criterion was recommended, since it provides less conservative results (i.e., the smallest sensitivity region) and does not predict as safe conditions which in fact are not so.

As mentioned above, all the previously examined criteria are based on some geometric feature of the temperature profiles. As a consequence, they can be used to describe only thermal runaway, and can be applied only to systems where a temperature profile can be defined. This limits the generality of these criteria, and motivates the introduction of the new criterion described in the next section.

### 3. The generalized criterion for parametric sensitivity

In general, for any given model, we can define the *normalized sensitivity* of any output of the model to any of its inputs. For example, with reference to the model given by (1) and (2), the *local normalized sensitivity* of the temperature  $v(s)$  with respect to any of the model parameters,  $\phi$  (such as  $v'$ ,  $\gamma$ ,  $n$  . . . ) is defined as follows)

$$s(v; \phi) = (\phi/v) (\partial v / \partial \phi), \quad (6)$$

When studying the parametric sensitivity behaviour of tubular chemical reactors, it is particularly important to control the magnitude of the hot-spot, i.e., of the maximum temperature value along the reactor length. To this aim, it is convenient to consider the *objective normalized sensitivity*

$$S(v^*; \phi) = (\phi/v^*) (\partial v^* / \partial \phi), \quad (7)$$

where  $v^*$  indicates the maximum temperature value. Let us now consider, for convenience, the pseudohomogeneous plug-flow reactor model given by (1) and (2), and analyse its behaviour in the  $v-x$  phase plane:

$$dv/dx = \alpha^\circ - \beta (v-1) / [(1-x)^n \exp[\gamma(v-1)/v]] \quad (8)$$

with initial condition:  $v = v'$  at  $x = 0$ . The hot-spot objective sensitivity  $S(v^*; \phi)$  with respect to the generic model parameter  $\phi$ , can be computed efficiently through suitable numerical techniques reported recently (Morbidelli & Varma 1987a). The sensitivity values are shown in figure 2 as a function of the Semenov number  $\psi = \alpha/\beta$ , for various different choices of the input parameter,  $\phi$ . In particular, the following five independent dimensionless parameters are considered:  $\psi$ ,  $\alpha$ ,  $\gamma$ ,  $n$  and  $v'$ . It appears that for increasing values of  $\psi$ , the sensitivity  $S(v^*; \phi)$  increases first, then goes through a maximum, and eventually decreases approaching zero. The region corresponding to large sensitivity values indicates a sharp increase in the magnitude of the hot-spot of the steady-state temperature profile, which represents the transition from low to high temperature operation. Thus, it appears reasonable to take the  $\psi$  value corresponding to the sensitivity maximum as the *critical condition*, separating safe from runaway operating conditions for the reactor. Thus for  $\psi < \psi_c$  the reactor operates in a safe regime, which for  $\psi > \psi_c$  it operates in the runaway region (Lacey 1983; Boddington *et al* 1983; Morbidelli & Varma 1987a).

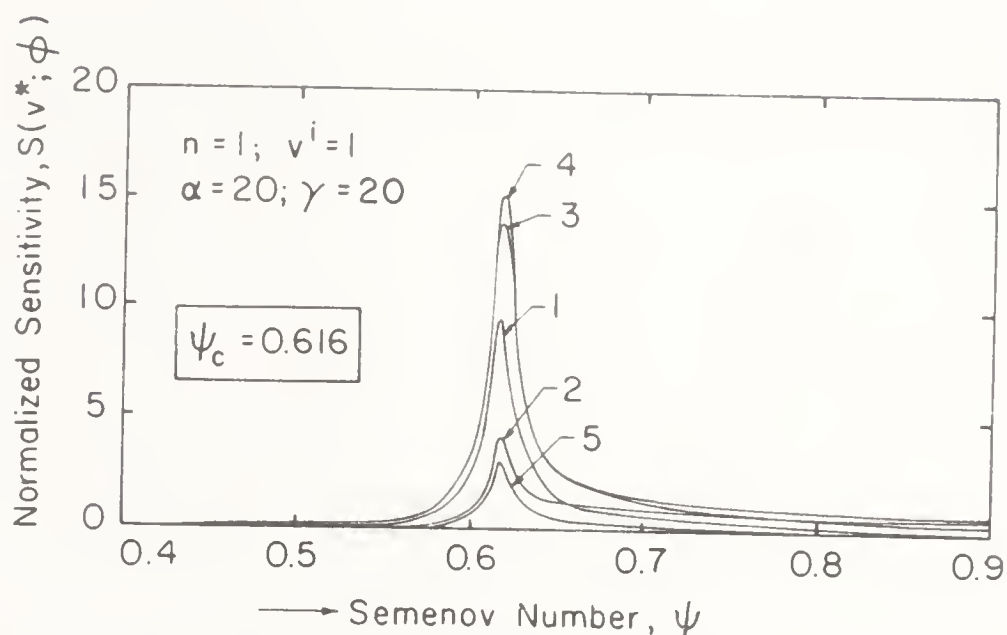


Figure 2. Normalized sensitivity,  $S(v^*; \phi)$  as a function of the Semenov number,  $\psi$ , for various input parameters,  $\phi$ : 1 =  $\psi^0$ , 2 =  $\alpha^0$ , 3 =  $v^i$ , 4 =  $\gamma$ , 5 =  $n$  [from Morbidelli & Varma 1987a].

Using the above definition of criticality it follows, in principle, that the sensitivity boundary  $\psi_c$  is a function of the particular input parameter  $\phi$  considered in the definition of sensitivity  $S(v^*; \phi)$ . However, it appears from the results shown in figure 2, that the sensitivity curve exhibits its maximum value at the *same*  $\psi$  value, independent of the particular choice of the input parameter,  $\phi$ . In other words, the reactor becomes simultaneously sensitive to small variations of *any* of its input parameters (whether they are operating conditions, inlet conditions, or kinetic and physicochemical parameters). This provides an *intrinsic* nature to the criterion reported above, which we can then refer to as a *generalized criterion for parametric sensitivity* (Morbidelli & Varma 1986b, 1987a.)

It is worth noting that such a criterion does not refer to any geometric feature of the reactor temperature profile, and in fact it can be applied to any reactor type (other than tubular) and to any characteristic of reactor behaviour (other than temperature). Examples of applications to such systems are reported in later sections.

In order to investigate more closely the sensitivity behaviour of the pseudohomogeneous tubular reactor (8), let us consider the critical values  $\psi_c$  reported in table 1 as a function of the heat of reaction parameter,  $\alpha$ , obtained by maximizing the objective sensitivity  $S(v^*; \phi)$  for various choices of the input parameter,  $\phi$ . It appears that for large values of  $\alpha$ , where runaway is a very strong phenomenon (i.e., leads to large temperature increase), all  $\psi_c$  values are identical to the third digit, independent of the particular parameter  $\phi$  considered.

This generalized character vanishes for smaller values of  $\alpha$ . However, it may be noted that significant differences among the various  $\psi_c$  values occur only for very low  $\alpha$  values, where the energy content of the reaction is so small that runaway is a mild phenomenon anyway. This behaviour is more easily understood by the sensitivity plots shown in figures 3 and 4, for activation energy values  $\gamma = 5$  and 10, respectively. It appears that for  $\alpha$  and/or  $\gamma$  values sufficiently large, the sensitivity peak is rather sharp and its magnitude is large. This is the case where thermal runaway is a significant phenomenon, and the generalized criterion mentioned

**Table 1.** Critical values  $\psi_c$ , as a function of  $\alpha$ , obtained by maximizing  $S(v^*; \phi)$  with respect to  $\psi$  for fixed  $\alpha$ ,  $\gamma$ ,  $v'$ , and  $n$ ;  $\gamma = \infty$ ,  $v' = 1$ ,  $n = 1$ .

$\alpha \rightarrow$	$\psi \rightarrow$	$\alpha^0$	$v'$	$\gamma$	$n$	
	(1)	(1)	(1)	(1)	(1)	(2)
3	1.66	44.3	4.78	2.43	2.53	*
4	1.54	5.88	2.63	1.96	1.99	*
5	1.36	2.58	1.80	1.58	1.58	2.38
7	1.05	1.22	1.13	1.10	1.09	1.09
10	0.781	0.794	0.787	0.786	0.784	0.758
20	0.545	0.545	0.545	0.545	0.545	0.545
30	0.490	0.490	0.490	0.490	0.490	0.490

\* No runaway for any  $\psi$ .

(1) Criterion based on the maximum in the  $S(v^*; \phi) - \psi$  curve;

(2) Criterion based on the simultaneous vanishing of second and third derivatives of  $v$  vs.  $x$  (Adler & Enig 1964).

above holds. On the other hand, for small  $\alpha$  and/or  $\gamma$  values (say,  $\alpha \lesssim 7$  and  $\gamma \lesssim 5$ ), the hot-spot sensitivity is always very small, so that it is actually not possible to talk about thermal runaway at all. This is the situation where the generalized criterion loses its generalized character, and its answer becomes a function of the particular input parameter,  $\phi$ , considered in the sensitivity analysis.

This behaviour has been found consistently in various different reacting systems, so that it can be concluded that in the parameter region where the generalized sensitivity criterion does not hold, the system may be considered non-sensitive, in the sense that thermal runaway would be a very mild phenomenon, and thus there is little need for the a priori definition of critical boundaries for safe reactor operation. When even under such conditions a sensitivity analysis is desired to be performed, then it has to be carried out separately for each of the input parameters,  $\phi$ , of interest. It should be noted that this separate analysis cannot be done using the

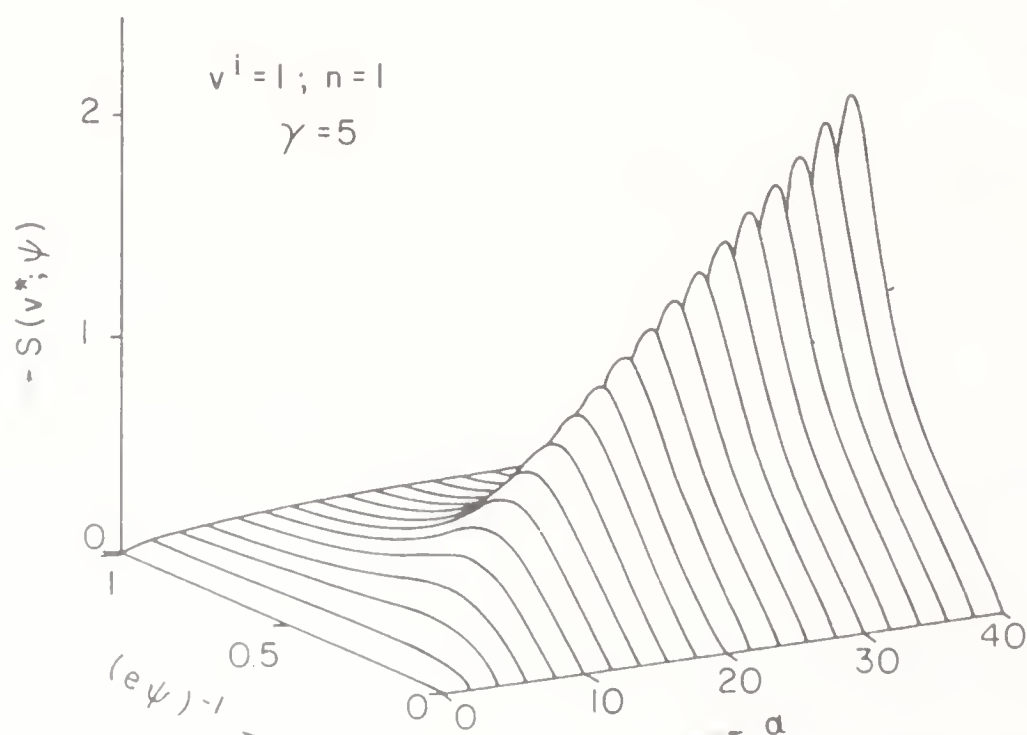


**Figure 3.** Normalized sensitivity,  $S(v^*; \psi)$  as a function of  $\psi$  and  $\alpha$ ;  $\gamma = 5$ ,  $v' = 1$ ,  $n = 1$  [from Morbidelli & Varma 1987a].



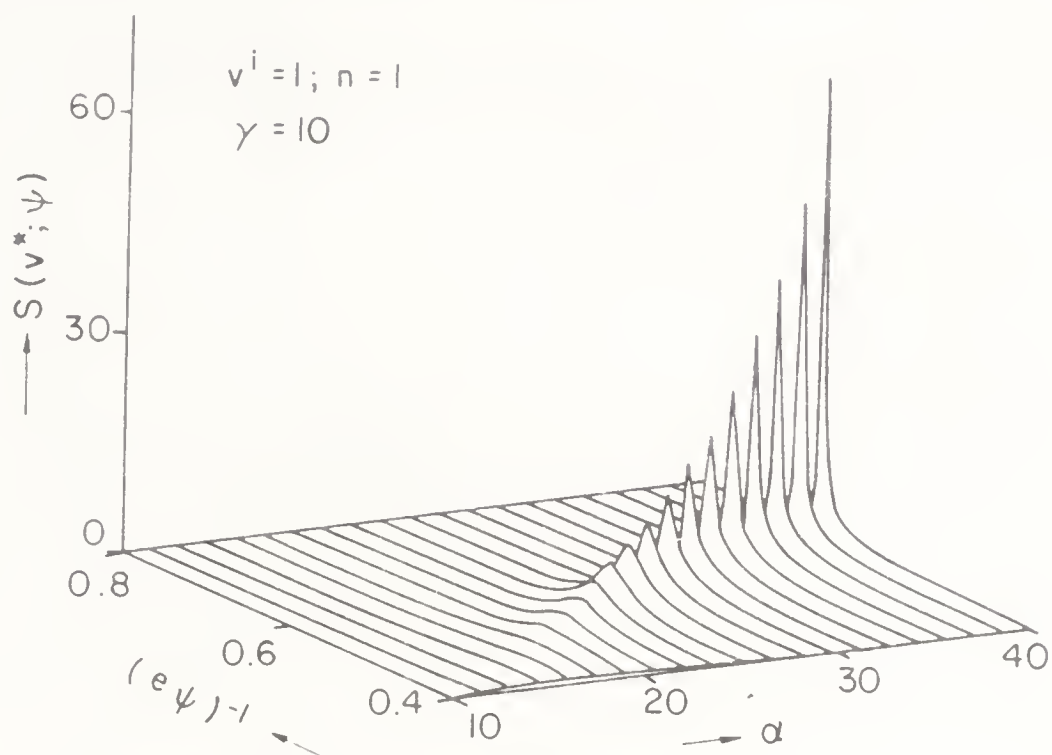


Figure 4. Normalized sensitivity,  $S(v^*; \psi)$  as a function of  $\psi$  and  $\alpha$ ;  $\gamma = 10$ ,  $v' = 1$ ,  $n = 1$  [from Morbidelli & Varma 1987a].

geometric sensitivity criteria examined previously, since they do not analyse separately the effects of the various parameters. In fact, such criteria refer to a generic sensitive behaviour of the system, thus implicitly assuming the generalized behaviour, which actually can be proven rigorously only by resorting to the detailed sensitivity analysis reported above.

A final point is the comparison between predictions of the generalized sensitivity criterion and of those based on the geometric feature of the temperature profiles. For this, the critical Semenov number as predicted by the Adler and Enig criterion, in the case of a pseudohomogeneous plug-flow reactor model (8), is also reported in table 1 as a function of the heat of reaction parameter,  $\alpha$ . It appears that for increasing  $\alpha$  values the critical Semenov number predicted by the Adler and Enig criterion approaches the corresponding value predicted by the generalized sensitivity criterion. This indicates that, when thermal runaway is a significant phenomenon, the two criteria yield the same answer. This supports the validity of the critical boundaries in the reactor parameter space reported earlier by Morbidelli & Varma (1982). These were computed through the Adler and Enig criterion for a pseudohomogeneous plug-flow reactor where an irreversible  $n$ th order reaction occurs, with no limitations on the activation energy,  $\gamma$ , or the inlet temperature,  $v'$ .

In the sequel, we report sensitivity analyses of some reacting systems of interest in applications, where the flexibility of the generalized sensitivity criterion is clearly demonstrated.

#### 4. Sensitivity analysis of a tubular catalytic reactor

Let us consider the heterogeneous one-dimensional plug-flow model of a catalytic reactor where an  $n$ th order irreversible reaction occurs. The catalyst particle is



described through the internal isothermal model (cf. Carberry 1975; Pereira *et al* 1979), using the following approximate expression for the effectiveness factor (cf. Froment & Bischoff 1979; Doraiswamy & Sharma 1984)

$$\eta = [3\Phi \coth(3\Phi) - 1]/3\Phi^2, \quad (9)$$

where  $\Phi$  is the normalized Thiele modulus

$$\Phi^2 = \Phi_w^2 (1 - x_p)^{n-1} f(v_p). \quad (10)$$

Note that the quantities with subscript  $p$  refer to the catalyst surface, so that the effectiveness factor in (9) accounts only for intraparticle mass transport resistance. Using the dimensionless quantities defined in the list of symbols, the mass and heat balances in the fluid and in the catalyst phases may be written as follows

$$dv/dx = \alpha^\circ - \beta(v-1)/[(1-x_p)^n f(v_p) \eta(x_p, v_p)], \quad (11)$$

$$x_p = x + (Le/\alpha^\circ)(v_p - v), \quad (12)$$

$$v_p = \dot{v} + (A_p \alpha^\circ / Le)(1 - x_p)^n f(v_p) \eta(x_p, v_p), \quad (13)$$

with initial condition:  $v = v^i$  at  $x = 0$ .

The sensitivity behaviour of catalytic reactors has been examined by Rajadhyaksha *et al* (1975) using the van Welsenaere & Froment (1970) criterion applied to the fluid temperature. In this work, simple analytical expressions were reported which describe the effects of mass and heat transfer limitations on the boundary between safe and runaway operating conditions for the reactor. It was noted that this approach accounts for runaway in the fluid phase, the so-called *global sensitivity*, but not for those cases where runaway is induced by the catalyst temperature, according to the *local sensitivity* phenomenon described by McGreavy & Adderley (1973). The latter occurs when the system approaches the situation where the derivative of the fluid to the particle temperature vanishes, as in the region of incipient multiplicity. In this case, small variations of the fluid temperature lead to large variations of the particle temperature, which are then responsible for promoting runaway.

In order to account for both global and local sensitivity behaviour, Morbidelli & Varma (1986a, 1987b) have applied the Adler and Enig criterion directly to the catalyst temperature versus conversion profile. This approach is valuable in applications where the quantity to be controlled is indeed the catalyst temperature, which is the one controlling both the reaction rate and selectivity, and also catalyst activity and durability.

An important aspect in the sensitivity study of heterogeneous reactors is the issue of steady state multiplicity, which has been discussed in detail elsewhere (Morbidelli & Varma 1986a). Without entering into details of the multiplicity analysis, the main conclusion may be summarized with arguments based on physical intuition. Thermal runaway corresponds to a situation where the catalyst temperature increases sharply, but yet remains a *continuous function*, along the reactor length. The occurrence of ignition from a low to a high conversion steady state for some particle along the reactor, as a consequence of its multiplicity behaviour, is a more drastic phenomenon, leading to a *discontinuous jump* of the catalyst temperature along the reactor length. Thus, considering steady state

conditions corresponding to increasing values of, say, the heat of reaction parameter  $\alpha$ , it is expected (and it has indeed been shown) that runaway conditions will always occur before (i.e. for smaller values of  $\alpha$ ) those involving some temperature ignition along the reactor. In other words, multiplicity can manifest itself only for situations which lie within the parametric sensitivity region, and thus it does not need to be considered for establishing the boundaries between safe and runaway operating conditions for the reactor.

Note that as discussed elsewhere (Morbidelli & Varma 1986a, 1986b), in order to derive the regions of parametric sensitivity, the case of catalyst particles operating in the high conversion steady state does not need to be considered. Strictly speaking, this is a non-sensitive condition; in this state, the temperature values are so high (of the order of those attained as a consequence of thermal runaway) that reactant is depleted soon after the inlet, and thus further runaway does not occur.

The generalized sensitivity criterion described above has been applied to the heterogeneous models 11–13 by Morbidelli & Varma (1986b). A typical behaviour of sensitivity of the catalyst temperature hot-spot with respect to the model parameter  $\phi$ ,  $S(v^*; \phi)$  is shown in figure 5, for various choices of  $\phi$ . As in the case of the pseudohomogeneous reactor previously examined, it appears that the sensitivity curve exhibits a sharp peak at a certain value of  $\alpha$ , corresponding to the critical value for runaway, which does not depend upon the particular parameter  $\phi$

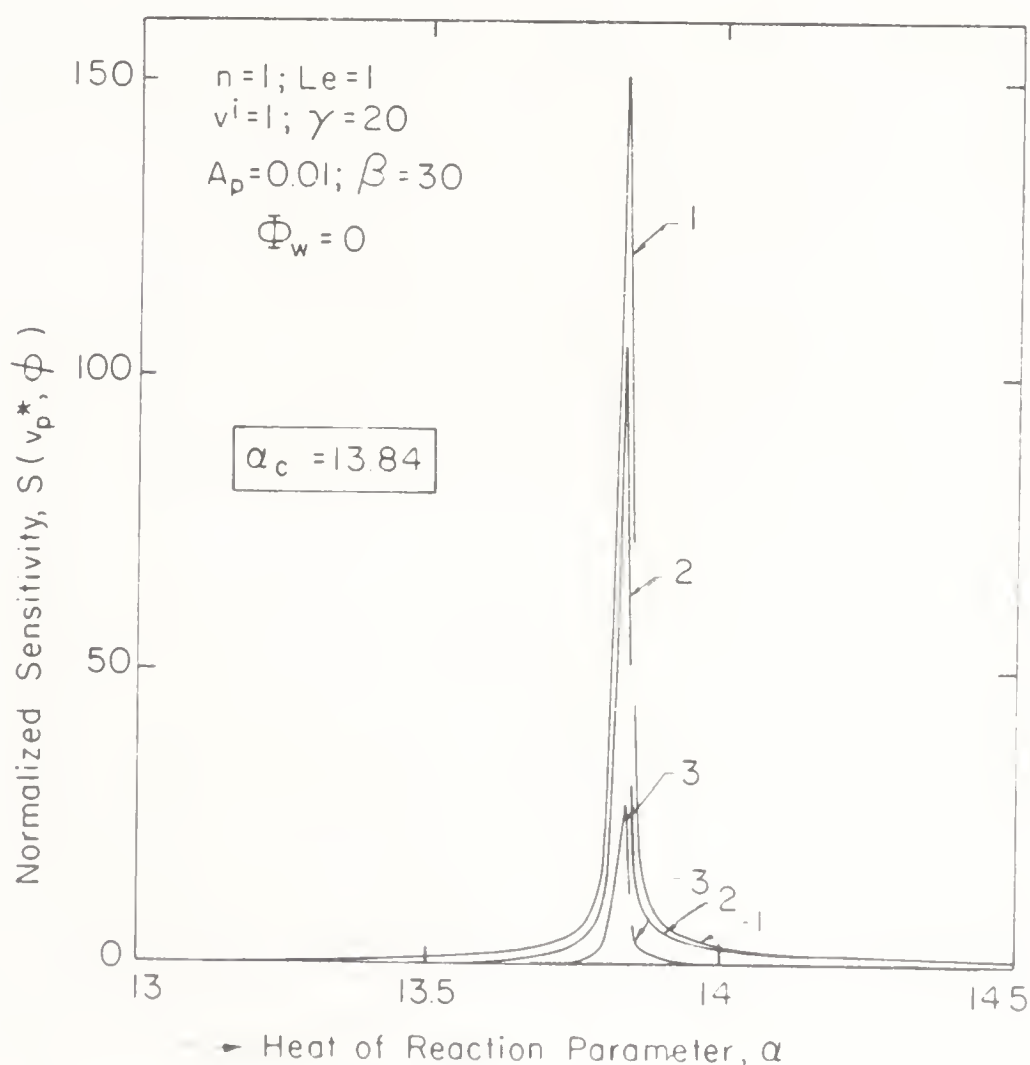


Figure 5. Normalized sensitivity,  $S(v_p^*; \phi)$  as a function of the heat of reaction parameter,  $\alpha$ , for various input parameters,  $\phi$ : 1 =  $v^i$ , 2 =  $\alpha^i$ , 3 =  $A_p$  [from Morbidelli & Varma 1986b].

considered in the definition of sensitivity. This confirms the validity of the generalized sensitivity criterion also in the case of heterogeneous catalytic reactors.

It should be emphasized that the same observations made earlier for pseudohomogeneous reactors hold true in this case also. Thus, for low heat of reaction and/or activation energy values, the answer to the criterion becomes dependent upon the particular model input parameter  $\phi$  under examination, thus indicating that the sensitivity character of the system is mild. On the other hand, for strongly sensitive systems, the critical boundaries predicted by this criterion are in good agreement with those obtained from the Adler and Enig original criterion, but applied to the catalyst temperature. This finding supports the reliability of the critical boundaries in the reactor parameter space computed through this criterion for a wide variety of operating conditions (Morbidelli & Varma 1986a, 1987b).

In order to verify the reliability of the conclusions reported above, the boundary between safe and runaway reactor operations predicted by the generalized sensitivity criterion has been compared with the experimental findings of Emig *et al* (1980). The experimental data refer to a fixed-bed reactor for vinyl acetate synthesis using supported zinc acetate as the catalyst. The results obtained are summarized in figure 6, where open and closed circles represent operating

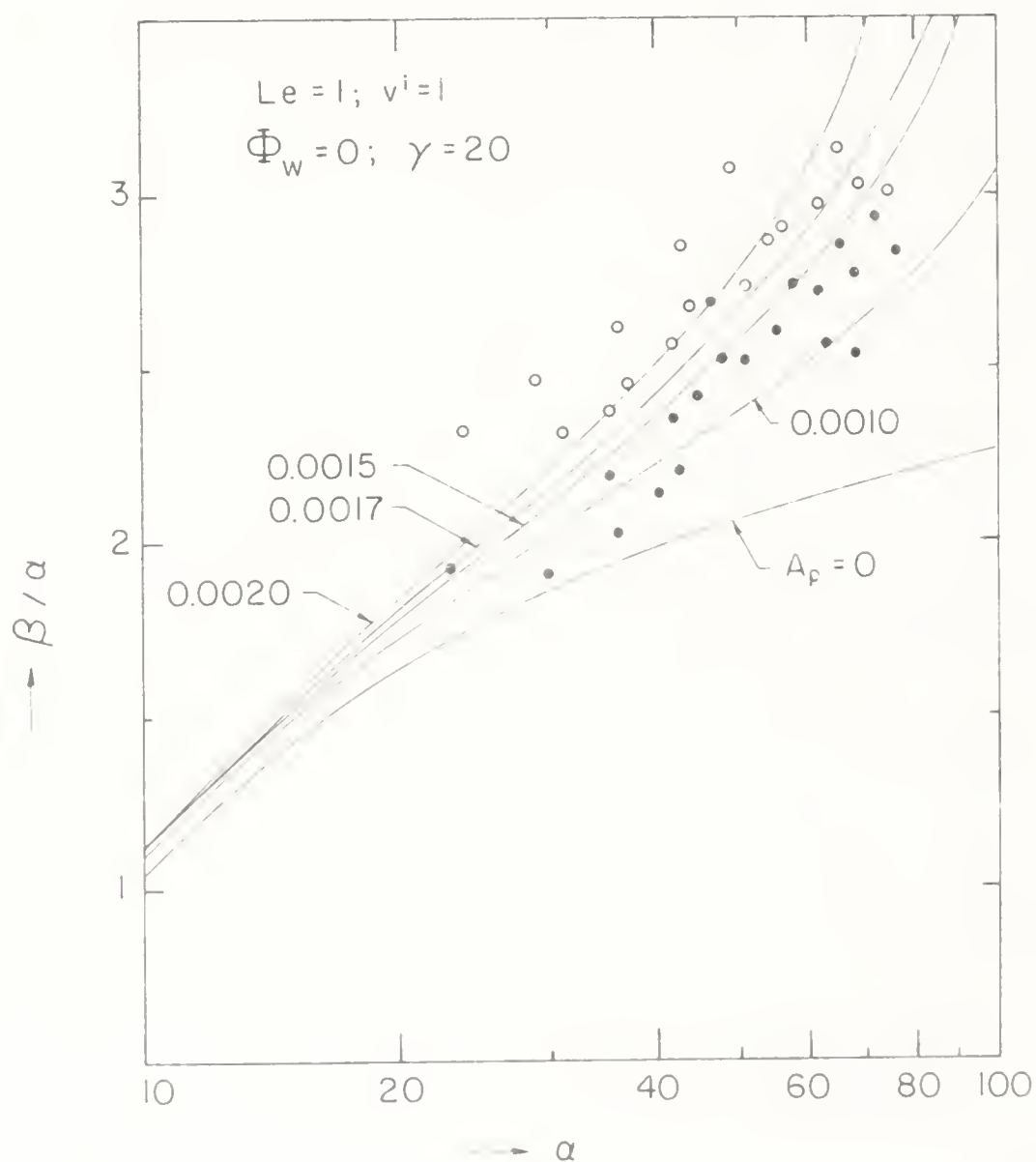


Figure 6. Comparison of the sensitivity region boundaries predicted by the sensitivity criterion and the experimental data of Emig *et al* (1980); experimental data: ○ = non-sensitive, ● = sensitive [from Morbidelli & Varma 1986b].



conditions for the reactor which were observed experimentally to exhibit non-sensitive and sensitive behaviour, respectively. Thus, the correct criticality curve predicted by the sensitivity criterion should separate the parameter space leaving all the open circles in the upper region and all the closed ones in the lower region. The curves shown in figure 6 were all computed through the generalized sensitivity criterion for various values of the mass transfer resistance parameter,  $A_p$ . It appears that the pseudohomogeneous model (i.e.  $A_p = 0$ ) does not properly represent the behaviour of the experimental system, which instead is reproduced well by the heterogeneous model accounting for mass and heat transfer resistances (see Morbidelli & Varma 1986b, for additional details).

## 5. Sensitivity analysis of a homogeneous CSTR

The homogeneous nonisothermal CSTR model is probably the most widely studied from the steady state multiplicity and transient behaviour points of view; however, very little has been reported about its sensitivity behaviour. This is readily understood since in a CSTR, there is no temperature profile – thus all previous criteria based on geometric considerations about such a profile cannot be applied. In a recent analysis, Barkleew (1984) identified the occurrence of runaway arbitrarily with the occurrence of multiplicity. More recently, Chemburkar *et al* (1986) have analysed sensitivity behaviour of the CSTR using the generalized sensitivity criterion. This can be done by evaluating the sensitivity of the outlet temperature,  $v$ , with respect to the generic model input parameter,  $\phi$ , i.e.  $S(v; \phi)$ . Consider the CSTR model in the following dimensionless form (Kauschus *et al* 1978):

$$\alpha^{n-1} - Da(1 + \alpha - v)^n \exp[\gamma(v - 1)/v]/(v - 1) = 0. \quad (14)$$

$\phi$  may be taken as any of the four independent model input parameters:  $\alpha$ ,  $Da$ ,  $\gamma$  and  $n$ . The outlet temperature sensitivity values  $S(v; \phi)$ , for each such choice of the input parameter  $\phi$ , are shown in figure 7. It appears that, again, a sensitivity peak appears identifying a critical value for the heat of reaction parameter,  $\alpha$ , which is independent of the particular choice of  $\phi$  – thus again leading to the generalized sensitivity criterion.

It is of interest to note that in the limit of large heat of reaction,  $\alpha$  and activation energy,  $\gamma$ , the critical Semenov number (defined as usual as the ratio between the rate of heat production and heat removal, i.e.,  $\psi = Da \gamma \alpha$ ) approaches the classical value  $e^{-1}$ . This indicates some intrinsic character of the sensitivity phenomenon, which brings together tubular and well-stirred reactors.

An important issue here again is the connection between sensitivity and multiplicity. Figures 8a and b show the outlet temperature and its sensitivity to  $\alpha$ ,  $S(v; \alpha)$  as a function of  $\alpha$  for two different values of  $Da$ . In the first case uniqueness prevails, but yet sensitivity can occur, and it is indeed possible to define a critical  $\alpha$  value beyond which runaway occurs. In the second case the reactor exhibits typical multiplicity behaviour, and the sensitivity peak degenerates into a sharp increase to an infinite value, which is reached precisely at the bifurcation point  $\alpha^*$ . Thus, in this case, but not in the first, sensitivity and multiplicity occur simultaneously. It is again confirmed that multiplicity occurs only in the sensitivity region, while the



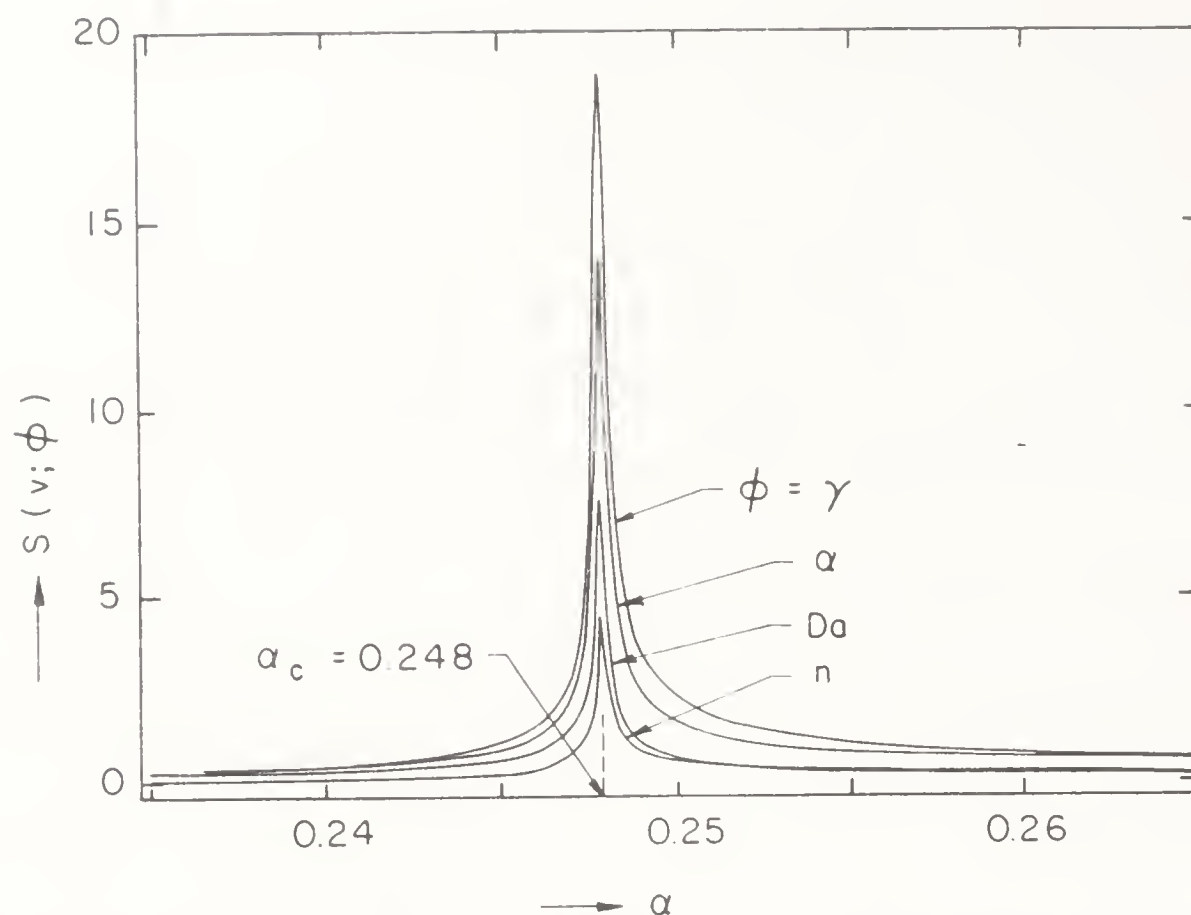


Figure 7. Behaviour of sensitivities  $S(v; \phi)$  with the dimensionless heat of reaction,  $\alpha$ , for a CSTR;  $Da = 0.11$ ,  $\gamma = 20$ ,  $n = 1$  [from Chemburkar *et al* 1986].

reverse is not true. This issue is discussed in detail elsewhere (Chemburkar *et al* 1986), and a conclusion with respect to practical applications is that the first objective should be to establish the boundary of the sensitivity region, since once this is avoided, multiplicity is also automatically avoided.

## 6. Sensitivity analysis of tubular reactors with complex kinetic schemes

An advantage of the generalized sensitivity criterion over the previous ones based on geometric features of the temperature profile, is the possibility of analysing the sensitivity of quantities other than the temperature hot-spot. This can be of great interest in applications, as for example in investigating the sensitivity of selectivity and/or yield in the case of multiple reactions, or the sensitivity of the molecular weight distribution in the case of polymerization reactors. Tjahjadi *et al* (1987) have recently analysed the sensitivity behaviour of a low density polyethylene tubular reactor using the generalized sensitivity criterion. The reaction scheme in this case is more complex, since it involves an initiation reaction, through the thermal decomposition of initiator, I,



a propagation reaction ,



where M denotes the monomer, and finally a radical termination reaction



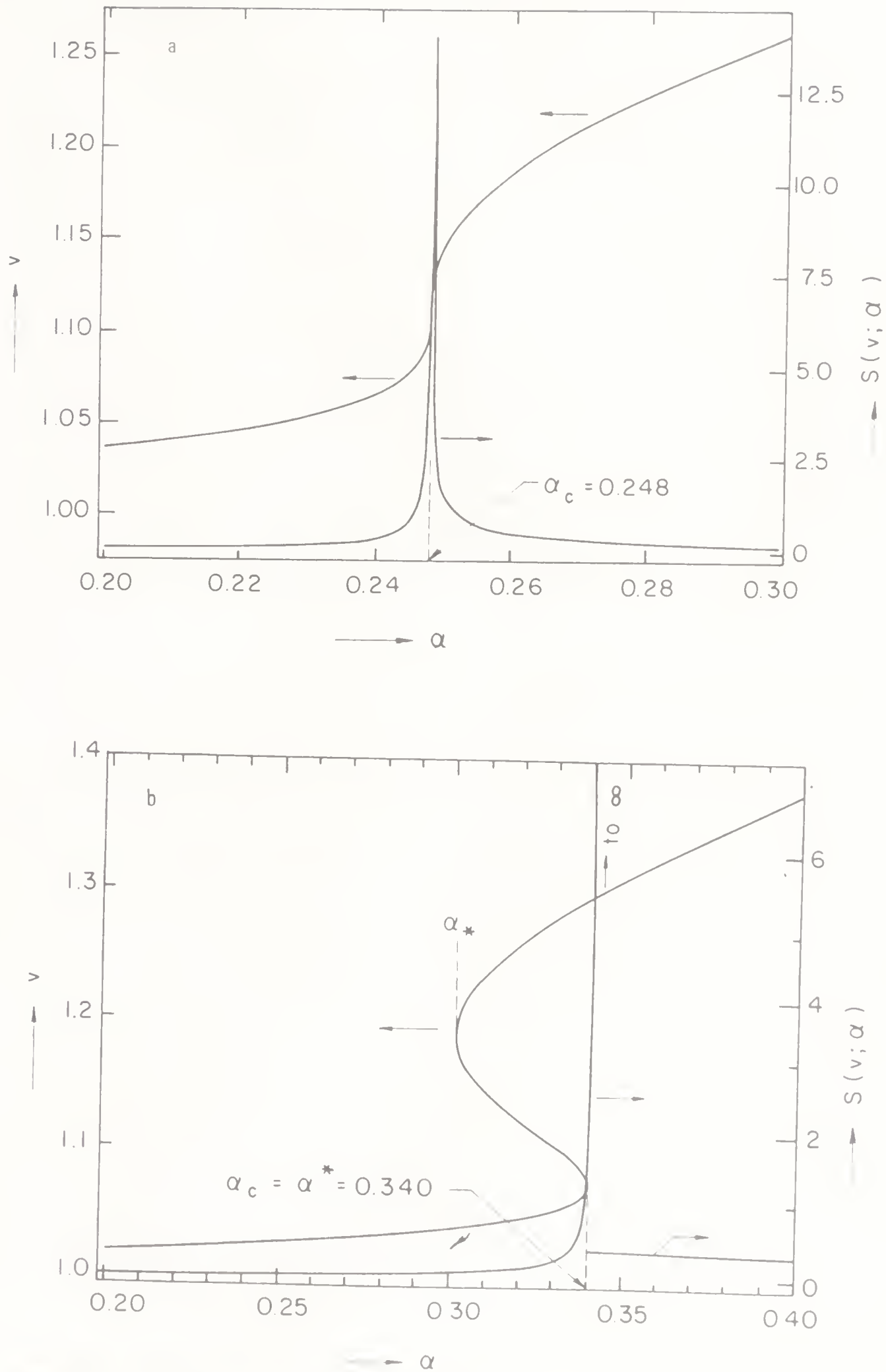


Figure 8. Effect of the dimensionless heat of reaction,  $\alpha$ , on  $v$  and  $S(v; \alpha)$  for a CSTR [from Chemburkar *et al* 1986] (a) Uniqueness region,  $Da = 0.11$ ,  $\gamma = 20$ ,  $n = 1$  (b) Multiplicity region,  $Da = 0.07$ ,  $\gamma = 20$ ,  $n = 1$ .

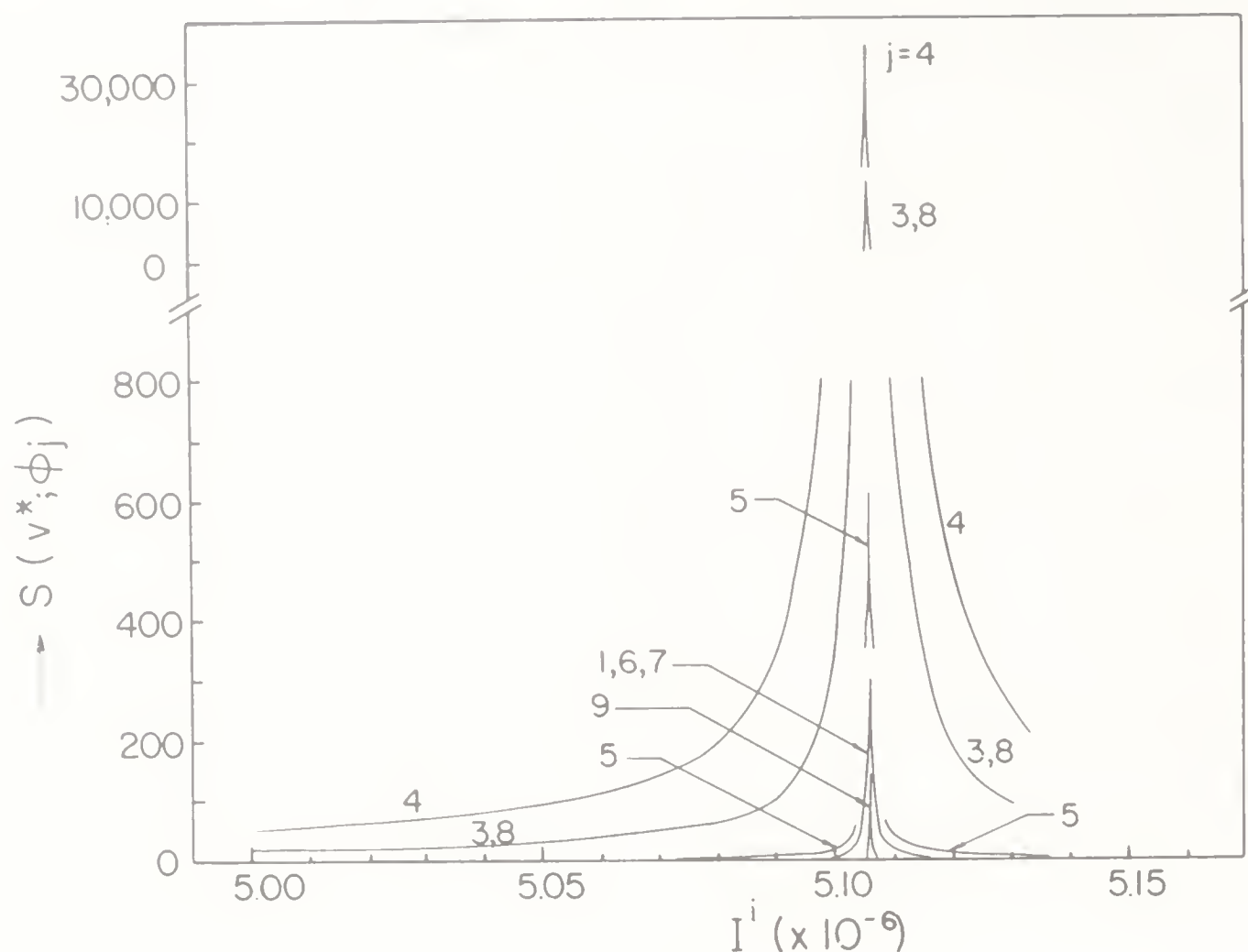


Figure 9. Normalized sensitivity  $S(v^*; \phi_j)$  as a function of the inlet initiator concentration,  $I^i$ , for a low density polyethylene reactor [from Tjahjadi *et al* 1987].

In this case several quantities can be taken in the sensitivity analysis. In figure 9 the sensitivity of the temperature maximum is shown as a function of the inlet initiator concentration,  $I^i$ , for various choices of the model input parameter,  $\phi_j$ . Without going into details, it is sufficient to mention here that the parameters  $\phi_j$  considered in figure 9 involve various characteristics of the system such as: initiator and monomer inlet concentrations, inlet temperature, heat transfer coefficient, activation energies of initiation, propagation and termination reactions etc. The typical behaviour of the sensitivity values shown in this figure demonstrates once again the reliability and flexibility of the generalized sensitivity criterion.

It is of interest to also study the sensitivity of other quantities, such as average molecular weight, or the variance of the molecular weight distribution, to the reactor operating conditions. Clearly, the sensitivity behaviour of these quantities is correlated to thermal sensitivity but their magnitudes depend on the particular operating conditions, and on the occurrence of other related phenomena, such as for example the gel-effect. Certainly, avoiding those regions in the reactor parameter space, where molecular weight sensitivity is significant, is of interest in the design of polymerization reactors, and this issue has also been discussed by Tjahjadi *et al* (1987).

## List of symbols

$a$	area of heat transfer, $\text{m}^2$ ,
$a_v$	particle surface area per unit reactor volume, $\text{m}^{-1}$ ,
$A$	$k(T_w)c^{l''-1}L/\bar{v}$ ,
$A_p$	mass transfer resistance parameter, $\rho_b k(T_w)c^{l''-1}/k_g a_v$ ,
$B$	$K(T_w)c^{l''}L(-\Delta H)\gamma/\rho_f C_p \bar{v} T_w$ ,
$B^\circ$	$B/\gamma$ ,
$c$	reactant concentration, $\text{mol}/\text{m}^3$ ,
$C$	$4LU/\bar{v}\rho_f C_p d_t$ ,
$C_p$	specific heat, $\text{J}/\text{kg K}$ ,
$d_t$	diameter of the reactor tube, $\text{m}$ ,
$Da$	Damkohler number, $V/c^{l''-1}k(T_m)/q$ ,
$D_e$	effective intraparticle diffusion coefficient, $\text{m}^2/\text{s}$ ,
$E$	activation energy, $\text{J}/\text{mol}$ ,
$f(v)$	$\exp[\gamma(v-1)/v]$ ,
$h$	interparticle heat transfer coefficient, $\text{J}/\text{m}^2 \text{K s}$ ,
$I$	initiator concentration, $\text{mol}/\text{m}^3$ ,
$k$	reaction rate constant, $\text{mol}(\text{m}^3/\text{mol})^m/\text{kg s}$ ,
$k_g$	interparticle mass transfer coefficient, $\text{m}/\text{s}$ ,
$L$	reactor length, $\text{m}$ ,
$Le$	Lewis number, $h/\rho_f C_p k_g$ ,
$n$	reaction order,
$P$	polymer radical concentration, $\text{mol}/\text{m}^3$ ,
$q$	volumetric flowrate, $\text{m}^3/\text{s}$ ,
$R$	ideal gas constant, $\text{J}/\text{K mol}$ ,
$s$	$z/L$ ,
$S(\lambda; \phi)$	normalized sensitivity of model output, $\lambda$ , to model input, $\phi$ ,
$S_p$	particle surface area, $\text{m}^2$ ,
$T$	temperature, $\text{K}$ ,
$T_m$	mean temperature, $(T' + \delta T_w)/(1 + \delta)$ ,
$U$	overall heat transfer coefficient, $\text{J}/\text{m}^2 \text{K s}$ ,
$v$	dimensionless temperature, $T/T_w$ ,
$v^*$	maximum value of dimensionless temperature,
$\bar{v}$	mean superficial velocity, $\text{m}/\text{s}$ ,
$V$	volume of the CSTR, $\text{m}^3$ ,
$V_p$	particle volume, $\text{m}^3$ ,
$x$	conversion, $(c' - c)/c'$ ,
$z$	reactor axial coordinate, $\text{m}$ ,
$\alpha$	dimensionless heat of reaction parameter, $B/A$ ; for CSTR: $(-\Delta H)c'/\rho_f C_p T_m(1 + \delta)$ ,
$\alpha^\circ$	$\alpha/\gamma$ ,
$\beta$	dimensionless heat transfer parameter, $C/A$ ,
$\gamma$	dimensionless activation energy, $E/RT_w$ ,
$\Delta H$	heat of reaction, $\text{J}/\text{mol}$ ,
$\delta$	$Ua/q\rho_f C_p$ ,
$\eta$	effectiveness factor,
$\rho_b$	catalyst bulk density, $\text{kg}/\text{m}^3$ ,



$\rho_f$	fluid density, $\text{kg/m}^3$ ,
$\rho_s$	catalyst particle density, $\text{kg/m}^3$ ,
$\Phi$	normalized Thiele modulus, $\Phi_w [f(v_p) (1+x_p)^{n-1}]^{1/2}$ ,
$\Phi_w$	normalized Thiele modulus, $(V_p/S_p)[(n+1)\rho_s k(T_w)c^{i^{n-1}}/2D_e]^{1/2}$ ,
$\phi$	generic input parameter of the model,
$\psi$	Semenov number, $\alpha/\beta$ ; for CSTR: $Da \gamma \alpha$ ,
$\psi^\circ$	$\psi/\gamma$ .

### Subscripts

$c$	critical condition,
$p$	catalyst particle surface,
$w$	reactor wall,

### Superscript

$i$	reactor inlet.
-----	----------------

## References

- Adler J, Enig J W 1964 *Combust. Flame* 8: 97–103
- Barkelley C H 1984 *ACS Symp. Ser.* 237: 337–359
- Bilous O, Amundson N R 1956 *AIChE J.* 2: 117–126
- Boddington T, Gray P, Kordylewski W, Scott S K 1983 *Proc. R. Soc. Lond.* A390: 13–20
- Carberry J J 1975 *Ind. Eng. Chem., Fundam.* 14: 129–131
- Chemburkar R M, Morbidelli M, Varma A 1986 *Chem. Eng. Sci.* 41: 1647–1654
- Dente M, Collina A 1964 *Chim. Ind.* 46: 752–761
- Doraiswamy L K, Sharma M M 1984 *Heterogeneous reactions: Analysis, examples and reactor design* (New York: John Wiley) Vol. 1
- Emig G, Hofmann H, Hoffmann U, Fiand U 1980 *Chem. Eng. Sci.* 35: 249–257
- Froment G F, Bischoff K B 1979 *Chemical reactor analysis and design* (New York: John Wiley)
- Kauschus W, Demont J, Hartmann K 1978 *Chem. Eng. Sci.* 33: 1283–1285
- Lacey A A 1983 *Int. J. Eng. Sci.* 21: 501–515
- McGreavy C, Adderley C I 1973 *Chem. Eng. Sci.* 28: 577–584
- Morbidelli M, Varma A 1982 *AIChE J.* 28: 705–713
- Morbidelli M, Varma A 1985 *Chem. Eng. Sci.* 40: 2165–2168
- Morbidelli M, Varma A 1986a *AIChE J.* 32: 297–306
- Morbidelli M, Varma A 1986b *Chem. Eng. Sci.* 41: 1063–1071
- Morbidelli M, Varma A 1987a *Chem. Eng. Sci.* (in review)
- Morbidelli M, Varma A 1987b *AIChE J.* (in review)
- Pereira C J, Wang J B, Varma A 1979 *AIChE J.* 25: 1036–1043
- Rajadhyaksha R A, Vasudeva K, Doraiswamy L K 1975 *Chem. Eng. Sci.* 30: 1399–1408
- Semenov N N 1928 *Z. Phys.* 48: 571–582
- Thomas P H, Bowes P C 1961 *Br. J. Appl. Phys.* 12: 222–229
- Tjahjadi M, Gupta S K, Morbidelli M, Varma A 1987 *Chem. Eng. Sci.* (in review)
- van Welsenaere R J, Froment G F 1970 *Chem. Eng. Sci.* 25: 1503–1516
- Zeldovich YaB, Barenblatt G I, Librovich V B, Makhviladze G M 1985 *The mathematical theory of combustion and explosions* (New York: Plenum Press)

# Olefin incorporation on supported FeCo alloy Fischer-Tropsch catalysts

K B ARCURI<sup>1</sup>, L H SCHWARTZ<sup>2</sup> and J B BUTT\*

Ipatieff Laboratory and Department of Chemical Engineering,  
Northwestern University, Evanston, IL 60201, USA

<sup>1</sup> Present Address: Exxon Research and Development Laboratories,  
Baton Rouge, LA 70821, USA

<sup>2</sup> Present Address: National Bureau of Standards, Gaithersburg,  
MD 20899, USA

**Abstract.** We have previously reported on the properties of silica-supported Fe, Co and FeCo alloy for the Fischer-Tropsch (FT) reaction, both at atmospheric pressure and up to 14 atm ( $14 \times 1.0133 \times 10^5$  Pa). The selectivity for C<sub>2</sub>-C<sub>3</sub> olefins reported in the literature for these catalysts (particularly FeCo) was found to be somewhat suppressed at higher pressures, although methanol production was enhanced. The present study is concerned with the possible role of olefin insertion on hydrocarbon chain growth and oxygenate production. Results for both ethylene and 1-pentene indicate some incorporation into the next higher carbon number product at low CO conversions, but not a significant effect on overall chain growth. There is a diminution of oxygenate formation with olefin-containing feeds for all catalysts and reaction conditions investigated (250°C, 1 and 7.8 atm). Present results do not exclude a role of olefin insertion in the mechanism of chain growth, but it seems to be a minor one at most.

**Keywords.** Fischer-Tropsch catalysts; iron-cobalt alloy catalysts; iron catalysts; cobalt catalysts; olefin incorporation in synthesis reactions; selectivity in synthesis reactions.

## 1. Introduction

Earlier work in this laboratory on the FeCo system has concentrated on possible enhancement of olefin production under typical Fischer-Tropsch conditions (Amelse *et al* 1981; Arcuri *et al* 1984). While some selectivity for olefin formation does exist for the alloy, it is suppressed at higher pressures probably by hydrogenation of olefinic intermediates. To investigate this in greater detail, and particularly with respect to competitive olefin incorporation or chain initiation, the

---

A list of symbols is given at the end of the paper

\*To whom correspondence should be addressed

present experiments with ethylene and 1-pentene containing feeds at constant CO/H<sub>2</sub> were undertaken.

A summary of early work on olefin incorporation in synthesis has been given by Eidus (1967). Iron and cobalt present an interesting contrast, since it is generally acknowledged that incorporation on iron occurs only to a small extent (Hall *et al* 1960; Satterfield *et al* 1983) while that on cobalt is much more pronounced (Pichler *et al* 1967; Kibby *et al* 1984). Much of the prior experience, however, has been with bulk materials (fused or precipitated) and a major purpose of the present work is to compare incorporation behaviour on the supported metals and to investigate the influence of alloying iron with cobalt in this regard.

## 2. Experimental

The basic apparatus and analytical methods have been described by Arcuri *et al* (1984). Further details, for the specific experiments here, are given by Arcuri (1982). The catalysts employed are 4.94 wt% Fe/SiO<sub>2</sub>, 4.61 wt% Co/SiO<sub>2</sub> and 3.85 (Fe) – 1.02 (Co) wt% on SiO<sub>2</sub>. The support was 80–100 mesh Davison 62 silica gel. Details of preparation, characterization and treatment are given by Arcuri (1982) and Arcuri *et al* (1984).

Reaction experiments were conducted in a standard differential reactor at a fixed temperature of 250°C and at total pressures of 1.0 and 7.8 atm ( $7.8 \times 1.0133 \times 10^5$  Pa). Comparisons were made both for activity and selectivity of the three catalysts using a pure 1/3 CO/H<sub>2</sub> feed and mixtures of the 1/3 composition containing either 5.4 mole % ethylene or 0.5 mole % 1-pentene. Purity of the reaction gases was as described by Arcuri *et al* (1984). Analysis for products, normally C<sub>1</sub> to C<sub>8</sub> plus CO<sub>2</sub> and methanol, was conducted with a tandem temperature-programmed GC system. This was capable of separating  $\alpha$ -olefin/*n*-paraffin components of each C<sub>1</sub> (to C<sub>8</sub>) hydrocarbon in approximately 30 min.

The catalysts are all of low percentage exposed, about 5%. Turnover frequency measurements for methane  $N_{\text{CH}_4}$  are based on these percentage exposed determinations via the method of Amelse *et al* (1981). There is, however, one difference in procedure here as compared to the results reported by Arcuri *et al* (1984). Because of the relatively large amounts of olefin in the feed gas accurate mass balances involving the olefin could not be obtained reliably owing to the inherent inaccuracies in gas chromatographic peak measurements ( $\pm 5\%$ ). Consequently the CO turnover frequencies and/or conversions could not be well measured in experiments with the olefin-containing feeds. Thus, we have made all product yield, activity, and selectivity comparisons among the various feeds at comparable conditions of gas hourly space velocity (GHSV, volume/volume-hr). Nominal CO conversion levels are, however, comparable to those reported by Arcuri *et al* (1984), ranging from about 1–10%.

## 3. Results and discussion

### 3.1 Methane activities in olefin enhanced feeds

In the case of Fe/SiO<sub>2</sub> there is a depression of methane formation for either the C<sub>2</sub> or C<sub>5</sub> enhanced feeds. A typical result at 7.8 atm is shown in figure 1. The



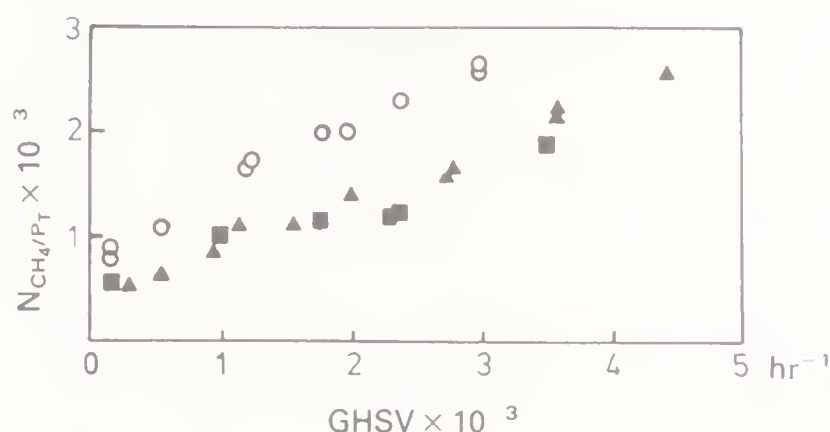


Figure 1. Methane turnover frequency vs. GHSV for Fe/SiO<sub>2</sub> with olefin enhanced feeds at 7.8 atm and 250°C. ○ = 1/3 CO/H<sub>2</sub>; ▲ = 5.4% C<sub>2</sub>H<sub>4</sub>; ■ = 0.5% 1-C<sub>5</sub>.

similarity of the depression of CH<sub>4</sub> activity for the two olefins, at very different concentrations, would suggest that methane activity is only partially dependent upon gas phase olefin concentration or that there is a large difference in chemisorption between the two olefins. Overall, the trend of  $N_{\text{CH}_4}$  with GHSV is the same with both olefins, which might be expected. However, for FeCo/SiO<sub>2</sub> methane conversion is independent of olefin feed concentration, decreasing (but in equal ratio for the two olefin feeds) with increasing CO conversion. The Co/SiO<sub>2</sub> is similar in this respect to FeCo/SiO<sub>2</sub>, with no significant effect of olefin on the observed  $N_{\text{CH}_4}$ . There is, thus, some interaction of CH<sub>4</sub> with Fe that would appear to be suppressed by the presence of Co. This is of interest because the FeCo/SiO<sub>2</sub>, demonstrated to be an alloy phase in this composition range (Arcuri 1982), normally is dominated by the Fe component. There is no evidence for CH<sub>4</sub> formation via hydrocracking for FeCo/SiO<sub>2</sub>, in agreement with the results of Hall *et al* (1960), but the story for Co/SiO<sub>2</sub> may be somewhat different, as discussed later.

### 3.2 Yields and selectivities

The following sections indicate in general the effects of olefin incorporation, including secondary hydrogenation, on the hydrocarbon product distribution. Since there are three feeds (including the pure CO/H<sub>2</sub>), two levels of pressure and three catalysts, the list of results can become rather extensive. We shall attempt to condense this as far as possible. There is also a conversion dependence (via GHSV) of results in certain cases. These are referred to as "low conversion" (1% CO conversion) and "high conversion" (3%) in reference to the pure CO/H<sub>2</sub> feed results, although results here are presented in terms of GHSV as explained above.

Product yields are presented as  $Y_i$  (moles product  $i$  produced/moles feed gas initially present) and are generally presented in the interpretation of chain growth into higher molecular weight products for both ethylene and 1-pentene feeds.

**3.2a CO/H<sub>2</sub> with ethylene feed:** For Fe/SiO<sub>2</sub> the 5.4 mole % C<sub>2</sub>H<sub>4</sub> in 1/3 CO/H<sub>2</sub> significantly increases both the propylene and 1-butene product yields, as shown in figure 2. Similar increases, but to a lesser extent, are observed for the corresponding paraffin yields (Arcuri 1982). The FeCo/SiO<sub>2</sub> is similar to Fe/SiO<sub>2</sub> in this respect, while Co/SiO<sub>2</sub> shows the same trends but is more reluctant (by about 50%) towards olefin production. At higher pressures (figure 3) the iron-containing catalysts give increased C<sub>3</sub><sup>+</sup> yields; there is a corresponding increase, but smaller, for Co/SiO<sub>2</sub>. In general then, the enhanced product for all C<sub>3</sub> and C<sub>4</sub> noted is indicative of some direct incorporation of ethylene in the chain, and a possible role



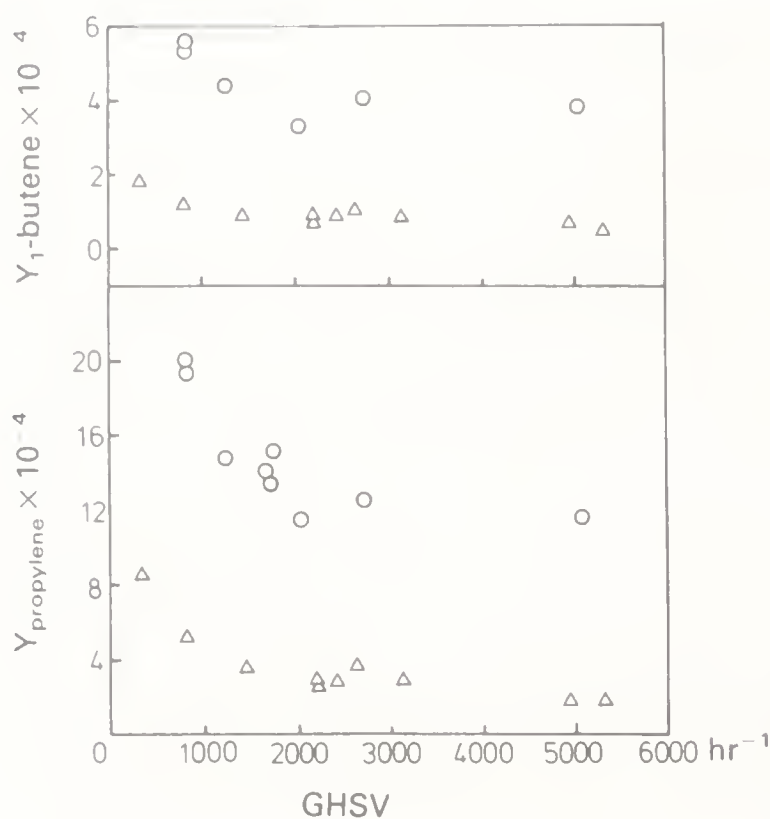


Figure 2. 1-Butene (top) and propylene (bottom) yields for Fe/SiO<sub>2</sub> with the ethylene feed at 1 atm and 250°C. O = 5.4% C<sub>2</sub>H<sub>4</sub>; Δ = 1/3 CO/H<sub>2</sub>.

as a chain initiator for linear chain products. Experimentally this is supported by the fact that the amount of ethylene consumed corresponds to the total molar increase in products.

There are conversion dependencies of C<sub>2</sub>H<sub>4</sub> incorporation that are not immediately obvious in interpretation. At 1 atm Co/SiO<sub>2</sub> consumes the most C<sub>2</sub>H<sub>4</sub>, since product increases are much larger than similar Fe-based catalysts C<sub>3</sub> and C<sub>4</sub> and appear to increase with conversion of CO. The iron catalyst has the smallest increase in C<sub>2</sub>H<sub>4</sub> consumption with conversion, although all are close given the experimental precision. It is clear, however, that higher pressure inhibits C<sub>2</sub>H<sub>4</sub> consumption; a comparison of figures 2 and 3 for propylene yield suggests a decrease of approximately 50% as the pressure is increased from 1 to 7.8 atm for the iron catalyst. Similar trends are noted for the other materials. There is, then, a notable decrease in olefin incorporation with pressure, independent of catalyst, and the understanding of secondary reactions such as hydrogenation and hydrocracking may be necessary to obtain an interpretation of this behaviour.

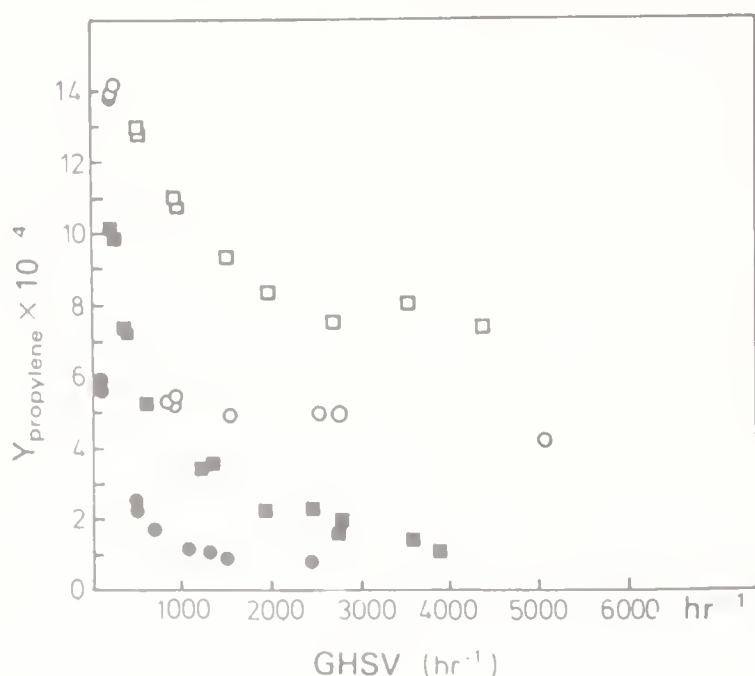


Figure 3. Propylene product yield vs. GHSV for Fe/SiO<sub>2</sub> and FeCo/SiO<sub>2</sub> with the ethylene feed at 7.8 atm and 250°C. □ = Fe/SiO<sub>2</sub>; 5.4% C<sub>2</sub>H<sub>4</sub>; ■ = Fe/SiO<sub>2</sub>; 1/3 CO/H<sub>2</sub>; ○ = FeCo/SiO<sub>2</sub>; 5.4% C<sub>2</sub>H<sub>4</sub>; ● = FeCo/SiO<sub>2</sub>; 1/3 CO/H<sub>2</sub>.

3.2b *Further interpretation of  $C_2H_4$  incorporation:* Biloen & Sachtler (1981) have suggested that  $C_2$  insertion may be significant in overall chain growth. We have seen in the previous data that there is significant incorporation of  $C_2$  into the chain for  $C_3$  but, in fact, this is less for  $C_4$  and is not really evident for higher C-number products. The result is not, in fact, very different from much earlier findings of Hall *et al* (1960) that ethylene can initiate reaction but does not propagate chain growth and that the primary reaction is hydrogenation.

The apparent conflict in these viewpoints can be largely resolved if one examines in more detail the fraction of ethylene consumed. For example, in figure 2 at a GHSV of  $1500\text{ hr}^{-1}$  for the Fe/SiO<sub>2</sub> catalyst, corresponding to a CO conversion of 3%, only 2.7% of the total feed ethylene actually undergoes chain growth reactions, and of this amount the majority appears as  $C_3$  products. A similar observation, with slightly different numbers, pertains to the other catalysts at both 1 and 7.8 atm total pressure (Arcuri 1982). Such low ethylene consumption fractions would indicate that readsorption of ethylene with subsequent chain initiation/insertion reactions is not a major pathway leading to the production of long chain hydrocarbon products.

In effect, the predominant reaction involving feed ethylene is hydrogenation to ethane, although there are some differences among the catalysts in this regard. The mole fraction ratio of ethylene to ethane is plotted as a function of GHSV in figure 4 for Fe/SiO<sub>2</sub> at both pressure levels. This ratio is approximately two times higher for the olefin-containing feed at one atm, while at 7.8 atm the olefin/paraffin ratio appears to be almost the same at lower GHSV for both feeds. Such results indicate that a significant fraction of the feed ethylene is undergoing hydrogenation; typical values would range from 30–50% of the total feed content dependent upon pressure and conversion level. A similar story exists for  $(X_{C_2}/X_{C_3})$ . The ratio is significantly higher in the ethylene containing feed, again indicative that the primary product of ethylene initiation/insertion is propylene; however again at lower GHSV (higher CO conversion) the ratio approaches comparable values for

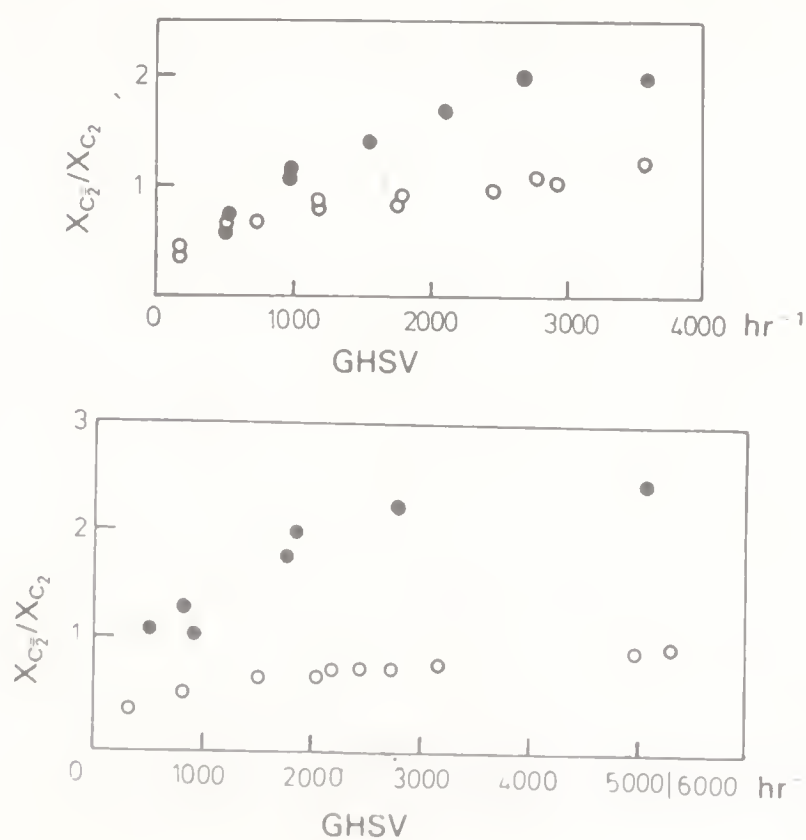


Figure 4. Ethylene to ethane mole fraction ratios vs. GHSV for Fe/SiO<sub>2</sub> at 7.8 (top) and 1 atm (bottom) and 250°C  
● = 5.4%  $C_2H_4$ ; ○ = 1/3  $CO/H_2$ .

both pure and ethylene-containing feed. The Co/SiO<sub>2</sub> is not as efficient for hydrogenation as Fe/SiO<sub>2</sub>, since under comparable conditions ( $X_{C_2^-}/X_{C_2}$ ) is about 5 times higher for the ethylene containing feed (vs 2 for Fe/SiO<sub>2</sub>), although the ratios for the two feed compositions also approach each other at higher CO conversions. A mild surprise is provided by FeCo/SiO<sub>2</sub>. This is illustrated in figure 5 for results at one atm. The ethylene/ethane ratios are identical over the entire range of conversions investigated, and of course the feed compositions studied are the same as for the other catalysts. Even at the higher pressure of 7.8 atm, ethylene/ethane remains the same for FeCo/SiO<sub>2</sub>. This is, in fact, one of the few instances in which the alloy seems to deviate from the pattern of dominance by the iron component.

Overall, thus, there is evidence for considerable C<sub>2</sub><sup>-</sup> hydrogenation activity for these catalysts, with C<sub>3</sub><sup>-</sup> following the same patterns. However, the activity of Fe/SiO<sub>2</sub>, which seems a surprisingly good hydrogenation catalyst, is almost completely suppressed by the incorporation of Co which may account at least quantitatively for the reportedly enhanced selectivity of the alloy for olefin formation.

### 3.3 Some details on hydrogenation

The previous section began with a discussion of olefin incorporation but ended up with a general discussion of hydrogenation. Some further detail on hydrogenation may be appropriate at this point. As stated above, a rather large fraction of the feed ethylene hydrogenates on Fe/SiO<sub>2</sub>. The basic indicator is the ethylene/ethane ratio, which for ethylene containing feeds can range from 0.5 to 30. If no feed ethylene undergoes hydrogenation these ratios would typically range from 70–100 for the experimental conditions employed. Even in the case of Co/SiO<sub>2</sub>, where comparable ratios vary from 1.0 to ≈ 10.0, there is a substantial amount of hydrogenation. In sum, one must conclude that the hydrogenation activity of the catalyst is very important in the interpretation of experiments such as these involving both

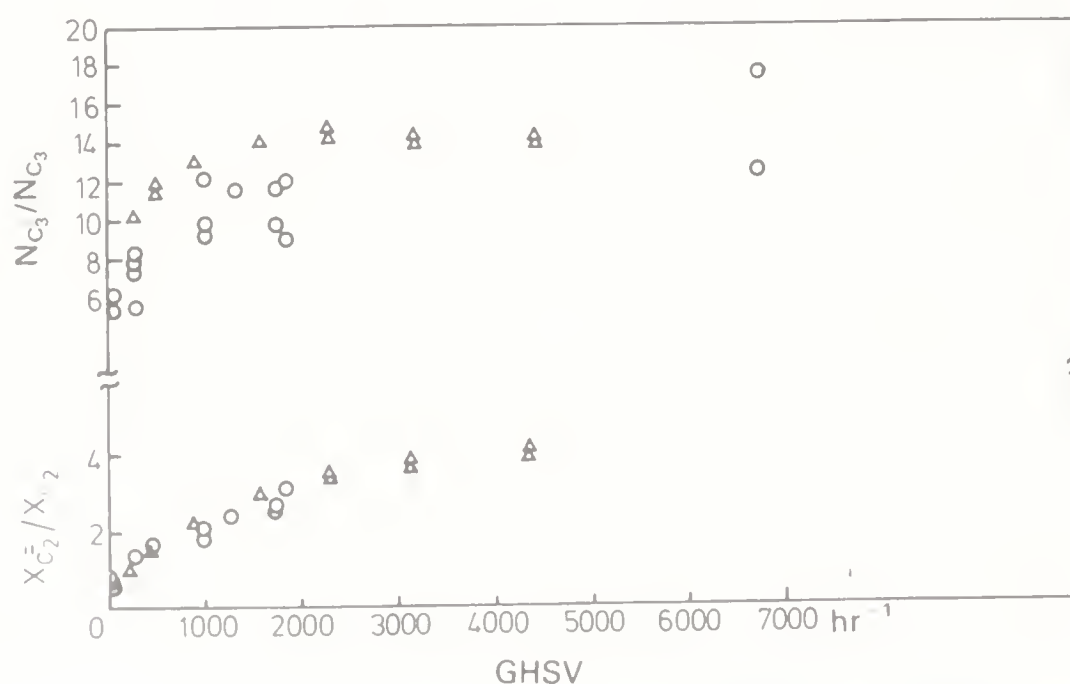


Figure 5. Ethylene to ethane mole fraction ratio and propylene to propane selectivity vs. GHSV for FeCo/SiO<sub>2</sub> with the ethylene feed at 1 atm and 250°C. Δ = 5.4% C<sub>2</sub>H<sub>4</sub>; ○ = C<sub>3</sub>H<sub>6</sub>.



synthesis activity and olefin incorporation. Arcuri (1982) has presented an argument that the number of active sites available for ethylene hydrogenation is proportional (approximately half) to those determined by hydrogen chemisorption (Amelse *et al* 1981). The calculation of active sites by this approach may not be quantitatively correct, since the hydrogenation mechanism on Pt-group surfaces may well be completely different from that on the Fe-based FT catalysts, but relative values should nonetheless be informative. Some representative results are presented in table 1. It is clear that hydrogenation activity follows a decreasing trend with increasing pressure and increasing conversion by this measure.

There are some exceptions (FeCo at 7.8 atm and Co at 1 atm), however, the rest of the results are sufficiently consistent to establish what we believe to be a general pattern. It is true, though, that the predominant trend for hydrogenation is apparently coupled with the observed decrease in CO activity presented before. The fact that hydrogenation activity normally decreases faster than CO activity with decreasing GHSV is shown in table 1. The question is then whether independent hydrogenation sites exist on the catalyst, different from those available for Fischer-Tropsch reactions. The answer is probably no, based on an accumulation of circumstantial evidence. A major factor is provided if a comparison is made between  $(X_{C_2^=}/X_{C_2})$  for the pure and ethylene-containing feeds. Figure 6 presents, for example, the values of this ratio for FeCo/SiO<sub>2</sub> at 1 and 7.8 atm. If a certain fraction of the sites is active only for ethylene hydrogenation, one would expect the olefin/paraffin ratio to be proportional to the olefin gas phase concentration at a given GHSV (or conversion), since dehydrogenation reactions are unlikely due to the relatively high hydrogen partial pressure. The introduction of 5.4% ethylene in the feed corresponds to a concentration of at least 50 times greater than normal ethylene concentrations at typical conversions employed with the pure CO/H<sub>2</sub> feed. If all gas phase components are competing for a finite fraction of specific hydrogenation sites one would reasonably expect the  $(X_{C_2^=}/X_{C_2})$  ratios to be much higher with the ethylene-containing feed at comparable conversions; however, no such competition is observed. This would, in itself, seem to rule out any important role of separate hydrogenation and FT sites for ethylene conversion.

Table 1. Ethylene hydrogenation activity.

Catalyst	GHSV (hr <sup>-1</sup> )	Pressure (atm)	Turnover (C <sub>2</sub> H <sub>6</sub> /site-s)	$N_{CO}/N_{C_2H_6}$
Fe/SiO <sub>2</sub>	5100	1.0	11.5	0.13
	4443	7.8	85.0	0.07
	526	7.8	14.0	0.50
FeCo/SiO <sub>2</sub>	4381	1.0	6.5	0.06
	2796	7.8	18.5	0.10
	467	7.8	17.0	0.08
Co/SiO <sub>2</sub>	24100	1.0	30.0	0.16
	1868	7.8	14.0	0.10
	142	7.8	5.0	0.30



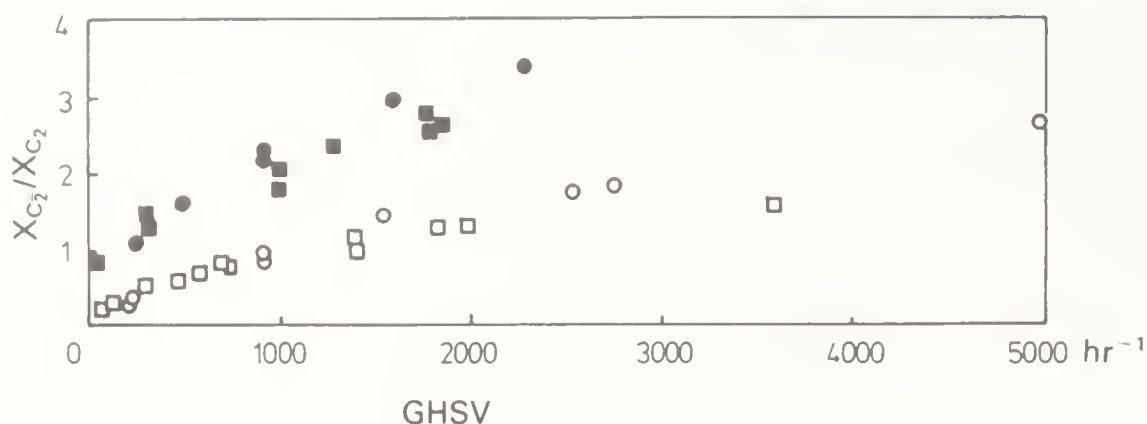


**Figure 6.** Comparison of ethylene to ethane mole fraction ratio for FeCo/SiO<sub>2</sub> with the ethylene feed at 1 and 7.8 atm and 250°C. ● = 5.4% C<sub>2</sub>H<sub>4</sub>, 1 atm; ■ = 1/3 CO/H<sub>2</sub>, 1 atm; ○ = 5.4% C<sub>2</sub>H<sub>4</sub>, 7.8 atm; □ = 1/3 CO/H<sub>2</sub>, 7.8 atm.

### 3.4 1-pentene feeds

The picture for 1-pentene feeds is not quantitatively very different from the results with ethylene-containing feeds. For the Fe/SiO<sub>2</sub> catalyst overall results are shown in figure 7. There is significant depression in the C<sub>2</sub><sup>+</sup> and C<sub>3</sub><sup>+</sup> olefin yields, probably by adsorption competition, and a modest increase in 1-hexene, by about 20%, that tends to disappear at higher GHSV. The fraction consumed of 1-pentene in incorporation reactions is less than 0.5% contained in the feed, and again most of this appears in the next highest C<sub>n</sub> product. There is little effect of pressure on this

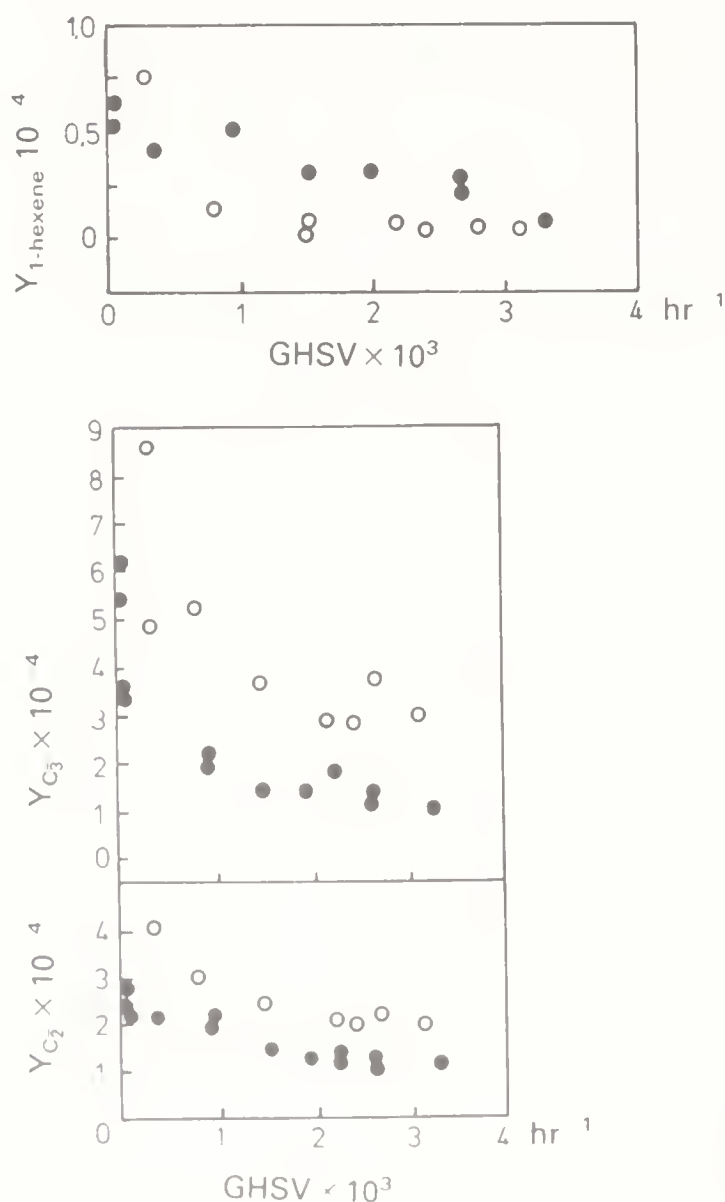


**Figure 7.** Various olefin yields vs. GHSV for Fe/SiO<sub>2</sub> with the 1-pentene feed at 1 atm and 250°C. ● = 0.5% 1-C<sub>5</sub>; ○ = 1/3 CO/H<sub>2</sub>.

pattern. However, for FeCo/SiO<sub>2</sub>, while there is still no change in low molecular weight products, hexene is substantially enhanced by primary insertion, though there remains a very low fraction of incorporation (about 1% at 3% CO conversion). There is evidence for some enhanced incorporation of pentene for FeCo compared to Fe, particularly at the higher pressure, that may be indicative of selectivity of the alloy for the chain growth of higher molecular weight products but, again, in view of the experimental uncertainty it is difficult to make a conclusive statement about this.

While the Fe and FeCo/SiO<sub>2</sub> catalysts are roughly the same for the pentene feeds, here the Co/SiO<sub>2</sub> provides the variation. There is still a low incorporation of the olefin (0.5%), and at one atmosphere not much change in either the low molecular weight products or in C<sub>6</sub>. However, at the higher pressure of 7.8 atm there is a significant increase in lower molecular weight hydrocarbons, and an apparently much higher incorporation of pentene. The basic results are shown in figure 8. These results are reflective of hydrocracking over Co/SiO<sub>2</sub> at the higher pressure, with substantial production of C<sub>2-5</sub>, and the incorporation of the feed pentene is much higher, 7%. The large increase in methane yield, about the same as C<sub>6</sub> in terms of feed consumption, may be due to the transformation of an  $\alpha$ -carbon in 1-pentene to a methylene species that can either hydrogenate or insert. This general pattern is not normally seen in catalytic hydrocracking, but it is definitely not a thermal mechanism. Some reaction pathways, involving dissociation of a diadsorbed species, are discussed by Arcuri (1982). These results are consistent with those of Pichler & Schulz (1970), although their observations were obtained at much higher conversion levels.

Aside from the fact that there is evidence for hydrocracking with 1-pentene feeds, little else contrasts with ethylene. Subsequent hydrogenations are similar, and there is no substantial evidence for significant incorporation into higher molecular weight products.

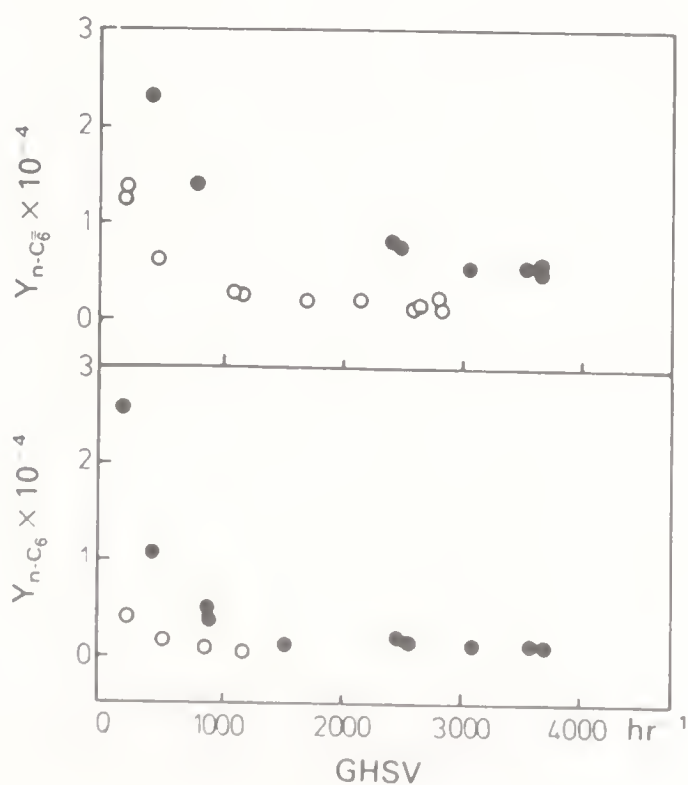


Figure 8. 1-Hexene (top) and *n*-hexane (bottom) yields vs. GHSV for Co/SiO<sub>2</sub> at 7.8 atm and 250°C. ● = 0.5% 1-C<sub>5</sub>; ○ = 1.3 CO/H<sub>2</sub>.

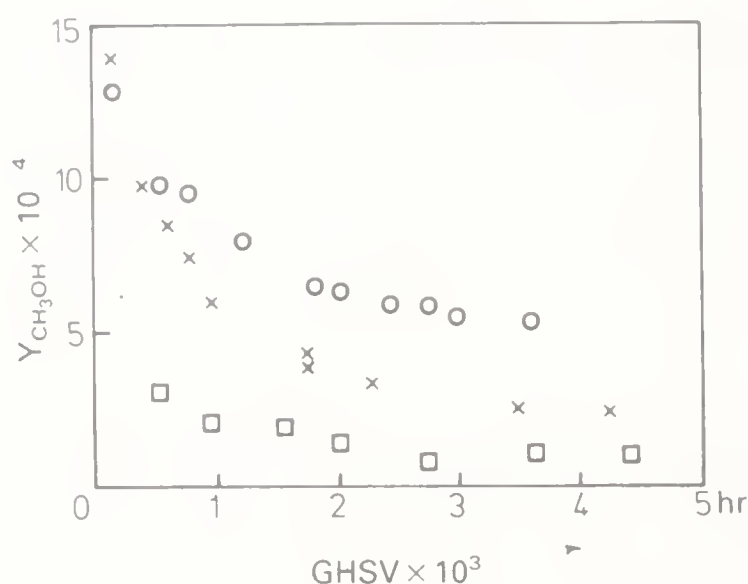


Figure 9. Methanol yield vs. GHSV for Fe/SiO<sub>2</sub> for olefin containing feeds at 7.8 atm and 250°C. □ = 5.4% C<sub>2</sub>H<sub>4</sub>; × = 0.5% 1-C<sub>5</sub>; ○ = 1/3 CO/H<sub>2</sub>.

### 3.5 Oxygenates

If we use Fe/SiO<sub>2</sub> as a basis, one may say that olefin addition depresses methanol formation under all conditions. Typical examples are given in figure 9. There is a smaller suppression for FeCo/SiO<sub>2</sub>, and not much change for Co/SiO<sub>2</sub>, but the latter is in any event a poor oxygenate producer under these conditions (Arcuri *et al* 1984). CO<sub>2</sub> yields seem insensitive to any condition of catalyst, temperature or pressure. It has been suggested that there is a common intermediate for CH<sub>3</sub>OH and CO<sub>2</sub> formation, but then, why is the methanol yield decreased by increased gas phase hydrocarbon concentrations? Certainly this argument cannot be supported by the present results, but more extensive experiments, perhaps with labelled oxygen, would be required further to resolve the matter.

### 3.6 Schulz-Flory-Anderson parameterization

Although some individual products such as C<sub>3</sub> or C<sub>6</sub> are affected by the feed olefin, as pointed out above, in general, overall product distributions are not much affected, even at relatively higher conversions. This becomes quite evident upon comparison of chain growth plots. A representative example is provided by Fe/SiO<sub>2</sub>, as shown in figure 10 for ethylene and figure 11 for 1-pentene at 1 atm. The pressure of ethylene has essentially no effect on the growth probability for C<sub>n</sub> > 4 products (chain growth parameter, α, of 0.45 vs. 0.42 for unadulterated feed). This may be somewhat unexpected in view of the increase in C<sub>3</sub> and C<sub>4</sub> yields because of ethylene insertion. However, these yield increases occur approximately in proportion to the carbon number in such a way as to increase the ln (Y<sub>i</sub>) values

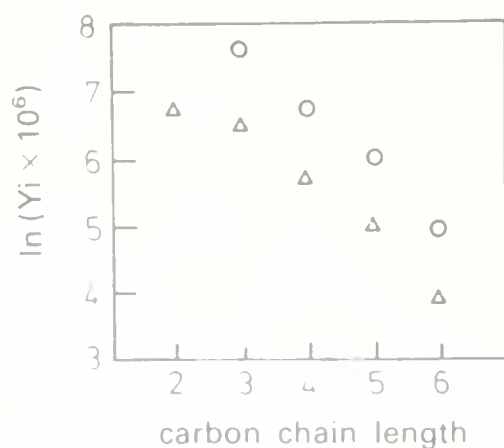


Figure 10. Product distribution plot for Fe/SiO<sub>2</sub> with the ethylene feed at 1 atm and 250°C. GHSV = 700 hr<sup>-1</sup>. ○ = 5.4% C<sub>2</sub>H<sub>4</sub>; △ = 1/3 CO/H<sub>2</sub>.

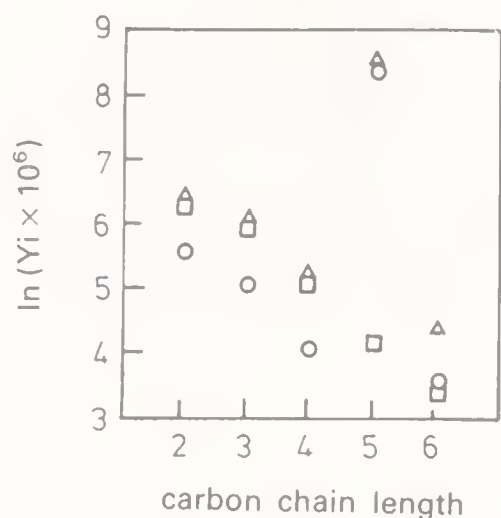


Figure 11. Product distribution plot for Fe/SiO<sub>2</sub> with the 1-pentene feed at 1 atm and 250°C. ○ = 0.5% 1-C<sub>5</sub>, GHSV = 1300 hr<sup>-1</sup>; α = 0.42; △ = 0.5% 1-C<sub>5</sub>, GHSV = 1000 hr<sup>-1</sup>; α = 0.45; □ = 1/3 CO/H<sub>2</sub>, GHSV = 1000 hr<sup>-1</sup>; α = 0.42.

while maintaining the same slope of the distribution plot. There is apparently an increase in  $\alpha$  for the 1-pentene feed ( $\alpha$  of 0.6 vs. about 0.45) but these values are based only on C<sub>3</sub> to C<sub>6</sub>. It was pointed out earlier that 1-pentene decreased C<sub>3</sub> and C<sub>4</sub> product yields, so the change in  $\alpha$  here is probably real, but because of the limited range of C<sub>i</sub> the absolute magnitude is probably not to be trusted. At 7.8 atm there is no change.

For the Co/SiO<sub>2</sub> catalyst there is a noticeable increase in growth probability ( $\alpha$  of 0.6 vs. 0.50) with ethylene feeds at 1 atm and comparable conversions. This result is illustrated in figure 12. The difference disappears at 7.8 atm, however, indicating a strong suppression of insertion with pressure. The increase in growth probability for Co/SiO<sub>2</sub> vs. Fe/SiO<sub>2</sub> at low pressure is most probably just a reflection of the lower hydrogenation activity of the former for ethylene. There is no noticeable effect of 1-pentene on the distributions for Co/SiO<sub>2</sub> at either pressure level.

The FeCo/SiO<sub>2</sub> shows no effect of any variable on the product distribution parameterization and in this sense would appear to be dominated by the iron component, a result that is not surprising in view of the overall catalyst composition.

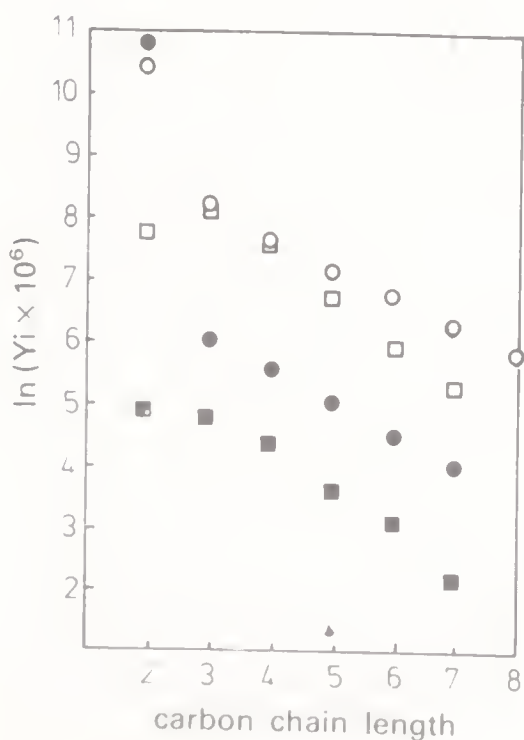


Figure 12. Product distribution plot for Co/SiO<sub>2</sub> with the ethylene feed at 1 atm and 250°C. ● = 5.4% C<sub>3</sub>H<sub>4</sub>, GHSV = 1000 hr<sup>-1</sup>; α = 0.62; ○ = 5.4% C<sub>3</sub>H<sub>4</sub>, GHSV = 3000 hr<sup>-1</sup>; α = 0.61; □ = 5.4% C<sub>3</sub>H<sub>4</sub>, GHSV = 700 hr<sup>-1</sup>; α = 0.47; ■ = 1/3 CO/H<sub>2</sub>, GHSV = 3000 hr<sup>-1</sup>; α = 0.50.

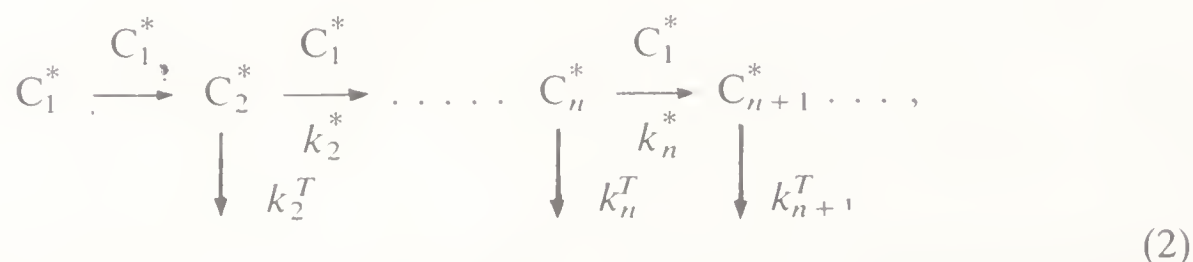


### 3.7 Mechanistic implications of distribution data

In the typical Schultz-Flory-Anderson parameterization the growth probability,  $\alpha$ , is a ratio of two reaction rates:

$$\alpha = r(\text{propagation})/[r(\text{propagation}) + r(\text{termination})], \quad (1)$$

Thus, in terms of an insertion mechanism involving a carbon monomer, we have:



where  $C_1^*$  is the insertion monomer,  $C_n^*$  the surface intermediate containing  $n$  carbon atoms,  $k_i^*$  the insertion rate constant and  $k_i^T$  the termination rate constant for  $C_i^*$ . This leads directly to an expression for  $\alpha$  in terms of the individual reaction rates of surface intermediate as:

$$\alpha = (k_i^* C_i^* C_i^*) / (k_i^* C_i^* C_i^* + k_i^T C_i^* C_i^*) \quad (3)$$

assuming that the termination rate constants are the same for each step in the insertion process, including hydrogenation, desorption or isomerization. If  $C_i^*$  can be assumed a constant and lumped into  $k_i^* \alpha$ , then:

$$\alpha = k_i^* / (k_i^* + k_i^T). \quad (4)$$

Now the pressure of added olefin concentrations in the feed stream should at least increase the concentrations  $C_x^*$ , where  $x$  is the carbon number corresponding to the added olefin. In this case, the above analysis would lead to:

$$1/\alpha = 1 + (k_i^T/k_i^*) \quad (5)$$

and the value of  $\alpha$  would be independent of the concentration of the growth reaction intermediates  $C_i^*$  so long as the basic approach of (2) is obeyed. Consequently any enhancement in  $C_i^*$  should result in an increase in the product yield and the slope determined by  $[\ln(Y_{i+1}) - \ln(Y_i)]$  should remain unchanged at steady conditions. This is generally observed in the present study, although the iron-containing catalysts do exhibit a small deviation from this behaviour. The exact reasons for this cannot be deduced from the experimental results here, but obviously are due to some deviations from the assumptions based on the insertion reaction scheme (2) used to obtain (4). Even though, for example, the total incorporation of ethylene from the olefin-containing feed is low, one can still estimate that surface concentrations  $C_2^*$  may well increase by a factor of 2 or 3 compared to normal synthesis conditions. In such an event,  $C_i^*$  may become the rate limiting reactant for all surface intermediates involving longer chain products and certainly severely to perturb the  $C_3$ - $C_4$  distributions. Other arguments can be made however and, in the light of present information, it is probably not worthwhile to belabour such philosophies further here.

### 3.8 Product selectivities

Arcuri (1982) presents an extensive documentation and discussion of the product selectivities obtained with the various feeds, three catalysts, two pressure levels and extent of conversion investigated. In fact, those data lead to no significant insights beyond those discussed above. Further, the small incorporation of olefin and apparently large changes in olefin/paraffin ratio make such measurements difficult to interpret quantitatively in the light of experimental uncertainty, and additional discussion herein is not necessary.

## 4. Conclusions

There is no real evidence from this work that either ethylene or 1-pentene, added in the feed, participate in the formation of reaction products by an insertion mechanism much beyond the next higher carbon number. Although there are some specific deviations among the individual catalysts, Fe/SiO<sub>2</sub>, Co/SiO<sub>2</sub> and FeCo/SiO<sub>2</sub>, we retain this as a general conclusion.

Incorporation of olefin in the adduct feeds is very low, although a high percentage of that adsorbed shows up in the next highest carbon number product. Hydrogenation appears to be important in determination of the incorporation of the feed olefin in chain growth. Even though Co/SiO<sub>2</sub> is a much less efficient hydrogenation catalyst than the iron-based materials, such activity, even for this material, is still sufficient to affect the incorporation of olefins into the product chain.

All olefin incorporation reactions, with all catalysts, are inhibited by increasing pressure. While we have data here only for two pressures, the trends seem to be sufficiently strong to make a statement. One might expect that, while none of the catalysts studied here are notable in the world of hydrogenation, their activities at higher pressures for hydrogenation are sufficient to remove olefin before it can incorporate into the chain. Hydrocracking may also be a possible mechanism for suppression of incorporation on the Co/SiO<sub>2</sub> catalysts, and presumably would be also be so with FeCo/SiO<sub>2</sub> catalysts of higher Co ratio than that employed here.

Production of oxygenated compounds was not a primary objective of the present research, yet some interesting results appear. There is quite a difference in the effect of added olefins on CH<sub>3</sub>OH and CO<sub>2</sub> formation. The former is decreased significantly, both with ethylene and 1-pentene, and the latter hardly at all under the various reaction conditions investigated. This is not in agreement with respect to various suggestions in the literature that there is a common intermediate for CH<sub>3</sub>OH and CO<sub>2</sub> formation. Of course here we deal only with the iron-cobalt system; other alloys could behave quite differently.

This paper is dedicated to Dr L K Doraiswamy on his sixtieth birthday. This research was supported by the Department of Energy, Office of Basic Energy Sciences, Contract DE-AC02-78ER04993. JBB would like to thank the Alexander von Humboldt-Stiftung for assistance in completion of this work and M Baerns for helpful discussion.

**List of symbols**

$C_1^*$	insertion monomer,
$C_n^*$	surface intermediate of $n$ carbon atoms,
$C_x^*$	surface intermediate from added olefin of carbon number $x$ ,
$K_i^T$	termination rate constant for $C_i^*$ ,
$k_i^*$	insertion rate constant,
$r$	rate of propagation or termination reaction,
$Y_i$	yield of product with carbon number $i$ ,
$\alpha$	chain growth probability parameter, equation (1).

**References**

- Amelse J A, Schwartz L H, Butt J B 1981 *J. Catal.* 72: 95–110  
Arcuri K B 1982 Ph. D. dissertation, Northwestern University, Evanston  
Arcuri K B, Schwartz L H, Piotrowski R D, Butt J B 1984 *J. Catal.* 85: 349–361  
Biloen P, Sachtler W M H 1981 *Adv. Catal.* 30: 165–216  
Eidus Y T 1967 *Russ. Chem. Rev.* 36: 338–351  
Hall W K, Kokes R J, Emmett P H 1960 *J. Am. Chem. Soc.* 82: 1027–1037  
Kibby C L, Pannell R B, Kobylinski T P 1984 *Prepr., Div. Pet. Chem., Am. Chem. Soc.* 29: 1113–1119  
Pichler H, Schultz H 1970 *Chem.-Ing.-Tech.* 42: 1162–1174  
Pichler H, Schultz H, Elstner M 1967 *Brennst.-Chem.* 48: 78–87  
Satterfield C N, Huff G A Jr, Summerhayes R 1983 *J. Catal.* 80: 486–490



# New strategies for separations through reactions

V G GAIKAR and M M SHARMA\*

Department of Chemical Technology, University of Bombay, Matunga, Bombay 400 019, India

**Abstract.** Separations through reactions can provide reliable and economically viable alternatives to established methods of separation, particularly for close boiling substances. New strategies in 'Dissociation Extraction' and 'Dissociation Extractive Crystallization' for separation of close boiling acidic/basic mixtures have been highlighted. Separations with aqueous solutions of hydrotrope and aqueous micellar solutions have been brought out. Separations by membranes with facilitated transport is potentially attractive.

**Keywords.** Separations through reactions; dissociation extraction; reactive crystallization; dissociation extractive crystallization; reactive distillation; separations with hydrotropes; micelles in separations; membrane separations; hydrometallurgical separations; separations with supercritical fluids.

## 1. Introduction

In chemical process industries separations of a variety of mixtures are frequently encountered and the cost of separation may dominate the capital investment and operational expenses. Quite often physical methods of separation, such as distillation, crystallization, solvent extraction followed by distillation and adsorption, are used, which exploit the differences in physical properties like boiling points, solubility, melting points etc. However, for systems having close boiling points or which are thermally unstable, these methods are either not applicable or not economically viable. In such cases the strategy of selective reactions may prove to be attractive. There is, therefore, a clear incentive to probe newer methods of separations through reactions to achieve better selectivity and higher throughput. An ideal situation would be where separation and the desired reaction are conducted simultaneously.

Separations through reactions have played a significant role in chemical industry from the early stages. The alkylation-dealkylation with isobutylene, with separation of alkylated products, has been successfully exploited for the separation of *m*-cresol/*p*-cresol (Stevens 1943). A similar strategy has been applied for separation of *m*-xylene/*p*-xylene mixtures by reacting the mixtures with acetaldehyde where *p*-xylene hardly reacts when *m*-xylene is present. Recently it has been claimed that *m*-xylene/*p*-xylene can be separated by fractional distillation in the presence of an organometallic compound where the relative acidities of the



different xylenes in exchanging hydrogen with metallic atoms is exploited (ANVAR 1975; Terill *et al* 1985; Cleary & Doherty 1985).

The method of sulphonation-desulphonation also finds application in the separations of xylenes, dichlorobenzenes etc.

It is known that  $\beta$ -picoline does not condense with benzaldehyde whereas  $\alpha$ - and  $\gamma$ -isomers yield corresponding stilbazoles; this method was used by Schwarz (1891) for the isolation and was proposed as a convenient way of separating  $\gamma$  and  $\beta$ -picolines. Another strategy exploited the greater susceptibility of  $\gamma$ -picoline and 2,6-lutidine to oxidation as compared to  $\beta$ -picoline (Coulson & Jones 1946).

The separation of methyl ethers of *m*-/*p*-cresols has been carried out very recently by selective oxidation with  $\text{MnO}_2$  where *p*-isomer reacted selectively to form substituted benzaldehyde (Millington *et al* 1986).

It is also possible to chlorinate *m*-cresol selectively, in the presence of a  $\text{CuCl}/\text{CuCl}_2/\text{HCl}$  system. The resulting mixture of 4-chloro-3-methyl phenol with 2-chloro derivative and *p*-cresol can be easily separated (Sharma 1985).

The removal of sulphur compounds like  $\text{H}_2\text{S}$ ,  $\text{RSH}$  and  $\text{COS}$  from  $\text{CO}_2$  is another large scale application of separations through reactions. The fast kinetics of  $\text{H}_2\text{S}$  and  $\text{RSH}$  with alkaline solutions and the manipulations of the operating conditions can lead to highly selective absorption of  $\text{H}_2\text{S}$  and  $\text{RSH}$  from their mixtures with  $\text{CO}_2$ . The use of hindered amines is a recent development in this field (Sarfori & Savage 1983); this was originally suggested by Sharma (1964).

$\text{C}_4$  olefins, found in a variety of streams in petrochemical plants and petroleum refineries, can be made free from vinyl acetylene by selective hydrogenation of vinyl acetylene to butadiene. Absorption in 50–60%  $\text{H}_2\text{SO}_4$  has been widely employed, in the past, for selective absorption of isobutylene from mixtures with butenes.

A recent state-of-art review by Sharma (1985) brings out different aspects of separations through reactions. This paper will be concerned with aspects which have not been discussed by Sharma.

The separation of close boiling, isomeric/nonisomeric, acidic/basic/neutral, substances provides the most attractive situation for exploitation of reactions. Dissociation extraction is an approach of significant industrial importance for the separations of acidic/basic close boiling mixtures. 'Dissociation extractive crystallization' and 'dissociation extractive distillation' are the newly emerging fields for separation of acidic/basic mixtures.

Separation by hydrotropes is yet another strategy by which separation factors for some systems can be enhanced many-fold.

Selective solubilization with micellar solutions can provide yet another strategy where reactions also can be imposed to increase the rate and the extent of solubilization.

Membrane processes supplemented by reactions or facilitated transport can provide answers in some of the difficult and/or energy-intensive situations.

## 2. Dissociation extraction

This two-phase technique of liquid-liquid extraction, applicable to acidic/basic mixtures, exploits the differences between the dissociation constants and distribution coefficients of the components of the mixture.

### 2.1 Liquid-liquid dissociation extraction

A dissociation extraction step involves equilibrating the mixture dissolved in a suitable water-immiscible organic solvent with an aqueous phase containing a stoichiometric deficiency of the neutralising agent. The term 'stoichiometric deficiency' implies that the amount of neutralising agent is just sufficient to neutralise the stronger component of the mixture. The competition between the components of the mixture for the neutralising agent results in the enrichment of the aqueous phase by the stronger component, while the organic phase gets enriched with the weaker component.

The following equation gives the value of separation factor for the separation of acids, HA and HB (HA is the weaker acid) and published data correlate well with this equation (Anwar *et al* 1974):

$$\alpha = \frac{D_A K_B}{D_B K_A} \left\{ \frac{N(\delta + 1) + T[(1/D_B) + (K_A/K_B)(\delta/D_A)]}{N(\delta + 1) + T[(1/D_B)(K_B/K_A) + (\delta/D_A)]} \right\}, \quad (1)$$

where  $D$  and  $K$  are distribution coefficients and dissociation constants, respectively, and

$$\left. \begin{aligned} N &\approx [A^-] + [B^-], \\ \delta &= [AH]_{\text{org}}/[HB]_{\text{org}}, \\ T &= [HA]_{\text{org}} + [HB]_{\text{org}}, \end{aligned} \right\} \text{ at equilibrium.}$$

After the initial theoretical development by Anwar *et al* (1971, 1973, 1974, 1979), this potentially attractive method of separation has been extensively exploited by Sharma and co-workers for a number of systems of industrial relevance. The separation of *N*-alkylanilines and chlorobenzoic acids (Laddha & Sharma 1978); the separation of chlorophenols, *p*-cresol (or *m*-cresol)/2,6-xylenol, chlorosubstituted cresols and xylenols (Wadekar & Sharma 1981b,c); *N*-substituted anilines, chloroanilines and nitroanilines (Jagirdar & Sharma 1981b) are a few of the systems which have been tried. Wadekar & Sharma (1981a) have given a state-of-art review of this process, covering the literature upto 1981.

### 2.2 Regenerative dissociation extraction

Sharma and co-workers have developed new regenerative processes so that the extractant can be reused; the cost of acid and alkali constitutes the dominant factor in separation via dissociation extraction. Wadekar & Sharma (1981b) suggested a thermal regenerative method for the recovery of weak neutralising agents like ammonia or methylamine from aqueous extracts. This could eliminate the solvent extraction of aqueous extract by a secondary highly polar solvent as suggested by Anwar *et al* (1979). Gaikar & Sharma (1984b) have proposed the method of carbonation of the aqueous extract to recover phenolics as a separate phase from the aqueous phase containing alkanolamines. Alkanolamines can be recycled for dissociation extraction step after desorption of carbon dioxide under boiling conditions; even CO<sub>2</sub> can be recycled.



### 2.3 Gas-liquid-solid dissociation extraction

Jagirdar & Sharma (1981b) have extended the liquid-liquid mode of dissociation extraction to the gas-liquid-solid mode of dissociation extraction. Very high values of separation factors, in the range of 4–40, were realised when anhydrous HCl gas was used to separate substituted anilines, chloroanilines and nitroanilines. Considerably high values of selectivity ( $\approx 100\%$ ) were observed when Gaikar & Sharma (1984a) applied this strategy for the separation of cumidines. Table 1 shows the separation factors for gas-liquid-solid dissociation extraction as compared to conventional liquid-liquid dissociation extraction. The process was also found to be thermally regenerative; the hydrochlorides of the bases can be decomposed by heating and the liberated HCl gas can be recycled. One particular advantage in this process for cumidines is that *p*-cumidine hydrochloride can be directly phosgenated to make the corresponding isocyanate; this is the dominant outlet for *p*-cumidine.

### 2.4 Selection of solvent and prediction of separation factor

The selection of a solvent for dissociation extraction to manipulate the ratio of distribution coefficients may be a crucial step to decide the highest possible separation factor. Gaikar & Sharma (1985) have given some guidelines based on thermodynamic considerations for the selection of solvents; solute-solvent interactions, solute-solute interactions and steric hindrance to the functional groups have been considered. Table 2 shows the improvement, sometimes of an order of magnitude, in the separation factor when a proper solvent was selected.

Gaikar & Sharma (1985) have also used the recent work on octanol-water distribution to propose a predictive method for  $\alpha$  in dissociation extraction. This work was followed by a complete predictive method for separation factor in dissociation extraction for any solvent (Gaikar 1986).

**Table 1.** Gas/liquid/solid vs liquid/liquid dissociation extraction.

System	$pK_a$ at 25°C	$\alpha$ in liquid/liquid dissociation extraction	Solvent	$\alpha$ in gas liquid/solid disassociation extraction	Gas (solvent)
<i>o</i> -Nitroaniline	-0.26	3.8 <sup>a</sup>	Nitro- benzene	40.0	HCl gas <sup>a</sup> (nitrobenzene)
<i>p</i> -Nitroaniline	1.00				
<i>o</i> -Chloroaniline	2.65	50 <sup>a</sup>	<i>p</i> -Xylene	6.6	HCl gas <sup>a</sup> ( <i>p</i> -xylene)
<i>p</i> -Chloroaniline	4.15				
N-ethylaniline	5.11	1.5 <sup>b</sup>	Benzene	43.0	HCl gas <sup>a</sup> ( <i>p</i> -xylene)
N,N-diethylaniline	6.45				
<i>o</i> -Cumidine	4.42	6.0 <sup>c</sup>	<i>n</i> -Heptane	700	HCl gas <sup>c</sup> ( <i>n</i> -heptane)
<i>p</i> -Cumidine	4.87	5.0 <sup>c</sup>	Cumene	approaching $\infty$	HCl gas <sup>c</sup> (cumene)
N-methylaniline	5.15	3.5 <sup>b</sup>	<i>p</i> -Xylene	48.5	HCl gas <sup>a</sup> ( <i>p</i> -xylene)
N,N-dimethylaniline	4.84	4.8 <sup>b</sup>			

$\alpha$  = Separation factor; <sup>a</sup> Jagirdar & Sharma (1981b); <sup>b</sup> Jagirdar & Sharma (1981a); <sup>c</sup> Gaikar & Sharma 1984a.

Table 2. Selection of solvent for dissociation extraction.

System	$pK_a$ at 25°C	Literature	Proper solvent	Solvent (separation factor)
Phenol	10.0	Benzene (1.9–2.4) <sup>a</sup>	Polar	<i>n</i> -Octanol <sup>d</sup> (5–6.8)
<i>o</i> -Chlorophenol	8.48	Di- <i>n</i> -butylether (4)	solvent	
2,6-Xylenol	10.62	Benzene (6–13) <sup>b</sup>	Inert	<i>n</i> -Heptane <sup>d</sup> (27–30)
<i>p</i> -Cresol	10.28	Di- <i>n</i> -butylether (4)	solvent	
<i>o</i> -Cresol	10.3	Benzene (~ 1) <sup>a</sup>	Polar	<i>n</i> -Octanol <sup>d</sup> (8–9.8)
6-Cl- <i>o</i> -cresol	8.09	Di- <i>n</i> -butylether (4.5)	solvent	
2,6-Xylidine	3.95	Di-butylether (2) <sup>b</sup>	Inert	<i>n</i> -Heptane <sup>d</sup> (10.2)
2,4-Xylidine	4.85		solvent	
<i>o</i> -Chloroaniline	2.65	<i>p</i> -Xylene (54) <sup>c</sup>	Inert	<i>n</i> -Heptane <sup>d</sup> (300–400)
<i>p</i> -Chloroaniline	4.15		solvent	

<sup>a</sup> Wadekar & Sharma (1981c); <sup>b</sup> Wadekar & Sharma (1981b); <sup>c</sup> Jagirdar & Sharma (1981b); <sup>d</sup> Gaikar & Sharma (1985).

## 2.5 Dissociation leaching

New strategies have been also developed for solid–liquid systems through dissociation leaching; it involves equilibrating the solid mixture with aqueous solutions of neutralising agent. Laddha & Sharma (1978) were the first to apply such a strategy to the separation of *o*-/*p*-chlorobenzoic acids where high selectivity towards *o*-chlorobenzoic acid was observed. Later, Wadekar & Sharma (1981c), utilized this strategy to separate solid mixtures of chloroxylenols. Recently, Jagirdar & Lawson (1984) have carried out the separation of mixtures of nitrophenols using this modified form of dissociation extraction.

A two-step process, selective solubilization in an organic solvent followed by dissociation extraction has been used by Jagirdar (1985).

Recently taken patents for the separations of dichloroanilines (Chang 1983) and of 2,6-xylenol/*p*-cresol (Mendiratta & Talley 1985) are clear indicators of the potential of dissociation extraction for industrial exploitation.

## 2.6 Dissociation extraction in the pharmaceutical industry

Dissociation extraction has also found applications in the pharmaceutical industry to separate lincomycin, an antibiotic, from lincomycin hexanoate esters or to separate flurbiprofen, a non-steroidal anti-inflammatory agent, from the associated impurity of 'dimeric acid (DA)' (Robinson & Cha 1985). It appears that alternate methods are either not practicable or are too expensive.

## 2.7 Separation of *m*-chloroperoxybenzoic acid/*m*-chlorobenzoic acid

In the manufacture of epoxides or certain sulfoxides *m*-chlorobenzoic acid ( $pK_a = 3.82$ ) is the by-product if the oxidation is carried out using *m*-chloroperoxybenzoic acid ( $pK_a = 7.3$ ). The peroxy *m*-chlorobenzoic acid is weaker and more lipophilic than the benzoic acid. If the solution of two acids in dichloromethane is stirred with a buffer solution of pH 7, the aqueous solution extracts 99% of *m*-chlorobenzoic acid (Brandström 1983). The existence of *m*-chlorobenzoic acid in the organic phase brings down the yield of the epoxide substantially and this unique application of dissociation extraction is commendable.



### 2.8 Recovery/separation of organic acids from dilute aqueous solutions

Removal of a variety of solutes from aqueous streams poses a challenging problem from the pollution abatement point of view as well as from an economic standpoint.

Reacting systems, like dissociation extraction, are likely to be economically viable alternatives. Jagirdar & Sharma (1980) have modified the strategy of dissociation extraction to separate formic/acetic/glycolic/oxalic acids by using stoichiometric deficiency of tri-octylamine (TOA) in a suitable organic solvent. The purification of glyoxal solution was also carried out in a similar manner (Jagirdar 1981).

Aromatic sulphonic acids, such as, *p*-toluene sulphonic, phenol sulphonic, nitrobenzene sulphonic etc. as encountered in aqueous waste streams of dyestuff, drug and pesticide industries, can be efficiently recovered through reactive extraction using TOA or dilaurylamine taken in 2-ethylhexanol, even in the presence of a large amount of sulphonic acid (Lodaya & Sharma 1985). Monoaromatic sulphonic acids were also selectively recovered from mixtures with disulphonic acids in aqueous solutions by extraction with TOA, dissolved in chlorobenzene, taken in a stoichiometrically deficient amount (Kroupa & Vrana 1986). Table 3 gives the data of recovery of some carboxylic and sulphonic acids from aqueous streams.

Krishnakumar & Sharma (1984) have recently demonstrated a novel strategy where a reaction system is used to recover phenolics from aqueous alkaline solutions through the formation of the esters of the phenolics with benzoyl chloride or *p*-toluene sulphonyl chloride using a phase transfer catalyst. Sasson *et al* (1981) have demonstrated a similar strategy to separate carboxylic acids and recover them

**Table 3.** Recovery and separation of carboxylic/sulphonic acids from dilute aqueous streams (Modified dissociation extraction).

System	$pK_a$ at 25°C	Extractant (solvent)	% Recovery	Separation factor
Formic acid	3.77	Trioctylamine <sup>a</sup>	52.6	9.5
Oxalic acid	1.27	( <i>o</i> -xylene)		
Acetic acid	4.76	Trioctylamine <sup>a</sup>	70.5	23.2
		( <i>o</i> -xylene)		
Monochloroacetic acid	2.81	(2-ethylhexanol)	56.6	24.2
Oxalic acid	1.27	Trioctylamine <sup>a</sup>	45.4	4.8
		( <i>o</i> -xylene)		
Glycolic acid	3.83	(benzene)	39.0	4.6
Monochloroacetic acid	2.81	Trioctylamine <sup>a</sup>	94.0	9.5
		( <i>o</i> -xylene)		
Dichloroacetic acid	1.29			
<i>p</i> -Toluene sulphonic acid H <sub>2</sub> SO <sub>4</sub>	—	Trioctylamine <sup>b</sup> (2-ethylhexanol)	67.6–97	17.4
<i>m</i> -Nitrobenzene sulphonic acid H <sub>2</sub> SO <sub>4</sub>	—	Trioctylamine <sup>b</sup> (2-ethylhexanol)	96	13–250

<sup>a</sup> Jagirdar & Sharma (1980); <sup>b</sup> Lodaya & Sharma (1985).

as esters under phase transfer catalytic conditions. The selectivity and removal of acidic materials from aqueous streams were very high, approaching 99. + %.

Kawabata *et al* (1981) have described a new method for the separation of carboxylic acids from aqueous solutions which involves treatment with cross-linked poly(4-vinylpyridine) followed by elution using methanol or other organic solvents. These cross-linked polymers showed an excellent capacity for removing carboxylic acids and the separation was attributed to the acid-base interaction between the pyridyl group of the polymer and the carboxyl group of the acid. The larger capacity of poly(4-vinylpyridine) for formic acid over acetic acid or for acrylic acid over propionic acid was attributed to the differences in acidity of these carboxylic acids.

An intriguing possibility is the use of a soluble polymeric amine in stoichiometric deficiency and then the use of membrane separation or ultrafiltration.

### 3. Reactive crystallization

The strategy of selective complexation of one of the components of the mixtures with an extracting agent has been followed by different investigators. Adductive or extractive crystallization has been used for a number of industrially important mixtures, such as, separation of *m*-/*p*-cresols by adductive crystallization with urea (Schering-Kahlbaum 1927) or with benzidine (Savitt & Othmer 1952), purification of Bisphenol A by formation of an adduct with phenol (Schuster 1974), separation of  $\gamma$ -/ $\beta$ -picolines/2,6-lutidine by forming crystalline products with urea (Riethof 1943) or phthalic acid (Grigorovskii & Kimen 1946).

#### 3.1 Separations using metal halide complexation

There has been a lot of activity in the separation of phenolic materials through metal halide complexation in the recent past. Leston (1983a,b,c) has claimed the efficacy of selective complexation with  $\text{CaBr}_2$  or  $\text{MgBr}_2$  in  $\text{EtOH}/\text{C}_6\text{H}_6$  for the separation of *p*-cresol/2-*t*-butyl-*p*-cresol, 3-thymol/4-thymol, hydroquinone/4-methyl pyrocatechol and other alkylated mixtures.

The separation of *m*- and *p*-cresols has also been achieved successfully by complexation with  $\text{CaBr}_2$  (Chemical Engineering News 1984). Recently Leston (1985) has reported the separation of close boiling amines, such as, mixtures of 3- and 4-picolines, 2,3,6-collidine/2,4,6-collidine, with  $\text{CaBr}_2$  in benzene or toluene as a medium.

#### 3.2 Separation through clathration

Clathration can be also included as a selective separation technique where clathrate-forming compounds like  $\alpha$ - (or  $\beta$ ) cyclodextrin form loose bonds with solutes, thus differentiating them in their size and molecular architecture.

*p*-Xylene was separated from *m*-xylene and ethylbenzene by forming such inclusion compound with metacyclophane (Teijn Ltd. 1985). Similarly *p*-cresol was separated from mixtures with *m*-cresol by formation of an inclusion compound with fluorene (Ube Industries Ltd. 1985).

The clathrates also have some molecular sieve potential. Dianin compound (4-*p*-hydroxyphenol-2,2,4-trimethyl chroman) and its thio analogue have hour-glass shaped cavities. The length of the cavity is somewhat less than the C-repeat



unit ( $\sim 11 \text{ \AA}$ ). Therefore it has remarkable capabilities of not only selecting certain isomers but of making a cut of paraffins upto  $n\text{-C}_7$  from  $n\text{-C}_8$  (Barrer 1986). This characteristic of clathrates, similar to zeolites, can be advantageous to separate even linear paraffins varying in chain length. Cyanometallates like  $\text{Zn}[\text{Fe}(\text{CN})_5\text{NO}]$  have been reported to separate  $\text{CO}_2$  from  $\text{CH}_4$  and 3-methylpentane from 2,2-dimethylpentane (Barrer 1986).

### 3.3 Separation of racemic mixtures

The synthesis of amino acids usually leads to racemic mixtures. In food or drug industry, the separation of the components by formation of distereoisomers is the most popular method of resolution where the racemic mixture is treated with an optically active reagent. For instance, DL-alanine can be separated by reaction with benzoyl chloride in aqueous alkaline solution to give N-benzoyl-DL-alanine, which on further reaction with (–) brucine can give an insoluble salt of N-benzoyl-D-alanine and a soluble salt of N-benzoyl-L-alanine (Streitwiser & Heathcock 1986).

The fact that organisms can use only one enantiomer of a racemic mixture can be exploited to separate such mixtures. The separation of DL-leucine by such biochemical method; N-acylation followed by addition of hog renal acylate (enzyme), has been achieved to get pure L-leucine (Greenstein & Winitz 1961).

Kinetic resolution of optical isomers exploits the difference in the rates of formation of diastereoisomers. An optically active compound may react with one of the isomers in racemic mixtures much faster than with another isomer. In ( $\pm$ ) mandelic acid, (+) isomer reacts faster with (–) menthol. If a limited quantity of (–) menthol is taken, the result is a mixture containing mainly (–) menthyl (+) mandelate and a very small quantity of (–) menthyl (–) mandelate (Greenstein & Winitz 1961). A similar strategy was demonstrated by Coisne and Pecker (1981) for ( $\pm$ )-mandelic acid isomers using an insoluble co-polymer functionalized by (+) alphas-methyl benzylamine. These examples have some resemblances to dissociation extraction in the principle of using stoichiometric deficient amount of the reacting species.

### 3.4 Dissociation extractive crystallization

Jagirdar & Sharma (1981b) and later Gaikar & Sharma (1984a,b) have observed substantial increase in the separation factor while using HCl gas to crystallize substituted anilines from organic solutions. Therefore, it is desirable to use an extracting agent which can form a complex with the stronger component of the mixture and come out as a separate phase, preferably as a solid crystalline phase.

When the solution of two components, A and B, A being the weaker component, in a suitable solvent, is contacted with an extracting agent C in a stoichiometric deficient amount the competition for C leads to an equilibrium reaction based on the relative strengths of two compounds as follows:



If, however, the complex  $\text{B} - \text{C}$  is sparingly soluble in the solvent it will crystallize out and the equilibrium shifts to the right, further precipitating  $\text{B} - \text{C}$  and this in turn will increase the extent of separation.

A wide variety of industrial mixtures of organic acids and bases, such as, 2,6-xyleneol/*p*-cresol, *N*-methylaniline/aniline, *N,N*-dimethylaniline/*N*-methylaniline, substituted anilines, guaiacol/*p*-cresol, 2,6-xyleneol/guaiacol etc., have been separated by dissociation extractive crystallization (Gaikar & Sharma 1987; A Mahapatra & M M Sharma, unpublished) and the separation factors for some of the systems are reported in table 4. Anhydrous sulphonic acids like *p*-toluene sulphonic, xylene sulphonic and piperazine were selected for crystallization of organic bases and phenolics, respectively. It was found that small impurities at 5–10% level can be removed in a single stage in some cases.

Crystallization can be also carried out from an aqueous phase provided the complex exhibits limited solubility in the aqueous phase. Such a strategy has proved to be useful for the separation of cumidines (Gaikar 1986), *m*-chloroaniline/*o*-anisidine (A Mahapatra & M M Sharma, unpublished) and 2,4,6-trichlorophenol/2,4-dichlorophenol/2,6-dichlorophenol (Gaikar 1986) using aqueous concentrated solutions of *p*-toluene sulphonic acid for anilines and aqueous solutions of monoethanol amine for chlorophenols. The separation factors for these systems are reported in table 5.

The separation factors obtained with dissociation extractive crystallization are very high, sometimes an order of magnitude higher than those obtained by conventional methods. In some cases, a single stage suffices to give complete separation.

There are various examples where such a strategy of reactive crystallization is being applied or is under development. For instance, alkyl or aryl diesters of phosphoric acid have been separated from equimolar mixtures by treating the mixture with  $\text{NH}_3(\text{g})$  and thus separating the ammonium salt of the monoester (Ludewig *et al* 1985). For mixtures containing 3,5,4-(MeO)<sub>2</sub>(OH)C<sub>6</sub>H<sub>2</sub>CHO and 3,4-MeO(OH)C<sub>6</sub>H<sub>3</sub>CHO when treated with  $\text{NH}_3$ , the complex of the former crystallized from aqueous methanolic solution in 99–100% purity (Gitchel *et al*

Table 4. Dissociation extractive crystallization.

System	$pK_a$ at 25°C	Extracting agent	Solvent	Separation factor
2,6-Xyleneol	10.62	Piperazine	<i>n</i> -Heptane	115–562 <sup>a</sup>
<i>p</i> -cresol	10.28			
<i>N</i> -methylaniline	3.5	<i>p</i> -TSA	<i>n</i> -Heptane + Toluene (90:10)	134 <sup>a</sup>
Aniline		<i>p</i> -XSA	-do-	267 <sup>a</sup>
<i>N</i> -Et-aniline	5.11	<i>p</i> -TSA	Toluene	18 <sup>a</sup>
Aniline		<i>p</i> -XSA	-do-	78 <sup>a</sup>
<i>o</i> -Chloroaniline	2.65	<i>p</i> -TSA	<i>n</i> -Heptane + Toluene (90:10)	Approaching $\infty^a$
<i>p</i> -Chloroaniline	4.15	<i>p</i> -XSA	<i>n</i> -Heptane	Approaching $\infty^a$
Guaiacol	9.93	Piperazine	Di- <i>i</i> -Pr- $\epsilon$ oc	16–52 <sup>b</sup>
<i>p</i> -Cresol	10.28			
Guaiacol	9.93	Piperazine	Di- <i>i</i> -Pr-ether	5–109 <sup>b</sup>
2,6-Xyleneol	10.62			

*p*-TSA = *p*-toluene sulphonic acid; *p*-XSA = *p*-xylene sulphonic acid; <sup>a</sup> Gaikar & Sharma (1986); <sup>b</sup> A Mahapatra & M M Sharma, unpublished.



Table 5. Dissociation extractive crystallization from aqueous phase.

System	$pK_a$ at 25°C	Extracting agent	Solvent	Separation factor
2,4,6-Trichlorophenol	6.37	Aq. MEA (1.0 M)	Toluene	20–83 <sup>a</sup>
2,4-Dichlorophenol	7.85		Di- <i>n</i> -butylether	17.84 <sup>a</sup>
2,6-Dichlorophenol	6.89			
<i>o</i> -Cumidine	4.42	Aq. <i>p</i> -TSA (3.0 M)	Toluene	73.5–95 <sup>b</sup>
<i>p</i> -Cumidine	4.87			
<i>m</i> -Chloroaniline	3.52	Aq. <i>p</i> -TSA (3.5 M)	Di- <i>i</i> -Pr-ether	19–137 <sup>c</sup>
<i>o</i> -Anisidine	4.52		Toluene	3–106 <sup>c</sup>

MEA = monoethanolamine; *p*-TSA = *p*-toluene sulphonic acid; <sup>a</sup> Gaikar & Sharma (1984b); <sup>b</sup> Gaikar & Sharma (1986); <sup>c</sup> Coisne & Pecker (1981).

1973). The complex formation can be superimposed on extraction; for instance, 2-allyl-6-chlorophenol and 2-allyl catechol are separated by treating the mixture, dissolved in alkaline solution, with boric acid and then extracting with benzene after adjustment of the pH of the solution. The addition of H<sub>3</sub>BO<sub>3</sub> increased the extraction of chlorophenol from 47.9% to 97.6% into the organic phase (Tamura *et al* 1986).

### 3.5 Purification of polyamines

Separation or recovery of polyamines, such as, diethylenetriamine, triethylenetetraamine etc. has been carried out from aqueous solutions by crystallizing the salts of these amines with *p*-toluene sulphonic acid. Here the separation by distillation may be difficult (Stapleton 1985).

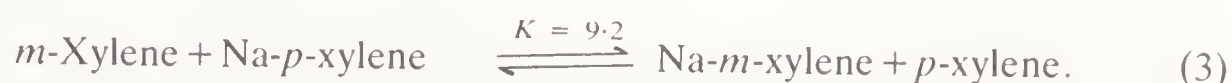
## 4. Reactive distillation

The strategy of an entrainer to modify the relative volatility of the mixture in extractive distillation is an attractive proposal for the separation of close boiling compounds. Reactions can be imposed on distillation and thus may lead to a promising method of separation. The idea of distillation with reactive entrainers is to introduce a third component into the distillation column so that reversible chemical reaction occurs. The reactive entrainer must be such that it is comparatively nonvolatile, it must be able to react selectively with one of the components forming nonvolatile products and the reaction must be reversible in order to facilitate recovery.

### 4.1 Separation of *m*-/*p*-xylenes

The concept of reactive distillation has been recently exploited by ANVAR (1975), Terrill *et al* (1985) and Cleary & Doherty (1985) for separation of *m*- and *p*-xylenes using organometallic compounds, such as, sodium-*p*-xylenes using organometallic compounds, such as, sodium-*p*-xylene-18-crown ether or phenylsodium and tertiary amines as chelating agents, dissolved in cumene as a reactive entrainer. The entrainer reacts selectively with *m*-xylene, retaining it in the liquid phase in

complex form, and thus produces a vapour rich in *p*-xylene. This example of xylenes indicated that it is possible to separate an industrial mixture of *m*- and *p*-xylene into 99.9% *p*-xylene in an 11-tray column. This method of reactive distillation exploits the difference in acidities of *m*-/*p*-xylenes. *p*-Xylene is much less 'acidic' than *m*-xylene, therefore, sodium preferentially attaches to *m*-xylene leaving *p*-xylene free to go overhead in a distillation column. The transmetallation reaction responsible for this separation is



#### 4.2 Dissociation extractive distillation

The principle of dissociation extraction can be extended to distillation as well. For instance, to a mixture of two acidic components is added a base of proper  $pK_a$  with a relatively high boiling point in stoichiometric deficient amounts. The stronger component is then expected to form a relatively non-volatile compound with the base and should be retained in the liquid phase. The distillation of such a mixture will create a vapour phase enriched in the weaker component. The addition of a neutralising agent, therefore, should increase the relative volatility of the mixture. This method of separation may be termed 'dissociation extractive distillation'. The set-up for this distillation may be similar to extractive distillation except that the extractive solvent is replaced by a proper acid or base and involves acid-base reaction on each plate in the liquid phase.

The counter-current contact of the downcoming neutralising agent with vapours depletes the stronger component from the vapour phase and enriches it in the liquid phase in the form of a complex which is assumed to be nonvolatile at column temperature. The weaker component is obtained as an overhead product while the stronger component can be recovered from the bottom product in a number of ways.

This idea has been tested on some of the systems, such as, 2,6-xylenol/*p*-cresol and 2,4-dichlorophenol/*p*-chlorophenol (Gaikar 1986); for both the systems the first component was enriched in the vapour phase. For a 2,6-xylenol/*p*-cresol mixture the relative volatility was increased to 3.2 in the presence of diethanolamine.

#### 4.3 Separation of ethanol/isopropanol

A similar idea was tested by Gassend *et al* (1985) for the separation of ethanol and isopropanol using different amines like pyridine, substituted cyclohexyl amines, ethylene diamines and substituted ethylene diamines in the presence of cyclohexane or toluene as diluents. The selectivity increase was from 2 to 22. The presence of N,N,N',N'-tetraethyldiaminocyclohexane increased the selectivity, i.e. relative volatility, by a factor of 22. This clearly shows the advantage of imposing chemical reaction on distillation.

Recently Oba (1986) has claimed that 2,3-dichloroaniline can be steam-distilled after addition of sulphuric acid to the mixtures of 2,3-/3,4-dichloroanilines. This is also an example of reactive distillation.



## 5. Separations with hydrotropes

The phenomenon of hydrotropy is related to increasing the solubility of sparingly soluble solutes in the aqueous phase in the presence of certain substances called hydrotropes. These substances include aryl sulphonic acids, their Na- and K-salts, salts of benzoic and substituted benzoic acids etc. Although the mechanism of hydrotropy is still not clear, it is believed to occur because of hydrogen-bonded complex formation between the solute and the hydrotrope.

These substances are under intensive investigation for enhancing the rates of heterogeneous reactions (Janakiraman & Sharma 1985, Pandit & Sharma 1987) and for separations (Gaikar & Sharma 1986). McKee (1946) was the first to use aqueous solutions of Na-xylene sulphonate to separate mixtures of aniline and dimethylaniline.

### 5.1 Extractive separations with hydrotropes

Gaikar & Sharma (1986) have recently used aqueous solutions of hydrotropes in extractive separations of various close boiling mixtures, such as, 2,6-xyleneol/*p*-cresol; *o*-chlorophenol/phenol; 2,4-dichlorophenol/*p*-chlorophenol; 6-chloro-*o*-cresol/*o*-cresol etc. Separation factors were in the range 10–68. Hydrotropy can be imposed on dissociation extraction, whenever applicable, to further increase the separation factor and percent extraction.

### 5.2 Separation of *o*-/*p*-chlorobenzoic acids

The strategy of selective solubilization using aqueous solutions of hydrotropes has been tried for separation of *o*-/*p*-chlorobenzoic acids (Gaikar 1986). The selectivity was found to be very high ( $\alpha \sim 400$ –2000), the percent extraction was higher as well.

A particular advantage of hydrotropic separation is the easy recovery of dissolved solutes from the solutions; simple dilution should allow the solute to come out or a solvent extraction using a polar solvent may suffice to recover the material.

### 5.3 Micelles in separations

The aggregates of surfactant molecules in the aqueous phase, above the critical micellar concentrations, may show considerably high selectivity in solubilization depending on the molar volume of the solute and the interactions which it can have with the functional groups of the surfactant. Hydrophobic interactions or hydrogen bonds are responsible for nonpolar or relatively polar solutes, while ionic interactions are predominant in the case of highly polar solutes.

It was shown by Nagarajan & Ruckenstein (1984) that aqueous solutions of dodecyltrimethyl ammonium chloride (DTAC) can remove small quantities of benzene from hexane-rich mixtures selectively ( $\alpha \sim 4$ ). The selectivity towards benzene was much higher ( $\alpha \sim 20$ –50) when the conventional surfactants were replaced by block copolymer micelles of poly[(ethylene oxide)-propylene oxide]

and of poly(vinyl pyrrolidone)-styrene (Nagarajan *et al* 1986).

The micellar solutions have been also employed for solid-liquid leaching, such as, extraction of vanillin and ethyl-vanilline from tobacco leaves (Borgerding & Hinze 1985).

## 6. Membrane separations

Membrane processes have been finding an increasing number of uses for the past decade as a result of the development of ultra-thin and highly permselective membranes. Reverse osmosis, ultrafiltration and electrodialysis are the fields still occupying a major fraction of membrane processes. But because of the development of asymmetric membranes and hollow fibre modules, gas separation by membranes is competing with the conventional processes, such as absorption, adsorption etc.

The separation of  $H_2$  in synthetic ammonia plants, and recovery of helium from natural gas are the early applications of gas separations by membranes. The separation of  $CO_2$  from natural gas, selective removal of  $H_2S$  from  $CO_2$  and enrichment of air in oxygen are the new processes under extensive research.

Reactive membranes or membranes with facilitated transport can augment the speed of separation and can also give very high selectivity.

### 6.1 Separation of $CO_2/CH_4$

An immobilized liquid membrane in the matrix of porous polymer can give very high values of fluxes as well as high values of the separation factor. For instance, monopositive ethylene diamine (EDA) ions when exchanged with persulphonic acid ionomer films, an ion exchange membrane, could give an increase of a factor of 26 in the flux of  $CO_2$  and also increase the separation factor for  $CO_2/CH_4$  by as high as 550 (Way *et al* 1984). The basic mechanism in this case is the diffusion controlled by reaction. The separation of  $CO_2$  from  $CH_4$  or from other hydrocarbons is important in natural gas processing and in enhanced oil recovery (EOR).

### 6.2 Separation of $H_2S/CO_2$

A similar strategy was tested for the separation of  $H_2S/CO_2$  from a coal gasifier gas by Matson *et al* (1977). The liquid membrane consisted of aqueous carbonate solutions. The slow kinetics of reaction of  $CO_2$  with carbonate as compared to instantaneous reaction of  $H_2S$  facilitates the selective removal of  $H_2S$ . Separation factors as high as 300 were obtained and the membrane could withstand pressures upto 20 atm.

### 6.3 Separation of $CO_2/O_2$

Ward & Robb (1967) exploited the carbon dioxide hydration catalysts – principally sodium arsenite – in the design of a novel membrane system for the removal of carbon dioxide from mixtures with oxygen; the separation factor was 4100.



#### 6.4 Removal of NO

Ward (1970) measured the facilitated flux of nitric oxide across a thin liquid film of ferrous chloride solution immobilized between two silicone support films. The NO reacts with  $\text{Fe}^{2+}$  reversibly:



The permeate, NO, can also be made to move against concentration gradient by the application of an electric field which interacts with the charged carrier (Bdzil *et al* 1973).

#### 6.5 Enrichment of air in oxygen

The enrichment of air in oxygen by supported liquid membranes with facilitated transport is another process being pursued by many investigators for medical applications (artificial lungs) and to improve combustion efficiency. Some of the Co complexes have shown promising success in enriching air in oxygen content upto 88% with separation factor of 30 as compared to the enrichment to 40% oxygen and separation factor 2 in the case of silicone rubber as the membrane material (Baker & Blume 1986).

#### 6.6 Separation of $\text{NH}_3/\text{H}_2\text{S}$

A combination of liquid membrane permeation and conventional steam stripping was used to separate  $\text{H}_2\text{S}$  and  $\text{NH}_3$  from waste streams by Cahn *et al* (1978).  $\text{NH}_3$  is allowed to react with acidic emulsion droplets while  $\text{H}_2\text{S}$  was stripped out of solution by steam.

#### 6.7 Separation of amino acids

A rather interesting application of electrolysis using ion exchange membranes is the separation of amino acids which because of their amphoteric nature can be protonated when the pH of the solution is lower than the isoelectric point (IP) thus forming positively charged species. Consequently different amino acids with different isoelectric points can be separated by pH adjustment and electrodialysis. For instance, L-alanine (IP = 6.1) and L-asparaginic acid (IP = 2.98) when placed in electrolysis chamber with pH 4, can move towards the cathode and the anode, respectively (Strathman 1984).

#### 6.8 Separation of xylenes

Xylene isomers have also been separated by a membrane which was apparently able to distinguish among their basicities. Polymer, which contained dinitrophenyl groups, gave selectivity of 2.8 for *m*-/*o*-xylenes and 2.4 for *m*-/*p*-xylenes (Chemtech 1986).

#### 6.9 Facilitated transport of monosaccharides through liquid membrane

The uphill transport of monosaccharides containing vicinyl -OH against the concentration gradient was carried out by Shinbo *et al* (1986) through bulk dichloromethane membrane containing phenylboronic acid and trioctylammonium

chloride (TOMA-Cl) as carriers. The rates of transport differed in the following order: fructose > galactose > glucose. The rates of transfer of species can be manipulated by controlling the pH of the receiving phase since the transport involves the neutralization reaction of phenylboronic acid and then the formation of an ion pair with  $\text{TOMA}^+$ .

#### 6.10 Separation of ethanol/water

Functional polymers, with a  $-\text{COOH}$  group, have been tried for the separation of ethanol-water mixtures (Yoshikawa *et al* 1986). A membrane obtained from acrylic acid-acrylonitrile was effective for selective separation of water from aqueous solutions of ethanol by pervaporation. High selectivity towards water was attributed to the H-bonding interaction between water and the acrylic acid unit in the membrane. On the other hand, a membrane from the acrylic acid-styrene copolymer preferentially permeated ethanol in the lower water feed concentration region.

#### 6.11 Separation of isomers of nitroaniline

Although a PVC membrane plasticized with isodecylphthalate permits the three isomers of nitroanilines to penetrate it in proportion to their relative concentration, when  $\alpha$ -cyclodextrin is added to the solution containing nitroanilines the relative ease of penetration of the *p*-isomer is reduced by 50 times (Anzai *et al* 1986). Nitro- and iodophenols are also expected to behave similarly. Cyclodextrins are known to form inclusion compounds with phenols and anilines and can differentiate between the isomers according to their structures.

#### 6.12 Membrane reactor

Vaughan (1985) of Varen Tech., USA, has patented a system to separate the oxidation product of cyclohexane; the products cyclohexanone/-ol are continuously separated by permeation through a fluorocarbon membrane with sulphonic acid groups, into an aqueous  $\text{HNO}_3$  solution for further oxidation to adipic acid.

### 7. Hydrometallurgical separations

The separations of metal ions in hydrometallurgy is yet another large scale application of separations through reactions; separation/processing of ores, precipitation of sulphides, separation of uranium, thorium, neptunium and plutonium in nuclear field, processing of electroplating wastes are few examples of industrial importance. The extraction of metals selectively into an organic solution by complexation has been one of the classical tools in differentiating and separating the cations of metals.

#### 7.1 Separation of uranium, plutonium and neptunium

These metal ions interact with tributyl phosphate (TBP) to form complexes that are soluble in organic solvents such as paraffins. Uranyl ion ( $\text{UO}_2^{2+}$ ) can be easily separated from plutonium or neptunium as they do not readily form neutral nitrate species and are not complexed with TBP (Thomson 1978).

Plutonium and neptunium can be separated by manipulating the conditions of the solution. The addition of ferrous sulphamate to create reducing conditions allows only neptunium to be recovered (Thomson 1978).

### 7.2 Removal of heavy metals from aqueous streams

For selective removal of highly toxic or valuable constituents from industrial waste containing heavy metal ions in low concentration, ultrafiltration can be effectively and economically applied when combined with a water-soluble macro-molecular complex which selectively binds certain metal ions (Stratmann & Kock 1978). Polymers used in such studies are polyethyleneimine, polyvinyl alcohol, polyvinylpyrrolidone and polyacrylic acid. For instance, at pH 4.2, a substantial amount of  $\text{Cu}^{++}$  was bound by polyethyleneimine, but  $\text{Fe}^{2+}$ ,  $\text{Ni}^{2+}$  and  $\text{Zn}^{2+}$  remained unaffected. The mercury-containing effluent from a chloralkaline electrolysis, at a level of 2 to 5 ppm, has also been made mercury-free by such a strategy.

Use of liquid membranes with facilitated transport and ion exchange membranes is also finding increasing application in the recovery of metal ions from aqueous streams.

### 7.3 Selective flocculation of ores

The processing of ores for enrichment of required metal uses selective flocculation by chelating agents or polymers.

Attia & Kitchner (1978) developed a selective flocculation process for the recovery of copper minerals from an oxidised ore. The selective flocculation separation of copper minerals, such as malachite, chalcocite from calcite, pyrite using the chelating agent, and polyacrylamide glyoxal bishydroxyanil (PAMG), has been reported.

LIX 65N also has been tried for selective chelation-flotation of the oxidised copper ore which is a highly selective commercial copper chelating extractant (Nagaraj & Somasundaram 1979).

### 7.4 Separation of zirconium from hafnium

Zirconium is specially desirable as a construction material for liquid-cooled atomic reactors of the thermal type. Naturally occurring zirconium ore contains hafnium (2 to 3%) which must be removed.

Chandler (1966) proposed a metathetical reaction between  $\text{HfCl}_4$  impurity in the feed and  $\text{ZrO}_2$  in the bed to yield nonvolatile  $\text{HfO}_2$  and  $\text{ZrCl}_4$  vapour while Newnham (1957) developed a method from an observation that different temperatures are required for the reduction of  $\text{ZrBr}_4$  and  $\text{HfBr}_4$  with Al to the respective tribromides.  $\text{HfCl}_4$  can be separated from  $\text{ZrCl}_4$  by reduction of the latter to nonvolatile  $\text{ZrCl}_3$  with subsequent sublimation of  $\text{HfCl}_4$ .

## 8. Separations with supercritical fluids

Separations with reactions can also be carried out using supercritical fluids. Shimshick (1983) has suggested supercritical  $\text{CO}_2$  for extraction of carboxylic acids



from alkaline fermentation broths.  $\text{CO}_2$  acts as an extractant and as a reactant for carboxylate ions in the alkaline solutions.

Separations of isomers of hydroxybenzoic acids (Krukoniš & Kurnik 1985) and Bisphenol isomers (Inoue *et al* 1985) have been tried successfully using supercritical  $\text{CO}_2$  as an extractant. This indicates that supercritical bases, such as, methyl amines may have some utility in separations of acidic isomeric/non-isomeric compounds.

## 9. Miscellaneous separations with reactions

### 9.1 Separation of *m*-/*p*-xylenes

Chlorination of *m*-/*p*-xylenes in alcoholic media gives very selective chloro-*m*-xylene. The rate of chlorination of *m*-xylene is 60 times higher than that of *p*-isomer (Bermecjo *et al* 1986).

### 9.2 Selective removal of HF

Asahi Glass of Japan have claimed that dispersion of an alkali metal aluminate in alcoholic media allows selective removal of HF from HCl down to 2–3 ppm; this gas mixture is encountered in the manufacture of Freons (Nashiro *et al* 1986).

### 9.3 Recovery and separation of nitric/hydrochloric acids

Haifa Chemicals, Israel, manufactures potassium nitrate by reacting solid potassium chloride with nitric acid in the presence of *n*-amyl alcohol which extracts hydrochloric acid generated in the reaction. The solvent from the reaction contains both hydrochloric and nitric acids and is fed to a washing battery. The washing with dilute nitric acid gives an aqueous stream which is further solvent-extracted with tributyl phosphate to remove nitric acid preferentially and this gives pure aqueous hydrochloric acid (Brunborg *et al* 1986).

### 9.4 Removal of silica from silicon carbide (SiC)

Oak Ridge National Laboratory (Chemical Week 1985) of USA has developed a novel process of purifying SiC by passing HF gas through SiC powder at 200–600°C, when reaction occurs between HF and  $\text{SiO}_2$ . The  $\text{SiO}_2$  content is reduced from 15% to 0.1–0.4%.

### 9.5 Selective removal of vinylidene olefin (VO)

Ethyl Corporation (Smith & Gerald 1985) have recently patented a process where VO impurity is selectively removed via reaction with  $\text{H}_2\text{S}$  or  $\text{RSH}$  with  $\text{H}_2\text{SO}_4$  as a catalyst.

### 9.6 Separation of nitration isomers of substituted benzenes

Monsanto (Nickson 1985) have claimed that the nitrated products of substituted benzenes can be reduced selectively with  $\text{Na}_2\text{S}/\text{NH}_4\text{Cl}$  in  $\text{EtOH-H}_2\text{O}$  at 75°C. The hindered  $\text{NO}_2$  remains unattacked.



### 9.7 Removal of aldehyde from ethylene oxide

Acetaldehyde can be removed from mixtures with ethylene oxide by refluxing the mixtures in the presence of 1–5% KOH and 3–5% PEG as a phase transfer catalyst (Wu *et al* 1985).

### 9.8 Separation of phenol from *p*-fluorophenol

Phenol, as an impurity, can be removed by selective reaction of phenol with phthalic anhydride with which 4-fluorophenol hardly reacts (Kawai *et al* 1985). This mixture should be amenable to separation by dissociation extraction.

### 9.9 Selective absorption of ethylene/CO

The toluene solutions of equimolar AgCl-AlCl<sub>3</sub> rapidly absorb ethylene from mixtures with CO selectively. The solutions showed no measurable absorption of CO (Hirai *et al* 1986a).

The toluene solutions of polystyrene protected aluminium CuCl absorb CO rapidly and the reaction becomes reversible at a temperature of 82°C (Hirai *et al* 1986b).

## 10. Scope for further work

There is considerable scope for further work in separations through reactions.

A predictive method for dissociation extractive crystallization would be highly desirable. The behaviour of the organic acids or bases in organic media is still an unexplored area. A sound knowledge of the acidities and basicities of the compounds in organic solvents would be necessary to predict the separation factor. Dissociation extractive crystallization may also provide directions for exploiting selective reactions in organic media.

Reactive distillation merits further systematic investigations. The knowledge of relative acidities/basicities in non-aqueous medium will be useful. The prediction of vapour-liquid equilibria in such cases requires a systematic study.

The separation of acidic or basic gaseous mixtures using stoichiometric amounts of reactant should be investigated.

Facilitated transport, particularly of acidic or basic gases using functional polymers, should be further investigated. Functional polymers can be of great value especially when separation is accompanied by the production of the desired compound.

Selective complexation followed by membrane separation may provide a cheaper method of recovering chemicals from waste streams.

Separations using hydrotropic solutions and micellar solutions may provide attractive methods of separation particularly for the removal of impurities. Reactions can also be imposed on these systems to increase the rate and extent of separation. There is also a need to study the basic mechanism of hydrotropy which can help in extending this method to various systems.

The use of acidic/basic supercritical fluids may be possible for separations of basic/acidic mixtures and may provide good separation factors.

There are great economic incentives to improve hydrometallurgical separations by selective reaction.

## 11. Conclusions

Separations through reactions may be attractive, compared to physical methods of separations, especially for close boiling mixtures. The cost of the separation can be reduced considerably if the reactions are reversible.

Dissociation extraction has been successfully applied to a number of close boiling acidic/basic mixtures. The selection of a proper solvent has improved the separation factor considerably.

Dissociation extractive crystallization is a promising method of separation and for certain systems a single stage may suffice to give complete separation. The separation of racemic mixtures has also proved the utility of reactive crystallization.

Selective solubilization or extraction by aqueous solutions of hydrotropes has given excellent separations. The use of micellar solutions with superimposed reaction may prove to be attractive.

Separations by reactive membranes or facilitated transport can provide answers in some of the difficult cases.

There is still considerable scope for developing new techniques and exploiting chemical reactions for separations.

This paper is dedicated to Dr L K Doraiswamy on his sixtieth birthday.

## References

- ANVAR (Agence Nationale de Valorisation de La Recherche) 1975 French Patent 1,378,951
- Anwar M M, Cook S T M, Hanson C, Pratt M W T 1974 *Proc. Int. Solvent Extraction Conf. ISEC* (London: Society of Chemical Industry) 1: 895-910
- Anwar M M, Cook S T M, Hanson C, Pratt M W T 1979 *Proc. Int. Solvent Extraction Conf. ISEC* (Toronto: Canadian Inst. of Mining and Met.) 2: 671-676
- Anwar M M, Hanson C, Patel A N, Pratt M W T 1973 *Trans. Inst. Chem. Eng.* 51: 151-153
- Anwar M M, Hanson C, Pratt M W T 1971a *Trans. Inst. Chem. Eng.* 49: 95-100
- Anwar M M, Hanson C, Pratt M W T 1971b *Proc. Int. Solvent Extraction Conf. ISEC* (London: Society of Chemical Industry) 2: 911-915
- Anzai J, Kobayashi Y, Veno A, Osa T 1986 *J. Appl. Polym. Sci.* 31: 1199-1208
- Attia Y A, Fuerstenau D W 1978 *Recent developments in separation science* (ed.) N N Li (West Palm Beach, FL: CRC Press) vol. 4, pp. 51-70
- Baker R W, Blume I 1986 *Chemtech.* 16: 233-238
- Barrer R M 1986 *Pure Appl. Chem.* 58: 1317-1322
- Bdzil J, Carlier C C, Fesch H L, Ward W J, Breiter M W 1973 *J. Phys. Chem.* 77: 846-854
- Bermejo J, Cabeza C, Blanco C G, Mainela S R, Martineg A 1986 *J. Chem. Technol. Biotechnol.* 36: 129-135
- Borgerding M F, Hinze W L 1985 *Anal. Chem.* 57: 2183-2190
- Bradström A 1983 *J. Mol. Catal.* 20: 93-98
- Brunborg I, Langham A, Barekat M 1986 *Nitric acid and fertiliser nitrates* (ed.) C Keleti (New York: Marcel Dekker Inc.) pp. 357-372
- Cahn R P, Li N N, Minday R M 1978 *Environ. Sci. Technol.* 12: 1051-1056
- Chandler H W 1966 US 3,276,862 *cf. Chem. Abst.* 65: 5020
- Chang T 1983 US 4,409,386
- Chem. Eng. News* 1984, 62(17): 31

- Chem. Eng. News* 1985 63(21): 60  
*Chem. Week* 1985, (September 25): 43-44  
*Chemtech.* 1986, 16(1): 57  
Cleary W, Doherty M F 1985 *Ind. Eng. Chem., Process Des. Dev.* 24: 1071-1073  
Coisne J M, Pecker J 1981 *Chimia* 35(3): 97 *cf* 1981 *Chem. Abstr.* 95: 42108  
Coulson E A, Jones J I 1946 *J. Soc. Chem. Ind.* 65: 169-175  
Frampton O D, Feldman J 1968 *Progress in separation and purification* (ed.) E S Perry (New York: Interscience Publishers) vol. 1, pp. 247-296  
Gaikar V G 1986 *Separations through reactions*, Ph.D thesis, University of Bombay  
Gaikar V G, Sharma M M 1984a *J. Sep. Process Technol.* 5: 49-52  
Gaikar V G, Sharma M M 1984b *J. Sep. Process Technol.* 5: 53-58  
Gaikar V G, Sharma M M 1985 *Solvent Ext. Ion Exch.* 3: 679-696  
Gaikar V G, Sharma M M 1986 *Solvent Ext. Ion Exch.* 4: 839-843  
Gaikar V G, Sharma M M 1987 *Ind. Eng. Chem. Res.* (in press)  
Gassend R, Duprat F, Gau G 1985 *Nouv. J. Chim.* 9: 703-705  
Gitchel W B, Diddams D G, Barrer J W 1973 US 3, 755, 456 *cf* 1973 *Chem Abstr.* 79: 115314  
Greenstein J P, Winitz M 1961 *Chemistry of amino acids* (New York: John Wiley and Sons)  
Grigorovskii A M, Kimen Z M 1946 *J. Appl. Chem. (USSR)* 18: 252-262  
Hirai H, Hara S, Komiyama M 1986a *Chem. Lett.* 2: 257-260  
Hirai H, Hara S, Komiyama M 1986b *Bull. Chem. Soc. Jpn.* 59: 109-116  
Inoue K, Hoyer G G, Bates S I 1985 US 4, 515, 574 *cf* 1985 *Chem. Abstr.* 103: 5999  
Jagirdar G C 1981 *Ind. Eng. Chem., Process. Des. Dev.* 20: 708  
Jagirdar G C 1985 *Ind. Eng. Chem., Process. Des. Dev.* 24: 886-887  
Jagirdar G C, Lawson F 1984 *J. Sep. Process Technol.* 5: 45-48  
Jagirdar G C, Sharma M M 1980 *J. Sep. Process Technol.* 1(2): 40-43  
Jagirdar G C, Sharma M M 1981a *J. Sep. Process Technol.* 2(9): 37-41  
Jagirdar G C, Sharma M M 1981b *J. Sep. Process Technol.* 2(4): 7-12  
Janakiraman B, Sharma M M 1985 *Chem. Eng. Sci.* 40: 2156-2157  
Kawabata K, Yoshida J, Tanigawa Y 1981 *Ind. Eng. Chem., Prod. Res. Dev.* 20: 386-390  
Kawai T, Suzuki H, Kaneda S 1985 German Offen DE 3, 421, 946 *cf* 1985 *Chem. Abstr.* 103: 6018  
Krishnakumar V K, Sharma M M 1984 *Ind. Eng. Chem., Process Des. Dev.* 23: 410  
Kroupa J, Vrana V 1986 Czech CS 2 17,523 *cf* 1986 *Chem. Abstr.* 104: 109289  
Krukonis V J, Kurnik R T 1985 *J. Chem. Eng. Data* 30: 247-249  
Laddha S S, Sharma M M 1978 *J. Appl. Chem. Biotechnol.* 28: 69-78  
Leston Q 1983a Kopper Co. Inc. US 4,423,523  
Leston Q 1983b Kopper Co. Inc. US 4,429,169 *cf* 1984 *Chem. Abstr.* 100: 138751  
Leston Q 1983c Kopper Co. Inc. US 4,424,381 *cf* 1984 *Chem. Abstr.* 100: 102937  
Leston Q 1985 *Chem. Eng. News* 63(21): 60  
Lodaya M P, Sharma M M 1985 *J. Sep. Process Technol.* 6: 34-39  
Ludewig D, Eiserback W, Feike E 1985 German DD 222,598 *cf* 1986 *Chem. Abstr.* 104: 149167  
Matson S L, Herrick C S, Ward W J 1977 *Ind. Eng. Chem., Process Des. Dev.* 16: 370-374  
McKee R H 1946 *Ind. Eng. Chem.* 38: 383-386  
Mendiratta A K, Talley J J 1985 US 4,547,596 *cf* 1986 *Chem. Abstr.* 104: 168111  
Millington J P, Jones A R, Hughes J A, Trofman J E 1986 Brit. Patent Appl. GB 2,164,935; *cf* 1986 *Chem. Abstr.* 105: 114728  
Nagaraj D R, Somasundaran P 1979 *Recent developments in separation science* (ed.) N N Li (West Palm Beach FL: CRC Press) vol. 4, pp. 81-94  
Nagarajan R, Borg M, Ruckenstein E 1986 *Langmuir* 2: 210-215  
Nagarajan R, Ruckenstein E 1984 *Surfactants in solution* (ed.) K L Mittal (New York: Plenum Press) vol. 2, pp. 923-948  
Nashiro M, Yarita T, Otsuka I, Nakano T, Hoshimoto T, Enomoto A 1986 Japan Kokai Tokyo Koho JP 6,136,102 *cf* 1986 *Chem. Abstr.* 104: 209454  
Newham I E 1957 *J. Am. Chem. Soc.* 79: 5415-5417  
Nickson T E 1985 Monsanto Co. US 4,503,276  
Oba H 1986 Japan Kokai Tokyo Koho JP 6105058; *cf* 1986 *Chem. Abstr.* 104: 186116  
Pandit A, Sharma M M 1987 *Chem. Eng. Sci.* (in press)  
Riethof G 1943 US 2,295,606 *cf* 1943 *Chem. Abstr.* 37: 1132



- Robinson R G, Cha D Y 1985 *Biotechnol. Prog.* 1: 18-25
- Sarlori G, Savage D W 1983 *Ind. Eng. Chem., Fundam.* 23: 239-249
- Sasson Y, Yonowich-Weiss M, Grushya E 1981 *Sep. Sci. Technol.* 16: 195-199
- Savitt S A, Othmer D F 1952 *Ind. Eng. Chem.* 44: 2428-2431
- Schering-Kahlbaum G A 1927 Brit. Patent 297,083
- Schuster L 1974 (BASF A-G) Brit. Patent 1,377,227 *cf.* 1975 *Chem. Abstr.* 103: 11129
- Schwarz A 1891 *Ber.* 24: 1676 *cf.* Coulson E A and Jones J I 1946 *J. Soc. Chem. Ind.* 65: 169-175
- Sharma M M 1964 *Kinetics of gas absorption* Ph.D. thesis, Cambridge University, England
- Sharma M M 1985 *J. Sep. Process Technol.* 6: 9-15
- Shimshick E J 1983 *Chemtech.* 13: 374-375
- Shinbo T, Nishimura K, Yamaguchi T, Sugiwa M 1986 *J. Chem. Soc., Chem. Commun.* 349-351
- Smith R S, Gerald Z Jr 1985 US 4,511,753 *cf.* 1985 *Chem. Abstr.* 103: 22168
- Stapelton I W 1985 *Aust. J. Chem.* 38: 633-636
- Stevens D R 1943 *Ind. Eng. Chem.* 35: 655-660
- Strathman H 1984 *J. Sep. Process Technol.* 5: 1-13
- Stratmann H, Kock K 1978 *Recent developments in separation science* (ed.) N N Li (West Palm Beach, FL: CRC Press) vol. 4, pp. 29-38
- Streitwiser A, Heathcock C H 1976 *Organic chemistry* (New York: Macmillan)
- Tamura M, Adachi K, Nakajima S, Otani Y 1986 Japan Kokai Tokyo Koho JP 6,168,434 *cf.* 1986 *Chem. Abstr.* 105: 172045
- Teijn Ltd. 1985 Japan Kokai Tokyo Koho JP 6,041,622 *cf.* 1985 *Chem. Abstr.* 100: 104682
- Terill D L, Sylvestre L F, Doherty M F 1985 *Ind. Eng. Chem., Process Des. Dev.* 24: 1062-1071
- Thomson M J 1978 *Recent developments in separation science* (ed.) N N Li (West Palm Beach, FL: CRC Press Inc.) vol. 4, pp. 215-224
- Ube Industries Ltd. 1985 Japan Kokai Tokyo Koho JP 6,112,730 *cf.* 1985 *Chem. Abstr.* 103: 214970
- Vaughen R J (Varen Tech.) 1985 US 4,532,347 *cf.* 1985 *Chem. Abstr.* 103: 162582
- Wadekar V V, Sharma M M 1981a *J. Sep. Process Technol.* 2: 1-15
- Wadekar V V, Sharma M M 1981b *J. Sep. Process Technol.* 2: 28-32
- Wadekar V V, Sharma M M 1981c *J. Chem. Tech. Biotechnol.* 31: 279-284
- Ward W J 1970 *AIChE J.* 16: 405-410
- Ward W J, Robb W L 1967 *Science* 156: 1481-1483
- Way J D, Noble R D, Reed D L, Ginlay G W, Baker L A 1984 Report submitted to National Bureau of Standards, Boulder CO. 80303, USA
- Wu Z, Zuo C, Sun H, Huang R 1985 *Hauxue Shijie* 26(7): 247-249 *cf.* 1985 *Chem. Abstr.* 103: 179987
- Yoshikawa M, Yukoshi T, Sami K, Ogata N 1986 *J. Polym. Sci.* 24: 1585-1589





# Theoretical foundation of cluster formation in supported liquid-phase catalysts

H LIVBJERG, T S CHRISTENSEN\*, T T HANSEN\*\*  
and J VILLADSEN

Department of Chemical Engineering, Technical University of Denmark, 2800 Lyngby, Denmark

\* Present address: Haldor Topsøe A/S, Lyngby, Denmark

\*\* Present address: Novo Industries A/S, Bagsværd, Denmark

**Abstract.** Despite the widespread use of supported liquid phase catalysts (SLPC) in industrial practice, the basic phenomenon of liquid dispersion which affects the diffusion rates of reaching components and gas-liquid interfacial area, is not well understood. The paper identifies the associated problems and formulates a model for the pore structure of real catalysts based on intersecting cylinders to study the effects of capillary forces. The formation of liquid clusters of dimensions larger than the pore dimensions and their subsequent effects on the performance of SLPC can be studied using this model. The model provides a basis for manipulating parameters that can reduce such cluster formation.

**Keywords.** Supported liquid phase catalysts; liquid clusters; liquid dispersion in porous solids.

## 1. Introduction

Supported liquid-phase catalysts (SLPC) form an important group of industrial catalysts. They are characterized by a liquid phase which is a catalyst for reactions between gas phase components. The liquid is dispersed in a porous solid to produce a large gas-liquid interface. SLPC are therefore particularly suited for catalysts with a low diffusion rate in the liquid phase.

The control of liquid dispersion is of considerable importance and is not well understood. It affects both the rate of diffusion in the liquid phase and the gas diffusion rate in the support pore structure. Since the activity of most SLPC is strongly reduced by diffusion resistance when the liquid loading becomes high, the liquid distribution invariably becomes one of the key factors in SLPC design.

It has been known for some time that the liquid distribution in a porous solid depends markedly on fractional loading  $\alpha$  of the pore volume (Villadsen 1978). At low  $\alpha$  the liquid phase is normally finely and uniformly dispersed by capillary forces. When  $\alpha$  is increased, however, part of the liquid eventually agglomerates to

---

A list of symbols is given at the end of the paper

flood regions of the pore structure much larger than pore size dimensions. The flooded regions are generally known as "clusters". Since they represent a poorly dispersed state of the liquid it becomes of obvious importance to study the factors which influence their formation. Very little is presently known about this subject.

A rigorous approach to liquid dispersion control is, however, complicated due to the highly irregular geometry of a typical support pore structure. It therefore seems worthwhile to approach the subject more carefully by first considering the behaviour of liquids in geometrically regular and simple pores.

## 2. Liquid distribution in model pores

### *The energetics of liquid distribution*

In a porous solid containing both a liquid and a gas phase any spontaneous change in the shape of the liquid phase will tend to minimize the surface Gibbs free energy (Adamson 1976):\*

$$G^s \equiv A a_L \gamma_{SL} + A (1 - a_L) \gamma_{SG} + A_{LG} \gamma_{LG}. \quad (1)$$

$A$  is the total surface area of the solid—of which a fraction  $a_L$  is covered by the liquid.  $A_{LG}$  is the gas-liquid interface area and  $\gamma_{SL}$ ,  $\gamma_{SG}$ , and  $\gamma_{LG}$  are interface tensions: solid-liquid, solid-gas, and gas-liquid respectively. We implicitly assume that the pores of the solid are so small that the influence of gravity on the liquid distribution is negligible.

In (1) we substitute Young's equation and introduce the adhesion tension  $\gamma_a$  (Adamson 1976)

$$\gamma_{LG} \cos \theta = \gamma_{SG} - \gamma_{SL} \equiv \gamma_a, \quad (2)$$

where  $\theta$  is the usual solid-liquid contact angle. The free energy is then expressed as

$$\begin{aligned} G^s &= A(\gamma_{SG} - a_L \gamma_a + a_G \gamma_{LG}) \\ &= A(\gamma_{SG} - a_L \gamma_{LG} \cos \theta + a_G \gamma_{LG}), \end{aligned} \quad (3)$$

where  $a_G$  is the normalized gas/liquid interface area:  $a_G = A_{LG}/A$ .

We wish to examine in detail the variation of  $G^s$  with the fractional liquid loading  $\alpha$ . The boundary conditions for this relation can be written immediately from (3): When  $\alpha = 0$  (no liquid in the pores) both  $a_L$  and  $a_G$  are zero, and

$$G_0^s = A \gamma_{SG} (\alpha = 0). \quad (4)$$

When  $\alpha$  changes from 0 to 1,  $a_G$  goes through a maximum. When  $\alpha = 1$ , the pores are completely flooded with liquid,  $a_L = 1$  and  $a_G = 0$ —if we neglect the small external particle surface,

$$G_1^s = A(\gamma_{SG} - \gamma_a), \text{ for } \alpha = 1. \quad (5)$$

The change in free energy between  $\alpha = 1$  and  $\alpha = 0$  is then

$$-(G_1^s - G_0^s) = -\Delta G^s = A \gamma_a. \quad (6)$$

---

\*The influence of liquid molecules held by surface forces in an adsorbed state at the gas/solid surface is neglected.

$-\Delta G^s$  is the total energy available for dispersion of the liquid. It is negative when the solid is not wetted by the liquid, i.e. when  $\theta > 90^\circ$ . This is the case for, e.g., some molten metal catalysts. These catalysts actually attract some practical interest since it is possible to design molten metal SLPC by a special preparation procedure by which the metal is trapped in the support structure (Adamson 1976; Kenney 1978; Villadsen & Livbjerg 1978; Villadsen *et al* 1980). They are, however, far less common than wetting catalysts and will not be further discussed here. Wetting catalysts have positive  $-\Delta G^s$  because the energy needed to disperse the liquid by increasing  $a_G$  is gained by wetting the solid surface, i.e., by increasing  $a_L$ . Therefore a suitable pore structure can produce stable liquid distributions with extremely large  $A_{LG}$  even by the spontaneous action of capillary forces.

The value of  $G^s$  for intermediate values of  $\alpha$  in the range  $0 < \alpha < 1$  is far more difficult to calculate because it is necessary to calculate the exact shape of the liquid to obtain  $a_L$  and  $a_G$  of (3). Physically meaningful solutions to this problem have to obey the following two criteria (Adamson 1976):

- 1) The contact angle along the three-phase border lines must at all points be equal to  $\theta$  of (2).
- 2) The curvature  $1/r_1 + 1/r_2$  of the gas-liquid interface must be the same throughout the pore structure.  $r_1$  and  $r_2$  are the two main radii of curvature.

Criterion 2 states that the pressure difference across the gas-liquid interface, i.e. the capillary pressure given by the Young-Laplace equation (Adamson 1976),

$$\Delta p = \gamma_{LG}(1/r_1 + 1/r_2), \quad (7)$$

remains constant. Together with criterion 1 it constitutes the condition for stability in the sense that  $dG^s$  of (3) is positive for all small perturbations in the shape and size of the gas-liquid interfaces.

It is known that such problems from the field of capillary theory may have several solutions—all satisfying the two stability criteria (Adamson 1976). We shall mainly concern ourselves with that particular solution for which  $G^s$  for a given  $\alpha$  attains its minimum value. The argument for emphasizing this particular solution is: Spontaneous processes due to a slow mobility of the liquid phase, e.g. evaporation, surface diffusion, or liquid flow, probably tend towards the global minimum, considering especially the long life time of a typical industrial catalyst. In this sense the distribution with minimum  $G^s$  is the most stable of all the solutions satisfying the stability criteria.

### Unit cells

To proceed further with the calculation of  $G^s$  for  $0 < \alpha < 1$  it is necessary to specify the geometry of the support pore structure. For simplification, we consider model pore structures which can be constructed by replication of the "unit cells" shown in figures 1–3:

### Channels with rhombic cross-section

The channels (figure 1) are assumed to be straight and infinitely long so that end effects can be ignored. It is thus essentially a two-dimensional distribution.



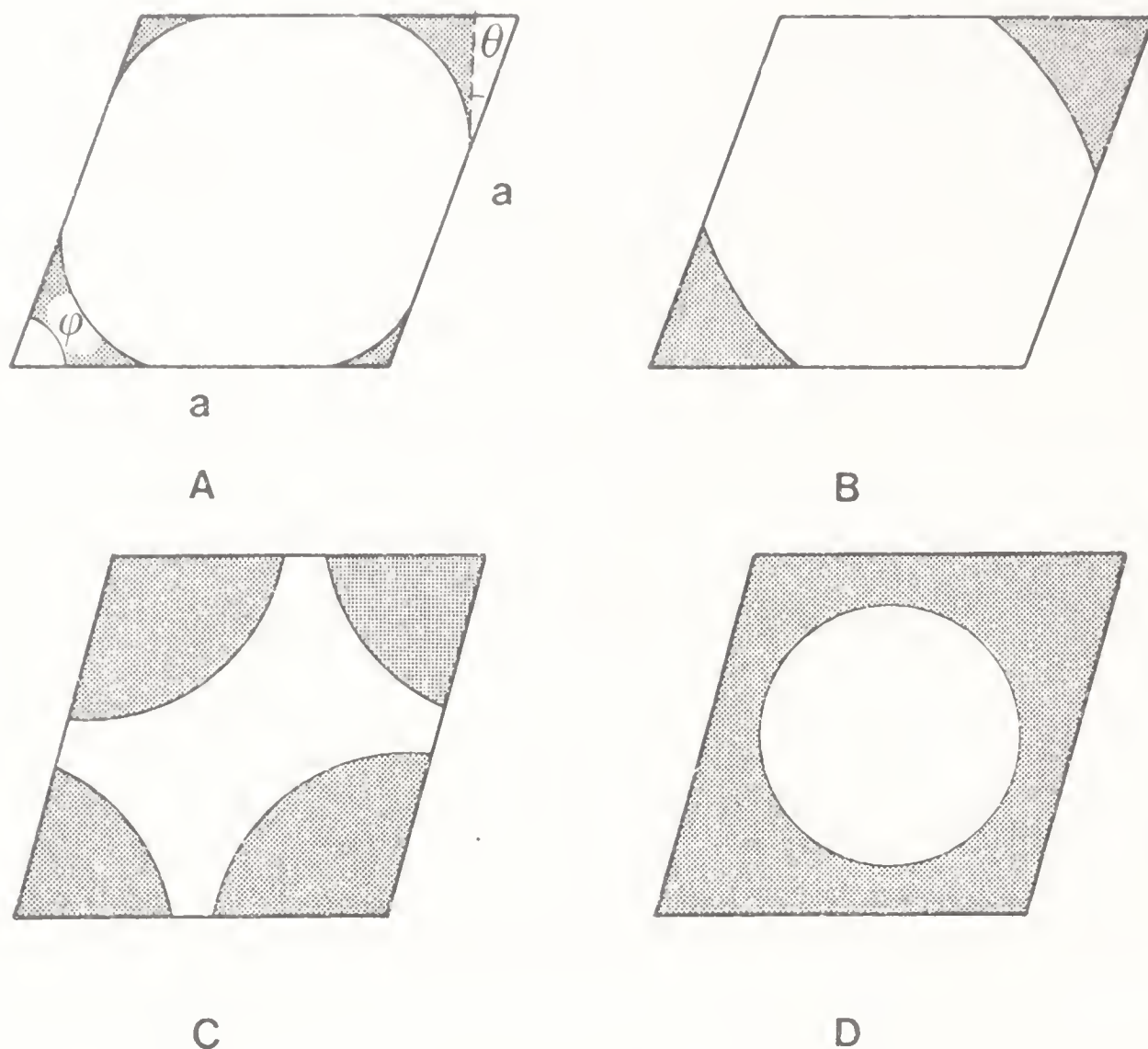


**Figure 1.** Distribution of a liquid in a channel with rhombic cross-section. A:  $\phi > 2\theta$ . B:  $\phi \leq 2\theta < \pi - \phi$ . C:  $2\theta \geq \pi - \phi$ . D: All  $\theta$ , when  $\alpha > 1 - (\pi/4) \cdot \sin \phi$ .

The gas-liquid interface is cylindrical with circular cross-section. It has an infinite radius of curvature  $r_2$  in a plane parallel to the channel axis, and a radius  $r_1$ —depending on  $\alpha$ —in a plane perpendicular to the channel. Figures 1A–C show three cases of different contact angle  $\theta$  in a channel with given  $\phi$ : if  $\phi > 2\theta$  there is liquid in all four corners of the rhomb. For  $\phi \leq 2\theta < \pi - \phi$  liquid cannot coexist in two corners with different angles because the curvatures have different signs, and for minimum  $G^s$ , all the liquid will assemble in the corner with the smallest angle which, for a given  $\alpha$ , yields the smallest  $a_G$  and the largest  $a_L$  [see (3)]. For  $2\theta \geq \pi - \phi$  it is possible to have liquid with identical, but negative curvature in all four corners. For large  $\alpha$ , i.e.  $\alpha > 1 - \pi \sin \phi/4$ , any of the three situations (figures 1A–C), ends up as in figure 1D with a cylindrical bubble surrounded by liquid. For a certain range of intermediate  $\alpha$ -values the picture can be either that shown in figure 1D or one of the 3 other distributions, i.e., two solutions may exist. The calculation of  $r_1$ ,  $a_L$ , and  $G^s$  for given values of  $\alpha$ ,  $\theta$ , and  $\phi$  is straightforward using (3) and elementary geometry.

#### *Stacked cylindrical rods*

This unit cell (figure 2) is formed by the void volume between the rods. Assuming infinitely long rods this is a two-dimensional distribution with  $1/r_2 = 0$ . Two different packing densities are considered: a loose quadratic arrangement in which

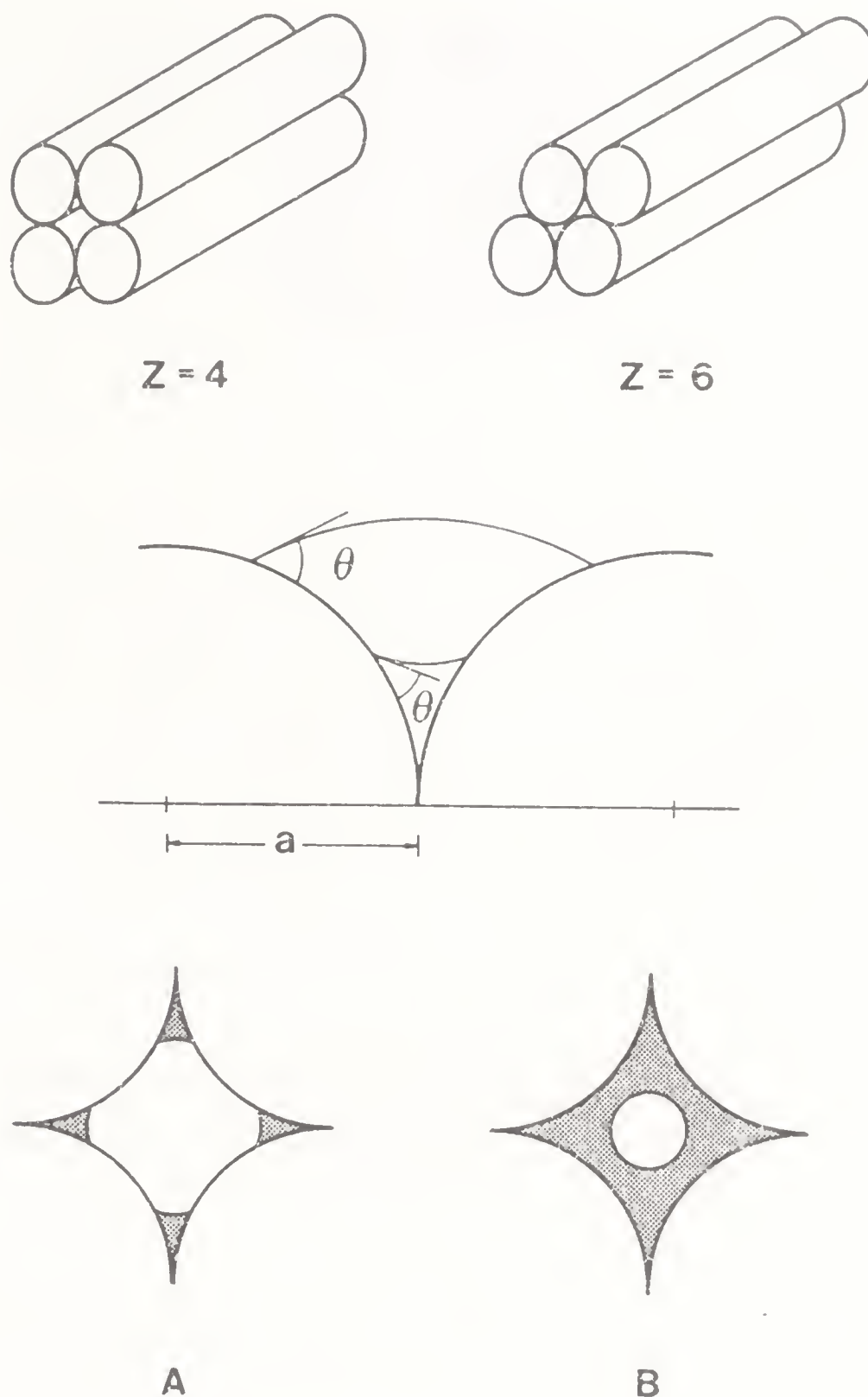


**Figure 2.** Distribution of a liquid in the void between stacked cylindrical rods with radius  $a$ . The two possible types of interfaces are shown in A and B for the quadratic arrangement of the stacking ( $Z = 4$ ). They are quite equivalent for the triangular stacking ( $Z = 6$ ).

the number of nearest neighbours for each rod is  $Z = 4$ , and the dense triangular arrangement with  $Z = 6$ . When  $\alpha$  is small the liquid accumulates in the vertices formed by the contact points. The curvature,  $1/r_1$ , varies in sign and value with  $\alpha$  (see figure 2). When  $\alpha > 0.3721$  for  $Z = 4$  or  $\alpha > 0.5337$  for  $Z = 6$  a cylindrical meniscus in a continuous liquid phase is possible. In a certain  $\alpha$ -range both solutions are possible.

Since all gas-liquid interfaces are cylindrical,  $G'$  of (3) can be calculated in a straightforward manner from elementary geometry.

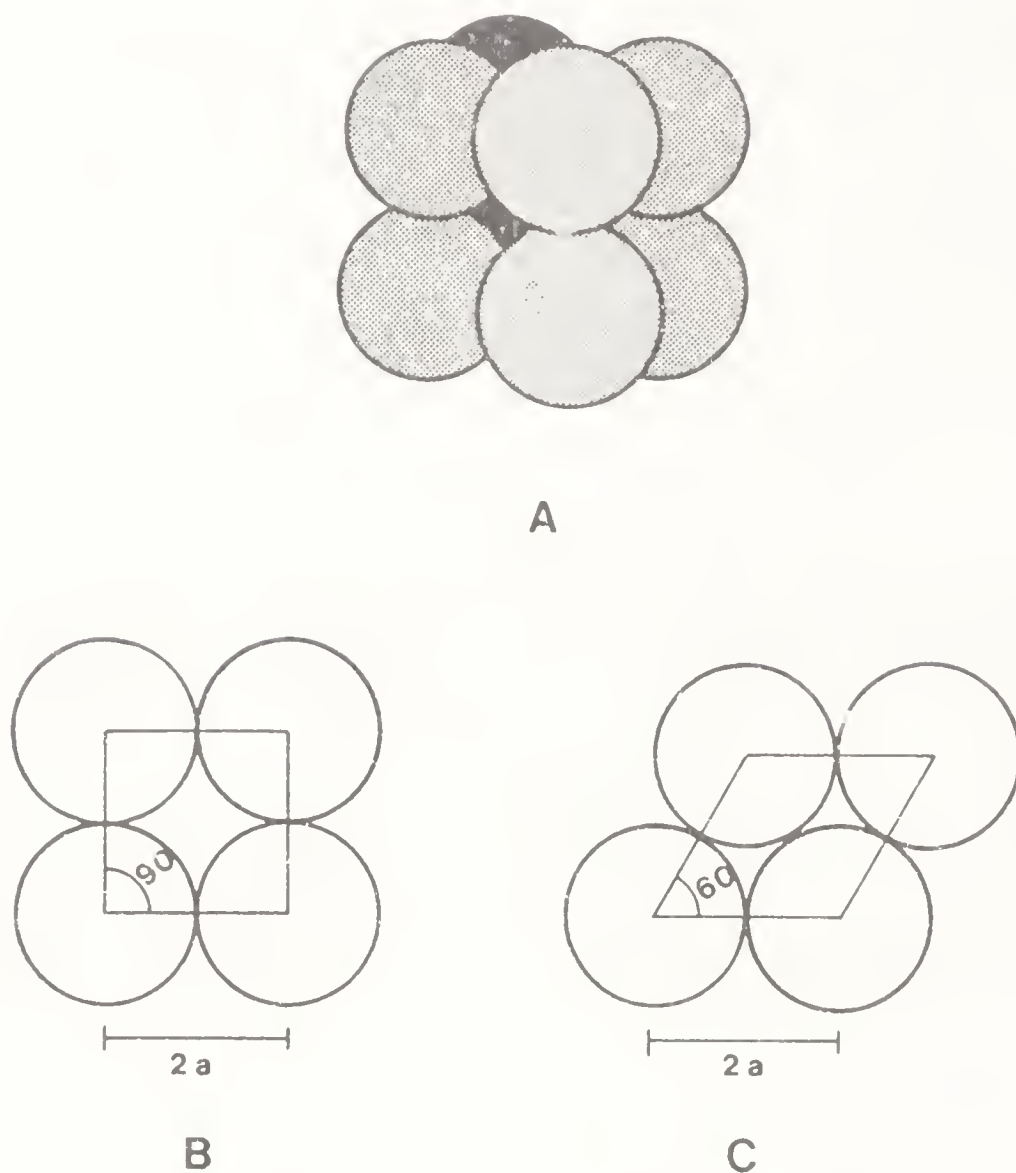


**Figure 3.** A: Porous structure in a stacking of spheres with radius  $a$ . B: The quadratic arrangement of the spheres in a layer of the loose packing with  $Z = 6$  (as in A), porosity 0.4764 and  $v_u = 3.8112 a^3$ . C: The rhombic arrangement of the spheres in a layer of the dense packing with  $Z = 12$ , porosity 0.2595, and  $v_u = 1.4681 a^3$ .

### *Packed spheres*

The pore structure is formed by the voids in a three-dimensional packing of ideal, identical spheres (figure 3). Two packing types with different densities are considered: 1) A loose "quadratic" structure with the spheres stacked one on top of the other, the number of contact points per sphere being  $Z = 6$ . 2) A dense "rhombic" packing with  $Z = 12$ . Properties of these structures are summarized in figure 3.

This three-dimensional structure has a more complicated gas-liquid interface geometry, and it is difficult to calculate  $G^*$ . Hence, we shall only treat this case for low liquid loading when the liquid forms isolated "rings" around the contact points—the so-called nodular region which turns out to be the only region of interest in terms of global stability due to cluster formation as shown below. This region has previously been treated by, e.g., Schubert (1982) who computed the capillary pressure of the stacked spheres structure. The equations describing the interface shape are derived in the following manner (Schubert 1922):

The interface is evidently cylinder-symmetrical on the centreline between two contacting spheres. Let  $\{z, y\}$  be cylinder coordinates.  $z$  is measured on the

centreline with  $z = 0$  at the point of contact between the spheres.  $y$  measures the distance from the centreline. The function  $y = f(z)$ —to be determined in the following—describes the interface shape. When the radii of curvature are expressed through  $f$  and inserted into the Young-Laplace equation (7), criterion 2 yields the differential equation:

$$\Delta p = \gamma_{LG} \left| \frac{(d^2y/dz^2)}{[1 + (dy/dz)^2]^{3/2}} - \frac{1}{y[1 + (dy/dz)^2]^{1/2}} \right|, \quad (8)$$

and by rearrangement:

$$d^2y/dz^2 = (\Delta p/\gamma_{LG}) [1 + (dy/dz)^2]^{3/2} + (1/y) [1 + (dy/dz)^2]. \quad (9)$$

Let  $z_1, y_1$  denote the point where all three phases meet (figure 4). The correct contact angle  $\theta$  of criterion 1 is ensured by

$$dy/dz = \tan \left( \frac{\pi}{2} - \beta - \theta \right), \text{ for } z = z_1. \quad (10)$$

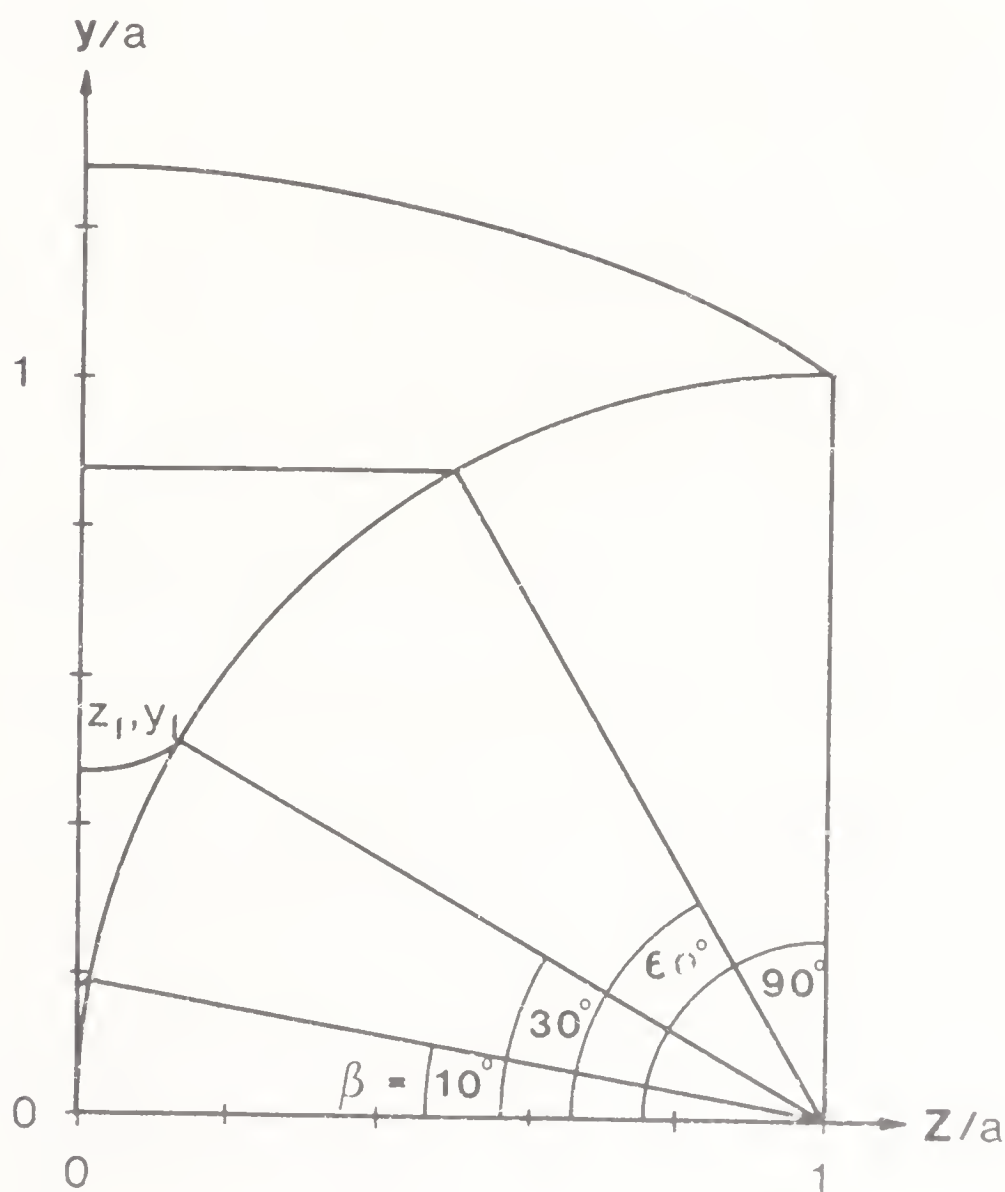


Figure 4. Distribution of a liquid between two spheres with radius  $a$ . The gas-liquid interface shape in cylindrical coordinates computed from (9) for a contact angle  $\theta = 30^\circ$  for different volumes of liquid.



Boundary conditions of (9) at  $z = 0$  and  $z = z_1$  are:

$$\begin{aligned} dy/dz &= 0, \text{ for } z = 0, \\ y &= y_1 = a \sin \beta, \text{ and} \\ z_1 &= a(1 - \cos \beta), \end{aligned} \quad (11)$$

at the three-phase boundary point.

The following numerical procedure is used to map the solution of (9) in terms of the surface energy for different liquid loadings (see Hansen 1983, Christensen 1985, for details): For a given value of the angle  $\beta$  (see figure 4) (9), with boundary conditions (11), is solved numerically by orthogonal collocation (Villadsen & Michelsen 1978). The solution contains the scalar factor  $\Delta p$ , and using (10) one finally obtains both  $y = f(z)$  and  $\Delta p$ . Knowing  $y = f(z)$  one subsequently computes the liquid volume  $v_l$ , the gas-liquid surface area  $s_l$ , and the solid-liquid surface area  $s_s$  connected with one contact point.

$$v_l = 2\pi \int_0^{z_1} y^2 dz - (2a^3/3)\pi (1 - \cos \beta)^2 (2 + \cos \beta), \quad (12)$$

$$s_l = 4\pi \int_0^{z_1} y [1 + (dy/dz)^2]^{1/2} dz, \quad (13)$$

$$s_s = 4a^2 \pi (1 - \cos \beta). \quad (14)$$

Referring to (3) one can now calculate the surface free energy  $G_s$  per unit cell except for the physical parameter  $\gamma_a$ :

$$A = 4\pi a^2, \quad a_G = \frac{1}{2} Z s_l / 4\pi a^2, \quad a_L = \frac{1}{2} Z s_s / 4\pi a^2, \quad (15)$$

and the fractional liquid loading  $\alpha$  is

$$\alpha = \frac{1}{2} Z v_l / v_u. \quad (16)$$

$v_u$  is the unit cell volume, i.e., the void volume per sphere. In figures 5–7 examples of calculations are shown.

To avoid the physical parameter  $\gamma_a$ , a dimensionless free energy function,

$$g^s = (G^s - G_1^s) / (-\Delta G^s) = 1 - a_L + a_G / \cos \theta, \quad (17)$$

is calculated as a function of  $\alpha$ .  $g^s$  varies from 1 at  $\alpha = 0$  to 0 at  $\alpha = 1$ . We shall refer to  $g^s$  as the energy dispersion function. For a given unit cell type the form of the  $g^s$  vs.  $\alpha$  relation depends only on the contact angle  $\theta$ .

#### *Uniform dispersion and cluster formation*

Let  $a_L''$  and  $a_G''$  denote the values of  $a_L$  and  $a_G$  of the most stable distribution in a single unit cell for a given  $\alpha$ .  $G_u^s$  is the corresponding minimal  $G^s$  value:

$$G_u^s = A(\gamma_{SG} - a_L'' \gamma_a + a_G'' \gamma_{LG}). \quad (18)$$

A dispersion in which all unit cells have identical distribution, a so-called uniform distribution, is obviously possible for the whole pore structure since criteria 1 and 2

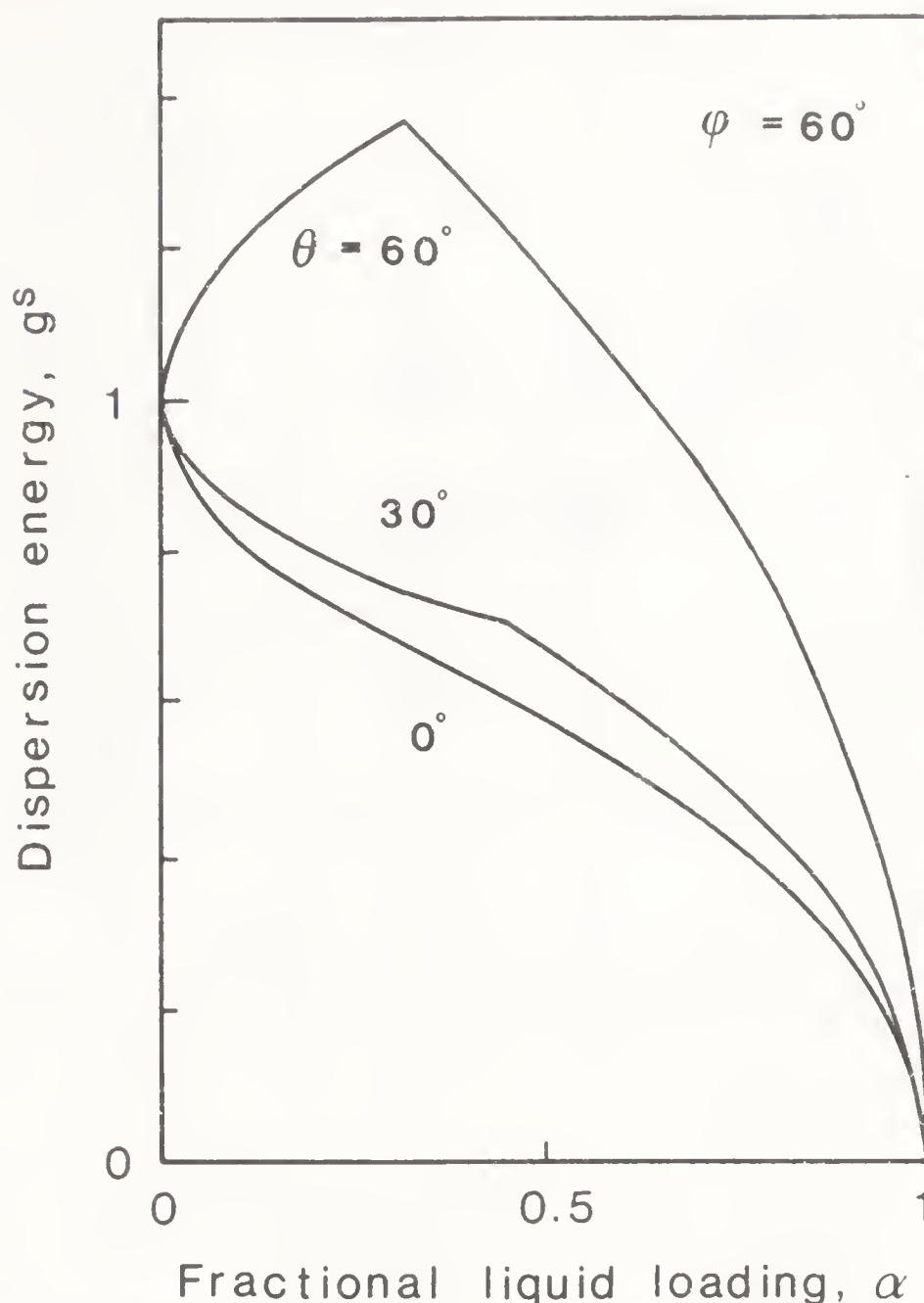


**Figure 5.** Dispersion energy relation for a uniform liquid distribution in the rhombic channels (figure 1) for different values of the contact angle  $\theta$ . The curves are for a corner angle  $\phi = 60^\circ$ . The break on the curves for  $\theta > 0$  marks the transition into the  $D$  distribution (see figure 1).

are both satisfied. The relationship between  $G_u^s$  and  $\alpha$  for a uniform distribution is exactly what is shown in the examples in figures 5–7 for different unit cell geometries.

We shall next examine the surface energy by the formation of liquid clusters i.e. large regions of the pore structure completely flooded with liquid (figure 8). Since the clusters have no “internal” gas-liquid interface they form stable distributions (i.e. satisfying criteria 1 and 2) together with any stable and uniform distribution surrounding the cluster. We assume that the clusters are so large that we can neglect the energy contribution from the interfaces along the “external” boundaries of the clusters. Then we can compute the surface energy for the composite structure of clusters surrounded by uniformly distributed liquid by adding together the energy for each of the two different regions:

$$G^s = (1 - \xi) G_u^s + \xi G_l^s. \quad (19)$$

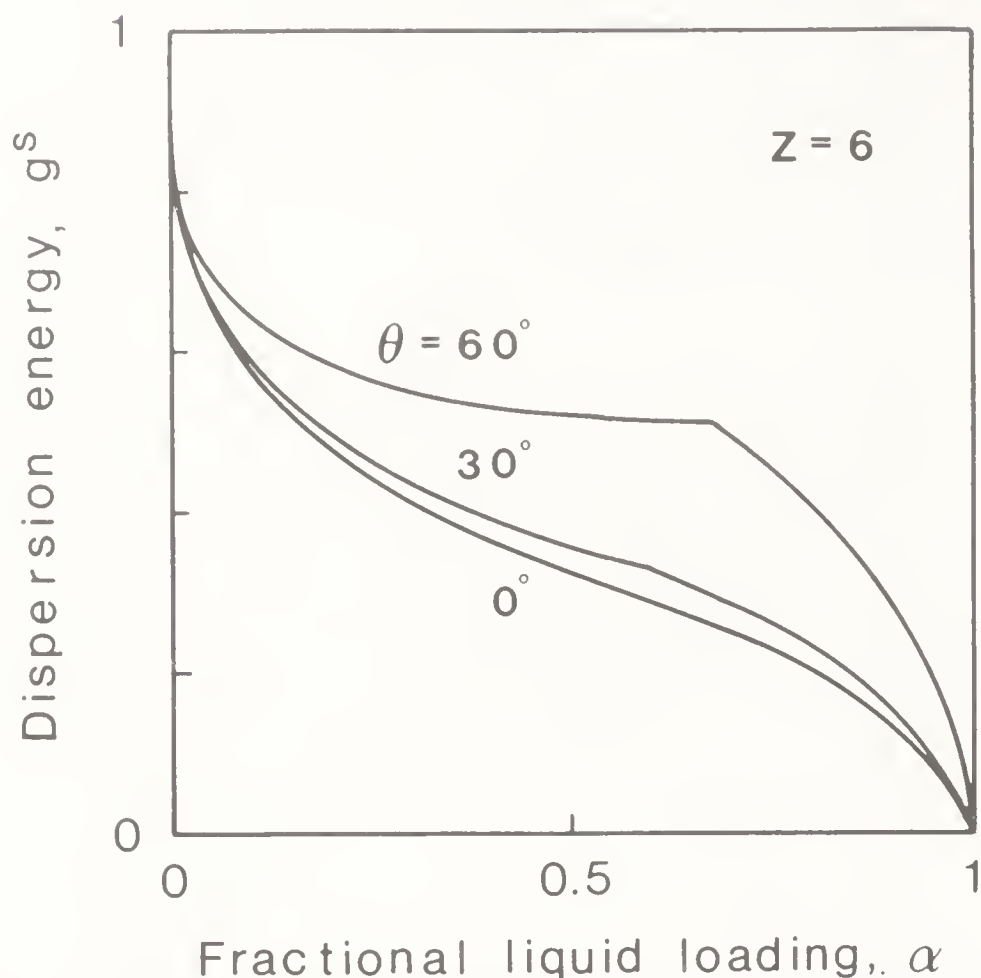


**Figure 6.** Dispersion energy relation for a uniform liquid distribution in the structure of stacked cylindrical rods (figure 2) for different  $\theta$ . The curves are for the dense arrangement with  $Z = 6$ . The breaks on the curves mark transition from A to B distribution (see figure 2).

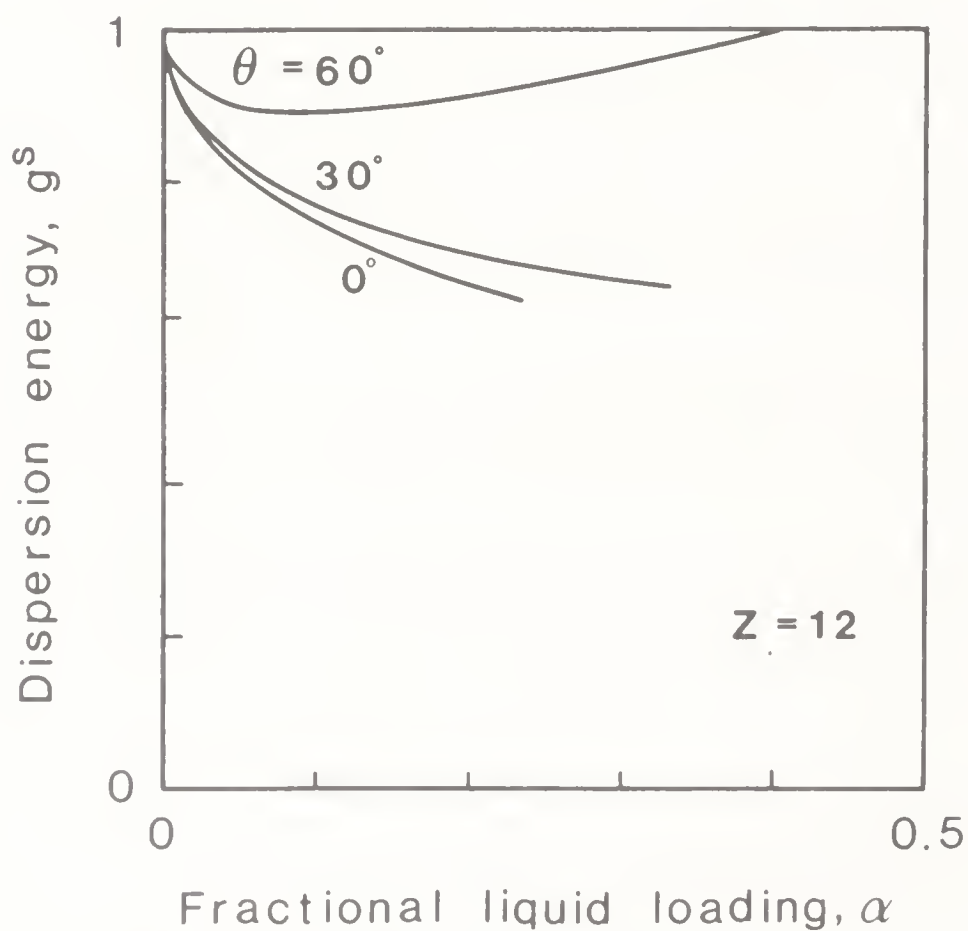


**Figure 7.** Dispersion energy relation for a uniform liquid distribution in the dense structure of stacked spheres ( $Z = 12$ ) for different  $\theta$ . The curves are constructed until the point of contact between liquid nodes.

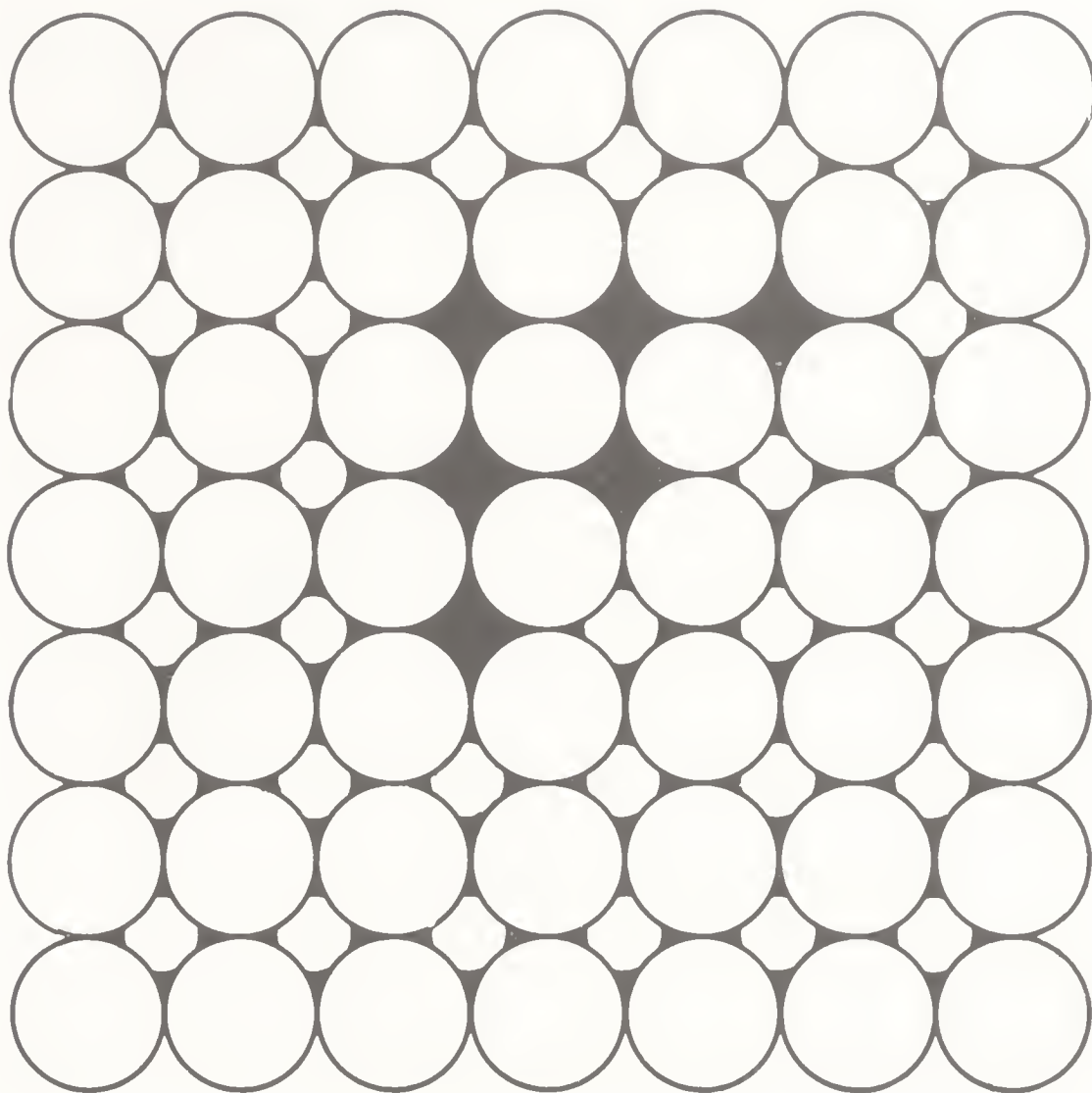


**Figure 8.** Schematic illustration of cluster formation in a pore structure of stacked spheres. The cluster is a region of the pore structure which is completely filled with liquid. It is surrounded by a uniformly distributed liquid.

Here  $G_u^s$  is the surface energy for the uniformly distributed phase that coexists with the clusters, (18), and which is characterized by liquid surface area  $a_G^u$ , surface coverage  $a_L^u$ , and liquid loading  $\alpha_u$ .  $G_1^s$  is the surface energy for the clusters, (5).  $\xi$  is the fraction of the pore volume  $V_p$  occupied by clusters:

$$V_p \alpha = V_p [(1 - \xi) \alpha_u + \xi] \quad \text{or} \\ \xi = (\alpha - \alpha_u) / (1 - \alpha_u), \quad (20)$$

where  $\alpha$  is the overall fractional liquid loading.

For constant  $G_u^s$ , (19) is a straight line on the  $\alpha, G^s$  diagram – connecting  $\alpha_u, G_u^s$  on the  $G_u^s$ -curve with  $\alpha = 1, G^s = G_1^s$ . Along this line the increase of  $\alpha$  is caused solely by expansion of the cluster region ( $\xi$ ) until finally, for  $\alpha = 1$ , the whole pore structure is flooded by liquid.

Examples of  $G^s, \alpha$ -relations for distributions with clusters are shown in figure 9 in terms of the dimensionless dispersion energy  $g^s$  in (17). Since we emphasize stability in the sense of minimal  $G^s$  it is evident from the computed  $G^s$ -relations that distributions with clusters are favoured when  $\alpha$  is high, but are less stable than uniform distributions for small  $\alpha$ . This behaviour is related to the S-shape of the  $g^s$  vs.  $\alpha$ -curve. When the  $g^s$ -curve has an inflection point one of the straight “cluster lines”, (19), is a tangent to the  $g^s$ -curve in the point for  $\alpha = \alpha_c$  (C in figure 9). If we



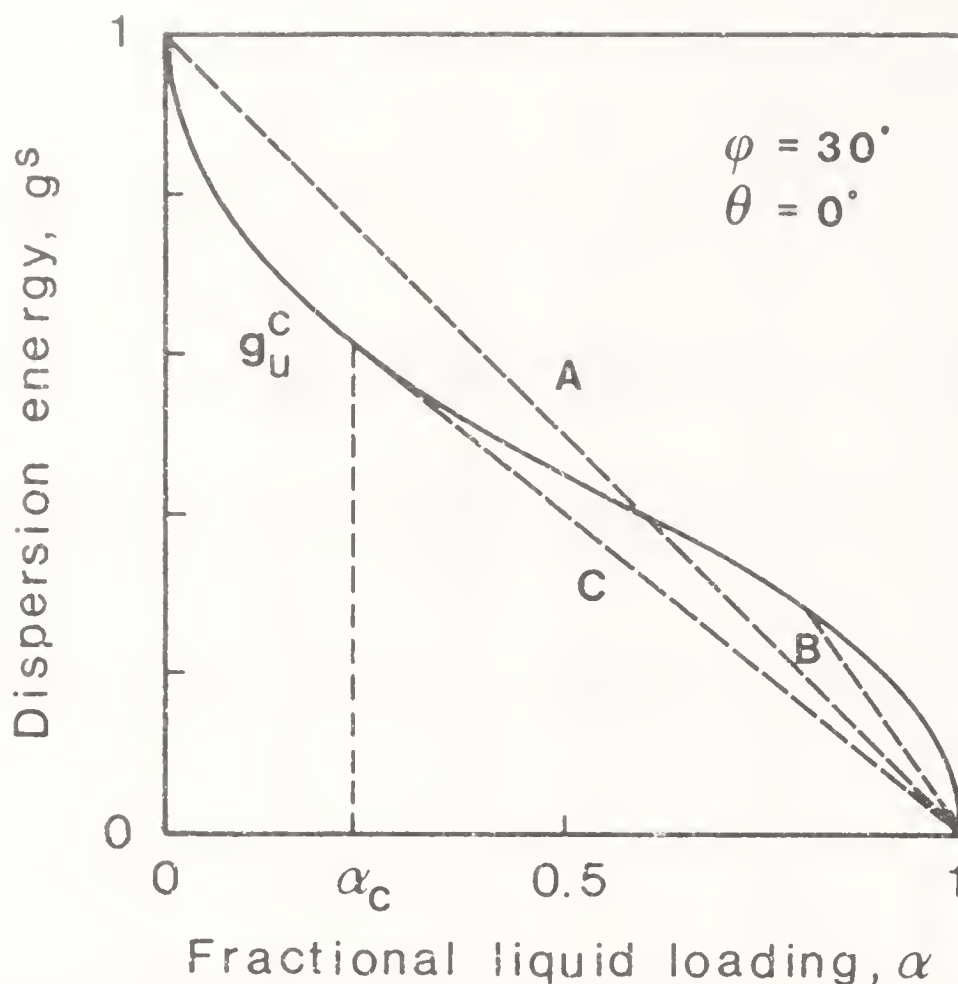


Figure 9. Dispersion energy relation for distribution of a liquid in the rhombic channels (figure 1) with  $\phi = 30^\circ$  and  $\theta = 0$ . The full curve is the energy relation for a uniform distribution. The broken lines are for cluster distribution (19); C is for the minimum dispersion energy which defines the saturation loading  $\alpha_c$ .

spline the  $g_u^s$ -curve for  $\alpha \leq \alpha_c$  with the tangent cluster line for  $\alpha > \alpha_c$  we clearly define the global minimum of  $G^s$  for the whole range:  $0 \leq \alpha \leq 1$ .

Consequently, the most stable liquid distribution is defined as follows: When  $\alpha \leq \alpha_c$  the liquid is uniformly distributed and no clusters are formed. When  $\alpha > \alpha_c$  all additional liquid forms clusters, and gradually expands the cluster region, leaving the surrounding region undisturbed in the uniformly distributed state it had for  $\alpha = \alpha_c$  – characterized by liquid interface  $a_G^u = a_G^c$  and surface coverage  $a_L^u = a_L^c$ . An appropriate name for  $\alpha_c$  is “saturation loading”. For  $\alpha > \alpha_c$  the spontaneous formation of uniformly distributed liquid from clusters is energetically impossible – at least by the action of capillary forces which in this respect are “saturated”.

In mathematical terms  $\alpha_c$  is defined as the point with identical slopes for the cluster and uniform distributions, respectively. For the cluster distribution differentiation of (19) with  $\alpha_u = \alpha_c$  yields:

$$(dG^s/d\alpha)|_{\alpha=\alpha_c} = (G_1^s - G_c^s) \frac{d\xi}{d\alpha} = (G_1^s - G_c^s)/(1 - \alpha_c),$$

or using (17):

$$-(dg_s/d\alpha)|_{\alpha=\alpha_c} = g_c^s/(1 - \alpha_c) = (1 - a_L^c + a_G^c/\cos \theta)/(1 - \alpha_c), \quad (21)$$

where  $G_c^s = G_u^s$  for  $\alpha = \alpha_c$ .

The slope of the uniform distribution curve is obtained by differentiation of (18) and substituting  $g^s$  of (17):

$$(dg_u^s/d\alpha)|_{\alpha=\alpha_c} = (da_L^u/d\alpha) - (1/\cos \theta) (da_G^u/d\alpha). \quad (22)$$

Elimination of the slopes yields the equation:

$$\{(da_L^u/d\alpha) - (1/\cos \theta) (da_G^u/d\alpha)\}_{\alpha=\alpha_c} = (1 - a_L^c + a_G^c/\cos \theta)/(1 - \alpha_c), \quad (23)$$

from which  $\alpha_c$  can be calculated.

Equation (23) is solved by iterative computation of  $a_G^u$ ,  $a_L^u$  for the individual unit cells by the methods described above. The derivatives on the LHS of (23) can be computed analytically for the "2-dimensional" unit cells and by numerical differentiation in the case of the "3-dimensional" stacked spheres unit cells.

For any point along the  $g_u^s$  vs.  $\alpha$ -curve we may define  $\Delta$  as the ratio between the "driving forces" for the formation of uniform and cluster distributions respectively.

$$\begin{aligned} \Delta &= (dg_u^s/d\alpha)/(dg_c^s/d\alpha) \\ &= \left\{ \frac{da_L^u}{d\alpha} - \frac{1}{\cos \theta} \frac{da_G^u}{d\alpha} \right\} (1 - \alpha) / \left[ 1 - a_L^u + \frac{a_G^u}{\cos \theta} \right]. \end{aligned} \quad (24)$$

For simplicity we shall in the following refer to  $\Delta$  as *the (uniform) distribution stability coefficient*.

If  $\Delta > 1$ , uniform distributions are energetically more stable than cluster distributions whereas cluster distributions are the most stable for  $\Delta < 1$ .  $\Delta = 1$  corresponds to (23) and defines the saturation loading  $\alpha_c$ .

The saturation loading depends on pore geometry in a broad sense. Once, the geometry has been fixed by, e.g., choosing one of the cells from figures 1–3,  $\alpha_c$  depends only on the contact angle  $\theta$ . Due to geometric similarity it is, of course, independent of the cell size  $a$ .

Figures 10–12 show that the saturation loading is very significantly affected by a variation of both geometry and contact angle. For a given geometry a decrease in contact angle increases the saturation loading which attains its maximum value for a contact angle of zero – an expected result since the capillary forces increase with decreasing contact angle. The saturation loading becomes zero when the contact angle becomes large – the exact limit depends on the pore geometry. In this case the clusters start to form immediately, and there is no precursor state characterized by globally stable, uniformly dispersed liquid. The energetics of this situation is clearly illustrated in figure 5 for  $\theta = 60^\circ$ .

For  $\theta = 0$  the saturation loading is  $\alpha_c = 0.139$  for the dense packing of the stacked spheres and 0.076 for the loose packing (figure 12). For the stacked cylinders the corresponding values are 0.274 for the dense and 0.200 for the loose packing (figure 11). For packings of either spheres or cylinders, the saturation loading varies inversely with the support porosity.

The properties of the rhombic channels in figure 1 are particularly interesting since they show a very pronounced influence of a geometric parameter on the

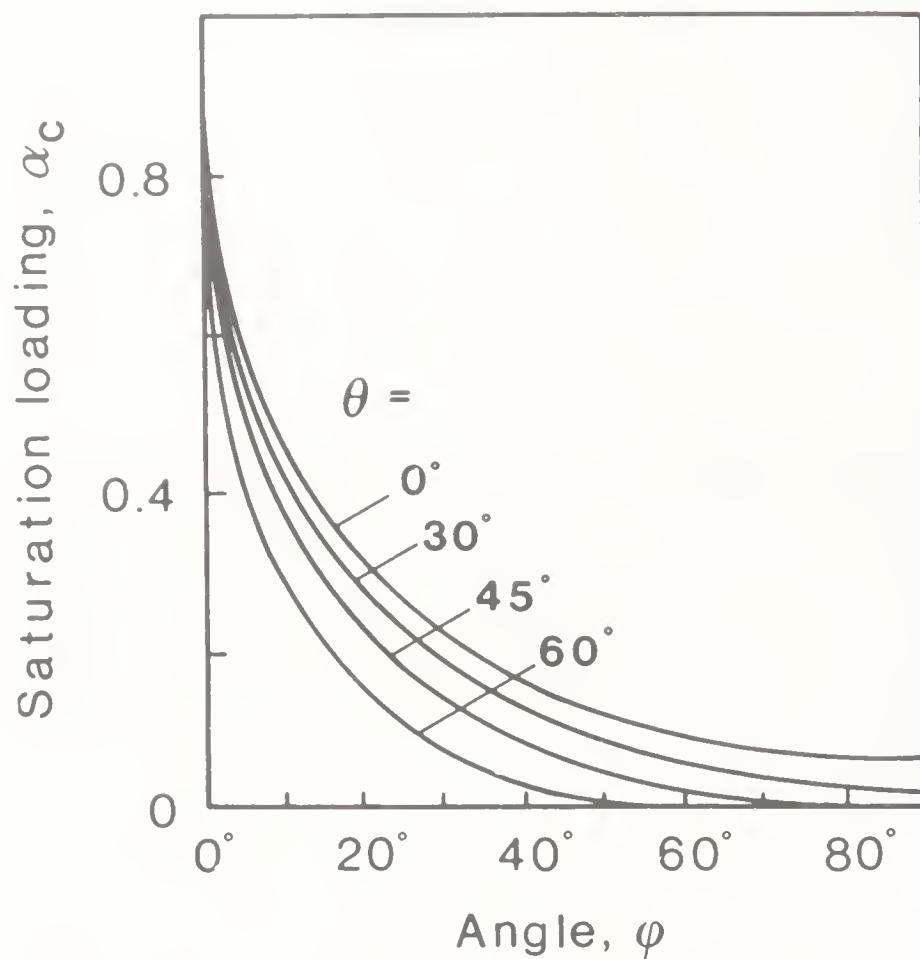


Figure 10. Saturation loading for the straight rhombic channels (figure 1) for different  $\theta$  and  $\phi$ .

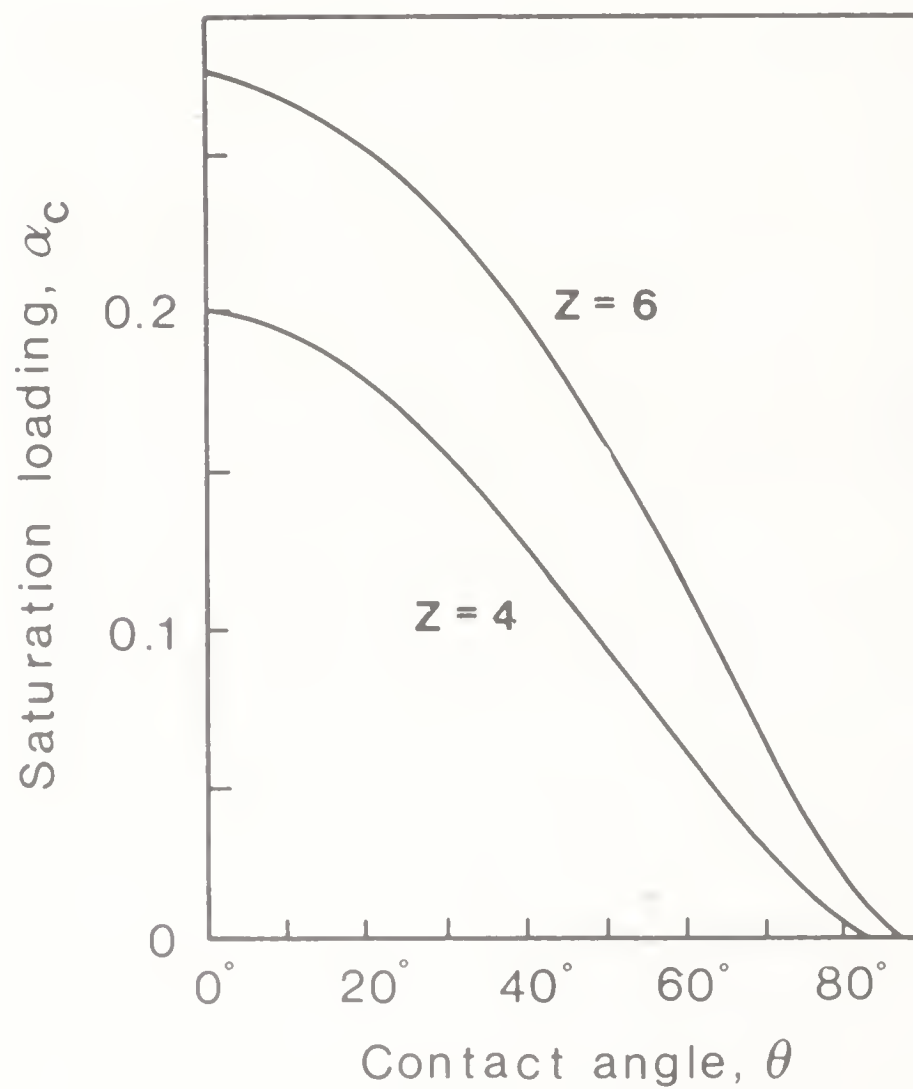


Figure 11. Saturation loading for the two structures of stacked rods (figure 2) as functions of the contact angle  $\theta$ .

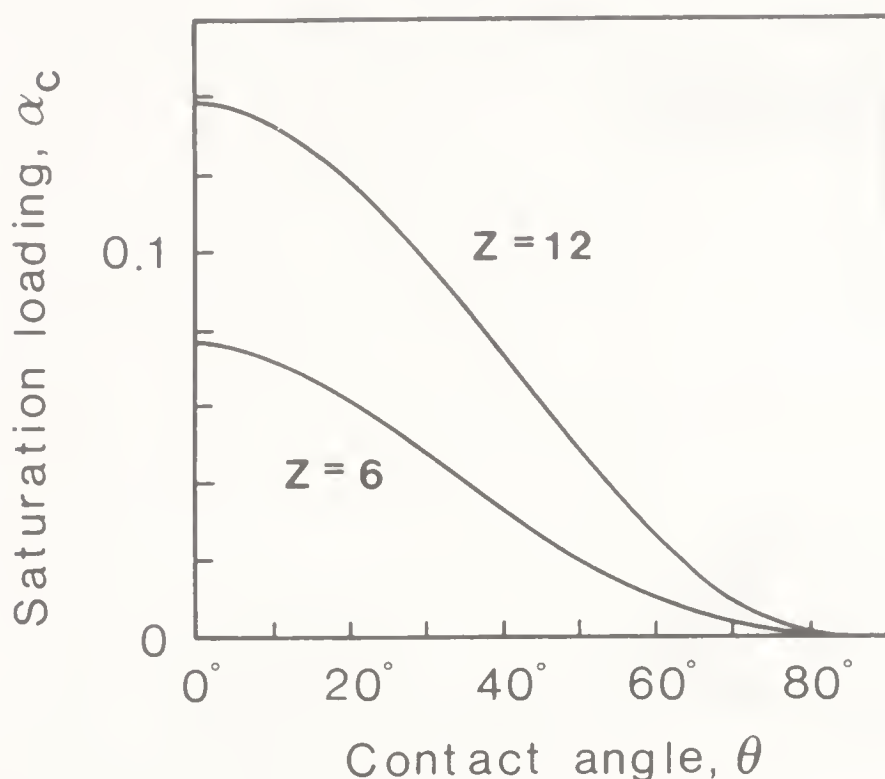


Figure 12. Saturation loading for the two structures of stacked spheres (figure 3) as functions of the contact angle  $\theta$ .

saturation loading. When the corner angle  $\varphi$  decreases, i.e. for a very elongated slit-like rhomb,  $\alpha_c$  increases, and the value 1 is approached. Undoubtedly, this behaviour is equivalent to the effect of the pore size distribution variance discussed below for general pore structures.

### 3. Liquid distribution in real pore structures

Having shown that the geometric parameters of the simple pore models significantly influence the stability of clusters, it becomes of great interest to analyse real pore structures in a way similar to that used for the model structures. This requires a geometric model of the pores which, although necessarily simplified, must be sufficiently realistic for an estimation of  $a_G$  and  $1 - a_L$  in (17). The model must be of a general nature and so flexible that it can be adjusted to reflect measurable properties of a given pore structure, such as porosity, surface area, and pore size distribution.

A pore model of long non-intersecting cylinders is widely used to characterize the size of pores in connection with standard experimental methods like the BET-method and mercury porosimetry (Gregg & Sing 1967). In this model the liquid, condensed in a pore, forms gas/liquid menisci only at the pore mouths of the external particle surface. The pores in a real porous solid, however, are highly interconnected. At the intersections the smaller pores can be accessed through pore mouths in the walls of larger pores. When there is liquid in the pore structure the gas/liquid interface tends to form in the pore mouths not only at the external but also at the internal surface. Therefore the non-intersecting cylinder model grossly underestimates  $a_G$  and must be modified in this respect to become useful.

#### *Pore model: Intersecting cylinders*

All pores are assumed to be cylindrical. The cylindrical walls of a pore consist partly of solid support surface and partly of the pore mouths of intersecting smaller



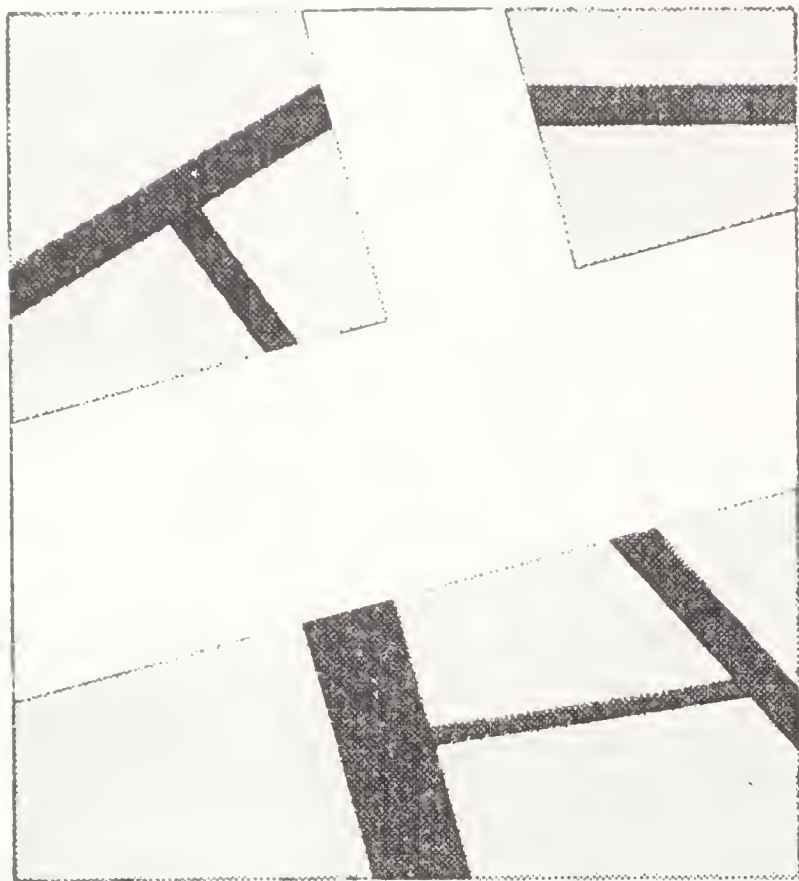


**Figure 13.** Schematic illustration of the intersecting cylinder model for a pore structure containing a uniformly dispersed liquid. White areas: gas; gray: solid; dark: liquid.

pores (figure 13). The total pore volume is  $v_p$ . The distribution of pore sizes is characterized by a distribution function

$$dV/dx = V_p f(x), \quad (25)$$

defined such that  $V_p f(x) dx$  is the volume of pores with radii in the range from  $x$  to  $x + dx$ .

Since the integral of  $v_p f(x) dx$  over all pore sizes equals  $V_p$ :

$$\int_0^\infty f(x) dx = 1. \quad (26)$$

The total surface area of the support is computed in the following way. The differential of the total surface area of the cylindrical walls for a given pore size  $x$  is:

$$dA' = (2/x) V_p f(x) dx. \quad (27)$$

$dA'$  is partly solid surface and partly pore mouth area. It is not possible to give an unambiguous definition of what is internal and what is external surface, since such a definition would require an arbitrary distinction between what is to be considered a pore rather than an external cavity in the catalyst particle. We shall find it useful to define an  $x$ -dependent "external surface" as that associated with all pores of size larger than the current pore size  $x$ . This "external surface" confines a body of solid volume  $V_s$  together with the pore volume of pores with radii less than  $x$ . We assume that the surface porosity of this "inner" body equals its volume porosity  $\epsilon_x$  (which is always less than or equal to the particle porosity  $\epsilon$ , see figure 13). Hence the solid surface area differential  $dA$  is derived from  $dA'$  by

$$dA = (1 - \epsilon_x) dA' = (V_s) / \left[ V_s + V_p \int_0^x f(y) dy \right] (2/x) V_p f(x) dx, \quad (28)$$

where the integral denotes the volume of pores with radii less than  $x$ .

By integration of (28) over all pore sizes we obtain the total solid surface area:

$$A = 2V_p \int_0^\infty (f(x) dx) / \left\{ x \left[ 1 + p \int_0^x f(y) dy \right] \right\}, \quad (29)$$

in which a porosity dependent parameter  $p$  is introduced by the definition:

$$p = V_p/V_s = \varepsilon/(1 - \varepsilon), \quad (30)$$

where  $\varepsilon$  is the overall porosity of the support.

### *Uniformly dispersed liquid*

In a homogeneous pore structure, pores of any given size are uniformly distributed throughout the pore structure. The intersecting cylinder model depicts the pores as an assembly of cylinders of finite average length, determined from the pore mouth area. When liquid is introduced in the pore structure we shall assume that any individual pore is either completely filled with liquid or with gas. If all pores of a given size range have the same liquid loading (i.e. either  $\alpha = 0$  or 1) the liquid in a homogeneous pore structure will be uniformly dispersed, i.e., no clusters are formed. The total wetted surface area is the sum of solid pore walls of all the liquid-filled pores [the integral of  $dA$  in (28) for these pores]. The gas/liquid surface area is the sum of all the liquid interfaces of the pore mouths at the boundary between gas-filled and liquid-filled pores. We shall assume that these interface areas are identical to the integral of  $\varepsilon_x dA$  of (27) for the relevant pore size ranges, thus avoiding a calculation of the exact curvature of the interface. This is a consequence of using a general model which avoids a detailed geometry at the single pore level. For reasons discussed below the approach is believed to lead to a meaningful estimation of  $g^s$  in spite of this simplification.

When the ranges of pore sizes have been specified for gas and liquid-filled pores, respectively,  $a_L$  and  $a_G$  are well defined by the pore model, and  $g^s$  of (17) can then be calculated. For a given liquid loading  $\alpha$ , the most stable uniform distribution, leading to minimal  $g^s$ , emerges as that for which all pores with radii  $x$  less than some  $r$  which depends on  $\alpha$  are filled with liquid, and all larger pores are gas-filled. In this case  $a_L$  attains a maximum value, and  $a_G$  is at a minimum value, since  $\varepsilon_x = \varepsilon$ , [(27)] is the smallest attainable pore surface porosity. This central concept is also generally accepted when studying capillary phenomena using the pore model of non-intersecting pores (Gregg and Sing 1967; Livbjerg *et al* 1974; Schubert 1982). Sometimes the liquid in an SLPC is visualized as an even layer covering the whole solid surface. For energetic reasons this distribution is very unlikely, yielding a large  $g^s$ -value due to a large  $a_G$ .

Microscopic investigations also qualitatively confirm the model of figure 13 as shown in figure 14.

For the most stable uniform distribution  $a_L$  and  $a_G$  are calculated as follows: Taking  $r$ , the radius of the largest pores filled with liquid, as the independent variable the liquid loading becomes

$$\alpha = \int_0^r f(x) dx. \quad (31)$$



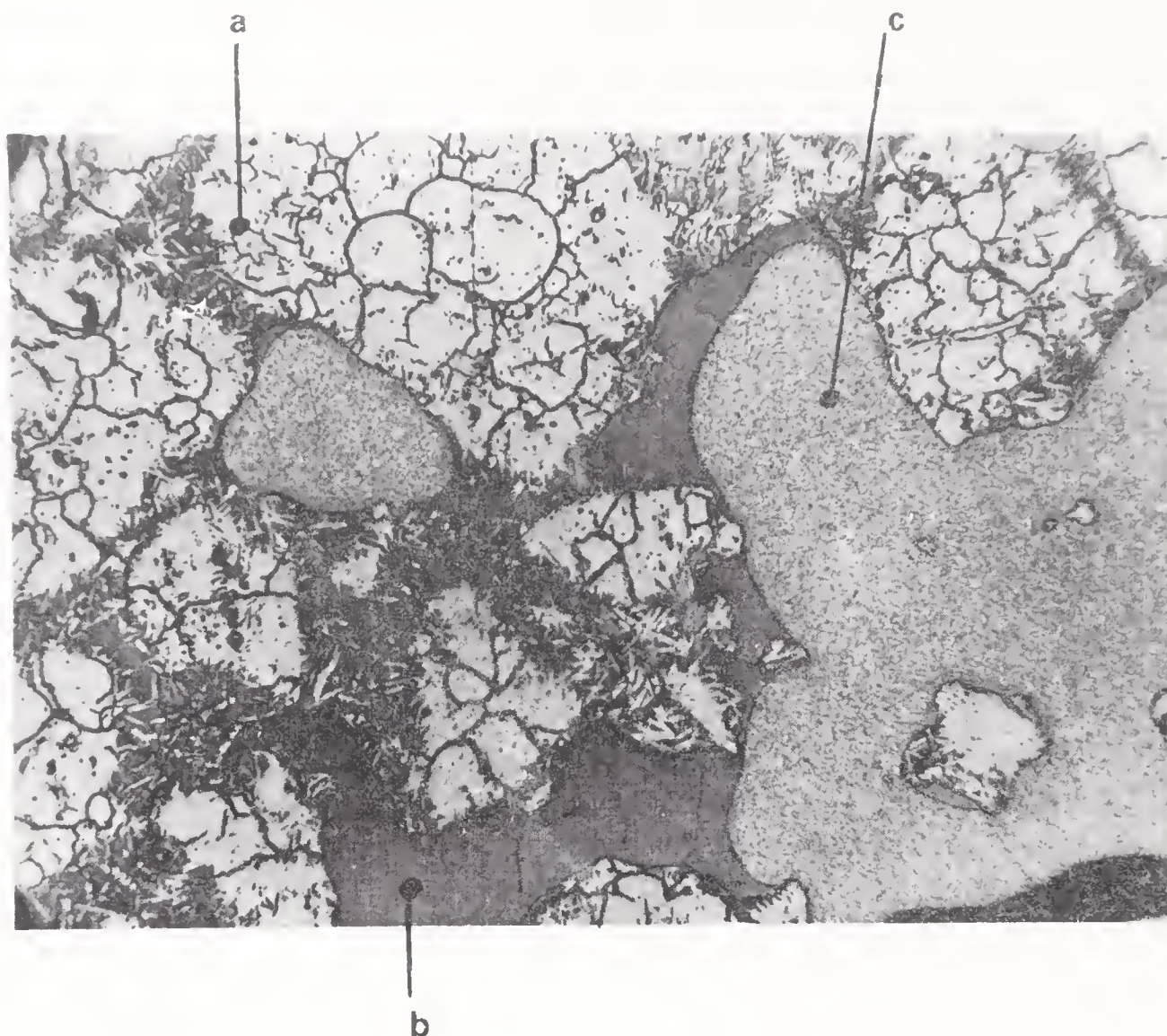


**Figure 14.** Micro-photo of a polished fracture surface of a  $V_2O_5-K_2S_2O_7/SiO_2$  sulphuric acid catalyst.

- a. The  $SiO_2$  skeleton interspersed with numerous small pores filled with the catalytically active salt melt.
- b. Salt melt, solidified to a glass when cooled from reaction temperatures of  $\sim 450^\circ C$ .
- c. Large gas-filled pore. Impregnated with plastic for preparation of the sample.

A support material with rather large pores, visible in optical microscope, has been used. The photo has been made with assistance from the Department of Mineral Industries, Technical University of Denmark.

The solid/liquid surface area associated with  $r$  is equal to the *solid* surface area of pores with radii less than  $r$ .  $a_L(r)$  is thus obtained by integration of  $d[A(x)]$  for  $0 < x < r$ , and dividing by the total solid surface area  $A$  defined in (29).

$$\begin{aligned}
 a_L(r) &= (2V_p/A) \int_0^r [(2/x) V_s f(x) dx] / \left[ V_s + \int_0^x V_p f(y) dy \right] \\
 &= \rho \int_0^r [f(x) dx] / x \left[ 1 + \rho \int_0^x f(y) dy \right], \quad (32)
 \end{aligned}$$

where the average cylinder diameter for the pore structure  $\rho$  is introduced by the usual definition:

$$\rho = 2V_p/A. \quad (33)$$

The gas/liquid interface area  $a_G$  is equal to the pore mouth area of pores with radii less than  $r$  along the surface of pores with radii greater than  $r$ . Since we assume that the surface porosity of the combined gas/solid and gas/liquid interfaces is equal to the volume porosity of the body confined by this surface we have

$$A_{LG}/[A_{LG} + A(1 - a_L)] = V_p \alpha / (V_s + V_p \alpha), \quad (34)$$

from which  $a_G$  is calculated as

$$a_G(r) = A_{LG}/A = p\alpha(1 - a_L). \quad (35)$$

In general the distribution function  $f(x)$  is not a simple function, and  $(\alpha, a_L)$  have to be computed numerically. Since  $\rho$  is not known initially we introduce the variable  $\beta$  defined as

$$\beta = a_L/\rho. \quad (36)$$

Substituting  $\beta$  into (32) and differentiating (31) and (32) with respect to  $r$  yields two ordinary differential equations which are readily solved by an o.d.e. package

$$\left. \begin{aligned} d\alpha/dr &= f(r), \\ d\beta/dr &= f(r)/r(1 + p\alpha) \end{aligned} \right\} \text{with } \alpha = \beta = 0 \quad (37)$$

$$\text{for } r = 0 \text{ (or } r = x_{\min}) \quad (38)$$

Since  $a_L = 1$  for  $\alpha = 1$ ,  $\rho$  is obtained from (36) as:

$$\rho = 1/\beta \text{ for } r \rightarrow \infty \text{ (or } r = r_{\max}). \quad (39)$$

From the  $(\alpha, \beta)$  vs.  $r$  relationship obtained by integration of (37) and (38), the dispersion energy  $g^s$  is calculated as a function of liquid loading  $\alpha$  using (17), (36) and (39).

The depth of the liquid segments is the distance which reaction components at any position have to diffuse from the gas/liquid interface into the liquid phase in order to access all catalytically active species dissolved in the liquid. For the uniform distribution this distance can be estimated by considering again the combined volume of the solid and liquid as one body confined by the pore walls of the gas-filled pores. The ratio between volume and surface for this body i.e. its "equivalent slab thickness"  $\delta_f$  is a measure of the average diffusion distance,

$$\delta_f = (V_p \alpha + V_s)/[A(1 - a_L + a_G)] = 1/2 \rho(\alpha + 1/p)/(1 - a_L + a_G). \quad (40)$$

### Formation of clusters

The stability of a uniform distribution towards formation of clusters can be estimated using (23) to compute the saturation loading or (24) to compute  $\Delta$  for a given liquid loading. The derivatives of  $a_L(r)$  and  $a_G(r)$  with respect to  $\alpha(r)$  can be derived from (35), (37) and (38):

$$da_L/d\alpha = (da_L/dr)/(d\alpha/dr) = \rho/r(1 + p\alpha), \quad (41)$$

$$da_G/d\alpha = (da_G/dr)/(d\alpha/dr) = (1 - a_L)p - [p\alpha\rho/r(1 + p\alpha)], \quad (42)$$

hence, from (24),

$$\Delta = \left[ \frac{\rho}{r(1 + p\alpha)} - \frac{p}{\cos \theta} \left\{ 1 - a_L - \frac{\alpha\rho}{r(1 + p\alpha)} \right\} \right] \frac{1 - \alpha}{1 - a_L + a_G/\cos \theta}. \quad (43)$$



### *Influence of pore structure properties*

The pore distribution of real catalyst carriers varies considerably. Structures with a large variation in pore size will often have an approximately Gaussian distribution on a logarithmic  $x$ -scale (see figure 16). However, many catalysts have two distinct peaks, corresponding to a "micro-macro" structure which results from sintering of micro-porous powder particles. Inspection of (37) and (38) shows that both  $a_L$  and  $a_G$  are invariant to the distribution mean  $\bar{x}$  i.e. the first moment of  $f(x)$  if the variance is proportional to  $\bar{x}^2$ . Thus, the relevant properties to consider are porosity, which appears separately in the equations, and the variance (and higher moments), i.e. the shape of  $f(x)$ .

Equations (37) and (38) were integrated for selected pore distribution functions  $f(x)$  of which four are shown in the appendix. These distributions were chosen to illustrate typical variations of industrial catalysts and catalyst carriers. For the triangular distribution  $g^s$  can even be calculated analytically as shown in the appendix. A comparison with the numerical results for this distribution function was used to test the numerical method. Figure 15 shows  $g^s$  vs.  $\alpha$  for log-normal distributions with different values of the variance  $\sigma^2$  (compare figure 16). The shape of the curves changes characteristically with  $\sigma$  from convex for large  $\sigma$  to concave for small  $\sigma$ , approaching an asymptote for  $\sigma \rightarrow 0$ . This change of shape is important for the stability of the liquid distribution as discussed above for figure 9. A better quantitative measure of the stability is provided by the function  $\Delta(\alpha)$  of (24) computed in figure 17. For small  $\sigma$ , i.e. a narrow pore size distribution,  $\Delta$  is less than one. This signifies poor dispersion properties with stable clusters in the whole  $\alpha$ -range, i.e., the saturation loading is zero. The  $g^s$ -curves are without the characteristic inflection point of the model pores treated above, and therefore the saturation loading changes abruptly from 0 to 1 when  $\sigma$  is increased a little beyond the value of 1/10 at which point  $\Delta$  becomes greater than one. When  $\sigma$  is further increased,  $\Delta$  increases markedly for all – and especially for small  $\alpha$ -values.

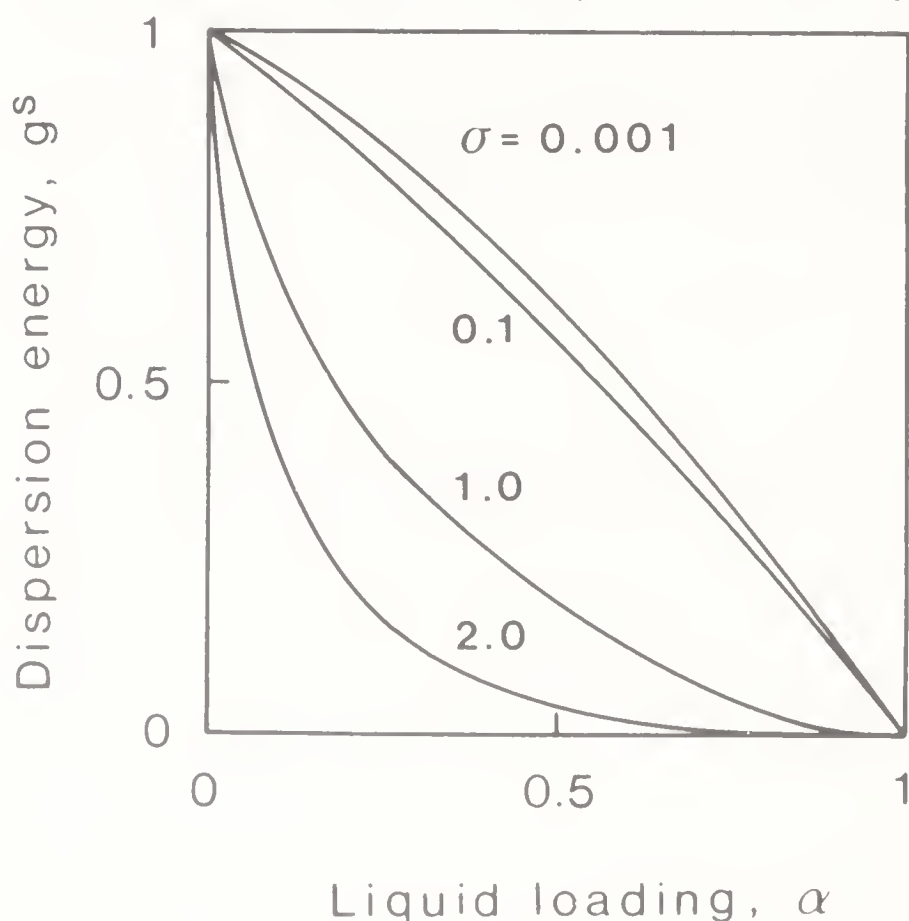


**Figure 15.** Dispersion energy relation for a log-normal pore distribution for different values of the distribution variance  $\sigma^2$ . Porosity: 0.5. Contact angle  $\theta = 0^\circ$ . Median for distribution  $\bar{x} = 1$ .

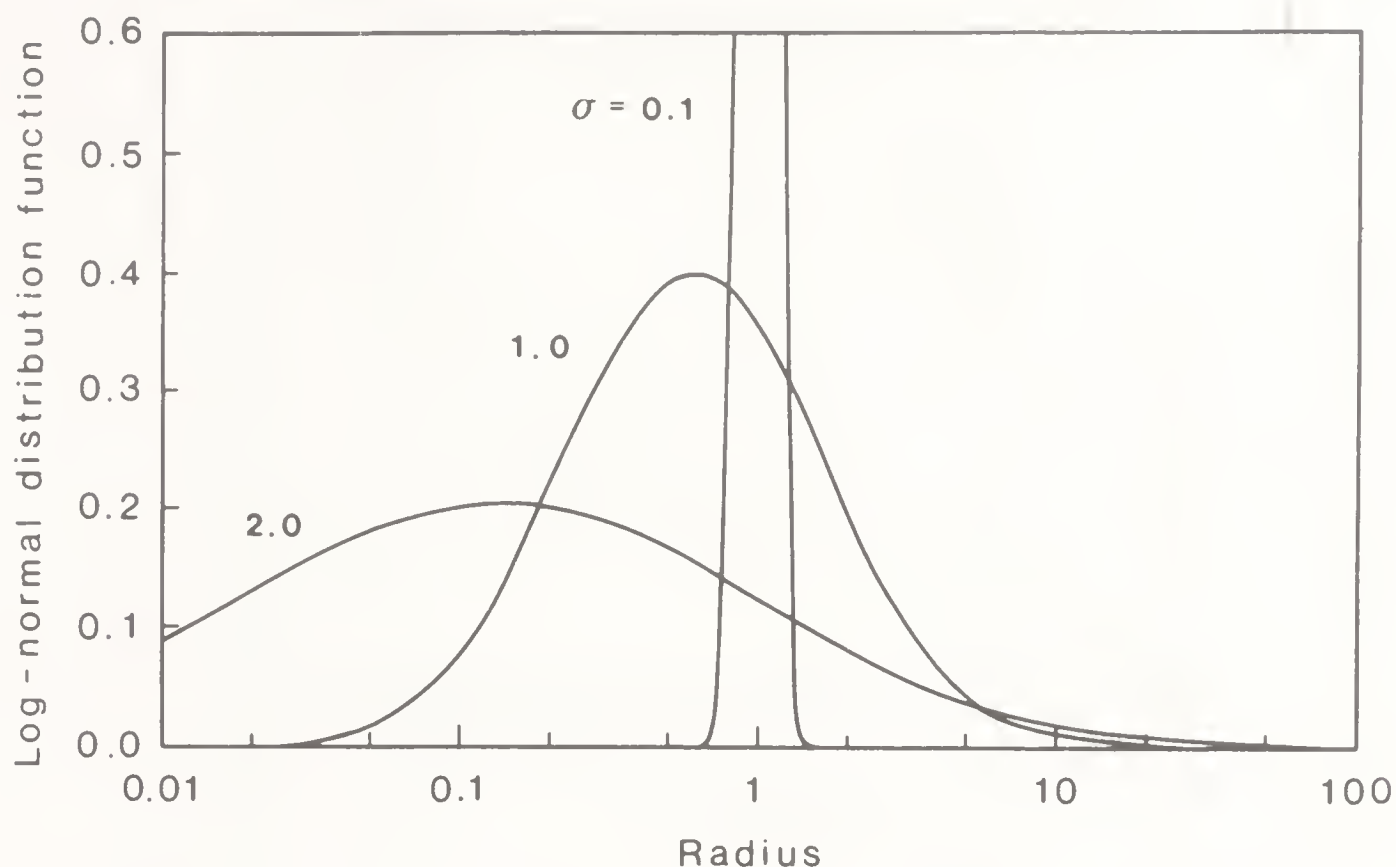


**Figure 16.** Log-normal pore distributions (appendix) for different values of the variance  $\sigma^2$ . The distributions are depicted as  $[dV/d \ln x = f(x) \cdot x]$  vs.  $(\ln x)$  which transforms the distribution into the normal error distribution curve. The curves are drawn for a constant median  $\bar{x} = 1$  for  $f(x)$  which explains the displacement of the maximum with changing  $\sigma$ . Actually this displacement is of no importance since  $g_s$  and  $\Delta$  are invariant to changes in  $\bar{x}$ .

This means that the uniform distribution becomes increasingly stable against cluster formation when the variance of the pore distribution function is increased.

This stabilizing effect of broadening the pore distribution was found for all other types of distribution functions investigated and seems to be connected mainly with the variance of the distribution. The higher moments i.e. the degree of symmetry of the pore distribution has a smaller influence. Figure 18 shows  $\Delta$  for log-triangular distributions with an extreme variation of distribution symmetry. The  $\Delta$  vs.  $\alpha$  relation is seen to be tilted somewhat in favour of small liquid loadings when the triangular distribution is reversed from a positive to a negative slope of the skew side. However, the overall level of stability is hardly affected and is again seen to depend basically on the variance expressed by the length of the base-line of the triangular distribution for  $f[\ln(x)]$ . The "variance effect" also stabilizes the uniform distribution in a bimodal pore structure. Figure 19 shows  $\Delta$  for different ratios of micro to total pore volume for a pore structure where micro and macro pores considered separately are narrowly distributed with poor dispersion stability. The composite structure with both micro and macro pores, however, provides an excellent dispersion stability in an important  $\alpha$ -range. The saturation loading for this structure proves to be the loading which fills the micro-pores since the curves cross  $\Delta = 1$  at this point.

Further analysis of bimodal structures shows that there can be more than one level of saturation loading (figure 20). Clusters may even be stable in the micro-pores without being stable in the macro-pores. The size of clusters formed in the micro-pores without traversing the macro-pores is limited by the size of the

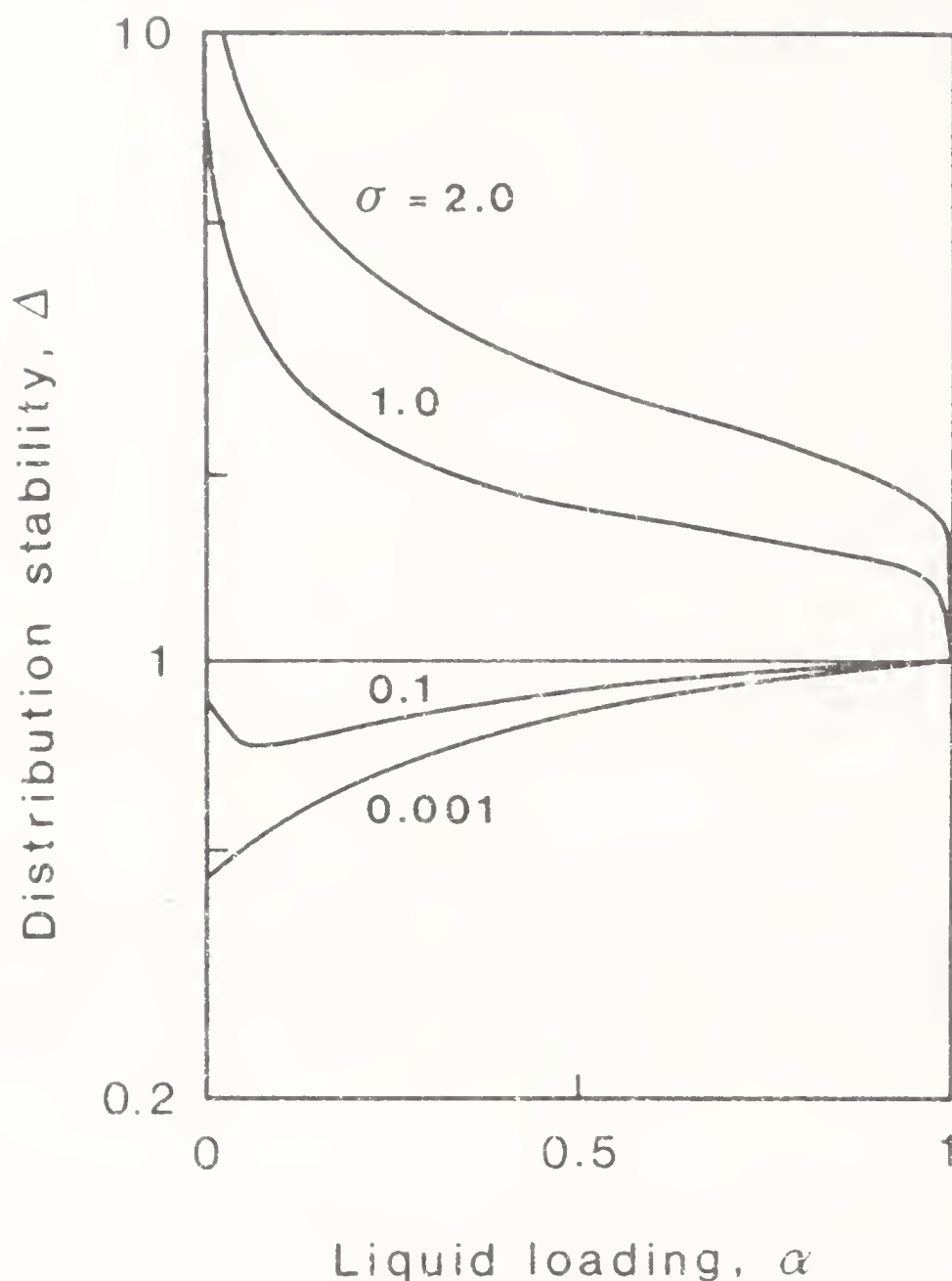


**Figure 17.** Stability of uniform distribution for log-normal pore distributions expressed as the parameter  $\Delta$ , (24), when  $\Delta < 1$  clusters are the most stable distribution. Data as for figure 15.

micro-particles, which have been sintered together to produce the bimodal structure. This holds also in the limit of completely saturated micro-pores, and it means that a bimodal pore structure can be used to control the liquid distribution, provided clusters are unstable in the macro-pores.

Figures 21 and 22 show the influence of contact angle and porosity. Predictably an increasing contact angle tends to destabilize a uniform distribution as also observed above for the unit cell models.

The porosity affects the number of pore intersections. If the porosity is increased for a given pore size distribution, the number of pore mouths, i.e. the pore wall porosity and hence the gas/liquid interface area, is likewise increased. Therefore a high porosity is not in itself desirable for the liquid dispersion since it may provoke the formation of clusters as shown in figure 22.

The effect of clusters – if they are formed – remains to be discussed. Uniformly dispersed, the liquid phase of an SLPC has very desirable properties with respect to diffusion influence. Figure 23 shows the diffusion depth  $\delta_f$  as given by (41). For values of porosity and liquid loading in the range of practical interest the diffusion



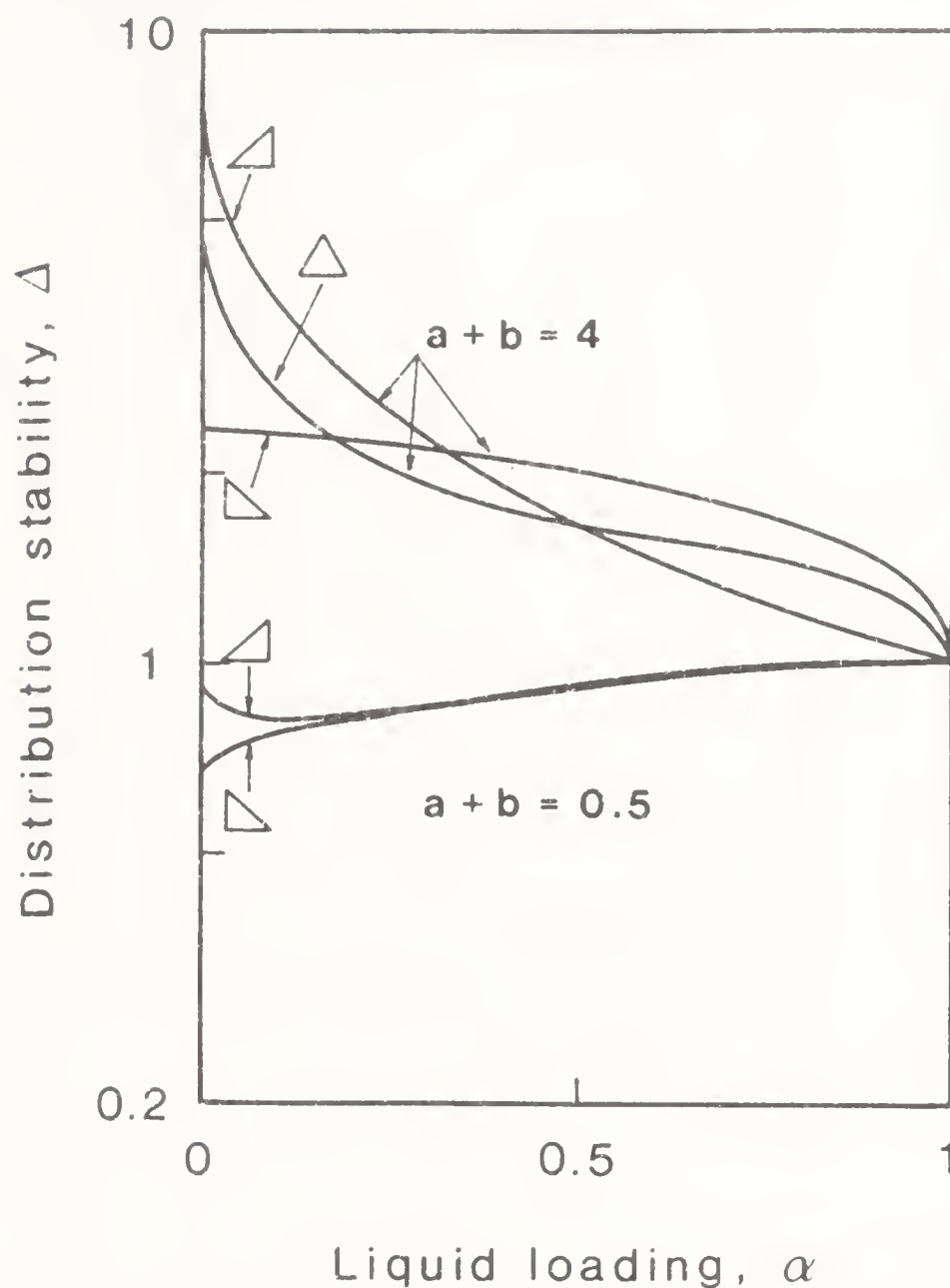


**Figure 18.** Distribution stability for log-triangular distributions (see appendix). The symbols denote the distribution symmetry i.e. symmetric ( $a = b$ ), nonsymmetric with a positive slope ( $b = 0$ ), and a negative slope ( $a = 0$ ). Porosity 0.5, contact angle  $\theta = 0^\circ$ .  $X_{\text{top}} = 1$ .

depth is of the same order of magnitude as the average pore size  $\rho$ . Thus,  $\delta_f$ -values of 100–1000 Å can be obtained straightaway in an SLPC, and this is presumably small enough to eliminate liquid diffusion influence in all but heterogeneous catalytic systems. A stable liquid phase with an equivalent degree of dispersion can hardly be obtained by any other method of practical interest.

On the other hand, the dimensions of liquid clusters are poorly defined, but observations show that they tend to approach particle dimensions. Hence they easily introduce a serious liquid diffusion barrier even if the diffusion rate is moderately high. For catalysts with a potentially slow diffusion rate, as for example some salt melt catalysts, clusters are practically inaccessible for catalytic reaction due to diffusion resistance. Therefore, clusters are generally very undesirable and the support material of an SLPC must be selected to minimize as far as possible the formation of clusters. A computation of distribution stability for the pore structures considered should prove useful for this purpose.



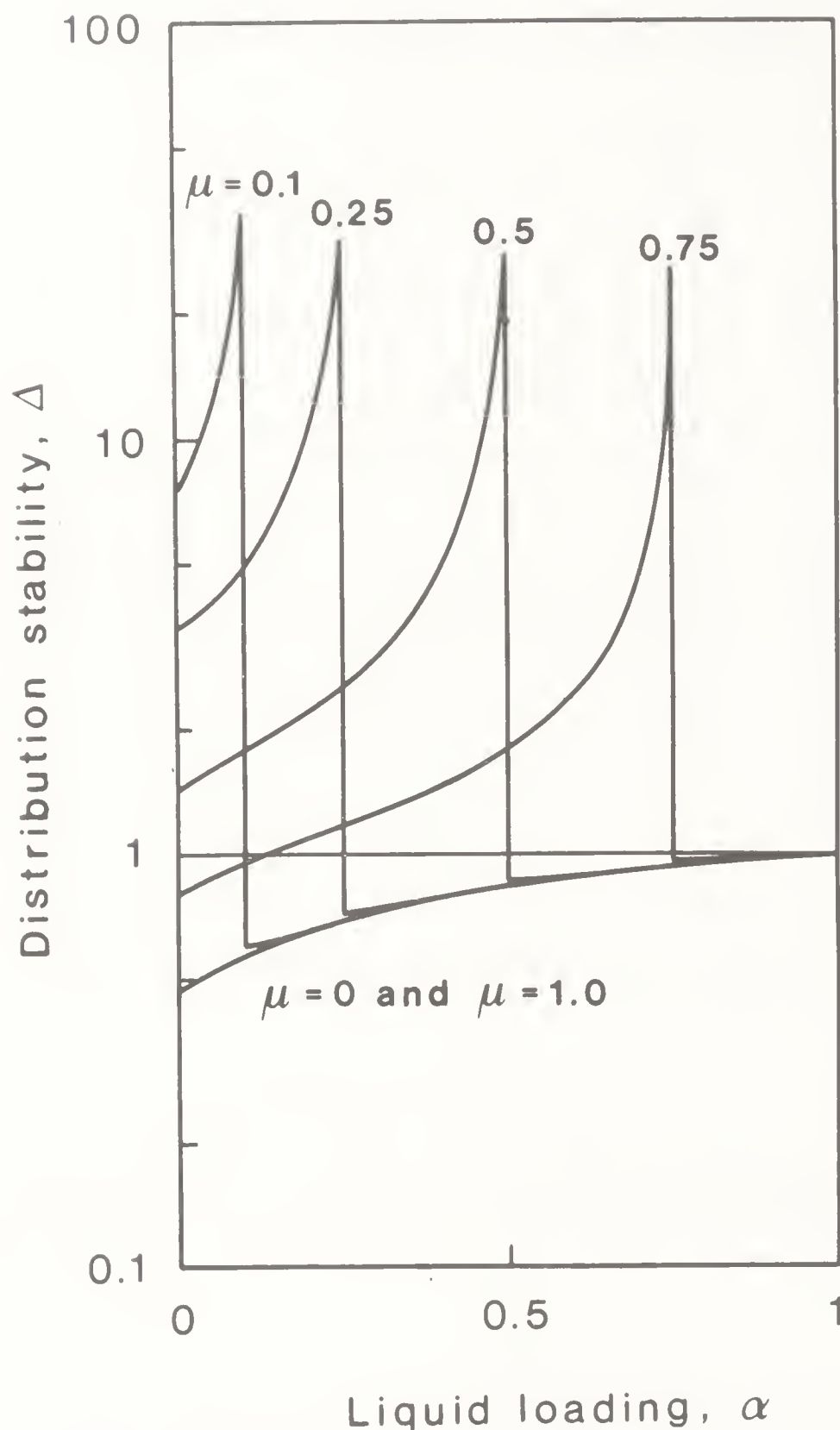


**Figure 19.** Liquid distribution stability, (24), for a log-normal, bimodal pore distribution (appendix).  $\bar{x}_1 = 1$ ,  $\bar{x}_2 = 25$ ,  $\sigma_1 = \sigma_2 = 0.01$ . Porosity  $\varepsilon = 0.5$ , contact angle  $\theta = 0^\circ$ ;  $\mu$  is the ratio of micro-pore to total pore volume.  $\mu = 0$  and 1 then denote unimodal distribution of macro- and micro-pores respectively.

### *Some model considerations*

The influence of liquid molecules held in an adsorbed state at the gas/solid surface has been neglected. This is probably justified for most SLPC because they use supports with rather large pores ( $\rho \approx 1000\text{--}5000 \text{ \AA}$ ) so that the amount of liquid adsorbed at the gas/solid surface can be considered to be negligible as compared to the total volume of liquid. The adsorbed liquid modifies the adhesion tension and also the catalytic activity especially when diffusion influence in the bulk liquid is

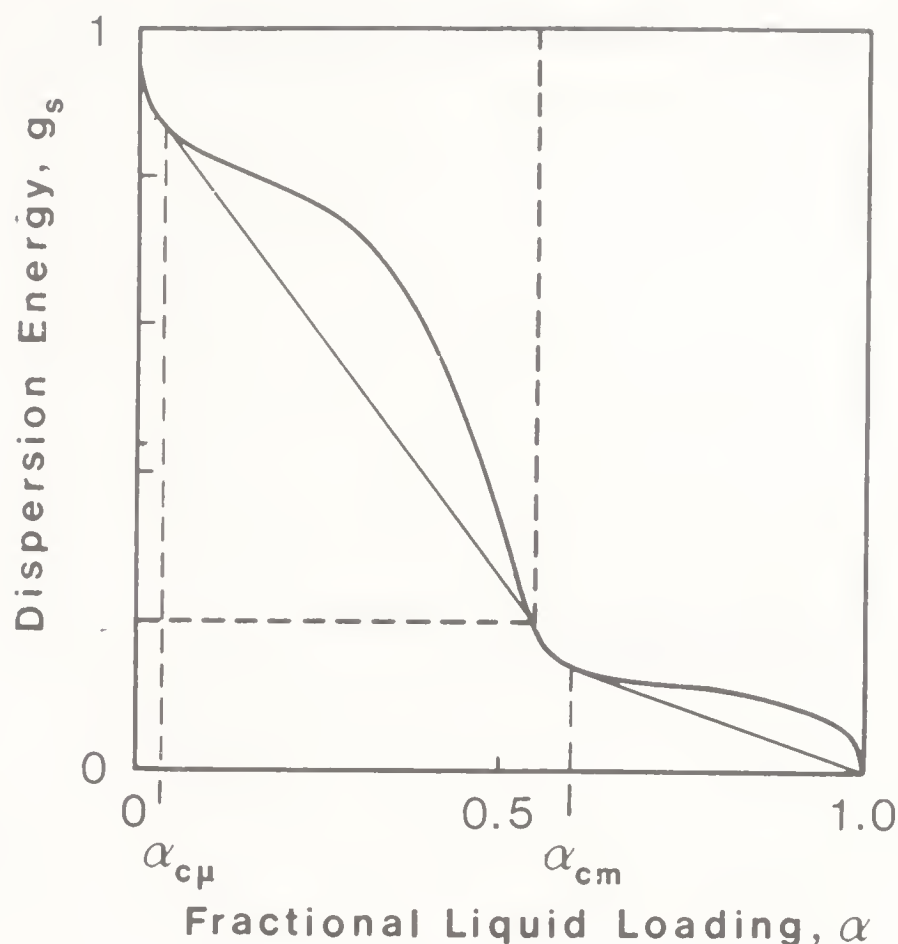


Figure 20. The dispersion energy relation for a bimodal ("micro-macro") pore structure (schematically). The part of the curve within the upper left quadrangle is the relation for the micro-porous particles considered separately.

severe. However, the criteria for cluster formation developed above remain unchanged as long as the dimension of the adsorbed layer is small compared to the pore size.

The approximation introduced by disregarding the correct curvature of the gas/liquid menisci is unavoidable since the detailed pore geometry is hardly ever known. It can be argued that the gas/liquid surface, if accurately calculated, may be somewhat larger than that computed from  $\epsilon_x$  because surface forces will increase the gas/liquid interface area at the expense of unwetted area, i.e. increasing  $a_G$  and  $a_L$  simultaneously. However, according to (17) such changes leave  $g^s$  relatively undisturbed and are therefore presumably of secondary importance. However, one may slightly overestimate the  $\alpha$ -value at which the solid is completely wetted. For large  $\alpha$  the uniform liquid distributions of the unit cell models treated above will all end up with a complete surface coverage ( $a_L = 1$ ) and a cylindrical or spherical gas bubble completely surrounded by liquid in each unit cell. The intersecting pore model, however, has unwetted solid ( $a_L < 1$ ) for all  $\alpha < 1$ . This discrepancy can be studied more closely by examining the asymptotic value of  $\Delta$  for  $\alpha \rightarrow 1$  using (24):

Intersecting pore model:	$\Delta_{\text{lim}} = 1,$
"2-dimensional" unit cells with a cylindrical bubble:	$\Delta_{\text{lim}} = 2/3,$
"3-dimensional" unit cells with a spherical bubble:	$\Delta_{\text{lim}} = 1/2.$

The difference between the intersecting pore model and the unit cell models is not alarming but confirms that the intersecting pore model underestimates the stability

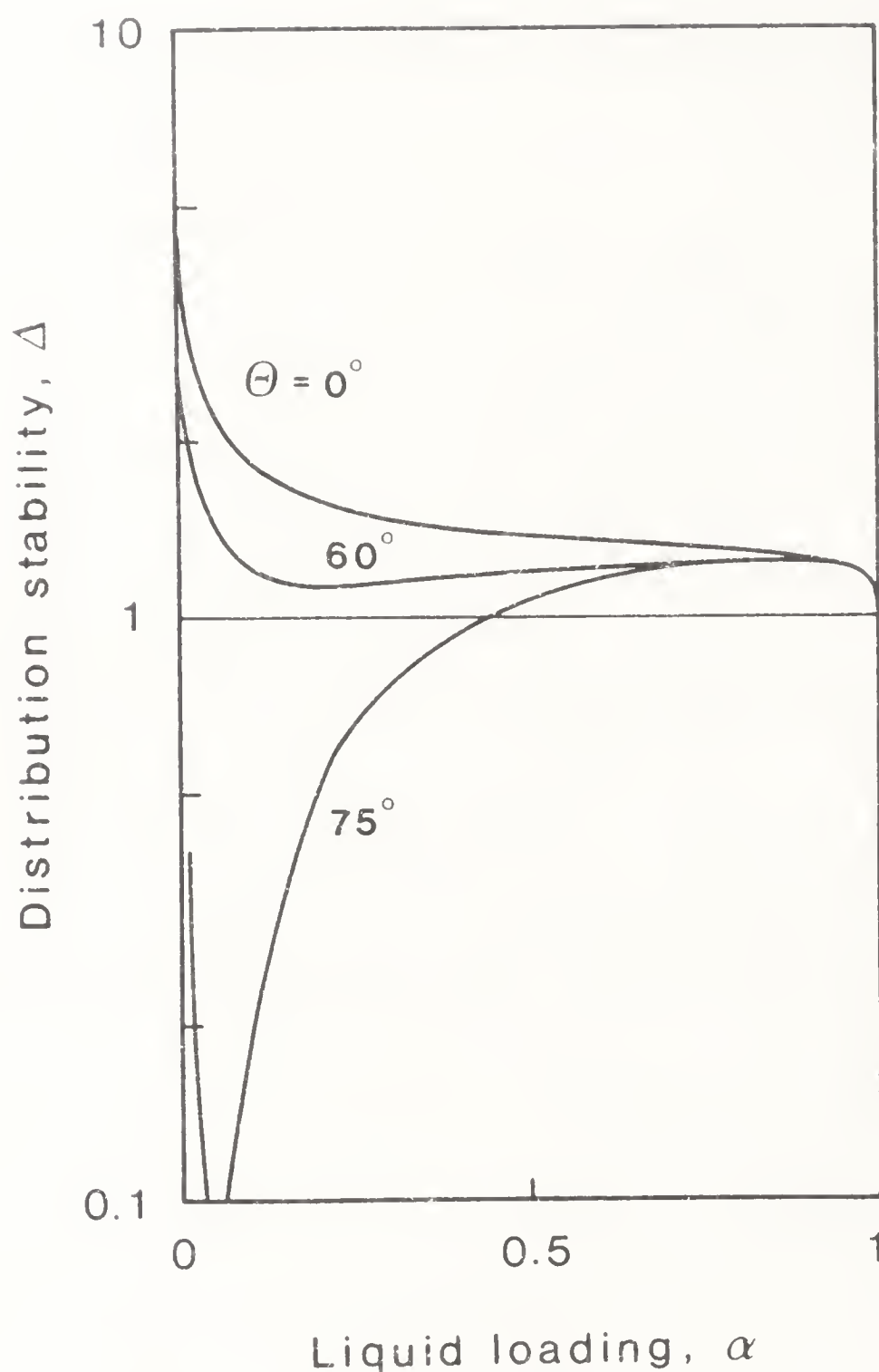


**Figure 21.** Liquid distribution stability as a function of contact angle. Log-normal pore distribution with  $\sigma = 0.6$ . Porosity,  $\varepsilon = 0.5$ .

of clusters at high liquid loading. Obviously, this error particularly obscures the saturation loading  $\alpha_c$  as a measure of the distribution stability which hence for the general pore model is better characterized using the complete  $\Delta(\alpha)$ -function rather than the single point  $\alpha_c$ .

When measuring pore distribution by mercury porosimetry for the intersecting pore model it is necessary to assume that the single pores are long enough that the correction for the curvature of the Hg-meniscus entering a pore mouth becomes unimportant. With this assumption it is easily seen that the distribution function  $f(x)$  for the intersecting and the non-intersecting pore models become identical, i.e. the distribution function used above is the usual pore distribution function. Other procedures would require a detailed knowledge of the pore geometry.

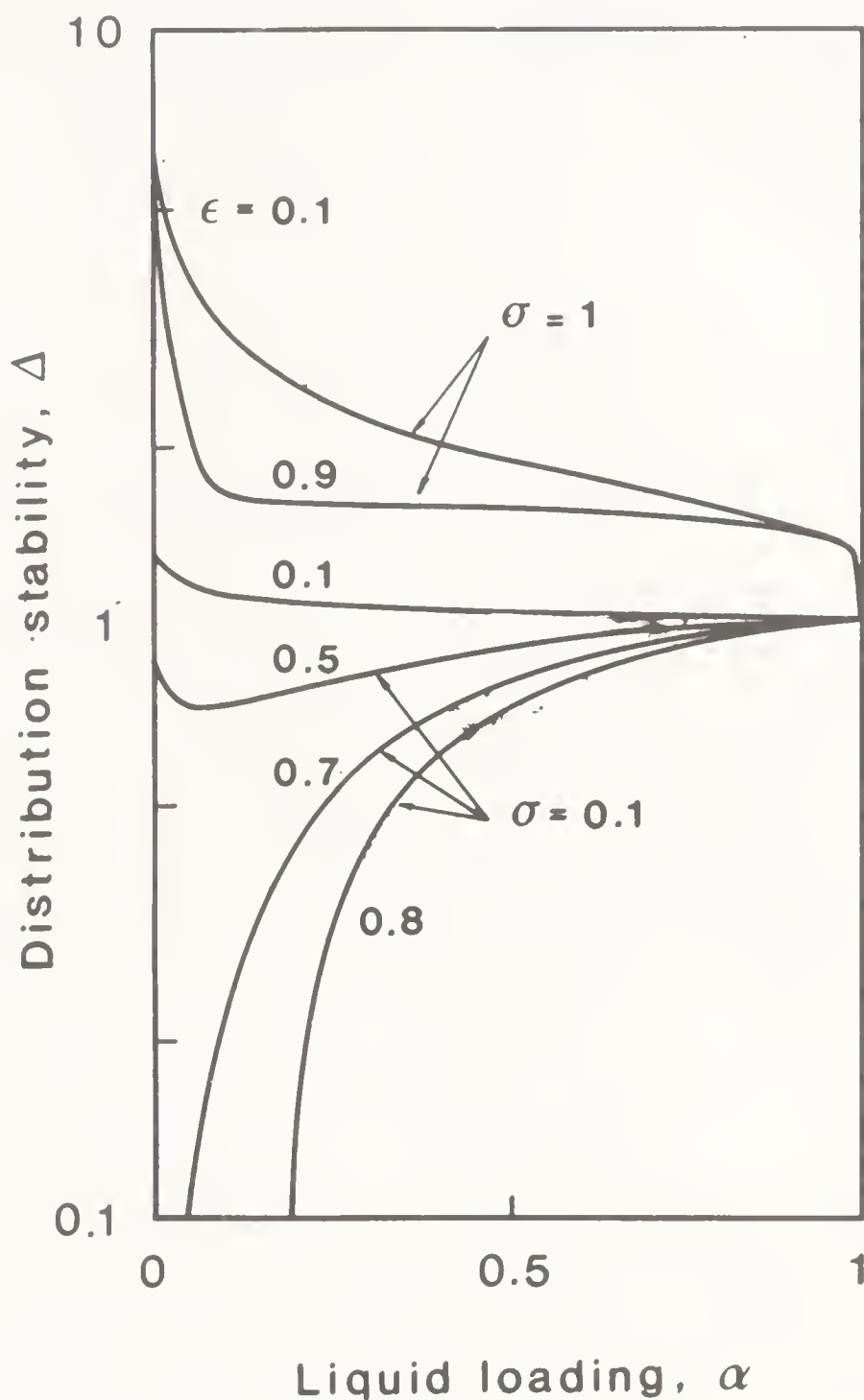


Figure 22. Influence of porosity on liquid distribution stability. The curves are shown for log-normal pore distributions with two values of the variance  $\sigma^2$ . Contact angle  $\theta = 0^\circ$ .

#### 4. Conclusion

The dispersion of the liquid phase in supported liquid phase catalysts is governed by capillary forces. A poor degree of dispersion may evoke a liquid diffusion influence deleterious to the catalytic properties. Therefore the support material must be designed to minimize such effects.

A model for the pore structure based upon intersecting cylinders is proposed for the analysis of capillary forces in real catalyst supports and is shown to agree qualitatively with exact calculations for model pore structures of simple geometry. It is shown by energetic arguments that the liquid can coalesce to flood continuous regions of the pore structure, much larger than pore dimensions. These regions are the so-called liquid clusters, which under unfavourable conditions, form the most stable liquid distribution.

The influence of liquid clusters has not previously been fully recognized, but we



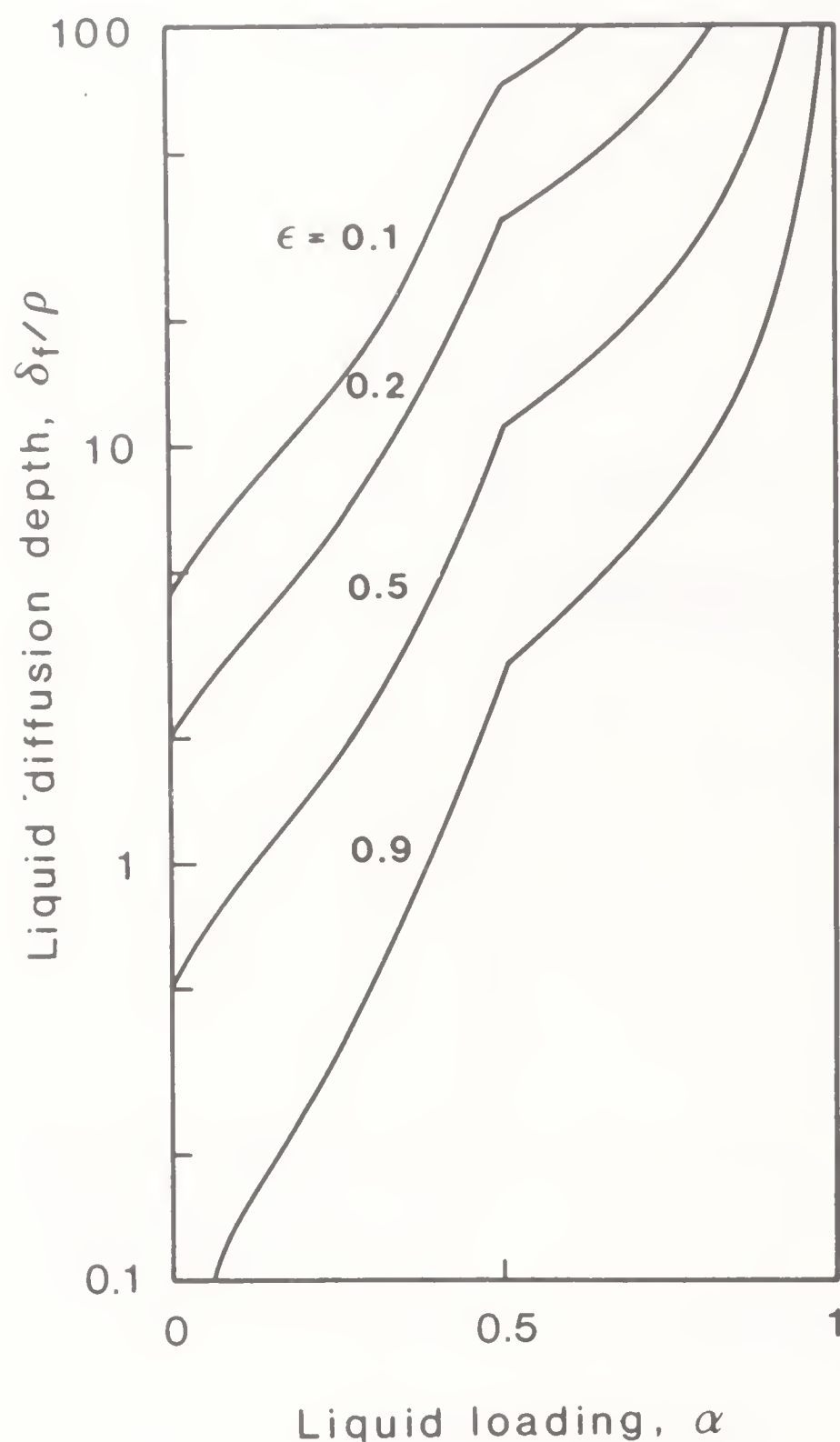


**Figure 23.** Variation of diffusion depth  $\delta_f$ , (40), with liquid loading and porosity,  $\epsilon$ . Bimodal, log-normal pore distribution with  $\mu = 0.5$ . Data as for figure 19.

now argue that in most SLPC, liquid diffusion influence is caused by an uncontrolled formation of clusters.

When designing SLPC, a number of parameters can be manipulated to reduce the likelihood of cluster formation. It is first of all important that the contact angle is small and that the support has a wide distribution of pore sizes. Our analysis of the influence of the pore distribution can be extended to any given industrial catalyst.

## Appendix

### Distribution functions

Triangular:

$$f(x) = \begin{cases} 0; & x < x_1 \\ 2/[a(a+b)] (x-x_1); & x_1 \leq x \leq c \\ 2/[b(a+b)] (x_2-x); & c \leq x \leq x_2 \\ 0; & x > x_2. \end{cases}$$

For this pore distribution function (37) and (38) can be solved analytically yielding:

$$\begin{aligned} \rho^{-1} &= \frac{1}{p(x_1^2 + \gamma_1^2)} \left\{ 2\gamma_1 \tan^{-1} \left( \frac{a}{\gamma_1} \right) - x_1 \ln \left[ \left( \frac{c}{x_1} \right)^2 \frac{\gamma_1^2}{(a^2 + \gamma_1^2)} \right] \right\} \\ &+ \frac{1}{p(x_2^2 - \gamma_2^2)} \left\{ \gamma_2 \ln \left( \frac{\gamma_2 + b}{\gamma_2 - b} \right) - x_2 \ln \left[ \left( \frac{x_2}{c} \right)^2 \frac{\gamma_2^2 - b^2}{\gamma_2^2} \right] \right\}, \\ \alpha &= \begin{cases} (r-x_1)/a(a+b); & x_1 \leq r \leq c, \\ 1/(a+b) \{ [(r-c)/b] (x_2 + b - r) \}; & c \leq r \leq x_2, \end{cases} \\ a_L &= \begin{cases} \frac{\rho}{p(x_1^2 + \gamma_1^2)} \left\{ 2\gamma_1 \tan^{-1} \left( \frac{r-x_1}{\gamma_1} \right) - x_1 \ln \left[ \left( \frac{r}{x_1} \right)^2 \frac{\gamma_1^2}{(r-x_1)^2 + \gamma_1^2} \right] \right\}; & x_1 \leq r \leq c, \\ \frac{\rho}{p(x_1^2 + \gamma_1^2)} \left\{ 2\gamma_1 \tan^{-1} \left( \frac{a}{\gamma_1} \right) - x_1 \ln \left[ \left( \frac{c}{x_1} \right)^2 \frac{\gamma_1^2}{a^2 + \gamma_1^2} \right] \right. \\ \quad + \frac{\rho}{p(x_2^2 - \gamma_2^2)} \left\{ \gamma_2 \ln \left[ \frac{(x_2 - r - \gamma_2)(b + \gamma_2)}{(x_2 - r + \gamma_2)(b - \gamma_2)} \right] \right. \\ \quad \left. \left. - x_2 \ln \left[ \left( \frac{r}{c} \right)^2 \frac{b^2 - \gamma_2^2}{(x_2 - r)^2 - \gamma_2^2} \right] \right\} \right\}; & c \leq r \leq x_2, \end{cases} \end{aligned}$$

where

$$\gamma_1^2 = a(a+b)/p; \quad \gamma_2^2 = b(a+b) (1 + 1/p).$$

### Logarithmic distributions

Real pore structures with a large variation of pore sizes are often better characterized by depicting their pore distribution on a logarithmic scale using a

logarithmic distribution function defined by:

$$dV/dy = f'(y); y = \ln x$$

so that  $f(x)$  of (25) becomes

$$f(x) = f'(\ln x)/x.$$

*Logarithmic-triangular distribution*

$$f(x) = \begin{cases} 0; & \ln x < \ln x_1, \\ \frac{2}{a(a+b)} \frac{(\ln x_2 - \ln x_1)}{x} & ; \ln x_1 \leq \ln x \leq \ln c, \\ \frac{2}{b(a+b)} \frac{(\ln x_2 - \ln x)}{x} & ; \ln c \leq \ln x \leq \ln x_2, \\ 0; & \ln x > \ln x_2, \end{cases}$$

where  $x_1$  and  $x_2$  are minimum and maximum radii, respectively, and

$$a = \ln(c/x_1); b = \ln(x_2/c).$$

*Log-normal distribution (figure 16)*

$$f(x) = \frac{1}{(2\pi)^{1/2} \sigma x} \cdot \exp \left\{ \frac{-[\ln(x/\bar{x}) + \sigma^2/2]^2}{2\sigma^2} \right\},$$

where  $\bar{x}$  is the median of  $f(x)$ , and  $\sigma^2$  is the variance of the distribution  $f'(y)$ .

*Bimodal log-normal distribution*

The pore structure contains both a micro and a macro-pore system each of which is log-normal distributed. The overall distribution function is obtained as the weighted sum of the two separate distribution functions:

$$f(x) = \frac{c \cdot \mu}{(2\pi)^{1/2} \sigma_1 x} \exp \left\{ \frac{-[\ln(x/\bar{x}_1) + \sigma_1^2/2]^2}{2\sigma_1^2} \right\} \\ + \frac{c(1-\mu)}{(2\pi)^{1/2} \sigma_2 x} \exp \left\{ \frac{-[\ln(x/\bar{x}_2) + \sigma_2^2/2]^2}{2\sigma_2^2} \right\}$$

where  $\bar{x}_1$ ,  $\bar{x}_2$ ,  $\sigma_1^2$  and  $\sigma_2^2$  are the median and variance for micro and macropores, respectively.  $\mu$  is the ratio of micro-pore volume to total pore volume. The normalization parameter  $c$  is computed to obtain:

$$\int_0^\infty f(x) dx = 1.$$

This paper is dedicated to Dr L K Doraiswamy on his sixtieth birthday.

### List of symbols

$a$	Unit cell size (figures 1–3) ( $m$ );
$a_G$	dimensionless gas/liquid interface, $a_G = A_{LG}/A$ ;
$a_L$	fraction of support surface covered by liquid (dimensionless);
$A$	support surface area ( $m^2/kg$ );
$A'$	total pore wall surface area including pore mouth areas ( $m^2/kg$ );
$A_{LG}$	gas-liquid interface area per kilogram support ( $m^2/kg$ );
$f(x)$	pore volume distribution function ( $m$ );
$g^s$	“dispersion energy” = dimensionless surface energy, (17), (dimensionless);
$G^s$	surface Gibbs free energy per kilogram support ( $J/kg$ );
$G_0^s, G_1^s$	value of $G^s$ for $\alpha = 0$ and $\alpha = 1$ , respectively;
$p$	defined by (30) (dimensionless);
$\Delta p$	capillary pressure ( $Pa$ );
$r$	radius of largest pores filled with liquid ( $m$ );
$r_1, r_2$	main radii of curvature ( $m$ );
$V_p$	support pore volume ( $m^3/kg$ );
$V_s$	skeletal volume of solid support ( $m^3/kg$ );
$x$	pore radius;
$\bar{x}$	distribution mean pore radius for given $f(x)$ ( $m$ );
$Z$	number of nearest neighbours for the stacked cylinders and spheres of figures 2 and 3 (dimensionless);
$\alpha$	fraction of support pore volume occupied by liquid (dimensionless);
$\beta$	angle (figure 4) (dimensionless);
$\beta$	variable defined by (36) ( $m^{-1}$ );
$\gamma_{SL}, \gamma_{SG}$	
$\gamma_{LG}$	interface tension ( $J/m^2$ );
$\gamma_a$	adhesion tension, (2), ( $J/m^2$ );
$\delta_l$	average diffusion length in the liquid ( $m$ );
$\Delta$	stability parameter for uniform distribution defined by (24), (dimensionless);
$\epsilon$	support porosity (dimensionless);
$\epsilon x$	porosity of body formed by solid and pores less than $x$ (dimensionless);



$\theta$	contact angle (dimensionless);
$\mu$	ratio of micro- to total pore volume (figure 19);
$\xi$	volume fraction of SLPC, occupied by clusters (20) (dimensionless);
$\rho$	average pore diameter defined by (33) ( $m$ );
$\sigma^2$	variance of distribution functions defined in the appendix ( $m^2$ );
$\varphi$	corner angle of channel cross-section (figure 1A) (dimensionless);

### Sub- and superscripts

$c$	saturation conditions where clusters start to form;
$s$	surface;
$u$	uniform liquid distribution,

### References

- Adamson A N 1976 *Physical chemistry of surfaces* 3rd edn (New York: Wiley Interscience)
- Christensen T S 1985 M.Sc. thesis, Institutet for Kemiteknik, Lyngby, Denmark
- Gregg S J, Sing K S W 1967 *Adsorption, surface area and porosity* (London: Academic Press)
- Hansen T T 1983 M.Sc. thesis, Institutet for Kemiteknik, Lyngby, Denmark
- Kenney C N 1978 *ACS Symp. Ser. 12*: 37
- Livbjerg H, Jensen K F, Villadsen J 1976 *J. Catal.* 45: 216–230
- Livbjerg H, Sørensen B, Villadsen J 1974 *3rd Int. Symp. Chem. React. Eng. Evanston, Adv. Chem. Ser.* 133: 242
- Schubert H 1982 *Kapillaritat in porösen feststoff-systemen* (Berlin: Springer-Verlag)
- Villadsen J, Livbjerg H 1978 *Catal. Rev. Sci. Eng.* 17: 203
- Villadsen J, Livbjerg H, Møller C E 1980 *US* 4, 224, 190
- Villadsen J, Michelsen M L 1978 *Solution of differential equation models by polynomial approximation* (Englewood Cliffs: Prentice Hall)

# Periodic operation of chemical reactors – a review of the experimental literature

PETER LEWIS SILVESTON

Department of Chemical Engineering, University of Waterloo,  
Waterloo, Ontario, Canada

**Abstract.** The decade 1970–80 has seen researchers focus on the dynamic behaviour of chemical reactors. This has led to active programmes in many countries exploring the use of periodic operation to improve reactor performance. Most of these explorations have centred on the use of periodic changes in reactant composition. In the time domain, these appear usually as concentration square waves; they lead to a time varying product composition, which averaged over a long enough period provides a constant mean. Periodic operation introduces new variables which can be utilized for reactor design or control. Among the variables that have been explored so far, frequency of the periodic changes and symmetry of the successive square waves have proved to be the most important. Research results demonstrate that periodic operation can offer higher activity per unit of catalyst load. There is no general physical explanation for the success of periodic operation, however.

**Keywords.** Periodic operation; catalyst activity; transient behaviour of reactors; catalytic reactors; cycling; chemical reactor dynamics.

## 1. Introduction

Reaction engineering textbooks and the instructional curricula that they are used in assume without discussion that chemical reactors should be operated at steady state. Is this mode of operation always the best choice? This question has engaged the attention of researchers world-wide for over fifteen years. Certainly, catalytic reactions under changing feed compositions or changing temperature exhibit excursions in product formation rates which exceed rates at steady state. However, if production targets are to be met, not all types of transient behaviour are permissible. Thus, researchers have focused their attention on periodic operations. In this mode, the reactor can always be kept in a transient state, while periodicity leads to a steady output if a long enough time for averaging the product transients is chosen.

Periodic operation is fairly widespread in the chemical industry. Catalysts lose activity with time due to poisoning or saturation with unwanted reaction products and it has become common practice to regenerate activity by an appropriate treatment of the catalyst. This is essentially a periodic operation. Even periodic catalyst replacement is an example of this mode of operation. In both these cases, the period is very long and the catalyst system can be assumed to be at steady state at any point in time. There are a few cases for which the period is short and approaches the time frames in which chemical reactions and transport processes occur. One such example is in catalytic cracking. However, when fluidized beds are used in this process, a mean, time invariant condition is maintained in the bed and possible advantages of periodic operation are not exploited.

There are other examples. Pulsating flows are used to increase mass transfer rates in extraction columns. Periodic operation using the same means has also been proposed to improve separation in distillation columns. As a consequence, periodic operation should not be viewed as a "new" mode of operation. Nevertheless, the application of periodic operation discussed in this review differs quite fundamentally from the catalysis examples mentioned above. Here this mode is being studied as a means of increasing catalyst activity, whereas in the examples mentioned it served to restore activity lost through use.

Application of periodic operation to heterogeneous catalytic reactors has been reviewed three times even though research activity has been underway for only about 15 years. Most of the early work employed control theory and used various forms of the strong and weak maximum principle to demonstrate better performance with periodic operation. This work was reviewed by Bailey in 1973 and again in an expanded version in 1977 (Bailey 1973, 1977). A review emphasizing Russian research was provided by Boreskov & Matros (1983). This review dealt with both experimental and theoretical studies, but concentrated on the latter. The Matros' reviews contain interesting studies making imaginative use of the thermal and ignition behaviour of heterogeneous reactions.

In this review, we will restrict consideration to concentration forcing which is perhaps the class of periodic operation that is the simplest to realize. Only the application to improved catalyst activity will be examined.

## 2. Periodic concentration forcing

Figure 1 illustrates this operation by comparing it with the steady state mode. The Fischer-Tropsch synthesis serves as an example. In the steady state mode, shown on the LHS of the figure, composition of the synthesis gas is maintained constant with time, whereas in the forcing mode it is periodically altered around a time averaged mean. The forcing mode appears on the RHS of the diagram. A consequence of the composition forcing is a time-varying product concentration, yield, or rate of formation. The latter is actually shown on the upper RHS of the figure. Because of the periodic character, the variation must occur around a mean. In our further discussion, this mean will be referred to as a time averaged rate, composition, or yield.

Variables introduced by periodic operation are cycle period or frequency, symmetry of the successive disturbances or waves and amplitude. All of these are



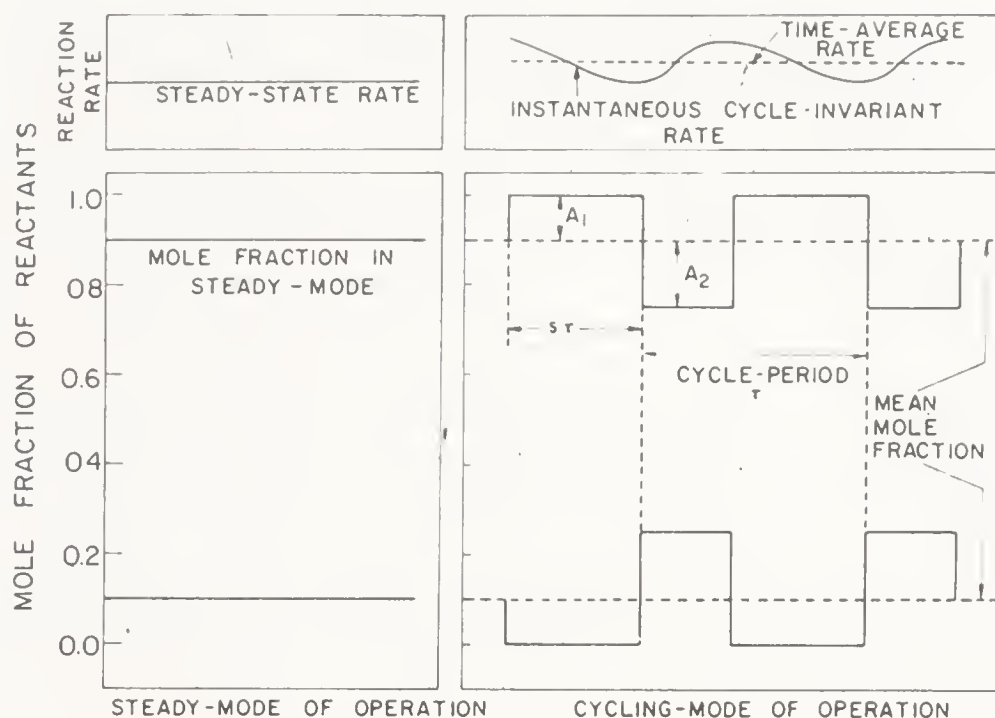


**Figure 1.** Schematic comparison of steady state and periodic operation (Silveston *et al* 1986).

defined in the figure:  $\tau$  is the period,  $s$  will be referred to as the cycle split in what follows and, if square waves are used, it alone measures symmetry.  $A$  measures amplitude, however, if  $s = 0.5$ , two amplitudes must be specified to fully describe periodic operation. Of course, if a certain time average reactant composition is to be maintained, as indicated in the figure,  $s$ ,  $A_1$ , and  $A_2$  are not independent. The time average composition is also a variable, but, of course, it is a variable in the steady state mode as well.

The influences of all the variables, shown in figure 1, on performance have been investigated. There are further variables, not shown, which have received just scant attention. These are wave shape and phase lag. Square waves are shown in the figure, but sinusoids or ramp functions could be used. Experimentally, square waves are the easiest to achieve. Furthermore, if the relaxation time of the chemical system is rapid, a square wave provides the maximum disturbance and may be necessary to shift the reaction system from steady state.

The phase lag in figure 1 is  $180^\circ$ , that is, a change in one reactant concentration occurs simultaneously as a change in the other reactant concentration, but in the opposite direction. Although all investigators have used this lag so as to preserve a constant flow rate through the reactor, other lags could be used. A phase lag of  $0^\circ$  would mean that both reactant concentrations would change simultaneously in the same direction. This could be accomplished while still preserving a constant flow rate by employing a diluent whose flow could be also adjusted periodically. The experimental complications introduced are not serious.

Only simple cycles involving two reactant compositions are shown in figure 1. Other operations are conceivable. For example, the compositions shown could be separated by additional composition states. A rather obvious choice would be to separate them by pure diluent. This might be attractive to eliminate mixing or to strip undissociated reactant from a catalyst surface. Two or more frequencies would be needed to describe this type of operation. Further reactor inputs could be periodically manipulated, such as flow rate or feed temperature. System inputs



such as reactor temperature could also be periodically varied. It would seem then that the number of variables which could be used to optimize performance is very large.

Ranges of the variables are not unlimited, however. Amplitudes, obviously, have limits because they must be greater than zero and cannot be infinite because concentrations are never negative. If stated in terms of mole fraction, as in figure 1, the maximum amplitude is 0.5 if  $s = 0.5$ . Cycle split, of course, has a range of 0 to 1.0.

Even cycle period is limited. If the period is long, periodic operation is simply switching between two steady states assuming a system such as shown in figure 1. The time average behaviour is uniquely defined by the cycle split,  $s$ , and the steady state performance corresponding to each of the feed compositions. In the literature, this situation is referred to as the quasi steady state limit. Figure 2 illustrates two possible situations depending upon the shape of the performance versus composition curve.

If the curve is convex, as in figure 2a, the quasi steady state will always be less than the steady state performance at the time average reactor feed composition. On the other hand, if the curve is concave, the quasi steady state performance will be better as figure 2b shows.

At the other extreme, if the period is very short, mixing in the reactor smooths the square wave and the system operates at steady state. However, if mixing is negligible, or the fraction of the reactor volume that can be characterized as well-mixed is small so that its mean residence time is very small, control theory postulates that another unique state of periodic operation, the relaxed steady state, will be found. If a kinetic model for the reaction exists, the performance at relaxed steady state can be predicted. The methodology is discussed by Horn & Bailey (1968), Matsubara *et al* (1973), and by Wilson & Rinker (1982). The latter investigators claim to have observed the relaxed steady state experimentally. The test for the existence of the state is that performance should become independent of period. Unfortunately, Wilson and Rinker did not apply this test in their study.

In the above study, reference has been made to long and short periods, but these are relative terms. Bailey (1973) defines long and short in terms of the relaxation time of the reactor system after it is subjected to a pulse or step change stimulation.

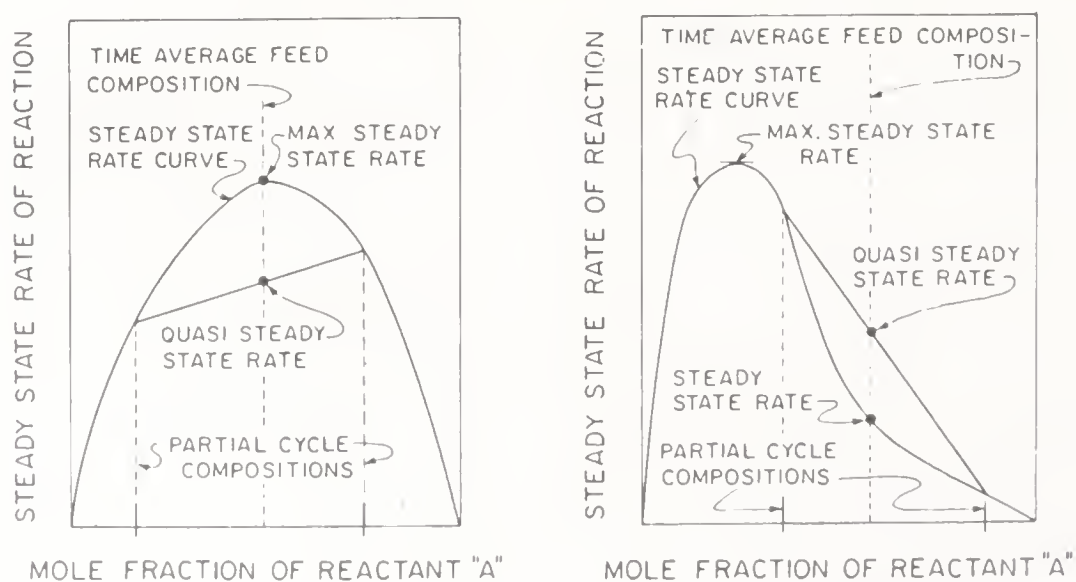


Figure 2. The quasi steady state limit in periodic operation (Hudgins 1986).

This time would be the time constant if the system is a linear one. The cycle period can be described as "long" or "short" if they differ by more than a factor of ten from the system relaxation time. The steady state limit is approached when the cycle period is equal to or less than the mean residence time in the well-mixed portion of the reactor.

One last consideration remains before turning to the experiment described in the literature. If a judgement is to be made as to whether or not periodic operation is superior to the steady state mode, a comparison must be made. But, what should be compared? Figure 1 suggests that the comparison should be made between the time average performance (such as rate) and the steady state performance at the time average reactor feed composition. An examination of figure 2b shows, however, that the quasi steady state performance could be better than the steady state one. Since this performance is an average of two steady state ones, it is also a steady state performance. A further possibility is that there is a steady state feed composition which offers a better performance than the time average one. Thus, comparison of the periodic operation time average with the best possible steady state performance is also valid. Figure 3 illustrates this situation. Data are for ammonia synthesis over an iron catalyst (Jain *et al* 1983a). Labelled points are those used in a study of periodic operation.

If an extreme operation of periodically switching between nitrogen and hydrogen with  $s = 0.5$  was used, the time average synthesis rate could be compared to the steady state rate at a hydrogen mole fraction of 0.5 (crudely, point *D* in the figure). To assess the benefit of periodic operation, however, it would be equally valid to compare the time average rate with the rate at point *C* which is the maximum steady state rate at the specified temperature, pressure and space velocity.

### 3. Implementation of periodic operation

Figure 4 shows one of the many laboratory versions of a periodically operating reactor. In this version, two solenoid valves switch flow paths. Each reactant has two flow paths furnished with needle valves so that the flow rates needed for the composition required in each portion of the cycle can be set. In the figure, the diluent flow is not switched, but this could easily be accomplished by adding a further solenoid valve and a further line equipped with a needle valve. Adding additional flow control lines and solenoid valves would permit the more complex

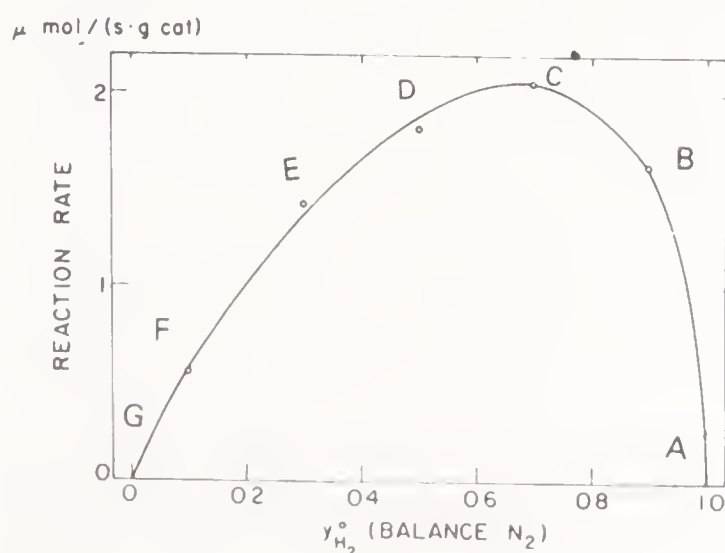


**Figure 3.** Ammonia synthesis rate under steady state as a function of composition at 400°C and 2.38 MPa (Jain *et al* 1983a).

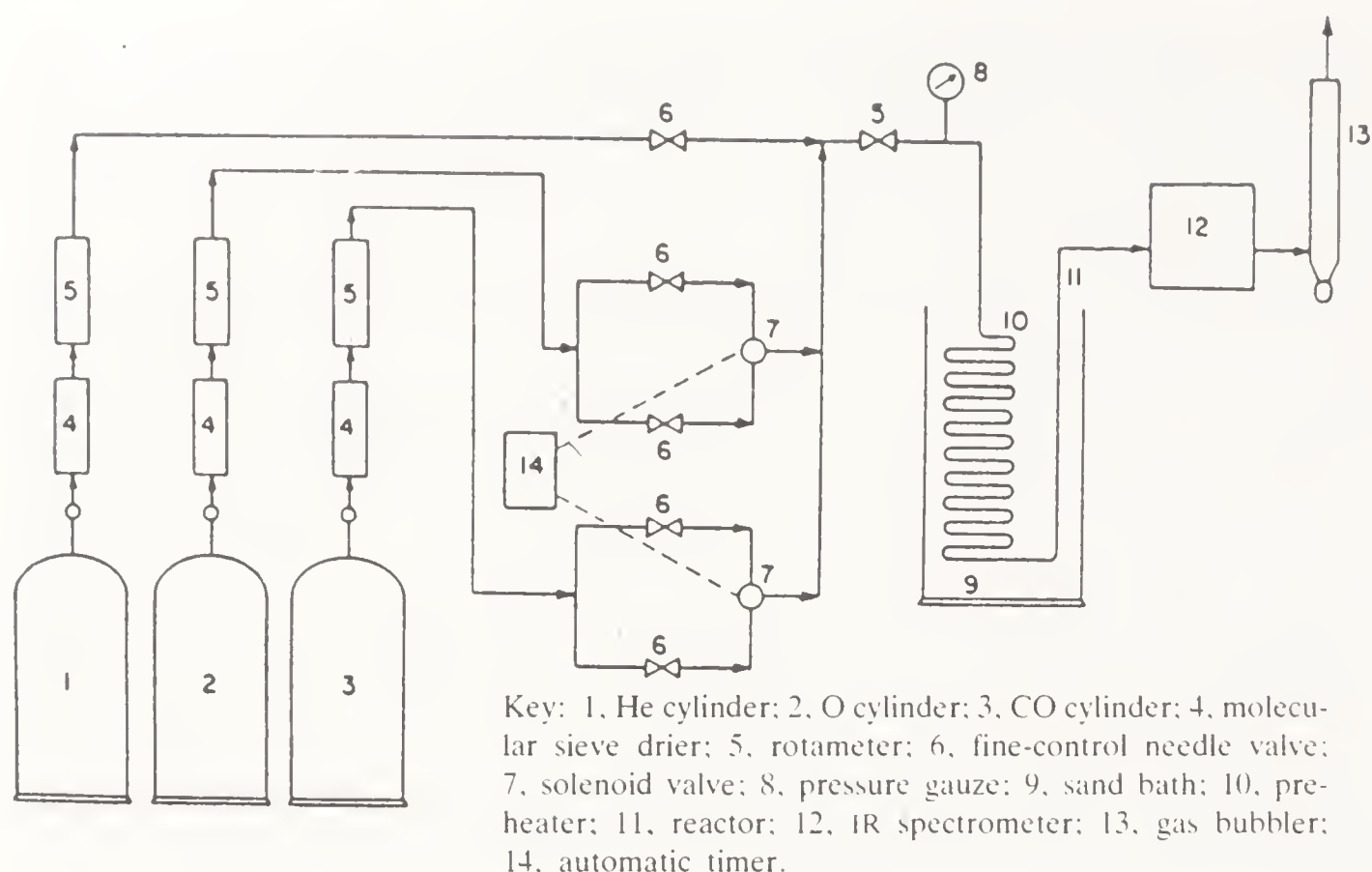


**Figure 4.** Schematic diagram of a periodically operating reactor using solenoid valves to generate the repetitive square waves (Abdul-Kareem *et al* 1980)

cycles discussed at the end of the previous section to be implemented. Wilson & Pinker (1982) use a system similar to the one shown in the figure, but replace the solenoid valves with a motor driven, multiport sampling valve.

An even simpler laboratory system replaces the parallel flow control lines before each solenoid valve with a single valve equipped line and uses cylinders containing the gas compositions needed for each part of the cycle (Feimer *et al* 1985; Cho & West 1984). Either two on-off valves or a single three-way solenoid valve, then, can be used for cycling between the feed cylinders.

If computer control is desired, the solenoid valves can be replaced by flow controllers whose set points are furnished by a computer. This latter system is currently in use in our laboratory, but we frequently use it together with cylinders containing the mixtures desired in the cycle (Adesina *et al* 1986). Of course, flow controllers can be used to produce periodic operation without a computer. In this case, the desired flow rate is set manually (Jain *et al* 1983; Nappi *et al* 1985).

The systems discussed above are satisfactory for atmospheric operation and periods greater than several minutes. Dead ending flows and the use of needle valves for control lead to flow pulses on switching that may last for several seconds. Pulse magnitude can be substantially reduced by switching from the reactor to a purge whose flow resistance matches the resistance in the reactor. Fast acting, properly tuned flow controllers provide the best solution to this problem.

Periodic operation can also be achieved by switching catalyst continuously between two reactors. The square wave is achieved by employing different feed compositions for each of the reactors. Carbova & Gau (1983) proposed a circulating bed system for the partial oxidation of benzene to maleic anhydride. Data on *o*-xylene oxidation obtained in such a reactor are given by Boreskov & Matros (1983) and the reactor is described. A circulating bed has been operated by



Du Pont (Contractor *et al* 1986) as a large bench scale plant. High selectivity in the partial oxidation of butane to maleic anhydride was demonstrated when the riser effluent was segregated from the oxidizing mixture fed to the fluidized bed catalyst regenerator.

The circulating bed seems to be the most inviting means to implement periodic operation on a commercial scale.

#### 4. Activity improvements

##### *Ammonia synthesis*

Three research groups have studied the synthesis. Wilson & Rinker (1982) and Jain *et al* (1982a,b, 1983, 1985) employed the same triply promoted iron catalysts and used temperatures between 325 and 425°C. In both studies, pressures were about one tenth of those employed commercially. Rambeau & Amariglio (1981, 1982) used a ruthenium catalyst. The experiments of Jain are more comprehensive than those of the other investigators so we will consider them first.

Jain employed a reaction system with a recycle reactor and a packed bed, near-adiabatic, integral reactor. These reactors, however, could not be run in parallel. The system is shown in its entirety in figure 5a. Careful attention was paid to achieving well-defined composition square waves; the apparatus for this purpose appears in figure 5b (Jain *et al* 1983). An IR spectrometer was used to detect ammonia. This permitted continuous observation of the response to square wave cycling. When the recycle reactor was used, the ammonia mole fraction in the effluent was held under 0.014. This is well below the equilibrium mole fraction at 400°C and 2.38 MPa so that only the synthesis rate was measured in these experiments.

Figure 3 plotted the steady state rate of synthesis versus reactant composition. Data were obtained in the recycle reactor. As discussed earlier, the quasi steady state rates are always below the steady state ones for this reaction system. Consequently, improvement through periodic operation would not be expected a priori. Figure 6 shows, however, that catalyst activity can be significantly raised by this operation.

The figure illustrates most of the phenomena associated with square wave cycling. The recycle reactor (Berty reactor) contains well-stirred dead volume above and below the catalyst bed. The mean residence time of this dead space as well as upstream well-mixed flow volumes was about one minute at the space velocity of 19000 hr<sup>-1</sup> used for most experiments. If a period of one minute and a cycle split of 0.5 was used with this reactor, each half-cycle would be 0.5 minutes. Mixing in this case would virtually smooth out the composition change so that cycling with a one-minute period should lead to a synthesis rate which closely approaches the steady state rate at the time averaged reactant composition. The bottom curve in figure 6 at a cycle split of 0.6 shows that this is just what happens as the cycle period shortens.

As the cycle period increases, transients associated with the composition switch disappear, so periodic operation becomes equivalent to mixing synthesis rates for steady state at the two half-period compositions. This is the quasi steady state case



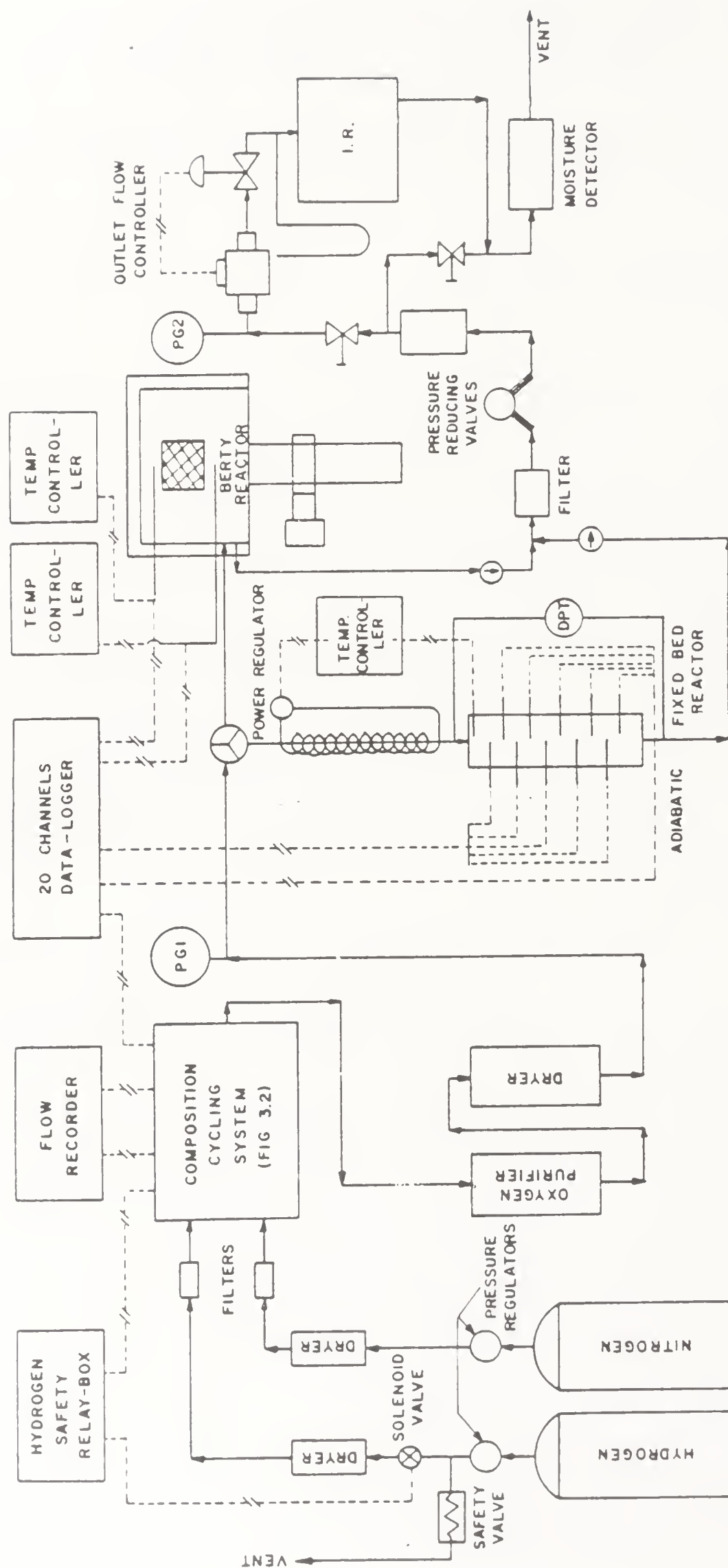


Figure 5. Experimental system employed by Jain *et al* (1982a, 1983, 1985) for the study of ammonia synthesis at 400°C and 2-38 MPa.

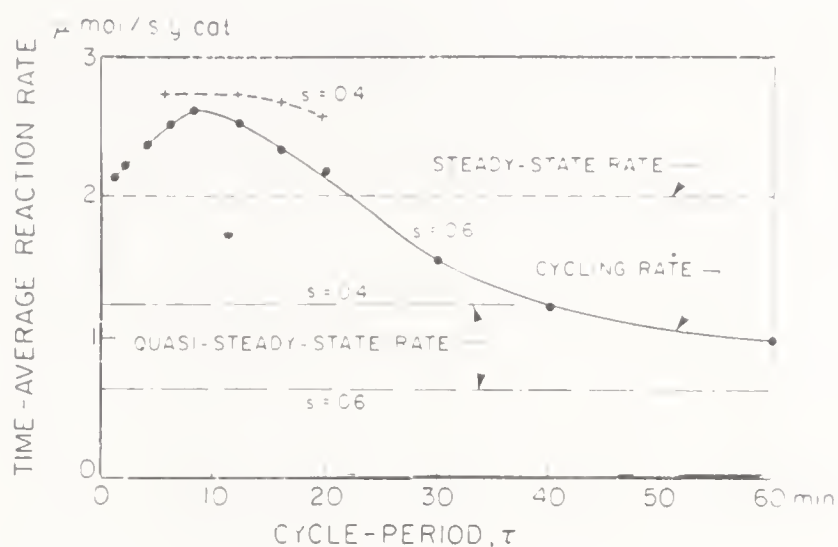


Figure 6. Effect of cycle period and split on the time averaged ammonia synthesis rate for a time averaged reactant mixture containing 75 vol.% hydrogen. Data obtained with a recycle reactor at 400°C, 2.38 MPa and  $SV = 19,000 \text{ hr}^{-1}$  (Jain *et al* 1983).

discussed earlier. In figure 6, the time averaged synthesis rate begins to approach the quasi steady state rate at periods of 60 minutes or greater. Independent measurements of the relaxation time after switching to a synthesis mixture from hydrogen found that almost 30 minutes are needed for steady state to be attained. Thus, for a 60-minute period and a 0.5 cycle split, each half-cycle would be 30 minutes long and steady state would be just attained at the end of each half-cycle. Most of the cycle would still be unsteady so that the rate would be greater than the quasi steady state one. This is what can be seen in figure 6.

Figure 6 indicates that period or cycle frequency is an important variable for periodic operation. There is a range for this variable in which the time averaged rate is significantly above the rate at the comparable steady state. Assuming an analogy with alternating current electrical networks, we refer to this range as resonance. Various experiments indicate that the period associated with this resonance corresponds to times after a composition disturbance for which the rate shows an overshoot.

The upper curve in figure 6 shows the time averaged synthesis rate at a cycle split of 0.4, but with the same time averaged reactant composition. The rate increase is even greater than that found at  $s = 0.6$  and a distinct maximum is seen no longer. Cycle split appears to be an important variable for periodic operation as figure 6 shows.

Wilson & Rinker (1982) used a packed bed microreactor and a multiport motorized valve immediately upstream to minimize upstream mixing. Periods as short as a second were used in their study. Figure 7 plots their measurements as the time averaged synthesis rate versus period. Measurements at different temperatures are shown, but in all cases the reactor feed alternated between pure nitrogen and pure hydrogen. The data were taken with cycle splits from 0.45 to 0.51. In order to display these rates on a single plot, the rates have been normalized by dividing them by the maximum steady state rates at the temperature and pressure used. The abscissa in the figure is logarithmic so that the measurements of Jain *et al* (1983) for alternating nitrogen and hydrogen feeds can be compared with those of Wilson and Rinker. The figure demonstrates that periodic operation can increase the ammonia synthesis rate, or in other words, the catalyst activity, appreciably beyond the best attainable at steady state at a given temperature and total pressure.

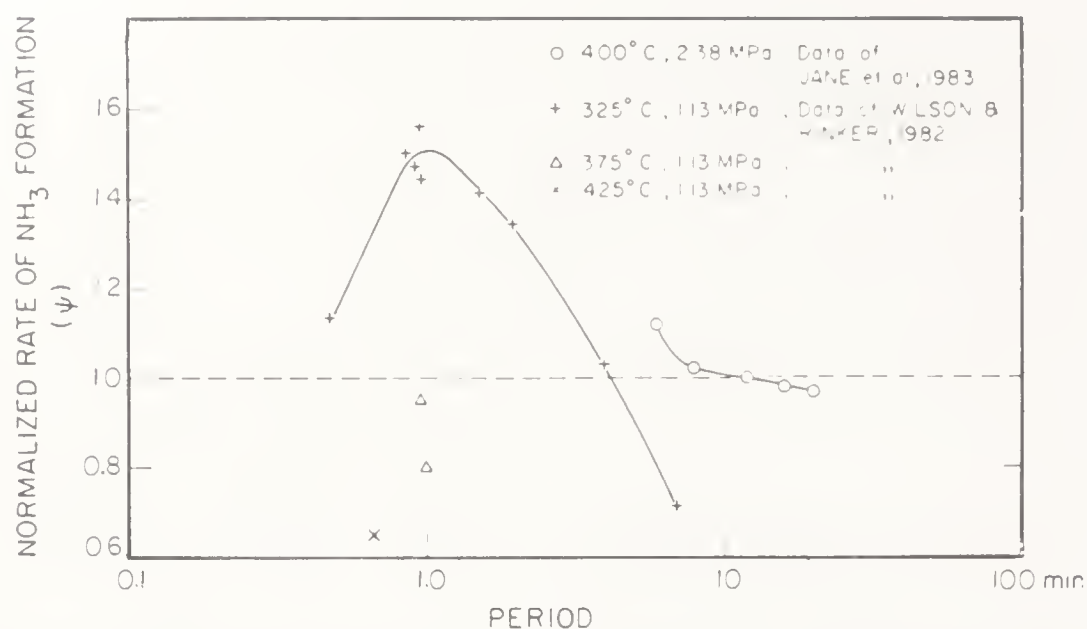


**Figure 7.** Normalized rates of ammonia synthesis over a triply promoted iron catalyst for periodic operation using alternating nitrogen and hydrogen feed streams and various operating conditions (data of Wilson & Rinker 1982; Jain *et al* 1983).

There appears to be some consistency between the measurements of the two research groups if the measurements at 325°C and 1.13 MPa are compared with those at 400°C and 2.38 MPa. However, the results of Wilson and Rinker in figure 7 show that the improvement decreases with increasing temperature, whereas Jain and co-workers found the opposite temperature effect. They also found that increasing pressure increased activity under periodic operation, whereas Wilson and Rinker observed a decrease. The reason for these divergent observations may be that Wilson and Rinker operated under conditions in which the reverse reaction was significant. Differing contributions of the reverse reaction under periodic operation and steady state could account for the temperature and pressure effects that they measured.

The improvement due to periodic operation at the same temperature and pressure are dramatically illustrated in figure 8. This figure summarizes all of Jain's data at 400°C. The area under the bottom curve is the region of steady state operation, that is, any rate in this region can be obtained by mixing the output of

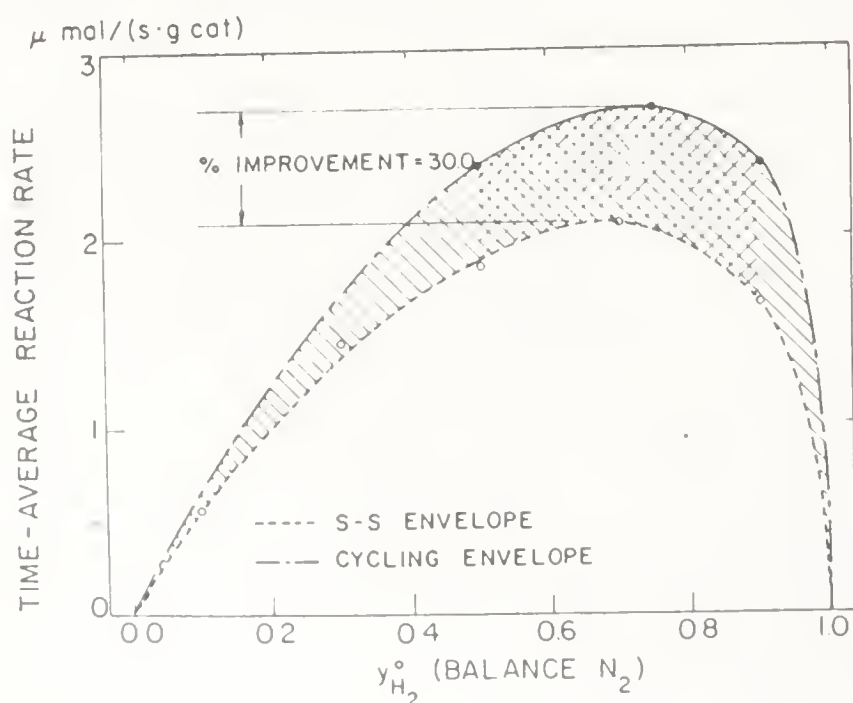


**Figure 8.** Comparison of catalyst activity for ammonia synthesis under steady state and periodic operation at 400°C and 2.38 MPa with a triply promoted iron catalyst (Jain *et al* 1983).



two or more reactors operating at steady state with different feed compositions. The curve itself is the rate attainable by a single reactor operating at the feed composition corresponding to the point. The upper curve defines the region of periodic operation. The curve itself is for a single reactor as before. Not all of this curve has been established experimentally. The experimentally confirmed portion bounds the double cross hatching in the figure; the remainder with single cross hatching is an estimate of the real behaviour.

Jain attempted to assess the effect of periodic operation under commercial ammonia synthesis conditions by performing experiments with industrial catalysts (Jain *et al* 1985) and in a near adiabatic, integral, packed bed reactor (Jain *et al* 1982). The former showed that diffusion interference reduced the improvement in activity for periodic operation when compared with measurements made on fine, diffusion interference free, catalysts. However, when compared with steady state measurements for particles of the same size, the improvements under periodic operation were virtually the same for fine and coarse catalyst particles.

With an integral reactor, synthesis rates were lower because of the reverse reaction. Nevertheless, periodic operation increased the time averaged rates to greater than those attainable under steady state. Indeed, a figure similar to that shown in figure 8 was obtained. The improvement over the maximum steady state synthesis rate was 25% compared with about 30% when a recycle reactor was used. The reduction was attributed both to mixing in the packed bed which diminished the amplitude of the concentration changes and to the reverse reaction.

#### *Sulphur dioxide oxidation*

Experiments on this system were carried out under conditions corresponding to the inlet and outlet of a commercial packed bed reactor. Both studies employed a commercial potassium promoted vanadia catalyst supported on diatomaceous earth. Unni *et al* (1973) used 30/40 mesh catalyst packed into a 0.6 cm tube (o.d) which was immersed in a fluidised sand bath. Measurements were made at 405°C and atmospheric pressure; variables in the study were cycling period, amplitude and the time averaged ratio of sulphur dioxide to oxygen. Figure 9 shows the effect of period on the time averaged oxidation rate at an amplitude of 0.3 and a time averaged reactant composition of 0.6, both defined in terms of the sulphur dioxide to oxygen ratio. The increase in oxidation rate is about 24% at a period of 4 hours. A resonance phenomenon is evident in the figure. When the period exceeds 6 hours, the oxidation rate falls towards the quasi steady state rate just as with ammonia synthesis. However, at periods below 2 hours, the time averaged oxidation rate appears to fall below the steady state rate. Why this should occur is not clear; it may reflect experimental error. The possible extent of this error is suggested by the data points shown in figure 8. The drop in the time averaged oxidation rate at periods under 2 hours cannot be explained by mixing prior to the catalyst bed because the residence time of dead volume upstream from the reactors which might be well-mixed amounted to less than a minute. Apparently short periods of less than one or two hours fail to excite this catalytic system.

Measurements were repeated at time averaged reactant ratios of 0.3 and 0.9. In both cases, a small increase in the time averaged oxidation rate of about 2 to 4% was observed. Amplitude (expressed in terms of the reactant ratio) strongly affected the improvement as figure 10 shows.



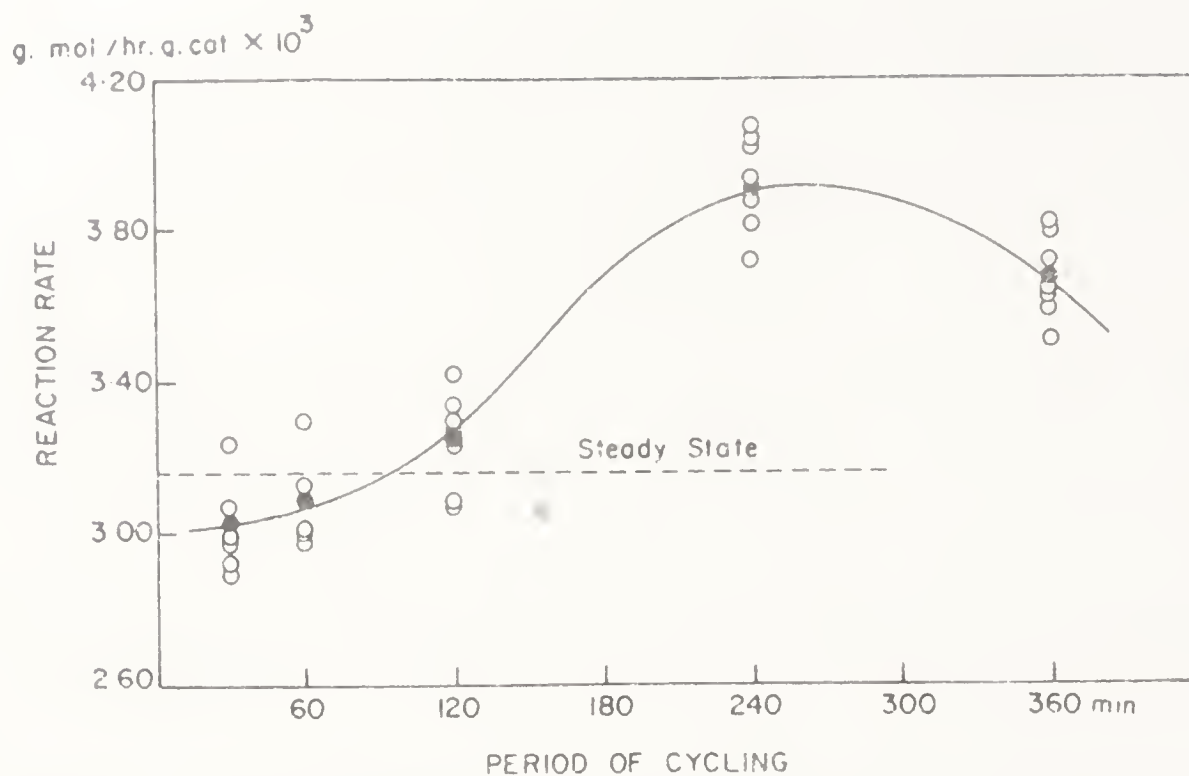


Figure 9. Comparison of steady state and periodic operation for the oxidation of sulphur dioxide over a commercial vanadia catalyst in a differential reactor at 405°C and atmospheric pressure (Unni *et al* 1973).

The data in the figure suggest an amplitude threshold for the oxidation reaction. A sharp drop-off at an amplitude of 0.6 corresponds to alternating feeds of oxygen and a reactant mixture. Symmetrical cycling was used, that is,  $s = 0.5$ , so sulphur dioxide was not fed to the reactor for half of a cycle. It should be kept in mind that cycling is not symmetrical with respect to reactant concentration.

When the procedure of Unni was applied to an integral reactor in which sulphur dioxide conversion was about 40%, no improvement in the oxidation rate was found, although a change in the sulphur trioxide partial pressure was observed after a composition change (Briggs *et al* 1977). To explore the application of periodic operation to this reaction system further, Briggs constructed a two-stage sulphur dioxide oxidation reactor which converted 90% of the sulphur dioxide feed in the first stage. The second stage consisted of a 2.5 cm tube (o.d.) packed with 12/20 mesh particles of the catalyst used by Unni. A pneumatically operated valve

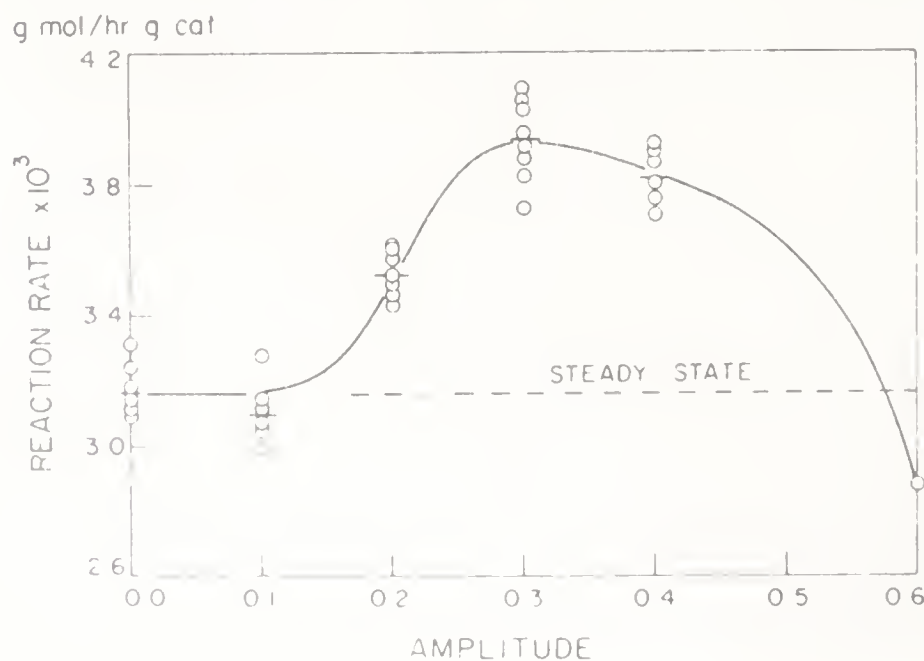


Figure 10. Effect of cycle amplitude on the time averaged rate of sulphur dioxide oxidation under periodic operation at 405°C and  $m = 0.6$  with  $s = 0.5$  and a period of 4 hours (Unni *et al* 1973).

switched the feed to the stage periodically from first stage effluent to nitrogen, air, oxygen, or even sulphur dioxide. Feed and effluent from the stage were monitored for sulphur trioxide by a modified mass spectrometer and for sulphur dioxide by chromatography after washing with sulphuric acid.

Experiments with this system (Briggs *et al* 1977) showed that cycling between the effluent from stage 1 and air with a period of 26 minutes raised the total conversion of the two-stage system to 98.7% from the 95.7% conversion obtained at steady state with stage 2 treating the effluent from stage 1. The improvement in activity in stage 2 due to periodic operation, thus, amounts to 53%. Reducing the period could have increased conversion further. Passing air or nitrogen over the catalyst at 406°C for several hours and then switching to stage 1 effluent gave overall sulphur dioxide conversions of 99.7% initially, which decayed to the steady state value over the next 24 hours. Equilibrium calculations indicated a conversion of 99.4% which suggests that the initial transient exceeds the thermodynamic limit.

Briggs *et al* (1980) and Silveston & Hudgins (1981) recognized that the high conversions achieved in periodic operation offered a means of controlling sulphur dioxide emissions from sulphuric acid plants. The equipment devised by Briggs was modified by doubling the second stage. Thus, with symmetrical cycling, the effluent from the first stage passed alternately to the first or second bed of the second stage. When one bed was being fed effluent from stage 1, the other bed was fed preheated air. Experiments were carried out with two mixtures. The first represented the composition when sulphur dioxide is supplied by burning sulphur in air, the second represented the composition from smelting of a sulphide ore. Results summarized in table 1 show a large improvement through periodic operation.

By sampling in successive cycles, it is possible to build up a time profile of the sulphur dioxide partial pressure leaving one of the beds in the second stage. Figure 11 shows this profile for the half-cycle with stage 1 effluent flowing to the bed. Data for the sulphur burning mixture are given. Results for periods of 10 and 20 minutes

**Table 1.** Periodic operation of the final converter stage in a sulphuric acid plant.

	Sulphur burning	Ore smelting
Feed composition		
sulphur dioxide	0.108	0.080
oxygen	0.152	0.062
nitrogen	0.740	0.858
Temperature in final stage °C	401	405
Sulphur dioxide conversion (%)		
<i>At steady state</i>		
Stage 1*	91.7	88.3
Stage 2	95.2	91.3
<i>Stage 2 under periodic operation</i>		
Period = 10 min	99.4	98.4
Period = 20 min	99.2	98.1
Period = 24 min	—	97.6
Equilibrium	99.5	98.7

\* For both steady state and periodic operation. Source: Briggs *et al* 1980.

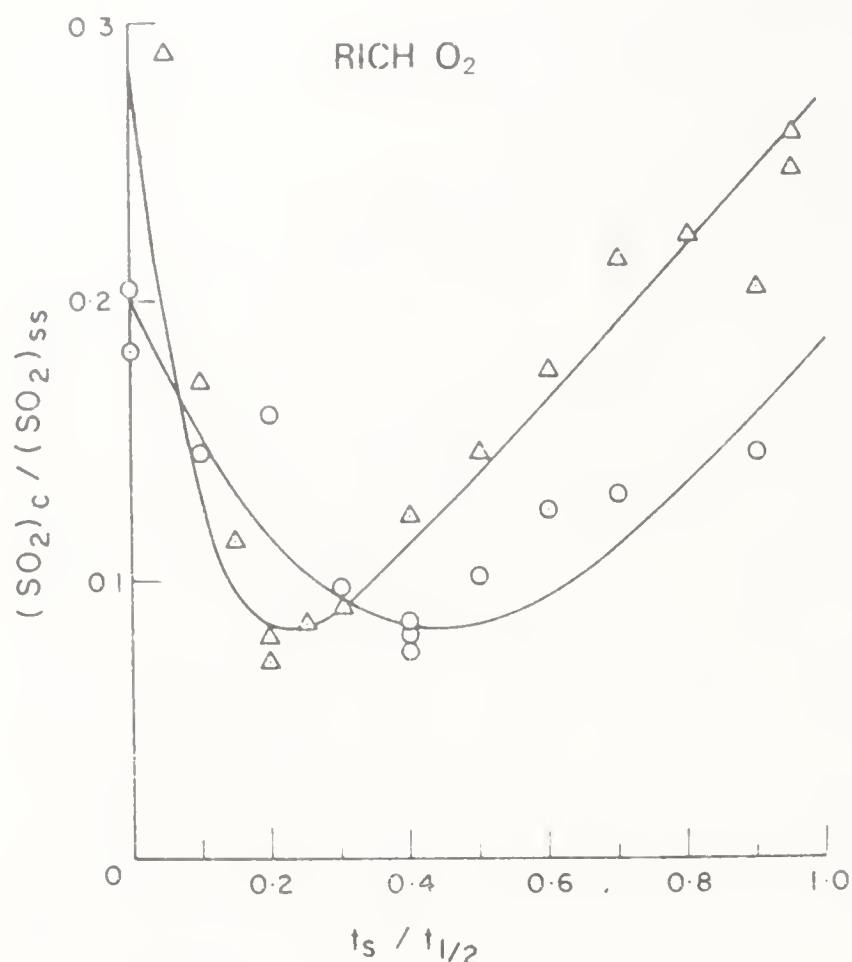


Figure 11. Normalized sulphur dioxide partial pressure in the effluent from stage 2 as a function of dimensionless time in the half cycle with stage 1 effluent (Briggs *et al* 1980).

can be seen. Since the values in table 1 are time averaged, substantially higher conversions could be achieved by using periods as short as 4 minutes.

#### Automotive catalysts

Periodic operation is a reality and not just an experimental curiosity for the catalytic muffler. Modern automobiles are fitted with closed loop control systems which maintain the air-fuel ratio near its stoichiometric value. One of the reasons for this is that noble metal three-way catalysts operate most efficiently under this condition. However, the control loop introduces a fluctuation in the air-fuel ratio which in turn causes periodic variations in the composition of the engine exhaust passed on to the muffler. As a consequence, periodic operation of the noble metal muffler catalysts has been given a good deal of attention. Research has been practice-oriented so that only cyclic variables close to those met in muffler operation have been studied. This makes comparison with the other experimental studies discussed in this paper difficult.

Early studies indicated that the fluctuating exhaust composition did not benefit three-way muffler performance. However, Schlatter *et al* (1983) using a Pt/Rh/Al<sub>2</sub>O<sub>3</sub> catalyst and symmetrical, square wave cycling found that CO conversion was higher than at steady state provided the time averaged exhaust composition was reducing. The benefits of cycling were confirmed by Taylor & Sinkevitch (1983) who used symmetric and asymmetric cycling of the air-fuel ratio. Cho & West (1984) employed a well-characterized 0.1 wt.% Pt/ $\gamma$  alumina catalyst to investigate the effect of Pt dispersion and depth of impregnation, mean reactant composition and operating temperature on the benefits of periodic operation.

Cho and West were not concerned with the cycle period or amplitude of the concentration swings. Symmetrical cycles containing 0.4 vol.% O<sub>2</sub>-0.2 vol.% CO



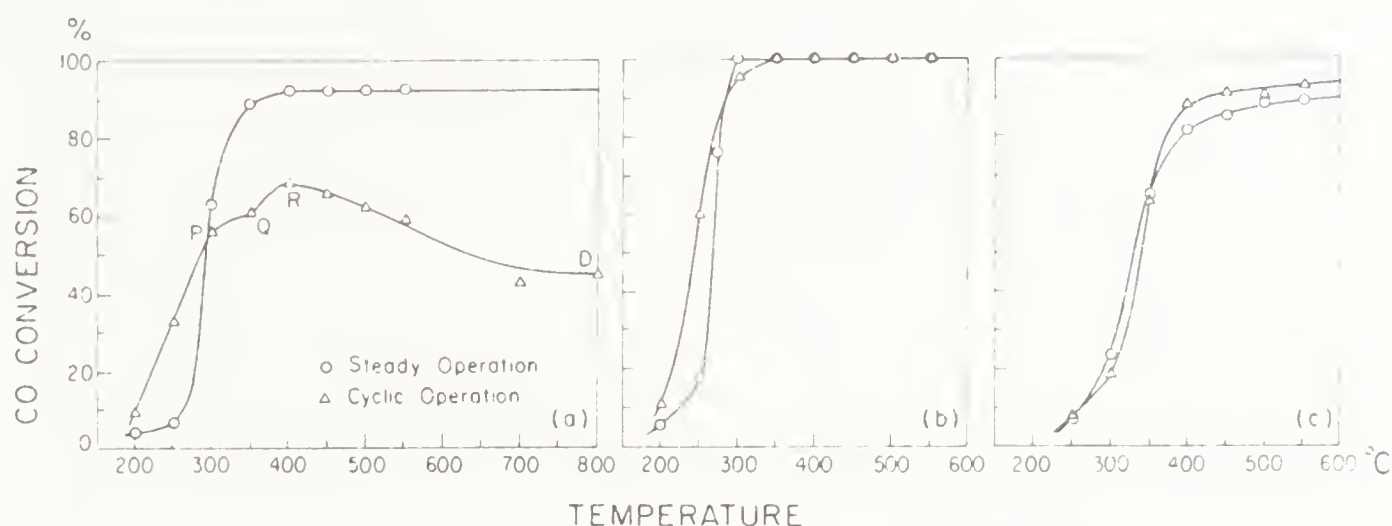


**Figure 12.** Effect of operating temperature and reactant composition on the relative CO conversion in steady state and periodic operation over a shell impregnated, poorly dispersed 0.1 wt.% Pt on  $\gamma$  alumina catalyst (Cho & West 1984).

and 0.2 vol.%  $O_2$ -1.0 vol.% CO were used for experiments with a mean stoichiometric reactant mixture. Figure 12 compares steady state and periodic operation as a function of the mean reactant composition and operating temperature. With stoichiometric reactants, periodic operation gives higher CO conversion below 300°C (figure 12a). If the reactant mixture is reducing (volume % CO twice that for the stoichiometric mixture), the behaviour reverses. Periodic operation is advantageous only above 350°C. Figure 12c shows that low temperatures favour periodic operation if the reactant mixture is oxidizing (volume % oxygen twice that for the stoichiometric mixture).

Figure 12 demonstrates clearly that cyclic operation can out-perform steady state operation under some reactant conditions for CO oxidation over a platinum catalyst. Cho and West found further that Pt dispersion and depth of impregnation changed the temperatures at which the cyclic out-performed steady state operation, but did not change the overall behaviour.

### *Carbon monoxide oxidation*

Not only is the catalytic oxidation important in automotive catalysis, it is a convenient reaction for study. The oxidation proceeds at low temperatures over noble metals, at moderate temperatures over many oxides and the product, carbon dioxide, is easily detected by IR spectrometry.

Cutlip (1979) used a 0.5 wt.% platinum on  $\gamma$  alumina catalyst. His study was directed at the mechanism of activity improvement under periodic operation so an exhaustive investigation of the cycling variables was not undertaken. Cutlip reasoned from studies on spontaneous oscillations of the oxidation rate that the coverage of the catalyst surface by adsorbed reactant was implicated, so his primary variables were the cycle split and temperature. He employed a recycle reactor and used alternating exposure of the catalyst charge to 2 vol.% CO and to 3 vol.% oxygen in argon. These compositions and the temperatures used (28 and 60°C) meant that Cutlip's experiments were performed in the region of steady state multiplicity.

Unlike experiments discussed heretofore, Cutlip observed a sharp resonance which is illustrated by figure 13 devised from his results. The cycle split in the figure



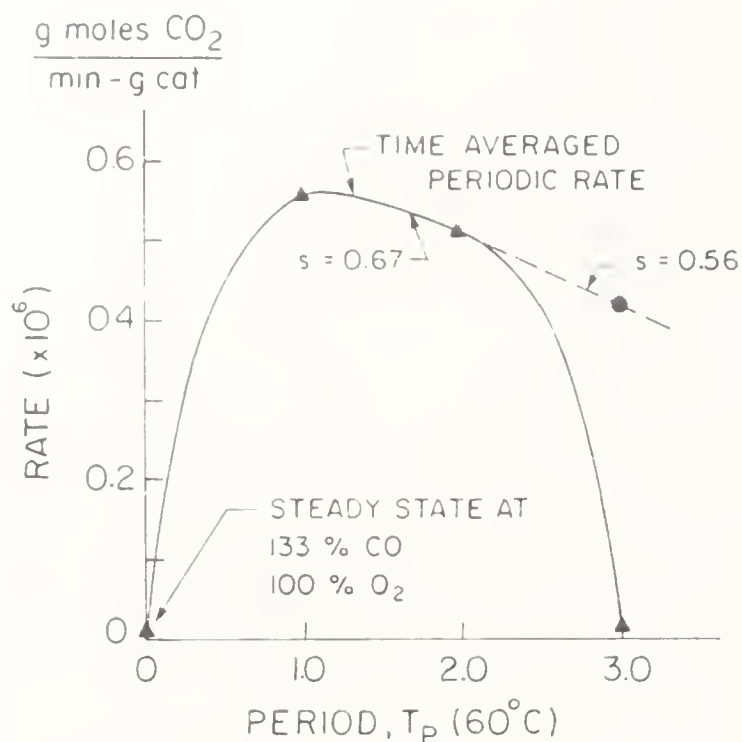


**Figure 13.** Comparison of steady state and periodic operation for the oxidation of carbon monoxide over a 0.5 wt.% Pt/ $\gamma$  alumina catalyst at 60°C and atmospheric pressure (Cutlip 1979).

is 0.67. At a 3-minute period, the oxidation rate has dropped to nearly zero. However, if a cycle split of 0.56 is used, there is just a small decrease in the time averaged rate. The steady state rate at the time averaged feed composition is shown by the point at zero period.

The importance of cycle split can be seen moreover in that the time averaged rate under periodic operation does not change with period in the range 1 to 3 minutes if the split is 0.5. This rate as well as the maximum rate in figure 13 equals the rate at the higher steady state for the multiplicity region.

Figure 14 plots reactant and product mole fractions leaving the reactor for a period = 3 minutes and  $s = 0.56$ . Because CO is limiting and conversion is high, very little CO was detected. The double oxygen peak may be explained by a surface saturated with CO when the feed is switched to 3% oxygen. Due to mixing in the recycle reactor, the oxygen partial pressure does not jump instantaneously. Some of the oxygen reacts with adsorbed CO freeing adsorption sites for  $O_2$ . Continued reaction between the adsorbates and the build up of oxygen on the surface drive

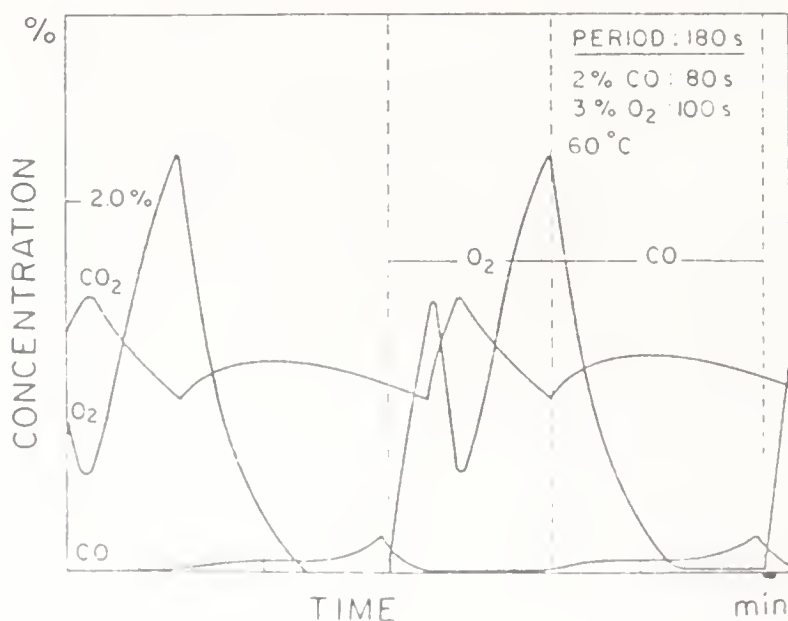


**Figure 14.** Reactor outlet mole fractions for CO oxidation over a 0.5 wt.% Pt/ $\gamma$  alumina catalyst at 60°C at a period of 3 minutes and a cycle split of 0.56 (Cutlip 1979).

down the oxygen partial pressure. As the surface fills with oxygen adatoms and the CO adatoms are consumed, the oxygen partial pressure builds up again, while the carbon dioxide partial pressure drops. The persistence of oxygen in the CO portion of the cycle and the double CO<sub>2</sub> peak indicate equilibrium adsorption of the reactants. Thus, figure 14 supports Cutlip's contention that the shifting reactant coverage of the surface during periodic operation is the source of the activity improvement.

A recent study of the platinum system is available (Barshad & Gulari 1985) with a more extensive variable study made under conditions for which carbon monoxide conversion was incomplete. Oxidation rates were measured under periodic operation and increases of several hundred percent over steady state were noted.

Waterloo researchers have investigated CO oxidation over platinum, nickel oxide, copper oxide and vanadia. Results for platinum and nickel oxide have not been published because they are incomplete and not always reproducible. Generally, symmetrical cycling at periods under 1 to 2 minutes results in catalyst activity substantially in excess of steady state activity (Hugo *et al* 1986). With a copper catalyst, a study of cycling frequency was not performed, but a curious, "wrong way" behaviour was seen following a composition change (Prokopowicz *et al* 1986). This was attributed to changing reactant concentrations on the catalyst surface (see figure 14 where the oxygen mole fraction in the gas decreases in the middle of the oxygen portion of the cycle).

A thorough study of periodic operation was performed for CO oxidation over a potassium promoted vanadia catalyst (Abdul-Kareem *et al* 1980a). Oxidation over this catalyst appears to proceed via a redox mechanism so the composition variable used by Abdul-Kareem was the ratio of carbon monoxide to oxygen partial pressure. It is the value of this ratio which makes the catalyst environment either oxidizing or reducing. The range from 0.12 to 1.1 was investigated. A helium diluent was used whose mole fraction was about 0.8. Steady state measurements indicated that the oxidation rate increased monotonically with the partial pressure ratio. Curvature of the rate versus ratio curve was small so that the quasi steady state rate was only about 10% below the steady state rate at the time averaged partial pressure ratio. In his study, Abdul-Kareem considered the effect of cycle period, amplitude and the time averaged partial pressure ratio on conversion under periodic operation.

Resonance was found for the three mean partial pressure ratios investigated as may be seen in figure 15. The period corresponding to the maximum oxidation rate depends on the mean partial pressure ratio, increasing from about 20 minutes at a ratio of 0.36 to 40 minutes at 0.86. A fourfold variation in amplitude was used, but this variable seemed to be important only for periods in the resonance region.

The shape of the curves in figure 15 suggest other regions of resonance. Additional experiments were carried out at 440°C and a partial pressure ratio of 0.86. Results of these experiments appear in figure 16. The increase in the oxidation rate over steady state at a period of 40 minutes is much larger than that seen in figure 15. Resonance peaks now are found around a period of 20 minutes and 2 minutes. Indeed the heights of these rate maxima suggest a harmonic progression at intervals of about 20 minutes. There may be a further small rate maximum at about 60 minutes. The two amplitudes investigated seem to have little influence on the position or magnitude of the rate maxima.

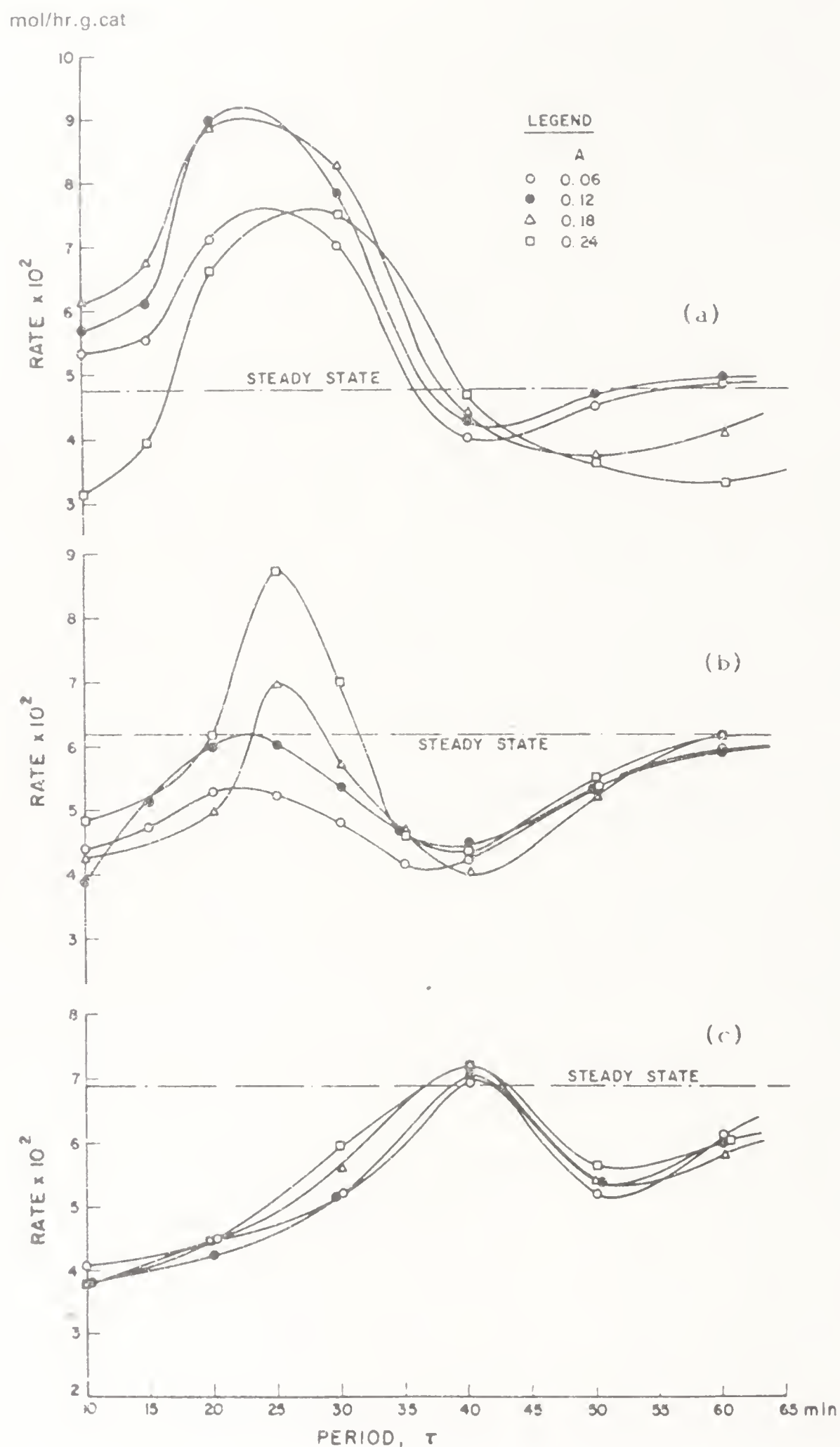


Figure 15. Variation of the time averaged oxidation rate with cycle period, cycle amplitude and mean reactant partial pressure ratio for a commercial vanadia catalyst at 395°C and atmospheric pressure (Abdul-Kareem *et al* 1980). (a)  $p\text{CO}/p\text{O}_2 = 0.36$  (b) = 0.56 (c) = 0.86.



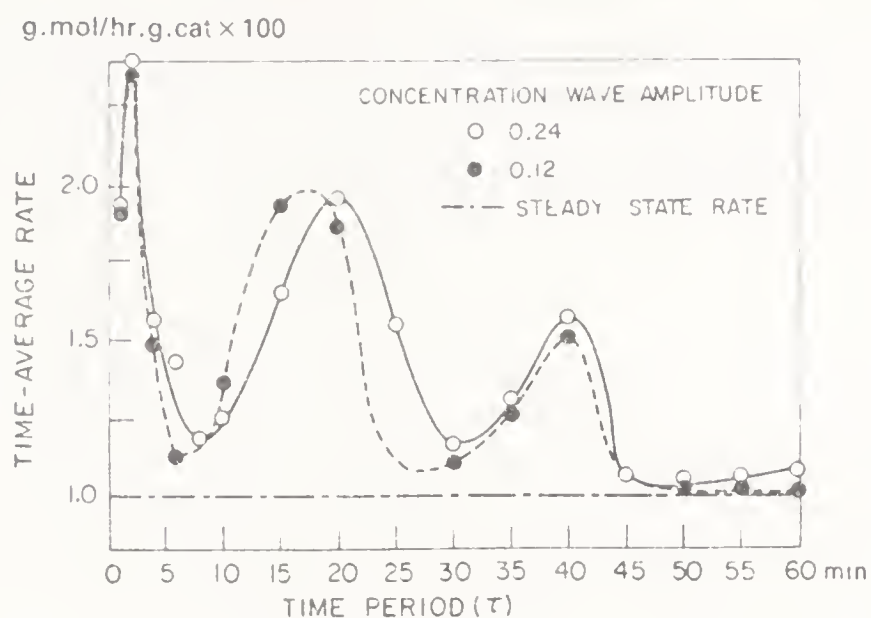


Figure 16. Variation of the time averaged rate of CO oxidation with cycling period at  $p_{\text{CO}}/p_{\text{O}_2} = 0.86$  and  $440^\circ\text{C}$  (Abdul-Kareem *et al* 1980b; Jain *et al* 1982c).

### Claus reaction

El Masry (1985) reported a study of the periodic operation of this reaction. A bauxite catalyst was used and all experiments were conducted at  $210^\circ\text{C}$  and  $107.5\text{ kPa}$ . Variables investigated were cycle period and split. Different time averaged feed compositions were used. Large relative increases in catalyst activity were found with periods of 2 to 4 minutes for the stoichiometric mixture of hydrogen sulphide and sulphur dioxide and for the two other reactant mixtures studied when periodic operation was carried out alternating between a feed containing only hydrogen sulphide and a reactant mixture feed. Periods greater than 4 minutes suppressed the Claus reaction rate below the steady state rate at the time averaged reactant mixture. If cycling was performed alternating between a feed containing only sulphur dioxide and reactant mixture, improvement was not observed regardless of the cycle period and split employed.

### Methanol synthesis

Commercial low pressure synthesis catalysts or copper-zinc water gas shift catalysts that are iron or nickel free are so selective towards methanol that the side reaction to methane can be neglected. The synthesis then can be treated as a single reaction system. An exploratory study was carried out to see if the low pressure synthesis over a copper-zinc catalyst could be activated by periodic operation (Nappi *et al* 1985). Experiments were carried out in a recycle reactor at  $2\text{ MPa}$  and  $350^\circ\text{C}$ . Two cycling modes were examined. In the first of these, carbon monoxide and hydrogen were the reactants and their partial pressures were varied cyclically and  $180^\circ$  out of phase. The second mode consisted of periodically dosing the reactant mixture with carbon dioxide. Carbon dioxide in low concentrations appears to prevent the slow deactivation of the copper-zinc catalyst. At mole fractions above several percent, this oxide participates in the reaction. Variables in these studies were cycle period and split.

Cycling between hydrogen and synthesis mixtures failed to show any improvement in the synthesis rate over the rate measured under steady state at the time averaged reactant composition. Because of mixing in the recycle reactor, one minute was the shortest period that could be used. For this period, the time averaged synthesis rate approached the steady state rate, but this reflected



smoothing of the composition switch through mixing. Carbon dioxide pulsing appeared to yield a small increase in activity assuming that at steady state the synthesis rate is proportional to the carbon dioxide concentration. Only limited measurements were made. This cycling mode is still under study.

### *Multiple reaction systems*

There are many studies of the effect of periodic operation on selectivity in the literature. It has been found that there are several cases where positive changes in selectivity arise from an activation of one of the reactions in the system network. We will consider some of these cases in this section. In other cases, selectivity was improved by throttling reactions which led to undesirable products (Al-Taie & Kerschenbaum 1978; Fiolitakis *et al* 1983; Silveston & Forrissier 1985). It is interesting to note that Jain *et al* (1983b) demonstrate that the models used in the seminal papers by Bailey & Horn (1969, 1972) result in better selectivity through throttling rather than by activating the formation of the desired product.

The partial oxidation of ethylene to ethylene oxide over a silver catalyst was studied by Renken *et al* (1976) using an integral packed bed reactor which was operated non-isothermally. At a constant 0.06 oxygen mole fraction, the ethylene mole fraction was symmetrically switched between 0.06 and 0.12. The nitrogen diluent was also varied to maintain a constant space velocity. Renken found that with proper choice of period the yield at all conversion but the highest increased under periodic operation. If ignition did not occur in the bed, cycle periods of 10 to 16 seconds gave the highest yields, whereas at high ethylene conversion under an ignition condition, a two second period was best. It was not clear from the measurements whether or not the ethylene oxide formation rate increases or the rate of further oxidation to carbon dioxide decreases.

There is no ambiguity about the next case to be considered. The hydrogenation of acetylene is a consecutive reaction catalyzed by nickel. Bilimoria & Bailey (1978) used an internally mixed (spinning basket) reactor in a study of the periodic operation of this hydrogenation at 166°C and nearly atmospheric pressure. The acetylene mole fraction was held constant at 0.10 while the hydrogen mole fraction cycled between 0.05 and 0.325. The mole fraction of the nitrogen diluent was varied concomitantly with hydrogen to maintain a constant space velocity. Chromatography was used to measure the hydrocarbon composition of the reactor effluent. Cycle period and split were the variables investigated by Bilimoria and Bailey.

Two commercial nickel catalysts were used by the investigators with slightly different results. Figure 17a shows the mole fraction of each hydrocarbon as a function of the time averaged hydrogen-ethylene ratio in the reactor feed when catalyst I was used. The feed ratio was varied by the cycle split so that a high ratio indicates a high split value. It is evident that periodic operation increases the formation rates of both ethylene and ethane. Only the ethane mole fraction in the effluent is shown for catalyst II in figure 17b. The shaded area in the figure reflects ongoing catalyst fouling during the experiments.

The period associated with the maximum rate of ethylene formation cannot be determined from figure 17a, except that it must be greater than 3 minutes. Increasing the period must sharply raise the formation rate because the ethane formation rate also increases between periods of 3 and 5 minutes. The mean

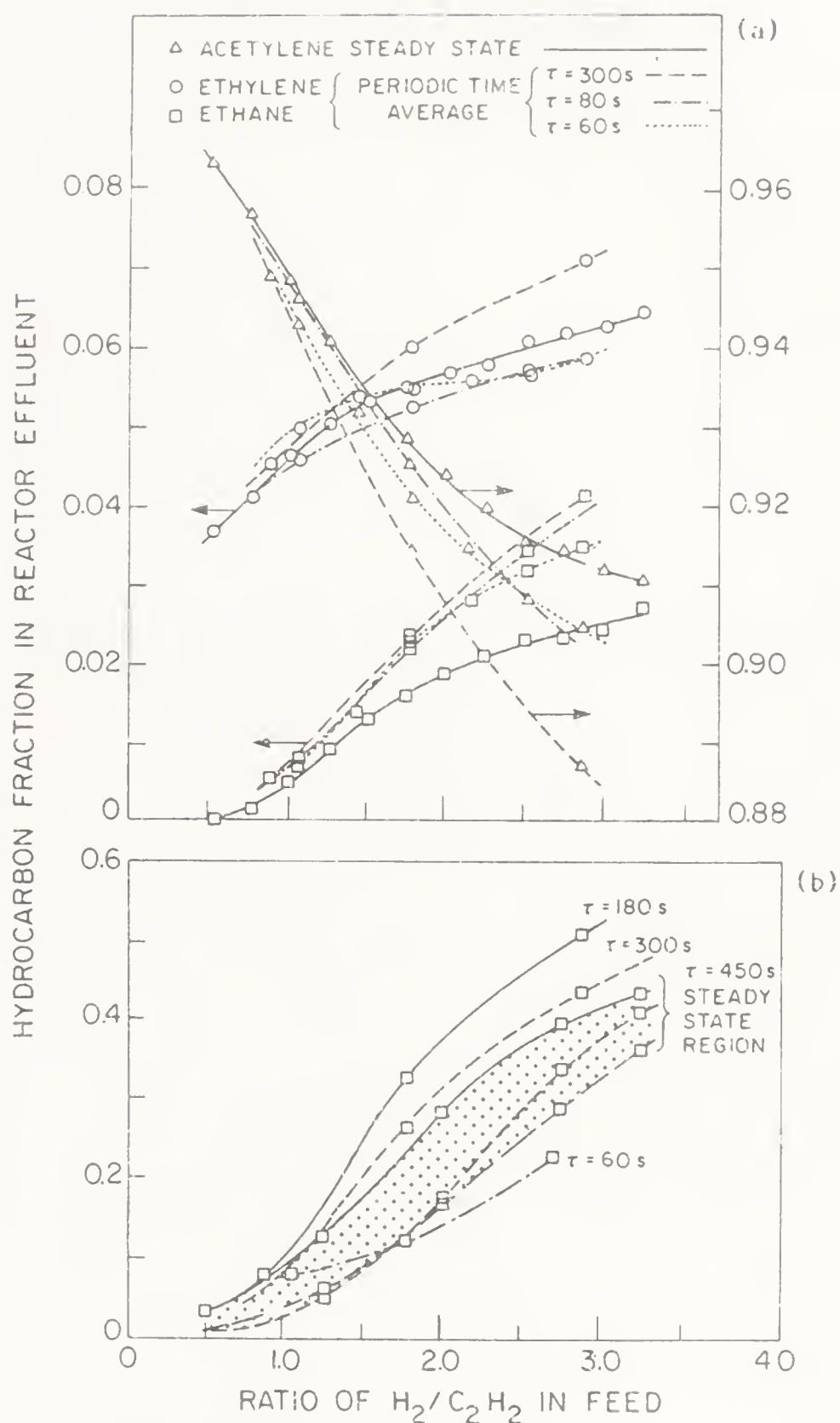


**Figure 17.** Effluent hydrocarbon mole fractions in the catalytic hydrogenation of acetylene versus cycle period and time averaged inlet composition for steady state and periodic operation at 166°C and 108 kPa (Bilimoria & Bailey 1978) – (a) catalyst I, (b) catalyst II.

residence time in the well-stirred reactor is about a minute, so the smoothing of the hydrogen concentration step change should force the behaviour at a period of 1 minute toward the steady state curve. Although this is the case for ethylene, it does not occur for ethane. Indeed, figure 17a indicates that cycle split is the more important variable rather than period.

For catalyst II, a resonance situation is evident from figure 17b. Ethane formation rates under periodic operation exceed steady state rates for periods



greater than 1 and less than 7.5 minutes. The cycle split seems to be less important for this catalyst than for catalyst I.

Periodic operation had a large effect on selectivity of the Fischer-Tropsch synthesis for the three catalysts studied by the Waterloo research group. Activation of these catalysts was also observed. The variables investigated in all studies were cycle period and split. Work was done on a copper promoted iron catalyst at 246°C and 384 kPa (Feimer *et al* 1985), on 0.5 wt.% ruthenium on alumina at 211°C and 440 kPa (Ross *et al* 1986), and on 62 wt.% cobalt on kieselguhr at 200°C and 115 kPa (Adesina *et al* 1986). For the most part, alternating feed streams of hydrogen and synthesis gas constituted the cycles. Experiments were performed in packed bed microreactors immersed in well-stirred oil baths. Residence times upstream of the reactor where mixing could occur were between 10 and 20 seconds so that little distortion of the step changes in reactant concentration occurred for periods equal or greater than one minute. Chromatography was used to measure product concentrations.

Results for the three catalysts have been pooled together in figure 18 despite differences in operating conditions by normalizing the time averaged synthesis rates with the steady state rate at the time averaged reactant composition. The cycle split is 0.5 (symmetrical cycles) for the ruthenium and cobalt catalysts and 0.7 for iron; split is defined in terms of the pure hydrogen feed.

It is evident that the activity of all three catalysts for methane formation improves under periodic operation if an appropriate cycle period is chosen. For the iron catalyst, the rate of formation is twice the steady state rate at a period of 1.5 minutes. Mixing has little effect for that period so the increase would be even greater if shorter cycle periods has been used. The increase is less for the other two catalysts. It seems to be independent of periods above forty minutes for the ruthenium catalyst. For cobalt, resonance is evident with the synthesis rate peaking at a period of about 40 minutes. Measurements at a cycle split of 0.5 using the iron catalyst showed just a 10% increase in the methane formation rate.

The behaviour of the other light hydrocarbons in figure 18 resembles that for methane. The cobalt catalyst is activated by periodic operation for all the products shown in the figure. The range of periods for this effect seem to be independent of the product. Periodic operation stimulates the formation of alkanes for all three catalysts as the plot for propane shows. This is not surprising as these catalysts are active for hydrogenation. The cause of this shift from alkene to alkane is certainly the periodic introduction of pure hydrogen. Both ruthenium and cobalt are activated by periodic operation for ethane and ethylene production. The activity increase is about 50% for ruthenium and almost twofold for cobalt. The normalized rate for the iron catalyst increases as the period decreases. This indicates that iron can be activated for these hydrocarbons by rapid cycling because mixing of the feed step change should be negligible at the periods used.

### *Polymerization reactions*

Although one of the earliest publications on periodic operation is a patent discussing the application to olefin polymerization over Ziegler-Natta catalysts (Claybaugh *et al* 1969) and the effect of concentration changes on molecular weight distribution have been known for some time (Laurence & Vasudevan 1968; Ray

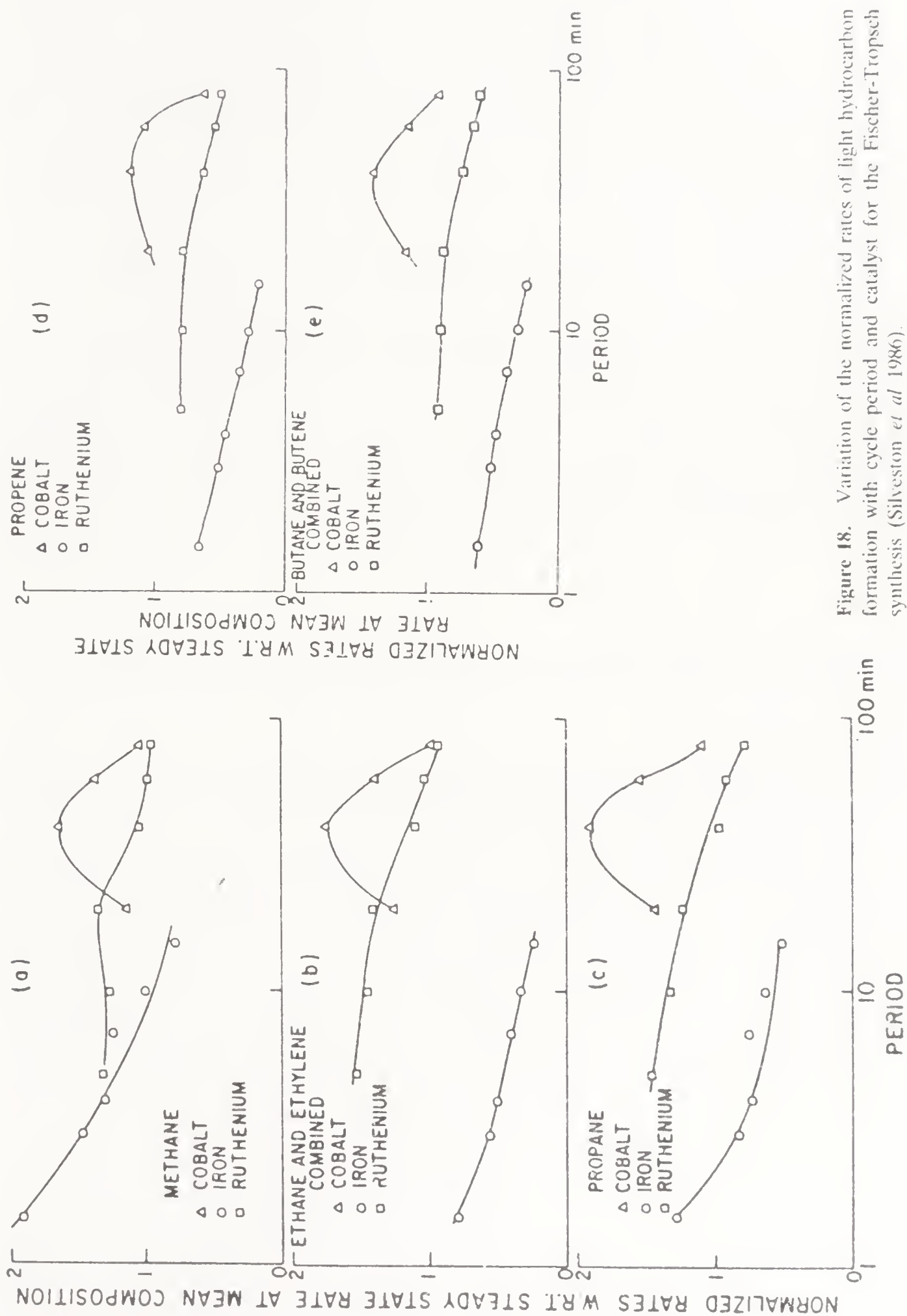


Figure 18. Variation of the normalized rates of light hydrocarbon formation with cycle period and catalyst for the Fischer-Tropsch synthesis (Silveston *et al* 1986).



1968), there appears to be just one experimental paper on the application of periodic operation to polymerization. Crone & Renken (1979) studied the polymerization of styrene in a toluene solvent using azo-*bis*-isobutylnitrile as the initiator. Measurements were made in continuous stirred tank reactors at 80°C. Periodic operation can be carried out in three ways: 1) both monomer and initiator concentrations can be varied, 2) monomer concentration can be held constant and initiator varied, and 3) initiator can be held constant and monomer varied. All three modes were used by Crone and Renken. Variations were achieved by halting the flow of monomer or initiator to the stirred reactor. Only the effect of period on performance was explored.

System activation is measured by monomer conversion and by the mean degree of polymerization. Crone and Renken found that monomer conversion increases above steady state if both monomer and initiator are varied periodically, but not for the other two modes of operation. The degree of polymerization was found to increase with cycle period for all three operational modes, but the largest increase occurred when just the monomer concentration was cycled. Both molecular weight distribution and conversion are influenced by periodic operation so Crone and Renken also compared the space-time yield of polymer having the same degree of polymerization and the same non-uniformity coefficient for steady state and periodic operation. Table 2 gives their results at different cycle periods.

## 5. Effect of cycling variables

In this section, we will summarize the experimental results outlined above with respect to those variables which have been studied the most to date.

### *Cycle period*

This variable has been found to affect reactor performance in all cases for which it has been considered. The resonance behaviour found in many of the experimental studies indicates its importance.

The term resonance has been used, perhaps, indiscriminately. If the analogy with electrical networks or structural systems is to be strictly followed, the term should be used only in cases where the periodic disturbance introduced in the gas phase interacts with the catalyst phase. Examples of this case are the multiple rate maxima shown in figure 16 for the oxidation of carbon monoxide over vanadia. Other possible cases are the hydrogenation of carbon monoxide over cobalt (figure 18), the hydrogenation of acetylene over nickel (figure 17) and sulphur dioxide

**Table 2.** Comparison of space-time polymer yields for the polymerization of styrene in toluene under steady state and periodic operation

Period (hours)	Ratio of steady state and periodic space time yields
0.5	1.04
3.0	1.18
4.0	1.23
6.0	1.45

Source: Crone & Renken (1979).

oxidation over vanadia (figure 9). In the remaining cases in which the rate or catalyst activity exhibits a maximum, the fall-off of activity at short cycle periods is the result of mixing in the reactor, while the fall-off at long periods results from the speed of the physico-chemical processes in the catalyst system. They are not strictly gas-solid interactions. Examples of these latter resonance cases are ammonia synthesis (figure 4), carbon monoxide oxidation over platinum (figure 13) and Fischer-Tropsch synthesis over iron (figure 18).

Perhaps the relaxed steady state whose existence in periodic operation is predicted by control theory occurs in situations where the resonance behaviour results from mixing in the reactor or this condition is obscured by such mixing. Wilson & Rinker (1982) claim to have found the relaxed steady state using periods of the order of several seconds (see figure 4). According to Bailey (1973, 1977), this state should be found when the cycle period is very much smaller than the physico-chemical relaxation time of the catalyst system. Jain's studies of relaxation after a step change (Jain 1982b; Li *et al* 1985) suggest that two processes occur with nitrogen pretreatment. The relaxation time of the fast process is about 5 minutes, while the time for the slow process is between 1 and 2 hours. With hydrogen pretreatment, the relaxation time appears to be several minutes. Thus, the experiments of Wilson and Rinker were carried out at periods consistent with the relaxed steady state. Mixing, even in their packed bed microreactor, seems to have interfered with the observation of that state.

### *Cycle amplitude*

This variable was examined in two studies: the oxidation of carbon monoxide and the oxidation of sulphur dioxide using the same vanadia catalyst. In the former, Abdul-Kareem *et al* (1980a) found an influence only in the resonance region and this was restricted to activity and not to the period at which the maximum rate was found (see figure 15). Jain *et al* (1982c) and Abdul-Kareem *et al* (1980b) found that amplitude had no effect on the time averaged rate versus period behaviour as may be seen in figure 16. Unni *et al* (1973) found a threshold effect, that is, a minimum amplitude for period to influence performance. Hudgins (1986) has pointed out that the threshold observation may be illusory and simply result from data scatter. Unni also observed a fall-off of activity at a high amplitude. However, just one data point led to this observation and this was taken at the unusual condition of alternating between reactants containing diluent and just oxygen or just sulphur dioxide.

The small effect of amplitude is surprising. Amplitude has a large effect on perceived catalyst activity in the quasi steady state, a limiting state for periodic operation: This is illustrated in figure 2a. Changing the end points in the figure causes a large change in the mean.

The quasi steady state performance depends uniquely on the shape of the steady state versus composition curve. If this curve is sharply convex as in figures 2a or 3, amplitude will have a large effect on the quasi steady state. On the other hand, if the curvature is small, the amplitude will have a negligible effect on performance. Hudgins (1986) observed that the carbon monoxide and sulphur dioxide oxidation experiments were carried out with compositions for which there is little curvature in the rate versus composition curve. He concluded that this may explain the small amplitude effect uncovered.



The discussion above has dealt only with symmetrical cycling ( $s = 0.5$ ). If cycling is asymmetrical, amplitude effects are confounded with cycle split. Experiments are still to be performed to untangle the effects of these two variables.

### *Cycle split*

Although cycle split has been varied in many experimental studies, a systematic study remains to be done. Often the amplitude and the time averaged reactant composition have varied concurrently with split. There are indications that it is an important variable. Cycle split is actually the variable in the Bilimoria & Bailey (1978) study of acetylene hydrogenation summarized in figure 17. Large differences in product mole fraction can be seen in figure 17a and this may reflect cycle split. In the discussion of the carbon monoxide hydrogenation experiments, it was mentioned that at a cycle split of 0.5 there was just a 10% increase in the time averaged methane formation rate above the comparable steady state rate, whereas in figure 18 the increase is about 90% when the cycle split is 0.7. There is also a significant cycle split effect in the ammonia synthesis data shown in figure 6. The maximum time averaged synthesis rate as well as the shape in the resonance region changes with a shift in the split from 0.4 to 0.6. Unfortunately, in the above data sets, amplitude varied as well as cycle split.

Cycle split is expected to be an important variable in periodic operation. It is well-known that the rates of elementary surface processes such as adsorption, surface diffusion and diffusion in the solid phase depended on the species involved. Similarly, reversible processes such as surface oxidation and reduction or crystallization will have different rates in the forward and reverse direction. The cycle split allows for these differences. It probably also allows for differences in adsorption equilibria which can result in near saturation of a surface by one reactant species and negligible adsorption of a second species under identical partial pressure and temperature.

### *Time averaged reactant composition*

Reactant composition affects the steady state rate. The time averaged composition would be expected to and does affect the periodic behaviour. Although not discussed in the previous section, Jain *et al* (1983a) examined the time averaged reactant composition effect on performance under periodic operation in the region surrounding the stoichiometric mixture. The period corresponding to the maximum in the synthesis rate seemed to depend on the mean composition, increasing as the hydrogen mole fraction increased. The maximum rate may also depend on composition, but Jain's data scatter and the relationship cannot be determined. There is also a composition effect in the CO oxidation data of Abdul-Kareem *et al* (1980a) shown in figure 15. It can be seen that as the CO/O<sub>2</sub> ratio increases from 0.36 to 0.86 the improvement in the catalyst activity declines until at 0.86 it becomes negligible.

## **6. Physical models for catalyst activity under periodic operation**

There appear to be at least three distinct models applicable to the various experimental observations discussed earlier. The observations of Briggs *et al* (1980)

are explained by periodic desorption of the sulphur trioxide product when the catalyst is flushed with air. The evidence for this is the sulphur trioxide level in the effluent after a switch from a reactant mixture to air is made. Further evidence is the large temperature fluctuations recorded in the bed after a composition switch is made. These are shown in figure 19.

Measurements were made with a reactor feed mixture from the burning of sulphur. The abscissa is dimensionless time. Both the air flushing and reactant mixture portions of the cycles are shown. In the former, temperature drops sharply after air is introduced because of sulphur trioxide desorption. The reactant mixture contains a large mole fraction of sulphur trioxide, hence adsorption occurs on the reverse switch and this appears as a sharp temperature rise.

Sulphur trioxide is strongly adsorbed by the vanadia catalyst and inhibits further oxidation at high sulphur dioxide conversions. Periodic operation simply strips the reaction product from the catalyst surface. The increase of rate in the half cycle after stripping more than compensates for the lapse in oxidation when the catalyst is flushed with air.

The product, carbon dioxide, is not strongly adsorbed on platinum, so another explanation for activity improvement must be sought for CO oxidation. Lynch (1984), responding to claims by Feimer *et al* (1982) and Jain *et al* (1983b) that adsorption/desorption models do not predict resonance, examined a continuous stirred tank reactor model which assumed that the dissociative adsorption of oxygen and the surface reaction between CO and O atoms are rate controlling. This model predicted a large increase in oxidation rate in a narrow range of periods, just as observed by Cutlip (1979) and shown in figure 13. It also predicted the double oxygen and carbon dioxide peaks shown in figure 14. Lynch's model

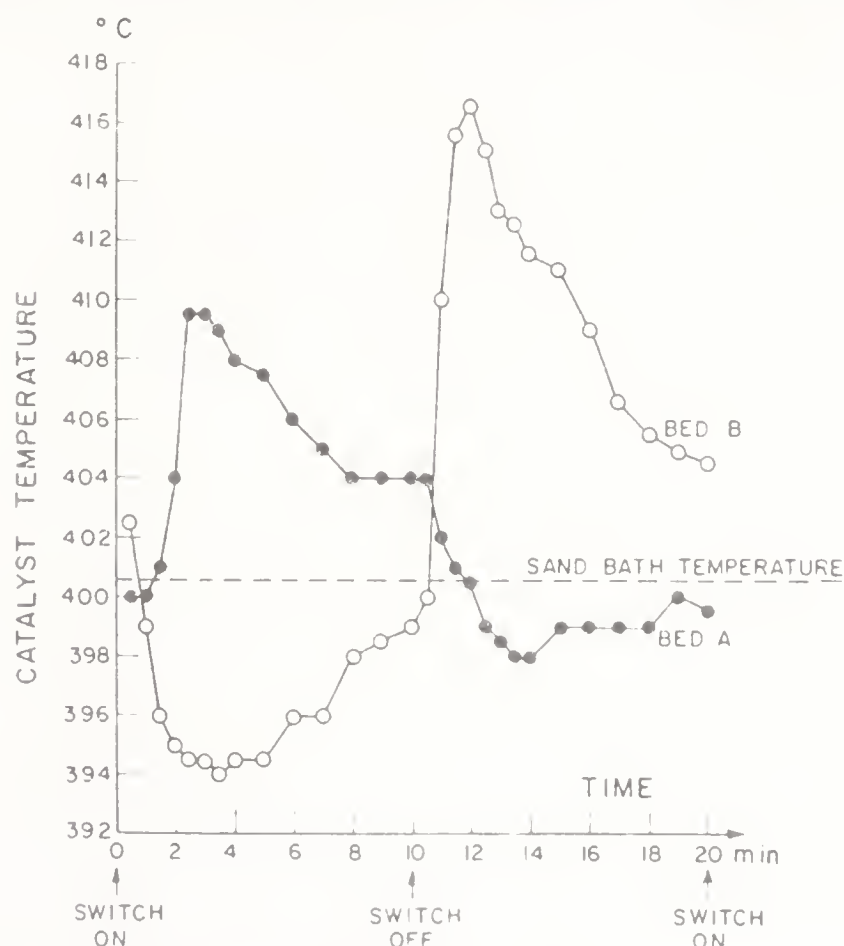


Figure 19. Temperature variation with time in the periodic operation of the second stage of a sulphur dioxide oxidation reactor (Briggs *et al* 1980).



predicts the existence of steady state multiplicity. Further investigations of the model show that the oxidation rates predicted under periodic operation result from a mixing of the upper and lower steady state rates. The maximum oxidation rate is always less than the rate at the upper steady state. The amplitudes used by Cutlip (1979) and Barshad & Gulari (1985) are partially or entirely within the region of steady state multiplicity. Consequently, improvements in activity observed experimentally for CO oxidation over platinum arise from periodically switching from the lower to the upper steady state.

The physical model behind Lynch's formulation is competitive adsorption on the catalyst surface, involving near-saturation by carbon monoxide as Cutlip supposed.

Steady state multiplicity is not found for CO oxidation over vanadia, for sulphur dioxide oxidation or for ammonia synthesis experiments discussed earlier. With the sulphur dioxide system, the 4-hour period associated with the rate maximum suggests that any explanation of resonance must involve diffusion in the melt phase known to exist with this catalyst (Unni *et al* 1973). Step change experiments with the iron ammonia synthesis catalyst indicated ammonia production for over an hour after the reactor feed had been switched from a synthesis mixture to hydrogen (figure 20). This is explained by the dissolution of atomic nitrogen in the iron catalyst (Jain *et al* 1982b). Hydrogen storage in the catalyst or on its surface was also indicated.

Catalyst activation can be explained then by assuming that the surface is blocked by nitrogen or reaction intermediate adatoms. Periodic pulsing with hydrogen strips the surface of these adatoms and utilizes the dissolved nitrogen stored in the catalyst bulk. In the other portion of the cycle, the hydrogen adatoms are consumed and the bulk nitrogen is replenished (Jain *et al* 1982b; Li *et al* 1985).

Recently, the physical explanation above was incorporated in a mathematical model which closely predicted the periodic operation observations of Jain *et al* (1983a). An essential part of Li's model was a lumped parameter resistance

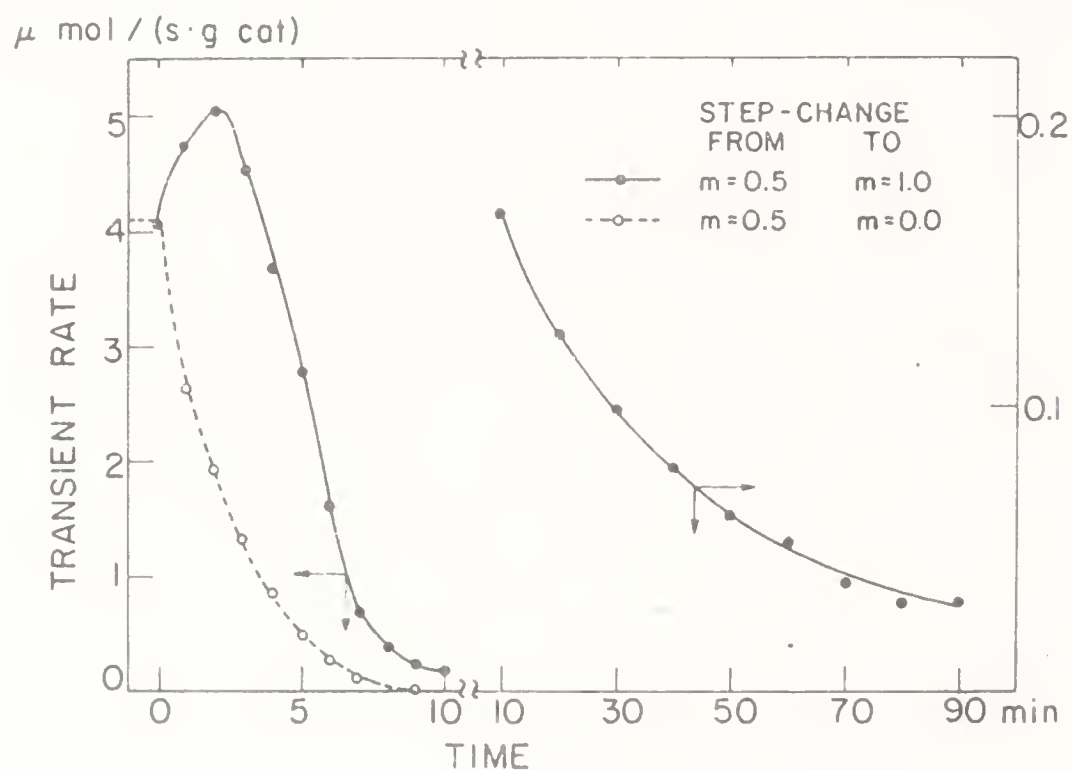


Figure 20. Ammonia production after a step change from a synthesis mixture to one of the reactants for a commercial ammonia synthesis catalyst at 400°C and 2.38 MPa (Jain *et al* 1982b).

controlling the movement of nitrogen atoms from storage to the active catalyst surface (Li *et al* 1985). It was not necessary to specify the location of storage in this model.

A version of Li's storage model was devised to reflect the assumed redox mechanism of sulphur dioxide oxidation over vanadia. The model predicted a resonance effect for this oxidation, but did not predict Unni's observations closely (Li *et al* 1986). It seems that storage models of the kind described above explain the resonance behaviour seen for redox catalysts (CO oxidation over vanadia) and the Fischer-Tropsch synthesis with cobalt and ruthenium catalysts.

There may be still other explanations. Feimer *et al* (1985) are able to predict the performance under periodic operation for C<sub>2</sub>+ products by adsorption/desorption models. However, a second pathway to methane that is activated by periodic operation must be assumed to explain the behaviour observed for this species. The multiple rate maxima seen for CO oxidation over vanadia (figure 16) remain to be explained, although Jain *et al* (1983b) have offered modelling suggestions.

## 7. Conclusions

This review of experimental studies of single and multiple reaction systems under periodic operation demonstrates that large increases in catalyst activity are possible. Only one system reported in the literature did not show a positive effect owing to this mode of reactor operation. The improvement achievable depends on cycle period, cycle split and the time averaged reactant composition. The role of cycle amplitude is uncertain.

Explanations of the effects observed experimentally require storage of a reactant species under conditions in which it cannot react directly or they require adsorption inhibition.

This paper is dedicated to Dr L K Doraiswamy on his sixtieth birthday. Preparation of this manuscript was assisted by funds from an operating grant of the Natural Sciences and Engineering Research Council of Canada.

## References

- Abdul-Kareem H K, Silveston P L, Hudgins R R 1980a *Chem. Eng. Sci.* 35: 2077-84
- Abdul-Kareem H K, Jain A K, Silveston P L, Hudgins R R 1980b *Chem. Eng. Sci.* 35: 273-282
- Adesina A A, Hudgins R R, Silveston P L 1986 *Can. J. Chem. Eng.* 64: 447-54
- Al-Taie A S, Kerschenbaum 1978 *ACS Symp. Series* 65: 512-25
- Bailey J E 1973 *Chem. Eng. Commun.* 1: 111
- Bailey J E 1977 in *Chemical reactor theory* (eds) L Lapidus and N R Amundson (Englewood Cliffs, NJ: Prentice Hall) pp. 758-813
- Bailey J E, Horn F J M 1969 *Ber. Bunsenges. Phys. Chem.* 73: 274-9
- Bailey J E, Horn F J M 1972 *Chem. Eng. Sci.* 27: 109-19
- Barshad Y, Gulari E 1985 *AIChEJ* 31: 649-58
- Bilimoria M R, Bailey J E 1978 *ACS Symp. Series* 65: 526-36
- Boreskov G K, Matros Yu Sh 1983 *Catal. Rev.-Sci. Eng.* 25: 551-590
- Briggs J P, Hudgins R R, Silveston P L 1977 *Chem. Eng. Sci.* 32: 1087-92
- Briggs J P, Kane D M, Hudgins R R, Silveston P L 1980 *Proc. 1st Int. Waste Treatment and Utilization Conf.*, Univ. of Waterloo, Waterloo, Ontario, Canada, pp. 521-33

- Carbova V R, Gau G 1983 *Can. J. Chem. Eng.* 61: 200-7
- Cho B K, West L A 1984 "Cyclic operation of Pt/Al<sub>2</sub>O<sub>3</sub> catalysts for CO oxidation", Research Publication GMR-4738, General Motors Research Laboratories, Warren, Michigan
- Claybaugh B E, Griffin J R, Watson A T 1969 US 3, 472, 829
- Contractor R M, Bergna H E, Horowitz H S, Blackstone C M, Malone B, Toradi C C, Griffiths B, Chowdhry U, Sleight A W 1986 "Butane oxidation to maleic anhydride over vanadium phosphate catalysts", preprint of contribution to the European Workshop on Selective Oxidation, Brussels, Belgium
- Crone G, Renken A 1979 *Ger. Chem. Eng.* 2: 337-42
- Cutlip M B 1979 *AIChEJ* 25: 502-8
- El Masry H 1985 *Appl. Catal.* 16: 301-13
- Feimer J L, Jain A K, Hudgins R R, Silveston P L 1982 *Chem. Eng. Sci.* 37: 1797-805
- Feimer J L, Silveston P L, Hudgins R R 1985a *Can. J. Chem. Eng.* 63: 86-92
- Feimer J L, Silveston P L, Hudgins R R 1985b *Can. J. Chem. Eng.* 63: 481-9
- Fiolitakis E, Schmid M, Hofmann H, Silveston P L 1983 *Can. J. Chem. Eng.* 61: 703-9
- Horn F J M, Bailey J E 1968 *J. Opt. Theo. Appl.* 2: 441-449
- Hudgins R R 1986 "Lecture notes on selected experimental studies of cycling operation of catalytic reactors", ENSIC, Univ. Nancy, Nancy, France
- Hugo A J, Jakelski D M, Stanitsas G, Sullivan G R, Hudgins R R, Silveston P L 1986 *Can. J. Chem. Eng.* 64: 349-51
- Jain A K, Hudgins R R, Silveston P L 1982a *ACS Symp. Ser.* 196: 97-107
- Jain A K, Hudgins R R, Silveston P L 1982b *Can. J. Chem. Eng.* 60: 809-11
- Jain A K, Hudgins R R, Silveston P L 1983a *Can. J. Chem. Eng.* 61: 824-832
- Jain A K, Hudgins R R, Silveston P L 1983b *Can. J. Chem. Eng.* 61: 46-9
- Jain A K, Hudgins R R, Silveston P L 1985 *Can. J. Chem. Eng.* 63: 166-9
- Jain A K, Silveston P L, Hudgins R R 1982c *ACS Symp. Ser.* 178: 267-275
- Laurence R L, Vasudevan G 1968 *Ind. Eng. Chem., Process Des. Dev.* 7: 427
- Li C-Y, Hudgins R R, Silveston P L 1985 *Can. J. Chem. Eng.* 63: 803-9
- Li C-Y, Hudgins R R, Silveston P L 1986 *Can. J. Chem. Eng.* (submitted)
- Lynch D T 1984 *Chem. Eng. Sci.* 39: 1325-8
- Matsumura M, Nishimura Y, Takahashi N 1973 *Chem. Eng. Sci.* 28: 1369-1377
- Nappi A O, Fabbicino L, Hudgins R R, Silveston P L 1985 *Can. J. Chem. Eng.* 63: 963-70
- Prokopowicz R A, Silveston P L, Hudgins R R, Irish D E 1986 *J. Catal.* (submitted)
- Rambeau G, Amariglio H 1981 *Appl. Catal.* 1: 291
- Rambeau G, Amariglio H 1982 *Appl. Catal.* 3: 273
- Ray W H 1968 *Ind. Eng. Chem., Process Des. Dev.* 7: 422-6
- Renken A, Mueller M, Wandrey C 1976 *Proc. 4th Int. Symp. Chem. Reaction Eng., Heidelberg, Germany* 3: 107-16
- Ross G S, Hudgins R R, Silveston P L 1986 *Can. J. Chem. Eng.* (accepted for publication)
- Schlatter J C, Sinkevitch R M, Mitchell P J 1983 *Ind. Eng. Chem. Prod. Res. Dev.* 22: 51
- Silveston P L, Hudgins R R 1981 *Environ. Sci. Technol.* 15: 419-22
- Silveston P L, Forrissier M 1985 *Ind. Eng. Chem. Process Des. Dev.* 24: 320-5
- Silveston P L, Hudgins R R, Adesina A A, Ross G S, Feimer J L 1986 *Chem. Eng. Sci.* 41: 923-8
- Taylor K C, Sinkevitch R M (1983) *Ind. Eng. Chem., Prod. Res. Dev.* 22: 45-50
- Unni M P, Hudgins R R, Silveston P L 1973 *Can. J. Chem. Eng.* 31: 623-9
- Wilson D H, Rinker R G 1982 *Chem. Eng. Sci.* 37: 343-355



# Classification of three-phase reactors

A TSUTSUMI, Y H KIM, S TOGAWA and K YOSHIDA

Department of Chemical Engineering, University of Tokyo,  
7-3-1 Hongo, Bunkyo-ku, Tokyo 113, Japan

**Abstract.** Cocurrent upward three-phase reactors with discontinuous gas phase can be classified into three types according to axial profile of solid concentration. These are: gas-sparged slurry reactors, three-phase bubble columns and three-phase fluidized beds. A map to characterize these three types of reactors was obtained as a function of both particle size and difference between densities of solid and liquid.

**Keywords.** Classification; three-phase reactors; gas-sparged slurry reactor; three-phase bubble column; three-phase fluidized bed.

## 1. Introduction

Gas-liquid-solid three-phase reactions are of great importance in chemical, petrochemical and biochemical processing and are carried out in various types of reactors. All the reactors have been studied comprehensively to elucidate mixing phenomena, heat and mass transfer mechanisms, and performance of some chemical reactions. The data so far obtained showed that the hydrodynamic characteristics of three-phase reactors are strongly dependent on flow directions, gas and liquid flow rates, geometric aspects, and physical properties of the solids and the liquids used.

This paper, therefore, proposes an idea for classifying various types of three-phase reactors into three categories based on the differences in hydrodynamic behaviour and to test its validity by both experimental study and analysis of published data.

## 2. Former studies

Epstein (1981) presented a taxonomy for three-phase fluidization according to the difference in operation modes such as flow directions of gas and liquid and in contacting patterns between particles and the surrounding gas and liquid, as shown in figure 1. Three-phase fluidized beds are simply divided into two categories, namely, cocurrent and countercurrent beds. Similar classification is possible for



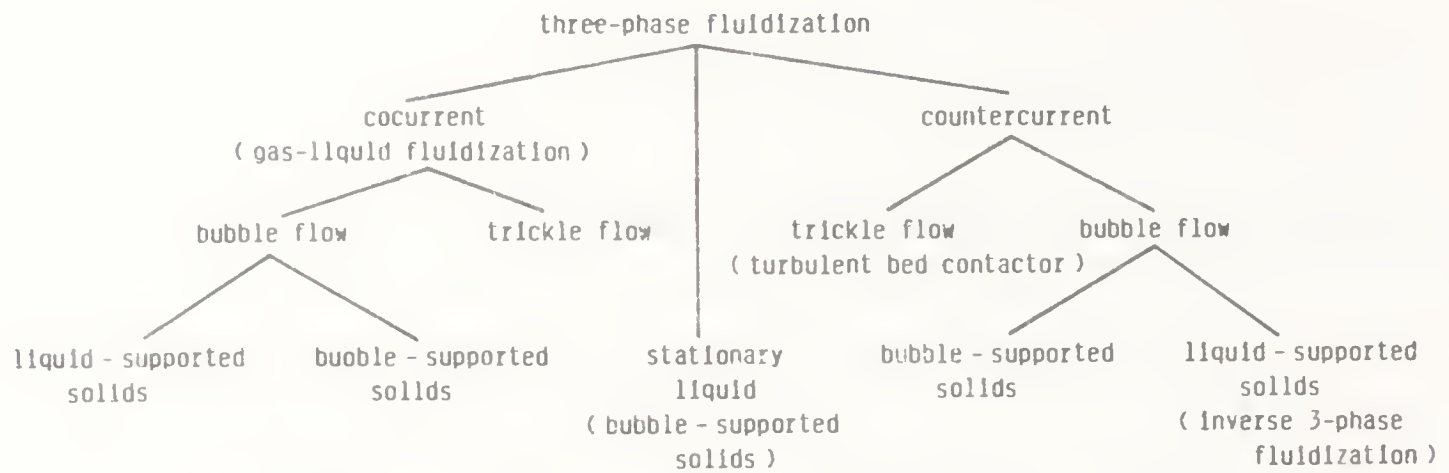


Figure 1. Taxonomy of three-phase fluidized beds (after Epstein 1981).

bubble column slurry reactors. This method is quite useful to pigeonhole many papers concerned with three-phase reactors but gives little information about mixing or transport properties.

It is very common to divide many types of reactors into two categories. The criteria and the definition are listed in table 1.

Farkas & Leblond (1969) pointed out early that the bubble column reactor is to be distinguished from the usual fluidized bed in that the gas does not lift and suspend the solid particles merely by its upward motion.

Epstein (1981) stated that three-phase bubble fluidization is distinguishable from bubble column slurry operation only in its use of large and/or heavier particles, which are not subject to the hydraulic transport characteristics of slurry operation when the liquid is moving.

Muroyama & Fan (1985) distinguished the three-phase fluidized-bed reactor from the gas-sparged slurry reactor. In the gas-sparged slurry reactor, the size of the solid particle is usually less than  $100\ \mu\text{m}$  in diameter, the volumetric fraction of the solids is less than 0.1, and particles are maintained in a suspended state by bubble agitation. In the three-phase fluidized bed, the particle size is relatively large, normally greater than  $200\ \mu\text{m}$ , and the volumetric fraction of the solid particles varies from 0.6 (packed state) to 0.2 (close to the dilute transport state). The particles are supported by the liquid phase and/or the gas phase. The bed of particles may expand non-uniformly with elutriation as in gas-solid fluidized beds, or it may expand uniformly without elutriation as in liquid-solid fluidized beds while the bubbles intensify the mixing of the solid particles.

Pandit & Joshi (1986) stated that the three-phase sparged reactors should be called gas-liquid-solid fluidized bed or slurry reactors, respectively, corresponding to batchwise or continuous mode of operation for solid particles. They further divided the behaviour of three-phase reactors into four regions according to the effects of particle size and solid concentration on bubble diameter.

In this manner, considerable discrepancy can be recognized in spite of many papers and the necessity of more definite criteria for classification remains.

### 3. Proposed method

For simplifying the discussion, only the case for cocurrent up-flow of both liquid and gas with  $\rho_s > \rho_l > \rho_g$  is considered. Among many modes of operation, this case appears to be the most important in industrial application.

Table 1. Classification of three-phase reactors

Investigator(s)	Reactor name and characteristics	
Østergaard (1968, p. 71)	<i>Bubble column slurry reactor</i> Fine particles with diameter of the order of 0.01 mm Momentum is transferred to the liquid phase by the movement of gas bubbles	<i>Gas-liquid fluidized bed</i> Relatively large particles < 6 mm  The liquid flows upwards through a bed of solid particles which is fluidized by the flowing liquid, while the gaseous phase moves as discrete bubbles through the liquid-fluidized bed
Epstein (1981)	<i>Bubble column slurry reactor</i>  Three-phase bubble fluidization is distinguishable from bubble column slurry only in its use of larger and/or heavier particles.	<i>Three-phase fluidized bed</i>
Kojima & Asano (1981, p. 79)	<i>Suspension-bubble column</i> $d_p < 1$ mm	<i>Gas-liquid fluidized bed</i> $d_p = 1 - 6$ mm Uniform solid distribution in the bed
Deckwer & Schumpe (1984)	<i>Slurry bubble column</i> Fluidization by gas induced liquid motion alone $d_p < 50$ $\mu$ m uniform distribution model $50 < d_p < 500$ $\mu$ m sedimentation-dispersion model	<i>Three-phase fluidized bed</i> Fluidization of large and heavy particles additionally requires cocurrent liquid flow $d_p > 1$ mm
Muroyama & Fan (1985)	<i>Gas-sparged slurry column</i> $d_p < 100$ $\mu$ m $\phi < 0.1$ Particles are maintained in suspended state by bubble agitation. Particles are carried in and out by the liquid stream.	<i>Gas-liquid-solid fluidized bed</i> $d_p > 200$ $\mu$ m $\phi = 0.2 - 0.6$ Particles are supported by the liquid phase and/or the gas phase Particles are supplied or withdrawn independently of the liquid stream
Darton (1985)	<i>Slurry reactor</i> $d_p < 0.5$ mm $\phi > 0.1$ Solid is suspended by flow of liquid Solid concentration gradient exists	<i>Three-phase fluidized bed</i> $d_p = 0.1 - 5$ mm $\phi = 0.1 - 0.5$ Solid is suspended by flow of gas no solid concentration gradient
Kato <i>et al</i> (1985)	<i>Bubble column with suspended solid particles</i> Operation with continuous feed and discharge of solid particles The terminal velocity of solid particles is smaller than bubble rising velocity	<i>Three-phase fluidized bed</i>  Batch operation of solid particles  The terminal velocity of solid particles exceeds several $\text{cm} \cdot \text{s}^{-1}$
Pandit & Joshi (1986)	<i>Slurry reactor</i> Solid phase is continuous	<i>Gas-liquid-solid fluidized bed</i> Solid phase is batchwise

### 3.1 Fluid dynamics

In table 1, there is general agreement that larger and/or heavier particles are used in three-phase fluidized bed than in slurry bubble column reactors. In the case of very large and/or heavy particles the bed consists of the upper dilute region (freeboard) and the lower dense region where the solid distribution is uniform. As the size and density of particles decrease, the entrainment of particles into the freeboard due to the rising gas bubbles is appreciable and particles get dispersed throughout the reactor, but the solid concentration, in general, decreases exponentially with axial height. The particles are suspended by momentum transferred from the gas phase to the solid phase via the liquid medium. When very small and/or light particles are used, the effect of settling velocity becomes insignificant. A uniform distribution over the reactor is expected and the solid dispersion coefficient is very close to that of the liquid.

As mentioned above, according to the axial profile of solid concentration, three-phase reactors may be divided into three categories: (a) gas-sparged slurry reactors, (b) three-phase bubble columns, and (c) three-phase fluidized beds, as shown in figure 2.

Most researchers used quite a few kinds of particles for studying hydrodynamic behaviour, so that experimental conditions were not enough to distinguish between three types of reactors. For instance, Kojima & Asano (1981, p. 79) and Deckwer & Schumpe (1984) made no distinction between gas-sparged slurry reactors and three-phase bubble columns, while Muroyama & Fan (1985) and Darton (1985, p. 495) did not distinguish three-phase bubble columns from three-phase fluidized beds.

### 3.2 Description of the three types of reactors

**3.2a Gas-sparged slurry reactors:** Particles are uniformly distributed over the reactor even for low gas velocity and the relative velocity between liquid and solid particles is almost zero. This system can be treated as a two-phase system by regarding the suspension as a pseudo-homogeneous phase. The slurry is agitated by turbulence induced by rising gas bubbles.

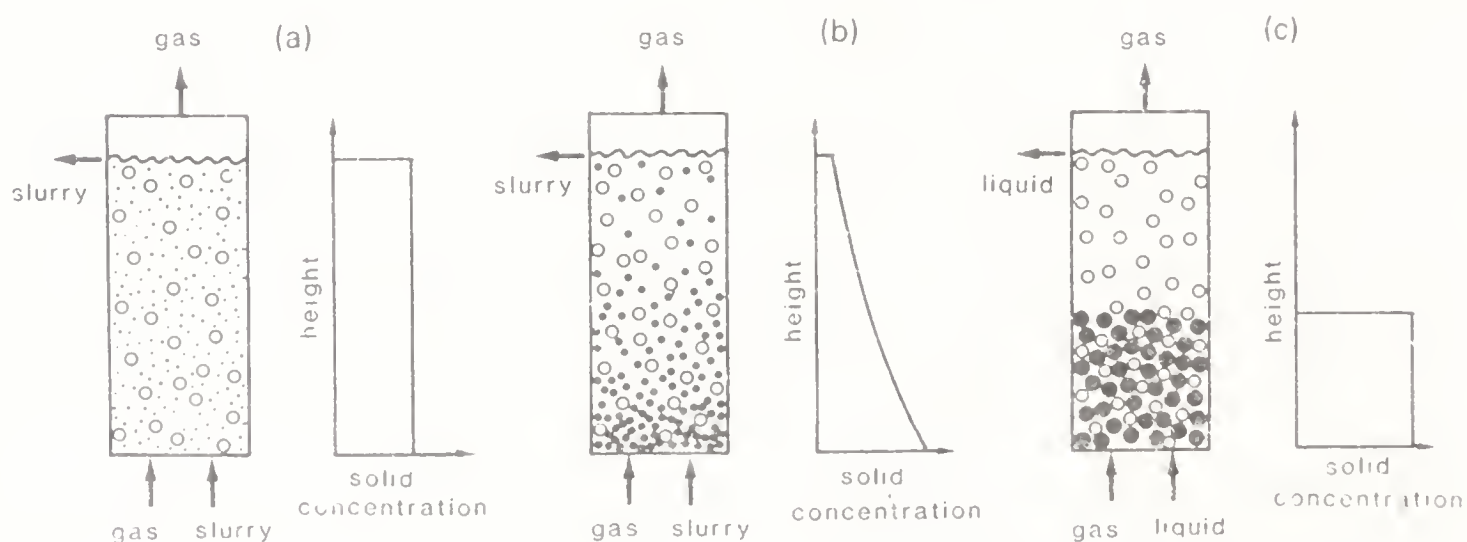


Figure 2. Three types of three-phase reactors, a. gas-sparged slurry reactor; b. three-phase bubble column; c. three-phase fluidized bed



3.2b *Three-phase bubble columns*: Particles, on the average, tend to sink, but are pushed upwards by the liquid flow which is also agitated by gas bubbles. Thus, a gradual decrease of solid concentration is found from the bottom to the top of reactor. The solid particles are suspended by the gas-induced liquid motion. The three-phase bubble column is designed such that the movement of particles by gravity is dominant in comparison with that by liquid turbulence due to the rising gas bubbles. The particles can be operated in either a batch or continuous manner.

3.2c *Three-phase fluidized beds*: The bed is divided into two regions. One is a lower dense region with concentrated solid particles and the other is an upper solid-free region. Solid distribution in the lower region is fairly uniform. Solid particles are fluidized by the upward flow of both gas and liquid phases directly, although the liquid phase is mainly responsible for maintaining the state of suspension. The liquid flows upwards through the bed of solid particles which is fluidized by the flowing liquid, while the gaseous phase moves as discrete bubbles through the liquid-fluidized bed. The solid operation is usually batchwise.

#### 4. Experimental

A flow diagram of the experimental setup is shown in figure 3. The main column made of transparent acrylic resin was 0.186 m in diameter and 2.5 m in height. The gas distributor was a copper perforated plate with 126 holes of diameter 1.0 mm. Taps for taking slurry samples were located along the column wall at 0.1 m intervals. Water and air were used as liquid and gas media respectively. Glass beads of 10 sizes ( $\rho_s = 2500 \text{ kg} \cdot \text{m}^{-3}$ ) and alumina particles of 8 sizes ( $\rho_s = 1664\text{--}2053 \text{ kg} \cdot \text{m}^{-3}$ )

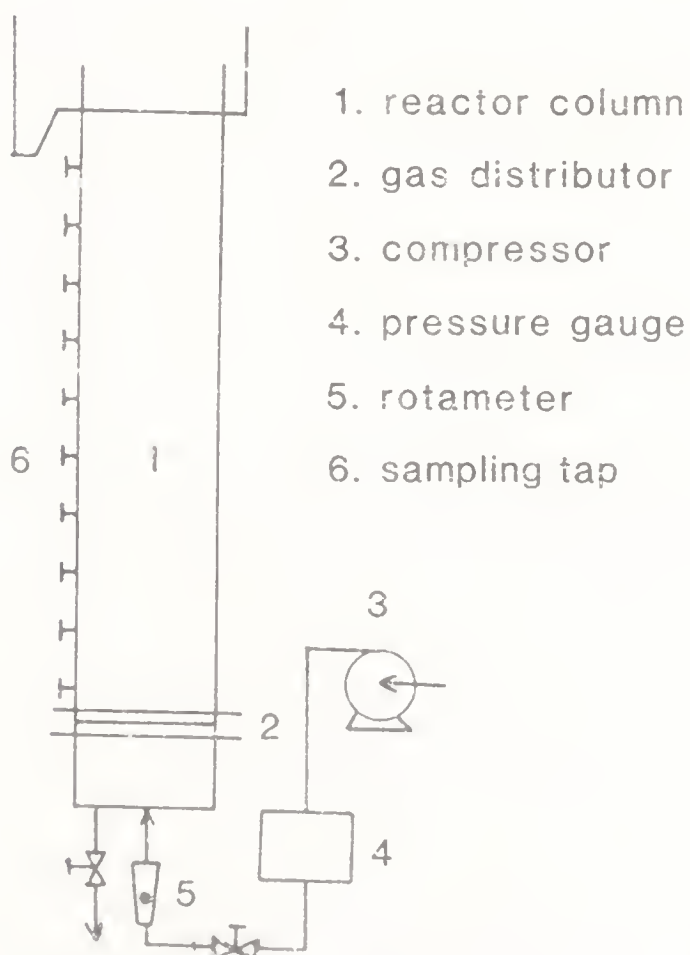


Figure 3. Flow sheet of experimental apparatus.



were suspended. The superficial gas velocity ranged from  $0.01$  to  $0.2 \text{ m} \cdot \text{s}^{-1}$ . After reaching a steady state slurry samples were taken out through the taps and weighed. Then the solid concentration was determined by drying and weighing the residue

## 5. Results and discussion

### 5.1 Axial distribution of solid concentration

Figure 4 shows the representative solid concentration data as a function of axial position of the column for glass beads of five particle sizes. Particles of diameter  $17$  and  $88 \mu\text{m}$  were distributed almost uniformly throughout the column. For particles above  $180 \mu\text{m}$ , gradual decrease of solid concentration from the bottom to top of the reactor was observed. In the case of particles larger than  $500 \mu\text{m}$ , there were unsuspended particles even at large gas velocity and the concentration of solid at

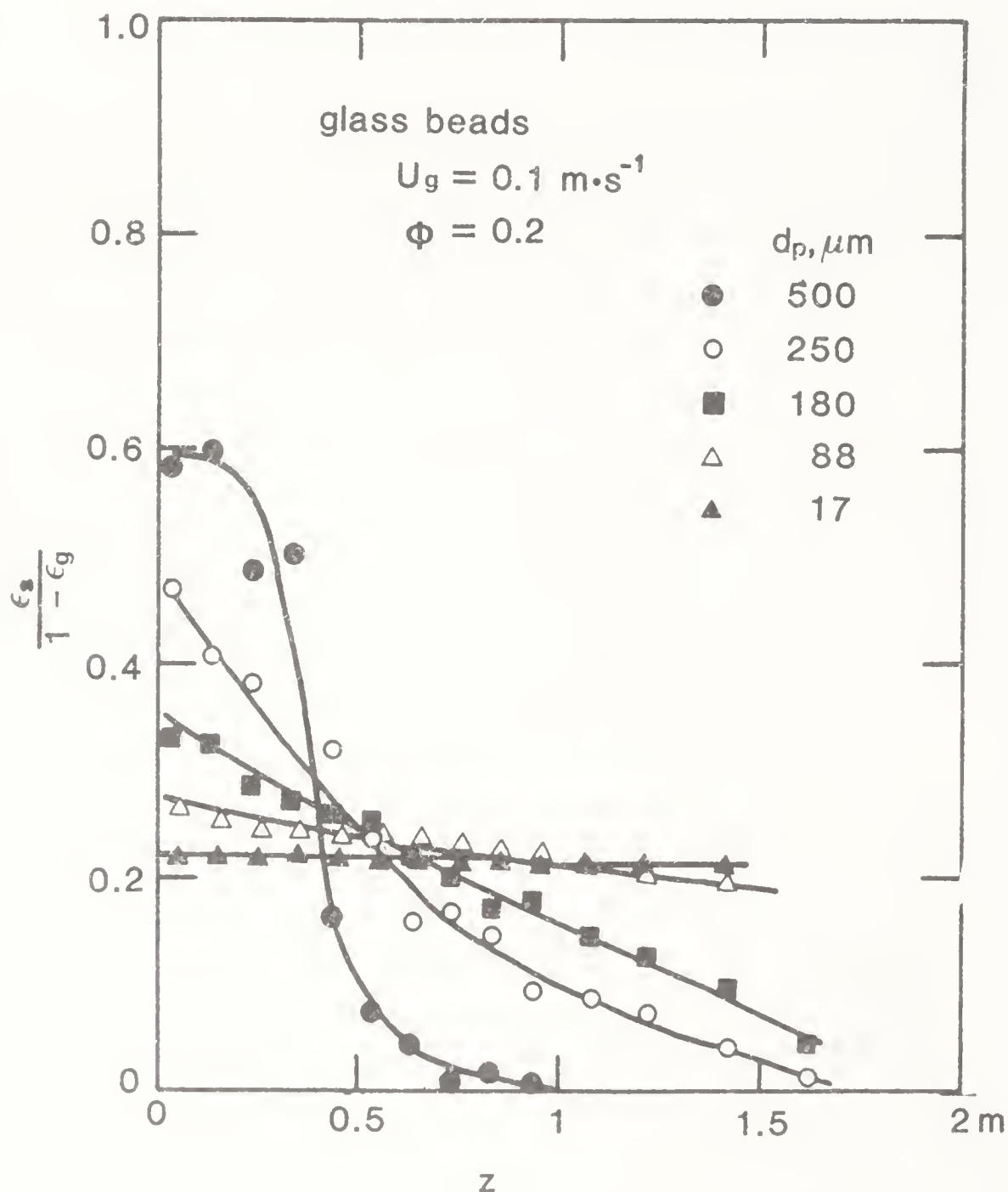


Figure 4. Solid concentration profiles for glass beads.

the top of the column was almost zero. The bed could be clearly divided into lower dense and upper lean regions by visual observation. Thus the criteria for three types of air-water-glass beads systems can be obtained as follows: gas-sparged slurry reactor,  $d_p < 180 \mu\text{m}$ ; three-phase bubble column  $180 < d_p < 500 \mu\text{m}$ ; three-phase fluidized bed,  $500 \mu\text{m} < d_p$ .

### 5.2 Effect of density

Figure 5 shows the profiles of solid concentration for alumina particles. A three-phase bubble column was formed when the particle size was  $700 \mu\text{m}$  as compared to the occurrence of fluidization for glass beads of the same size. Particle density was found to be an important factor for determining the type of three-phase systems.

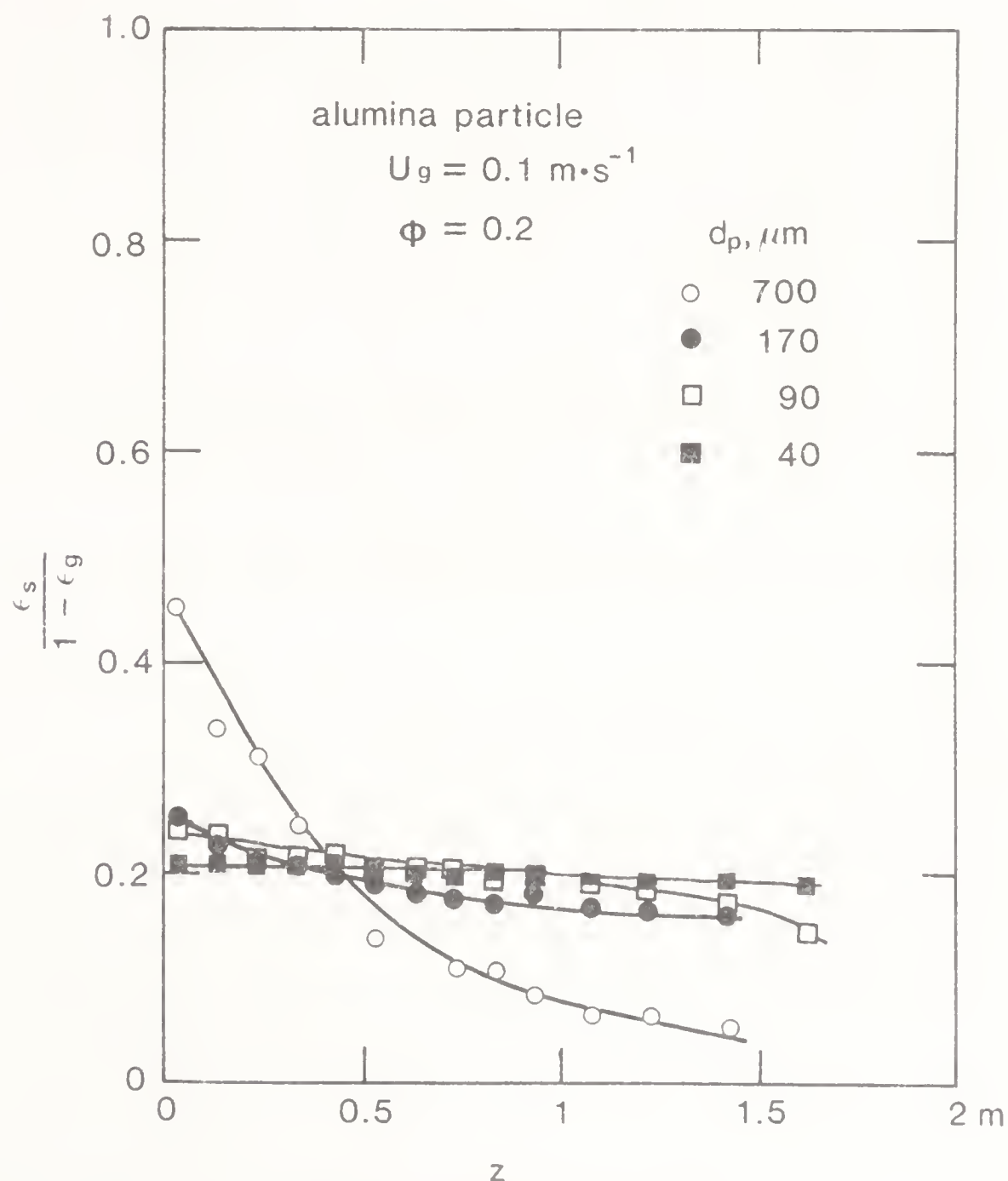


Figure 5. Solid concentration profiles for alumina particles.

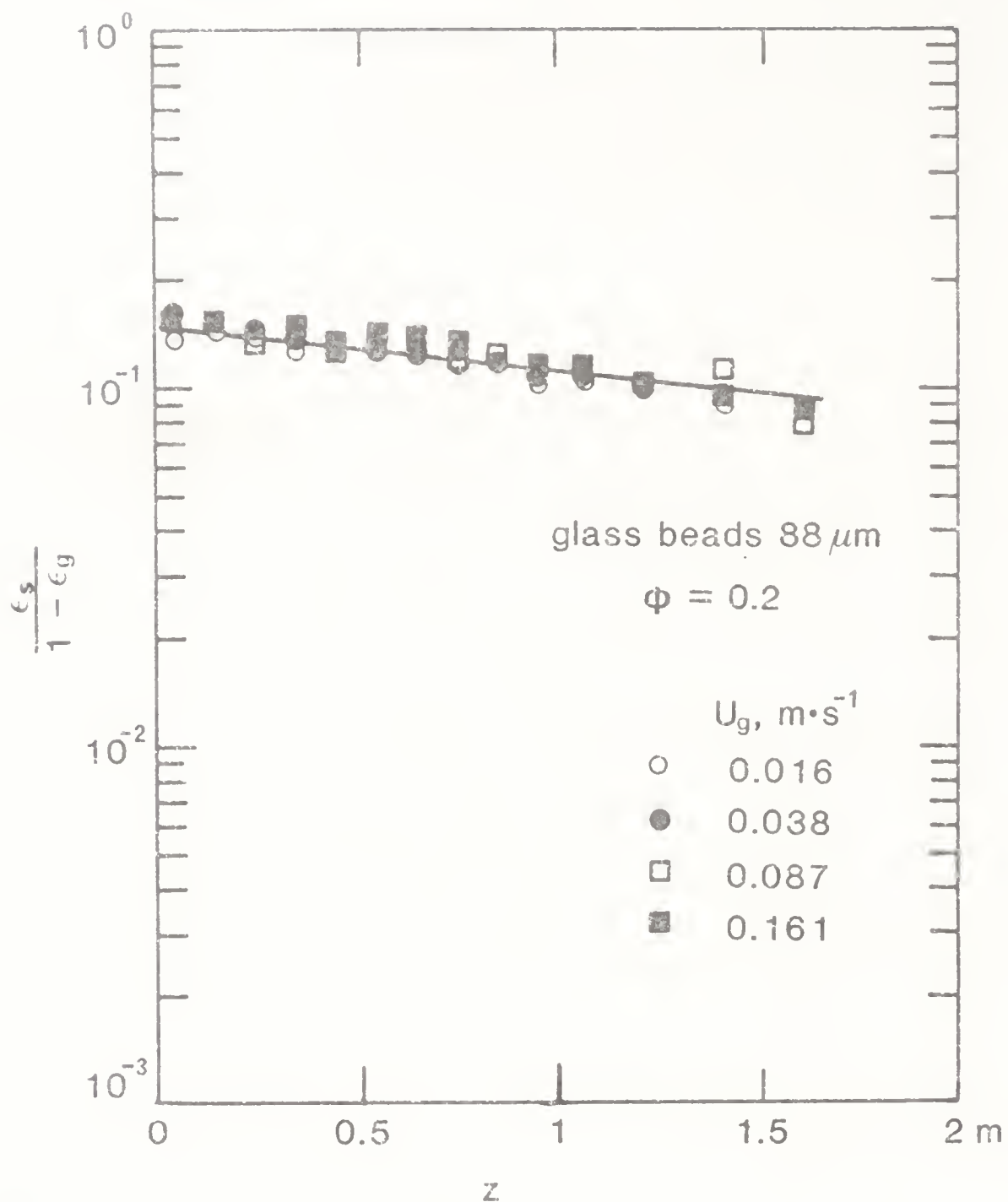


Figure 6. Effect of gas velocity on solid concentration profile for 88  $\mu\text{m}$  glass beads.

### 5.3 Effects of gas velocity and solid content

Solid concentration profiles are related to gas velocity, as shown in figures 6 and 7. In the regime of the gas-sparged slurry reactor, solid concentration profiles were little affected by gas velocity, as shown in figure 6. Even at low gas velocities all the particles were well-suspended. On the other hand, as the loading of solid particles increased, an unsuspended zone was formed just above the distributor, when particle size was larger than 180  $\mu\text{m}$  and the gas velocity was low, as shown in figure 7. Besides, the increase of solid content reduced the settling velocity of particles, resulting in more uniform concentration profile of solids, as shown in figure 8. The transition therefore, from bubble column regime to gas-sparged slurry regime is expected to occur with increase in gas velocity and solid content. It is, however, very hard to clearly distinguish between these two regimes only from the profiles of solid concentration.

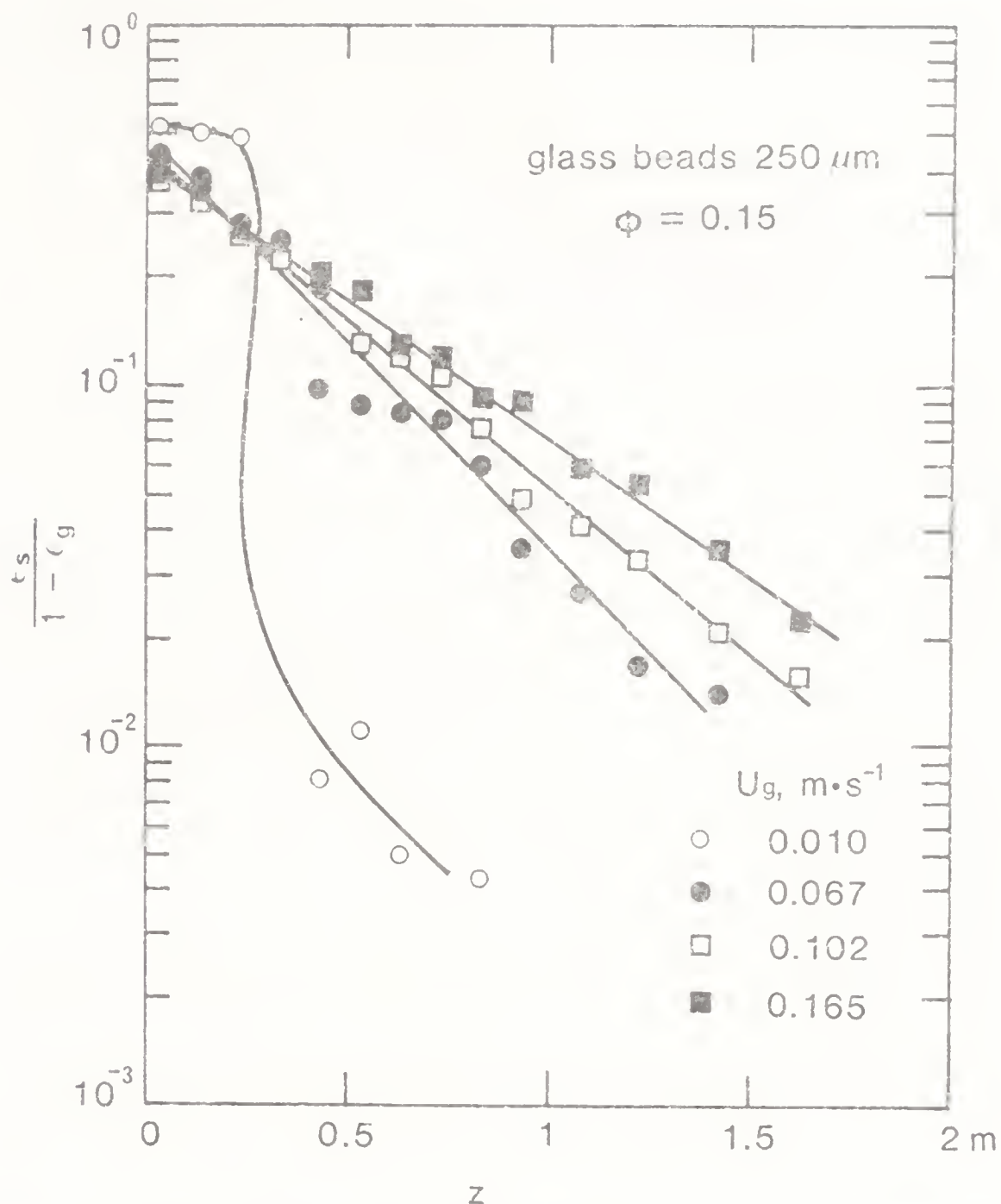


Figure 7. Effect of gas velocity on solid concentration profile for 250  $\mu\text{m}$  glass beads.

#### 5.4 Map for classifying reactor types

As described in the preceding sections, the size and density of solid particles have a great effect on their axial distribution in the reactors. In addition, both the liquid and gas velocities are relatively low in cocurrent upflow operations even in the case of three-phase fluidization, and consequently have small influence on solid dispersion. Thus, three regimes of reactor types may be characterized by density difference ( $\rho_s - \rho_l$ ) and mean particle size. Experimental data on the mode of solid concentration profile of the present work were plotted in relation to these two factors, as shown in figure 9. In this figure, the values of these two factors obtained from many authors who have commented on the mode of solid profile are also plotted. It is shown that cocurrent upward three-phase reactors are classified into three domains, where the boundary between (b) and (c) is clear, while the boundary between (a) and (b) has some overlaps. They should be explained by taking the effects of gas and liquid velocities and solid content into account.

Figure 10 shows the typical operation conditions used in industrial applications of



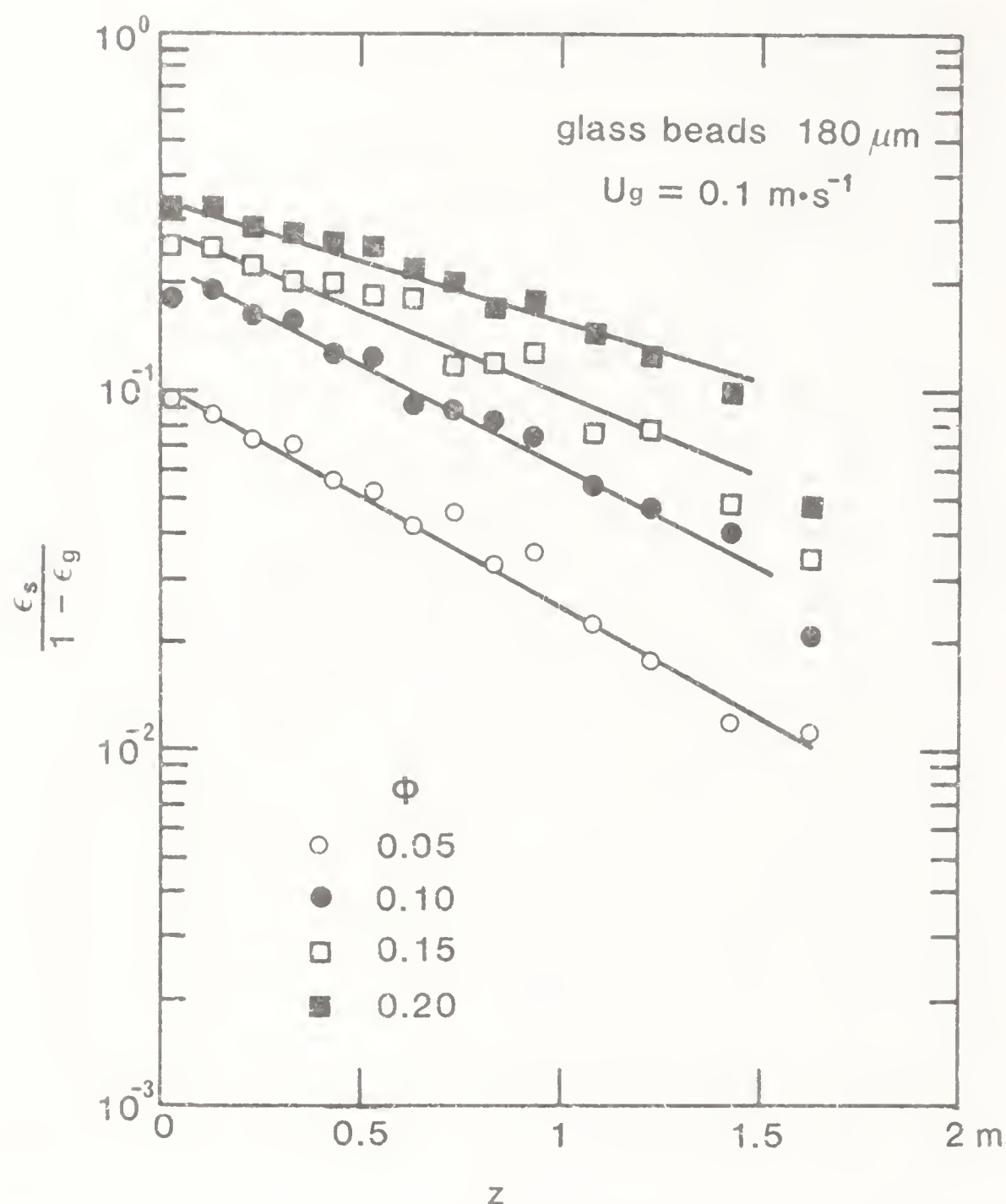
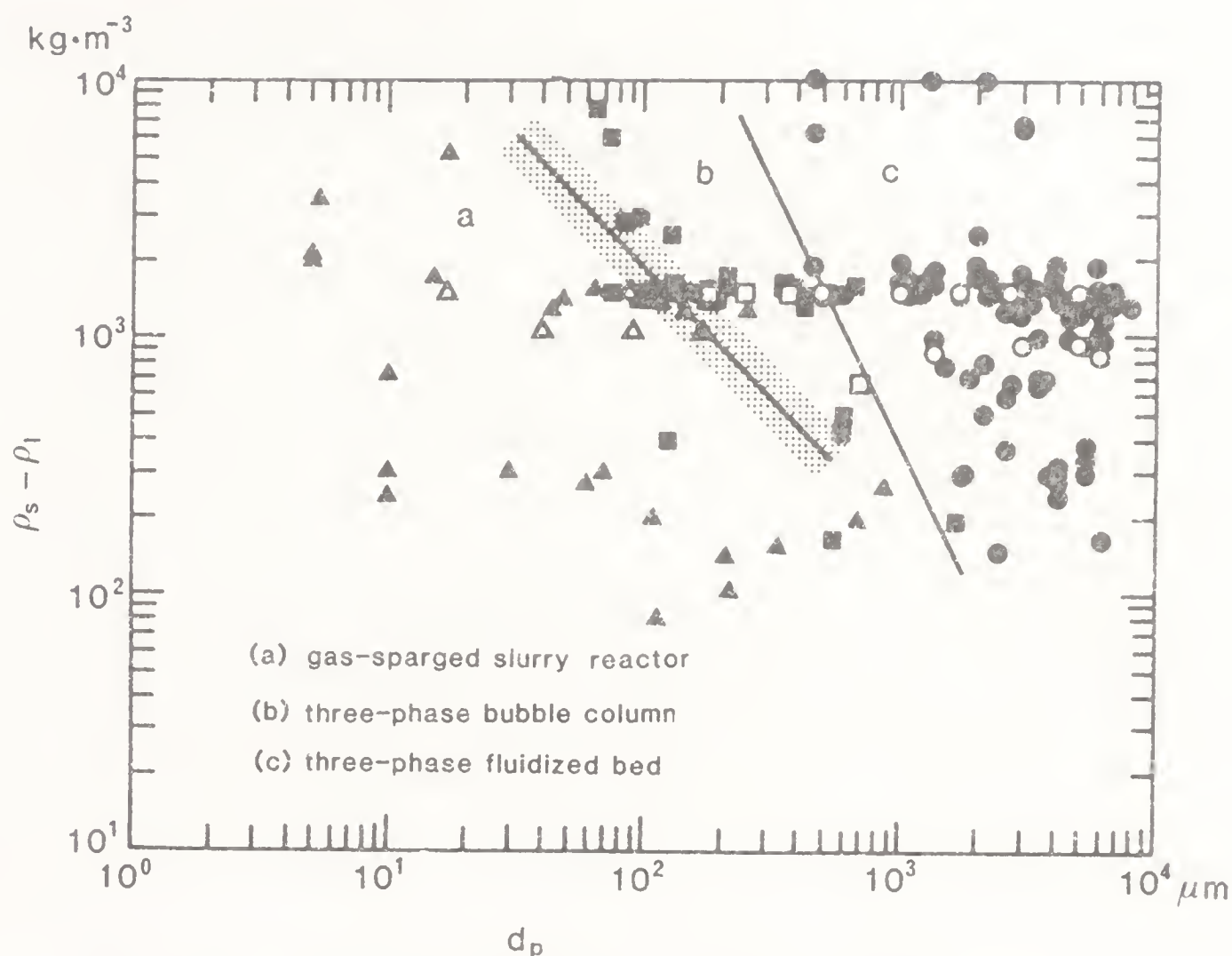


Figure 8. Effect of solid content on solid concentration profile for  $180\ \mu\text{m}$  glass beads.

three-phase reactors on the proposed classifying map. Figure 10 substantiates information lacking in figure 9 and also indicates the areas needing further research.

## 6. Conclusions

An idea for classifying cocurrent upward three-phase reactors is proposed. It is shown that they can be divided into three types such as gas-sparged slurry reactors, three-phase bubble columns, and three-phase fluidized beds by considering the differences in solid concentration profiles appearing in the axial direction of reactors. Experiments were carried out to find out substantial factors affecting the solid concentration profiles, and a classification map of three-phase reactors was drawn in the relation between the density difference ( $\rho_s - \rho_l$ ) and the mean particle size.



**Figure 9.** Classification map for three-phase reactors. (Open and closed signs stand for present work and data previously published, respectively). (a). Triangles – gas-sparged slurry reactors. (Kawamura *et al* 1965; Imafuku *et al* 1968; Deckwer *et al* 1980; Sanger & Deckwer 1981; Kara *et al* 1982; Capuder & Koloini 1984; Kelkar *et al* 1984; Kojima *et al* 1984). (b). Squares – three-phase bubble column reactors. (Roy *et al* 1964; Imafuku *et al* 1968; Farkas & Leblond 1969; Kato *et al* 1972; Kojima & Asano 1980, p. 79; Capuder & Koloini 1984; Kojima *et al* 1984; Smith & Ruether 1985; Smith *et al* 1986). (c). Circles – three-phase fluidized bed reactors. (Stewart & Davidson 1964; Dakshinamurty *et al* 1971, 1972; Bruce & Revel-Chion 1974; Kim *et al* 1975; Blum & Toman 1977; Baker *et al* 1978; Begovich & Watson 1978, p. 190; Dhanuka & Stepanek 1978, p. 179; Lee & Al-Dabbagh 1978, p. 184; Soung 1978; Morooka *et al* 1982; Alvarez-Cuenca *et al* 1983; Kim & Kim 1983; Fan *et al* 1984; Muroyama *et al* 1984; Catros & Bernard 1985; Chiu & Ziegler 1985; Kato *et al* 1985; Saberian-Broudjenni *et al* 1985).

### List of symbols

$d_p$	particle diameter, $\mu\text{m}$ ;
$U_g$	gas velocity, $\text{m} \cdot \text{s}^{-1}$ ;
$z$	axial distance from the distributor, m;
$\epsilon$	holdup;
$\rho$	density, $\text{kg} \cdot \text{m}^{-3}$ ;
$\phi$	volume fraction of solid.

### Subscripts

$g$	gas;
$l$	liquid;
$s$	solid.

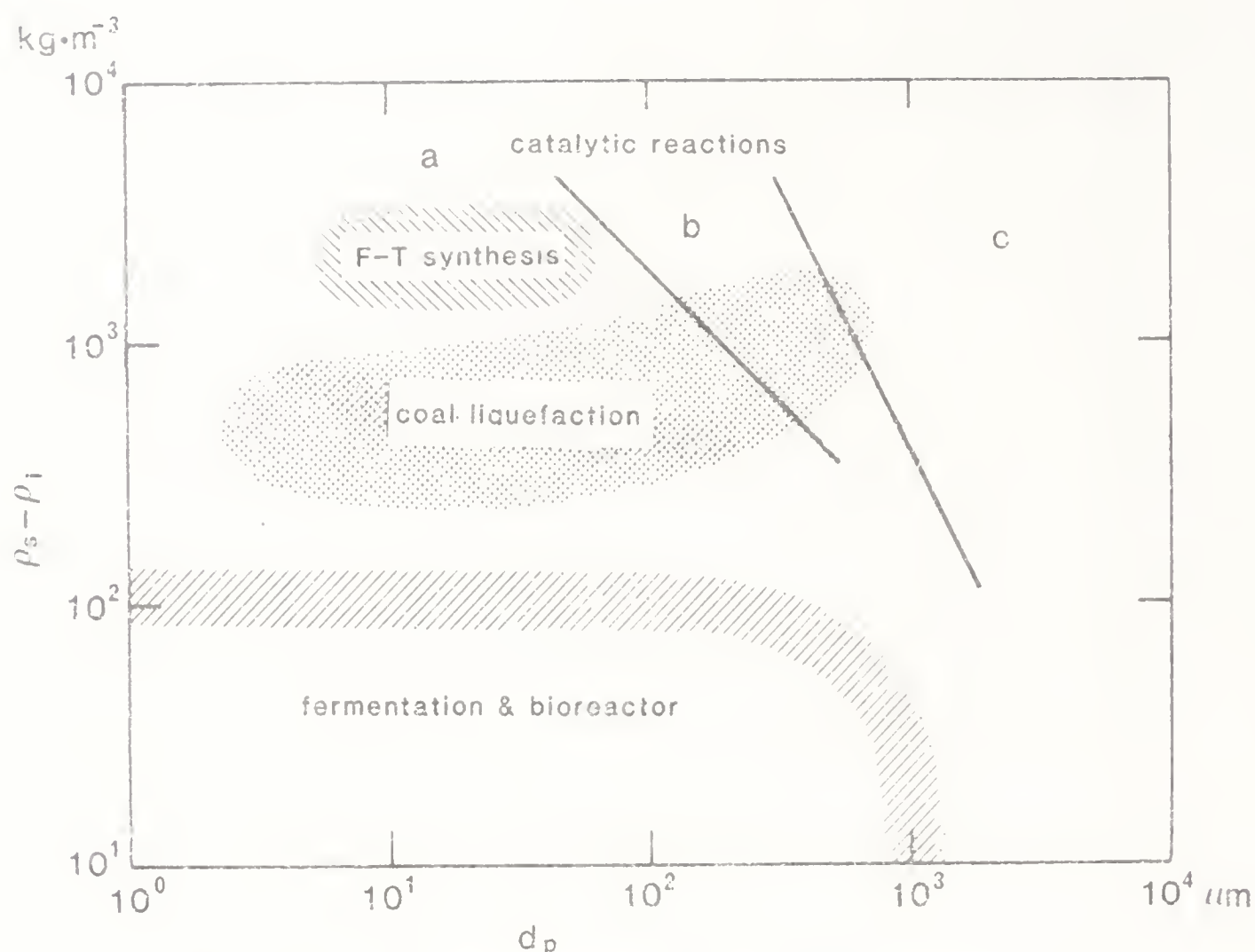


Figure 10. Relationship between reactor types and application field.

This paper is dedicated to Dr L K Doraiswamy on his sixtieth birthday

## References

- Alvarez-Cuenca M, Baker C G J, Bergougnou M A, Nerenberg M A 1983 *Can. J. Chem. Eng.* 61: 58–63
- Baker C G J, Armstrong E R, Bergougnou M A 1978 *Powder Technol.* 21: 195–204
- Begovich J M, Watson J S 1978 *Fluidization* (eds) J F Davidson, D L Kearns (Cambridge: Univ. Press)
- Blum D B, Toman J J 1977 *AIChE Symp. Ser.* 73 (161): 115–120
- Bruce P N, Revel-Chion L 1974 *Powder Technol.* 10: 243–249
- Capuder E, Koloini T 1984 *Chem. Eng. Res. Des.* 62: 255–260
- Catros A, Bernard J R 1985 *Powder Technol.* 44: 159–168
- Chiu T-M, Ziegler E N 1985 *AIChE J.* 31: 1504–1509
- Dakshinamurty P, Subrahmanyam V, Rao J N 1971 *Ind. Eng. Chem., Process Des. Dev.* 10: 322–328
- Dakshinamurty P, Rao K V, Subbaraju R V, Subrahmanyam V 1972 *Ind. Eng. Chem., Process Des. Dev.* 11: 318–319
- Darton R C 1985 *Fluidization* 2nd edn (eds) J F Davidson, R Clift, H Harrison (London: Academic Press)
- Deckwer W-D, Louisi Y, Zardi A, Ralek M 1980 *Ind. Eng. Chem., Process Des. Dev.* 19: 699–708
- Deckwer W-D, Schumpe A 1984 *Ger. Chem. Eng.* 7: 168–177
- Dhanuka V R, Stepanek J B 1978 *Fluidization* (eds) J F Davidson, D L Kearns (Cambridge: Univ. Press)
- Epstein N 1981 *Can. J. Chem. Eng.* 59: 649–657
- Fin L-S, Hwang S-J, Matsuura A 1984 *AIChE Symp. Ser.* 80 (234): 91–97
- Farkas E J, Leblond P F 1969 *Can. J. Chem. Eng.* 47: 215–217
- Imatuku K, Wang T-Y, Koide K, Kubota H 1968 *J. Chem. Eng. Jpn.* 1: 153–158

- Kara S, Kelkar B G, Shah Y T, Carr N L 1982 *Ind. Eng. Chem., Process Des. Dev.* 21: 584-594
- Kato Y, Nishiwaki A, Fukuda T, Tanaka S 1972 *J. Chem. Eng. Jpn.* 5: 112-118
- Kato Y, Morooka S, Kago T, Saruwatari T, Yang S-Z 1985 *J. Chem. Eng. Jpn.* 18: 308-313
- Kawamura K, Sasano T, Mifune A 1965 *Kagaku Kogaku* 29: 693-699
- Kelkar B G, Shah Y T, Carr N L 1984 *Ind. Eng. Chem., Process Des. Dev.* 23: 308-313
- Kim S D, Baker C G J, Bergougnou M A 1975 *Can. J. Chem. Eng.* 53: 134-139
- Kim S D, Kim C H 1983 *J. Chem. Eng. Jpn.* 16: 172-178
- Kojima H, Asano K 1980 *Kagaku Kogaku Ronbunshu* 6: 46-52
- Kojima H, Asano K 1981 *Ryudoso Kogaku* (Japan: Gakkai Shuppan Center)
- Kojima H, Iguchi A, Asano K 1984 *Can. J. Chem. Eng.* 62: 346-351
- Lee J C, Al-Dabbagh N 1978 *Fluidization* (eds.) J F Davidson, D L Keairns (Cambridge: Univ. Press)
- Morooka S, Uchida K, Kato Y 1982 *J. Chem. Eng. Jpn.* 15: 29-34
- Muroyama K, Fan L-S 1985 *AIChE J.* 31: 1-34
- Muroyama K, Fukuma M, Yasunishi A 1984 *Can. J. Chem. Eng.* 62: 199-208
- Østergaard K 1968 *Advances in chemical engineering* (eds) T B Drew, G R Cokerlet, J W Hoopes, T Vermulen (New York: Academic Press)
- Pandit A B, Joshi J B 1986 *Chem. Eng. Res. Des.* 64: 125-157
- Roy N K, Guha D K, Rao M N 1964 *Chem. Eng. Sci.* 19: 215-225
- Saberian-Broudjenni M, Wild G, Midoux N, Charpentier J C 1985 *Can. J. Chem. Eng.* 63: 553-564
- Sanger P, Deckwer W-D 1981 *Chem. Eng. J.* 22: 179-186
- Smith D N, Ruether J A 1985 *Chem. Eng. Sci.* 40: 741-754
- Smith D N, Ruether J A, Shah Y T, Badgujar M N 1986 *AIChE J.* 32: 426-436
- Soung W Y 1978 *Ind. Eng. Chem., Process Des. Dev.* 17: 33-36
- Stewart P S B, Davidson J F 1964 *Chem. Eng. Sci.* 19: 319-321





# Effect of particle size on gas holdup in three-phase reactors

Y H KIM, A TSUTSUMI and K YOSHIDA

Department of Chemical Engineering, University of Tokyo, 7-3-1 Hongo, Bunkyo-ku, Tokyo 113, Japan

**Abstract.** Gas holdups were measured in a batch three-phase cocurrent column in which glass beads ranging from 17 to 5000  $\mu\text{m}$  were suspended up to 20 vol %. The effect of particle size on gas holdup was found to be different in three types of reactors such as the gas-sparged slurry reactors, three-phase bubble columns and three-phase fluidized beds. An increase of particle size reduced gas holdup in three-phase bubble columns, while raising it in gas-sparged slurry reactors and three-phase fluidized beds. The maximum and minimum gas holdup were observed respectively for particle size of about 88–250  $\mu\text{m}$  and 500  $\mu\text{m}$ , but the values of particle size were dependent on solid content and gas velocity.

**Keywords.** Three-phase reactors; gas holdup; gas-sparged slurry reactor; three-phase bubble column; three-phase fluidized bed.

## 1. Introduction

In the preceding paper, Tsutsumi *et al* (1987) classified three-phase reactors into three types: (a) gas-sparged slurry reactors, (b) three-phase bubble columns, and (c) three-phase fluidized beds, according to the difference in solid concentration profiles.

A few papers concerned with gas holdup in three-phase reactors have reported the effect of particle size. Table 1 summarizes their experimental conditions. The effects of particle size and solid content in the three-phase bubble column was investigated by Kato *et al* (1972). They found that the larger particles showed a somewhat smaller gas holdup at low gas velocity. In addition, an increase in solid content gave a decrease of gas holdup but the effect became insignificant at high gas velocities. The data for the gas-sparged slurry reactor were reported by Kara *et al* (1982) with solid content up to 40 wt %. They stated that the increase in particle size reduces the gas holdup, though the effect becomes smaller for larger solid particles, and that gas holdup decreases with solid content. Similar trends for the change in gas holdup have been recently reported by Sada *et al* (1986) for the gas-sparged slurry reactor using 40 and 96  $\mu\text{m}$  glass beads.

Table 1. Gas holdup studies in three-phase reactors.

Investigators	Particles	$d_p$ ( $\mu\text{m}$ )	$\rho_s$ ( $\text{kg}\cdot\text{m}^{-3}$ )	Solid (wt%)	Reactor type*
Kato <i>et al</i> (1972)	Glass beads	63–177	2520	0–14	b
Kara <i>et al</i> (1982)	Mineral ash, coal	10	1300	0–40	a
		30, 70	1300	0–40	a
Sada <i>et al</i> (1986)	$\text{Ca}(\text{OH})_2$ ,	7	2240	0–20	a
	Glass beads	40, 96	2480	0–20	a
Begovich & Watson (1978)	Glass beads,	4600	2240		c
	alumina beads,	6200	1990	–	c
	plexiglas beads	6300	1170		c
Michelsen & Østergaard (1970)	Glass beads	1000	2670		
		3000	2450	–	c
		6000	2630		
Dhanuka & Stepanek (1978)	Glass beads	1980, 4080, 5860	2960	–	c
Patwari <i>et al</i> (1986)	Glass beads	3000	2533		
		5000	2530	–	c
		8000	2514		

\* a, gas-sparged slurry reactor; b, three-phase bubble column; c, three-phase fluidized bed

On the other hand, in the three-phase fluidized bed using large and/or heavy particles, it was reported that the gas holdup increased with particle size. Michelsen & Østergaard (1970) observed that bubble break-up occurs in beds of 6000  $\mu\text{m}$  large particles operated at high liquid flow rates and low gas velocity. In the bubble break-up regime, gas holdup was greater than that in the corresponding solid free systems, and increased with gas velocity. In beds of 1000 and 3000  $\mu\text{m}$  small particles at low liquid flow rates, bubble coalescence was important. Gas holdup characterized by a non-uniform bubble size distribution and by formation of large slugs decreased. The bed expansion in this regime first decreased rapidly with gas velocity but again increased at very high gas velocity.

Dhanuka & Stepanek (1978, p. 179) and Patwari *et al* (1986) reported that the gas holdup was lower than that in the gas-liquid system and increased as particle size became larger.

Begovich & Watson (1978, p. 190) reported that, by combining the gas holdup with 169 points obtained from the literature on three-phase fluidized beds, the gas holdup increased with particle size.

Recently, Pandit & Joshi (1986) investigated the effect of particle size on bubble diameter using glass beads with a wide range of particle size from 50 to 2000  $\mu\text{m}$ . The conditions covered all three types of reactors. When the particle size increased, the bubble diameter decreased, unlike the gas-liquid two-phase system. The minimum bubble diameter was obtained at the particle size of about 100  $\mu\text{m}$ . The bubble diameter increased with particle size in the range of 100–500  $\mu\text{m}$ . A maximum bubble diameter was reached at particle size of about 500  $\mu\text{m}$ . Beyond this size, the bubble diameter again decreased with particle size. Thus, it was shown that the minimum and the maximum gas holdup exist at the particle size where the maximum and the minimum bubble diameter are formed, respectively.

These studies indicated as follows: (1) The gas holdup in three-phase fluidized bed with 1000–2000  $\mu\text{m}$  small particles was lower than that in the corresponding

solid-free or 3000–6000  $\mu\text{m}$  larger particle systems. (2) The reduction in the gas holdup due to the presence of the solid or increase of particle size was commonly observed in three-phase bubble columns. (3) The gas holdup behaviour was strongly dependent upon the flow regimes. In the bubble coalescence regime, considerable reduction in the gas holdup took place with bubble diameter. On the other hand, in the bubble breakage regime, the gas holdup increased with bubble diameter.

In the present study, systematic measurements were conducted to elucidate the effect of particle size on gas holdup in all three types of reactors. Glass beads with a wide range of particle size from 17 to 5000  $\mu\text{m}$  were suspended up to 20 vol % in water and air media.

## 2. Experimental

The same reactor shown in the preceding paper was used. Solid properties are summarized in table 2. The flow rate of air supplied from the compressor was controlled by a pressure gauge and a rotameter in the range of 1–250  $\text{Nl} \cdot \text{min}^{-1}$ .

The gas holdup was defined as the volume percentage of gas by the bed height difference between the expanded and the settled states, in the following:

$$\varepsilon_g = (H_e - H_s)/H_e. \quad (1)$$

The measurement of gas holdup was made at gas velocity in the range of 0.01–0.2  $\text{m} \cdot \text{s}^{-1}$  with solid concentration up to 20 vol %.

## 3. Results and discussion

Figure 1 shows representative data on gas holdup in two and three-phase systems. The gas holdup of three-phase systems was less than that of air-water two-phase systems.

Table 2. Properties of glass beads used.

Nominal particle size ( $\mu\text{m}$ )	Average particle size ( $\mu\text{m}$ )	Density ( $\text{kg} \cdot \text{m}^{-3}$ )
17	17	2480
63–105	88	2500
149–210	180	2500
210–297	250	2500
297–420	370	2500
420–590	500	2500
840–1190	1000	2500
1410–2000	1700	2500
2000–3400	2700	2500
4500–5500	5000	2500



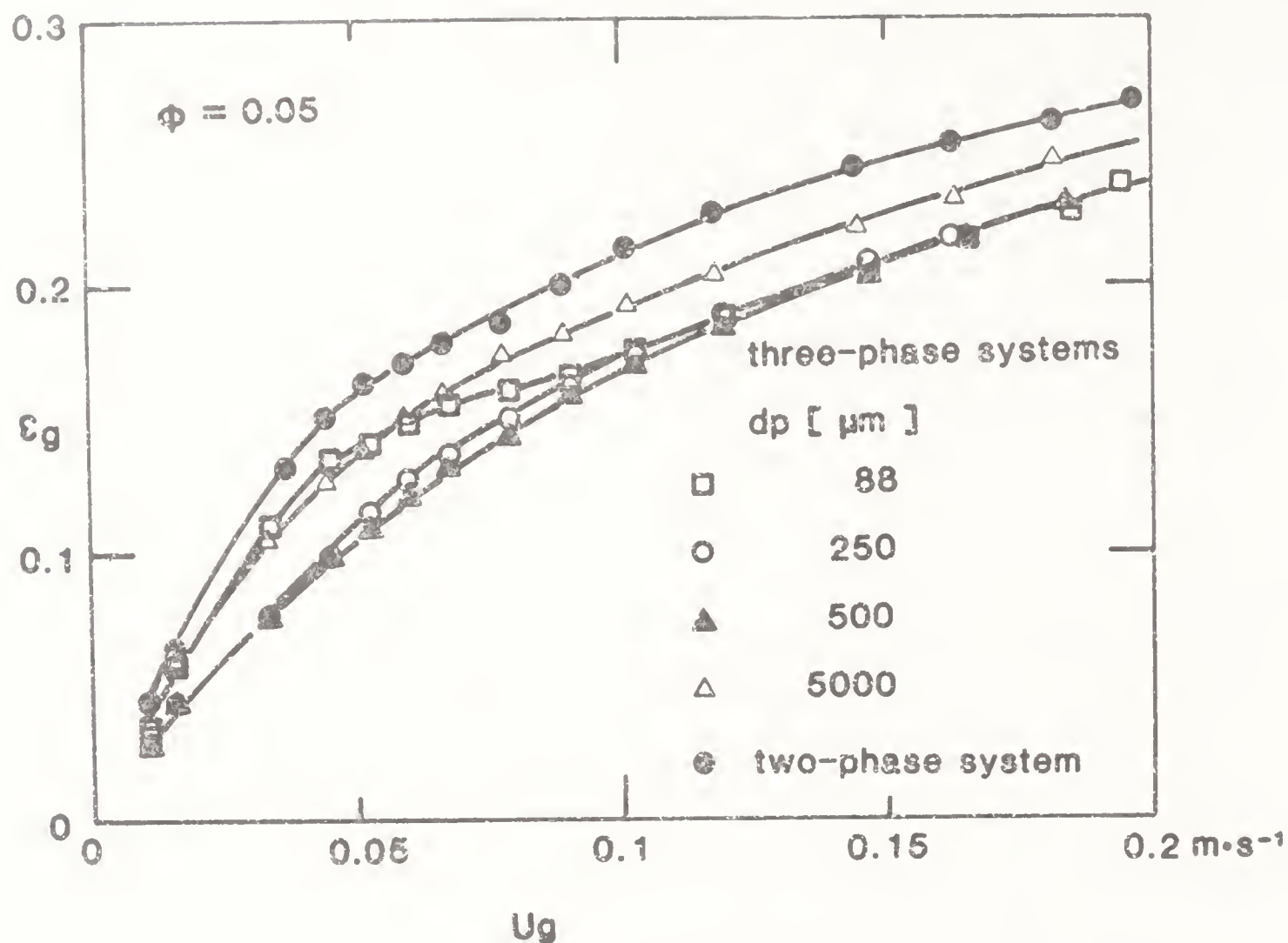


Figure 1. Representative data on gas holdup in two- and three-phase reactors.

### 3.1 Bubble flow behaviour

Wallis (1969) has characterized the upward movement of bubble swarms into three separate flow regimes: bubbly flow, churn-turbulent and slug flow.

At low gas velocities below  $0.05 \text{ m} \cdot \text{s}^{-1}$ , uniformly dispersed small bubbles rose through the column, i.e., homogeneous bubbly flow appeared. The gas holdup increased linearly with gas velocity. When the gas velocity increased above  $0.05 \text{ m} \cdot \text{s}^{-1}$ , a transition from a homogeneous bubbly flow to a heterogeneous churn-turbulent flow occurred. In the heterogeneous churn-turbulent flow, bubble coalescence took place to form a few large bubbles with high rising velocity. Hence, the increase of gas velocity did not significantly raise the gas holdup, as shown in figure 1. In all experiments, the critical values of gas velocity for the transition from bubbly to churn-turbulent flow, were  $0.04\text{--}0.05 \text{ m} \cdot \text{s}^{-1}$  being independent of particle size and solid content, as shown in figures 1 and 2. It is concluded that the presence of particles promotes bubble coalescence which reduces the gas holdup in all regimes, but has little influence on the transition of bubble flow regimes.

### 3.2 Effect of particle size

Figure 3 shows the effect of particle size on gas holdup at a solid content of 5 vol %. The dependence of gas holdup on particle size was found to differ entirely in each type of three-phase reactors. In the gas-sparged slurry reactor, gas holdup increased with particle size. In the three-phase bubble column, gas holdup

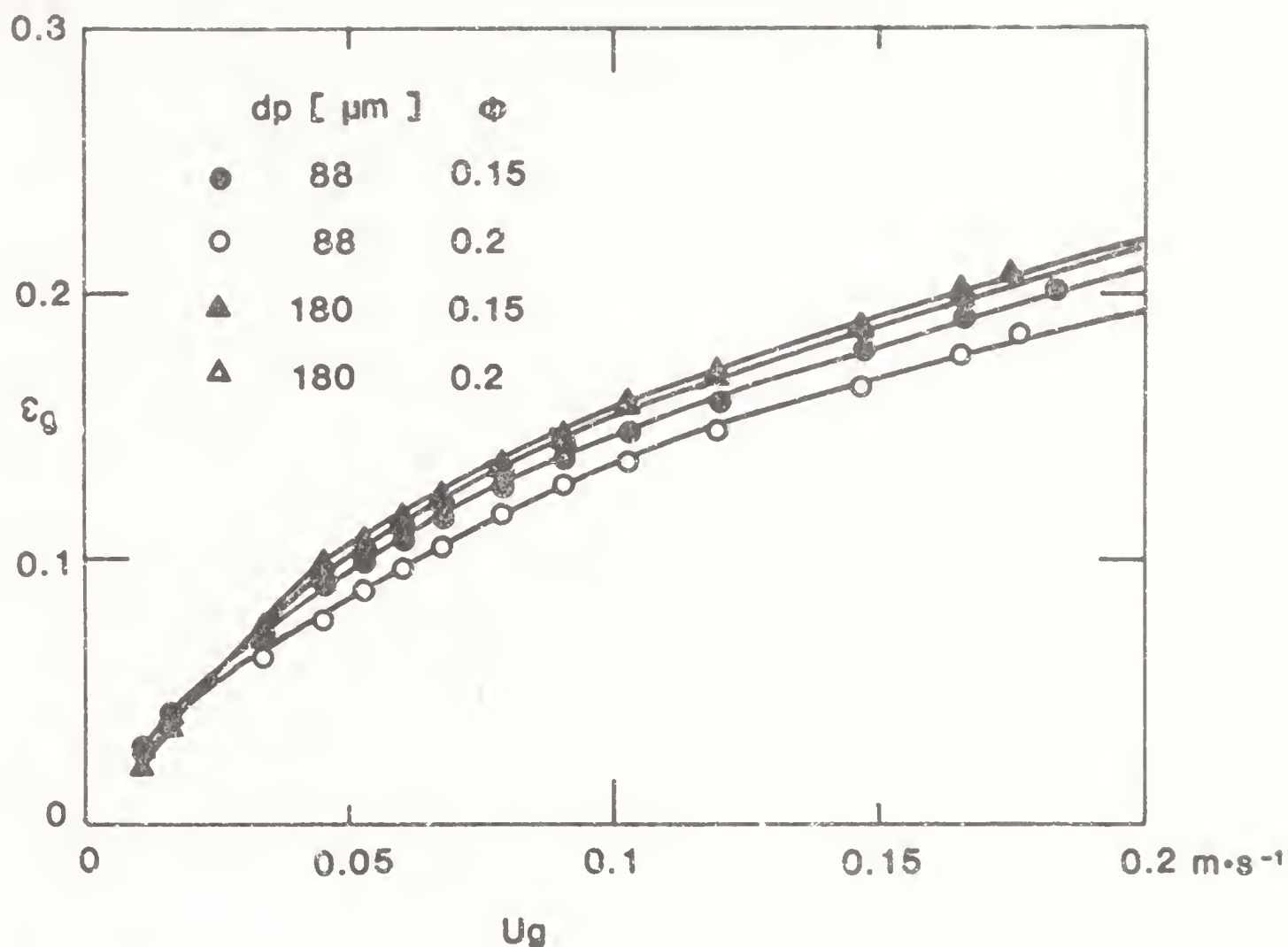


Figure 2. Relationship between gas velocity and gas holdup by changing particle size and solid content.

decreased with particle size. Therefore, a maximum gas holdup appears at the boundary between gas-sparged slurry reactor and three-phase bubble column. In the three-phase fluidized beds, gas holdup increased with particle size, so that a minimum gas holdup was observed at the boundary between the three-phase bubble column and the three-phase fluidized bed. These phenomena became less predominant with the increase of gas velocity.

It was found that the particle size showing a maximum gas holdup increases with gas velocity at the transition from homogeneous bubbly flow to heterogeneous churn-turbulent flow. This implies that as the gas velocity increases in this range, the transition from three-phase bubble column to gas-sparged slurry reactors takes place because of a significant agitation by rising gas bubbles (Tsutsumi *et al* 1987). However, the particle size showing a minimum gas holdup was independent of gas velocity.

Figure 4 shows the effect of solid content on gas holdup. In the gas-sparged slurry reactor, the gas holdup decreased with increase of solid content. This effect was more pronounced at lower solid content. On the other hand, in the three-phase bubble column and the three-phase fluidized bed, it was found that the increase of solid content does not reduce the gas holdup.

Figure 5 shows that, when the solid content increased from 5 to 20 vol %, the particle size showing maximum gas holdup was changed from 180  $\mu\text{m}$  up to about 250  $\mu\text{m}$ . Comparing with the result of Pandit & Joshi (1986) which showed that the

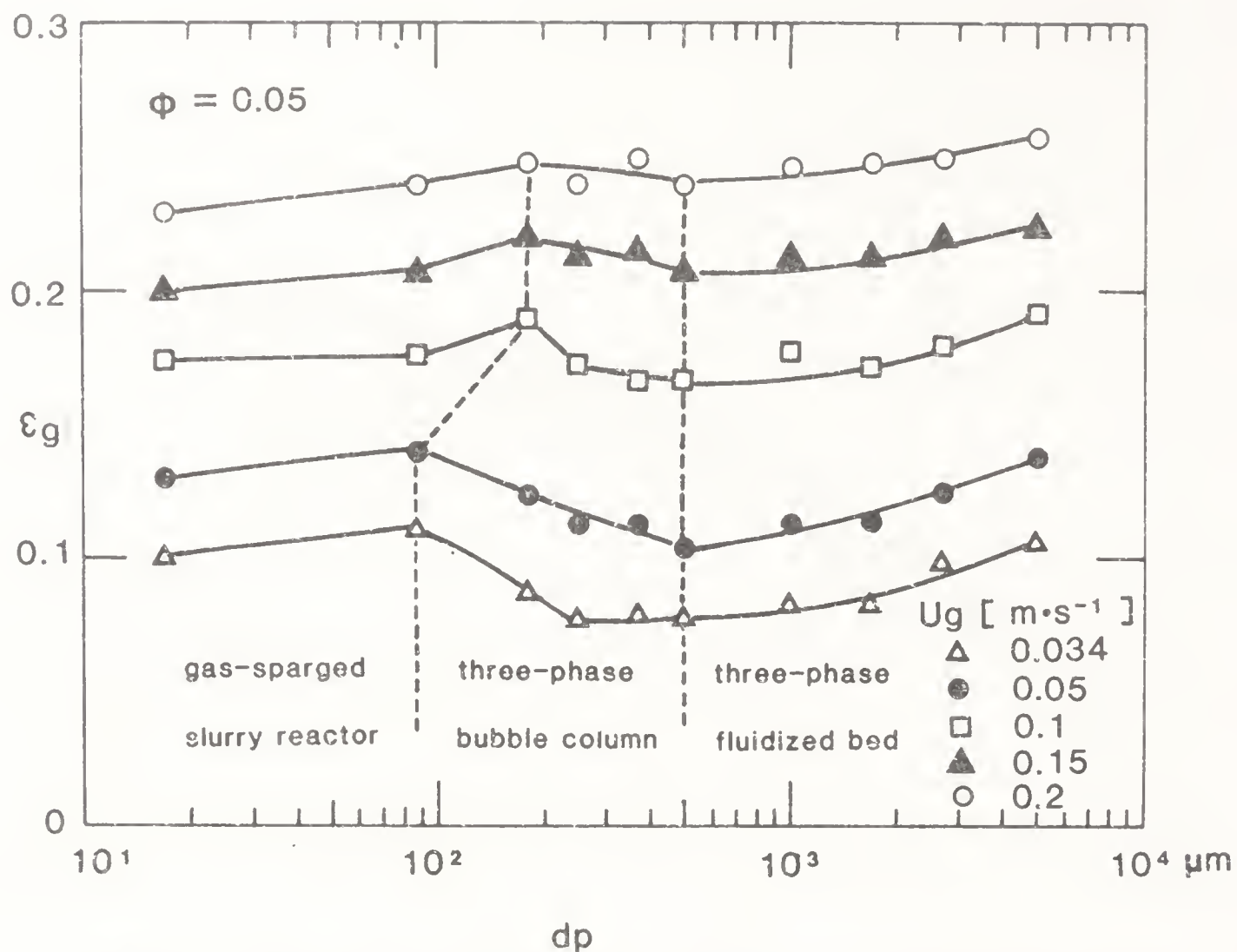


Figure 3. Relationship between particle size and gas holdup by changing gas velocity.

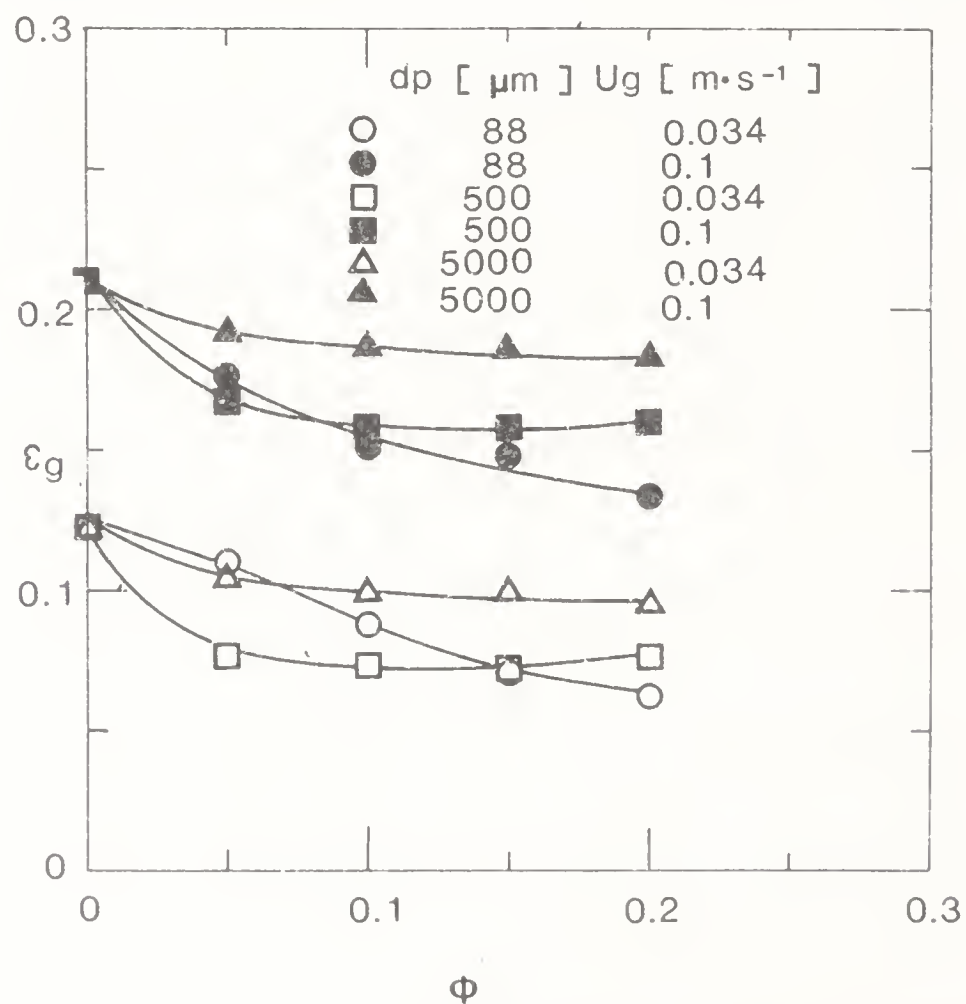


Figure 4. Effect of solid content on gas holdup.

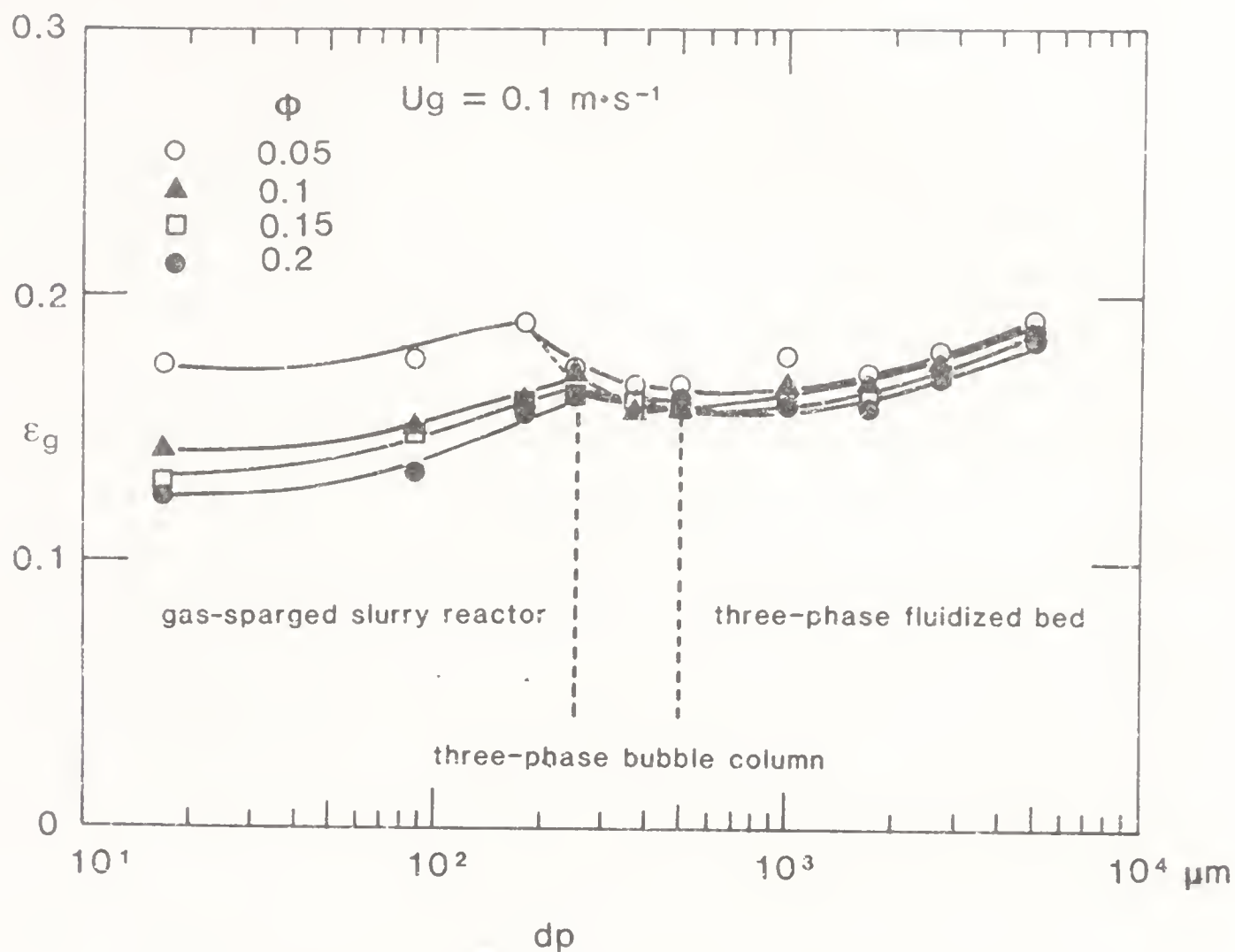


Figure 5. Effect of particle size on gas holdup with respect to solid content.

minimum bubble diameter, i.e., maximum gas holdup was obtained at about  $100\ \mu\text{m}$ , it can be said that the particle size showing the maximum gas holdup increased with solid content. However, there was no change in particle size showing the minimum gas holdup with respect to solid content. This suggested that the region of the gas-sparged slurry reactor extends with solid content. In addition, it showed that solid content up to 20 vol % has little effect on the regime of a three-phase fluidized bed.

#### 4. Conclusions

Effects of particle size on gas holdup in each type of three-phase reactors were shown experimentally at various solid contents and gas velocities. As the particle size increased, the gas holdup increased in both gas-sparged slurry reactors and three-phase fluidized beds, but decreased in three-phase bubble columns. The particle size showing the maximum gas holdup increased with solid content and gas velocity in the transition range from homogeneous bubbly flow to heterogeneous churn-turbulent flow, but there was no change in the particle size showing the minimum gas holdup in the range of up to a solid concentration of 20 vol %.



**List of symbols**

$d_p$	particle diameter, $\mu\text{m}$ ;
$H_e$	height of expanded bed, m;
$H_s$	height of settled bed, m;
$U_g$	gas velocity, $\text{m}\cdot\text{s}^{-1}$ ;
$\varepsilon_g$	gas holdup;
$\rho_s$	particle density, $\text{kg}\cdot\text{m}^{-3}$ ;
$\phi$	volume fraction of solid.

This paper is dedicated to Dr L K Doraiswamy on his sixtieth birthday.

**References**

- Begovich J M, Watson J S 1978 *Fluidization* (eds.) J F Davidson, D L Keairns (Cambridge: University Press)
- Dhanuka V R, Stepanek J B 1978 *Fluidization* (eds.) J F Davidson, D L Keairns (Cambridge: University Press)
- Kara S, Kelkar B G, Shah Y T, Carr N L 1982 *Ind. Eng. Chem., Process Des. Dev.* 21: 584–594
- Kato Y, Nishiwaki A, Fukuda T, Tanaka S 1972 *J Chem. Eng. Jpn.* 5: 112–118
- Michelsen M L, Østergaard K 1970 *Chem. Eng. J.* 1: 125–157
- Pandit A B, Joshi J B 1986 *Chem. Eng. Res. Des.* 64: 125–157
- Patwari A N, Nguyen-Tien K, Schumpe A, Deckwer W-D 1986 *Chem. Eng. Commun.* 40: 49–65
- Sada E, Kumazawa H, Lee C, Iguchi T 1986 *Ind. Eng. Chem., Process Des. Dev.* 25: 472–476
- Tsutsumi A, Kim Y H, Togawa S, Yoshida K 1987 *Sādhanā* 10: 247–259
- Wallis G B 1969 *One-dimensional two-phase flow* (New York: McGraw-Hill)

# Recent advances in the analysis and design of trickle-bed reactors

P A RAMACHANDRAN, M P DUDUKOVIĆ and P L MILLS<sup>†</sup>

Chemical Reaction Engineering Laboratory, Department of Chemical Engineering, Washington University at St. Louis, Missouri 63130, USA

<sup>†</sup> Monsanto Company, 800N Lindbergh Boulevard, St. Louis, Missouri 63167, USA

**Abstract.** This paper summarizes some progress in our understanding of trickle-bed reactors. The particular topics discussed in this review are the basic hydrodynamics, flow regime transition, pressure drop and holdup calculations, use of tracers, modelling of partial wetting effects, reactor design of and catalyst testing in trickle beds. The rapid advances made in these areas are critically examined and some problems which need further investigation are outlined.

**Keywords.** Multiphase reactors; trickle beds.

## 1. Introduction

Trickle-beds, which are packed-beds of catalyst with cocurrent flow of liquid and gas reactants, represent an important class of three-phase reactors. If reactor significance was judged by the tonnage of material processed, trickle-beds would be among the most important ones due to their widespread use in the petroleum industry in processes such as hydrodesulphurization, denitrogenation, demetallization and hydrocracking. They are also used in chemical processing mainly in hydrogenation and oxidation reactions. Typical applications include hydrogenation of nitrocompounds, aniline etc., synthesis of butynediol, production of sorbitol etc. Trickle-beds are also well-suited for the oxidation of dilute aqueous solutions of organic pollutants and hence have potential applications in waste water treatment. They can also be used in operations with immobilized cells or enzymes which require liquid substrates and oxygen or where CO<sub>2</sub> is formed as a product.

When dealing with gas and liquid reactants that need to be processed on a solid catalyst, immobilized cells or enzymes, one can choose between slurry systems and packed bed operation. Catalyst slurries, i.e., finely powdered suspended catalyst particles in the 20  $\mu\text{m}$  to 200  $\mu\text{m}$  range, are used in mechanically agitated

autoclaves, bubble columns and gas-lift reactors while somewhat larger particles are employed in three-phase fluidized beds. Catalyst pellets in the 0.08 to 0.32 cm range are used in packed-beds with cocurrent, downflow or upflow, and countercurrent gas-liquid flow. Germain *et al* (1979, p. 265) compare the relative merits of packed-beds and slurry reactors and conclude that, overall, the packed-beds are to be preferred due to their flow pattern that approaches plug flow, high catalyst loading per unit volume of the liquid, low energy dissipation rate (an order of magnitude lower than in slurry reactors) and much greater flexibility with respect to production rates and operating conditions used. The only marked disadvantages are their intolerance of highly exothermic reactions and their impracticality for systems with rapidly deactivating catalysts.

In spite of their advantages, the potential of trickle-bed reactors has never been fully utilized in chemical processing in partial hydrogenations, partial oxidations, desulphurizations, hydroformylations or in pollution abatement, fermentations and other biochemical reactions. The reason seems to lie in the difficulties associated with trickle-bed design which exceed those encountered with other reactor types. While scale-up of trickle-bed reactors in petroleum processing for certain types of known feeds is well established as an art, *a priori* prediction of trickle-bed performance or scale-up from small laboratory units for feeds and processes for which previous know-how does not exist is still considered very risky and is simply not done. This is due to the fact that phenomena in trickle-beds are incompletely understood and are not readily quantified.

In view of the complexities associated with trickle-beds, it is not surprising that considerable research has been done in this area. A number of review articles on trickle-bed reactors are available which summarize the progress in this area (Satterfield 1975; Goto *et al* 1977; Gianetto *et al* 1978; Shah 1979; Ramachandran & Chaudhari 1983; Herskowitz & Smith 1983; Dudukovic & Mills 1983, 1986; Gupta 1985, p. 515; Hanika & Stanek 1985, p. 1029). In view of the rapid advances that are being made in this area, it is appropriate to supplement these reviews with new developments and this is one of the objectives of this paper. In addition, the paper addresses the research needs in this area. Although the review is not exhaustive in its literature coverage, all the major new research trends are discussed.

The primary focus is on the developments in the subareas listed below in which significant work has been done in the recent years:

1. Flow regime transition;
2. pressure drop and holdup correlations;
3. use of tracers in trickle-beds;
4. influence of partial wetting;
5. reactor design equations;
- and 6. catalyst testing in trickle-beds.

## 2. Flow regime transition

Flow pattern in the trickle-bed can be classified into three regimes; (i) At low liquid rate, the flow pattern is trickling where the liquid trickles over the packing in essentially laminar flow. Here the presence of the gas does not significantly affect the flow of the liquid and this flow regime is therefore called a low interaction regime (LIR). The presence of the gas mainly alters the flow area available for the



liquid and this regime is alternatively also known as the 'geometric' interaction regime.

(ii) At higher gas and/or liquid rates, we observe rippling or pulsing flow. Here, pulses of liquid with entrained gas bubbles periodically pass through the column at regular frequencies. In this region the interaction between the gas and liquid pulses is very high and the regime is also known as the high interaction regime (HIR). As there is significant momentum exchange at the gas-liquid interface the regime is also known as the 'hydrodynamic' interaction regime.

(iii) At very high liquid rates and relatively low gas rates, the liquid becomes a continuous phase and the gas flows as a dispersed phase in the form of bubbles. This regime is referred to as the dispersed bubble flow regime.

Normal laboratory and commercial reactors are operated in the trickle or pulse flow regime. The transition between the two regimes is not very sharp and is usually characterized by an increase in the root mean square pressure fluctuations for a relatively small increase in the gas or liquid flow rates. Operation in the trickle flow regime ensures a large liquid residence time and provides a large single pass conversion of the liquid reactant. This is therefore useful for reactions which are kinetically controlled. Operation in the pulsing regime provides a dramatic increase in the mass transfer coefficients and is therefore suitable for relatively fast mass transfer limited reactions. Flexibility for changing the operating gas and liquid rates is also greater in the pulsing regime. Studies comparing the two regimes for reacting system are lacking and are needed to enable a rational choice of the operating gas and liquid velocities. Operation with very low liquid velocities in the trickle flow regime is common in commercial hydrodesulphurization reactors. Here in some cases the catalyst particle may not be completely wetted and the complexities associated with incomplete wetting are discussed in §7.

In order to properly interpret the experiments, it is necessary to know in which regime the reactor is operating for a given condition. It is also necessary to know whether the same flow regime will be maintained when one scales up from laboratory to pilot or commercial scale reactors. A number of studies have therefore been devoted to this subject. In one of the early studies, Charpentier & Favier (1975) used the Baker (1954) coordinate plot to demarcate the flow regime transition line. Separate flow maps were provided for foaming and non-foaming systems. Additional early work in this area has been provided by Specchia & Baldi (1977), Chou *et al* (1977), Fukushima & Kusaka (1977) and Talmor (1977).

The flow map of Charpentier & Favier (1975) is very useful for the practitioner when one views the transition as a zone rather than a sharp line. The flow map has been represented in analytical form by Duduković & Mills (1986) which leads to the following approximate criterion for maintaining trickle flow conditions.

$$\rho_L u_L \leq (\rho_L u_L)_{cr} \text{ and } \rho_G u_G / \epsilon_B \lambda < 1, \quad (1)$$

where  $(\rho_L u_L)_{cr}$  is the smaller of the two mass velocities evaluated in the following:

$$(\rho_L u_L)_{cr} = 10^3 \rho_G u_G / \lambda \psi, \quad (2a)$$

$$(\rho_L u_L)_{cr} = 5.45 [\epsilon_B \lambda / \rho_G u_G]^{0.22} (\epsilon_B / \psi), \quad (2b)$$

where

$$\lambda = [\rho_G \rho_L / \rho_{air} \rho_w]^{1/2}, \quad (3)$$



$$\psi = (\sigma_w/\sigma_L) [(\mu_L/\mu_w) (\rho_w/\rho_L)^2]^{1/3}. \quad (4)$$

with SI units being used. When  $\rho_L u_L > (\rho_L u_L)_{cr}$  and  $\rho_G u_G/\epsilon_B \lambda < 1$ , transition to pulsing flow occurs and at  $\rho_G u_G/\epsilon_B \lambda > 1$ , transition to spray flow occurs.

Recent studies have focussed more attention on the fundamental hydrodynamics and some of the trends in this area will now be reviewed.

The theoretical models for calculating the onset of pulsing is based on the analysis of flow in capillaries with restriction. Based on this approach, Sicardi & Hofmann (1982) proposed a model of a channel with constriction as shown in figure 1. Pulsing is assumed to occur when the large liquid waves occlude the channel. The channel diameter,  $d_{co}$ , is taken as  $4\epsilon_B/a_p$  and the parameter which takes into account the irregularity of the channel is the width of the protrusion,  $b$ , or an equivalent tortuosity factor  $\theta$  defined as  $2b/d_{co}$ . From dimensional analysis the following correlation was obtained for  $[A/h]$  at the onset of pulsing. (Here  $A$  is the maximum amplitude of the waves formed on the liquid surfaces and  $h$  is the mean film thickness. These parameters are shown in figure 1.)

$$[A/h]_p = C[\tau_i \epsilon_B/\sigma_L a_p]^\alpha, \quad (5)$$

where the subscript  $p$  denotes the onset of pulsing and  $\tau_i$  is the interfacial drag at pulsing inception. The constant  $C$  is assumed to be a function of only the tortuosity factor  $\theta$ . The value of  $[A/h]_p$  can also be related to the liquid saturation,  $\omega (= \epsilon_l/\epsilon_B)$  by the following equation:

$$[A/h]_p = \frac{1}{2} [(1-\omega)/\omega]_p \{1 + [1 + \{\omega/(1-\omega)\}]_p\}^{1/2}, \quad (6)$$

The interfacial drag  $\tau_i$  can be related to the pressure drop in the system by the following equation:

$$(\tau_i)_p = [-\Delta P/\Delta L]_p \epsilon_B (1-\omega)_p/a_p. \quad (7)$$

The value of  $C$  was found to be independent of packing diameter and was a function of only the packing shape. From the analysis of data on various packings such as Raschig rings, ceramic cylinders, glass beads and glass cylinders it was found that  $C = 16.2$  and  $\alpha = 0.5$ . The model is empirical based on dimensional

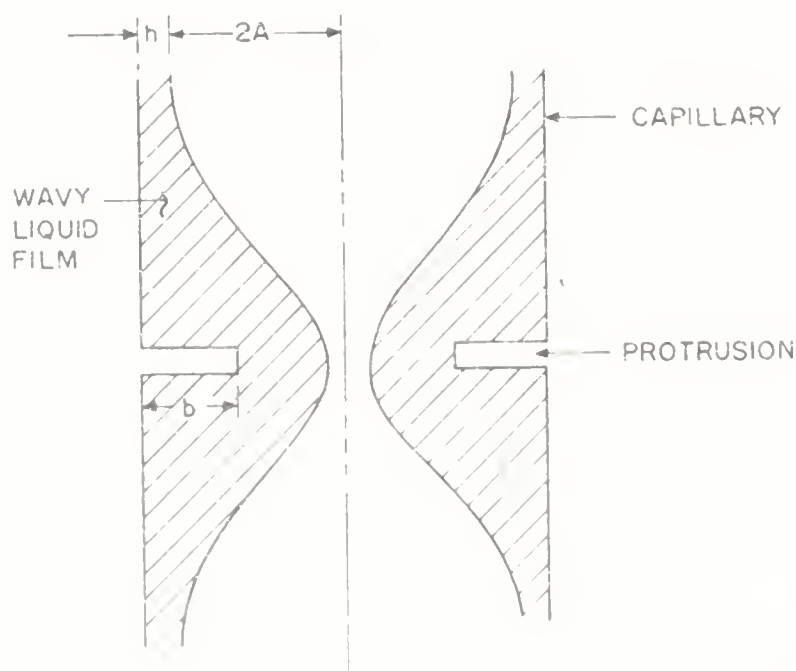


Figure 1. Schematic of a channel with constrictions used in the model of Sicardi & Hofmann (1982).

analysis. It provides a relation between the pressure drop [(7)] and liquid saturation [(5) and (6)] at the onset of pulsing. Alternately, if a reasonable correlation is available for calculations of pressure drop and saturation, then the equations can be used to determine the liquid velocity required for the onset of pulsing. This can be done by equating (5) and (6) and leads to the following simplified equation:

$$[-\Delta P/\Delta L]_{\text{Pulsing}} = 2.5 \times 10^{-3} a_p^2 \sigma_L \varepsilon_B^{0.2} / (\varepsilon_L)_{\text{Pulsing}}^{2.2} \quad (8)$$

A similar approach was used by Dimenstein & Ng (1986). The conceptual sketch of the flow geometry used in their work is shown in figure 2. The model predicts the following equation for the gas velocity at the onset of pulsing:

$$u_G = \varepsilon_B(1 - \alpha) \{ (2/\rho_G) [(4\sigma_L/d_p) - \sigma_L g (d_p/2)] \}^{1/2} \quad (9)$$

Here,  $\alpha$  is the fraction of the cross-sectional area of the void space occupied by liquid which was related to the external average liquid saturation in the bed.

$$\alpha = 4[(1 - \omega)^{1/2} - (1 - \omega)] \quad (10)$$

In this method the effect of liquid velocity on the onset of pulsing comes only indirectly through the liquid holdup factor [parameter  $1 - \alpha$ ]. The interstitial gas velocity necessary to cause pulsing is a constant which depends only on the packing diameter and physical properties. Also, for a certain range of packing size the RHS of (9) can become zero and the correlation is then no longer valid. For small particles and for air-water system the correlation agrees with the experimental data reasonably well.

Blok & Drinkenberg (1982) proposed that the liquid velocity required for pulsing to occur is a constant for a certain packing material. The correlation suggested was that the liquid phase Froude number at pulsing inception is a constant

$$u_l^2 / (\varepsilon_L^2 \rho_L^2 g d_p) = 0.08 \text{ to } 0.09 \quad (11)$$

Blok & Drinkenburg (1982) postulated two mechanisms for the pulse triggering process. First is liquid blocking of some of the passages among packing particles which occurs stochastically. The gas flow either breaks through or bypasses such blockages. At higher liquid flow rates this occurs more frequently and may

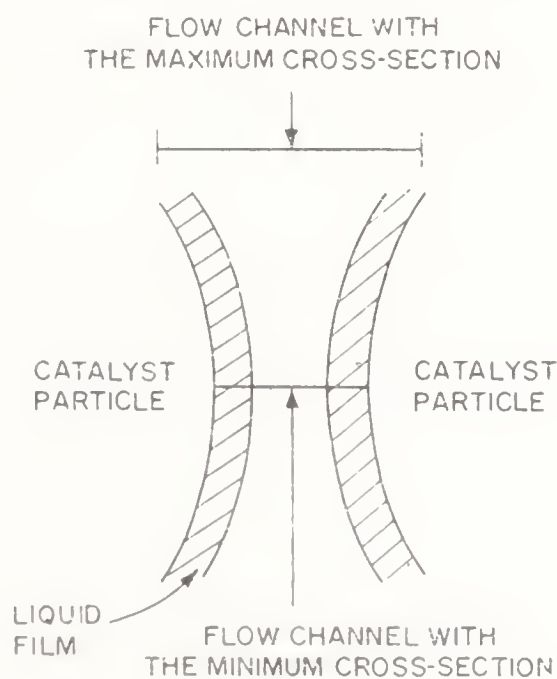


Figure 2. Sketch of the flow geometry used to predict pulsing in the model of Dimenstein & Ng (1986)

sometime lead to the blocking of a large part of the cross-section for flow. When the liquid holdup has reached a certain level, the total blockage starts moving. This corresponds to the onset of pulsing. The mechanism suggests that stochastic components need to be introduced in any model to calculate the conditions for flow transition.

The above discussion indicates the need for substantial work in this area. More data are clearly needed for large diameter columns and porous packings. Most of the studies have been done with nonporous packings. The reported capillary models (approach used by Hofmann and Sicardi, Ng etc.) need to be rigorously solved by finite element methods to explore their true behaviour and relationship to observed bed behaviour. Both steady state and transient hydrodynamics need to be simulated. The transient simulations provide useful information on the onset of flow instabilities. Single capillary models can then be incorporated using percolation concepts into a bed scale model to take into account the randomness of the bed. It may also be necessary to introduce stochastic components into the model. For practitioners, experimental information on the effect of operating variables such as column diameter, packing diameter, pressure, temperature etc., on the onset of pulsing would clearly be useful. For preliminary calculations the flow chart proposed by Talmor (1977) is useful as it covers a wide range of physical properties. For a quick calculation the flow map of Charpentier & Favier (1975) or the approximate criterion of Blok & Drinkenburg (1982) would be used.

### 3. Pressure drop and holdup

For predicting the pressure drop and holdup in trickle-beds, it has been found convenient to consider the low interaction and high interaction regimes separately.

#### 3.1 Low interaction regime: Pressure drop

Specchia & Baldi (1977) proposed a model for the calculation of pressure drop on the basis that the gas flow in the bed is restricted by the presence of the liquid. The effective porosity then is  $\epsilon_{\text{eff}} = \epsilon_B - \epsilon_{ls} - \epsilon_{ld}$ . Now the Ergun equation is used with this modified porosity to correlate the frictional pressure drop.

$$\delta_{LG} = \frac{C_1}{d_p^2} \frac{\mu_G u_G (1 - \epsilon_{\text{eff}})^2}{\epsilon_{\text{eff}}^3} + \frac{C_2}{d_p} \frac{\rho_G u_G^2 (1 - \epsilon_{\text{eff}})}{\epsilon_{\text{eff}}^2} \quad (12)$$

It was suggested that  $C_1$  and  $C_2$  be determined for single phase flow of gas in a prewetted bed. In this case  $\epsilon_{\text{eff}} = \epsilon_B - \epsilon_{ls}$ . A knowledge of static holdup is necessary when using the procedure. Values of  $C_1$  and  $C_2$  obtained for the air-water system on some packings are shown below:

Packing	$C_1$	$C_2$
2.5 mm Raschig rings	316	4.0
4 mm Raschig rings	517	3.4
6 mm Raschig rings	384	3.4
3 mm spheres	227	1.52



Since both the knowledge of the pressure drop for gas flow in a prewetted bed and static liquid holdup are necessary in using this method for new systems, the method is not predictive but provides rational means for correlation of experimental data.

In a recent study Saez & Carbonell (1985) used the relative permeability approach to correlate the pressure drop and liquid holdup.

The starting equation for the approach of Saez and Carbonell is the single phase momentum balance for the gas and liquid phase using the Ergun equations. The Ergun equation provides an expression for the frictional interaction between the solid packings and the (single) flowing phase. The effect of the second flowing phase is now incorporated by defining a relative permeability. Thus, the following equations are obtained for the phase averaged pressure drop for the gas and liquid phases:

$$-\frac{d\langle P_L \rangle}{dx} + \rho_L g = \left[ \frac{A}{k_\beta} \frac{Re_L^*}{Ga_L^*} + \frac{B}{k_{\beta i}} \frac{Re_L^{*2}}{Ga_L^*} \right] \rho_L g, \quad (13)$$

$$-\frac{d\langle P_G \rangle}{dx} + \rho_g g = \left[ \frac{A}{k_\gamma} \frac{Re_G^*}{Ga_G^*} + \frac{B}{k_{\gamma i}} \frac{Re_G^{*2}}{Ga_G^*} \right] \rho_G g, \quad (14)$$

where

$k_\beta$  and  $k_{\beta i}$  are the liquid phase relative permeabilities for the viscous and inertial regimes and  $k_\gamma$  and  $k_{\gamma i}$  are the corresponding values for the gas phase. The parameters  $A$  and  $B$  are the constants in the Ergun type model for frictional pressure drop. The parameters  $Re_L^*$  and  $Ga_L^*$  are defined as follows:

$$Re_L^* = \rho_L u_L d_e / (1 - \varepsilon_B) \mu_L \varepsilon_l, \quad (15)$$

$$Ga_L^* = \rho_L^2 g d_e^3 \varepsilon_B^3 / \mu_L^2 (1 - \varepsilon_B)^3, \quad (16)$$

with corresponding definitions for  $Re_G^*$  and  $Ga_G^*$ .

The liquid and gas side pressures are related to the capillary pressure which is difficult to estimate in packed beds.

In the absence of significant surface tension interactions or for the case where the capillary pressure does not change with axial position we have

$$d\langle P_L \rangle / dx = d\langle P_G \rangle / dx. \quad (17)$$

Using the above relationship in (13) and (14) and rearranging, the following correlation is obtained for liquid holdup

$$\frac{A}{k_\beta} \frac{Re_L^*}{Ga_L^*} + \frac{B}{k_{\beta i}} \frac{Re_L^{*2}}{Ga_L^*} - \frac{\rho_G}{\rho_L} \left[ \frac{A}{k_\gamma} \frac{Re_G^*}{Ga_G^*} + \frac{B}{k_{\gamma i}} \frac{Re_G^{*2}}{Ga_G^*} \right] = 1. \quad (18)$$

Using the available experimental data, the relative permeabilities were correlated as a function of the reduced saturations

$$\delta_\beta = (\varepsilon_B - \varepsilon_{ls}) / (\varepsilon_B - \varepsilon_{ls}), \quad (19)$$

and

$$S_\gamma = \varepsilon_G / \varepsilon_B. \quad (20)$$



The following correlations were obtained

$$k_{\beta} = k_{\beta i} = \delta_{\beta}^{2.43}, \quad (21)$$

$$k_{\gamma} = k_{\gamma i} = S_{\gamma}^{4.8}, \quad (22)$$

Once the holdup is calculated from the trial-error solution of (18) the pressure drop can be calculated from (14). The parameters  $A$  and  $B$  were assigned values of 180 and 1.8, respectively, which is consistent with the original work of Ergun (1952). The method had a mean absolute deviation of 12.7% for liquid holdup and 21.9% for the pressure drop.

Rao (1979) and Rao & Drinkenburg (1983) proposed a correlation for the low interaction regime which can be represented as

$$\delta_{LG} = \{\delta_{GW}/[1 - (\epsilon_{ld}/\epsilon_B)]^3\} - \rho_G g, \quad (23)$$

where  $\delta_{GW}$  is the single phase pressure drop for the gas phase flowing in a prewetted bed. The model represented by (23) is also referred to as the geometric interaction model.

A common basis for comparison of the various correlations for pressure drop is the parameter  $\Delta P/\Delta P_w$ , where  $\Delta P_w$  is the pressure drop for flow of gas phase alone in a prewetted bed (Sicardi *et al* 1986). The values of  $\Delta P/\Delta P_w$  for the various correlations have been summarized by Sicardi *et al* (1986). The agreement between the various correlations and experimental data is reasonable when  $\Delta P/\Delta P_w$  is plotted as a function of  $(\epsilon_B - \epsilon_{ls})/(\epsilon_B - \epsilon_l - \epsilon_{ls})$ . A typical comparison plot is shown in figure 3.

### 3.2 Low interaction regime: Liquid holdup

Liquid holdup is the fractional volume of liquid in a reactor and is defined as the volume of liquid per unit column volume. Liquid saturation is the liquid volume per unit void volume. In porous packings the liquid holdup will be the sum of the internal (liquid held in the pores of the catalyst) and the external holdup. The internal holdup can be calculated as  $\epsilon_p(1 - \epsilon_B)$  when the inner pores of the particles are completely filled with the liquid. This conclusion is based on laboratory scale reaction or tracer studies and is valid for systems operating close to isothermality. The external holdup can then be calculated as:

$$\epsilon_l = \epsilon_{IT} - \epsilon_p(1 - \epsilon_B). \quad (24)$$

The external holdup can be divided into a static or residual holdup,  $\epsilon_{ls}$  and a dynamic or free draining holdup  $\epsilon_{ld}$

$$\epsilon_l = \epsilon_{ls} + \epsilon_{ld}. \quad (25)$$

A large number of correlations have been proposed for liquid holdup and these have been summarized by Gianetto *et al* (1978). Some correlations are for the total external holdup while others correlate the static and dynamic holdup separately.

The correlation of Sato *et al* (1973) is based on 2.6 to 24.3 mm glass spheres and is as follows:

$$\epsilon_l/\epsilon_B = 0.185a_t^{1/3} \chi^{0.22}, \quad (26)$$

where  $a_t$  is the surface area of the particles per unit volume of the column based on a modified diameter of the particle.

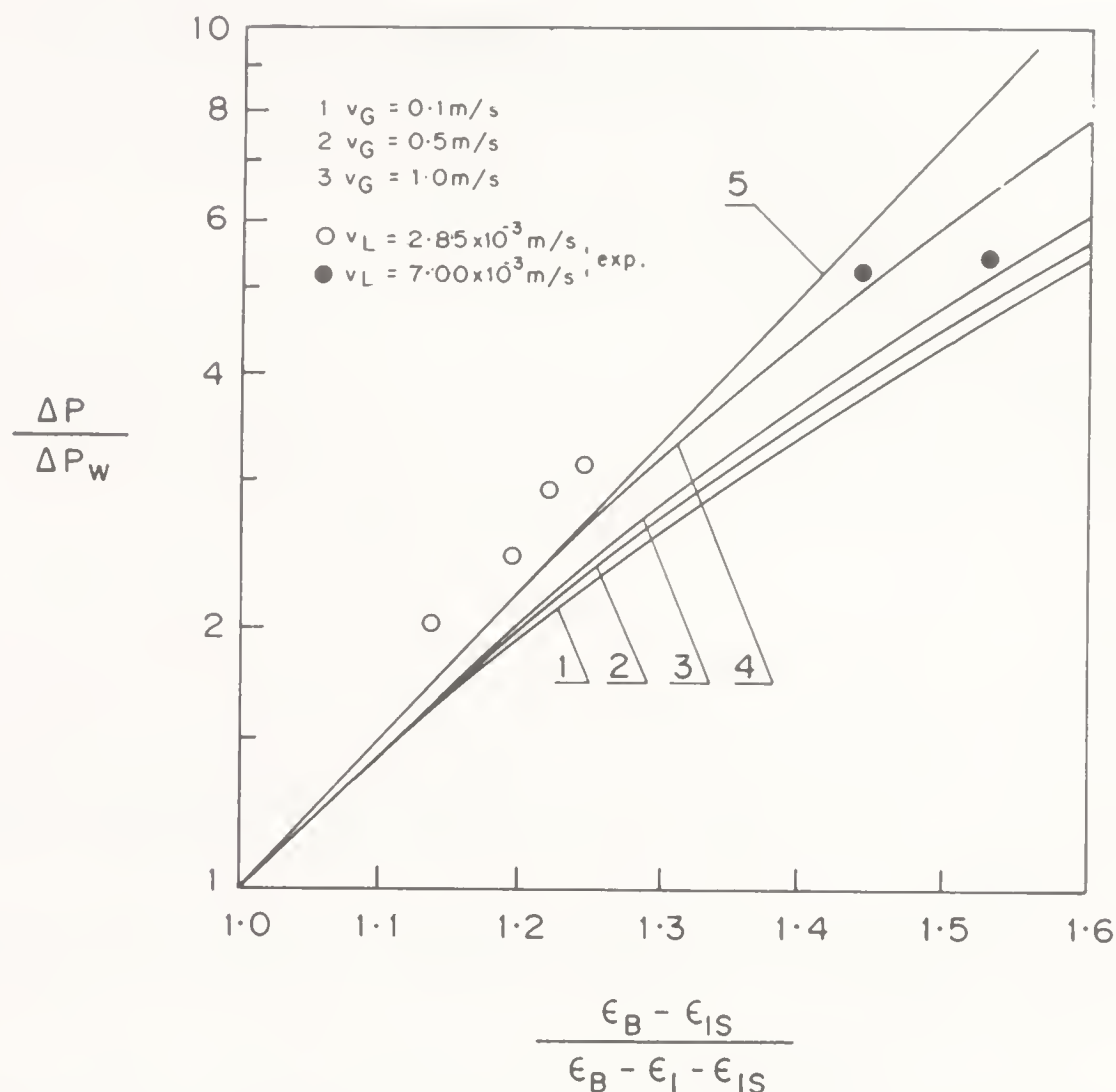


**Figure 3.** Comparison plot for various models for pressure drop prediction. Adapted from Sicardi *et al* (1986). Packings: 6 mm glass sphere; system: air-water.

$$a_l = 6(1 - \epsilon_B)/d_p^*, \quad (27)$$

where  $d_p^*$  is the diameter of the particle modified to account for wall effects.

$$d_p^* = \frac{d_p}{1 + [4d_p/6d_T(1 - \epsilon_B)]}. \quad (28)$$

Midoux *et al* (1976) proposed the following correlation for  $\epsilon_l$  based on 3 mm glass and catalyst spheres and  $1.8 \times 6$  and  $1.4 \times 5$  mm catalyst cylinders:

$$\epsilon_l/\epsilon_B = 0.66\chi^{0.81}/(1 + 0.66\chi^{0.81}), \text{ for } 0.1 < \chi < 80. \quad (29)$$

The parameter  $\chi$  in (26) and (29) is the square root of the ratio of pressure drop for gas and liquid flowing alone in the bed. This correlation is valid for nonfoaming systems for all hydrodynamic regimes, and for foaming systems for low interaction regimes. A separate correlation for foaming systems at high interaction regimes has been proposed by these authors.

Some correlations consider  $\epsilon_{ls}$  and  $\epsilon_{ld}$  separately, and these have a stronger theoretical basis, since  $\epsilon_{ld}$  is affected by all the operating parameters, while  $\epsilon_{ls}$

mainly depends on liquid and solid physical properties. The following correlation was proposed for  $\varepsilon_{ls}$  by Saez & Carbonell (1985):

$$\varepsilon_{ls} = 1/(20 + 0.9 Eo^*), \quad (30)$$

where  $Eo^*$  is a modified Eötvös number defined as

$$Eo^* = \rho_L g d_c^2 \varepsilon^2 / \sigma_L (1 - \varepsilon)^2. \quad (31)$$

Specchia & Baldi (1977) proposed the following correlation for predicting  $\varepsilon_{ld}$ , which is based on a voluminous amount of data for 6 mm glass spheres, 2.7 and 5.4 mm glass cylinders, and 6.4, 10.3 and 22 mm Raschig rings.

$$\varepsilon_{ld}/\varepsilon_B = 3.86 Re_L^{0.545} (Ga_L^*)^{-0.42} [a_p d_p / \varepsilon_B]^{0.65}, \quad \text{for } 3 < Re_L < 470, \quad (32)$$

where  $Ga_L^*$  is a modified Galileo number defined as

$$Ga_L^* = d_p^3 \rho_L (g \rho_L + \delta_{LG}) / \mu_L^2. \quad (33)$$

A correlation for liquid holdup based on the relative permeability concept was developed by Saez & Carbonell (1985). This correlation is discussed in §3.1 on pressure drop [see (18)].

El-Hisnawi *et al* (1981) proposed the following correlation for the dynamic external liquid holdup.

$$\varepsilon_{ld} = 2.02 \varepsilon_B Re_L^{0.344} Ga_L^{-0.197} \quad (34)$$

This correlation is based on extensive data on porous packing. At low liquid flow rates the external surface of the catalyst may not be completely wetted. For such cases, the following correlation was proposed by Mills & Duduković (1981, 1982):

$$\varepsilon_{ld} = 1.74 f_w^{2/3} [Re_L / Ga_L^*]^{1/3} (a_p d_p)^{2/3} \quad (35)$$

The term  $f_w$  is defined as the fraction of the external liquid surface which is wetted by the catalyst. The theoretical model for film flow over a single sphere and concepts from percolation theory were used to develop this correlation.

Holdup predictions based on these correlations are on the average within 35% of each other. Attempts to introduce dimensionless numbers that contain surface tension effects led to no improvements in matching the available data. It appears that the effect of surface tension on the total liquid holdup comes mainly through the static holdup. For practical calculations the correlations of Specchia & Baldi (1977) and Mills & Duduković (1981) have proved to be useful.

### 3.3 High interaction regime

In the high interaction regime (pulsing flow) the empirical correlation of Turpin & Huntington (1967) is commonly used for calculation of the pressure drop. These authors used the friction factor defined by the following equation to correlate the pressure drop data:

$$\delta_{LG} = (2u_G^2 \rho_G / d_{pe}) f_{GL}, \quad (36)$$

where  $d_{pe}$  is an equivalent particle diameter defined by:



$$d_{pl} = \frac{2}{3} (d_p \varepsilon_B) / (1 - \varepsilon_B). \quad (37)$$

The two-phase friction factor is then correlated by the following equation (Specchia & Baldi 1977):

$$\ln f_{GL} = 7.82 - 1.30 \ln \left[ \frac{Z}{\psi^{1.1}} \right] + 0.573 \ln \left[ \frac{Z}{\psi^{1.1}} \right]^2, \quad (38)$$

where

$$Z = Re_G^{1.167} / Re_L^{0.767}, \quad (39)$$

and

$$\psi = (\sigma_w / \sigma_L) [\mu_L / \mu_w (\rho_w / \rho_L)^2]^{1/3}. \quad (40)$$

The liquid holdup in the high interactive regime was also correlated by Specchia and Baldi using the parameter  $Z$ .

$$\varepsilon_{ld} = 0.123 \varepsilon_B (Z / \psi^{1.1})^{-0.312} [a_p d_{pc} / \varepsilon_B]^{0.75} \quad (41)$$

Experimental measurements of the holdup data and the corresponding actual liquid velocities indicate that a part of the liquid in the pulsing regime travels at a high velocity, which is comparable to the actual gas velocity. The fraction of the liquid travelling at high velocity probably corresponds to the liquid in excess of that required to cause pulsing. The analogy between this and a gas-solid fluidized bed is worth noting here. In a fluidized bed, the gas in excess of that required for minimum fluidization travels as a bubble phase. It appears that there is a hydrodynamic similarity between the fluidized bed and the pulsing trickle-bed and this analogy should be exploited in further basic studies.

Rao & Drinkenburg (1985) analyzed pulsing flow regime from a fundamental hydrodynamic point of view. They divide the column into two regions, (i) a region of large liquid holdup occupied by the pulse and (ii) a region of low liquid holdup in a gas continuous regime. The schematic of a pulsing trickle-bed proposed by Rao & Drinkenburg (1985) is shown in figure 4. The liquid pulse sweeps through the column at a frequency  $f_p$ . Figure 4, therefore, shows an instantaneous snapshot of

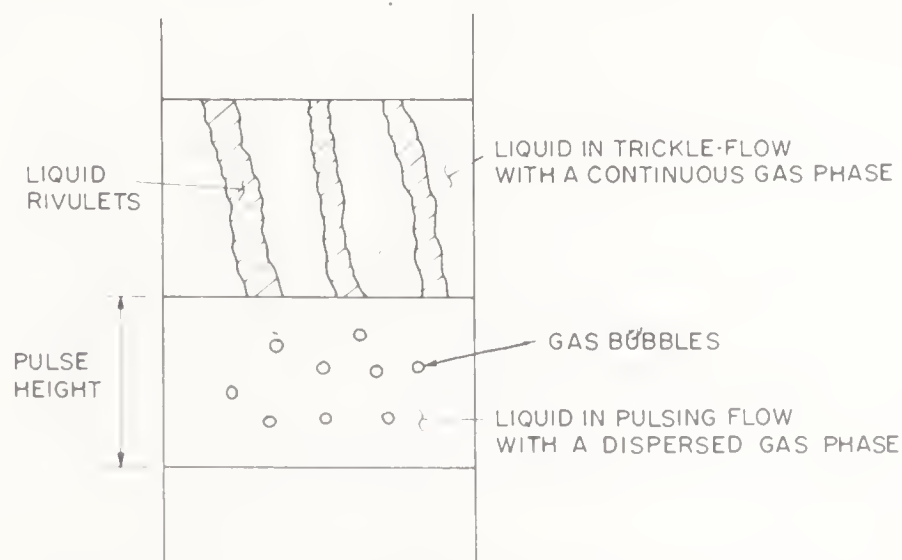


**Figure 4.** Schematic of the model for a pulsing regime proposed by Rao & Drinkenburg (1985).



the column. If the pulse velocity is  $v_p$  then the number of pulses per unit column height is  $f_p/v_p$  and therefore the fraction,  $H_{PT}$ , of a unit column height occupied by the pulse is equal to  $N_p H_p$  where  $H_p$  is the pulse height.

The pressure drop is assumed to consist of three independent contributions: (i) pressure drop due to geometric interaction in the gas continuous region, (ii) pressure drop due to geometric interaction in the pulse, and (iii) additional contribution due to dynamic interaction in the pulse regime resulting from the gas bubble formation, liquid acceleration and liquid turbulence. The pressure drop per unit column height can therefore be expressed as

$$\delta_{LG} = (1 - H_{PT})\delta_{LG,GC} + H_{PT} \delta_{LG,P} + \delta_{LG,B} + \delta_{LG,M} + \delta_{LG,A}, \quad (42)$$

where,

$\delta_{LG,GC}$  is the pressure drop contribution from the gas continuous region (trickling flow part of the column),

$\delta_{LG,P}$  = pressure drop contribution from the pulsing part of the column,

$\delta_{LG,B}$  = extra pressure drop due to gas dispersion into the pulse,

$\delta_{LG,M}$  = pressure drop due to mixing and turbulence in the liquid pulse,

$\delta_{LG,A}$  = pressure drop due to liquid acceleration as the liquid enters a pulse.

Equations have been developed for calculating each of the above pressure drop contributions by Rao & Drinkenburg (1985). For the sake of brevity, those equations are not reproduced here. A satisfactory fit of the experimental data ( $\pm 30\%$ ) was obtained by using their model. The pressure drop due to bubble dispersion and pressure drop due to liquid acceleration were found to be comparable to each other at low liquid rates. At higher rates the bubble dispersion pressure drop dominates over the acceleration pressure drop. The mixing pressure drop was not found to be important.

The above model results in a large number of basic parameters to characterize the flow in a trickle-bed. These are pulse frequency, pulse velocity, pulse height, liquid holdup in the trickling part of the pulse and liquid holdup in the pulsing part. These hydrodynamic parameters were measured in an earlier paper by Blok & Drinkenburg (1982). The total liquid holdup was determined by a tracer technique and the pulse properties were determined by conductivity measurements with two sets of conductivity cells (wire mesh nettings) placed 5 cm apart. The time difference between the minimum resistance values for the two signals, in combination with the distance between the two electrode sets, provides the value of pulse velocity. The conductivity cell was also calibrated separately by operating in the gas continuous flow regime using independent liquid holdup measurements by tracer techniques. Using these calibrations, the pulse holdup and base holdup (that in the trickling part of the column) could be measured. Pulse frequency would be measured by noting the time at which the minimum resistance value is attained at either of the two conductivity probes. In a recent study Christensen *et al* (1986) used a microwave probe to determine the flow parameters for the pulsing regime. A two-dimensional rectangular column was used in this work. It was observed that the pulse did not span the entire column cross-section unlike the case of small diameter columns.

A model to calculate the pressure drop in pulsing flow was also developed by

Dimenstein & Ng (1985). The model is similar to the approach of Rao and Drinkenburg and the pressure drop is calculated as the sum of the two contributions from the pulsing and trickling part of the column. For each of these calculations a form of Ergun equation was used. Additional contribution to pressure drop resulting from the liquid acceleration as the liquid enters a pulse was introduced. The contributions of liquid deceleration and gas dispersion was not accounted for unlike in the work of Rao and Drinkenburg. Further, the Ergun coefficient for a dry bed was used. The model appears to be satisfactory at moderate gas flow rates. Further work is clearly needed along these directions especially using porous catalysts for experiments.

#### 4. Conduit models for trickle-beds

A periodically constricted tube has proven to be a useful model to represent single phase flow through packed beds (see Pendse *et al* 1983, for instance). Insights into a number of transport processes in a packed bed such as axial dispersion, solid-liquid mass transfer etc., could be obtained through simulation of flow in a periodically constricted tube. It is therefore likely that a periodically constricted tube will serve as a useful model for study of flow behaviour in trickle-beds. This requires the simulation of two-phase flow in such a geometry, which is a considerably more complex problem than the problem of simulation of single phase flow. Saez *et al* (1986) obtained a numerical solution for a cubic array of spheres for the viscous flow regime by finite element techniques. A schematic of the geometry used in their work is shown in figure 5. The simulated results were used to predict the relative permeabilities of the gas and liquid. The predicted solutions indicate that the relative permeability is a strong function of the surface tension forces, contrary to experimental observations. The discrepancy may be due to the fact that inertial forces were neglected in the solution of the Navier-Stokes equation. Gyure & Krantz (1983) have shown that the inertial effects are of extreme importance in the problem of free surface flow over a sphere. In a recent study done in our laboratory, Holub (unpublished) simulated the flow including the inertial effects. Two significant differences were observed when the inertial effects were included in

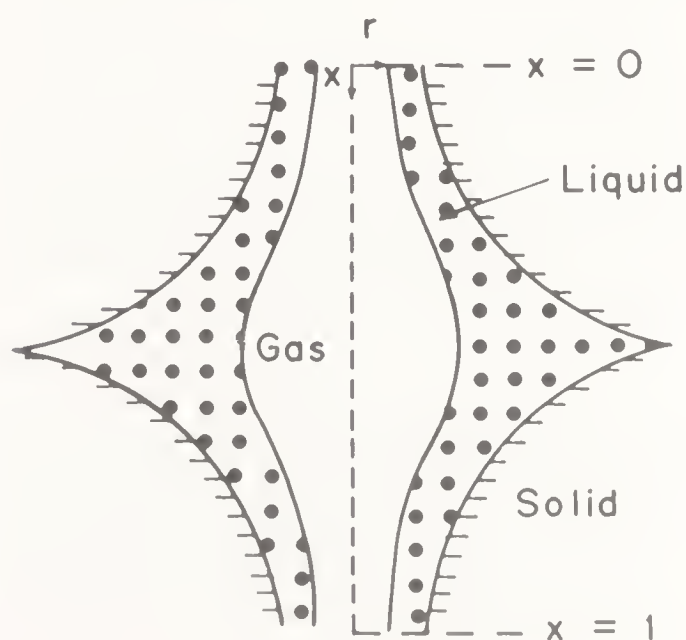


Figure 5. Schematic of the conduit model to simulate trickle-beds used by Saez *et al* (1986) and Holub (unpublished).



the computations: (i) the gas-liquid interface shape becomes flatter indicating a reduced role of surface tension which is consistent with experimental trends, (ii) a recirculating flow developed near the solid surface. Work is currently in progress in correlating the basic trickle-bed design parameters using this approach.

The constricted tube model does not fully represent the liquid mixing that takes place at packing junctions. For this purpose, more complex pore space models used to study the transport phenomena in porous media are likely to prove useful. The single constricted capillary forms a basic unit cell here and these pore space models essentially consist of constricted capillaries connected in series and/or in parallel and have proved successful in predicting the various phenomena such as hysteresis etc. (Hysteresis behaviour has also been observed in trickle-beds with nonporous packings as shown by Kan & Greenfield 1978, and others.) Van Brakel (1975) has provided a useful summary of the various models. Alternatively, the constricted capillaries could be connected using the percolation concepts (Crine *et al* 1980) to develop a model for the flow in trickle-beds. The advantage of using the two-phase flow in constricted tubes to represent the various bonds in the percolation context is that considerable basic physics can be imbedded into the model. Significant progress in this direction can be expected in the near future.

## 5. Use of tracers

A number of basic design parameters in trickle-beds can be obtained using tracers. Due to the heterogeneous nature of the system, the interpretation of tracer data is more complicated as compared to single phase systems. This section of the paper summarizes the progress in this area.

Nonvolatile nonadsorbing tracers have been traditionally used to evaluate liquid holdup and backmixing. These studies have been summarized by Schwartz *et al* (1976), Duduković & Mills (1986) and Ramachandran & Chaudhari (1983).

Following the work of Schneider & Smith (1968) and of Colombo *et al* (1976), the first and second moment equations for a pulse input are

$$\mu_1 = (L/u_L) [\epsilon_I + (1 - \epsilon_B) (\epsilon_p + \rho_p K'_A)], \quad (41)$$

and

$$\begin{aligned} \mu'_2 = & [(2/Pe) - (2/Pe^2) (1 - e^{-Pe})] \mu_1^2 \\ & + [6(1 - \epsilon_B)R^2L/u_L] (\epsilon_p + \rho_p K'_A)^2 [(1/45D_e) + (1/9k_sR)]. \end{aligned} \quad (42)$$

Equation (42) is based on the assumption that the adsorption rate is very rapid and that axial dispersion can be used to describe the flow pattern of the external liquid. For a nonadsorbing tracer (i.e.,  $K'_A = 0$ ), (41) can be expressed as

$$\mu_1 = \epsilon_{IT}L/u_L, \quad (43)$$

where  $\epsilon_{IT}$  is the total (external as well as internal) liquid holdup and is defined by (24). Liquid holdup can therefore be obtained from the measured first moments. For an adsorbing tracer an additional contribution of the adsorption equilibrium constant to  $\mu_1$  results as indicated by (41). The adsorption acts as a time delay for the process.

In the case of a partially wetted catalyst, Schwartz *et al* (1976) suggested a modified equation for the first moment:

$$\mu_1 = (L/u_L) [\varepsilon_{IT} + f_i(1 - \varepsilon_B)\rho_p K'_A], \quad (44)$$

where  $f_i$  is the wetted fraction of the total internal area of the catalyst. The basis for the derivation of (44) is that adsorption occurs only from the wetted portions of the catalyst, and hence the factor  $f_i$  appears in the second term of (45).

The measurement of the first moment using both an adsorbable and a nonadsorbable tracer under identical operating conditions can therefore be used to predict the fraction of the internal area wetted by the catalyst. This can be done by measuring  $\mu_1$  for an adsorbing and nonadsorbing tracer in a trickle-bed as well as in a liquid filled bed at identical flow rate. Using these data,  $f_i$  can be directly calculated as

$$f_i = [(\mu_{1TB})_{\text{adsorbing}} - (\mu_{1TB})_{\text{nonadsorbing}}] / [(\mu_{1LF})_{\text{adsorbing}} - (\mu_{1LF})_{\text{nonadsorbing}}], \quad (45)$$

where the subscripts TB and LF refer to trickle-bed and liquid full operations, respectively.

Equation (45) is model independent based on the sound theoretical background of the central volume principle (Buffham & Kropholler 1973). The experimental data show that the internal pore filling is complete for moderately isothermal conditions probably due to capillary action.

The second moment data may be useful in determining the axial dispersion coefficient (Schwartz *et al* 1976) but the results are accurate only for nonporous packings. This is because the spread in tracer response is a combined effect of axial dispersion and intraparticle diffusion for porous particles. (The second term on the RHS of (42) is often much larger than the first term which represents the contribution of axial dispersion.) Methods of decoupling the external nonidealities will be discussed in §6.

Tracer methods can also be used to evaluate the external contacting efficiency in trickle-bed. External contacting efficiency refers to the fraction of the external catalyst surface wetted by the liquid. The evaluation of this parameter by tracer methods is however not well defined and no theoretical basis is available. If one uses the equations derived by Suzuki & Smith (1970) and Sagara *et al* (1970), an effective intraparticle diffusivity can be calculated from the measured variance of the impulse response of a completely wetted pellet for a nonvolatile tracer. The intraparticle diffusivity calculated from the experimental impulse response in trickle-beds from this model is found to be less than the value obtained by independent means (for example from tracer experiments from a liquid full operation which ensures complete wetting). This apparent difference in intraparticle diffusivity was attributed due to the effects of incomplete external contacting by Colombo *et al* (1976) who proposed the formula

$$f_w = [(D_e)_{\text{Trickle bed}} / (D_e)_{\text{Liquid full}}]^{1/2}. \quad (46)$$

The results of  $f_w$  computed by this method did not however agree well with other experimental evidence. To correct for that Baldi & Gianetto (1980) suggested the following equation:

$$f_w = [(D_e)_{\text{Trickle bed}} / (D_e)_{\text{Liquid full}}]^{1/2}. \quad (47)$$



This formula provides data that seem to be in agreement with reaction studies (Mills & Duduković 1981, 1982) but lacks a firm theoretical basis. How tracer data should be properly interpreted and contacting efficiency extracted is an important question that needs to be answered.

In a recent study, Ramachandran *et al* (1986b) analysed theoretically the dynamic response of a catalyst particle whose external surface is only partially wetted. This leads to a new type of transient mixed boundary value problem which can be solved by a dual series technique. The solutions presented in the Laplace domain provides a method for determining the external contacting efficiency without the need for involving any heuristic arguments as done in earlier studies. Preliminary results indicate that a single exponent for the diffusivity ratio such as 0.5 or 1 may not be found for the entire range of contacting efficiencies and the exponent would be a function of the contacting efficiency.

## 6. Decoupling tracer response

As indicated in the last section, the measured tracer response is a combined effect of the global (axial dispersion, nonuniform distribution, bypassing etc.) and local or particle scale (incomplete contacting, intraparticle diffusion etc.) nonidealities and it is necessary to decouple the effects in order that the tracer data can be effectively used for scaleup and also for diagnostics of malfunctioning units. Recently, considerable progress has been made in this area (Kennedy & Jafee 1986; Ramachandran *et al* 1986a) and the key points will now be reviewed without going into detailed derivations.

The procedure is based on the assumption that the nonvolatile nonadsorbing tracer follows the path that a nonvolatile reactant would take. We also assume that the system can be divided into two regions (the bulk liquid and the catalyst) which communicate with each other through a transfer or exchange coefficient. Generalization to systems with more than two regions is straightforward and might be necessary to include effects such as bypassing or presence of static holdup, etc., but is not dealt with explicitly here.

The dynamic response of a nonadsorbing nonvolatile tracer can be represented as

$$\mathcal{L}(C_L) = \varepsilon_l \partial C_L / \partial t + k_{ex} [C_L - C_p], \quad (48)$$

where  $C_L$  is the concentration of the tracer in the external liquid (whose holdup is  $\varepsilon_l$ ),  $C_p$  is the concentration of tracer corresponding to the particle phase,  $\mathcal{L}$  is a differential or algebraic operator characterizing the nonidealities of flow of the external fluid,  $k_{ex}$  is the exchange or mass transfer coefficient between the two regions and  $t$  is the time elapsed since tracer was introduced.

To illustrate this equation more clearly, if the axial dispersion model is used for the external liquid, then  $\mathcal{L}$  takes the form:

$$\mathcal{L}(C_L) = D_{EL} \frac{\partial^2}{\partial x^2} (C_L) - u_L \frac{\partial}{\partial x} (C_L). \quad (49)$$

Taking the Laplace transform of (48) one obtains

$$\mathcal{L}(\bar{C}_L) = \varepsilon_L s \bar{C}_L + k_{ex}(\bar{C}_L - \bar{C}_p). \quad (50)$$

Using a model for the dynamic response of the catalyst particle, the quantity  $(\bar{C}_L - \bar{C}_p)$  can be expressed as

$$\bar{C}_L - \bar{C}_p = \bar{C}_L H(s), \quad (51)$$

where  $H(s)$  now represents a particle scale transfer function.

Using this relationship, (50) can be represented as

$$\mathcal{L}(\bar{C}_L) = \varepsilon_L \bar{C}_L \left[ s + \frac{k_{ex} H(s)}{\varepsilon_l} \right] = \varepsilon_l \bar{C}_L p, \quad (52)$$

where

$$p = s + k_{ex} H(s)/\varepsilon_l. \quad (53)$$

The dynamic response of a tracer which stays only in the external fluid can be expressed in Laplace domain as

$$\mathcal{L}\bar{C}_{L,e} = \varepsilon_l s \bar{C}_{L,e}, \quad (54)$$

where the subscript  $e$  is used to indicate that the measured response represents only the external nonidealities.

The analogy between (52) and (54) provides a method for isolating the residence time distribution of the external fluid alone. The procedure is as follows. From the actual experimentally obtained response in the time domain of the nonadsorbing nonvolatile tracer we obtain the response in the Laplace domain for various values of  $s$  by integration as shown below:

$$\bar{C}_{L1}(s) = \int_0^\infty e^{-st} C_{L1}(t) dt, \quad (55)$$

where the subscript 1 indicates the outlet of the reactor.

To start with we assume a model for particle scale contacting. This gives us a specific form for  $H(s)$ . For each value of  $s$ , one can calculate  $p = s + k_{ex}(H(s)/\varepsilon_l)$  and group the data as  $\bar{C}_{L1}$  vs  $p$ . Then  $\bar{C}_{L1}(p)$  gives directly the nonidealities of the external fluid in the Laplace domain and the exit age density function for the external fluid can be obtained by inversion of  $C_{L1}(p)$ , i.e.,  $C_{L1}(t) = \mathcal{L}^{-1}\{\bar{C}_{L1}(p)\}$ . The procedure is shown schematically in figure 6.

If the tracer were of the adsorbing type with a linear isotherm, the above procedure is still valid provided the necessary modification to  $H(s)$  is made to include the effects of adsorption. Use of adsorbing vs non-adsorbing tracer now offers the possibility of discriminating between the assumed particle scale models. Experiments with several tracers of different adsorptivity can be performed. The correct particle scale model should result in the identical model for sojourn times for the external fluid. This procedure (two independent experiments with nonadsorbing and adsorbing tracer) then determines both the particle scale and bed scale transfer functions uniquely.

The response of the external liquid in the Laplace domain can also be used to

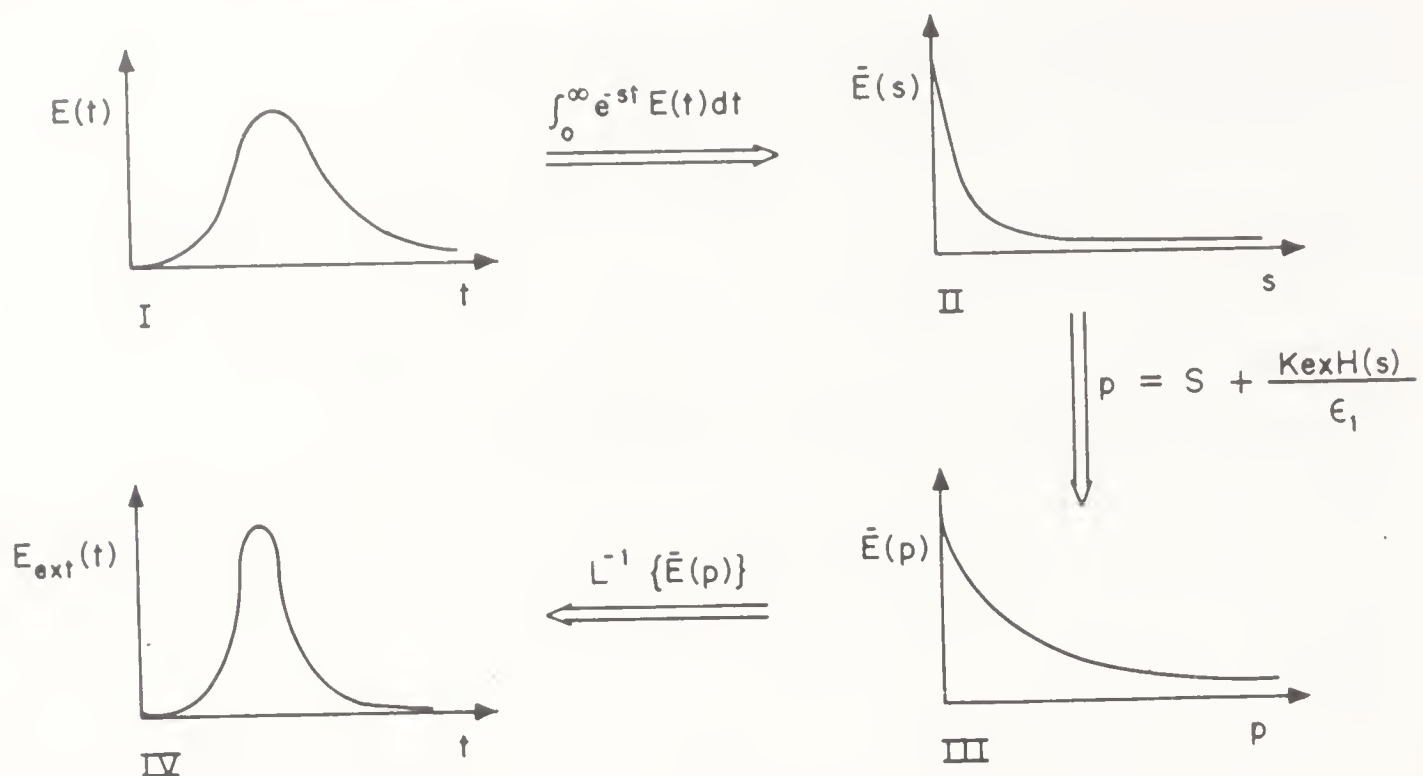


Figure 6. Procedure to decouple external liquid transfer function from the measured tracer response.

calculate the conversion of a first order liquid limiting reaction:

$$1 - X_s = \bar{C}_{L1,e} p = k_{ex} H(k_p) / \epsilon_l \quad (56)$$

where  $k_p$  represents the rate constant for a first order reaction per unit catalyst pore volume. Thus, if  $k_p$  is known from independent measurement the conversion can be predicted in the trickle-bed reactor and matched with experiments. This will provide an additional check on the consistency of the data.

Kennedy & Jaffee (1986) used a similar procedure to determine the flow maldistribution in trickle-beds. The particle transfer function was assumed to be that for a completely wetted spherical catalyst. The form of  $H(s)$  for this case is given by Ramachandran & Smith (1979a).

$$H(s) = (D_e/k_s R) \{ (\epsilon_p s / D_e)^{1/2} R \coth [ (\epsilon_p s / D_e)^{1/2} R ] - 1 \} / [ 1 + (D_e/k_s R) \{ (\epsilon_p s / D_e)^{1/2} R \coth [ (\epsilon_p s / D_e)^{1/2} R ] - 1 \} ]. \quad (57)$$

It may be noted here that the contribution of the solid-liquid mass transfer is often negligible in the above equation. This would simplify the transfer function even further.

The flow maldistribution in the external fluid could be isolated by this method. Using the transfer function of the external fluid, Kennedy and Jaffee modelled the reactor as two zones with unequal mass flux but otherwise in ideal plug flow (figure 7). The impact of the flow distribution on the reactor performance was estimated by coupling a kinetic model to the flow model.

The above procedure for decoupling the transfer function was applied to an industrial reactor by Ramachandran *et al* (1986b). A tracer curve for an industrial reactor is shown in figure 8. The corresponding overall response in the Laplace domain  $\bar{C}_{L1}(s)$  and the response of the external fluid alone obtained by the decoupling procedure  $\bar{C}_{L1,e}(p)$  is shown in figure 9. If the external fluid were in plug flow the Laplace response would be given as  $1 - \exp(-\bar{t}s)$ , where  $\bar{t}$  is the mean



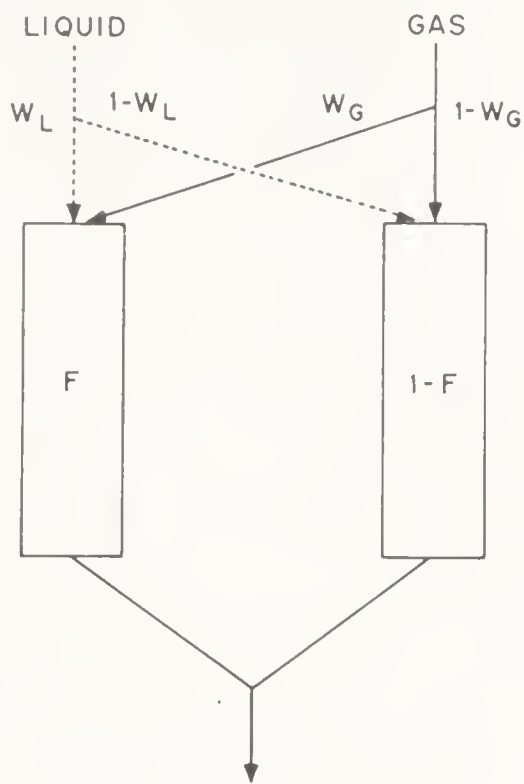


Figure 7. Reactor model for industrial scale trickle-beds proposed by Kennedy & Jaffee (1986).

residence time of the liquid in the reactor. This response is also shown in figure 9 for comparison. It is seen that the flow pattern of the external liquid in the industrial reactor deviates considerably from plug flow behaviour.

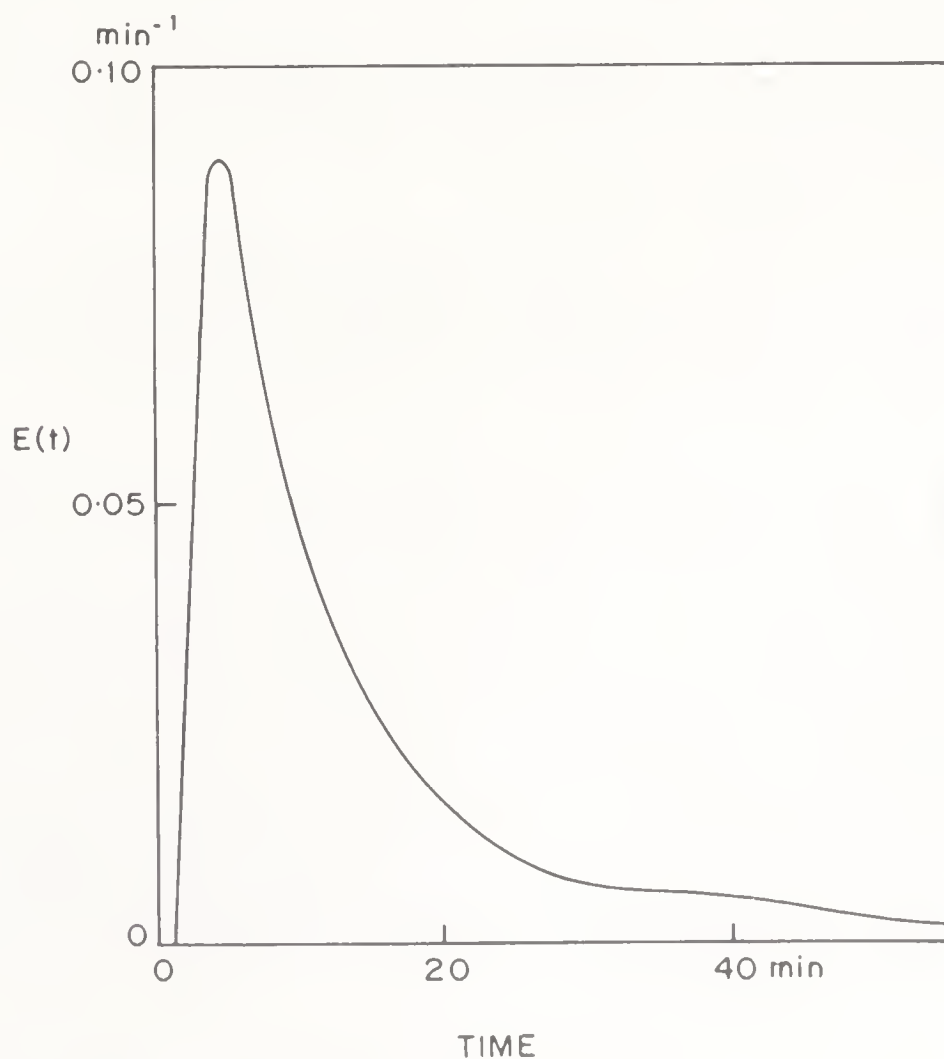


Figure 8. Tracer curves for a 2.1 m diameter industrial reactor.



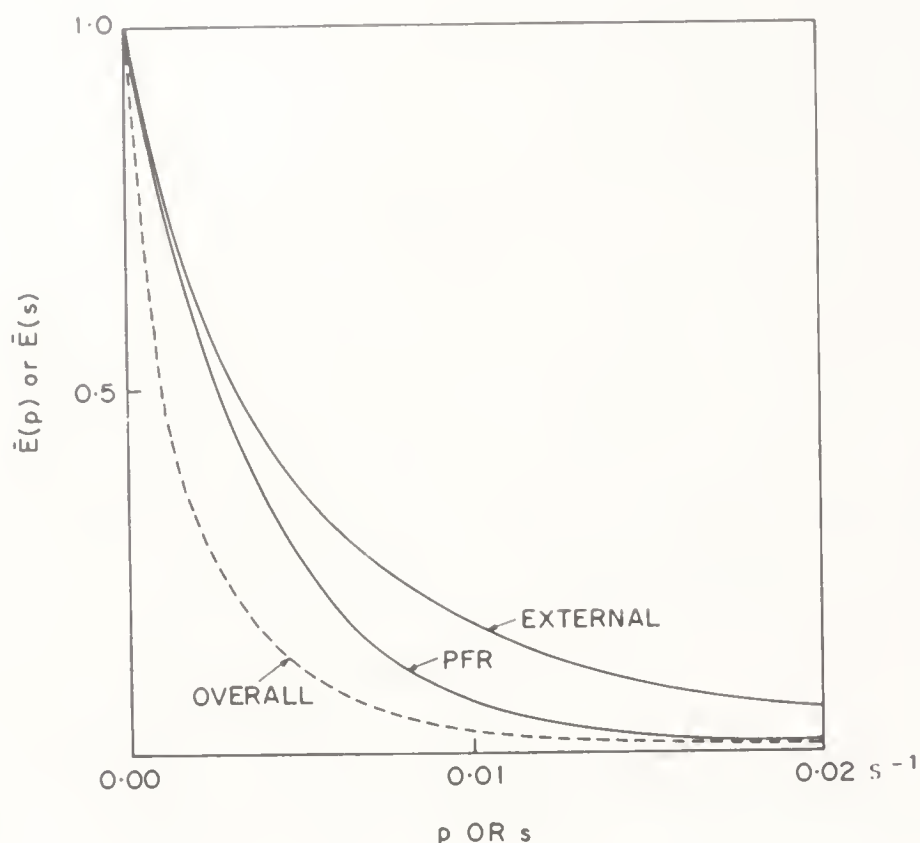


Figure 9. Tracer response in Laplace domain for the industrial reactor.

## 7. Influence of partial wetting

At low liquid superficial velocities ( $< 0.5$  to  $0.6$  cm/s) the external surface of the catalyst is not completely wetted. The fraction of the external area wetted by the liquid is referred to as the contacting efficiency and can be determined by tracer methods as discussed in §5. El-Hisnawi *et al* (1981) measured this important parameter and correlated the results by the following equation:

$$f_w = 1.617 Re_L^{0.1461} Ga_L^{-0.0711}. \quad (58)$$

This correlation is based on an extensive database on four different hydrocarbon solvents on porous packing and predicts experimental results within an accuracy of  $\pm 10\%$ . The effect of partial wetting on the reactor performance will now be discussed.

A partially wetted catalyst can be modelled by considering either a slab, cylinder or sphere whose external surface is divided into a liquid covered and a gas covered, part as shown in figure 10. (The gas covered part may actually be covered by a very thin liquid film which does not alter this conceptual model significantly.) It can also be assumed that the internal pores are completely wetted which is a valid assumption for isothermal or mildly exothermic systems. The model equations are of the mixed boundary value type and can be solved by the dual series method developed by Mills & Duduković (1979) for first order gas or liquid limiting reactions. As a simplified approximate solution, the overall effectiveness factor of a partially wetted catalyst can be obtained as the weighted sum of the effectiveness factors for totally wetted and totally dry pellets (Ramachandran & Smith 1979b). This expression can be generally written as

$$\eta_{o,TB} = f_w \eta_w + (1 - f_w) \eta_D, \quad (59)$$

where  $\eta_w$  is the effectiveness factor of an actively wetted pellet and  $\eta_D$  is an

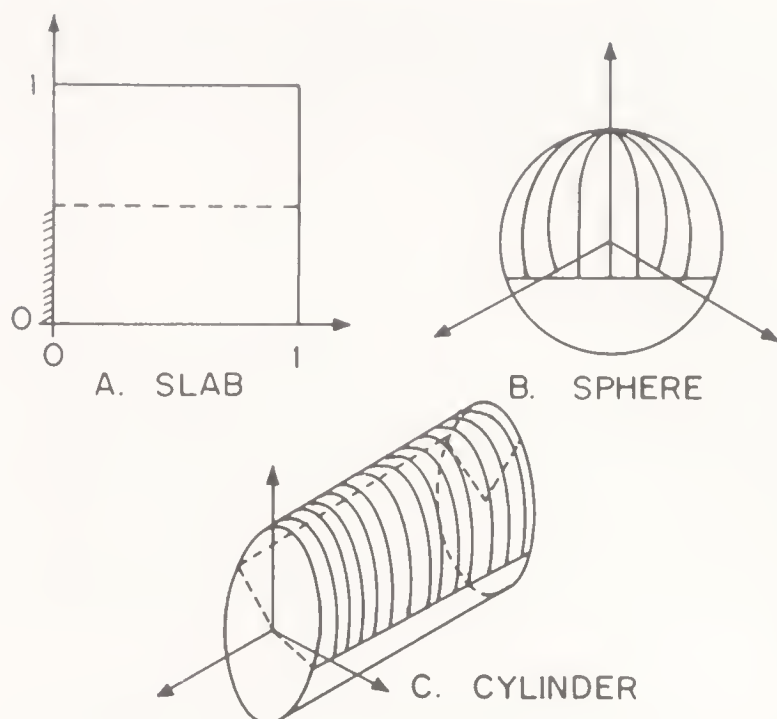


Figure 10. Representation of partial external wetting for various catalyst shape adapted from Mills & Duduković (1979).

effectiveness factor of a dry or an inactively wetted pellet. The equations  $\eta_w$  and  $\eta_D$  for a slab geometry are as follows:

$$\eta_w = 1/[(\phi^2/Bi_w) + (\phi/\tanh \phi)], \quad (60)$$

$$\eta_D = 1/[(\phi^2/Bi_D) + (\phi/\tanh \phi)], \quad (61)$$

where  $Bi_w$  and  $Bi_D$  are the Biot numbers for the wet and dry portions defined as  $k_{s,w}R/D_e$  and  $k_{s,D}R/D_e$  respectively. Here  $\phi$  is the Thiele modulus for a first-order reaction.

The corresponding equations for cylindrical and spherical geometry have been provided by Mills & Duduković (1980). The maximum error between the approximate solution and the exact solution is 12.8% for a gas limiting reaction and 38% for a liquid limiting reaction.

When the limiting reactant is in the liquid phase, the expression for the overall effectiveness factor of a partially wetted catalyst can be expressed as

$$\eta_{D,TB} = (f_w/\phi) \tanh (\phi/f_w)/[1 + (\phi/Bi_w) \tanh (\phi/f_w)]. \quad (62)$$

This expression is useful for analysing performance data on commercial hydrodesulphurization. It is seen that the overall effectiveness factor depends on three independent parameters  $f_w$ ,  $k_s(Bi_w)$  and  $D_e$  in addition to the rate constants and a simple power law correlation of the type  $\eta_o \propto u_L^\beta$  is unlikely to be valid over the entire range. This also explains the fact that when the commercial hydrodesulphurization data were plotted as  $(1-X)$  vs  $(1/LHSV)$  on a log-log scale a unique slope was not obtained and the slope varied from 0.53 to 0.92 (Paraskos *et al* 1975).

For power-law kinetics, analytical solutions based on the dual series method are not possible. The exact numerical solution can be approached using Galerkin finite element method as shown in a recent work by Mills *et al* (1986). In an earlier paper, Goto *et al* (1981) solved this problem by using a finite difference scheme with a fixed grid size. The solution accuracy can be improved by the finite element method since it is possible to use fine meshes in regions of steep concentration gradients. The diffusional characteristics of catalyst particles of irregular geometry such as trilobes, stars, macaroni or wagon wheels which are patented shapes used in

residuum hydrotreating (Dautzenberg 1984) can also be easily simulated using finite elements. Additional work in this direction may be necessary to find the optimum catalyst shape for hydrotreating processes.

## 8. Reactor design

Mills & Duduković (1983) proposed a generalized dispersion model for isothermal trickle-beds that include incomplete external contacting and compared various limiting cases of the model to experimental trickle-bed performance data using the hydrogenation of  $\alpha$ -methylstyrene as a test reaction. It should be noted that at atmospheric pressure, at which the experiments were conducted, this reaction is gas reactant (hydrogen) limited. Some of the performance equations, that were included, are as follows:

1. Completely wetted pellets with internal diffusion resistance controlling as typically encountered in basket reactors.
2. Completely wetted pellets with gas-to-liquid mass transfer resistance controlling.
3. Completely wetted pellets with liquid-to-solid mass transfer resistance controlling.
4. Partial externally wetted pellets with finite mass transfer resistance at the actively wetted catalyst surface with negligible mass transfer resistance at the inactive wetted catalyst surface.
5. Partial externally wetted pellets with unequal, finite mass transfer resistances at the actively and inactive wetted catalyst surfaces. The results can be summarized as follows: the model equation for case 1 always greatly overpredicted the measured trickle-bed conversion; while the model predictions for cases 2 and 3 were substantially less than the experimental values when the literature correlations for gas-liquid and solid-liquid mass transfer coefficients were used. The model predictions for case 4 underpredicted the experimental conversion for smaller values of space time but gave significant overprediction at larger values of liquid space time. Good agreement between the experimental and predicted values were obtained for case 5 except at very low liquid velocities. A comparison between the experimental and model predicted results is shown in figure 11 for two different reaction solvents (hexane and cyclohexane) along with the external contacting parameter ( $f_w$ ) values predicted by the correlation of El-Hisnawi *et al* (1981).

The experimental results are significantly lower than the theoretical results at low liquid velocity. Beaudry *et al* (1986) developed a model to explain these discrepancies. The model views the trickle-beds as consisting of particles which are completely dry, half wetted and fully wetted. The overall effectiveness factor is obtained by combining the effectiveness factors for these particles in the following manner

$$\eta_o = (1 - f_w)^2 \eta_D + 2(1 - f_w)f_w \eta_{Dw} + f_w^2 \eta_w, \quad (64)$$

where the subscripts  $D$ ,  $Dw$  and  $w$  represent dry, half wetted and fully wetted particles, respectively. For a nonvolatile reactant  $\eta_D = 0$ . For a half wetted slab, the nonvolatile reactant (such as  $\alpha$ -methyl styrene) can be supplied to the pellet



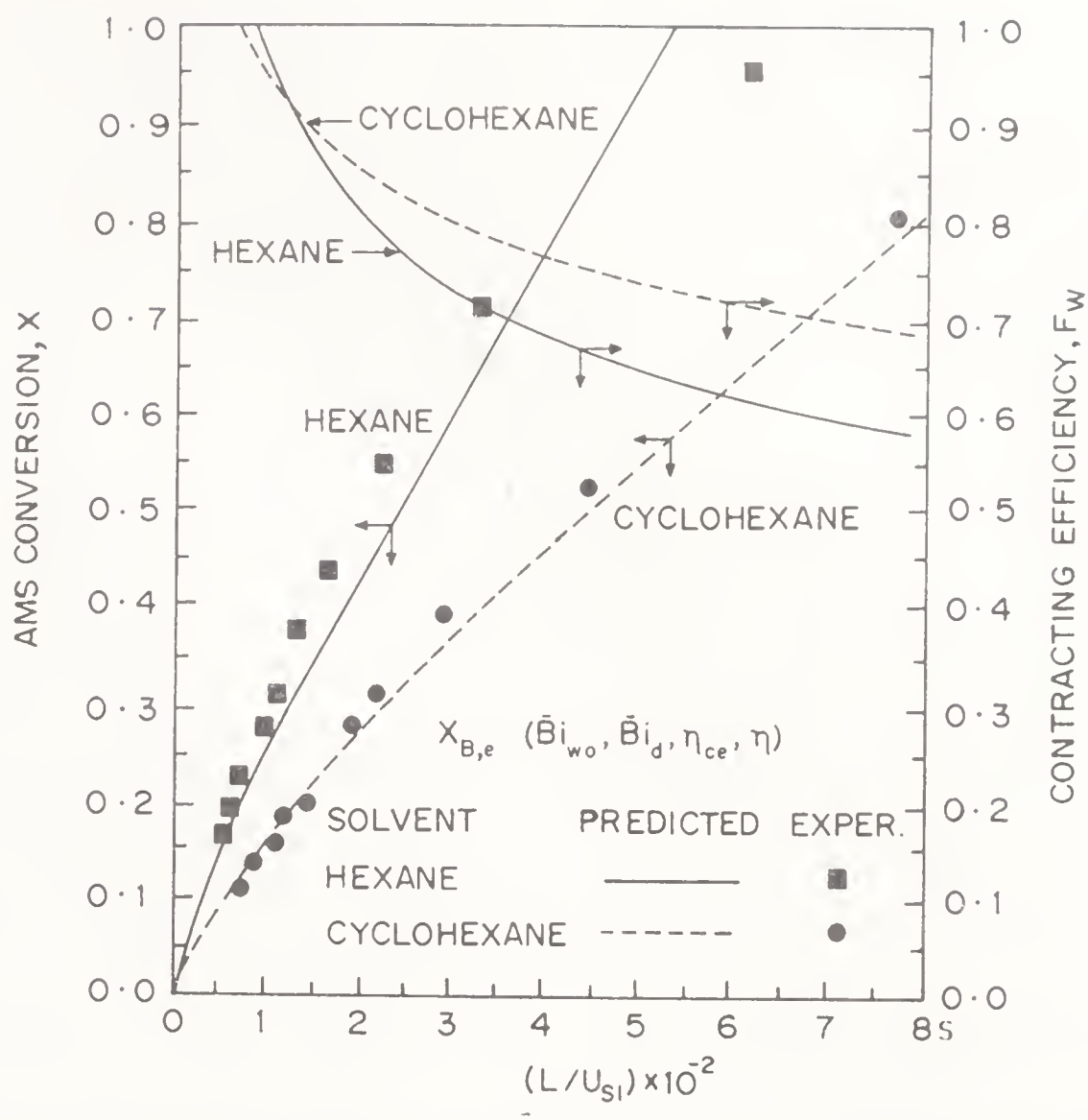


Figure 11. Experimental and model predicted conversion for  $\alpha$ -methyl styrene (AMS) hydrogenation in a laboratory scale trickle-bed reactor adapted from Mills & Duduković (1983).

only from the actively wetted surface. If the rate of reaction is relatively fast then a depletion zone with no liquid phase reactant can occur near the dry surface as shown in figure 12. This could occur even when the liquid phase reactant is in considerably large stoichiometric excess compared to the gas phase reactant ( $H_2$ ). The formation of this depletion zone over some of the pellets explains the observed reduced reaction rate at lower liquid velocities. The model predicts the experimental data reasonably well over the entire range of liquid velocities.

## 9. Volatility effects

There are a number of situations where one or more components in the liquid phase could be volatile. For example, in hydrodesulphurization processes, due to the large variation in the chemical composition of the feedstock, some of the components in the feed may be volatile. A more important situation occurs in hydrocracking where some of the cracked products are light fractions which have appreciable volatility compared to the feedstock (fuel oil). In many cases in chemical processing, a volatile solvent could be added to the reactant in order to remove the heat of reaction and to maintain temperature control. Finally,



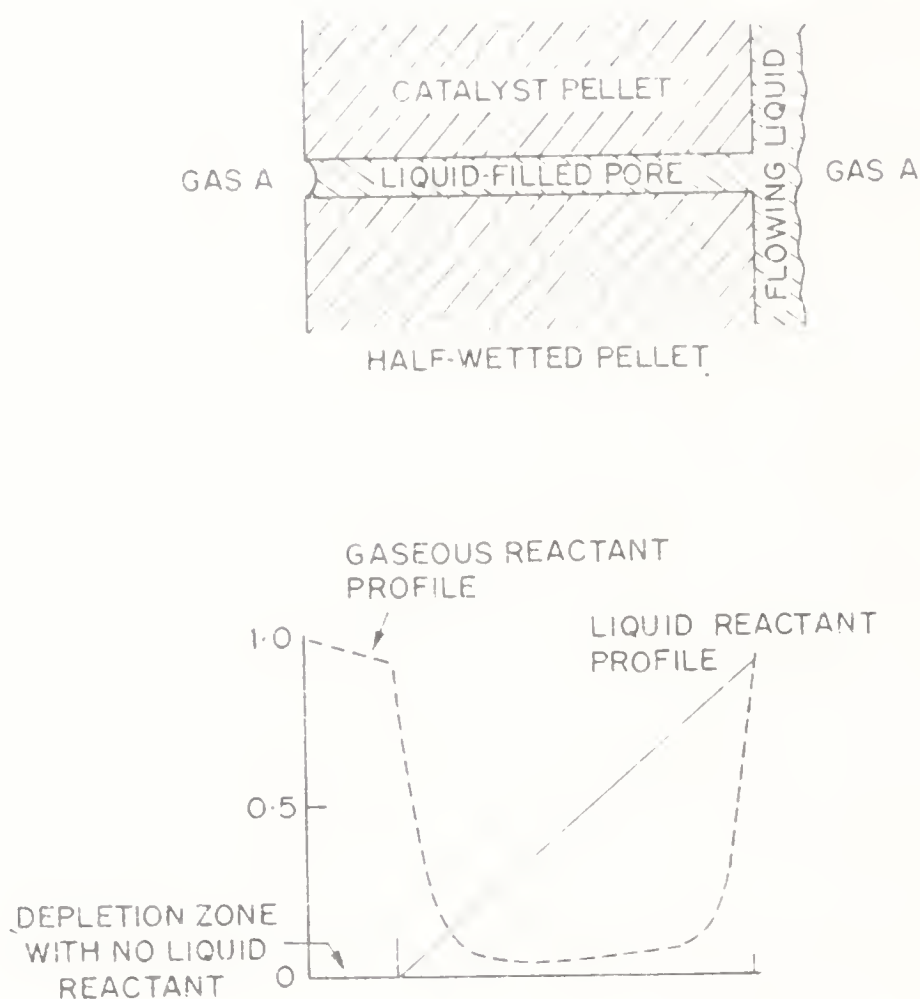


Figure 12. Schematic of a slab which is wetted only on one side and the development of a depletion zone for the liquid phase reactant (Beaudry *et al* 1986).

interpretation of reaction data from a laboratory reactor could lead to errors if one of the liquid phase components is volatile and the effect of volatility is not accounted for (Smith & Satterfield 1986). In spite of the fact that there are a variety of situations where the volatility effects are important, there have been only few analyses of this problem. Collins *et al* (1985) developed a simple isothermal model for that case assuming that the vapour phase and the liquid phase are at equilibrium at all points in the reactor. Transport effects were not accounted for and the analysis was for a first order liquid reactant limiting case. A related study of Akgerman *et al* (1985) extended the analysis to various other kinetic schemes (second-order etc.). Complete catalyst wetting was assumed in these models. Ruecker *et al* (1986) incorporated the effect of partial wetting in a simplified model. The non-isothermal case was analyzed by Hook *et al* (1986) by imposing an empirically fitted temperature profile in the system. The heat effects due to reaction and solvent volatilization cannot be properly accounted for by the procedure (i.e., when temperature profile is empirically fitted). The latter solvent latent heat effects are particularly important for the situation where the heat of reaction is removed by adding a volatile solvent. Hence, it is necessary to perform additional analysis in trickle-bed reactors for partially volatile liquid phase systems.

Recent experimental studies of Smith & Satterfield (1986) also demonstrate the importance of liquid reactant volatility under certain conditions. It was shown by these authors that for a specified liquid hourly space velocity, in a trickle-bed reactor, the degree of conversion of a reactant of appreciable volatility will usually decrease with increasing gas/liquid ratio. The magnitude of this effect will be larger, the higher the order of reaction. For systems with appreciable reactant/product volatility, the selectivity will also be affected by gas-liquid flow ratio when multiple reactions are taking place. No theoretical analysis or experimental confirmation of

this has been published. Such a work will be useful in determining the optimum gas-liquid ratio to be used in chemical processing.

Fundamental studies on exothermic reactions in trickle-beds are lacking. Kim & Kim (1981) have developed some equations for predicting the pore dry out due to heat effects. Barkelaw & Gambhir (1983) have provided some rules for prevention of hot spots in trickle-bed reactor. The use of these rules assures safe operation of adiabatic trickle-bed reactors. Multiple steady states have been experimentally observed by Hanika *et al* (1976). Although a comprehensive model is lacking, considerable progress in these directions could be expected in the next decade.

## 10. Catalyst testing

In industrial practice trickle-bed reactors are customarily used for catalyst testing in either one of the following two cases:

- a) It is necessary to develop the scale-up parameters for design of a commercial trickle-bed reactor. Measurement of kinetics and studies of catalyst deactivation would be the major task here.
- b) It is necessary to compare new catalysts under simulated plant conditions for potential use in existing large scale trickle-beds. Catalyst screening, kinetics, reactor simulation and deactivation studies would be undertaken now.

When comparing different catalysts in trickle-bed reactors it is important to clearly establish what the basis for comparison is. Preferably the catalysts should have the same size and shape and should be tested in the same reactor. Normally, comparisons are made with respect to activity, selectivity, life, mechanical properties and costs. Unfortunately, there is no uniformly accepted definition of catalyst activity. The commonly used measures of activity are:

- i) temperature required for a given conversion,
- ii) conversion achieved at given temperature,
- iii) space velocity required for a given conversion at given temperature,
- iv) overall reaction rate at given conditions,
- v) kinetic parameters from experimental studies.

Duduković & Mills (1987) recommend that criterion (iii) be used for catalyst comparison in trickle-bed reactors. The success of this procedure depends on three groups of assumptions: (a) the ratio of the catalyst activities is equal to the ratio of observed reaction rates per unit mass of catalyst, (b) that the reaction rate form is the same on various catalysts, and that (c) the trickle-bed behaves as an ideal plug flow reactor with no interphase and intraparticle gradients. Within a relatively narrow range of temperatures (30°C for some systems and over 60°C for others) it is likely that an  $n$ th order power law form can describe the apparent kinetics and assumption (a) will appear satisfied. Assumption (b) should hold for catalysts that have similar active sites and act on the same molecular functional groups. Assumption (c) demands a lot of trickle-bed reactor, i.e., absence of reactor scale radial gradients, negligible interphase and intraparticle gradients. Careful interpretation of experimental data would be needed if assumption (c) is not satisfied. Details are available in an unpublished report by Mills & Duduković (1987) which will appear soon and are not presented here.

## 11. Summary

This paper summarizes some progress in our understanding of trickle-bed reactors. The recent trend is to correlate the basic hydrodynamic parameters such as flow transition, pressure drop, holdup etc., on the basis of fundamental hydrodynamic models as opposed to purely empirical models used in the past. Separate hydrodynamic models may be necessary for trickle and pulse flow regimes due to additional complexities associated with pulse flow. Significant progress has also been made in our understanding of pulse flow. Analysis of flow in idealized complex geometries which would simulate a trickle-bed porous medium is an active field of research.

Use of tracers to estimate design parameters in trickle-beds such as holdups, contacting efficiency etc., is now a well-established procedure. Advances have been made in developing procedures to decouple bed scale and particle scale nonidealities in trickle-beds. Application to tracer data obtained in industrial size reactors is an active research project in both academia and industry.

Use of a partially wetted catalyst in the shape of a slab, cylinder or sphere, as a model to analyse trickle-bed reactor data has proven to be successful. Although such a simplified picture may be somewhat removed from reality, it provides a reasonable method for assessing the role of incomplete external wetting on reactor performance. Systems with nonlinear kinetics have also been recently simulated using this approach as well as cases where both the reactants could become limiting even though one reactant may be in large stoichiometric excess. Considerable work remains to be done in the area of reactor modelling and experimental verification of systems with volatile liquid phase components, non-isothermal and adiabatic reactions, reactor stability etc.

This paper is dedicated to Dr L K Doraiswamy on his sixtieth birthday. Dr Doraiswamy initiated a significant research programme in the area of multiphase reactors at NCL, Pune, resulting in a number of new technologies, several well-cited publications and a book in this area. One of the authors of this review (P A Ramachandran) had the privilege and pleasure of associating with this group and is grateful to the constant encouragement provided by Dr Doraiswamy.

This work could not have been possible without the industrial support to the Chemical Reaction Engineering Laboratory (CREL) at Washington University and Drs P A Ramachandran and M P Duduković would like to thank all the industrial sponsors of CREL.

## List of symbols

$a_p$	external area of particles per unit volume of reactor;
$a_t$	surface area $a_p$ based on a modified diameter $d_p^*$ in (27);
$A, B$	Ergun constants in (13) and (14);
$Bi_D, Bi_w$	Biot number for the dry and wet portions of the catalyst defined as $(k_{s,D}R)/D_e$ and $(k_{s,w}R)/D_e$ , respectively;
$C$	empirical constant in (5);



$C_L$	concentration of tracer in the external liquid;
$C_{L1}$	concentration of tracer in the outlet liquid;
$\bar{C}_L, \bar{C}_{L1}$	Laplace transform of the concentrations;
$C_p$	representative concentration in the particle phase;
$d_e$	packing equivalent diameter defined as $6(\text{volume of particle})/(\text{external area})$ ;
$d_p$	average diameter of catalyst particles;
$d_{pe}$	equivalent diameter of particle defined by (37);
$d_T$	diameter of the reactor;
$D_e$	intraparticle diffusivity of the tracer or reactant;
$D_{EL}$	axial dispersion coefficient of the liquid phase;
$E(t)$	exit age distribution of the liquid phase;
$E_o$	modified Eotvos number defined by (31);
$f_i$	fraction of the total area of the catalyst (internal and external) wetted by the liquid;
$f_p$	pulse frequency;
$f_w$	contacting efficiency or the fraction of the external area wetted by the liquid;
$g$	acceleration due to gravity;
$Ga_L$	Galileo number $d_p^3 g \rho_L^2 / \mu_L^2$ ;
$Ga_L^*$	modified Galileo number defined by (16) in Saez-Carbonell model or defined by (33) for Specchia-Baldi model;
$Ga_G^*$	modified Galileo number for gas defined in a manner similar to (16);
$H_p$	pulse height of individual pulses;
$H_{PT}$	fraction of the reactor height occupied by the pulses;
$H(s)$	particle scale transfer function;
$k_\beta, k_{\beta i}$	liquid phase relative permeability for the viscous and inertial regime, respectively;
$k_\gamma, k_{\gamma i}$	gas phase relative permeabilities in the viscous and inertial regimes respectively;
$k_{ex}$	exchange coefficient between the bulk phase and the particle phase;
$k_p$	rate constant for a first-order liquid phase reaction based on particle pore volume;
$k_{s,D}$	overall mass transfer coefficient from the gas phase to catalyst surface through the dry portions of the catalyst;
$k_{s,w}$	mass transfer coefficient from the gas to catalyst through the wet portions;
$k_s$	solid-liquid mass transfer coefficient;
$K'_A$	adsorption equilibrium constant for tracer for linear adsorption isotherm;
$L$	total height of the reactor;
$\mathcal{L}$	operator describing the nonidealities in the flow of the external liquid;
$p$	modified Laplace transform parameter defined by (53);
$Pe$	liquid phase Peclet number $u_L L / D_{EL}$ ;
$P$	pressure;
$\langle P_L \rangle$	phase-averaged pressure in liquid (or gas with the corresponding subscript);
$R$	radius of the catalyst pellet;



$Re_i^*$	modified Reynolds number for liquid phase defined by (15). A similar expression holds for $Re_G^*$ ;
$Re_L$	Reynolds number for the liquid $d_p u_L \rho_L / \mu_L$ ;
$s$	Laplace transform variable;
$sy$	reduced saturation of the gas defined by (20);
$t$	time elapsed since the introduction of tracer;
$u_G$	superficial velocity of the gas;
$u_L$	superficial velocity of the liquid;
$v_p$	pulse velocity;
$x$	axial distance;
$X$	conversion of the liquid phase reactant;
$Z$	parameter defined by (39);
$\alpha$	fraction of the throat area occupied by liquid;
$\delta_G$	pressure drop per unit bed height for a packed bed with only gas flowing;
$\delta_L$	pressure drop per unit bed height with only liquid flowing;
$\bar{\delta}_{LG}$ or $\Delta P / \Delta L$	/pressure drop per unit bed height in two-phase flow;
$\delta_\beta$	reduced saturation of liquid defined by (19);
$\varepsilon_\beta$	bed voidage;
$\varepsilon_l, \varepsilon_{ld}, \varepsilon_{ls}$	external, dynamic, static, and total liquid holdup, respectively;
$\varepsilon_{IT}$	
$\varepsilon_p$	particle porosity;
$\varepsilon_{eff}$	effective porosity for gas flow in a wetted bed $= \varepsilon_\beta - \varepsilon_{ls}$ ;
$\eta_{oTB}$	overall effectiveness factor in a trickle-bed;
$\eta_D, \eta_w$	effectiveness factor for the dry portion, and the wet portion of the catalyst, respectively;
$\eta_{Dw}$	effectiveness factor for a slab which is wetted only on one side;
$\lambda$	parameter defined by (3);
$\mu_1, \mu_2$	first and second absolute moments of the response curve for a pulse tracer;
$\mu_L, \mu_w$	viscosity of liquid, and water, respectively;
$\rho_{air}, \rho_G, \rho_L, \rho_w$	density of air, gas, liquid, and water, respectively;
$\tau_i$	interfacial drag in the model of Sicardi & Hofmann (1980);
$\phi$	Thiele modulus for a first-order catalytic reaction;
$\omega$	liquid saturation $\varepsilon_l / \varepsilon_\beta$ ;
$\chi$	parameter defined as $(\delta_L / \delta_G)^{0.5}$ ;
$\psi$	parameter defined by (4).

## References

- Akgerman A, Collins M, Hook B D 1985 *Ind. Eng. Chem., Fundam.* 24: 398–401  
 Baker O 1954 *Oil Gas J.* 53: 185–189  
 Baldi G, Gianetto A 1980 Paper presented at the NATO Advanced Study Institute on Multiphase Reactors, Vimiero, Portugal  
 Barkelew C H, Gambhir B S 1983 *ACS Symp. Ser.* 237: 61–72

- Beaudry E G, Mills P L, Duduković M P 1986 Paper presented at the World Congress in Chemical Engineering, Tokyo
- Blok J R, Drinkenburg A A H 1982 *Chem. Eng. J.* 25: 89–99
- Buffham B A, Kropholler H W 1973 *Chem. Eng. Sci.* 28: 1081–1089
- Charpentier J C, Favier M 1975 *AIChE J.* 21: 1213–1218
- Chou T S, Worley F L, Luss D 1978 *Ind. Eng. Chem. Fundam.* 18: 279–283
- Collins G M, Hess R K, Akgerman A 1985 *Chem. Eng. Commun.* 35: 281–291
- Colombo A, Baldi G, Sicardi S 1976 *Chem. Eng. Sci.* 31: 1101–1108
- Christensen G, McGovern S J, Sundaresan S 1986 *AIChE J.* 32: 1677–1681
- Crine M, Marchot P, L'Homme A 1980 *Chem. Eng. Sci.* 35: 51–58
- Dautzenberg F M 1984 Paper presented at the Catalytica Associates Seminar, Santa Clara, California
- Dimenstein D M, Ng K M 1985 *Chem. Eng. Commun.* 41: 215–219
- Dimenstein D M, Ng K M 1986 *AIChE J.* 1: 115–122
- Duduković M P, Mills P L 1986 *Encyclopedia of fluid mechanics*, (Houston: Gulf Publishing Company) Chap. 32
- Duduković M P, Mills P L 1987 Catalyst Testing in Trickle-Beds, Catalytic Report on Catalyst Testing, Catalytic, Palo Alto, CA.
- Ergun S 1952 *Chem. Eng. Prog.* 48: 89–94
- El-Hisnawi A A, Duduković M P, Mills P L 1981 *ACS Symp. Ser.* 196: 421–430
- Fukushima S, Kusaka K 1978 *J. Chem. Eng. Japan.* 11: 241–249
- Germain A, L'Homme A, Lefebvre 1979 in *Chemical engineering of gas-liquid reaction*, (Liege, Belgium: CEBEDOC)
- Giannetto A, Baldi G, Speechia V, Sicardi S 1978 *AIChE J.* 24: 1087–1104
- Goto S, Lakota A, Levec J 1981 *Chem. Eng. Sci.* 36: 157–162
- Goto S, Levec J, Smith J M 1977 *Catal. Rev. Sci. Eng.* 15: 187–247
- Gupta R 1985 in *Handbook of fluids in motion*, (eds) N P Cheremisinoff and R Gupta
- Gyure D C, Krantz W B 1983 *Ind. Eng. Chem. Fundam.* 22: 405–410
- Hanika J, Sporka K, Ruzicka V 1976 *Chem. Eng. J.* 12: 193–197
- Hanika H, Stanek S 1985 in *Handbook of heat and mass transfer* (ed) N P Cheremisinoff (Houston: Gulf Publishing Co.) vol. 25
- Herskowitz M, Smith J M 1983 *AIChE J.* 29: 1–18
- Hook B D, Collins G M, Akgerman A 1986 *Chem. Eng. Commun.* 28: 213–221
- Kan K M, Greenfield P F 1978 *Ind. Eng. Chem. Process Des. Dev.* 17: 482–485
- Kennedy C R, Jaffee S B 1986 *Chem. Eng. Sci.* 41: 845–853
- Kim D H, Kim Y G 1981 *J. Chem. Eng. Jpn.* 14: 311–317
- Midoux N, Favier M, Charpentier J C 1976 *J. Chem. Eng. Jpn.* 9: 350–357
- Mills P L, Duduković M P 1979 *Ind. Eng. Chem.* 18: 139–149
- Mills P L, Duduković M P 1980 *Chem. Eng. Sci.* 35: 1557–1570
- Mills P L, Duduković M P 1981 *AIChE J.* 27: 893–904
- Mills P L, Duduković M P 1982 *AIChE J.* 28: 526–534
- Mills P L, Duduković M P 1983 *ACS Symp. Ser.* 237: 37–51
- Mills P L, Lai S, Duduković M P, Ramachandran P A 1986 *Finite element solution of partially wetted catalyst* (to be published)
- Paraskos J A, Frayer J A, Shah Y T 1975 *Ind. Eng. Chem. Process Des. Dev.* 14: 315–322
- Pendse H, Chiang H W, Tien C 1983 *Chem. Eng. Sci.* 38: 1137–1150
- Ramachandran P A, Beaudry E, Duduković M P, Mayer F X 1986a. Paper presented AIChE Annual Meeting, Miami Beach, paper 84f
- Ramachandran P A, Chaudhari R V 1983 *Three phase catalytic reactors* (London: Gordon & Breach)
- Ramachandran P A, Duduković M P, Mills P L 1986b *Chem. Eng. Sci.* 41: 855–862
- Ramachandran P A, Smith J M 1979a *Chem. Eng. Sci.* 34: 75–91
- Ramachandran P A, Smith J M 1979b *AIChE J.* 25: 538–542
- Rao V G 1979 Ph.D. thesis, I.I.T., Madras
- Rao V G, Drinkenburg A A H 1983 *Can. J. Chem. Eng.* 61: 158–167
- Rao V G, Drinkenburg A A H 1985 *AIChE J.* 31: 1010–1018
- Ruecker C M, Mensik M A, Akgerman A 1986 *Chem. Eng. Commun.* 41: 279–287
- Saez A E, Carbonell R G 1985 *AIChE J.* 31: 52–57
- Saez A E, Carbonell R G, Levec J 1986 *AIChE J.* 32: 353–357

- Sagara M, Schneider P, Smith J M 1970 *Chem. Eng. J.* 1: 47–54  
Sato Y, Hirose T, Takahashi, Toda M 1973 *J. Chem. Eng. Jpn.* 6: 315–321  
Satterfield C N 1975 *AIChE J.* 21: 209–228  
Schneider P, Smith J M 1968 *AIChE J.* 14: 762–771  
Schwartz T G, Weger E, Duduković M P 1976 *AIChE J.* 22: 894–904  
Shah Y T 1979 *Gas-liquid-solid reactor design*, (New York: McGraw-Hill)  
Sicardi S, Gerhard D, Hofmann H 1986 *Chem. Eng. Commun.* 42: 1–9  
Sicardi S, Hofmann H 1980 *Chem. Eng. J.* 20: 251–253  
Sicardi S, Hofmann H 1982 *Chem. Eng. J.*  
Smith C M, Satterfield C N 1986 *Chem. Eng. Sci.* 41: 839–844  
Specchia V, Baldi G 1977 *Chem. Eng. Sci.* 32: 515–523  
Suzuki M, Smith J M 1970 *AIChE J.* 16: 882–884  
Talmor E 1977 *AIChE J.* 23: 868–874  
Turpin J L, Huntington R L 1967 *AIChE J.* 13: 1196–1202  
Van Brakel J 1975 *Powder Technol.* 11: 205–211

# Lumping analysis in the presence of measurement error

KENNETH B BISCHOFF<sup>1</sup> and PAMELA G COXSON<sup>2</sup>

<sup>1</sup> Department of Chemical Engineering, University of Delaware, Newark, DE 19716, USA

<sup>2</sup> Department of Mathematics, The Ohio State University, Columbus, OH 43210, USA

**Abstract.** A review of the analysis of our earlier paper is presented, where systems mathematics is utilized to define in a direct way the conditions for exact lumping of monomolecular first-order kinetic systems. A new extension is to show that a system that is exactly lumpable in a batch reactor will follow the same lumping in any reactor type. In addition, our new approach shows how cluster analysis provides a useful way to analyse approximate lumping. This is especially important when measurement error is present, since the implementation of a successful lumping scheme must be viewed in the context of the errors.

**Keywords.** Lumping analysis; monomolecular first-order kinetic systems; cluster analysis; measurement error.

## 1. Introduction

The mathematical basis of lumping analysis was introduced by Wei & Kuo (1969) and Kuo & Wei (1969), who showed how large monomolecular systems could be well represented by lower order monomolecular systems under certain circumstances. The lumped pseudo-species are formed from the real chemical species which have "similar" behaviour over time. Wei and Kuo defined the "Principle of Invariant Response" as when the lumped system is also first-order and its time behaviour is independent of the composition of the species within each lump. The mathematical criterion for this will be discussed below.

Weekman (1979) presented a review of lumping, discussing how practical situations can utilize this theoretical framework, and also providing many examples. He also pointed out some remaining problems: how to choose the lumps from large sets of kinetic data; how to incorporate error analysis, since even relatively large lumped systems can only be justified for very precise data. Coxson & Bischoff (1987a) (henceforth called I) have addressed the first of these, with theoretical justification in Coxson & Bischoff (1987b) (henceforth called II). The purpose of this paper is to present beginning analysis of the second problem area, in the context of our previous work. The specific example that will be used is that of



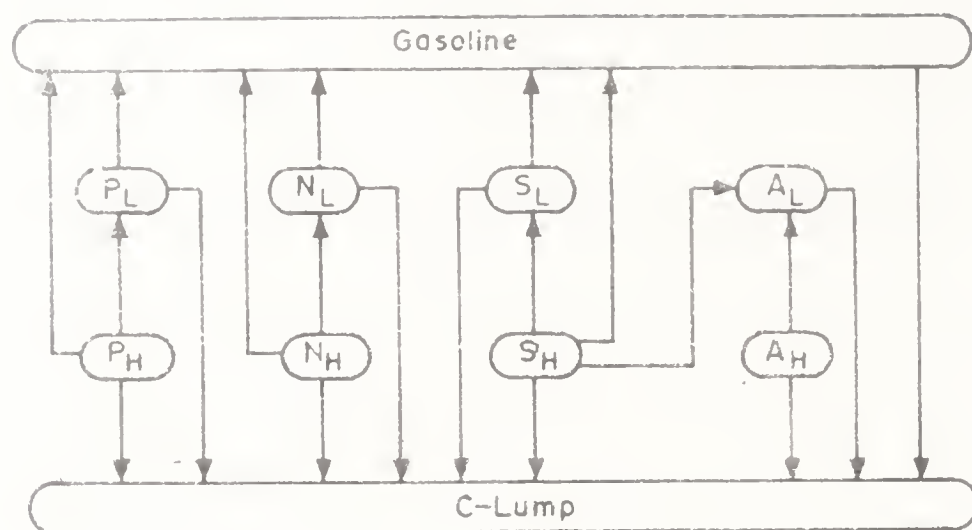


Figure 1. The ten lump species:  $P_H$  = wt. % paraffinic molecules,  $650^\circ\text{F}_+$ ;  $N_H$  = wt. % naphthenic molecules,  $650^\circ\text{F}_+$ ;  $S_H$  = wt. % aromatic side chains,  $650^\circ\text{F}_+$ ;  $A_H$  = wt. % carbon atoms among aromatic rings,  $650^\circ\text{F}_+$ ;  $P_L$  = wt. % paraffinic molecules,  $430^\circ$ – $650^\circ\text{F}$ ;  $N_L$  = wt. % naphthenic molecules,  $430^\circ$ – $650^\circ\text{F}$ ;  $S_L$  = wt. % aromatic side chains,  $430^\circ$ – $650^\circ\text{F}$ ;  $A_L$  = wt. % carbon atoms among aromatic rings,  $430^\circ$ – $650^\circ\text{F}$ ;  $G$  = gasoline lump ( $\text{C}_5$ – $430^\circ\text{F}$ );  $C$  = C-lump  $\text{C}_1$  to  $\text{C}_4$  + coke).

the Mobil "10-lump cracking model" of Jacob *et al.* (1976) shown in figure 1, and we will analyse the issues that occur when this is further lumped.

## 2. Linear reaction systems and lumping

An  $n$ -species monomolecular reacting system can be represented by the linear differential equations

$$dx(t)/dt = Kx(t), \quad (1)$$

where  $x(t)$  is the  $n$ -dimensional species composition vector at time  $t$ , and  $K$  is the reaction rate coefficient matrix. For an initial composition  $x(0) = x_0$ , the solution to (1) is  $x(t) = e^{Kt}x_0$ .

Real experimental data is usually taken at discrete intervals,  $\tau$ , with time  $t_h = h\tau$ . It is shown in I that the equivalent discrete form of the kinetic equation (1) is

$$x(h+1) = Gx(h), \quad (2)$$

with

$$G = e^{K\tau}. \quad (3)$$

The solution to (2) is  $x(h+1) = G^h x_0$ , and this form is often more convenient in the analysis.

Lumping is the construction of a reduced order system that reproduces the overall behaviour of the full system, and is mathematically represented by multiplying the composition  $n$ -vector,  $x(t)$ , by a  $(l \times n)$  lumping matrix to give the  $l$ -lumps represented by a pseudo-composition  $l$ -vector  $z(t)$ :

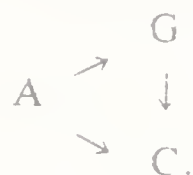
$$z(t) = Lx(t) \quad (4)$$

Wei & Kuo (1969) defined proper lumping as when each chemical species is

included in one, and only one, lump. An example of a lumping matrix for a four-species system that lumps species 1 and 2 and also species 3 and 4 into a two-pseudospecies lumped system is

$$L = \begin{bmatrix} 1 & 1 & 0 & 0 \\ 0 & 0 & 1 & 1 \end{bmatrix}.$$

Another example is for the 10-lump cracking model when all the gasoil feedstock components are lumped, keeping gasoline and coke + light ends separate (numbered as shown in figure 1), leading to the classical 3-lump scheme:



Then, the lumping matrix is

$$L = \begin{bmatrix} 1 & 1 & 1 & 1 & 1 & 1 & 1 & 1 & 0 & 0 \\ 0 & 0 & 0 & 0 & 0 & 0 & 0 & 0 & 1 & 0 \\ 0 & 0 & 0 & 0 & 0 & 0 & 0 & 0 & 0 & 1 \end{bmatrix}.$$

This is also a proper lumping matrix.

The concept of exact lumping of Wei and Kuo is the principle of invariant response described above. Here, the lumped system must also follow monomolecular kinetics:

$$\begin{aligned} z &= Lx = LKx \\ &= K_z z = K_z Lx. \end{aligned}$$

From the last equations, Wei & Kuo (1969) proved that the necessary and sufficient condition for exact lumping is that

$$LK = K_z L. \quad (5)$$

Equivalently, for the discrete system,

$$LG = G_z L. \quad (5a)$$

In II, we show the close connection of lumping analysis with concepts of modern systems theory. In particular, observability and controllability theorems can be used to establish mathematical criteria for lumpability; one example is II, theorem 3:

"A finite  $n$ -dimensional time invariant linear kinetic system with system matrix  $F$  ( $K$  or  $G$ ) is exactly lumpable by the lumping matrix  $L$  if and only if

$$\text{Rank} \begin{bmatrix} L \\ LF \end{bmatrix} = \text{Rank } L. \quad (6)$$

Criterion (6) provides a particularly simple test for exact lumpability in that we only need observe whether or not the rows of  $LF$  are linear combinations of the rows of  $L$ . Another result from II is that when the full system matrix  $F$  is known, the theory

of generalized matrix inverses can be used to directly find the lumped system matrix from (5) as

$$F_z = LFL^T \text{Diag}[1/n_1, 1/n_2, \dots, 1/n_m],$$

where  $n_i$  is the number of species in the  $i$ th lump. This is much simpler than the procedure of Wei & Kuo (1969).

Another question that can be asked is, if the lumping analysis is carried out in a batch reactor (as implied above), is the lumped system valid in any other reactor type? The answer is yes, as shown by the following. For the full monomolecular system, the outlet concentrations for an arbitrary residence time distribution  $E(t)$  is (e.g., Froment & Bischoff 1979):

$$x = \int_0^{\infty} E(t) e^{Kt} x_0 dt.$$

Then, for the lumped system,

$$z = Lx = \int_0^{\infty} E(t) L e^{Kt} dt.$$

Now,

$$\begin{aligned} L e^{Kt} &= L[I + Kt + (1/2!)K^2t^2 + (1/3!)K^3t^3 + \dots] \\ &= L + LKt + (1/2!)LK^2t^2 + \dots \end{aligned}$$

Now with (5),

$$\begin{aligned} LK &= K_z L \\ LK^2 &= (LK)K = (K_z L)K = K_z(K_z L) \end{aligned}$$

Thus,

$$\begin{aligned} L e^{Kt} &= L + K_z t L + (1/2!)K_z^2 t^2 L + \dots \\ &= [I + K_z t + (1/2!)K_z^2 t^2 + \dots] L \\ &= e^{K_z t} L, \end{aligned}$$

and so

$$\begin{aligned} z &= \int_0^{\infty} E(t) e^{K_z t} L x_0 dt \\ &= \int_0^{\infty} E(t) e^{K_z t} z_0 dt. \end{aligned} \tag{7}$$

Therefore, an exact lumping scheme determined in a batch reactor carries through for any arbitrary reactor RTD, and is generally applicable. Similar results were found by Wei & Kuo (1969) for reaction with diffusion, when all the diffusivities were equal.

### 3. Approximate lumping

An organized way to decide on which species might be lumped is to consider the response matrix. The concept is to construct a matrix, each column of which is the system response to a feed of pure chemical species  $j$ . The  $h$ th step response matrix is

$$R_h = \begin{bmatrix} r_{ij}^h \end{bmatrix} \quad \begin{matrix} i = 1, \dots, l \\ j = 1, \dots, n \end{matrix}$$

where  $r_{ij}^h$  is the quantity of (lumped) pseudo-species  $i$  at time  $h\tau$  if the initial composition is  $x(0) = (0 \dots 0 \underset{j}{1} 0 \dots 0)^T$ . It can be shown that theoretically (see I) :

$$R_h = MF^h,$$

if the full system matrix,  $F$ , is known. Of equal importance, however, is that the response matrix elements can be determined entirely from experiment, from the definition. Make  $n$  experiments, each starting with one pure chemical species (other feeds are also possible), and measure the kinetics at time intervals  $h = 1, \dots, n$ . Choose the coarsest lumping scheme that can give the essential information – in the cracking example, this is three lumps, since gasoil, gasoline, and coke + light ends must at least be kept separate – and then construct the elements according to (4). A specific example will be shown below. That this is sufficient to decide upon any finer lumping schemes is discussed in II, and proved mathematically in Coxson (1985).

The decision of what to lump with what is simple in principle: look at all the columns of the response matrix, and combine those chemical species that have a similar response. For exactly lumpable systems, this is indeed easy, since the species to be lumped will have identical columns in the response matrix. However, for only approximately lumpable systems, a systematic, objective method is needed to decide which species are allowed to be lumped, with what error. This judgement is even more difficult in the presence of measurement errors, which will be discussed below.

The approach proposed in I is to use the techniques of cluster analysis, a statistical technique that examines sets of data and determines whether they “cluster” into similarity classes (see, e.g., Anderberg 1973). Ward’s method, illustrated below, begins by putting each data set into a cluster by itself. At each step in the procedure, two of the clusters are “fused”, with a criterion of minimization of the increment of the total within group error sum of squares caused by the fusion. Various issues of local vs. global minima are briefly discussed in I.

If this algorithm is applied to the 10-lump cracking model, using rate coefficient values from Gross *et al* (1976), the clustering results shown in table 1 are obtained (see I for details).

Several interesting observations can be made from the above table. One is that the error increase does not change uniformly with each decrease in the number of lumps; sometimes more lumping causes a large increase in the error. Other changes in the error seem to be a consequence of the chemical nature of the process



Table 1. Clustering results obtained using rate coefficient values\*

Cluster pattern	Number of clusters	Error increase	Total error
1 2 3 4 5 6 7 8	7	0.0190	0.0190
1 1 3 4 5 6 7 8	6	0.0777	0.0967
1 1 3 4 5 6 5 8	5	0.1328	0.2295
1 1 3 4 3 1 3 8	4	0.3081	0.5376
1 1 2 4 3 1 3 4	3	1.4391	1.9767
1 1 1 4 1 1 1 4	2	1.4739	3.4506
1 1 1 1 1 1 1 1	1	7.8138	11.2644

\* From Gross *et al.* (1976)

(although the algorithm is purely mathematical). For example, it is important to keep the aromatics separate (increase of 7.81, >200%). The other lumping schemes also satisfy chemical intuition. The next split is to differentiate the nonaromatics into heavy paraffins plus naphthenes ( $x_1, x_2, x_6$ ) and side chains plus light paraffins ( $x_3, x_5, x_7$ ). These seem reasonable, since naphthenes are more difficult to crack (ring-breaking) and are probably approximately similar to heavy paraffins, and also most of the side chains would be expected to be not too long, and similar to light paraffins. Further improvement results when the heavy aromatics ( $x_4$ ) are differentiated from the light aromatics ( $x_8$ ). The next refinement is to separate the heavy side chains ( $x_3$ ) from the light paraffins plus light side chains ( $x_5, x_7$ ), which is not unreasonable. The light paraffins ( $x_5$ ) are then separated from the light side chains ( $x_7$ ), and they would be expected to have somewhat different reactivities. Finally, the heavy paraffins are separated from the light plus heavy naphthenes, which seems reasonable based on the chemical nature of the molecules. Clearly, the real chemical patterns are included in even this smoothed "data".

#### 4. Lumping with measurement error

It would intuitively seem that with measurement errors a criterion for adequate lumping would be, when the error of lumping is at the level of error in the data, any further retirement of the lumped kinetic scheme would not be justified. There is also the question of whether the same lumps are found by the cluster analysis without and with errors in the measurements. In order to get some estimates of this, simulations were made with the 10-lump scheme with random uniform noise, both additive and relative, of magnitude  $\pm 10\% \dots 50\%$ . An example of such a simulation is given in table 2.

Observations from these simulations are the following. Overall, the clustering technique is rather robust. This is evidenced by the fact that, even with  $\pm 50\%$  measurement error, the same overall cluster patterns are found. Occasionally, in cases where there was very little clustering error from one step to the next, a reversal in patterns is found but the original noise-free pattern is recovered within one or two further steps. Because the error increase in the clustering algorithm is a sum of squares, the additional error in this calculation due to the observation error will be proportional to the variance of the observation error.

A more exact analysis would require repeated calculations to form an ensemble

Table 2. Simulations made with a ten-lump scheme

Cluster pattern *	Error increase	Total error
$\pm 10\%$ error		
1 2 3 4 5 2 7 8	0.0437	0.9437
1 1 3 4 5 1 7 8	0.0869	0.1306
1 1 3 4 5 1 5 8	0.149	0.280
1 1 3 4 3 1 3 8	0.324	0.604
1 1 1 4 1 1 1 8	1.454	2.058
1 1 1 4 1 1 1 4	1.541	3.60
1 1 1 1 1 1 1 1	7.85	11.45
$\pm 20\%$ error		
1 2 3 4 5 1 7 8	0.0751	0.0751
1 1 3 4 5 1 7 8	0.1613	0.2364
1 1 3 4 5 1 5 8	0.2066	0.443
1 1 3 4 3 1 3 8	0.2797	0.723
1 1 3 4 3 1 3 4	1.491	2.214
1 1 1 4 1 1 1 4	1.620	3.834
1 1 1 1 1 1 1 1	7.43	11.26
$\pm 30\%$ error		
1 2 3 4 5 1 7 8	0.1927	0.1927
1 1 3 4 5 1 7 8	0.2791	0.4718
1 1 3 4 5 1 5 8	0.2891	0.7609
1 1 3 4 3 1 3 8	0.4787	1.240
1 1 1 4 1 1 1 8	1.645	2.887
1 1 1 4 1 1 1 4	2.02	4.91
1 1 1 1 1 1 1 1	8.32	13.22
$\pm 50\%$ error		
1 2 3 4 5 6 5 8	0.3670	0.3670
1 2 3 4 5 2 5 8	0.5529	0.9200
1 2 3 4 3 2 3 8	0.5744	1.494
1 1 3 4 3 1 3 8	0.8319	2.326
1 1 1 4 1 1 1 8	1.908	4.234
1 1 1 4 1 1 1 4	1.948	6.183
1 1 1 1 1 1 1 1	8.28	14.47

\* Noise free data (see text)

of results, simulating the error distributions in this way. Some of this has been done, and some interesting patterns have been found. We are not yet clear as to how to analyse these results, but from statistical considerations, some sort of  $F$ -test criterion would seem to be appropriate. The exact details of this are yet to be worked out.

The connection of this work with Dr Doraiswamy is that the senior author was invited to present a plenary lecture at ICREC-1 in 1984, where a very preliminary form of the work (unpublished) was presented. We would like to present this current status report in honour of Dr Doraiswamy on the occasion of his sixtieth birthday.

## References

- Anderberg M R 1973 *Cluster analysis for applications* (New York: Academic Press)  
 Coxson P G 1985 *IEEE Trans. Autom. Control* AC-30: 478-480

- Coxson P G, Bischoff K B 1987a *Ind. Eng. Chem. Res.* (to appear)
- Coxson P G, Bischoff K B 1987b *Ind. Eng. Chem. Res.* (to appear)
- Froment G F, Bischoff K B 1979 *Chemical reactor analysis and design* (New York: Wiley)
- Gross B, Jacob S M, Nace D-M, Voltz S E 1976 US 3.960. 707
- Jacob S M, Gross B, Voltz S E, Weekman V W 1976 *AIChE J* 22: 701-713
- Kuo J C W, Wei J 1969 *Ind. Eng. Chem., Fundam.* 8: 124-133
- Weekman V W Jr 1979 *AIChE Monograph Ser.* No. 11: 3-29
- Wei J, Kuo J C W 1969 *Ind. Eng. Chem., Fundam.* 8: 114-123

# Supercritical fluid extraction of Chinese Maoming oil shale with water and toluene

T FUNAZUKURI and N WAKAO\*

Department of Chemical Engineering, Yokohama National University,  
Yokohama, Japan 240

**Abstract.** Chinese Maoming (Guangdong Province) oil shale was subjected to supercritical fluid extraction with water and toluene, respectively, in a batch autoclave. Yields of organic matter were greater with toluene than with water, and more organic compounds of high molecular weight were extracted with toluene than with water, although the weight losses of the oil shale with toluene and water were almost the same. Yield distributions of *n*-alkanes were also almost the same, irrespective of the solvent.

**Keywords.** Supercritical fluid extraction; supercritical extraction; oil shale; supercritical water; supercritical toluene.

## 1: Introduction

Attention has been focused on supercritical fluid extraction (SFE) of organic matter from coal. Coal SFE started with toluene solvent (Whitehead & Williams 1975; Bartle *et al* 1975, 1979a,b; Tugrul & Olcay 1978; Ceylan & Olcay 1981), and later, various organic solvents (Kershaw & Jezko 1982; Bartle *et al* 1982; Amestica & Wolf 1984; Kershaw 1984a,b), and hydrogen donor solvents (Kershaw & Overbeek 1984) have also been used.

More recently supercritical (SC) water has also been employed. Easy separation of the extracts from their mixtures with water is also one of the advantages of using water as a solvent. Deshpande *et al* (1984) pointed out, in SFE of coal, that SC water acts not only as a solvent but as a species reacting with extractable components. Houser *et al* (1986) also found that SC water is active in decomposing organic compounds, especially those containing heteroatoms. As a matter of fact, much work has recently been done to examine the effects of SC water on the extraction yields of organic matter from coal and also on upgrading the extracts. Not only plain water but aqueous solutions have been used. Towne *et al* (1985) employed aqueous quinoline solutions and tetralin solutions, Barton (1983) used water with

---

\*To whom correspondence should be addressed



catalysts in the presence of hydrogen, and Amestica & Wolf (1986) employed carbon monoxide with water and catalysts, and aqueous quinolines and tetralin solutions.

Compared to coal SFE, fewer studies have so far been carried out on SFE of oil shale. Zhu *et al* (1982) and Qin *et al* (1984a,b) carried out extraction of Chinese oil shales with SC toluene. McKay *et al* (1983a,b) tested Green River oil shale with SC water in the presence of carbon dioxide and with SC mixtures of water and organic solvents such as toluene, methylene chloride and methanol.

In this study, SFE of Chinese Maoming oil shale was carried out with water and toluene. The oil shale was also subjected to Soxhlet extraction with tetrahydrofuran (THF).

## 2. Experiments

Chemical compositions of the Maoming oil shale employed in this study are listed in table 1 and the experimental conditions in table 2. Crushed particles (0.35–0.84 mm) of the oil shale were placed in a 0.7-litre autoclave (with a stirrer installed) and a certain amount of solvent was introduced into it. The autoclave was heated by an external heating element at 8.5 K/min to an intended temperature, and it was kept at this temperature for a certain period of time. The autoclave was then quickly cooled down with a fan and opened. In some cases, the autoclave was quickly cooled and opened as soon as it reached the intended temperature. It will be mentioned in §3 whether or not the data are those obtained by maintaining the autoclave at the intended temperature for one hour.

The residual solid and the liquid mixture of the oil extracted and the solvent were recovered. The residual solid was washed with THF, and thereafter dried and weighed. Also, THF was introduced into the autoclave, which was then heated at about 380 K for an hour to recover the oil adhering to the walls. The THF solution was placed in a rotary evaporator, where the THF evaporated, and the oil left

**Table 1.** Analyses of Maoming oil shale.

<i>Proximate analysis:</i>	
Volatile matter	28.6 wt% <sup>a</sup>
Fixed carbon	2.9
Ash	66.5
Moisture (as received)	2.0
<i>Ultimate analysis:</i>	
Carbon	20.20 wt% <sup>b</sup>
Hydrogen	3.07
Nitrogen	0.68
Sulphur	0.46
<i>Compositions of dried oil shale:</i>	
Carbonate mineral (HCl leaching)	16.7 wt% <sup>b</sup>
Silicate mineral (HF-HCl leaching)	65.1
Bitumen (Soxhlet extraction with THF)	0.7
Kerogen (residue)	17.5

<sup>a</sup> kg/kg-undried oil shale x 100; <sup>b</sup> kg/kg-dry oil shale x 100.

**Table 2.** Experimental conditions.

Sample employed	Maoming oil shale	
Sample size	0.35–0.84 mm	
Weight ratio of oil shale to solvent	0.08–0.3	
Extraction temperature and pressure		
	<i>Water</i>	<i>Toluene</i>
Temperature, K	593–773	593–700
Pressure, MPa	11–25	16–25
Critical temperature, K	647	592
Critical pressure, MPa	22.0	4.11
Reduced temperature	0.917–1.19	1.00–1.18
Reduced pressure	0.50–1.14	3.89–6.08

behind was separated into two parts, one containing toluene soluble (TS) (or in some cases cyclohexane soluble, CS) components and the other with toluene insoluble (TIS) (or cyclohexane insoluble, CIS) components. Using *n*-pentane, ethyl ether, chloroform and methanol, the TS (or CS) components were further solvent-fractionated by adsorption chromatography. A column (of 1.0 cm diameter) consisting of an activated alumina bed (of 10 cm length) followed by a silica gel bed (of 100 cm length) was used for the chromatography.

Elemental analyses for C and H were determined by a combustion method.

Average molecular weights of the oils extracted were determined by a vapour pressure osmometer (Hitachi model 115) with benzene solution and benzil as a standard.

<sup>1</sup>H-NMR spectra of the oils extracted were recorded at 90 MHz by an FT-NMR spectrometer (FX 90Q model, JEOL) with CDCl<sub>3</sub> solution and tetramethylsilane as a lock signal.

Shimadzu GC-7A, equipped with a flame ionization detector and an OV-1 fused silica capillary column (25 m × 0.25 mm I.D.), was employed to analyse aliphatic components of the extracts. The column was heated at 4 K/min from 323 K to 523 K, and maintained at this temperature for 30 minutes. An integrator (Hitachi D-2000 model) was used to count the GC signals.

Molecular weight distributions of the oils extracted were measured, at wavelength 254 nm, by a liquid chromatograph (Hitachi model 655A), equipped with a UV detector and a Gelpack (GL-A120, Hitachi) column (8 mm I.D. × 500 mm). Tetrahydrofuran at a flow rate of 0.5 ml/min was employed as the mobile phase.

A Soxhlet extraction for fine powder (0.075–0.15 mm) of the oil shale was also performed with THF for 48 hours at 3–5 minutes/cycle.

### 3. Results and discussion

Figure 1 shows the relationships between the weight loss of the oil shale and the final temperature, for extraction with water and toluene. For all the runs shown in this graph, the temperature was raised at 8.5 K/min from room temperature to an intended high temperature, and then maintained at this final temperature for one hour. During this one-hour period the pressure was maintained at 22+ MPa, when

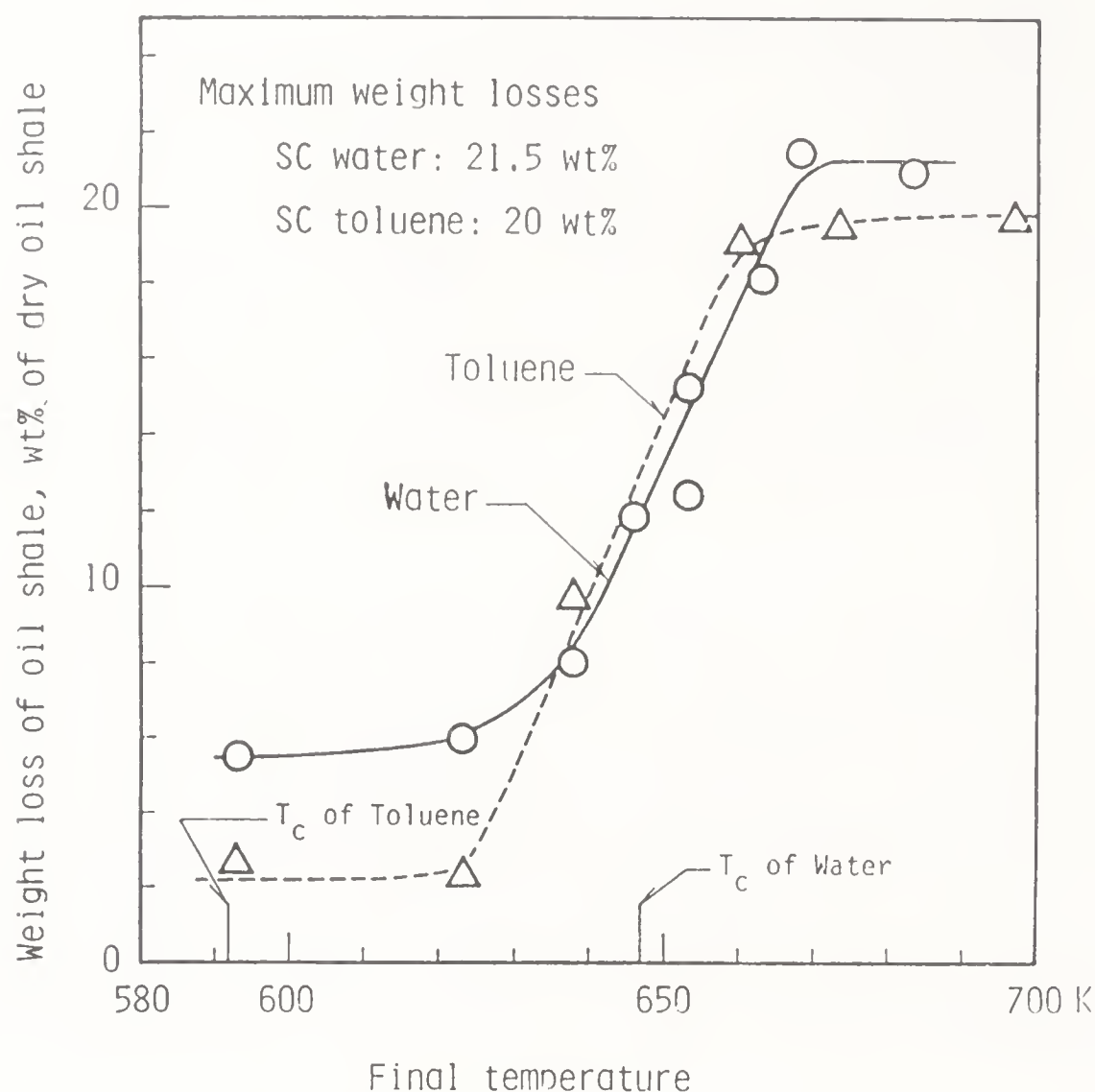


**Figure 1.** Weight loss vs. temperature, for extraction with water and toluene, autoclave being heated to the final temperature and maintained at this temperature for one hour.

temperature was above the critical, and at the saturated vapour pressure, when temperature was below the critical. Weight ratios of the oil shale to the solvents were nearly 0.08. Each data point was obtained from a separate run. In the case of both water and toluene, most of the weight losses occurred at temperatures from about 620–670 K. However, at temperatures lower than about 620 K and higher than about 670 K the weight losses were larger with water than with toluene. The weight losses with water levelled off at temperatures higher than about 670 K.

From separate SFE runs with water and toluene at 673 K and 22+ MPa for extraction time longer than 2 hours the maximum weight losses were found to be 21.5 wt% and 20 wt%, respectively.

Figures 2 and 3 (for the same experiments as in figure 1) show the yield vs. temperature curves for the TS and TIS components, respectively. Total yields of the oil extracted (TS plus TIS) with water are lower than those with toluene. It shows that more inorganics and less organics are extracted with water than with toluene. Also, figure 2 shows that the yields of the TS components with water decrease at temperatures higher than about 670 K. It suggests that the extracts are further decomposed at high temperatures.

Qin *et al* (1984b) observed that polymerization of toluene was noticeable at temperatures higher than 673 K in SFE of Maoming oil shale with toluene. Also Kershaw (1984a) estimated, in SFE of Australian coal with toluene at 723 K, that 17 wt% of the total extracts were the pyrolysis products of toluene, such as bibenzyl

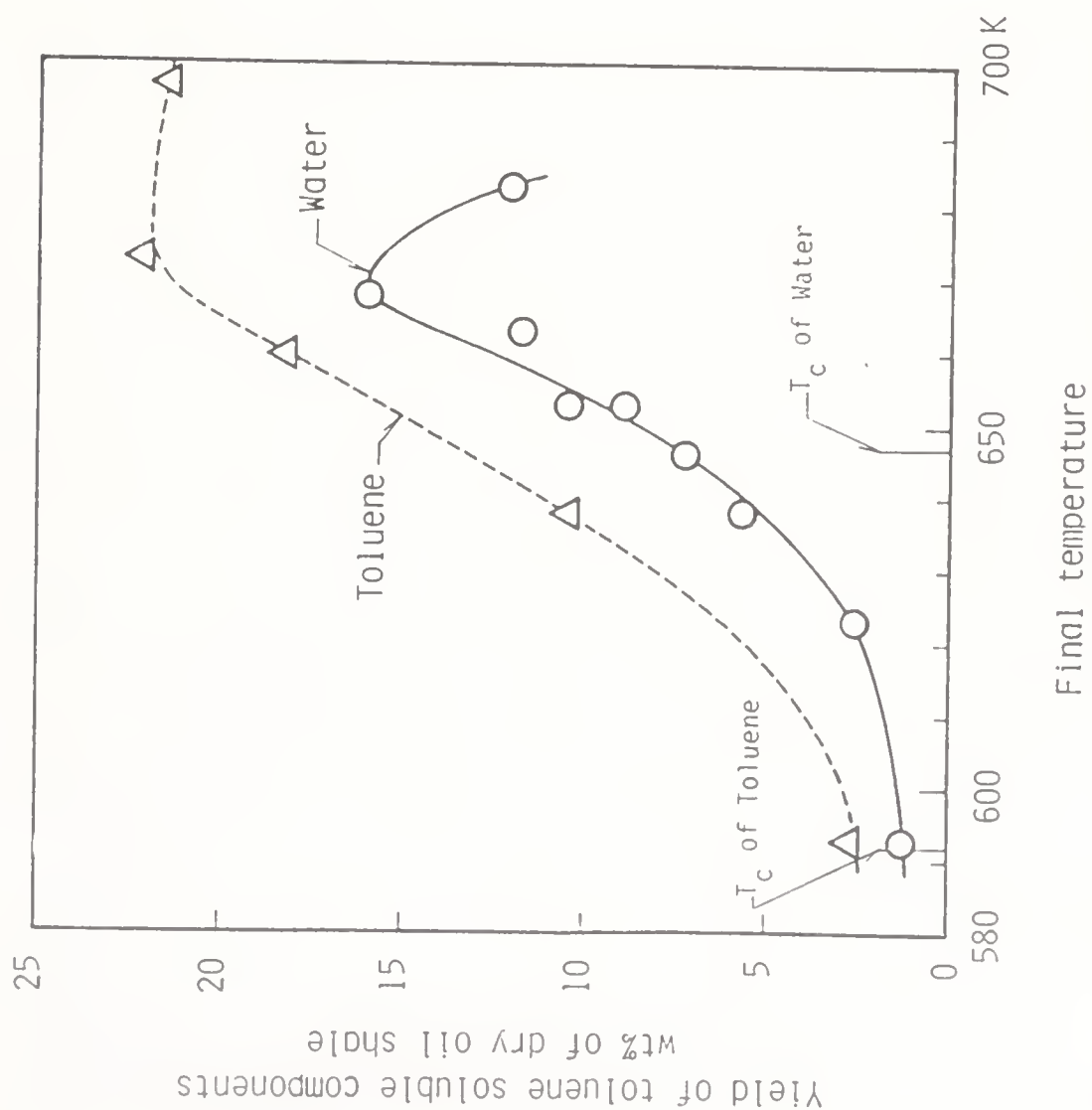


**Figure 2.** Yields of TS components of the oils extracted with water and toluene (the same experiments as shown in figure 1).

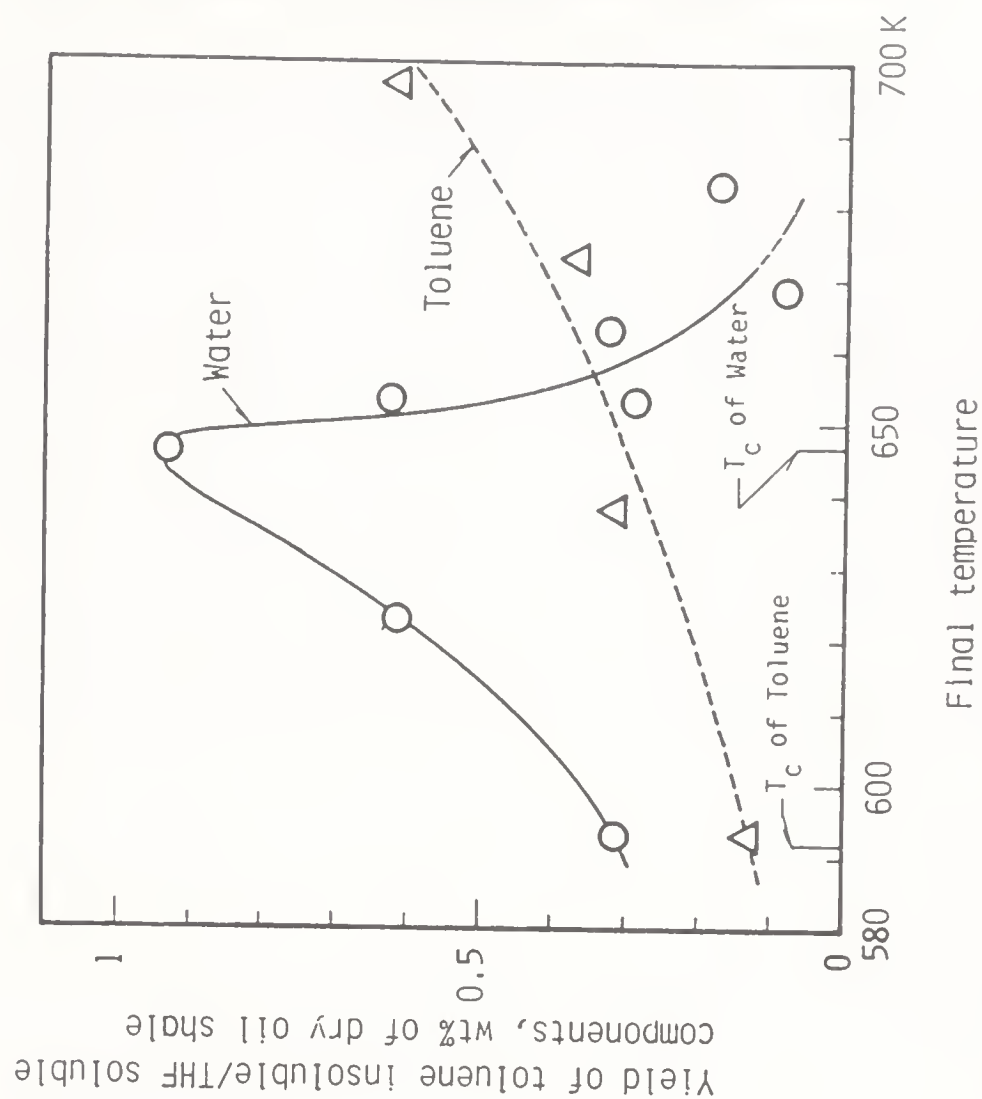


**Figure 3.** Yields of TIS components of the oils extracted with water and toluene (the same experiments as shown in figure 1).



and its isomers, dimethylbiphenyls, methyldiphenylmethanes etc. As a matter of fact, in the present SFE experiments at temperatures higher than 673 K the weight losses of the oil shale (plotted in figure 1) are slightly (1–2 wt%) less than the sum of the TS (figure 2) and the TIS components (figure 3). It is presumed from the work of Qin *et al* (1984b) and of Kershaw (1984a) that this difference in mass balance would also result from pyrolysis of the solvent toluene.

Figure 3 shows that the TIS components obtained from SFE with water are highest at about 645 K, while those with toluene increase with the increase in temperature. At temperatures higher than about 645 K, the TIS components extracted from SFE with water, which are an order of magnitude less than those of the TS components, are found to decrease as the temperature increases further. This may be an indication of reactions of supercritical water with the TIS components.

Figure 4 shows GPC molecular weight distributions of the oils extracted with water and toluene at the final condition of 22+ MPa and 673 K (heated at 8.5 K/min from room temperature to 673 K; the autoclave was cooled down and

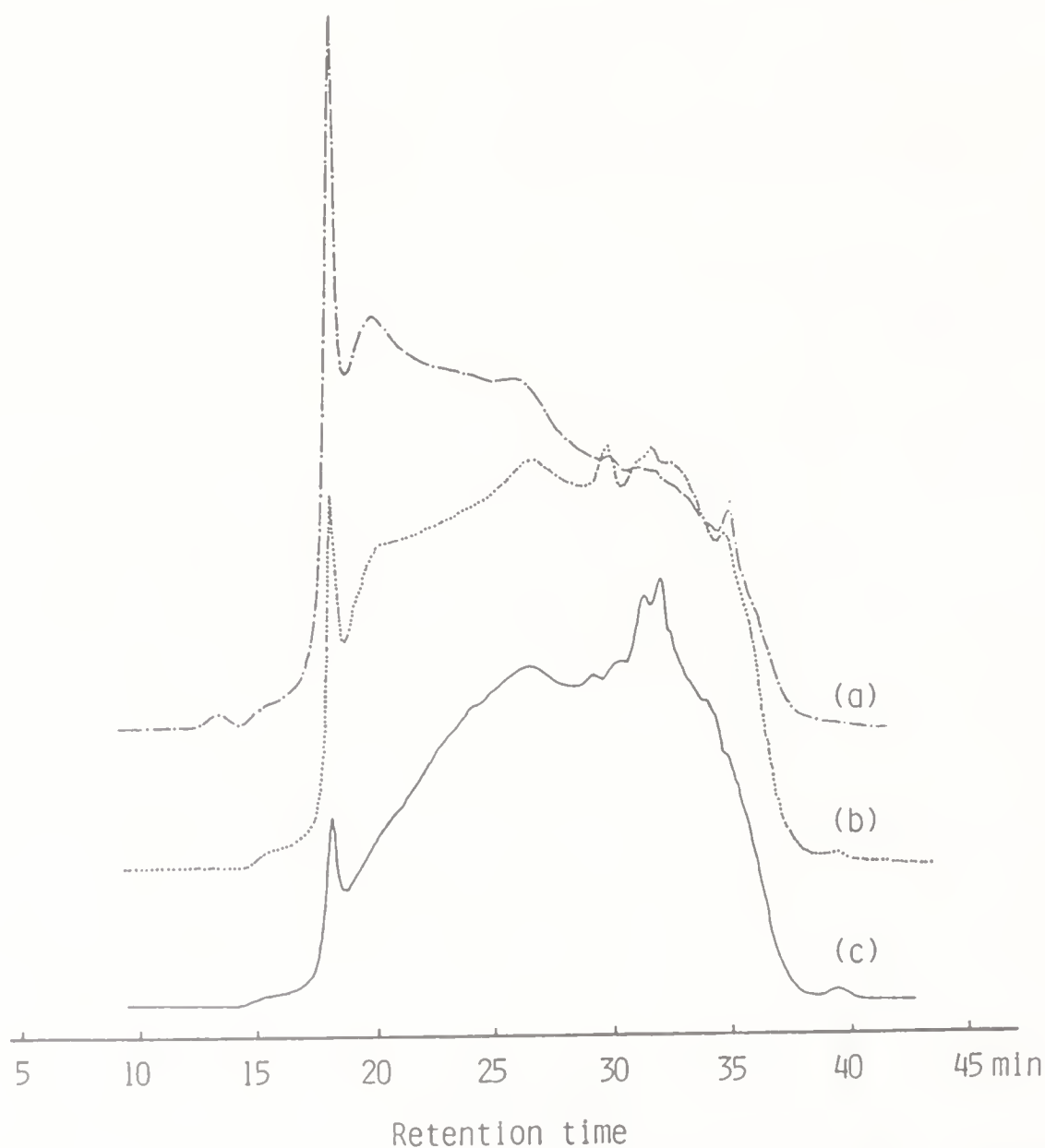
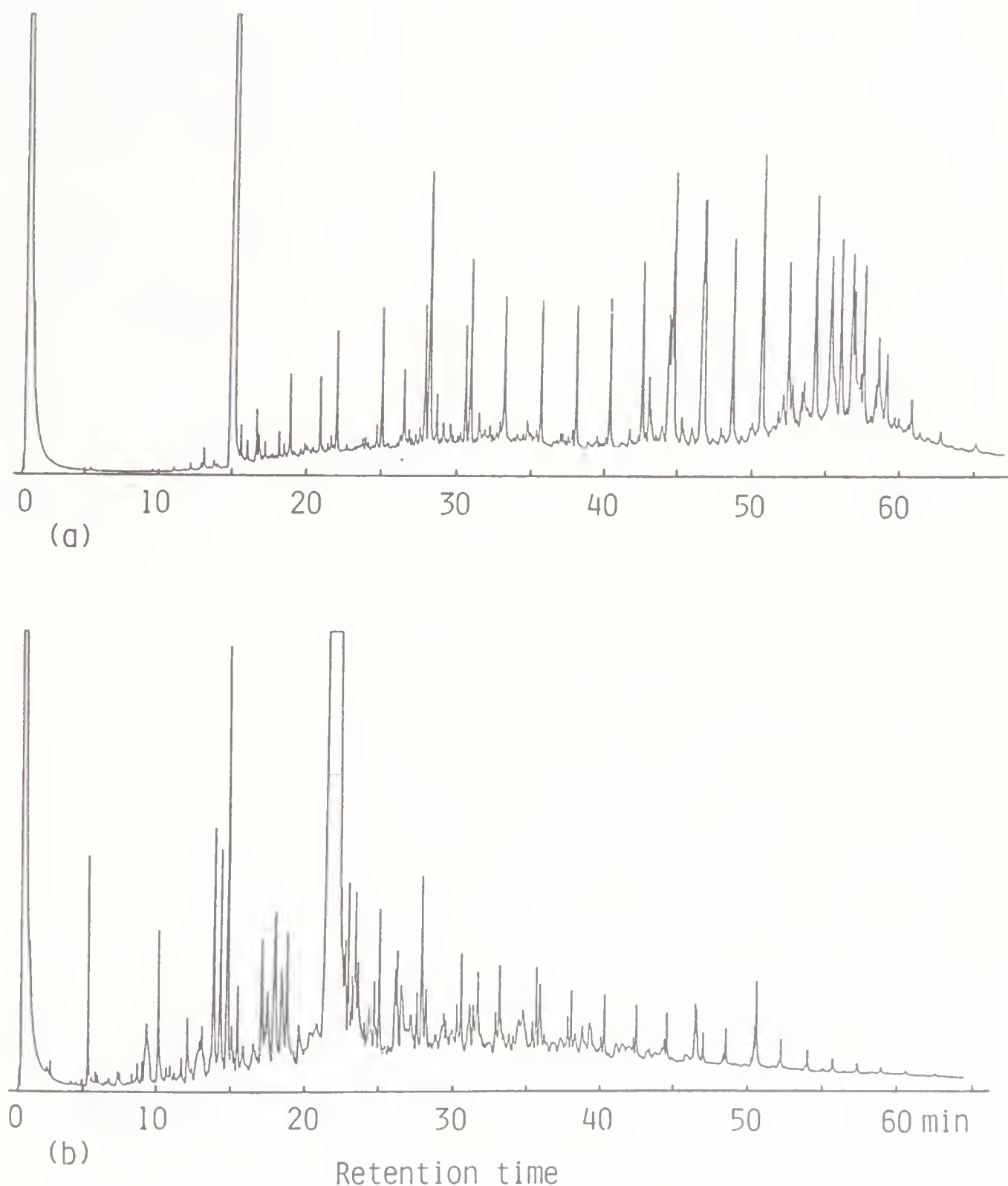


Figure 4. GPC scans of the extracts: (a) SFE with toluene (at final condition of 673K and 22+ MPa; heated at 8.5 K/min from room temperature and then cooled quickly when the temperature reached 673K); (b) SFE with water [same as in (a)]; (c) Soxhlet extraction.

opened). A GPC molecular weight distribution of the oil obtained from Soxhlet extraction with THF is also included in figure 4. In the analyses of the oils extracted with SC water and SC toluene and of Soxhlet extracts, almost the same quantities of the oils were injected into the GPC: about  $2\ \mu\text{l}$  0.01 g-oil/ml-tetrahydrofuran solutions. The GPC scan of the oil extracted from SFE with water (curve b in figure 4) and that of the oil obtained from Soxhlet extraction with THF (curve c) are similar to each other, whereas more organic compounds of high molecular weight are found to be extracted with SC water than in the Soxhlet. The GPC scan of the oil



**Figure 5.** Chromatograms of *n*-pentane eluates of the oils extracted with SC water: (a) SFE at final condition of 653K and 23 MPa for 1.7 hr (including a transient heating period of 0.7 hr); (b) SFE at final condition of 708K and 22+ MPa for 1.8 hr (including a transient heating period of 0.8 hr).

extracted with SC toluene (curve a) is considerably different from curves b and c, especially in the range of high molecular weight.

Figures 5a and b show typical chromatograms of *n*-pentane eluates of the oil extracted with SC water, subjected to SFE under conditions of (a) 653K and 23 MPa for 1.7 hr (including a transient heating period of 0.7 hr), and (b) 708K and 22+ MPa for 1.8 hr (including a transient heating period of 0.8 hr). Chromatogram (a) is similar to that of the oil (although not shown in this paper) obtained with SC toluene. Aliphatic compounds from C11 to C34, mostly of *n*-alkanes, are found in chromatogram (a). Patterns of *n*-alkanes of C11–C34 similar to chromatogram (a) have been observed with the oil extracted from SFE of coal with toluene by Bartle *et al* (1979c), and also with the extracts obtained from toluene SFE of Maoming oil shale by Qin *et al* (1984a). Chromatogram (b) shows that more light molecular weight components and less heavy components are obtained at higher temperature extraction with SC water. This indicates that thermal decomposition of heavy species occurred at high temperature.

Figure 6 shows the relative peak areas of *n*-alkanes (in the range from C11 to C31) of the extract obtained from the oil shale with SC water and SC toluene at 653K and 22+ MPa for 1.7 hr (including a transient heating period of 0.7 hr). As depicted, SC water and SC toluene extract almost the same amounts of C11–C31 *n*-alkanes. In SFE with water the TS components extracted were equivalent to 14.1 wt% of the dry oil shale, while in SFE with toluene it was 18.6 wt% of the dry oil shale. However, almost the same amount of *n*-pentane eluate was obtained with SC water (3.4 wt% of dry oil shale) and with SC toluene (3.0 wt%).

Separate experiments were also carried out under conditions where the autoclave was heated at 8.5 K/min and was quickly cooled down and opened as soon as it

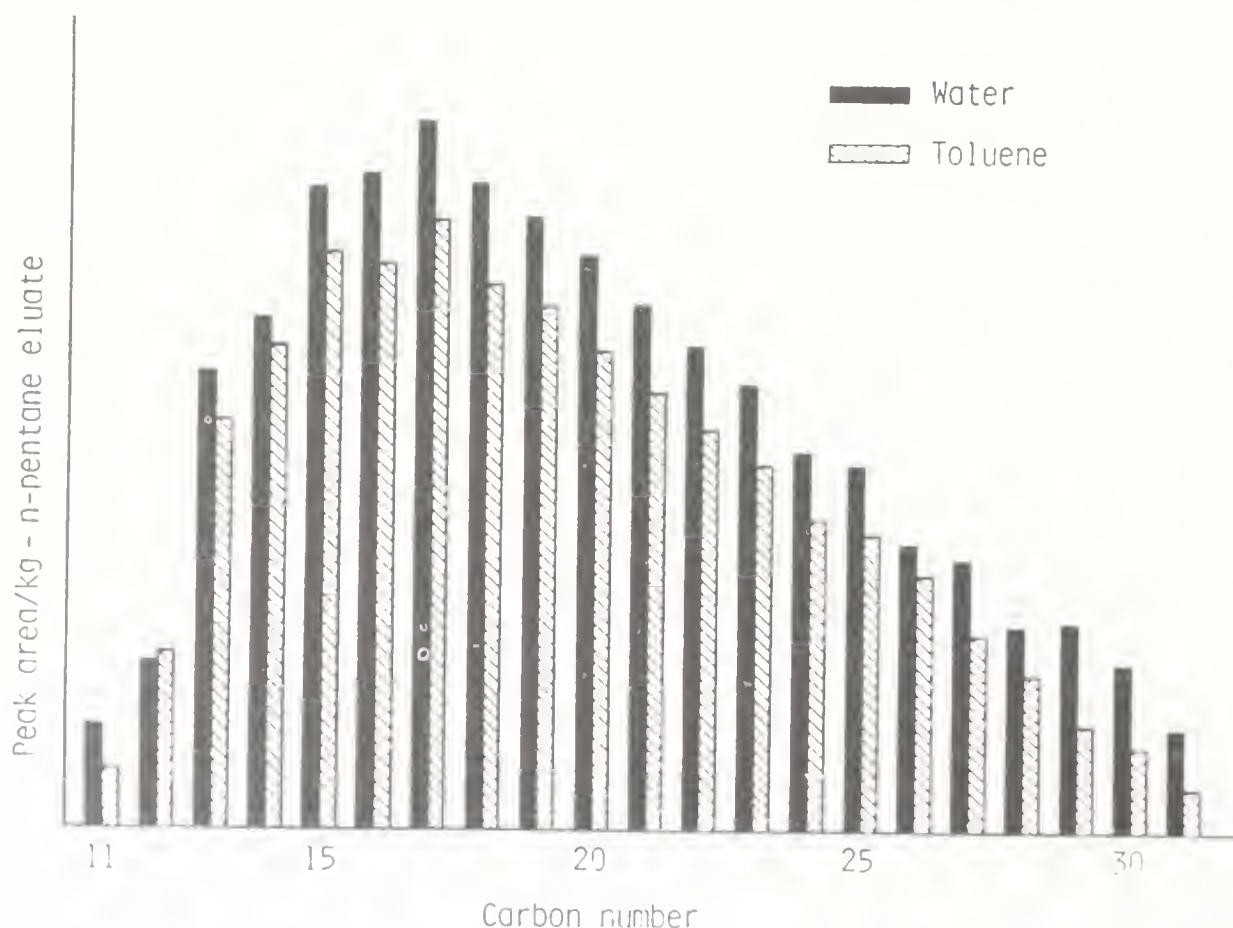


**Figure 6.** Relative yields of *n*-alkanes of the oils extracted with SC water and SC toluene, 653K and 22+ MPa for 1.7 hr (including a transient heating period of 0.7 hr).

reached a prescribed temperature, and the oils extracted were examined. Figure 7 shows, in terms of the relative peak area vs. carbon number, the aliphatic components (straight-chain and branched alkanes and alkenes) of the oils obtained at various prescribed temperatures. As depicted, the yield distribution at 593 K is similar to that of the Soxhlet extracts. Also the yields increase as the extraction temperature increases to 708 K. This increase is due to depolymerization of kerogen, as pointed out by Qin *et al* (1984b). However, a considerable decrease in the yield is observed at 773 K. This decrease is obviously due to the decomposition of kerogen at high temperature.

Table 3 shows two sets of the data obtained from SFE with water, one when the autoclave was opened as soon as the extraction temperature reached 673 K, and the other when the autoclave was kept for one hour after reaching 673 K. The autoclave pressure at 673 K was 22+ MPa. It is found that more chloroform and methanol

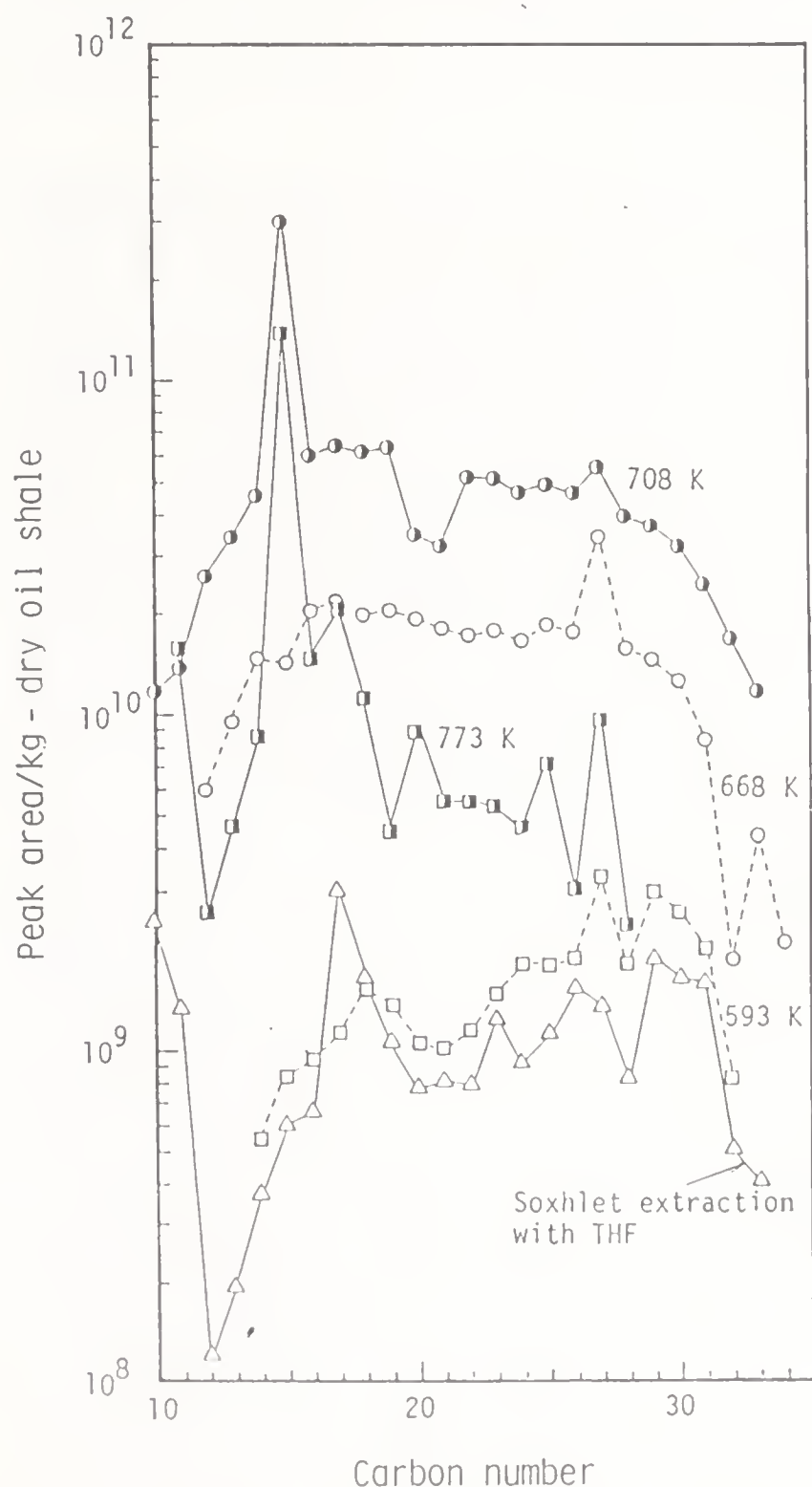


**Figure 7.** Relative yields of aliphatic components of the oils extracted with water; those obtained by Soxhlet extraction.



**Table 3.** Yields of extract components

	Soxhlet extraction with THF	SFE with water at 673K and 22+ MPa	
		for 0 hr <sup>b</sup>	for 1 hr <sup>c</sup>
Solid weight loss, wt% <sup>a</sup>	0.701	13.2	21.1
Cyclohexane-soluble components, wt% <sup>a</sup>	0.592	8.46	14.1 <sup>d</sup>
<i>n</i> -Pentane eluate, wt% <sup>a</sup>	0.157	3.43	3.34
Ethyl ether eluate, wt% <sup>a</sup>	0.218	2.61	2.74
Chloroform eluate, wt% <sup>a</sup>	0.0112	0.504	4.06
Methanol eluate, wt% <sup>a</sup>	0.0861	0.536	1.49
Cyclohexane-insoluble/THF- soluble components, wt% <sup>a</sup>	0.104	0.839	0.235 <sup>e</sup>

<sup>a</sup> kg/kg-dry oil shale x 100;<sup>b</sup> heated at 8.5K/min from room temperature and cooled quickly when the temperature reached 673K;<sup>c</sup> heated from room temperature to 673K at 8.5K/min and maintained at this temperature for one hour;<sup>d</sup> Toluene soluble components, wt% of dry oil shale;<sup>e</sup> Toluene insoluble components, wt% of dry oil shale.

eluates or polar substances were obtained and solid weight decreased further when the solid was subjected to a longer period of extraction, while *n*-pentane and ethyl ether eluates were little affected by the extraction period. Also, it is found that a small amount of TIS/CIS was obtained. The data from the Soxhlet extraction are also listed in table 3. The sample weight loss and the CS components extracted from the Soxhlet extraction with THF were considerably lower than those of SFE with toluene.

Table 4 shows the average molecular weight, aromatically ( $f_a$ ), percentage weight aromatic carbon ( $C_A$ ), C and H of various eluates of the oils obtained from the oil shale with SC water (extraction: 653 K, 22+ MPa, 1.7 hr including a transient period of 0.7 hr). Some Soxhlet extraction data are also shown in table 4. Also, the oil obtained with SC water is found to have an overall  $f_a$  of 0.30. This agrees with the data ( $f_a = 0.32$ – $0.34$ ) measured by Qin *et al* (1984b) from a continuous SFE of Maoming oil shale with toluene at 653–673 K and 15–20 MPa.

**Table 4.** Various eluates of the oil extracted with SC water; oil obtained from Soxhlet extraction with THF.

	Eluate	(MW) <sub>av</sub> <sup>a</sup>	$f_a^b$	$C_A^c$	C	H	Atomic H/C
SFE with water at 653K and 22+ MPa for 1.7hr (including a transient period of 0.7 hr)	<i>n</i> -Pentane	270	–	–	83.5	12.9	1.84
	Ethyl ether	345	0.237	27.0	83.0	11.9	1.71
	Chloroform	340	0.284	20.8	80.6	10.6	1.57
	Methanol	480	0.366	33.7	78.6	9.61	1.46
Soxhlet extraction with THF		150	0.270	–	74.9	10.3	1.64

<sup>a</sup> Average molecular weight;<sup>b</sup> aromaticity determined by the method of Brown & Ladner (1960);<sup>c</sup> percentage weight aromatic carbon determined by the method of Knight & Jenkins (1972).

#### 4. Conclusions

From the experiments on SFE of Maoming oil shale the following conclusions were obtained:

- 1) More organic components of high molecular weight and less inorganics are extracted with SC toluene than with SC water, although the total weight loss of the solid sample is almost the same, not being dependent on the solvent (toluene or water).
- 2) Average molecular weight and amount of the oil extracted are largest with SC toluene, followed by SC water and then Soxhlet extraction.
- 3) The extracts obtained from SC toluene and SC water have almost the same yield distributions of aliphatic compounds.

This paper is dedicated to Dr L K Doraiswamy on his sixtieth birthday.

#### References

- Amestica L A, Wolf E E 1984 *Fuel* 63: 227-230  
Amestica L A, Wolf E E 1986 *Fuel* 65: 1226-1232  
Brown J K, Ladner W R 1960 *Fuel* 39: 87-96  
Bartle K D, Ladner W R, Martin T G, Snape C E, Williams D F 1979a *Fuel* 58: 413-422  
Bartle K D, Calimli A, Jones D W, Matthews R S, Olcay A, Pakdel H, Tugrul T 1979b *Fuel* 58: 423-428  
Bartle K D, Jones D W, Pakdel H, Snape C E, Calimli A, Olcay A, Tugrul T 1979c *Nature* 277: 284-287  
Bartle K D, Jones D W, Pakdel H 1982 *Sep. Sci. Technol.* 17: 167-181  
Bartle K D, Martin T G, Williams D F 1975 *Fuel* 54: 226-235  
Barton P 1983 *Ind. Eng. Chem., Process Des. Dev.* 22: 589-594  
Ceylan R, Olcay A 1981 *Fuel* 60: 197-200  
Deshpande G V, Holder G D, Bishop A A, Gopal J, Wender I 1984 *Fuel* 63: 956-960  
Houser T J, Tiffany D M, Michael Z L, McCarville E, Houghton M E 1986 *Fuel* 65: 827-832  
Knight S A, Jenkins G I 1972 *Chem. Ind. (London)* 5 August: 614-616  
Kershaw J R 1984a *Fuel Process Technol.* 9: 235-250  
Kershaw J R 1984b *Liq. Fuels Technol.* 2: 385-394  
Kershaw J R, Jezko J 1982 *Sep. Sci. Technol.* 17: 151-166  
Kershaw J R, Overbeek J M 1984 *Fuel* 63: 1174-1177  
McKay J F, Chong S L, Gardner G W 1983 *Liq. Fuels Technol.* 1: 259-287  
McKay J F, Chong S L 1983 *Liq. Fuels Technol.* 1: 289-324  
Qin K Z, Wang R A, Jia S S, Lao Y X, Guo S H 1984a Structural characterization of supercritical gas extracts and residues of Fushun and Maoming oil shale, Preprint of *Pan-Am. Chem. Soc. Div. Fuel Chem.* 29(3): 104-112  
Qin K Z, Wang R A, Jia S S 1984b *Energy Sources* 7: 237-255  
Tugrul T, Olcay A 1978 *Fuel* 57: 415-420  
Towne S E, Shah Y T, Holder G D, Deshpande G V, Cronauer D C 1985 *Fuel* 64: 883-889  
Whitehead J C, Williams D F 1975 *J. Inst. Fuel* 48: 182-184  
Zhu Y, Yang H, Xiong K, Xue W 1982 Investigation on supercritical gas extraction of Chinese coal and oil shale, presented at Pan-Pacific Synfuels Conference, Tokyo, Vol. 1: 268-275



## Author Index

ANVAR	164, 172	<i>see</i> Gianetto A	270, 276
Abdul-Kareem H K	222, 233–235, 241, 242	Barekat M	
Adachi K		<i>see</i> Brungorg	179
<i>see</i> Tamura M	172	Barenblatt G I	
Adamson A N	186, 187	<i>see</i> Zeldovich Ya B	134
Adderley C I	140	Barkelew C H	143, 293
Adesina A A	222, 238	Barrer J W	
<i>see</i> Silveston P L	239	<i>see</i> Gassend R	173
Adler J	134–136, 138	<i>see</i> Gitchel	171
Akgerman A	292	Barrer R M	170
<i>see</i> Collins G M	292	Barreteau D	49–51, 53, 55, 57
<i>see</i> Hook B D	292	Barshad Y	233, 244
<i>see</i> Ruecker C M	292	Bartle K D	307, 314
Al-Dabbagh N	257	Barton P	307
Al-Taie A S	236	Bates S I	
Albright L F	88	<i>see</i> Inoue K	179
Alfani F	88	Bdzil J	176
Alvarez-Cuenca M	257	Beaudry E	
Amariglio H	223	<i>see</i> Ramachandran P A	284, 286
Amelse J A	149, 150, 155	Beaudry E G	290, 292
Amestica L A	308	Beeckman J W	88
Amstrong E R		Begovich J M	257, 262
<i>see</i> Baker C G J	257	Bergna H E	
Amundson N R	75	<i>see</i> Contractor R M	223
<i>see</i> Olson K E	88, 133	Bergougnou M A	
Ananth M S	99	<i>see</i> Alvarez-Cuenca M	257
Anderberg M R	303	<i>see</i> Baker C G J	257
Angelino H	50, 53, 57	<i>see</i> Kim S D	257
<i>see</i> Barreteau D	50, 57	Bermejo J	179
Anwar M M	165	Bernard J R	257
Anzai J	177	Best R J	53, 57
Arcuri K B	149–151, 153, 155, 157, 158, 161	Bhatia S K	103, 111
Argyriou D T	71	Bilimoria M R	236, 237, 242
Aris Rutherford	1	Biloen P	153
Asano K	249, 250, 257	Bilous O	133
<i>see</i> Kojima H	257	Bischoff K B	89, 140
Attia Y A	178	<i>see</i> Deshpande G V	299, 302
		Bishop A A	
Badgujar M N		<i>see</i> Deshpande G V	307
<i>see</i> Smith D N	257	Blackstone C M	
Bailey J E	218, 220, 236, 237, 241, 242	<i>see</i> Contractor R M	223
Baker C G J	257	Blano C G	
<i>see</i> Kim S D	257	<i>see</i> Bermejo J	179
<i>see</i> Alvarez-Cuenca M	257	Blok J R	273, 274, 280
Baker L A		Blum D B	257
<i>see</i> Way J D	175	Blume I	176
Baker O	271	Boddington T	136
Baker R W	176	Boreskov G K	218
Baldi G	271, 274, 278, 279, 283	<i>see</i> Nagarajan R	222
<i>see</i> Colombo A	282, 283	Borg M	



- see* Nagarajan R 175  
 Borgerding M F 175  
 Borwanker J D 72  
     *see* Ramkrishna D 72  
     *see* Shah B H 71, 76, 77  
 Botty M C 88  
 Bowes P C 134, 135  
 Bradstrom A 167  
 Breiter M W 176  
     *see* Bdzil J 176  
 Brereton C M H 35, 43, 45, 47  
 Briggs J P 228–230, 242, 243  
 Brito-Alayon A 87, 88  
 Brown J K 316  
 Bruce P N 257  
 Brungorg I 179  
 Buffham B A 283  
 Bukur B Dragomir 13, 25, 27  
 Burkell J J 42  
 Butt J B 149–151, 155  
     *see* Amelse J A 149, 150, 155  
     *see* Arcuri K B 149–151, 158  
 Byrne A 89  
  
 Cabeza C  
     *see* Bermejo J 179  
 Cahn R P 176  
 Calimli A  
     *see* Bartle K D 307, 314  
 Campbell D L  
     *see* Jahnigh C E 35  
 Cankurt N T 35, 45  
 Capuder E 257  
 Car N L  
     *see* Kara S 261, 262  
 Carberry J J 140  
 Carbonell R G 275, 278  
     *see* Saez A E 281  
 Carbova V R 222  
 Carlier C C  
     *see* Bdzil J 176  
 Carr N L  
     *see* Kara S 257  
 Carr N L  
     *see* Kelkar B G 257  
 Catros A 257  
 Ceylan R 307  
 Cha D Y 167  
 Chang T 167  
 Chang W  
     *see* Georgakis C C 103, 111, 115  
 Chaouki J 35  
     *see* Wu R L 44  
 Charpentier J C 271, 274  
     *see* Midoux N 270, 277  
     *see* Saberian-Broudjenni M 257  
 Chaudhary R V 270, 282  
  
 Chavarie C 14  
 Chemburkar R M 143–145  
 Chemical Engineering News 169  
 Chemical Week 179  
 Chemtech 176  
 Chiang H W  
     *see* Pendse H 281  
 Chiu T-M 257  
 Cho B K 222, 230, 231  
 Chong L B  
     *see* McKay J F 308  
 Chou T S 271  
 Chowdhry U  
     *see* Contractor R M 223  
 Christensen M 280  
 Christensen T S 185, 192  
 Claybaugh B E 238  
 Cleary W 164, 172  
 Coisne J M 172  
 Collina A 135  
 Collins G M 292  
     *see* Akgerman A 292  
     *see* Hook B D 292  
 Colombo A 282, 283  
 Contractor R M 223  
 Cook S T M  
     *see* Anwar M M 165  
 Costa E C 124  
 Coulson E A 164  
 Coxson P G 299, 303  
 Crine M 282  
 Cronauer D C  
     *see* Towne S E 307  
 Crone G 240  
 Cutlip M B 231, 232, 243, 244  
  
 Dabke N S 1  
 Dakessian V 87, 88  
     *see* Byrne A 89, 91  
 Dakshinamurty P 257  
 Daly J G  
     *see* Bukur D B 27  
 Daradimos G  
     *see* Reh L 37, 43  
 Darton R C 18, 25, 28, 249, 250  
 Dassori C G 115  
 Dautzemberg F M 50, 290  
 Davidson J F 57, 58, 60, 65, 71, 83,  
     85, 104, 121, 257  
     *see* Darton R C 18, 25  
 Davis M E 249, 250, 257  
 Deckwer W-D  
     *see* Patwari A N 262  
 Demont J  
     *see* Kauschus 143  
 Dente M 135  
 Deshpande G V 307

- see* Towne S E 307  
 Dhanuka V R 257, 262  
 Diddmas D G  
     *see* Gitchel W B 171  
 Dimenstein D M 273, 281  
 Doherty M F  
     *see* Terill D L 164, 172  
 Doraiswamy L K 99, 103, 111–117, 124, 140  
     *see* Dabke N S 1  
     *see* Jayaraman V K 14, 32, 33,  
     *see* Prasannan P C 103, 116, 124  
     *see* Rajadhyaksha R A 140  
     *see* Tambe S 1  
 Drinkenberg A A H 273, 274, 276, 279, 280, 281  
 Dudukovic M P 105, 269–271, 278, 282, 284,  
     288–291, 293  
     *see* Beaudry E G 290, 292  
     *see* El-Hisnawi A A 278, 288, 290  
     *see* Mills P L 270, 289  
     *see* Ramachandran P A 284, 286  
     *see* Schwartz T G 282, 283  
 Duprat F  
     *see* Gassend R 173  
  
 Edius Y T 150  
 Eiserback W  
     *see* Ludewigh D 171  
 El Masry H 235  
 El-Hisnawi A A 278, 288, 290  
 El-Kady F Y A  
     *see* Mann R 88  
 Elder H W 50  
 Elstner M  
     *see* Pichler H 150  
 Emig G 142  
 Emmett P H  
     *see* Hall W K 150, 151, 153  
 Enigh J W 134–136, 138  
 Epstein N 247–249, 257  
 Ergun S 276  
 Evans J W 111  
     *see* Szekely J 99, 103  
  
 Fabbricino L  
     *see* Nappi A O 222, 235  
 Fan L-S 248–250, 257  
     *see* Peters M H 14, 15, 17, 28, 30  
 Farkas E J 248, 257  
 Favier M 271, 274  
     *see* Madoux N 277  
 Feike E  
     *see* Ludewig D 171  
 Feimer J L 222, 238, 243, 245  
     *see* Silveston P L 239  
 Ferelov V B  
     *see* Gavrilov V Y 88  
 Fesch H L  
     *see* Bdzil J 176  
     Fiand U  
         *see* Emig G 142  
     Fiolitakis E 236  
     Forrissier M 236  
     Fraye J A  
         *see* Paraskos J A 289  
     Freyer C 14, 18, 19, 27, 28, 31, 32  
     Froment G F 88, 89, 135, 140, 302  
         *see* Johnson B H 88  
     Fuerstenau D W 178  
     Fukuda T  
         *see* Kato Y 261, 262  
     Fukuma M  
         *see* Muroyama K 257  
     Fukushima S 271  
     Funazukuri T 307  
     Furusaki S 15  
  
 Gaikar V G 163, 165–167, 170–174  
 Gambhir B S 293  
 Gardner G W  
     *see* McKay J F 308  
 Gassend R 173  
 Gau G 222  
 Gavrilov V Y 88  
 Geldart D 18, 36  
 Georgakis C C 103, 111, 115  
 Gerald Z Jr 179  
 Gerhard D  
     *see* Sicardi S 276, 277  
 Germain A 270  
 Gianetto A 270, 276, 283  
 Gibson J B 104  
     *see* Westmoreland P R 102, 104  
 Gigorovskii A M 169  
 Ginlay G W  
     *see* Way J D 175  
 Gitchel W B 171  
 Gopal J  
     *see* Deshpande G V 307  
 Goto S 270, 289  
 Grace J R 14, 35, 43–45  
     *see* Wu R L 45  
 Graf R 37  
 Gray P  
     *see* Boddington T 136  
 Greenfield P F 282  
 Greenstein J P 170  
 Greg S J 199, 201  
 Griffin J R  
     *see* Claybaugh B E 238  
 Griffiths B  
     *see* Contractor R M 223  
 Gross B 303, 304  
     *see* Jacob S M 300

- Grushya E  
    *see* Sasson Y 168
- Guha D K  
    *see* Roy N K 257
- Gulari E 233, 244
- Guo S H  
    *see* Qin K Z 308, 310, 312, 314, 316
- Gupta R 270
- Gupta S K  
    *see* Tjahjadi M 144, 146
- Gustafson S S 69  
    *see* Sweet I R 69, 71, 85
- Gyure D C 281
- Haldeman R G 88
- Hall W K 150, 151, 153
- Hanika H 270
- Hanika J 293
- Hansen T T 185, 192
- Hanson C  
    *see* Anwar M M 165
- Hara S  
    *see* Hirai H 180
- Harrison D 57, 58, 60, 65, 71, 83, 85  
    *see* Darton R C 18, 25
- Harrison D P 104, 116  
    *see* Westmoreland P R 102, 104
- Hartge E U 44
- Hartmann K  
    *see* Kauschus W 143
- Heathcock C H 170
- Herrick C S  
    *see* Matson S L 175
- Herskowitz M 270
- Hess R K  
    *see* Collins G M 292
- Hindmarsh A C 121  
    *see* Sohn H Y 121
- Hinze W L 175
- Hirai H 180
- Hirose T  
    *see* Sato Y 276
- Hirsan I 42
- Hirsch M 37
- Hoffman T W  
    *see* Shaw I D 14
- Hoffmann U  
    *see* Emig G 142
- Hofmann H 272, 274  
    *see* Emig G 142  
    *see* Fiolitakis E 236  
    *see* Sicardi S 276, 277
- Holder G D  
    *see* Deshpande G V 307  
    *see* Towne S E 307
- Hollinden G A 50
- Hoogendoorn J C 37
- Hook B D 292  
    *see* Akgerman A 292
- Horn F J M 220, 236
- Horowitz H S  
    *see* Contractor R M 223
- Hoshimoto T  
    *see* Nashiro M 179
- Houghton M E  
    *see* Houser T J 307
- Houser T J 307
- Hoyer G G  
    *see* Inoue K 179
- Huang R  
    *see* Wu Z 180
- Hudgins R R 220, 229, 241, 243  
    *see* Abdul-Kareem H K 222, 233–235, 241, 242  
    *see* Adesina A A 222, 238  
    *see* Briggs J P 228–230, 242, 243  
    *see* Feimer J L 222, 238, 243, 245  
    *see* Hugo A J 233  
    *see* Jain A K 221–223, 225, 226, 227, 235, 236, 241–245  
    *see* Li C–Y 241, 244, 245  
    *see* Prokopowicz R A 233  
    *see* Ross G S 238  
    *see* Silveston P L 239  
    *see* Unni M P 227, 228, 241, 244
- Huff G A Jr  
    *see* Satterfield C N 150
- Hughes J A  
    *see* Millington J P 164
- Hughes R 87, 88  
    *see* Byrne A 89, 91  
    *see* Sampath B S 122
- Hugo A J 233
- Huntington R L 278
- Hwang S-J  
    *see* Fan L-S 257
- Iguchi A  
    *see* Kojima H 257
- Iguchi T  
    *see* Sada E 261, 262
- Imafuku K 257
- Inoue K 179
- Iovtchev K  
    *see* Barreteau D 55
- Irish D E  
    *see* Prokopowicz R A 233
- Jacob S M 300  
    *see* Gross B 303, 304
- Jafee S B 284, 286, 287
- Jagirdar G C 165–168, 170
- Jagnigh C E 35
- Jain A K 221–223, 225–227, 235, 236, 241–245  
    *see* Abdul-Kareem H K 222, 233, 234, 235, 241, 242

- see* Feimer J L 222, 238, 243, 245  
 Jakelski D M 233  
     *see* Hugo A J  
 Jalan Vinod 99, 100, 108  
 Janakiraman B 174  
 Janssen K 37  
     *see* Hirsch M  
 Jayraman V K 14, 32  
 Jezko J 307  
 Jia S S 308, 310, 312, 314, 316  
     *see* Qin K Z  
 Johnson B H 88  
 Johnson S H 121  
     *see* Sohn H Y  
 Jones A R 164  
     *see* Millington J P  
 Jones D W 307, 314  
     *see* Bartle K D  
 Jones J I 164  
 Joshi J 248, 249  
 Joshi J B 262, 265  
  
 Kago T 249  
     *see* Kato Y  
 Kai T 15  
 Kan K M 282  
 Kane D M 229, 230, 242, 243  
     *see* Briggs J P  
 Kaneda S 180  
     *see* Kawai T  
 Kara S 257, 261, 262  
 Kato K 13, 14, 28  
 Kato Y 249, 257, 261, 262  
     *see* Morooka S  
 Kauschus W 143  
 Kawabata K 169  
 Kawai T 180  
 Kawamura K 257  
 Kelkar B G 257  
     *see* Kara S  
     *see* Kato Y  
 Kennedy C R 284, 286, 287  
 Kenney C N 187  
 Kerschenbaum 236  
 Kershaw J R 307, 310, 312  
 Kibby C L 150  
 Kim C H 257  
 Kim D H 293  
 Kim S D 257  
 Kim Y G 293  
 Kim Y H 247, 257, 261  
     *see* Tsutsumi A  
 Kimen Z M 169  
 Kitchner 178  
 Knight S A 316  
 Knowlton T M 42  
 Kobayashi Y  
     *see* Anzai J 177  
     Kobro H 43, 45  
     Kobylinski T P 150  
         *see* Kibby C L  
     Kock K 178  
     Koide K 257  
         *see* Imafuku K  
     Kojima H 249, 250, 257  
     Kokes R J 150, 151, 153  
         *see* Hall W K  
     Kolini T 257  
     Komiyama M 180  
         *see* Hirai H  
     Kondepudi D K 1  
     Kordylewski W 136  
         *see* Boddington T  
     Krantz W B 281  
     Krishnakumar V K 168  
     Kropholler H W 283  
     Kroupa J 168  
     Krukonis V J 179  
     Kubota H 257  
         *see* Imafuku K  
     Kulkarni B D 1  
         *see* Dabke N S  
         *see* Tambe S S  
     Kumazawa H 261, 262  
         *see* Sada E  
     Kunii D 13  
     Kuo J C 299–302  
     Kurnik R T 179  
     Kusaka K 271  
     Kwauk M 45  
  
 L'Homme A 282  
     *see* Crine M  
     *see* Germain A  
 La Nauze R D 18, 25  
     *see* Darton R C  
 Lacey A A 136  
 Laddha S S 167  
 Ladner W R 316  
 Laguerie C 49–51, 53, 55, 57, 65  
     *see* Barreteau D 50, 51, 55, 57  
 Lai S 270, 289  
     *see* Mills P L  
 Lakota A 289  
     *see* Goto S  
 Lamba H S 105  
 Langham A 179  
     *see* Brungorg I  
 Lao Y X 308, 310, 312, 314, 316  
     *see* Qin K Z  
 Laurence R L 238  
 Lawson F 167  
 Leblond P F 248, 257  
 Lee C



- see Sada E 261, 262  
 Lee J C 257  
 Lefebvre  
   see Germain A 270  
 Leston O 169  
 Levec J  
   see Goto S 270  
   see Saez A E 281  
 Levenspiel O 13, 103  
 Li C-Y 241, 244, 245  
 Li N N  
   see Cahn R P 176  
 Li Y 45  
   see Hartge E U 44  
 Librovič V B  
   see Zeldovich Ya B 134  
 Lim C J 35, 45  
   see Wu R L 44  
 Lindner B 116  
 List H L  
   see Argyriou D T 71  
 Litz W 15  
 Livbjerg H 185, 187, 201  
   see Villadsen J 187  
 Lodaya M P 168  
 Louisi Y  
   see Deckwer W-D 257  
 Ludewig D 171  
 Luss D  
   see Chou T S 271  
   see Olson K E 88  
 Lynch D T 243  
  
 Mainela S R  
   see Bermejo J 179  
 Makhviladze G M 134  
   see Zeldovich Ya B 134  
 Malone B  
   see Contractor R M 223  
 Mann R 88  
 Marchot P  
   see Crine M 282  
 Martin H Z  
   see Jahnigh C E 35  
 Martin T G  
   see Bartle K D 307  
 Martineg A  
   see Bermejo J 179  
 Massoth F E 89  
 Matros Yu Sn 218, 222  
 Matsen J M 37  
 Matson S L 175  
 Matsubara M 220  
 Matsuura A  
   see Fan L-S 257  
 Matthews R S  
   see Bartle D K 307  
  
 Mayer F X  
   see Ramachandran P A 284, 286  
 McCarville E  
   see Houser T J 307  
 McDonnell C F  
   see Albright L F 88  
 McGinnis P H 20  
 McGovern S J  
   see Christensen G 280  
 McGreavy C 140  
 McKay J F 308  
 McKee R H 174  
 Mendiratt A K 167  
 Menon P G 88  
 Mensik M A  
   see Rurrker C M 292  
 Michael Z L  
   see Houser T J 307  
 Michelsen M L 192, 262  
 Midoux N 277  
   see Saberian-Broudjenni M 257  
 Mifune A  
   see Kawamura K 257  
 Millington J P 164  
 Mills P L 269, 270, 288–291, 293  
   see Beaudry E G 290, 292  
   see El-Hisnawi A A 278, 288, 290  
   see Ramachandran P L 286  
 Minday R M  
   see Cahn R P 176  
 Mitchell P J  
   see Schlatter J C 230  
 Moller C E  
   see Villadsen J 187, 192  
 Moore I R  
   see Mann R 88  
 Morbidelli M 133, 135–143  
   see Chemburkar R M 143–145  
   see Tjahjadi M 144, 146  
 Mori S 13, 14, 60  
 Morooka S 257  
   see Kato Y 249  
 Mueller M  
   see Renken A 236  
 Muralidhar R 69  
 Muroyama K 248–250, 257  
  
 Nace D M 88, 257  
   see Gross B 303, 304  
 Nader J E 50  
 Nagaraj D R 178  
 Nagarajan R 174, 175  
 Nakajima S  
   see Tamura M 172  
 Nakano T  
   see Nashiro M 179  
 Nappi A O 222, 235

- Nascimento C A O 89  
 Nashiro M 179  
 Nasif N 25, 27, 29, 30  
     *see* Bukur D B 27  
 Nelson G W 1  
 Nerenberg M A 257  
     *see* Alvarez-Cuenca M 257  
 Ng K M 273, 281  
 Nguyen-Tien K 262  
     *see* Patwari A N 262  
 Nishimura K 176  
     *see* Shinbo T 176  
 Nishimura Y 220  
     *see* Matsubara M 220  
 Nishiwaki A 257, 261, 262  
     *see* Kato Y 257, 261, 262  
 Noble R D 175  
     *see* Way J D 175  
  
 Oba H 173  
 Ogata N 177  
     *see* Yoshikawa M 177  
 Olcay A 307  
     *see* Bartle K D 307, 314  
 Olson K E 88  
 Orlickas A 14  
     *see* Shaw I D 14  
 Osa T 177  
     *see* Anzai J 177  
 Østergaard K 249, 262  
 Otani Y 172  
     *see* Tamura M 172  
 Othmę D F 169  
 Otsuka I 179  
     *see* Nashiro M 179  
 Overbeek J M 307  
 Ozawa Y 88  
  
 Pakdel H 307, 314  
     *see* Bartle K D 307, 314  
 Pandit A 174  
 Pandit A B 248, 249, 262, 265  
 Pannell R B 150  
     *see* Kibby C L 150  
 Paraskos J A 289  
 Partridge B A 18  
     *see* Rowe P N 18  
 Parvinian M 96  
 Patel A N 165  
     *see* Anwar M M 165  
 Patwari A N 262  
 Pecker J 172  
 Pendse H 281  
 Pereira C J 140  
 Pereyra V 22  
 Perlmutter D D 103, 111  
 Peters M H 14, 15, 17, 28, 30  
 Petersen V 37, 43  
     *see* Reh L 37, 43  
 Pichler H 150, 157  
 Piotrowski R D 149–151, 158  
     *see* Arcuri K B 149–151, 158  
 Planck C J 88  
 Potter O E 14, 18, 19, 27, 28, 31, 32  
     *see* Stephens G K 13  
 Prasannan P C 103, 116, 124  
 Pratt M W T 165  
     *see* Anwar M M 165  
 Prausnitz J M 104  
     *see* Reed R C 104  
 Prokopowicz R A 233  
  
 Qin K Z 308, 310, 312, 314, 316  
  
 Rachkovskaya L N 88  
     *see* Gavrilov V Y 88  
 Rajadhyaksha R A 140  
 Ralek M 257  
     *see* Deckwer W-D 257  
 Ramachandran P A 99, 103, 111, 115–117, 124, 269, 270, 284, 286, 288  
     *see* Mills P L 270, 289  
     *see* Prasannan P C 103, 116, 124  
 Ramkrishna D 69, 71, 72, 75, 76, 289  
     *see* Shah B H 71, 76, 77  
     *see* Sweet I R 69, 71, 85  
 Rambeau G 223  
 Ranade P V 116  
 Rao J N 257  
     *see* Dakshinamurty P 257  
 Rao M N 257  
     *see* Guha D K 257  
 Rao V G 276, 279–281  
 Ravikumar V 1  
     *see* Tambe S S 1  
 Ray W H 238  
 Reed D L 175  
     *see* Way J D 175  
 Reed R C 104  
 Reh L 35, 37, 43, 47  
 Reilly P M 14  
     *see* Shaw I D 14  
 Renken A 236, 240  
 Revel-Chion L 257  
 Richardson J T 89  
 Riethof G 169  
 Rinker R G 220, 222, 223, 225, 226, 241  
 Robb W I 175  
 Robinson R G 167  
 Ross G S 238  
     *see* Silveston P L 239  
 Rowe P N 18  
 Roy N K 257  
 Ruckenstein E 174

- see* Nagarajan R 175  
 Ruecker C M 292  
 Ruether J A 257  
*see* Smith D N 257  
 Ruzicka V 293  
*see* Hanika J 257  
  
 Saberian-Broundjenni M 153  
 Sachtler W M H 261, 262  
 Sada E 275, 278, 281  
 Saez A E 283  
 Sagara M 177  
 Sami K 95, 122  
*see* Yoshikawa M 257  
 Sampath B S 257  
 Sanger P 89, 91  
 Santamaria-Ramiro J M 164  
*see* Byrne A 249  
 Sarfori G 257  
 Saruwatari T 257  
*see* Kato Y 257  
 Sasano T 168  
*see* Kawamura K 276  
 Sasson Y 104, 150, 270, 292  
 Sato Y 164  
 Satterfield C N 169  
 Savage D W 282  
 Savitt S A 283  
 Schneider P 169  
*see* Sagara M 230  
 Schering-Kahlbaum G A 236  
 Schlatter J C 236  
 Schmid M 236  
*see* Fiolitakis E 37, 43  
 Schmidt H W 190, 201  
*see* Reh L 88  
 Schubert H 157  
 Schulman B L 150  
 Schultz H 249, 250  
*see* Pichler H 262  
 Schumpe A 169  
*see* Patwari A N 149, 150, 155  
 Schuster L 149, 150  
 Schwartz L H 164  
*see* Amelse J A 37  
*see* Arcuri K B 136  
 Schwarz A 282, 283  
 Schwieger B 134  
 Scott S K 37  
*see* Boddington T 177  
 Scwartz T G 282, 283  
 Semenov N N 134  
 Serbent R 37  
*see* Hirsch M 71, 76, 77  
 Shah B H 72  
*see* Ramkrishna D 115, 270  
 Shah Y T 257, 261, 262  
  
*see* Kara S 157  
*see* Kelkar B G 289  
*see* Paraskos J A 257  
*see* Smith D N 307  
*see* Towne S E 141, 163–168, 170–172, 174  
 Sharma M M 140  
 Shaw I D 104  
 Sherwood T K 88  
*see* Reed R C 178  
 Shettigar U R 176  
 Shimshick E J 71  
 Shinbo T 272, 274, 276, 277  
 Shinnar R 282, 283  
*see* Argyriou D T 270, 276, 277  
 Sicardi S 217, 239  
*see* Colombo A 222, 233–235, 241, 242  
*see* Gianetto A 222, 238  
 Silveston P L 228–230, 242, 243  
*see* Abdul-Kareem H K 222, 238, 243, 245  
*see* Adesina A A 236  
*see* Briggs J P 233  
*see* Feimer J L 238  
*see* Fiolitakis E 233  
*see* Hugo A J 221–223, 225–227, 235, 236, 241–245  
*see* Jain A K 241, 244, 245  
*see* Li C-Y 222, 235  
*see* Nappi A O 233  
*see* Prokopovicz R A 238  
*see* Ross G S 227, 228, 241, 244  
*see* Unni M P 116  
 Simonsson D 13  
 Sinclair R J 199, 201  
*see* Stephens G K 230  
 Singh K S W 230  
 Sinkevitch R M 230  
*see* Schlatter J C 50  
 Slack A V 223  
 Sleight A W 257  
*see* Contractor R M 103, 111, 116, 117, 119, 124, 270, 282, 283, 286, 288, 292  
*see* Goto S 270, 289  
*see* Sagara M 283  
 Smith D N 179  
 Smith J M 307, 314  
*see* Bartle K D 99, 121  
 Sohn H Y 99, 103  
*see* Szekely J 178  
 Somasundaram P 1  
 Song Xiao-Hui 201  
 Sorensen B 116  
*see* Livbjerg H 257  
 Sotirchos S V 271, 274, 278, 279  
 Soung W Y  
 Specchia V

- |                             |                    |                             |                    |
|-----------------------------|--------------------|-----------------------------|--------------------|
| <i>see</i> Gianetto A       | 270, 276, 277      | Tierney J W                 | 115                |
| Sporka K                    |                    | Tiffany D M                 |                    |
| <i>see</i> Hanika J         | 293                | <i>see</i> Houser T J       | 307                |
| Sreeramamurthy R            | 88                 | Tjahjadi M                  | 144                |
| Stanek S                    | 270                | Toda M                      |                    |
| Stanitsas G                 |                    | <i>see</i> Sato Y           | 276                |
| <i>see</i> Hugo A J         | 233                | Togawa S                    | 247                |
| Stapleton I W               | 172                | <i>see</i> Tsutsumi A       | 261, 265           |
| Stepanek J B                | 257, 262           | Toman J J                   | 257                |
| Stephens G K                | 13                 | Toradi C C                  |                    |
| Stevens D R                 | 163                | <i>see</i> Contractor R M   | 223                |
| Stewart P S B               | 257                | Towne S E                   | 307                |
| Stratmann H                 | 178                | Trofman J E                 |                    |
| Streitwiser A               | 170                | <i>see</i> Millington J P   | 164                |
| Subrahmanyam V              |                    | Tsutsumi A                  | 247, 261, 265      |
| <i>see</i> Dakshinamurthy R | 257                | Tugrul T                    | 307                |
| Sugiwa M                    |                    | <i>see</i> Bartle K D       | 307, 314           |
| <i>see</i> Shinbo T         | 176                | Turpin J L                  | 278                |
| Sullivan G R                |                    | Ube Industries Ltd.         | 169                |
| <i>see</i> Hugo A J         | 233                | Uchida K                    |                    |
| Summerhayes R               |                    | <i>see</i> Morooka S        | 257                |
| <i>see</i> Satterfield C N  | 150                | Unni M P                    | 227, 228, 241, 244 |
| Sun H                       |                    |                             |                    |
| <i>see</i> Wu Z             | 180                | Van Brakel J                | 282                |
| Sundaresan S                |                    | Van Deempter J J            | 13, 88             |
| <i>see</i> Christensen G    | 280                | Van Hoote G                 | 50                 |
| Suzuki H                    |                    | Van Welsenaere R J          | 135, 140           |
| <i>see</i> Kawai T          | 180                | Varma A                     |                    |
| Suzuki M                    | 283                | <i>see</i> Chemburkar R M   | 143–145            |
| Sweeney T L                 |                    | <i>see</i> Pereira C J      | 140                |
| <i>see</i> Peters M H       | 14, 15, 17, 28, 30 | <i>see</i> Tjahjadi M       | 144, 146           |
| Sweet I R                   | 69, 71, 85         | Vasudeva K                  | 133, 135–143       |
| Sylvestve L F               |                    | <i>see</i> Rajadhyaksha R A | 140                |
| <i>see</i> Terill D L       | 164, 172           | Vasudevan G                 | 238                |
| Szekely J                   | 99, 111            | Vaughan R J                 | 177                |
| <i>see</i> Georgakis C C    | 103, 111, 115      | Veno A                      |                    |
|                             |                    | <i>see</i> Anzai J          | 177                |
| Takahashi N                 |                    | Villadsen J                 | 185, 187, 192      |
| <i>see</i> Matsubara M      | 220                | <i>see</i> Livbjerg H       | 201                |
| Takahashi T                 | 88, 92             | Vizcarra-Mendoza M          | 50, 51, 53, 63, 65 |
| Takahaski                   |                    | <i>see</i> Laguerie C       | 51                 |
| <i>see</i> Sato Y           | 276                | Voltz S E                   |                    |
| Talley J J                  | 167                | <i>see</i> Gross B          | 303, 304           |
| Talmor E                    | 271, 274           | <i>see</i> Jacob S M        | 300                |
| Tambe S S                   | 1                  | Vrana V                     | 168                |
| Tamura M                    | 172                |                             |                    |
| Tanaka S                    |                    | Wadekar V V                 | 165, 167           |
| <i>see</i> Kato Y           | 257, 261, 262      | Wadsworth M E               | 99                 |
| Tanigawa Y                  |                    | Wakao N                     | 307                |
| <i>see</i> Kawabata K       | 169                | Wallis G B                  | 264                |
| Taylor K C                  | 230                | Wandrey C                   |                    |
| Teijn Ltd.                  | 169                | <i>see</i> Renken A         | 236                |
| Terill D L                  | 164, 172           | Wang J B                    |                    |
| Thomas P H                  | 134, 135           | <i>see</i> Pereira C J      | 140                |
| Thomson M J                 | 177, 178           | Wang R A                    |                    |
| Tien C                      |                    |                             |                    |
| <i>see</i> Pendse H         | 281                |                             |                    |



- see* Qin K Z 308, 310, 312, 314, 316  
 Wang T-Y  
     *see* Imafuku K 257  
 Ward W J 175, 176  
     *see* Bdzil J 176  
     *see* Matson S L 175  
 Watanabe K 88, 92  
 Watson A T 238  
 Watson C C  
     *see* Johnson B H 88  
 Watson J S 257, 262  
 Way J D 175  
 Weekman V W Jr 299  
     *see* Jacob S M 300  
 Wegar E  
     *see* Schwartz T G 282, 283  
 Wei J 299-302  
 Welther C  
     *see* Albright L F 88  
 Wen C Y 13, 14, 28, 60  
 Wender I  
     *see* Deshpande G V 307  
 Werther J  
     *see* Hartge E U 44  
 West L A 222, 230, 231  
 Westmoreland P R 102, 104  
 Whitehead J C 307  
 Wild G  
     *see* Saberian-Broudjenni M 257  
 Williams D F 307  
     *see* Bartle K D 307  
 Wilson D H 220, 222, 223, 225, 226, 241  
 Winitz M 170  
 Wolf E E 88, 307  
 Woodburn T 50  
 Woolard I N M 18  
 Worley F L  
     *see* Chou T S 271  
 Wright C  
     *see* Byrne C 89, 91  
 Wu R L 44  
 Wu Z 180  
 Xiong K  
     *see* Zhu Y 308  
 Xue W  
     *see* Zhu Y 308  
 Yamaguchi T  
     *see* Shinbo T 176  
 Yang H  
     *see* Zhu Y 308  
 Yang S-Z  
     *see* Kato Y 249  
 Yarita T  
     *see* Nashiro M 179  
 Yasunishi A  
     *see* Muroyama K 257  
 Yates J G 53, 57, 70, 76, 84  
 Yerushalmi J 35, 45  
 Yi Duran H  
     *see* Barreteau D 51, 55  
     *see* Laguerie C 51  
 Yonowich-Weiss M  
     *see* Sasson Y 168  
 Yoshida J  
     *see* Kawabata K 169  
 Yoshida K 247  
     *see* Tsutsumi A 261, 265  
 Yoshikawa M 177  
 Yu Ch-C  
     *see* Sampath B S 122  
 Yu H-Ch 116  
 Yokoshi T  
     *see* Yoshikawa M 177  
 Zaidi A  
     *see* Deckwer W-D 257  
 Zeldovich Ya B 134  
 Zhu Y 308  
 Ziegler E N 257  
 Zuo C  
     *see* Wu Z 180

## Subject Index

- Catalyst activity
  - Periodic operation of chemical reactors – a review of the experimental literature 217
- Catalytic reactors
  - Periodic operation of chemical reactors – a review of the experimental literature 217
- Catalyst regeneration
  - Coking and regeneration of fixed bed catalytic reactors 87
- Chemical reactors
  - Parametric sensitivity and runaway in chemical reactors 133
- Chemical reactor dynamics
  - Periodic operation of chemical reactors – a review of the experimental literature 217
- Circulating fluidized bed reactor
  - Circulating fluidized bed reactor design and operation 35
- Classification
  - Classification of three-phase reactors 247
- Cluster analysis
  - Lumping analysis in the presence of measurement error 299
- Cobalt catalysts
  - Olefin incorporation on supported FeCo alloy Fischer-Tropsch catalysts 149
- Coking
  - Coking and regeneration of fixed bed catalytic reactors 87
- Counter-current backmixing model
  - The counter-current backmixing model for fluid bed reactors – computational aspects and model modifications 13
- CuO/Al<sub>2</sub>O<sub>3</sub>
  - Gas desulphurization by sorption of CO<sub>2</sub> on CuO/Al<sub>2</sub>O<sub>3</sub> solid sorbent in a counterflow multistage fluidized bed reactor: Experimental analysis and modelling of the reactor 49
- Cycling
  - Periodic operation of chemical reactors – a review of the experimental literature 217
- Desulphurization
  - Gas desulphurization by sorption of CO<sub>2</sub> on CuO/Al<sub>2</sub>O<sub>3</sub> solid sorbent in a counterflow multistage fluidized bed reactor: Experimental analysis and modelling of the reactor 49
- Dissociation extraction
  - New strategies for separations through reactions 163
- Dissociation extractive crystallization
  - New strategies for separations through reactions 163
- Experimental data
  - Gas desulphurization by sorption of CO<sub>2</sub> on CuO/Al<sub>2</sub>O<sub>3</sub> solid sorbent in a counterflow multistage fluidized bed reactor: Experimental analysis and modelling of the reactor 49
- Fischer-Tropsch catalysts
  - Olefin incorporation on supported FeCo alloy Fischer-Tropsch catalysts 149
- Fluid bed reactors
  - The counter-current backmixing model for fluid bed reactors – computational aspects and model modifications 13
- Fluidization
  - Population balance modelling of bubbling fluidized beds II. Axially dispersed dense phase 69
- Gas holdup
  - Effect of particle size on gas holdup in three-phase reactors 261
- Gas-solid reactions
  - A comparative study of mathematical models for gas-solid non-catalytic reactions 99
- Gas-sparged slurry reactor
  - Classification of three-phase reactors 247
  - Effect of particle size on gas holdup in three-phase reactors 261
- Heterogeneous reaction kinetics
  - Transient analysis of the particle-pellet model with structural changes in the solid phase 115
- Hot gas desulphurisation
  - A comparative study of mathematical models for gas-solid non-catalytic reactions 99
- Hydrometallurgical separations
  - New strategies for separations through reactions 163
- Iron-cobalt alloy catalysts
  - Olefin incorporation on supported FeCo alloy Fischer-Tropsch catalysts 149
- Iron catalysts
  - Olefin incorporation on supported FeCo alloy Fischer-Tropsch catalysts 149
- Kondepudi's pitchfork reaction
  - A global study of Kondapudi's pitchfork 1

- Liquid clusters
  - Theoretical foundation of cluster formation in supported liquid-phase catalysis 185
- Liquid dispersion in porous solids
  - Theoretical foundation of cluster formation in supported liquid phase catalysis 185
- Lumping analysis
  - Lumping analysis in the presence of measurement error 299
- Mathematical modelling
  - The counter-current backmixing model for fluid bed reactors – computational aspects and model modifications 13
- Mathematical models
  - A comparative study of mathematical models for gas-solid non-catalytic reactions 99
- Measurement error
  - Lumping analysis in the presence of measurement error 299
- Membrane separation
  - New strategies for separations through reactions 163
- Micelles in separation
  - New strategies for separations through reactions 163
- Modelling
  - Gas desulphurization by sorption of  $\text{CO}_2$  on  $\text{CuO}/\text{Al}_2\text{O}_3$  solid sorbent in a counterflow multistage fluidized bed reactor: Experimental analysis and modelling of the reactor 49
- Monomolecular first-order kinetic systems
  - Lumping analysis in the presence of measurement error 299
- Monte Carlo simulation
  - Population balance modelling of bubbling fluidized beds. II. Axially dispersed dense phase 69
- Multistage fluidized bed
  - Gas desulphurization by sorption of  $\text{CO}_2$  on  $\text{CuO}/\text{Al}_2\text{O}_3$  solid sorbent in a counterflow multistage fluidized bed reactor: Experimental analysis and modelling of the reactor 49
- Multiphase reactors
  - Recent advances in the analysis and design of trickle-bed reactors 269
- Non-catalytic gas-solid reactions
  - Transient analysis of the particle-pellet model with structural changes in the solid phase 115
- Non-catalytic reactions
  - A comparative study of mathematical models for gas-solid non-catalytic reactions 99
- Olefin incorporation in synthesis reactions
  - Olefin incorporation on supported FeCo alloy Fischer-Tropsch catalysts 149
- Oil shale
  - Supercritical fluid extraction of Chinese Maoming oil shale with water and toluene 307
- Parametric sensitivity
  - Parametric sensitivity and runaway in chemical reactors 133
- Periodic operation
  - Periodic operation of chemical reactors – a review of the experimental literature 217
- Population balances
  - Population balance modelling of bubbling fluidized beds. II. Axially dispersed dense phase 69
- Reactive crystallization
  - New strategies for separations through reactions 163
- Reactive distillation
  - New strategies for separations through reactions 163
- Reactor hydrodynamics
  - Circulating fluidized bed reactor design and operation 35
- Reactor models
  - Parametric sensitivity and runaway in chemical reactors 133
- Runaway behaviour
  - Parametric sensitivity and runaway in chemical reactors 133
- Selectivity in synthesis reactions
  - Olefin incorporation on supported FeCo alloy Fischer-Tropsch catalysts 149
- Separation through reactions
  - New strategies for separations through reactions 163
- Separations with hydrotropes
  - New strategies for separations through reactions 163
- Separations with supercritical fluids
  - New strategies for separations through reactions 163
- Silica-alumina bead catalyst
  - Coking and regeneration of fixed bed catalytic reactors 87
- Sorption
  - Gas desulphurization by sorption of  $\text{CO}_2$  on  $\text{CuO}/\text{Al}_2\text{O}_3$  solid sorbent in a counterflow multistage fluidized bed reactor: Experimental analysis and modelling of the reactor 49
- Stable steady state
  - A global study of Kondepudi's pitchfork 1
- Stirred tank reactor
  - A global study of Kondepudi's pitchfork 1
- Structural changes
  - Transient analysis of the particle-pellet model with structural changes in the solid phase 133

- Supercritical extraction  
  Supercritical fluid extraction of Chinese Maoming oil shale with water and toluene 307
- Supercritical fluid extraction  
  Supercritical fluid extraction of Chinese Maoming oil shale with water and toluene 307
- Supercritical water  
  Supercritical fluid extraction of Chinese Maoming oil shale with water and toluene 307
- Supercritical toluene  
  Supercritical fluid extraction of Chinese Maoming oil shale with water and toluene 307
- Supported liquid-phase catalysts  
  Theoretical foundation of cluster formation in supported liquid-phase catalysis 185
- Three-phase bubble column  
  Classification of three-phase reactors 247  
  Effect of particle size on gas holdup in three-phase reactors 261
- Three-phase fluidized bed  
  Classification of three-phase reactors 247  
  Effect of particle size on gas holdup in three-phase reactors 261
- Three-phase reactors  
  Classification of three-phase reactors 247  
  Effect of particle size on gas holdup in three-phase reactors 261
- Transient behaviour of reactors  
  Periodic operation of chemical reactors – a review of the experimental literature 217
- Transfer processes  
  Circulating fluidized bed reactor design and operation 35
- Trickle beds  
  Recent advances in the analysis and design of trickle-bed reactors 269







# ACADEMY PUBLICATIONS IN ENGINEERING SCIENCES

General Editor: R Narasimha

Volume 1. The Aryabhata Project (eds U R Rao, K Kasturirangan)

Volume 2. Computer Simulation (eds N Seshagiri, R Narasimha)

Volume 3. Rural Technology (ed. A K N Reddy)

Volume 4. Alloy Design (eds S Ranganathan, V S Arunachalam, R W Cahn)

...attempt in bringing together a series of articles, written by eminent scientists of India and abroad... Academy deserves all praise in bringing out these two timely issues.

*Powder Metall. Assoc. India, Newslett.*

Volume 5. Surveys in Fluid Mechanics (eds R Narasimha, S M Deshpande)

An informal and stimulating publication... (provides) a survey of many important topics in Fluid Mechanics.... All the papers are of excellent technical content and most are very well written. Many include lengthy reference lists, which are as useful as the body of the paper... The publishing quality is very good...

*IEEE Journal of Ocean Engineering*

... The general level (of papers) is high... Several are likely to have wide appeal... Judging by the invited lectures, the Asian Congresses of Fluid Mechanics are off to a good start.

*Journal of Fluid Mechanics*

Volume 6. Wood Heat for Cooking (eds K Krishna Prasad, P Verhaart)

...interesting and stimulating account of technical thinking on the wood stove problem up to date... excellent collection of valuable and thought-provoking investigations on the subject.

*Rev. Projector (India)*

Volume 7. Remote Sensing (eds B L Deekshatulu, Y S Rajan)

...Several contributions are specifically addressing topics of national interest, however, the majority of the papers is of general interest for a wide community. The book can serve not only as an inventory of the Indian activities, but also as a textbook on techniques and applications of remote sensing.

*Photogrammetria*

...particularly refreshing...

*Int. J. Remote Sensing*

Volume 8. Water Resources Systems Planning (eds M C Chaturvedi, P Rogers)

...It is well got up and very well printed and forms a valuable addition to our limited literature on Water Resources of India.

*Curr. Sci.*